

Leveraging 1,2-Azaborine's Distinct Electronic Structure to Access New Building Blocks:

Author: Cameron Reed McConnell

Persistent link: <http://hdl.handle.net/2345/bc-ir:108607>

This work is posted on [eScholarship@BC](#),
Boston College University Libraries.

Boston College Electronic Thesis or Dissertation, 2019

Copyright is held by the author. This work is licensed under a Creative Commons Attribution 4.0 International License (<http://creativecommons.org/licenses/by/4.0>).

Boston College
The Graduate School of Arts and Sciences
Department of Chemistry

LEVERAGING 1,2-AZABORINE'S DISTINCT ELECTRONIC STRUCTURE TO
ACCESS NEW BUILDING BLOCKS

A dissertation

By

CAMERON REED MCCONNELL

Submitted in partial fulfillment of the requirements
for the degree of
Doctor of Philosophy

May 2019

© copyright by CAMERON REED MCCONNELL

2019

LEVERAGING 1,2-AZABORINE'S DISTINCT ELECTRONIC STRUCTURE TO
ACCESS NEW BUILDING BLOCKS

By

CAMERON REED MCCONNELL

Dissertation Advisor:

Professor Shih-Yuan Liu

ABSTRACT: Described herein are three projects that derive from in-depth studies of the distinct electronic structure of monocyclic 1,2-dihydro-1,2-azaborine (heretofore referred to as simply 1,2-azaborine). In the first chapter, the first comprehensive review of the late-stage functionalization methods available for 1,2-azaborines as well as their bicyclic and polycyclic (BN-PAH) counterparts is presented. In the second chapter, the development of a general method for both C4 and C5 functionalization based on the building block approach is described. The distinct electronic structure of 1,2-azaborine enables the chemical separation and further functionalization of C4 and C5 borylated isomers. In the second part, the C4, C5, and C6 isomers of BN-styrene analogues were prepared using the newly developed azaborine building blocks. The corresponding polymers were synthesized and extensively characterized in order to compare the effects of the BN-bond positioning relative to the polymer chain. In the fourth and final chapter, 1,2-azaborine-containing phosphine ligands featuring a P-B bond are synthesized. A comparative electronic structure analysis is performed between the BN-phosphine ligands and their direct all-carbon counterparts.

Dedicated to:

My late grandfather and role model, Carl Bardman.

It was a privilege to know you.

ACKNOWLEDGMENTS

I will be forever grateful to my advisor, Professor Liu, for guiding me through the PhD process. Professor Liu is not only committed to the endeavor of scientific research but he is also passionate about teaching and the academic development of his students. I appreciate everything he has taught me, from the intricacies of chemical kinetics to critical thinking skills to the philosophy and practice of being meticulous. I know that the skills and knowledge I have acquired working in the Liu lab will serve me well in future endeavors.

I would like to thank Professor Jeff Byers and Professor James Morcken for taking the time to serve on my thesis committee and for offering their invaluable insights and advice. Professor Byers's physical organic course and Professor Morcken's synthesis course were foundational to my chemistry knowledge. I would also like to thank Professor Fredrik Haeffner for his patient efforts at teaching me computational chemistry; he was an essential collaborator in my thesis work.

Dr. Jacob Ishibashi and Dr. Rich Burford are incredible scientists and great friends. Jacob's critical approach to research and Rich's discipline and work ethic are inspirational. I consider myself very fortunate to have worked with them and I appreciate their support and mentorship.

Thanks to Dr. Andrew Baggett, Dr. Alec Brown, and Dr. Zachary Giustra for welcoming me to the Liu lab. It was a pleasure to work with such helpful and friendly senior colleagues. I also greatly appreciate the friendship and camaraderie of my classmate Katie Boknevitc as well as my younger colleagues Yuanzhe Zhang, Ricky Alvarado, Jon Deegan, Jeremy Armand, and the rest of the Liu lab crew. I also appreciate the help of my undergrad mentee, Keri Steiniger. I couldn't ask for better lab mates.

Special thanks go out to Dale Mahoney, Dr. Marek Domin, Dr. Ian Parr, Dr. Thusitha Jayasundera (TJ), and the rest of the BC office and instrument staff whose hard work and professionalism made it possible for me to conduct my research.

Thanks to my undergraduate advisor Professor Robert A. Stockland, Jr. for helping me get to BC and to Dr. Charles Verenna for getting me started on my chemistry journey. Thanks to Professor Philippe Dubois for making me a better student and a better person.

None of this would have been possible without the love and commitment of my family. My grandparents, Carl and Marion and Walter and Isabel, inspire me. My parents, Jeff and Christine, provided me with every conceivable advantage and opportunity. Curt and Collin, my brothers, and the rest of my extended family have always provided the utmost love and support.

Finally, I owe an incredible amount of gratitude to my wife, Daria Tuzhikova. Daria always provided unwavering support in the face of the many challenges brought on by the PhD process while still pushing me on to greater achievements. Thanks for always being on my team.

List of Abbreviations

Ac: acetyl	DPPF: bis(diphenylphosphino)ferrocene
AIBN: 1,1'-azobisisobutyronitrile	DSC: differential scanning calorimetry
atm: atmosphere(s)	dtbpy: 4,4'-di- <i>tert</i> -butyl-2,2'-dipyridyl
azaborine: monocyclic 1,2-dihydro-1,2-azaborine	Et: ethyl
B ₂ pin ₂ : bispinacolatodiboron	ESP: electrostatic potential
BDE: bond dissociation energy	GPC: gel permeation chromatography
Bn: benzyl	h: hour(s)
Boc: <i>tert</i> -butoxycarbonyl	HMBC: heteronuclear multiple bond correlation
Bu: <i>n</i> -butyl	HMQC: heteronuclear multiple quantum coherence
cod: 1,5-cyclooctadiene	HOMO: highest occupied molecular orbital
Cp: cyclopentadienyl	HPLC: high performance liquid chromatography
Cp*: pentamethylcyclopentadienyl	HRMS: high resolution mass spectrometry
Cy: cyclohexyl	ICy: 1,3-bis(1-cyclohexyl)imidazolin-2-ylidene
CV: cyclic voltammetry	LAH: lithium aluminum hydroxide
Da: Daltons	LDA: lithium diisopropyl amide
dan: 1,8-diaminonaphthalene	LUMO: lowest unoccupied molecular orbital
DART: direct analysis in real time	Me: methyl
dba: dibenzylidene diacetone	
DDQ: 2,3-dichloro-5,6-dicyanobenzoquinone	
DFT: density functional theory	
DMF: N,N-dimethylformamide	
DMSO: dimethylsulfoxide	

Mes: 2,4,6-trimethylphenyl	TD-DFT: time-dependent density
MIDA: N-methyliminodiacetic acid	functional theory
MTBE: <i>tert</i> -butylmethyl ether	TEP: Tolman Electronic Parameter
nbd: norbornadiene	TF: trifluoromethanesulfonyl
NBS: N-bromosuccinimide	T _g : glass transition temperature
NHC: N-heterocyclic carbene	TGA: thermogravimetric analysis
NICS: nucleus independent chemical shift	THF: tetrahydrofuran
NMO: N-methylmorpholine-N-oxide	TMSCl: trimethylsilyl chloride
NMR: nuclear magnetic resonance	TOF: turnover frequency
OMe: methoxy	UV-PES: ultra violet photoelectron spectroscopy
Ph: phenyl	
pin: pinacol	
PPh ₃ : triphenylphosphine	
ppm: parts per million	
PS: polystyrene	
RAFT: reversible addition-fragmentation chain transfer	
RCM: ring closing metathesis	
RSE: resonance stabilization energy	
RT: room temperature	
St: styrene	
<i>t</i> -Bu: <i>tert</i> -butyl	
TBS: <i>tert</i> -butyldimethylsilyl	
TBSCl: <i>tert</i> -butyldimethylsilyl chloride	

TABLE OF CONTENTS
Chapter 1: Late-Stage Functionalization of BN-Heterocycles

1.1 Introduction: 1,2-azaborines.....	1
1.1.1 BN/CC Isosterism in Benzene and its Analogues.....	1
1.1.2 Improvements in the Synthesis of 1,2-azaborines.....	3
1.1.3 Properties of 1,2-azaborines.....	6
1.2 Introduction: Late-Stage Functionalization of 1,2-azaborines.....	10
1.3 Monocyclic 1,2-azaborines.....	14
1.3.1 Electrophilic Aromatic Substitution (EAS).....	14
1.3.1.1 <i>C3 Substitution</i>	14
1.3.1.2 <i>C5 Substitution</i>	15
1.3.2 C-H Borylation.....	17
1.3.3 Cross-Coupling.....	18
1.3.3.1 <i>Suzuki-Miyaura Cross-Coupling</i>	18
1.3.3.2 <i>Negishi Cross-Coupling</i>	20
1.3.4 Nucleophilic Substitution.....	21
1.3.4.1 <i>BN Disubstitution</i>	21
1.3.4.2 <i>Boron Substitution with Anionic Nucleophiles</i>	23
1.3.4.3 <i>Boron Substitution with Neutral Nucleophiles</i>	24
1.3.4.4 <i>Boron Substitution of N-TBS, B-Cl Synthons</i>	25
1.3.4.5 <i>C3 Substitution</i>	26
1.3.5 Electrophilic Substitution at Nitrogen.....	27
1.3.5.1 <i>Deprotonation of N-H Substituted Azaborines</i>	27
1.3.5.2 <i>Deprotection of N-Silyl Substituted Azaborines</i>	28
1.3.6 B-X Activation.....	29
1.3.6.1 <i>B-Cl Activation</i>	30

1.3.6.2 <i>B-H Activation</i>	31
1.3.6.3 <i>B-C Activation</i>	31
1.3.7 BN-Styrene Reactivity.....	33
1.3.8 Diels-Alder.....	35
1.4 BN-Naphthalenes.....	37
1.4.1 EAS.....	37
1.4.1.1 <i>Halogenation</i>	37
1.4.1.1 <i>Acylation</i>	39
1.4.2 Borylation.....	41
1.4.3 Cross-Coupling.....	43
1.4.3.1 <i>Cross-Coupling of 1,2-Naphthalenes</i>	44
1.4.3.2 <i>Cross-Coupling of 9,10-Naphthalenes</i>	48
1.4.4 Nucleophilic Substitution.....	49
1.4.5 Benzylic Functionalization.....	51
1.4.6 Electrophilic Substitution.....	52
1.5 BN-Polycyclic Aromatic Hydrocarbons (PAHs).....	52
1.5.1 EAS.....	53
1.5.2 Cross-Coupling.....	56
1.5.3 Nucleophilic Substitution.....	57
1.5.4 Electrophilic Substitution at Nitrogen.....	58
1.5.5 B-X Activation.....	58
1.6 Distinct Reactivity of BN-Heterocycles.....	59
1.7 Conclusions.....	60

Chapter 2: Accessing New Regioisomeric Building Blocks of 1,2-Azaborine via Resolution Chemistry Enabled by 1,2-Azaborine's Distinct Electronic Structure

2.1 Introduction.....	62
2.1.1 Chapter Overview.....	62
2.1.2 Building Block Approach to Azaborine Synthesis.....	65
2.1.3 Regio- and Chemo-selective Reactions of Boronic Esters.....	67
2.2 Electronic Structure Analysis of C4 and C5 Borylated Azaborines.....	72
2.3 Oxidation with <i>N</i> -methylnmorpholine- <i>N</i> -oxide (NMO).....	74
2.4 Iridium-Catalyzed Protodeborylation.....	76
2.5 Transesterification with Diethanolamine.....	78
2.6 Functionalization of the 4- and 5- Positions of the 1,2-Azaborine.....	80
2.7 Conclusions.....	82
2.8 Experimental Section.....	83
2.8.1 General.....	83
2.8.2 Syntheses.....	83
2.8.3 Kinetic and Thermodynamic Experiments.....	88
2.8.4 Computational Details.....	97
2.8.5 NMR Spectra.....	126

Chapter 3: Changing up BN-Styrenes: Effect of Substitution Pattern on the Free Radical Polymerization and Polymer Properties

3.1 Introduction: BN-Containing Polymers.....	142
3.2 Monomer Synthesis.....	145
3.3 Electronic Structure Calculations.....	146
3.4 Polymerizations.....	148

3.5 Thermal and Spectral Properties of Monomers and Polymers.....	152
3.6 Conclusions.....	155
3.7 Experimental Section.....	157
3.7.1 General Methods.....	157
3.7.2 Materials.....	157
3.7.3 Monomer Synthesis.....	158
3.7.4 Homopolymerizations.....	173
3.7.5 2D NMR Spectra.....	184
3.7.6 Copolymerizations.....	190
3.7.7 Calculations.....	198

**Chapter 4: Synthesis, Electronic Structure Characterization, and Comparative
Analysis of 1,2-Azaborine-Containing Phosphine Ligands**

4.1 Introduction: Phosphine Ligands.....	235
4.1.1 The Role of Phosphine Ligands in Catalysis.....	235
4.1.2 Measuring the Properties of Phosphine Ligands.....	236
4.1.3 The Effect of Ligand Choice on Palladium-Catalyzed Cross-Couplings.....	241
4.1.4 Prior Examples of P-B Containing Ligands.....	246
4.1.5 Proposal for a New 1,2-Azaborine-Containing Phosphine Ligand.....	259
4.2 Synthesis and Characterization of BN-Phosphine Ligands.....	260
4.2.1 Synthesis of BN-Phosphine Ligands.....	260
4.2.2 Evaluation of Steric Parameters.....	261
4.2.3 Evaluation of Electronic Parameters.....	262
4.2.3.1 <i>UV-PES and DFT Studies</i>	262
4.2.3.2 <i>Determination of the Tolman Electronic Parameter</i>	264

4.3 Conclusions.....	266
4.4 Experimental Section.....	267
4.4.1 General Considerations.....	267
4.4.2 Synthetic Details.....	267
4.4.3 X-ray Crystal Structure Determination of 4.41 and 4.43	269
4.4.4 Electronic structure analysis of azaborine-phosphine ligand by UV-PES and quantum calculations.....	297
4.4.5 Cone Angle Determination.....	303
4.4.6 NMR Spectra.....	304
4.4.7 IR Spectra.....	312

Chapter 1

Late-Stage Functionalization of BN-Heterocycles

1.1 Introduction: 1,2-Azaborines

1.1.1 BN/CC Isosterism in Benzene and its Analogues

The replacement of a C=C bond with an isoelectronic and isosteric BN bond is known as BN/CC isosterism.¹ The two pairs of atoms share the same number of valence electrons, 4 from each carbon versus 5 and 3 from the nitrogen and boron, but exhibit different properties. A comparison between ethane (H₃CCH₃) and ammonia borane (H₃NBH₃) illustrates the potential differences between a CC and BN compound. Ethane is an inert gas at room temperature while ammonia borane is a solid (m.p. = 104 °C).² Ethane has no dipole moment and its C-H bonds are weakly acidic, and consequently exhibits weak intermolecular interactions; in contrast, ammonia borane is a highly polar molecule where the N-H bonds are somewhat acidic and the B-H bonds somewhat hydridic.² The introduction of the two different heteroatoms into a molecule will lead to at least a local dipole moment, and it will modify the nature of the frontier molecular orbitals. These electronic structural changes will result in new electronic and optical properties. BN isosteres of all-carbon compounds present an opportunity to alter the properties of molecules of interest across many fields of applied chemistry, driving an ever-expanding interest in BN chemistry.³

¹ For reviews of BN/CC isosterism in aromatic and other conjugated systems see: (a) Bosdet, M. J. D.; Piers, W. E. *Can. J. Chem.* **2009**, *87*, 8-29; (b) Campbell, P. G.; Marwitz, A. J. V.; Liu, S.-Y. *Angew. Chem. Int. Ed.* **2012**, *51*, 6074-6092. (c) Wang, X.-Y.; Wang, J.-Y.; Pei, J. *Chem. Eur. J.* **2015**, *21*, 3528-3539; (d) Bonifazi, D.; Fasano, F.; Lorenzo-Garcia, M. M.; Marinelli, D.; Oubaha, H.; Tasseroul, J. *Chem. Commun.* **2015**, *51*, 15222-15236; (e) Morgan, M. M.; Piers, W. E. *Dalton Trans.* **2016**, *45*, 5920-5924; (f) Helten, H. *Chem. Eur. J.* **2016**, *22*, 12972-12982.

² Liu, Z.; Marder, T. B. *Angew. Chem. Int. Ed.* **2008**, *47*, 242-244.

³ For a recent perspective on the field, see Giustra, Z. X.; Liu, S.-Y. *J. Am. Chem. Soc.* **2018**, *140*, 1184-1194.

Arenes are a ubiquitous motif found across many fields of chemistry,^{1b} and accordingly BN/CC isosterism in arenes has received significant attention. Until the 1950's, borazine, the inorganic version of benzene, was the only known BN arene.⁴ In 1958, Dewar replaced a single C=C bond of a polycyclic aromatic hydrocarbon (PAH) with a BN bond, making BN/CC isosterism reality in a seminal example of a hybrid organic/inorganic BNC arene (Figure 1.1a).⁵ The first azaborine, **1.1**, is a BN analogue of phenanthrene; Dewar⁶ and White⁷ later prepared the first monocyclic, 1,2-azaborines, **1.2** and **1.3**, respectively. Monocyclic azaborines, the isosteres of benzene **1.4**, have three possible isomers, the 1,2- (**1.5**), 1,3- (**1.6**), and 1,4-azaborine (**1.7**) (Figure 1.1b). Liu synthesized the parent compound of the 1,2 isomer⁸, while lightly substituted versions of the 1,3 **1.8**⁹ and 1,4-azaborine **1.9**¹⁰ were published by Liu and Braunschweig, respectively (Figure 1.1c).

⁴ Stock, A.; Pohland, E. *Ber. Dtsch. Chem. Ges.* **1926**, 59, 2210-2215.

⁵ Dewar, M. J. S.; Kubba, V. P.; Pettit, R. *J. Chem. Soc.* **1958**, 3073-3076.

⁶ Dewar, M. J. S.; Marr, P. A. *J. Am. Chem. Soc.* **1962**, 84, 3782.

⁷ White, D. G. *J. Am. Chem. Soc.* **1963**, 85, 3634-3636.

⁸ Marwitz, A. J. V.; Matus, M. H.; Zakharov, L. N.; Dixon, D. A.; Liu, S.-Y. *Angew. Chem. Int. Ed.* **2009**, 48, 973-977.

⁹ Chrostowska, A.; Xu, S.; Lamm, A. N.; Mazière, A.; Weber, C. D.; Dargelos, A.; Baylère, P.; Graciaa, A.; Liu, S.-Y. *J. Am. Chem. Soc.* **2012**, 134, 10279-10285.

¹⁰ Braunschweig, H.; Damme, A.; Jimenez-Halla, J. O. C.; Pfaffinger, B.; Radacki, K.; Wolf, J. *Angew. Chem. Int. Ed.* **2012**, 51, 10034-10037.

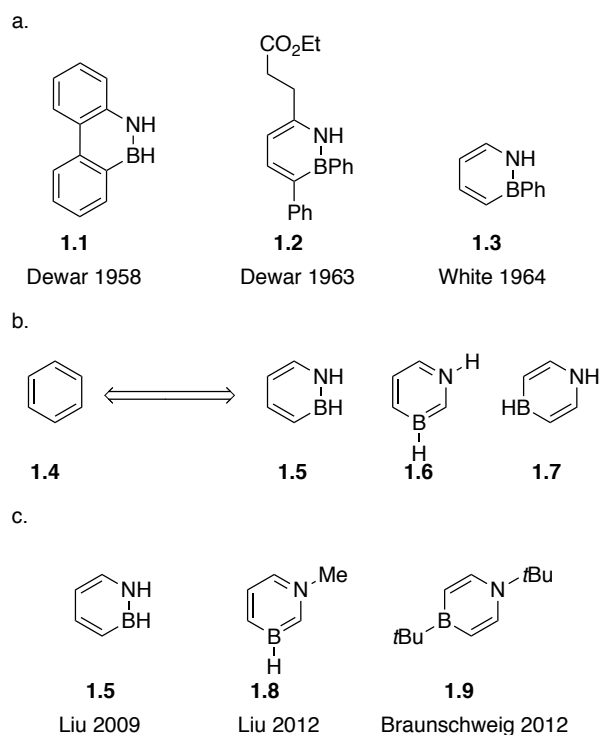


Figure 1.1. a) Early examples of BN arenes; b) Parental BN isosteres of benzene; c) Least-substituted examples of BN isosteres of benzene.

Over the ensuing decades, BN/CC isosterism in arenes has been demonstrated to be a viable strategy for expanding chemical space, spreading to fields where the arene structural motif is common such as materials, organometallic, biomedical, and synthetic chemistry.³ While there are rich chemistries in BN-containing polycyclic aromatic hydrocarbons as well as BN/CC isosterism in non-aromatic compounds, these topics are beyond the scope of this introduction.¹¹ Instead, this introduction will focus on the chemistry of monocyclic azaborines and in particular the 1,2-isomer.

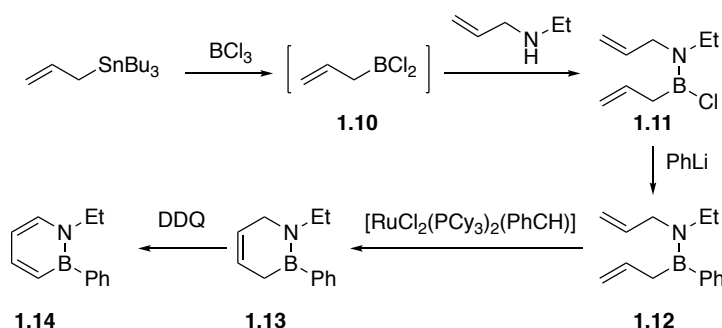
1.1.2 Improvements in the Synthesis of 1,2-azaborines

Dewar and White pioneered BN/CC isosterism in arenes, publishing examples of polycyclic as well as substituted monocyclic BN arenes.^{5,6,7} Dewar recognized the

¹¹ For more information on BN-PAHs, see: (a) Bosdet, M. J. D.; Piers, W. E. *Can. J. Chem.* **2009**, *87*, 8-29. (b) Campbell, P. G.; Marwitz, A. J. V.; Liu, S.-Y. *Angew. Chem. Int. Ed.* **2012**, *51*, 6074-6092. (c) Wang, X.-Y.; Wang, J.-Y.; Pei, J. *BN Chem. - Eur. J.* **2015**, *21*, 3528-3539. (d) Morgan, M. M.; Piers, W. E. *Dalton Trans.* **2016**, *45*, 5920-5924. (e) Huang, J.; Li, Y. *Front. Chem.* **2018**, *6*. For more information on BN/CC isosterism in non-aromatic compounds, see: Staubitz, A.; Robertson, A. P. M.; Sloan, M. E.; Manners, I. *Chem. Rev.* **2010**, *110*, 4023-4078.

potential utility of azaborines in a publication where he prepared water-soluble azaborines as potential neutron capture therapy agents.¹² However, interest in the field largely died off after the 1960's due to the limitations in scope and yield of the methods used to prepare BN arenes. In the early 2000's, Ashe revived interest in BN arenes by introducing a mild, efficient synthetic route based on a ring-closing metathesis/oxidation procedure to access 1,2-azaborine **1.14** (Scheme 1.1).¹³ Allyltributylstannane first undergoes transmetalation with boron trichloride to form *in-situ* generated allylborondichloride **1.10**. Addition of N-ethylallylamine yields adduct **1.11**, which is then substituted with phenyllithium at boron to furnish diallyl adduct **1.12**. An RCM reaction is performed on **1.12** to yield **1.13**, which subsequently undergoes oxidation with DDQ to finally yield aromatic 1,2-azaborine **1.14**.

Scheme 1.1. Mild synthesis of 1,2-azaborine.



In 2007, Liu introduced an important innovation to Ashe's RCM-based synthetic route that allowed for the preservation of the reactive B-Cl bond.¹⁴ The new synthetic route diverges at diallyl-adduct **1.11**; instead of installing a functional group at boron via nucleophilic addition, adduct **1.11** undergoes RCM to afford ring-closed product **1.15** (Scheme 1.2). Subsequent oxidation with palladium on carbon maintains

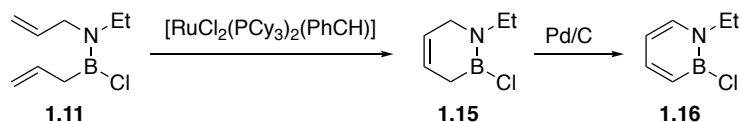
¹² Dewar, M. J. S.; Hashmall, J.; Kubba, V. P. *J. Org. Chem.* **1964**, *29*, 1755-1757.

¹³ Ashe, A. J.; Fang, X. *Org. Lett.* **2000**, *2*, 2089-2091.

¹⁴ Marwitz, A. J. V.; Abbey, E. R.; Jenkins, J. T.; Zakharov, L. N.; Liu, S.-Y. *Org. Lett.* **2007**, *9*, 4905-4908.

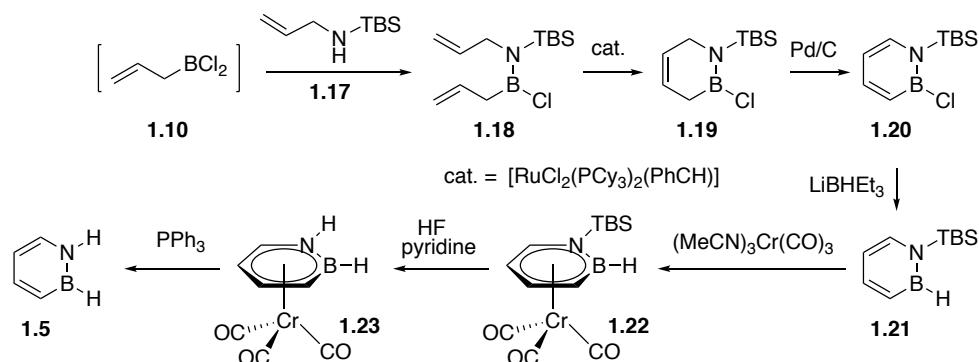
the B-Cl bond in synthon **1.16**, which is better suited to the preparation of libraries of B-substituted azaborines.

Scheme 1.2. Preparation of an *N*-alkyl, *B*-Cl 1,2-azaborine synthon.



In 2009, the Liu group made a landmark discovery in the chemistry of 1,2-azaborines with the publication of the parent 1,2-azaborine **1.5**.⁸ The key to unlocking the elusive parent 1,2-azaborine structure was the development of 1,2-azaborine synthon **1.20** which features a removable TBS group on the nitrogen (Scheme 1.3). Fully aromatic azaborine is still accessed via the same sequence of adduct **1.18** formation with allylamine **1.17** and **1.10**, RCM to form **1.19**, and oxidation to form **1.20**. It should be noted that **1.20** is a versatile azaborine synthon that features a removable TBS protecting group as well as a chloride leaving-group on the boron; methods for functionalizing compound **1.20** will be fully detailed in this chapter. Reduction of the B-Cl bond in **1.20** with lithium triethylborohydride affords **1.21**, which subsequently binds to chromium to furnish piano-stool complex **1.22**. Removal of the TBS group with HF pyridine is followed by decomplexation with triphenylphosphine to afford **1.5**, albeit in low yield (10% isolated yield).

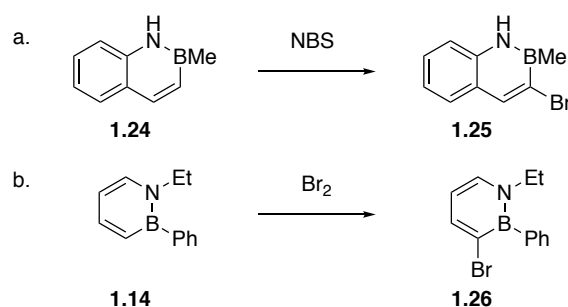
Scheme 1.3. Synthesis of parent 1,2-azaborine.



1.1.3 Properties of 1,2-azaborines

From the earliest days of azaborine chemistry, Dewar made observations that were consistent with the aromatic nature of azaborines.¹⁵ He noted that 2,1-azaboronaphthalene has a similar UV-VIS spectrum to its isostere naphthalene, suggesting its aromatic character. In addition, it was observed that the BH substituted 2,1-azaboronaphthalene was resistant to hydrolysis in alkaline solution, evidence for its aromatic stability. In another publication, 2,1-azaboronaphthalene derivatives **1.24** were shown to undergo electrophilic aromatic substitution at the 3 position to yield **1.25**, reactivity associated with aromatic compounds (Scheme 1.4a).¹⁶ Ashe later demonstrated similar reactivity with 1,2-azaborines, where **1.14** is brominated at the 3 position to furnish **1.26** (Scheme 1.4b).¹⁷ However, more definitive experimental and theoretical evidence for the aromatic character of azaborines did not arrive until the work by Ashe, Liu, and others.

Scheme 1.4. Electrophilic aromatic substitutions of 1,2-azaborines.



NMR spectra of various 1,2-azaborines by Ashe revealed ¹H NMR chemical shifts consistent with the presence of aromatic ring current effects.¹⁸ Nucleus independent chemical shift (NICS) calculations are also consistent with the aromatic character of 1,2-azaborine.^{11b} Aside from the magnetic field induced by ring-current

¹⁵ Dewar, M. J. S.; Dietz, R. *J. Chem. Soc.* **1959**, 2728-2730.

¹⁶ Dewar, M. J. S.; Dietz, R. O. *Y. J. Org. Chem.* **1961**, 26, 3253-3256.

¹⁷ Pan, J.; Kampf, J. W.; Ashe, A. *J. Org. Lett.* **2007**, 9, 679-681.

¹⁸ Ashe, A. J., III; Fang, X.; Fang, X.; Kampf, J. W. *Organometallics* **2001**, 20, 5413-5418.

effects,¹⁹ certain structural parameters are also associated with aromaticity. Aromatic compounds are cyclic and exhibit bond lengths that fall between typical single and double bonds.²⁰ Unlike conjugated systems, bond lengths throughout the aromatic framework are often similar due to electron delocalization. Liu and co-workers sought to provide structural evidence for the aromaticity of azaborines by preparing a series of reference heterocycles to compare with the fully delocalized structure of 1,2-azaborine.²¹

The Liu group prepared another series of cyclohexene analogues, this time in order to experimentally measure the resonance stabilization energy (RSE) of 1,2-azaborine.²² RSE is a measure of the additional energetic stabilization engendered by the cyclic arrangement of a conjugated system compared to the corresponding number of isolated double bonds.²³ The RSE can be measured by comparing the heats of hydrogenation of the aromatic compound in question with a series of reference compounds. Kistiakowsky and co-workers employed the technique in 1936 to measure the RSE of benzene, found to be 36 kcal mol⁻¹.²³ Enthalpies of hydrogenation for the azaborine system were determined by reaction calorimetry and the RSE of azaborine was found to be 16.6 ± 1.3 kcal mol⁻¹.²² While significantly lower than that of benzene, the RSE value for azaborine is on par with those of other heterocycles such as pyrrole (RSE ≅ 21 kcal mol⁻¹) and furan (RSE ≅ 15 kcal mol⁻¹).²⁴ One interesting consequence of this lower RSE value is that unlike their all-carbon

¹⁹ Dauben, H. J.; Wilson, J. D.; Laity, J. L. *J. Am. Chem. Soc.* **1968**, *90*, 811-813.

²⁰ Krygowski, T. M.; Cyrański, M. K. *Chem. Rev.* **2001**, *101*, 1385-1420.

²¹ Abbey, E. R.; Zakharov, L. N.; Liu, S.-Y. *J. Am. Chem. Soc.* **2008**, *130*, 7250-7252.

²² Campbell, P. G.; Abbey, E. R.; Neiner, D.; Grant, D. J.; Dixon, D. A.; Liu, S.-Y. *J. Am. Chem. Soc.* **2010**, *132*, 18048-18050.

²³ Kistiakowsky, G. B.; Ruhoff, J. R.; Smith, H. A.; Vaughan, W. E. *J. Am. Chem. Soc.* **1936**, *58*, 146-153.

²⁴ Burford, R. J.; Li, B.; Vasiliu, M.; Dixon, D. A.; Liu, S.-Y. *Angew. Chem. Int. Ed.* **2015**, *54*, 7823-7827.

analogues, certain 1,2-azaborines can undergo Diels-Alder reactions with highly activated dienophiles, similar to other heterocycles such as furan.²⁴

In addition to structural, reactivity, and aromatic properties of 1,2-azaborine, the physical and electronic properties have also been extensively studied.^{8,25} In 2012, Liu and Chrostowska published an extensive electronic structure analysis of 1,2-azaborine based on UV-photoelectron spectroscopy (UV-PES), supported by DFT calculations.²⁶ UV-PES is the measurement of kinetic energy of electrons emitted by a molecule that has absorbed UV photons, which provides information about the ionization energies of filled molecular orbitals.²⁷ Molecular orbital energies may be determined from the data. For benzene, the first band at 9.25 eV represents the ionization energy of the degenerate HOMOs of π symmetry (Figure 1.2). The next bands at 11.53 and 12.36 represent a set of degenerate orbitals of σ symmetry and the fully symmetrical π_3 orbital. Comparing these data with the results for 1,2-azaborine, the introduction of the polarized BN bond lifts the degeneracy of the orbitals and raises the HOMO energy level. The ionization energy at 8.6 corresponds to the HOMO of azaborine and is comparable to the π_1 of benzene. Contributing to the HOMO-1 at 10.3 are the nitrogen lone pair as well the π -bonding between C(3), C(4), and C(5), analogous to the π_2 of benzene. σ orbitals account for the electrons ejected at 11.1 and 12.0. The fifth ionization band at 12.7 is the π_3 equivalent of benzene. This comparison of the UV-PE spectra clearly shows a significant change in the electronic structure caused by the replacement of a C=C bond with a B-N bond.

²⁵ Abbey, E. R.; Lamm, A. N.; Baggett, A. W.; Zakharov, L. N.; Liu, S.-Y. *J. Am. Chem. Soc.* **2013**, *135*, 12908-12913.

²⁶ Chrostowska, A.; Xu, S.; Lamm, A. N.; Mazière, A.; Weber, C. D.; Dargelos, A.; Baylère, P.; Graciaa, A.; Liu, S.-Y. *J. Am. Chem. Soc.* **2012**, *134*, 10279-10285.

²⁷ Turner, D. W.; Baker, C.; Baker, A. D.; Brundle, C. R. *Molecular Photoelectron Spectroscopy*; Wiley-Interscience: New York, 1970.

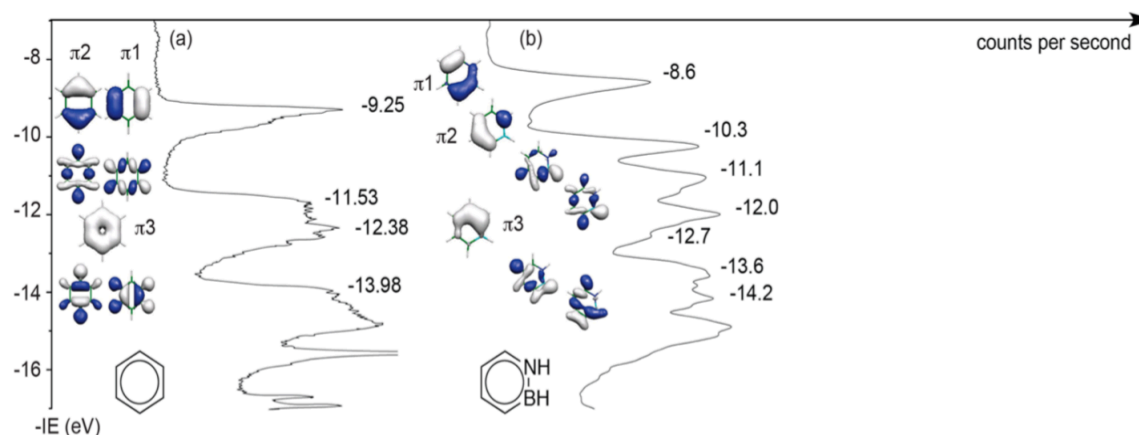


Figure 1.2. UV-PES spectra of benzene and 1,2-azaborine.²⁶

Other electronic properties of azaborine were determined through detailed calculations involving DFT and ab-initio methods.²⁶ A significant dipole of 2.15 D was determined for 1,2-azaborine (Table 1.1). Electrostatic potential (ESP) maps indicate the dipole points toward the C(3) and boron atoms; the B-H is hydridic while the N-H is protic. As discussed previously, the azaborine HOMO is higher than that of benzene, however the LUMO of azaborine, 0.6 eV, is calculated to be lower than that of benzene at 1.1 eV. It follows that the HOMO-LUMO gap of azaborine, 8.2 eV, is reduced compared to that of benzene, 9.5 eV. Introduction of the polar BN bond has a noticeable effect on the UV-VIS/absorption of 1,2-azaborine and BN compounds more generally. The λ_{max} of 1,2-azaborine (269 nm) is bathochromically-shifted compared to that of benzene (255 nm).

Table 1.1. Calculated electronic properties of benzene and 1,2-azaborine. CAM-B3LYP/6-311G(d,p) Ground- and First Excited-State Dipole Moments (Debye) and MP2/6-311G(d,p) Electrostatic Potential Surface Map at the 0.001 Electron au⁻³ Density Isocontour Level (from +12.55 to -12.55 kcal/mol), Δ SCF IE, HOMO, LUMO Energies and HOMO-LUMO Gap, EA (calculated with 6-311++G(d,p)), Δ (EA + IE), First HOMO \rightarrow LUMO UV Transition (calculated with 6-311++G(d,p)).²⁶

	benzene	1,2-azaborine
Electrostatic potential map		
Dipole Moment (D)	0	2.15
HOMO (ev)	-8.4	-7.7
LUMO (ev)	1.1	0.6
HOMO-LUMO gap (ev)	9.5	8.2

Clearly, introducing a BN bond in an arene has significant effects on the electronic properties, from the polarity to the energy levels and the aromaticity. In contrast, the changes to the steric properties induced by the BN bond are relatively minor. The isosteric relationship between benzene and 1,2-dihydro-1,2-azaborine provides an opportunity to alter the electronic properties of a given molecule without changing its steric properties. Due to the ubiquity of the phenyl structural motif across many fields of chemistry, one can envision a large number of potential applications to leverage the effects of BN/CC isosterism.

1.2 Introduction: Late-Stage Functionalization of 1,2-azaborines

As interest in BN/CC isosterism in arenes has increased significantly over the last few decades, so has the need for access to more complex derivatives.^{28,29,30,31} In particular, applications of BN-containing arenes are emerging in the fields of

²⁸ For an overview of BN/CC isosterism in aromatic compounds, see: Bosdet, M. J. D.; Piers, W. E. *Can. J. Chem.* **2009**, *87*, 8-29.

²⁹ For a history of azaborine chemistry, see: Campbell, P. G.; Marwitz, A. J. V.; Liu, S.-Y. *Angew. Chem. Int. Ed.* **2012**, *51*, 6074-6092.

³⁰ For recent developments in azaborine chemistry, see: Bélanger-Chabot, G.; Braunschweig, H.; Roy, D. K. *Eur. J. Inorg. Chem.* **2017**, (38-39), 4353-4368.

³¹ For a perspective on the applications of azaborines, see: Giustra, Z. X.; Liu, S.-Y. *J. Am. Chem. Soc.* **2018**, *140*, 1184-1194.

materials chemistry,^{32,33} biomedical chemistry,³⁴ ligand design in homogeneous catalysis,³⁵ and more recently, in organic synthesis.³⁶ The burgeoning of applications of BN-containing arenes, and in particular 1,2-azaborines, is tied to advances in the late-stage functionalization of the heterocyclic core. In this context, late-stage functionalization means any method used to install a functional group after the azaborine heterocycle has been assembled. A comparison of two syntheses of 1,2-azaborines by the Ashe¹³ and Liu¹⁴ groups illustrates the potential advantages of a late-stage functionalization approach to BN-heterocycles (Scheme 1.5). In the early-stage synthesis, the boron substituent is installed at an early stage and therefore the subsequent ring-closing and oxidation steps would need to be optimized for each new substituent. In contrast, the fully aromatic 1,2-azaborine **1.16** with the B-Cl leaving group provides flexibility in terms of functionalization without the need for additional reaction optimization. More importantly, the late-stage functionalization method is more amenable to the synthesis of libraries of compounds.

³² For an overview, see: (a) Wang, X.-Y.; Wang, J.-Y.; Pei, J. *BN Chem. - Eur. J.* **2015**, *21*, 3528-3539. (b) Morgan, M. M.; Piers, W. E. *Dalton Trans.* **2016**, *45*, 5920-5924. (c) Huang, J.; Li, Y. *Front. Chem.* **2018**, *6*.

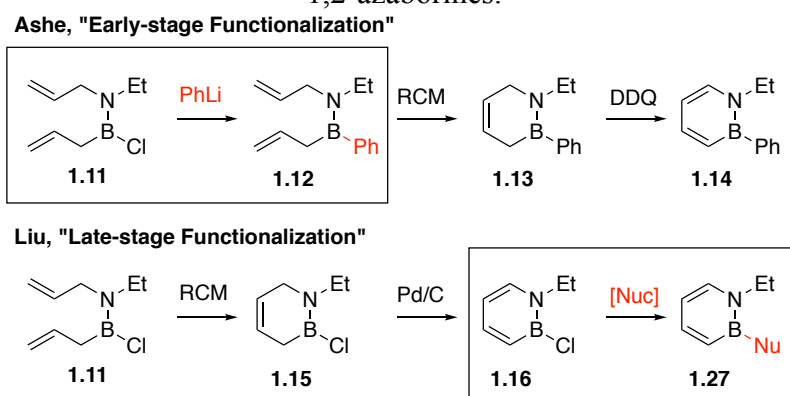
³³ For selected examples, see: (a) Helten, H. *Chem. -Eur. J.* **2016**, *22*, 12972-12982. (b) Wan, W.-M.; Baggett, A. W.; Cheng, F.; Lin, H.; Liu, S.-Y.; Jakle, F. *Chem. Comm.* **2016**, *52*, 13616-13619. (c) Thiedemann, B.; Gliese, P. J.; Hoffman, J.; Lawrence, P. G.; Sonnichsen, F. D.; Staubitz, A. *Chem. Comm.* **2017**, *53*, 7258-7261. (d) Ishibashi, J. S. A.; Dargelos, A.; Darrigan, C.; Chrostowska, A.; Liu, S.-Y. *Organometallics* **2017**, *36*, 2494-2497. (e) Liu, Z.; Ishibashi, J. S. A.; Darrigan, C.; Dargelos, A.; Chrostowska, A.; Li, B.; Vasiliu, M.; Dixon, D. A.; Liu, S.-Y. *J. Am. Chem. Soc.* **2017**, *139*, 6082-6085. (f) van de Wouw, H. L.; Awuyah, E. C.; Baris, J. I.; Klausen, R. S. *Macromolecules* **2018**, *51*, 6359-6368. (g) Matsui, K.; Oda, S.; Yoshiura, K.; Nakajima, K.; Yasuda, N.; Hatakeyama, T. *J. Am. Chem. Soc.* **2018**, *140*, 1195-1198. (h) Nakatsuka, S.; Yasuda, N.; Hatakeyama, T. *J. Am. Chem. Soc.* **2018**, *140*, 13562-13565.

³⁴ (a) Vlasceanu, A.; Jessing, M.; Kilburn, J. P. *Bioorg. Med. Chem.* **2015**, *23*, 4453-4461. (b) Rombouts, F. J.; Tovar, F.; Austin, N.; Tresadern, G.; Trabanco, A. A. *J. Med. Chem.* **2015**, *58*, 9287-9295. (c) Lee, H.; Fischer, M.; Shoichet, B. K.; Liu, S.-Y. *J. Am. Chem. Soc.* **2016**, *138*, 12021-12024. (d) Zhao, P.; Nettleton, D. O.; Karki, R.; Zecri, F. J.; Liu, S.-Y. *ChemMedChem* **2017**, *12*, 358-361.

³⁵ (a) Segawa, Y.; Yamashita, M.; Nozaki, K. *J. Am. Chem. Soc.* **2009**, *131*, 9201-9203. (b) Bailey, J. A.; Haddow, M. F.; Pringle, P. G. *Chem. Comm.* **2014**, *50*, 1432-1434. (c) Sun, F.; Huang, M.; Zhou, Z.; Fang, X. *RSC Advances* **2015**, *5*, 75607-75611. (d) Xu, S.; Zhang, Y.; Li, B.; Liu, S.-Y. *J. Am. Chem. Soc.* **2016**, *138*, 14566-14569. (e) McConnell, C. R.; Campbell, P. G.; Fristoe, C. R.; Memmel, P.; Zakharov, L. N.; Li, B.; Darrigan, C.; Chrostowska, A.; Liu, S.-Y. *Eur. J. Inorg. Chem.* **2017**, 2207-2210. (f) Wang, G.; Liu, L.; Wang, H.; Ding, Y.-S.; Zhou, J.; Mao, S.; Li, P. *J. Am. Chem. Soc.* **2017**, *139*, 91-94.

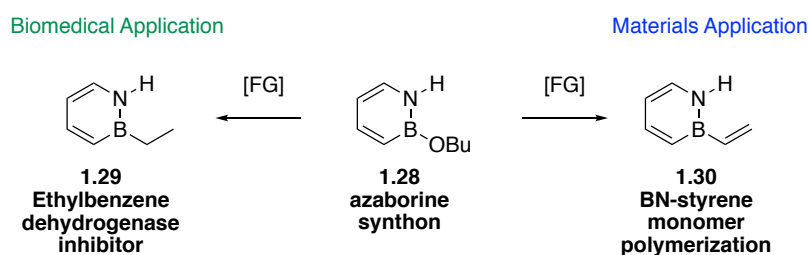
³⁶ (a) Burford, R. J.; Li, B.; Vasiliu, M.; Dixon, D. A.; Liu, S.-Y. *Angew. Chem., Int. Ed.* **2015**, *54*, 7823-7827. (b) Edel, K.; Yang, X.; Ishibashi, J. S. A.; Lamm, A. N.; Maichle-Mössmer, C.; Giustra, Z. X.; Liu, S.-Y.; Bettinger, H. F. *Angew. Chem., Int. Ed.* **2018**, *57*, 5296-5300.

Scheme 1.5. Early-stage versus late-stage functionalization approaches for preparing 1,2-azaborines.



Scheme 1.6 illustrates the utility of 1,2-azaborine synthons for accessing libraries of useful molecules via late-stage functionalization. 1,2-Azaborines for applications in biomedical and materials chemistry have been accessed from the synthon **1.28** via substitution of the boron atom (Scheme 1.6). Addition of an ethyl group afforded ethylbenzene analogue **1.29** which was evaluated as a potential substrate for the enzyme ethylbenzene dehydrogenase;³⁷ addition of a vinyl group afforded BN-styrene **1.30** which was applied in a polymerization study.^{33b}

Scheme 1.6. Applications of 1,2-azaborine via late-stage functionalization.



While several published reviews cover limited examples of late-stage functionalization of azaborines, there is no comprehensive review of the subject. The aim of this chapter is to provide all of the available methods for the late-stage functionalization of 1,2-azaborines, including monocyclic 1,2-azaborine as well as BN-naphthalenes and higher-order BN-polyaromatic hydrocarbons (PAHs) (Figure

³⁷ Knack, D. H.; Marshall, J. L.; Harlow, G. P.; Dudzik, A.; Szalaniech, M.; Liu, S.-Y.; Heider, J. *Angew. Chem. Int. Ed.* **2013**, *52*, 2599-2601.

1.3). This chapter serves as a practical guide for engaging in azaborine research and covers the synthetic toolbox available for functionalizing each azaborine.

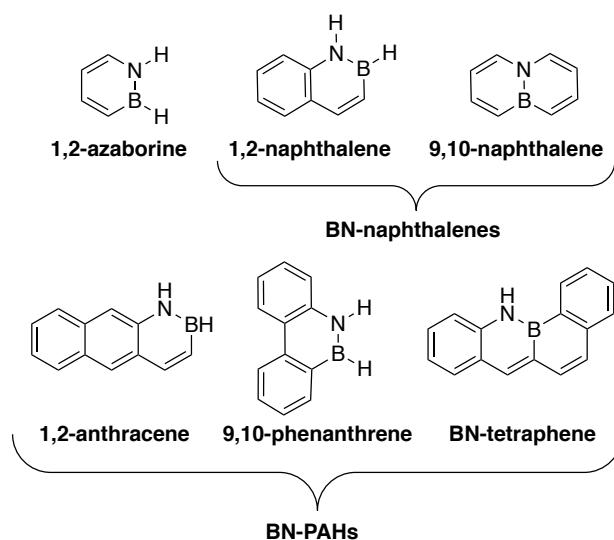


Figure 1.3. Examples of BN-containing arenes.

While much progress is yet to be made, the functionalization of 1,2-azaborines has seen substantial development in the past few years. Some of this progress has come from harnessing the unique reactivity of 1,2-azaborines,³⁶ but the majority of developments in late-stage functionalization are a result of adapting established arene chemistry to BN-containing substrates.¹⁷ Regardless of the type of reactivity, developing methods to elaborate the azaborine core is essential to increasing the number of potential applications. 1,2-azaborines provide challenges and opportunities compared to functionalizing their all-carbon counterparts. The susceptibility of certain BN-compounds to degradation by water or oxidation represents a significant hurdle in developing new synthetic methods. On the other hand, the presence of the BN bond provides access to inherent selectivity not available to all-carbon compounds, as the azaborine's lower symmetry renders each position of the azaborine electronically distinct. In this review, the available synthetic methods for each 1,2-azaborine will be described. By presenting each type of reaction as a subsection within the section for

each azaborine, the review will demonstrate both the published methods as well as gaps that remain to be addressed in the literature.

1.3 Monocyclic 1,2-azaborines

1.3.1 Electrophilic Aromatic Substitution (EAS)

1.3.1.1 C3 Substitution

One of the hallmark reactions of aromatic compounds is electrophilic aromatic substitution (EAS). In 2007, Ashe first demonstrated that monocyclic 1,2-azaborines could undergo EAS. Compound **2.1** undergoes rapid reaction with molecular bromine, installing a bromine with complete regioselectivity at the C3 position (Scheme 1.7a).¹⁷ According to calculations,²⁶ the C3 and C5 positions of the 1,2-azaborine are the most electron-rich, and are thus expected to undergo electrophilic attack. Halogenation opens a suite of well-developed reactions for converting aryl halides into a host of functionalized arenes (*vide infra*). The building block azaborine **1.20**³⁸ also reacts with bromine to afford C3-Br **1.31** in high yield (Scheme 1.7b).³⁹ This triply orthogonal azaborine synthon can be further functionalized at the N, B, and C3 positions. Fang developed an alternative method for bromination with CuBr₂ as the bromine source and acetyl chloride as an activating agent (Scheme 1.7c).⁴⁰ In another publication by the Fang group, the C3 position of **1.32** underwent electrophilic attack with NIS activated by AlCl₃ in high yield (Scheme 1.7d).⁴¹

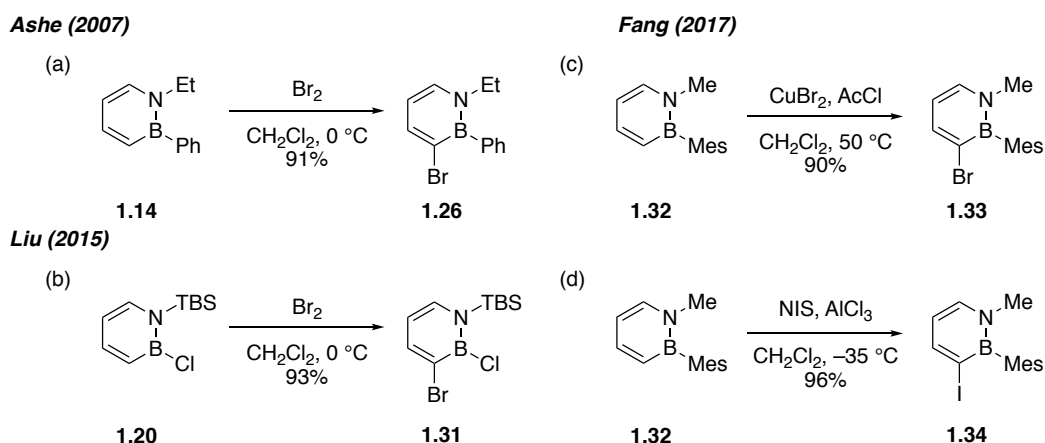
³⁸ This compound is now commercially available from www.strem.com, catalog number 05-0150. Accessed on 3/7/2019.

³⁹ Brown, A. N.; Li, B.; Liu, S.-Y. *J. Am. Chem. Soc.* **2015**, *137*, 8932-8935.

⁴⁰ Zhang, Y.; Dan, W.; Fang, X. *Organometallics* **2017**, *36*, 1677-1680.

⁴¹ Zhang, Y.; Sun, F.; Dan, W.; Fang, X. *J. Org. Chem.* **2017**, *82*, 12877-12887.

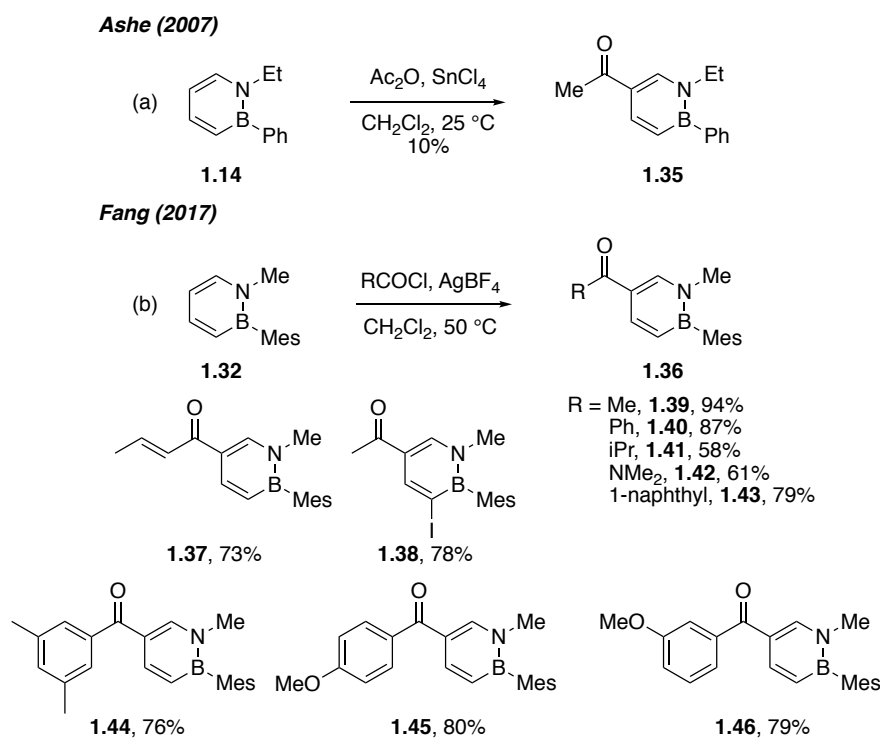
Scheme 1.7. Halogenation of various 1,2-azaborines through EAS.



1.3.1.2 C5 Substitution

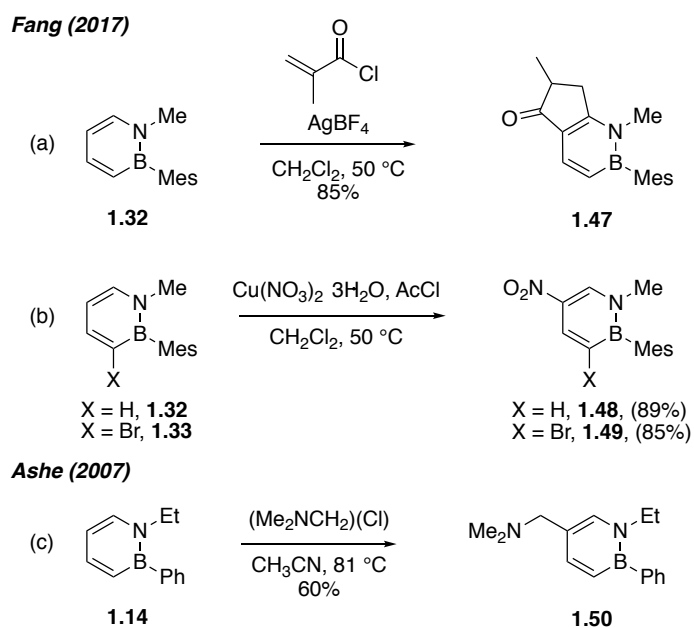
While the C3 position of the 1,2-azaborine attacks halogen electrophiles, the C5 position tends to engage in Friedel-Crafts reactivity. Ashe also reported the first example of C5 substitution; Friedel-Crafts acetylation of compound **1.14** proceeds in poor yield in the presence of acetic anhydride and SnCl_4 (Scheme 1.8a).¹⁷ The 10% yield of acetylated **2.17** and messy product mixture suggest significant side-reactivity. Fang built on the work of Ashe to develop an improved Friedel-Crafts acylation method for N-methyl, B-mesityl-substituted azaborine **1.32** (Scheme 1.8b).⁴¹ The mesityl (Mes = 2,4,6-trimethylphenyl) group is known to provide robustness to the azaborine heterocycle against unwanted side reactions such as oxidative degradation. AgBF_4 activates various acylchlorides at 50 °C in CH_2Cl_2 to Friedel-Crafts reaction with 1,2-azaborines **1.32** or **1.34**. Preference for substitution at the C5 instead of the C3 position may be explained by the presence of the bulky mesityl group. Intriguingly, when the reaction was performed with AlCl_3 , no regioselectivity was observed. The substrate table for the reaction with AgBF_4 includes alkanoyl, alkenoyl, and aroyl chlorides as well as one example of a carbamic chloride, compounds **1.39-1.46**. Absent from the substrate table are more electron-deficient substrates, as they could not be activated with AgBF_4 .

Scheme 1.8. Acylation of 1,2-dihydro-1,2-azaborines at the C5 position.



Other types of C5 substitution reactions are displayed in Scheme 1.9. As part of their acylation work, the Fang group investigated the reaction between **1.32** and methacryloyl chloride, which produced BN-indanone analogue **1.47** (Scheme 1.9a).⁴¹ According to the proposed mechanism, **2.14** first undergoes C5 Friedel-Crafts acylation followed by a Nazarov cyclization at the C6 position. In another publication, Fang and co-workers developed a procedure for the regioselective nitration of **1.32** and **1.33** (Scheme 1.9b).⁴⁰ In the presence of a metal nitrate hydrate and acetyl chloride a nitro group is installed at the C5 position in good yield, likely via a radical mechanism. In the presence of radical scavengers only compound **1.39** was observed as a product. Ashe demonstrated another non-acyl substituent could be added to the C5 position (Scheme 1.9c). N,N-dimethylmethyleiminium chloride reacts cleanly with **1.14** in refluxing acetonitrile to afford **1.50** in moderate yield, adding another example of a C5 selective reaction.¹⁷

Scheme 1.9. Other C5 functionalization methods by Ashe and Fang.



1.3.2 C-H Borylation

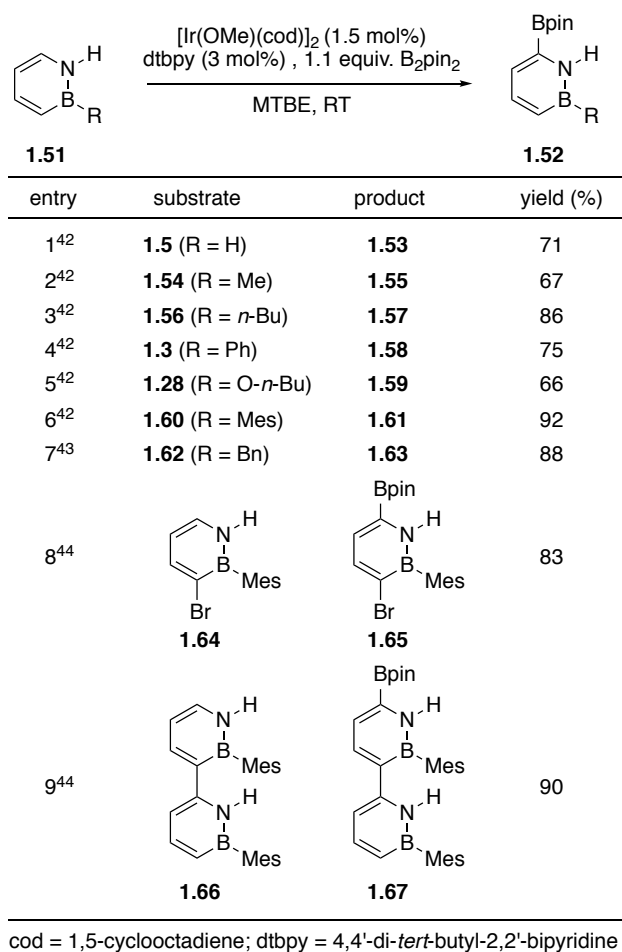
In addition to halogens, boronate esters are a versatile platform for forming bonds to arenes. C-H borylation proceeds at room temperature with complete regioselectivity for the most acidic C6-H position of parent azaborine **1.5** (Scheme 1.10).⁴² The preference for borylating the 1,2-azaborine ring is maintained in the presence of a phenyl ring within the same molecule as in **1.3**, as well as in direct competition experiments with benzene itself. Various groups are tolerated in the reaction, including alkyl,⁴³ aryl, and the alkoxide group at the boron position as well as the Br group at the C3 position (e.g., **1.64**).⁴⁴

⁴² Baggett, A. W.; Vasiliu, M.; Li, B.; Dixon, D. A.; Liu, S.-Y. *J. Am. Chem. Soc.* **2015**, *137*, 5536-5541.

⁴³ Baggett, A. W.; Liu, S.-Y. *J. Am. Chem. Soc.* **2017**, *139*, 15259-15264.

⁴⁴ Baggett, A. W.; Guo, F.; Li, B.; Liu, S.-Y.; Jäkle, F. *Angew. Chem. Int. Ed.* **2015**, *54*, 11191-11195.

Scheme 1.10. Substrate table for the C-H borylation of 1,2-azaborines.



1.3.3 Cross-Coupling

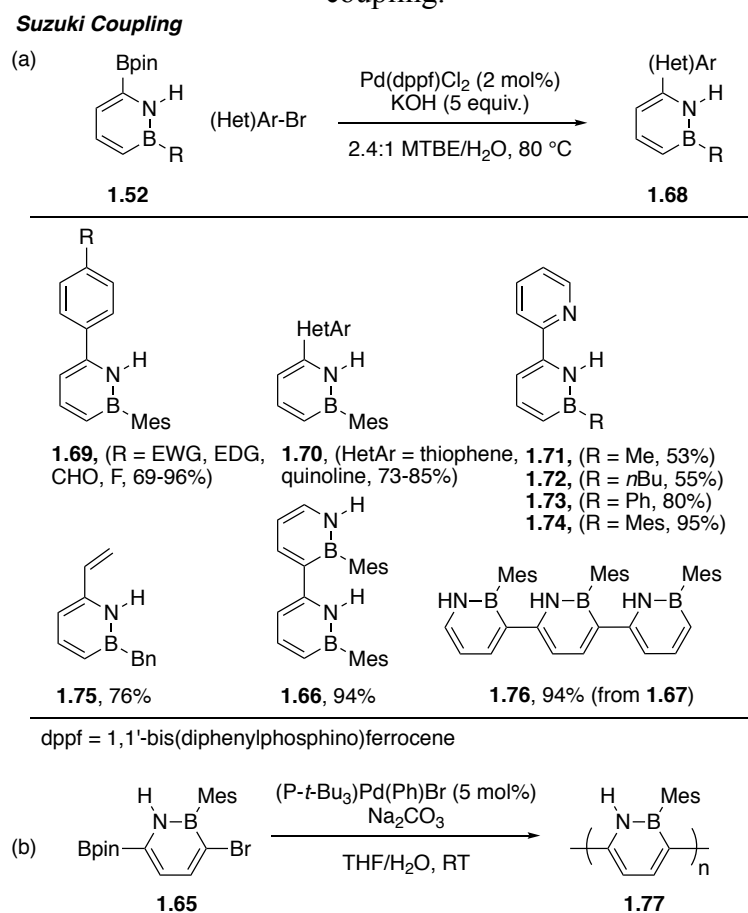
1.3.3.1 Suzuki-Miyaura Cross-Coupling

Optimization of a Suzuki-Miyaura cross-coupling for 1,2-azaborines followed the development of C-H borylation. In the presence of Pd(dppf)Cl₂ and KOH at 80 °C in MTBE/H₂O, many substituted phenyl bromides, heteroaryl bromides, and one example of an alkenyl bromide⁴³ undergo cross-coupling with C₆ borylated azaborines **1.52** (Scheme 1.11a).⁴² The cross-coupled products **1.68** with *B*-alkyl or *B*-aryl substituents were prepared with the aforementioned conditions. 1,2-azaborine can also be coupled to itself by reacting borylated **1.61** with brominated **1.64** to form dimer **1.66** (Scheme 1.11a).²¹ Another iteration of borylation and subsequent coupling between dimer **1.67** and brominated **1.64** produces trimer **1.76**. With some adjustment

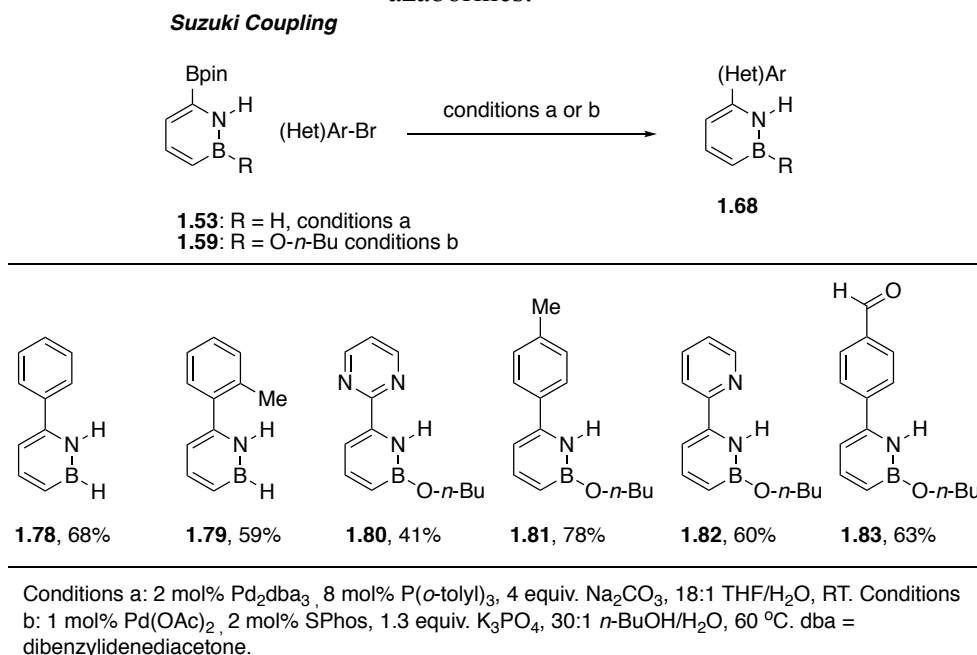
to the reaction conditions, C6 borylated, C3 brominated **1.65** functions as a monomer in a Suzuki-Miyaura polymerization process to afford polymer **1.77** (Scheme 1.11b).²¹

1,2-Azaborines bearing B-H or B-OR substitution generally required milder conditions, as these compounds are susceptible to hydrolysis (Scheme 1.12). Thus, the borylated parent 1,2-azaborine **1.53** undergoes the cross-coupling reaction at room temperature promoted by the more mild base Na₂CO₃ solubilized with minimal water. Under the room temperature conditions, compound **1.59** maintains its *n*-butoxide substituent at the boron position in an *n*-BuOH/H₂O solvent system. While the acidic N-H bond could theoretically participate in a competitive Buchwald-Hartwig coupling, only the Suzuki coupling products were observed.

Scheme 1.11. a) Suzuki-Miyaura cross-coupling of borylated 1,2-azaborines. b) Polymerization of C6-borylated, C3-brominated monomer via Suzuki-Miyaura cross-coupling.



Scheme 1.12. Suzuki-Miyaura cross-coupling of *B*-H and *B*-O-*n*Bu substituted 1,2-azaborines.

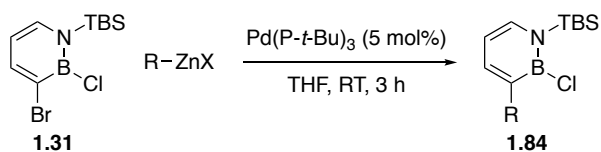


1.3.3.2 Negishi Cross-Coupling

Just as C-H borylation opened up the possibility for Suzuki-Miyaura coupling of 1,2-azaborines at the C6 position, so too did bromination provide access to cross-coupling methods at the C3 position. For synthon **1.31** (Scheme 1.13), Negishi cross-coupling was selected due to the ready availability and low toxicity of zinc reagents as well as their functional group compatibility.³⁹ In addition, Negishi couplings do not require borophilic additives. The catalyst Pd(P-*t*-Bu₃)₂ promotes cross-coupling between alkyl, alkenyl, and aryl zinc halides and **1.31** at room temperature (Scheme 1.13). The labile B-Cl bond remains intact, and thus the boron position can be subsequently functionalized (*vide infra*). No background reactivity with zincates was observed in the absence of catalyst.

Scheme 1.13. Negishi Cross-Coupling of C3-Br 1,2-azaborine **1.31**.

Negishi Coupling



entry	R-ZnX	yield (%) ^a
1	<i>n</i> -Pr-ZnBr	1.85 , 87
2	1-phenylvinyl-ZnBr	1.86 , 97
3	vinyl-ZnBr	1.87 , 69
4	2-(1,3-dioxan-2-yl)ethyl-ZnBr	1.88 , 69
5	4-chlorophenyl-ZnI	1.89 , 83
6	3,4,5-trifluorophenyl-ZnBr	1.90 , 91

^aYield determined by ¹H NMR.

1.3.4 Nucleophilic Substitution

For hydrocarbon-based arenes and other heterocycles, nucleophilic substitutions typically require highly activated substrates (e.g. 2-fluoropyridine) and/or harsh conditions involving strong nucleophiles and high temperatures.⁴⁵ The vacant p-type orbital on the boron atom of the 1,2-azaborine renders the boron position susceptible to nucleophilic attack. Thus, more mild conditions and a greater variety of nucleophiles can typically be employed with BN heterocycles. This section details numerous examples of nucleophilic substitution at the boron atom as well as selected examples of substitution-type reactions at the C3 position.

1.3.4.1 B-N Disubstitution

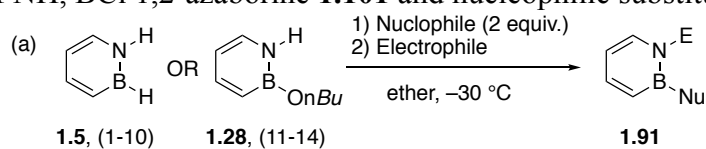
In 2011 Liu and coworkers investigated the reactivity of the parental 1,2-azaborine **1.5** with strong nucleophiles and developed a one-pot method for disubstitution at the N and B positions of the 1,2-azaborine.⁴⁶ Adding two equivalents of a strong nucleophile such as *n*-BuLi to parent 1,2-azaborine **1.5** induces the boron-hydride to act as a leaving-group, leading to a substitution reaction (Scheme 1.14a,

⁴⁵ Terrier, F. The S_NAr Reactions: Mechanistic Aspects. In *Modern Nucleophilic Aromatic Substitution*; Wiley: Hoboken, NJ, 2013; pp 1-94.

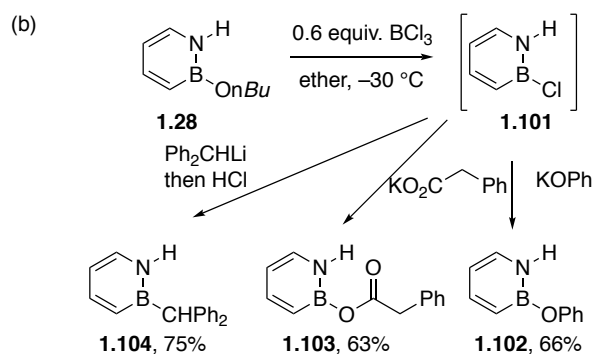
⁴⁶ Lamm, A. N.; Garner, E. B.; Dixon, D. A.; Liu, S.-Y. *Angew. Chem. Int. Ed.* **2011**, *50*, 8157-8160.

entries 1-10). One equivalent of the *n*-BuLi deprotonates the acidic N-H, and the resulting amide can then be quenched with an electrophile, yielding disubstituted **1.91**. The disubstitution reaction with respect to 1,2-azaborines was later expanded to include an alkoxide leaving-group on boron (Scheme 1.14a, entries 11-14).²⁵ Suitable nucleophiles include alkyl, alkenyl, aryl, and alkynyl organometallic reagents and electrophiles susceptible to attack by the nitrogen atom of the 1,2-azaborine in this one-pot procedure include proton, chlorotrimethylsilane, iodomethane, and benzylchloride.

Scheme 1.14. a) Nucleophilic substitution reaction of 1,2-azaborine. b) *In-situ* generation of NH, BCl 1,2-azaborine **1.101** and nucleophilic substitution at boron.



entry	M-Nu	E-X	product	yield (%)
1	Na-O <i>t</i> Bu	H-Cl	1.92	63
2	K-Oallyl	H-Cl	1.93	79
3	Li- <i>t</i> Bu	H-Cl	1.94	81
4	Li- <i>n</i> Bu	H-Cl	1.56	80
5	Li-Ph	H-Cl	1.3	98
6	BrMg-vinyl	H-Cl	1.30	59
7	BrMg-≡-Ph	H-Cl	1.95	71
8	Li- <i>n</i> Bu	TMS-Cl	1.96	89
9	Li- <i>n</i> Bu	Me-I	1.97	67
10	Li- <i>n</i> Bu	Bn-Cl	1.98	60
11	BrMg-vinyl	H-Cl	1.30	62
12	Li- <i>n</i> Bu	H-Cl	1.56	83
13	Li-Me	Me-I	1.99	49
14	Li-Me	TMS-Cl	1.100	63

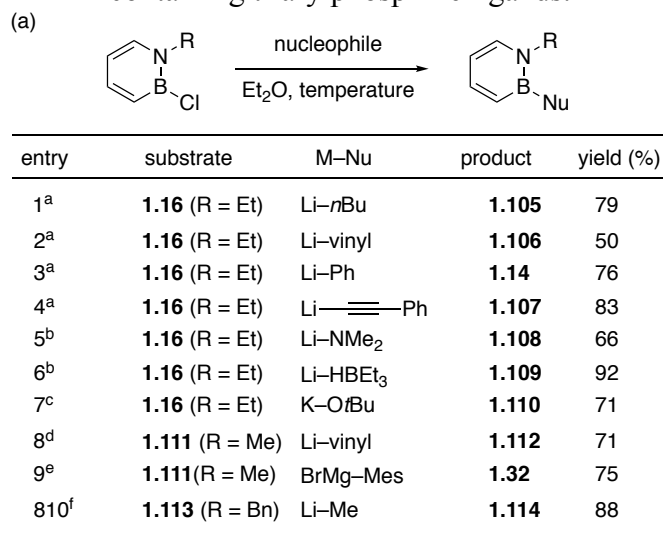


While alkoxides are suitable nucleophiles for the parent **1.5** they are unable to displace the *n*-butoxide group in **1.28**. Instead, ligand exchange between the 1,2-azaborine-alkoxide **1.28** and borontrichloride *in-situ* generates the more reactive *B*-Cl **1.101**, which then can undergo substitution with potassium phenoxide, potassium phenylacetate, or the hindered diphenylmethyllithium (Scheme 1.14b).²⁵

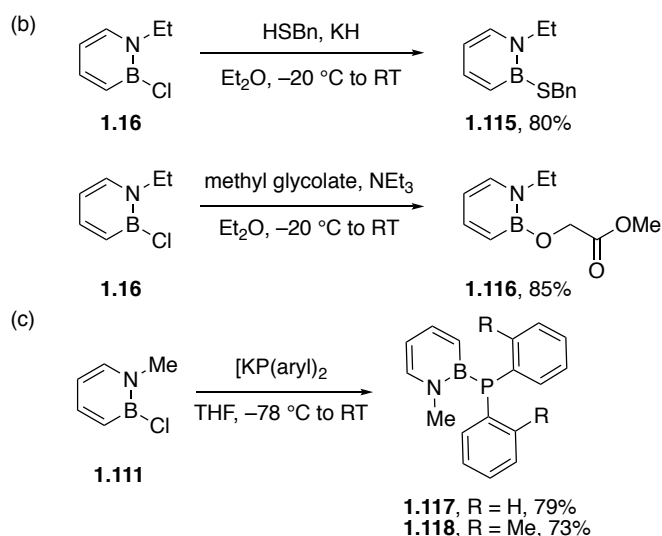
1.3.4.2 Boron Substitution with Anionic Nucleophiles

Many examples now exist for the simple nucleophilic displacement at the boron position of a 1,2-azaborine, in particular when the leaving-group is a halide. In 2007, the Liu group introduced an *N*-alkyl-*B*-Cl substituted 1,2-azaborine synthon to allow general access to *B*-substituted 1,2-azaborines.¹⁴ The scope with respect to the nucleophiles is quite broad, including various N-, O-based nucleophiles and alkyl, alkenyl, and aryl organometallic reagents (Scheme 1.15a). In addition to the *N*-Et azaborine **1.16**,¹⁴ examples of *N*-Me-(compound **1.111**),^{33c,40} and *N*-Bn substituted 1,2-azaborine (compound **1.113**) have been reported.²⁴ Substitution at boron is also possible with nucleophiles generated *in-situ* with non-nucleophilic bases such as KH and Et₃N (Scheme 1.15b).¹⁴ Phosphides can also displace the chloride leaving-group, forming azaborine-containing triarylphosphine ligands **1.117** and **1.118** (Scheme 1.15c).^{35e}

Scheme 1.15. a) Nucleophilic substitution of *N*-alkyl-*B*-Cl 1,2-azaborines. b) Substitution with *in-situ* generated nucleophiles. c) Synthesis of 1,2-azaborine-containing triarylphosphine ligands.



^a –78 °C to RT, ^b –20 °C to RT, ^c –10 °C to RT, ^d –91 °C to RT, ^e –35 °C to RT, ^f RT,

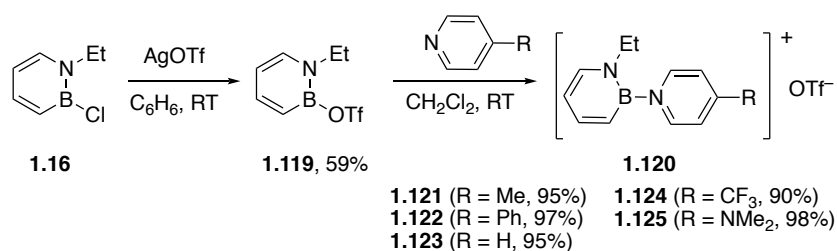


1.3.4.3 Boron Substitution with Neutral Nucleophiles

Neutral nucleophiles are in general not capable of displacing the chloride from the boron atom. However, when the chloride is replaced with the triflate (OTf[–]) leaving-group, pyridines become suitable nucleophiles to form cationic adducts **1.120** from the *B*-OTf-substituted 1,2-azaborine **1.119** (Scheme 1.16).⁴⁷

⁴⁷ Marwitz, A. J. V.; Jenkins, J. T.; Zakharov, L. N.; Liu, S.-Y. *Angew. Chem. Int. Ed.* **2010**, *49*, 7444–7447.

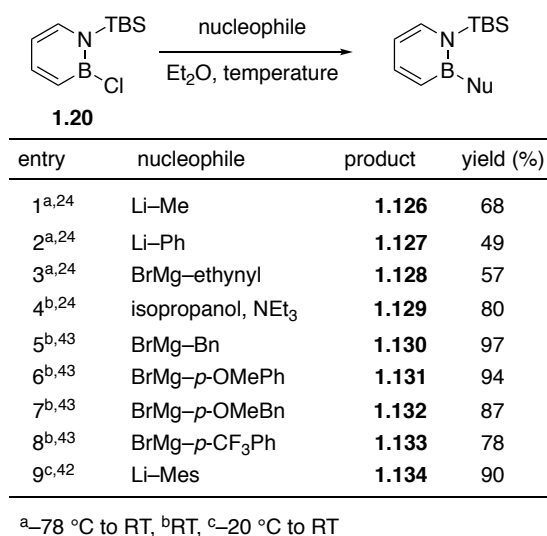
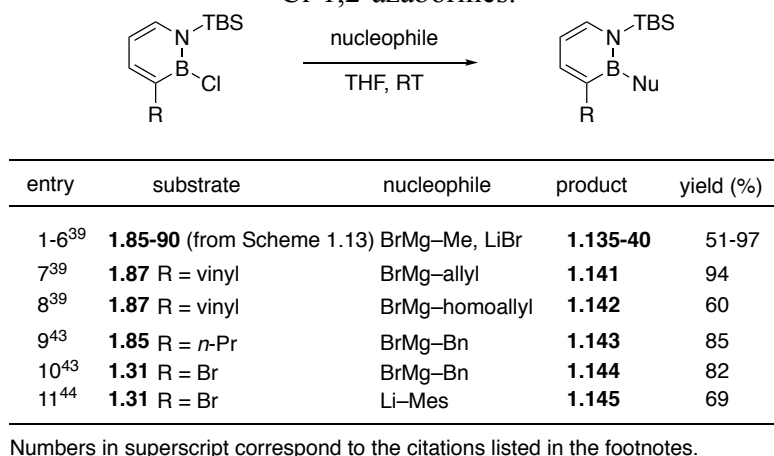
Scheme 1.16. Preparation of azaborine cations via reaction with B-OTf **1.119**.



1.3.4.4 Boron Substitution of N-TBS, B-Cl Synthon

The commercially available *N*-TBS-*B*-Cl 1,2-azaborine **1.20** has emerged as a foundational building block for the chemistry of monocyclic 1,2-azaborines and thus deserves special mention. In addition to the chloride leaving-group on boron, the TBS protecting group on nitrogen serves as a handle for late-stage functionalization. Compound **1.20** can be difunctionalized in a simple process: nucleophilic addition at the boron position followed by removal of the *N*-TBS group and subsequent functionalization at the nitrogen position. The scope of nucleophiles includes alkyl, aryl, alkynyl and benzylic organometallic species; non-anionic nucleophiles such as isopropanol can also be added in the presence of exogenous base (Scheme 1.17). For *N*-TBS, *B*-alkyl- or aryl-substituted 1,2-azaborines, the *N*-TBS group can subsequently be removed with TBAF (*vide infra*, Scheme 1.22).

Nucleophilic addition at the boron position is also possible with sterically more hindered C3-substituted *N*-TBS-*B*-Cl-1,2-azaborine (Scheme 1.18). C3-vinyl substituted 1,2-azaborines **1.141** and **1.142** were converted to BN-analogues of indenyl anion and naphthalene, respectively.³⁹ In the case of C3-brominated substrate **1.31**,⁴⁴ it appears that addition to boron with organolithium reagents occurs more rapidly than lithium-halogen exchange at the C3-Br position.

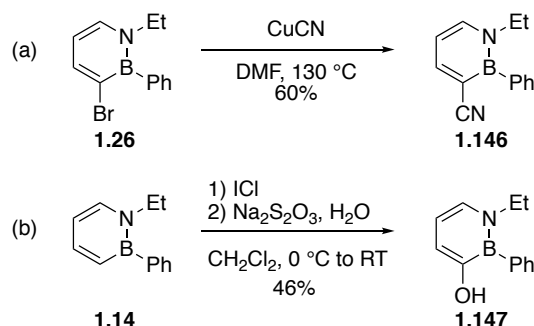
Scheme 1.17. Nucleophilic substitution of *N*-TBS-*B*-Cl 1,2-azaborine.**Scheme 1.18.** Nucleophilic addition to sterically hindered C3-substituted *N*-TBS-*B*-Cl-1,2-azaborines.

1.3.4.5 C3 Substitution

Ashe has reported additional transformations of C3-halide substituted 1,2-azaborine beyond cross-coupling chemistry.¹⁷ For example, C3-brominated 1,2-azaborine **1.26** is converted to cyano-substituted **1.146** with CuCN at elevated temperature (Scheme 1.19a).¹⁷ Reportedly, the synthesis of a 1,2-azaborine-phenol

1.147 has been accomplished presumably via a C3-iodinated 1,2-azaborine intermediate (Scheme 1.19b).⁴⁸

Scheme 1.19. Nucleophilic substitutions at C3 position of azaborine.



1.3.5 Electrophilic Substitution at Nitrogen

1.3.5.1 Deprotonation of *N*-H Substituted Azaborines

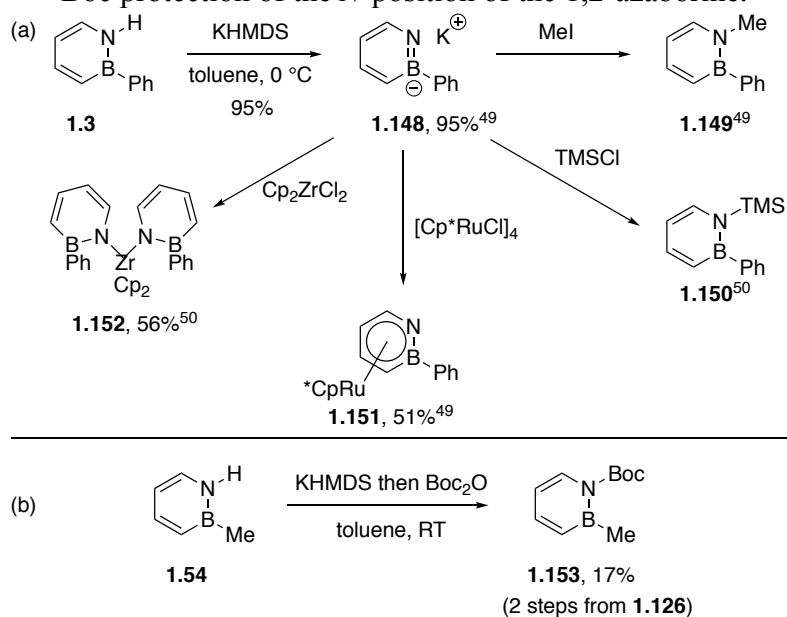
The pK_a of the azaborine N-H bond is approximately 24, much more acidic than the other C-H positions on the ring, which have pK_a 's between 43 and 47.⁴² Ashe demonstrated that strong amide bases such as LDA⁴⁹ or KHMDS⁵⁰ can generate amide **1.148** from *N*-H substituted **1.3** in high yield (Scheme 1.20a). Compound **1.148** can be isolated as a solid and then reacted with various electrophiles such as MeI⁴⁹ or TMSCl⁵⁰ to afford **1.149** and **1.150**, respectively. Complexes of 1,2-azaborine with transition metals (e.g., Ru(II)⁴⁹ or Zr(IV)⁵⁰) can also be synthesized from **1.148**. Liu demonstrated that deprotonation of 1,2-azaborine **1.54** followed by quenching with di-*tert*-butyldicarbonate furnishes the *N*-Boc protected 1,2-azaborine **1.153** (Scheme 1.20b).²⁴ Liu also demonstrated that epoxides can serve as suitable electrophiles for 1,2-azaborine anions such as **1.154** to produce β -amino alcohols **1.155** (Scheme 1.21).⁴³

⁴⁸ Intriguingly, the ¹¹B NMR shift of compound **1.147** (28 ppm) typically indicates the presence of a B-O bond.

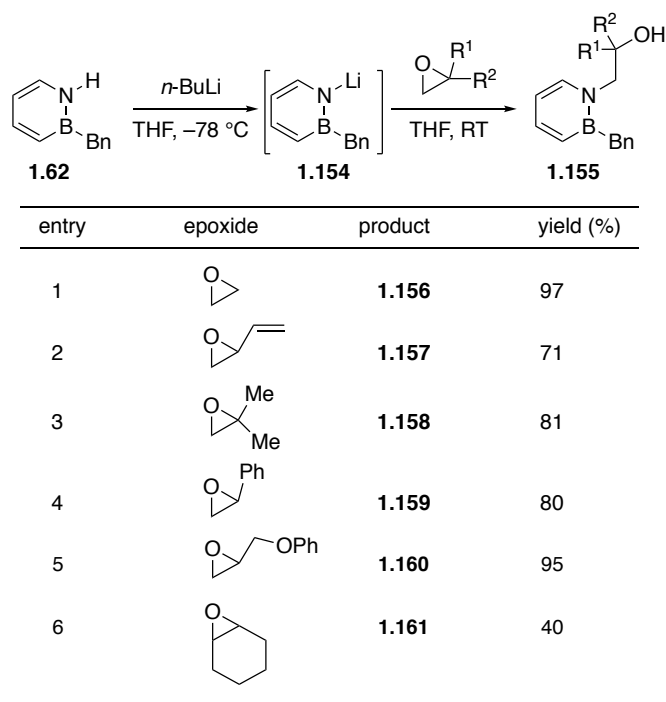
⁴⁹ Pan, J.; Kampf, J. W.; Ashe, A. J. *Organometallics* **2004**, *23*, 5626-5629.

⁵⁰ Pan, J.; Kampf, J. W.; Ashe III, A. J. *Organometallics* **2008**, *27*, 1345-1347.

Scheme 1.20. a) Generation of amide **1.148** and *N*-substitution with electrophiles. b) Boc protection of the *N*-position of the 1,2-azaborine.



Scheme 1.21. Reaction between 1,2-azaborine amide **1.154** and epoxides.

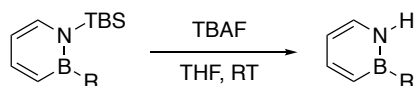


1.3.5.2 Deprotection of *N*-Silyl Substituted Azaborines

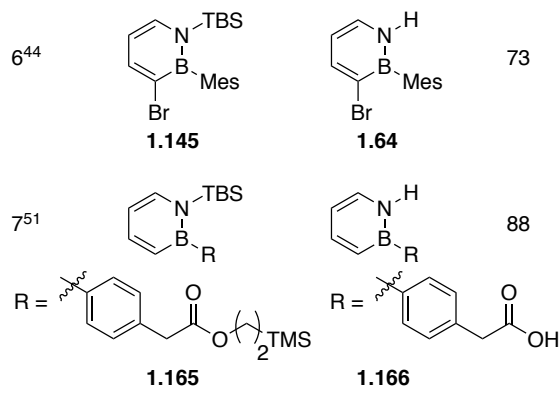
An alternative method for generating amides such as **1.148** or **1.154** is to treat an *N*-silyl protected 1,2-azaborine with TBAF; the intermediate amide can then be

quenched for example with a proton to afford the corresponding *N*-H-1,2-azaborine. Examples include *N*-TMS⁴⁹ and *N*-TBS-substituted 1,2-azaborines (Scheme 1.22).^{33b,24,42,43,44,51}

Scheme 1.22. Removal of the *N*-TBS protecting group of 1,2-azaborine.



entry	substrate	product	yield (%)
1 ²⁴	1.126 (R = Me)	1.54	62
2 ⁴²	1.134 (R = Mes)	1.62	74
3 ⁴³	1.130 (R = Bn)	1.64	63
4 ⁴³	1.132 (R = <i>p</i> -OMeBn)	1.162	72
5 ^{33b}	1.163 (R = <i>p</i> -styrene)	1.164	72



1.3.6 B-X Activation

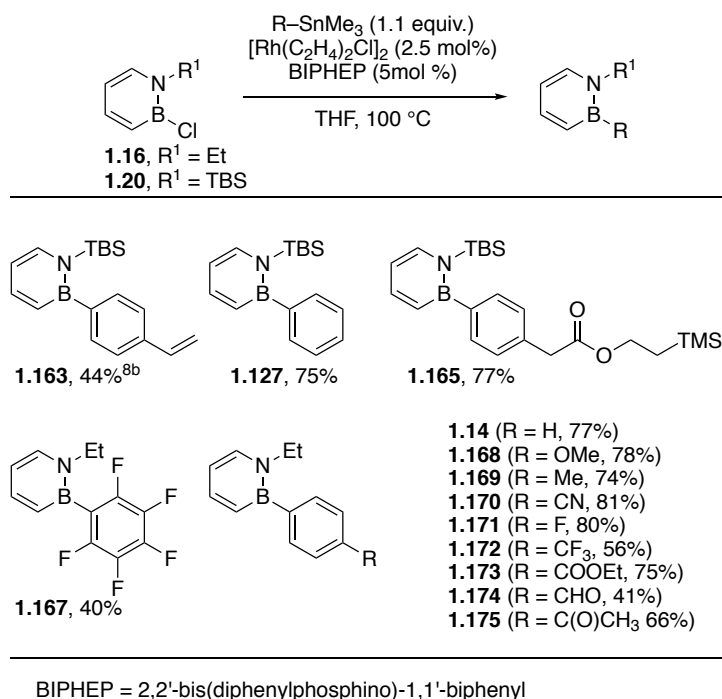
In addition to the direct displacement of a suitable leaving-group (e.g., H, Cl, OR) at the boron position with a nucleophile via an addition/elimination process, a boron substituent can be installed by transition-metal catalyzed *B*-X activation chemistry. This section summarizes methods for functional group interconversions at the boron position mediated by rhodium and copper complexes.

⁵¹ Rudebusch, G. E.; Zakharov, L. N.; Liu, S.-Y. *Angew. Chem. Int. Ed.* **2013**, *52*, 9316-9319.

1.3.6.1 B-Cl Activation

In 2013, the Liu group described a Rh-catalyzed arylation of B-Cl substituted 1,2-azaborines **1.16** and **1.20** with arylstannanes (Scheme 1.23).⁵¹ Mechanistic studies reveal that the reaction proceeds by a series of transmetalations, first between the Rh catalyst and the arylstannane followed by the transfer of the aryl group from Rh to the 1,2-azaborine. A wide variety of arylstannanes are tolerated including those containing esters, aldehydes, ketones, and arylstannanes bearing electron-withdrawing, and electron-donating groups. The BN-analogue of felbinac, a non-steroidal anti-inflammatory drug, was prepared with the key bond-forming step being the arylation of **1.20** to afford **1.165** followed by global deprotection with TBAF to yield BN felbinac **1.166** (see Scheme 1.22 for its structure).

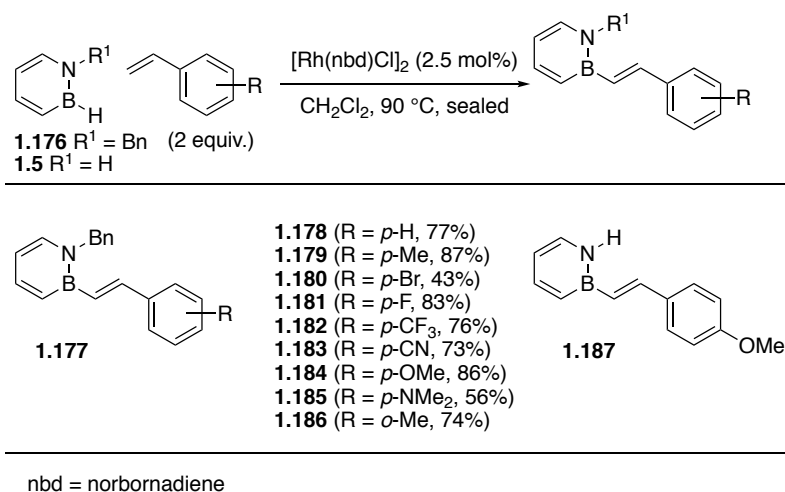
Scheme 1.23. Rh-catalyzed arylation of B-Cl 1,2-azaborines.



1.3.6.2 B-H Activation

In addition to Rh-catalyzed B-Cl arylation, the Liu group also demonstrated B-H activation with a Rh-catalyst.⁵² While the relatively non-hydridic B-H bond does not participate in hydroboration in the absence of promoters, a Rh-catalyst can effect the dehydrogenative borylation of styrenes (Scheme 1.24). A variety of BN-stilbenes have been prepared with this method, including the BN-analogue **1.187** of the biologically active 4-methoxy-*trans*-stilbene. Only the *trans*-BN stilbenes were isolated under the reaction conditions among possible products (e.g., *cis*-stilbene or hydroboration products). A potential mechanism may involve an oxidative addition of the B-H bond to Rh followed by a β -migratory insertion of the Rh-B bond into the styrene substrate. Subsequent β -hydride elimination would produce the desired *trans* BN stilbene product and a Rh dihydride complex which hydrogenates a second styrene substrate to restart the catalytic cycle.⁵²

Scheme 1.24. Rh-catalyzed B-H activation of 1,2-azaborines.



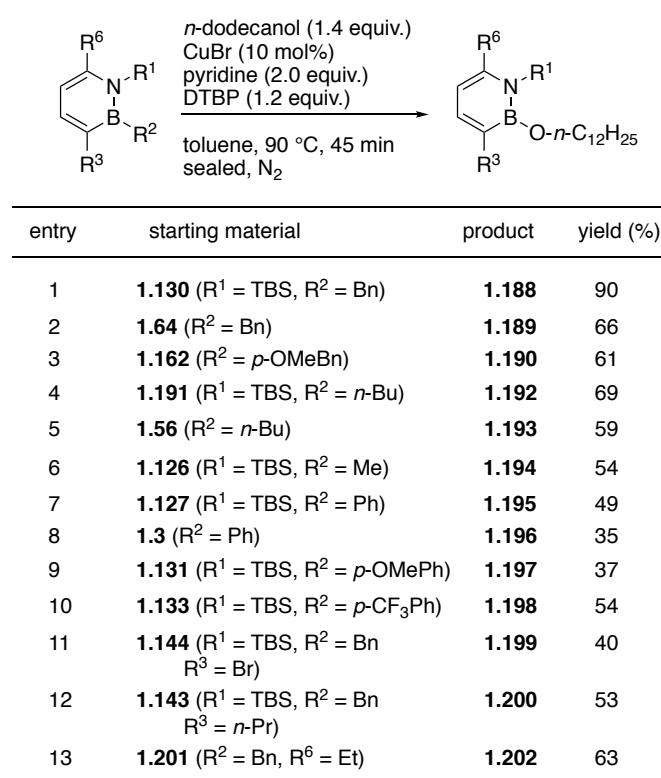
1.3.6.3 B-C Activation

As previously shown, *B*-alkoxide groups of 1,2-azaborines are readily modifiable by nucleophilic substitution chemistry, however, they oftentimes are

⁵²Brown, A. N.; Zakharov, L. N.; Mikulas, T.; Dixon, D. A.; Liu, S.-Y. *Org. Lett.* **2014**, *16*, 3340-3343.

incompatible with other late-stage transformations. On the other hand, carbon-based boron groups, particularly arenes, provide chemical robustness to the 1,2-azaborines and prevent side-reactions. In 2017, the Liu group reported a reaction that exchanges *B*-alkyl or *B*-aryl moieties for a *B*-alkoxide fragment.⁴³ This formal oxidation process allows carbon-based groups to function as a protecting group for the boron position that can be later transformed to the easily modifiable alkoxide moiety. Thus, under the optimized conditions, a Cu(I) compound mediates the homolytic cleavage of the B-C bond in the presence of pyridine with di-*tert*-butylperoxide (DTBP) as the stoichiometric oxidant (Scheme 1.25).

Scheme 1.25. Cu-catalyzed B-R activation and oxidation of 1,2-azaborines.



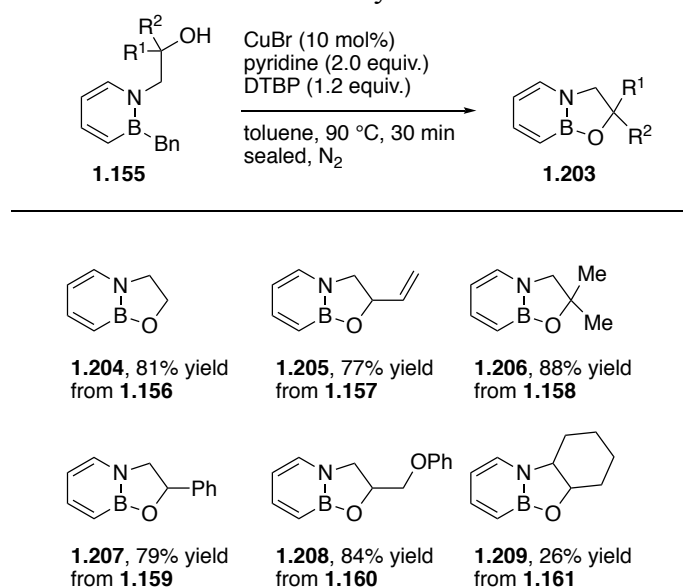
DTBP = di-*tert*-butylperoxide; if not specified, the corresponding R group is H.

Functional groups at the C6-, N-, and C3-positions are tolerated, including the *N*-TBS and the free *N*-H group. *B*-Alkyl, in particular *B*-benzyl substituted 1,2-azaborines are good substrates. *B*-Phenyl groups, as in **1.127**, **1.3**, **1.131**, **1.133** are

removed in modest yield, possibly due to decreased stability of the putative sp^2 -based phenyl radical. Notably, a C3-Br substituted 1,2-azaborine is a suitable substrate for the reaction, albeit with modest yield (Scheme 1.25, entry 11).

An intramolecular version of the *B*-alkyl to *B*-alkoxide exchange reaction was also demonstrated. *B*-Benzyl-substituted 1,2-azaborines **1.155**, accessed via ring-opening reaction of 1,2-azaborine anions with epoxides (Scheme 1.21), engage in the intramolecular displacement of *B*-alkyl groups to afford BN-dihydrobenzofurans **1.203** (Scheme 1.26).⁴³

Scheme 1.26. Intramolecular Cu-catalyzed *B*-R activation and oxidation of 1,2-azaborines to form BN-dihydrobenzofuran isosteres.

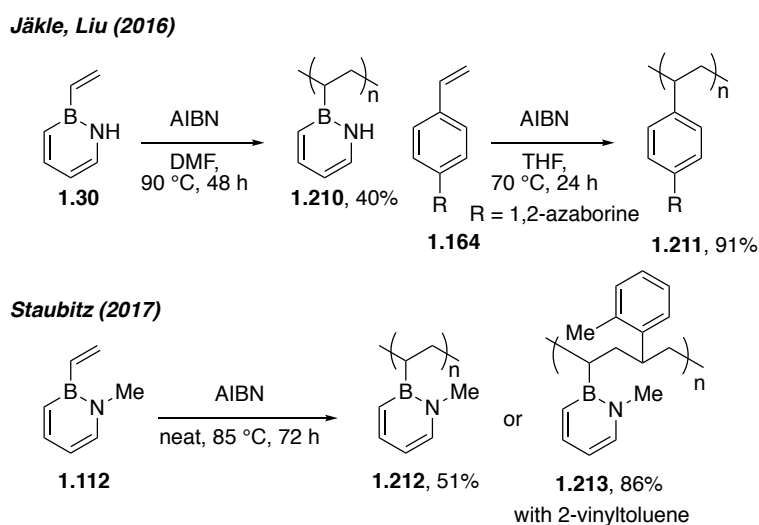


1.3.7 BN-Styrene Reactivity

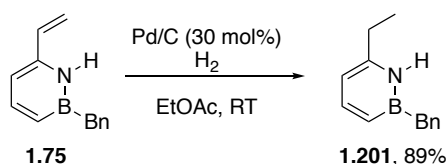
Like their all-carbon counterparts, BN-styrenes polymerize in the presence of free-radical initiators and also undergo controlled RAFT polymerization. Jäkle and Liu established that high molecular weight, atactic polymers can be obtained from the polymerization of monomer **1.30**; the lower reactivity and yield compared to styrene was attributed to the decreased stability of the benzylic radical that is formed adjacent to boron during the polymerization process (Scheme 1.27).^{33b} The polymerization of the BN-analogue of *para*-vinylbiphenyl **1.164** was also reported; yields comparable to

the all-carbon analogue were observed. Staubitz reported the polymerization of *N*-Me monomer **1.112** but obtained higher molecular weights and slightly improved reactivity compared to *N*-H monomer **1.30**.^{33c} The Staubitz group was also able to copolymerize **1.112** with 2-vinyltoluene. The resulting copolymer had a composition of approximately 3:2 (BN:CC) and its NMR characterization suggests a relatively random monomer distribution. The random nature of the copolymer as well as reaction progress monitoring by ¹H NMR suggest the rates of polymerization of the two monomers amongst themselves and with one another must be in the same order of magnitude. In another example of BN-styrene late-stage functionalization, the Liu group performed hydrogenation of the vinyl group in compound **1.75** (Scheme 1.28).⁴³

Scheme 1.27. Free-radical polymerization of vinyl-containing azaborines.



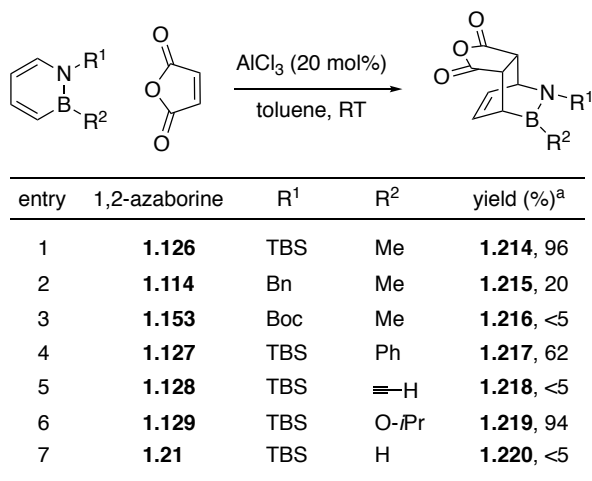
Scheme 1.28. Hydrogenation of C6-vinyl azaborine.



1.3.8 Diels-Alder

While benzene does not typically engage in Diels-Alder reactions, it was found that 1,2-azaborine undergoes [4+2] cycloaddition with activated dienophiles.²⁴ With a resonance stabilization energy (RSE) of about 32 kcal mol⁻¹, benzene lacks sufficient thermodynamic driving force to break its aromaticity and engage in a thermal cycloaddition. On the other hand, parent azaborine **1.5** has an RSE of about 19 kcal mol⁻¹ which situates it between two heterocycles known to engage in cycloaddition reactions, pyrrole (21 kcal mol⁻¹) and furan (15 kcal mol⁻¹). 1,2-azaborines react smoothly with maleic anhydride in the presence of a catalytic amount of AlCl₃ to afford the corresponding *endo*-cycloadducts; however, the reaction is highly sensitive to the nature of the boron and nitrogen substituents of the 1,2-azaborine (Scheme 1.29).

Scheme 1.29. Diels-Alder reaction of 1,2-azaborines with maleic anhydride.



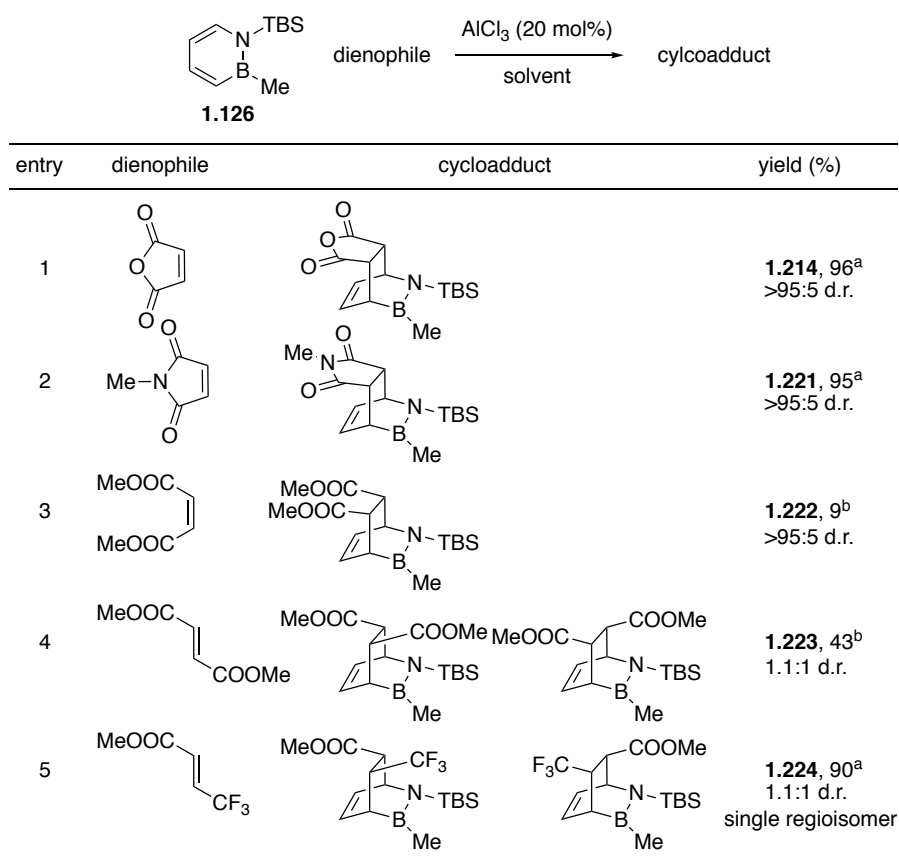
^aYield determined by ¹H NMR.

High yields were obtained with the TBS group on nitrogen and Me or O-*i*Pr on boron. Yields fell precipitously when R¹ was changed to Boc or when R² was changed to H or alkyne. *B*-H and *B*-alkynyl 1,2-azaborines display increased measures of aromaticity (e.g., NICS and RSE evaluated by calculation) relative to *B*-alkyl or *B*-

alkoxy 1,2-azaborines. Increased aromaticity corresponds to reduced Diels-Alder reaction free energy of the former compounds relative to the latter.²⁴

The scope of dienophiles was limited to highly activated substrates (Scheme 1.30). Reactions between 1,2-azaborine and less-activated dienophiles (Scheme 1.30, entries 3,4) never went to completion, regardless of the conditions. High diastereoselectivities were observed with *cis*-alkenes but selectivity was eroded with *trans*-alkenes. Reaction with the unsymmetrical alkene in entry 5 led to a single regioisomer, consistent with the more nucleophilic nature of the C3 and more electrophilic nature of the C6.

Scheme 1.30. Diels-Alder reaction of azaborine **1.126** with activated dienophiles.



Yield determined by ¹H NMR. ^atoluene, RT, 12 h. ^bCH₂Cl₂, 50 °C, 12h

1.4 BN-Naphthalenes

Some of the reactions described for 1,2-azaborines have also been optimized for BN-naphthalenes: primarily the 1,2 and 9,10 isomers and to a lesser extent the 2,1 isomer. For the purpose of this review, the prefix numbers refer to the positions of the nitrogen (first number), and boron (second number) with respect to the labelling convention of the corresponding hydrocarbon motif. Dewar pioneered the synthesis of 1,2- and 9,10-BN-naphthalenes and their “late-stage” functionalization. Molander and Fang later improved these methods for the 1,2-BN-naphthalene and 9,10-BN-naphthalene, respectively.

1.4.1 EAS

1.4.1.1 Halogenation

Similar to their monocyclic counterparts, BN-naphthalenes are attacked by electrophiles at the most electron-rich position which is typically the carbon adjacent to boron atom. In the case of 1,2-BN-naphthalene, Dewar first demonstrated that the C3 position is selectively halogenated.¹⁶ Molander later refined the EAS reaction for 1,2-BN-naphthalene, both improving reaction yields and greatly increasing the substrate scope (Scheme 1.31a).⁵³ Alkyl and H substituents are tolerated at nitrogen and alkyl, aryl, heteroaryl, and alkenyl substituents are tolerated at boron. Doubling the equivalents of bromine led to secondary bromination at the C6 position (Scheme 1.31b). Bromination at C6 also occurs when the C3 position is already substituted (Scheme 1.31c).

The most nucleophilic positions of the 9,10-BN-naphthalene are the C4 and C5 carbon positions adjacent to boron. Fang developed a halogenation procedure for

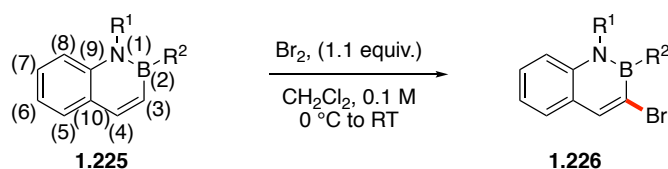
⁵³ Molander, G. A.; Wisniewski, S. R. *J. Org. Chem.* **2014**, *79*, 6663-6678.

9,10-BN-naphthalene using *N*-halosuccinimides promoted by AlCl₃ (Scheme 1.32).⁵⁴

Repeating the process with the same or a different halogenating reagent installs a second halide at the C5 position.

Scheme 1.31. a) Bromination of 1,2-BN-naphthalene. b) Dibromination of 1,2-BN-naphthalene. c) Bromination of C3-substituted 1,2-BN-naphthalene.

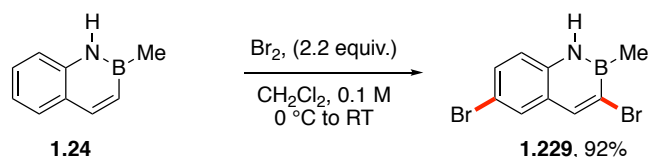
(a) **C3 Bromination**



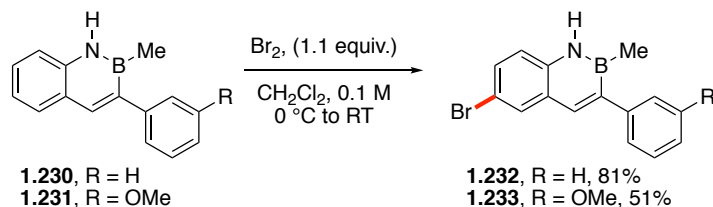
R¹ = H, Bn, allyl
R² = alkyl, aryl (EDG and EWG), heteroaryl, alkynyl
22 examples, 25-99% yield



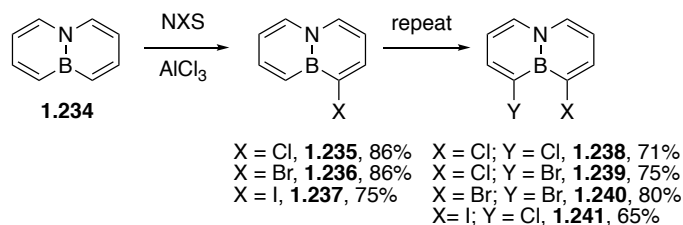
(b) **C6/C3 Dibromination**



(c) **C6 Bromination**



Scheme 1.32. Mono and dihalogenation of 9,10-BN-naphthalene.



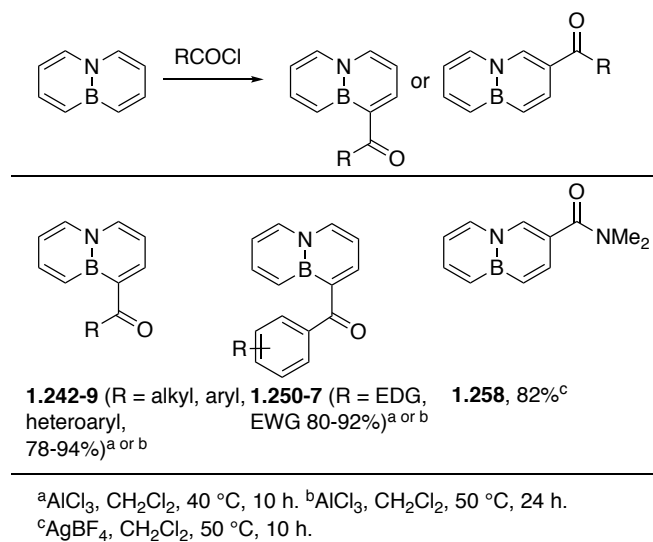
conditions: NXS (1.0 equiv.), AlCl₃ (1.0 equiv.) CH₂Cl₂, -35 °C to RT

⁵⁴ Sun, F.; Lu, L.; Huang, M.; Zhou, Z.; Fang, X. *Org. Lett.* **2014**, *16*, 5024-5027.

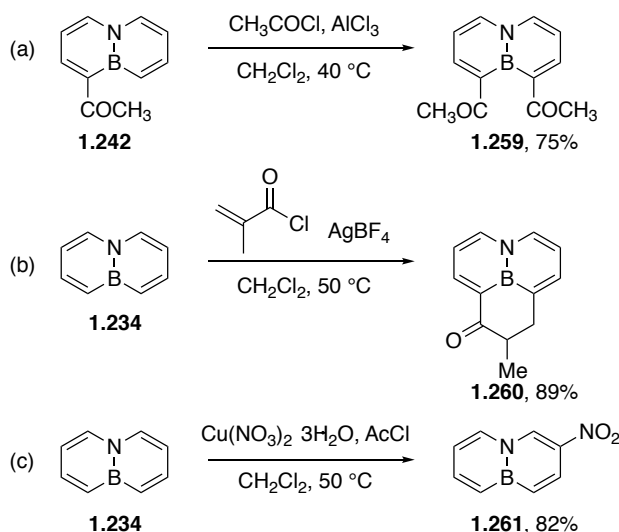
1.4.1.2 Acylation

Acylation of 9,10-BN-naphthalene has also been demonstrated by Fang. Acylation of the C4 position with acyl chlorides proceeds in good to excellent yield with either AlCl_3 or AgBF_4 as the Lewis-acid promoter (Scheme 1.33).⁴¹ Aroyl and alkanoyl chlorides were effective substrates in the acylation reaction and all furnished C4 BN-naphthyl ketones. Dimethylcarbamoyl chloride was the exception, which yielded the C2 isomer **1.258**. Repeating the acylation procedure with acetylated **1.242** produced bisacetylated compound **1.259** (Scheme 1.34a). A BN-phenaleonone adduct was accessible via a tandem acylation, cyclization of **1.260** with methacryloyl chloride (Scheme 1.34b). Fang and coworkers also extended their metal-nitrate mediated nitration to 9,10-BN-naphthalene, which installs a nitro group at C2 position (Scheme 1.34c).¹⁷

Scheme 1.33. Acylation of BN-naphthalene.



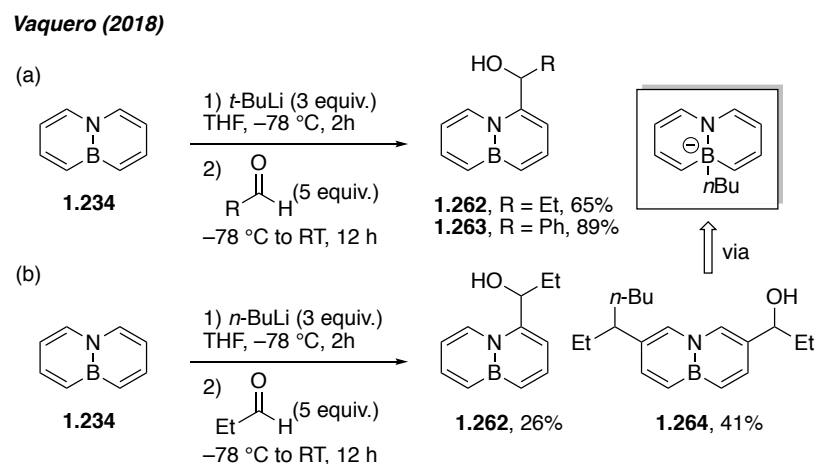
Scheme 1.34. a). Acylation of BN-aryl ketone **1.242**. b) BN-phenalene **1.260** prepared via-acylation-cyclization procedure. c) Nitration of BN-naphthalene **1.234**.



In 2018, Vaquero reported a complementary approach to the acylation reaction described by Fang and demonstrated the installation of an acyl group at the C1 position of 9,10-BN-naphthalene.⁵⁵ Treating **1.234** with a strong base such as *t*-BuLi leads to deprotonation of the most acidic C1-proton (Scheme 1.35a). Subsequent treatment of the C1-lithiated BN heterocycle with aldehydes furnishes alcohols **1.262-3** in good yield. The Vaquero group then discovered that the use of the more nucleophilic *n*-BuLi (vs. *t*-BuLi) activates both the C2 and C7 positions of 9,10 naphthalene for EAS reactions with aldehydes (Scheme 1.35b). While the expected acid-base chemistry occurs to form deprotonation product **1.262**, the authors observed the formation of difunctionalized **1.264** in modest yield. *n*-BuLi activates compound **1.234** to EAS via initial addition to the boron atom to form a borate. The quenching of the empty *p*-orbital on boron frees the nitrogen lone pair to participate in enamine-like reactivity, leading to EAS β to the nitrogen. It is worth noting that one of the benzylic hydroxy groups has been replaced with an *n*-butyl group.

⁵⁵ Abengózar, A.; Fernández-González, M. A.; Sucunza, D.; Frutos, L. M.; Salgado, A.; García-García, P.; Vaquero, J. J. *Org. Lett.* **2018**, *20*, 4902-4906.

Scheme 1.35. a) C1 acylation of 9,10-BN-naphthalene. b) C2, C7 difunctionalization of 9,10-BN-naphthalene via activation with *n*-BuLi.



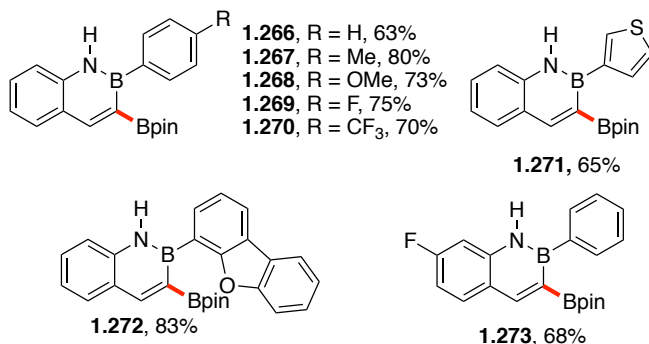
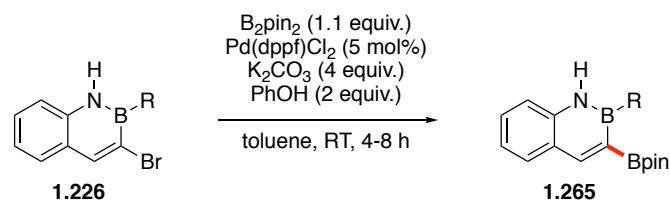
1.4.2 Borylation

The previous section covered methods for preparing halogenated 1,2-BN-naphthalenes as electrophilic building blocks. This section will describe the synthesis of BN naphthalene nucleophilic building blocks. Molander demonstrated that brominated 1,2-BN-naphthalenes **1.226** can undergo Miyaura borylation at the C3 position (Scheme 1.36a).⁵⁶ C3-borylated azaborines **1.265** can subsequently be converted to BF₃K salts **1.274-7** in good yields (Scheme 1.36b).

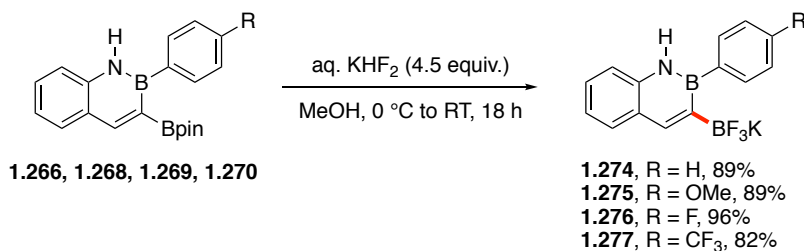
⁵⁶ Compton, J. S.; Saeednia, B.; Kelly, C. B.; Molander, G. A. *J. Org. Chem.* **2018**, *83*, 9484-9481.

Scheme 1.36. a) Miyaura borylation of 3-bromo-1,2-BN-naphthalenes. b) Conversion of 3-Bpin-1,2-BN-naphthalenes to corresponding BF₃K salts.

(a) **C3 Miyaura Borylation**



(b) **BF₃K Salt Formation**



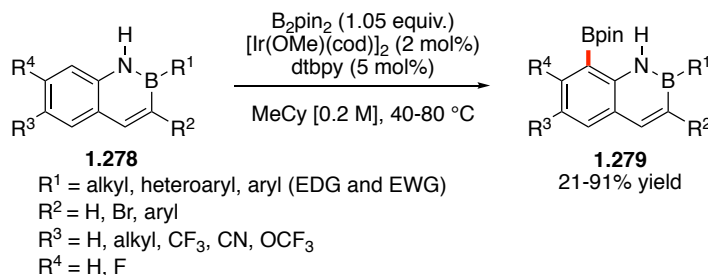
Both boron reagents **1.265** and **1.274** are suitable substrates for Suzuki cross-coupling reactions (*vide infra*). Along with Miyaura borylation, Molander also described the selective C-H borylation of 1,2-BN-naphthalenes at the C8 position (Scheme 1.37a).⁵⁷ Alkyl and aryl substituents at B (R²), aryl and bromo substituents at C3 (R³), and alkyl, CF₃, CN, and ether substituents at C6 (R⁶) are all tolerated. Anything larger than a proton on N or a proton or fluorine on C7 (R⁷) would sterically preclude borylation at the C8 position. The first C-H borylation is generally selective for the C8 position. A second Bpin can also be selectively installed at the C6 position to yield **1.280** in the presence of excess B₂pin₂ with elevated temperatures (Scheme

⁵⁷ Davies, G. H. M.; Jouffroy, M.; Sherafat, F.; Saeednia, B.; Howshall, C.; Molander, G. A. *J. Org. Chem.* **2017**, *82*, 8072-8084.

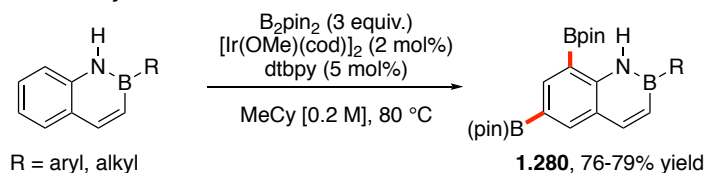
1.37b). When the C8 position is sterically blocked, as in *N*-Me substituted **1.281**, standard C-H borylation conditions lead to a mixture of C7 and C6 borylated isomers in a 70:30 ratio favoring the C7 isomer (Scheme 1.37c).

Scheme 1.37. a) C-H borylation at C8 position of *N*-H-1,2-BN-naphthalene. b) Bisborylation at C8 and C6 positions of 1,2-BN-naphthalene. c) Monoborylation at C7 and C6 positions of *N*-substituted 1,2-BN-naphthalene.

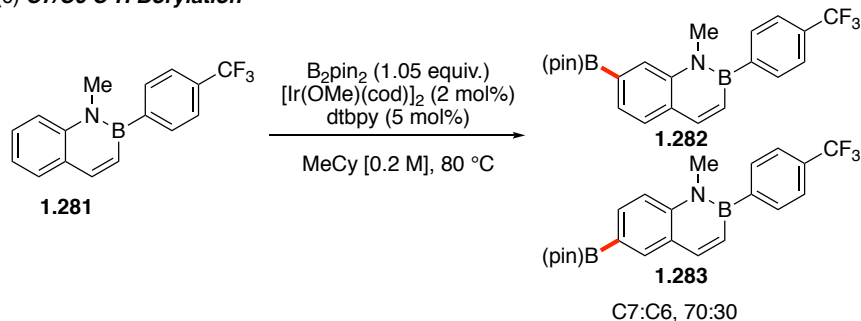
(a) **C8 C-H Borylation**



(b) **C8/C6 C-H Borylation**



(c) **C7/C6 C-H Borylation**



1.4.3 Cross-Coupling

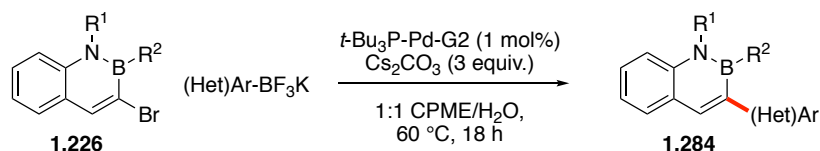
Molander, Fang, and Pei have all contributed to the cross-coupling chemistry of BN-naphthalenes. Molander has published extensively on the cross-coupling of 1,2-BN-naphthalenes, detailing a number of methods for functionalizing the C3, C6, and C8 positions totalling in the hundreds of substrates. Pei has demonstrated cross coupling at the C4 position of 1,2-BN-naphthalene, while Fang published cross-coupling methods for the 9,10 isomer of BN-naphthalene.

1.4.3.1 Cross-Coupling of 1,2-BN-naphthalenes

C3 brominated 1,2-BN-naphthalenes **1.226** engage in Suzuki cross-coupling with aryl BF₃K salts in modest to excellent yields (Scheme 1.38a).⁵³ Changing the catalyst and solvent broadened the scope of BF₃K coupling partners to include alkenyl substrates (Scheme 1.38b).⁵⁸ *N*-Alkyl, *B*-aryl substituted **1.286** serves as the electrophilic partner in the Kumada coupling of aryl Grignard reagents (Scheme 1.38c).⁵⁹

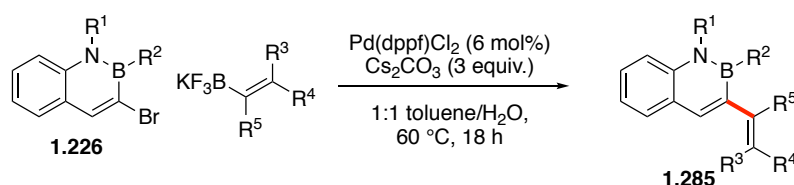
Scheme 1.38. Suzuki cross-coupling of 3-bromo-1,2-BN-naphthalenes and a) aryl BF₃K reagents; b) alkenyl BF₃K reagents. c) Kumada cross-coupling of 3-bromo-1,2-BN-naphthalenes and aryl Grignard reagents.

(a) **C3 Suzuki Coupling with Aryl Nucleophiles**



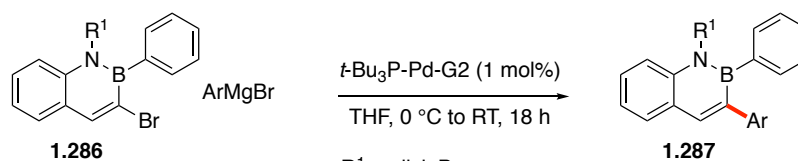
R¹ = H, alkyl, allyl, Bn
R² = alkyl, aryl, heteroaryl
39 examples, 24-98% yield

(b) **C3 Suzuki Coupling with Alkenyl Nucleophiles**



R¹ = H, allyl, Bn R³ = H, alkyl
R² = alkyl, aryl R⁴ = H, alkyl
R⁵ = H, alkyl
25 examples, 69-98% yield

(c) **C3 Kumada Coupling**



R¹ = allyl, Bn
5 examples, 73-89% yield

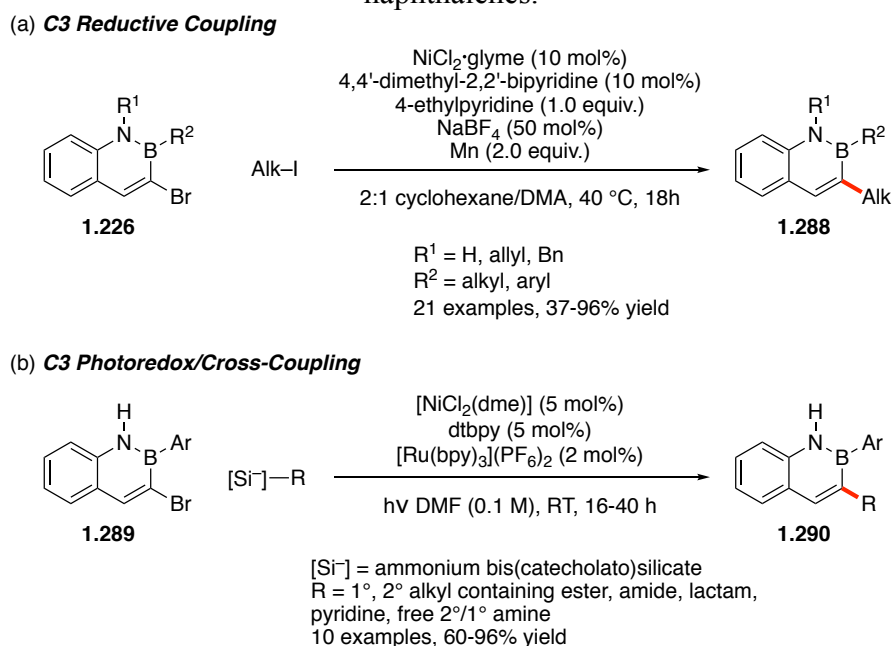
t-Bu₃P-Pd-G2 = chloro[bis(tri-*tert*-butylphosphine)]-[2-(2'-amino-1,1'-biphenyl)]-palladium(II).

⁵⁸ Molander, G. A.; Wisniewski, S. R.; Etemadi-Davan, E. *J. Org. Chem.* **2014**, *79*, 11199-11204.

⁵⁹ Molander, G. A.; Wisniewski, S. R. *J. Org. Chem.* **2014**, *79*, 8339-8347.

In order to extend the scope of cross-coupling reactions of 1,2-BN-naphthalenes to include alkyl reagents, Molander et al. developed the reductive cross-coupling of BN heteroaryl bromides and alkyl iodides.⁶⁰ Optimal conditions for the reductive cross-coupling include a Ni-catalyst supported by a bipyridine ligand, 4-ethylpyridine and NaBF₄ as additives, and Mn as the reductant (Scheme 1.39a). Cross-coupling of various alkyl iodides proceeds in modest to excellent yield. Molander et al. subsequently expanded the scope of alkyl coupling partners to include more sensitive functional groups, especially those susceptible to reduction, by developing a photoredox/nickel dual catalytic functionalization.⁶¹ The base-free method for derivatizing BN-naphthalene with ammonium bis(catecholato)silicates occurs at room temperature and is promoted by a Ni-catalyst and a Ru-photocatalyst (Scheme 1.39b). Functional groups such as esters, amides, lactams and even free amines are tolerated for the reaction.

Scheme 1.39. a) Reductive cross-coupling of 3-bromo-1,2-BN-naphthalenes and alkyl iodides. b) Photoredox/Nickel dual-catalytic functionalization of 3-bromo-1,2-BN-naphthalenes.

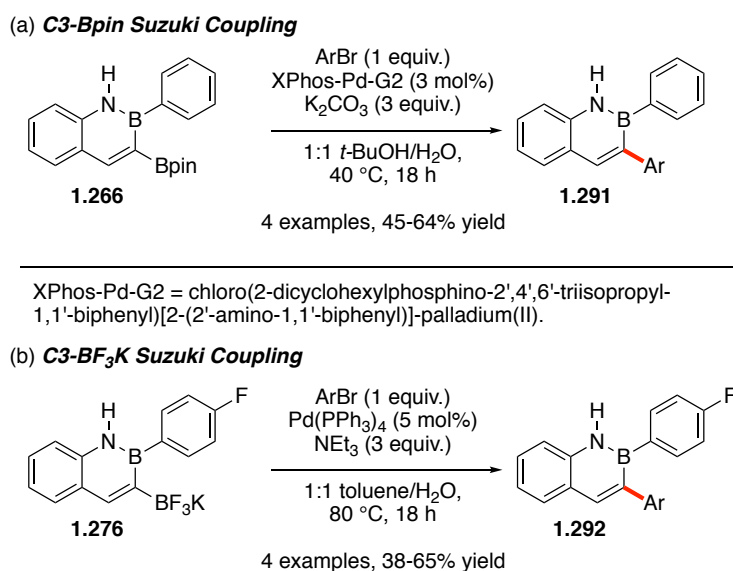


⁶⁰ Molander, G. A.; Wisniewski, S. R.; Traister, K. M. *Org. Lett.* **2014**, *16*, 3692-3695.

⁶¹ Jouffroy, M.; Davies, G. H. M.; Molander, G. A. *Org. Lett.* **2016**, *18*, 1606-1609.

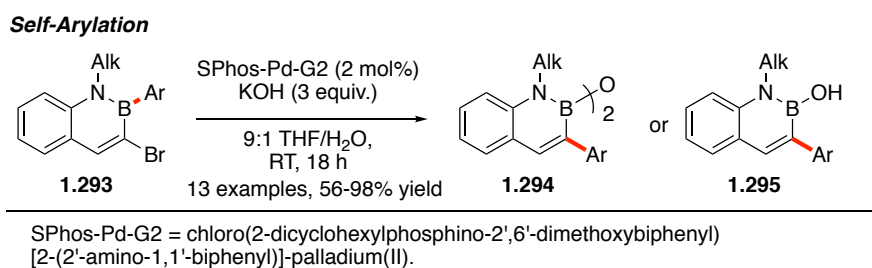
1,2-BN-naphthalenes also serve as the nucleophilic partner in a cross-coupling reaction. C3-boron pinacol ester **1.266** (Scheme 1.40a) and C3-BF₃K salt **1.276** (Scheme 1.40b) readily undergo Suzuki-Miyaura cross-coupling reactions.⁵⁶

Scheme 1.40. a) Cross-coupling of C3-Bpin-1,2-BN-naphthalene. b) Cross-coupling of C3-BF₃K-1,2-BN-naphthalene.



Molander et al. also developed a method for C3 functionalization via Suzuki cross-coupling where the BN-naphthalene contains both the nucleophile and the electrophile.⁵⁹ This self-arylation occurs when a *B*-aryl, C3-bromo BN-naphthalene is treated with a palladium catalyst and strong base; the *B*-aryl group undergoes a net migration to the C3 position (Scheme 1.41). A crossover experiment revealed that in fact the self-arylation is an intermolecular process. The boron atom of the BN-naphthalene is hydrolyzed during the self-arylation, and the reaction affords a mixture of anhydride **1.294** and alcohol **1.295**. Treating the anhydride with KOH in THF/H₂O converts it to the hydroxy compound.

Scheme 1.41. Self-arylation of 1,2-BN-naphthalenes.

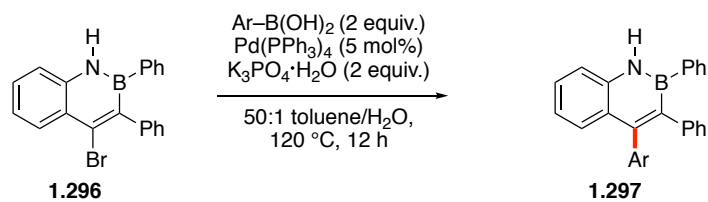


Suzuki cross-coupling has been deployed as a functionalization method for other positions on the 1,2-BN-naphthalene ring, including the C4, C6, and C8 positions. Using a bottom-up synthesis, Pei incorporated a bromine atom at the C4 position that serves as a handle for cross-coupling to afford a triaryl substituted BN-naphthalene core **1.297** (Scheme 1.42a).⁶² Cross-coupling of bisbrominated **1.229** or mono-C6-brominated **1.299** with aryl-BF₃K reagents affords the corresponding C3,C6 substituted naphthalenes (Scheme 1.42b,c).⁵³ The reactions depicted in Schemes 1.42b and c can also be performed with alkenyl-BF₃K reagents (cf. Scheme 1.38b).⁵⁸ The reductive cross-coupling method depicted in Scheme 1.39a has also been applied to compound **1.299**.⁶⁰ Suzuki-Miyaura coupling is also effective with C8-Bpin **1.301** and a variety of aryl bromides (Scheme 1.42d).⁵⁷

⁶²Zhuang, F.-D.; Han, J.-M.; Tang, S.; Yang, J.-H.; Chen, Q.-R.; Wang, J.-Y.; Pei, J. *Organometallics* **2017**, *36*, 2479-2482.

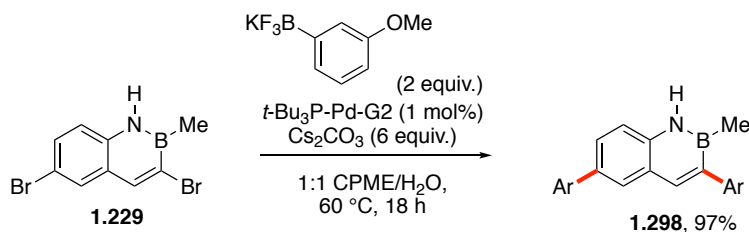
Scheme 1.42. a) Suzuki coupling at the C4 position of 1,2-BN-naphthalene; b) C3 and C6 positions; c) C6 position; d) C8 position.

(a) **C4 Suzuki Coupling**

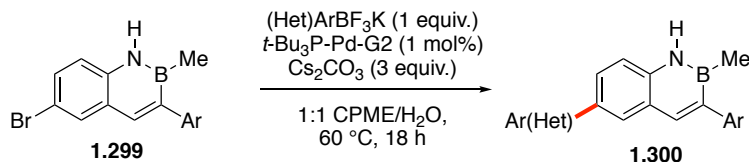


3 examples, 75-91% yield

(b) **C3/C6 Suzuki Coupling**

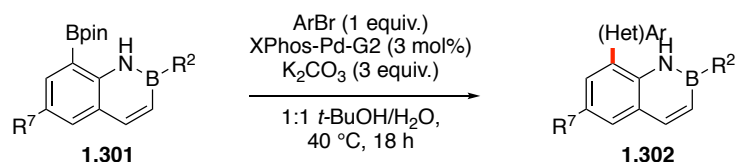


(c) **C6 Suzuki Coupling**



3 examples, 69-86% yield

(d) **C8 Suzuki Coupling**



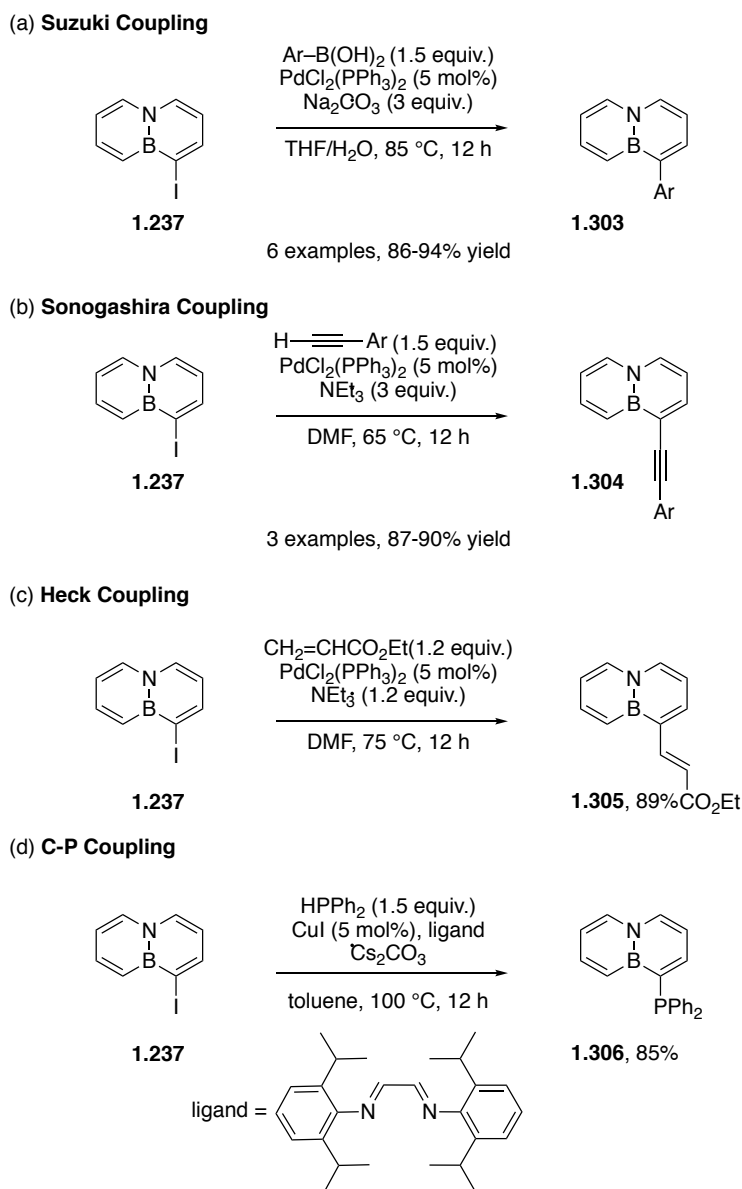
R^2 = alkyl, aryl
 R^7 = CN, OCF_3
 17 examples, 58-99% yield

1.4.3.2 Cross-Coupling of 9,10-BN-naphthalenes

Fang described cross-coupling methods to functionalize 9,10-BN-naphthalenes, including Suzuki coupling (Scheme 1.43a), Sonogashira coupling (Scheme 2.39b), and Heck reaction (Scheme 1.43c).⁵⁴ Several examples of arylboronic acids, alkynes as well as one example of an alkene engage in coupling with the C4-iodo compound **1.237**. Diaryl phosphines also function as nucleophiles in

a coupling reaction with **1.237** to form BN-containing phosphine ligand **1.306** (Scheme 1.43d).⁶³

Scheme 1.43. a) Suzuki coupling of 9,10-BN-naphthalene; b) Sonogashira coupling; c) Heck reaction; d) C-P coupling.



1.4.4 Nucleophilic Substitution

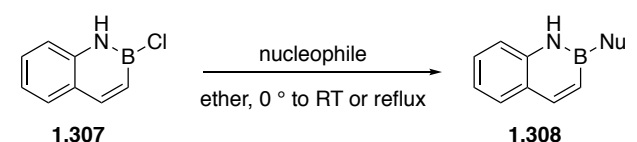
Dewar first reported the synthesis and functionalization of the 1,2-BN-naphthalene in 1959.¹⁵ Incorporating a B-Cl bond into the synthesis allowed for ready functionalization of the product at the boron position via nucleophilic substitution,

⁶³ Sun, F.; Huang, M.; Zhou, Z.; Fang, X. *RSC Advances* **2015**, *5*, 75607-75611.

albeit in modest yields. An excess amount of hydride or methyl or phenyl Grignard reagents displace the chloride in *N*-H, *B*-Cl 1,2-BN-naphthalene **1.307** to afford substituted **1.308** after aqueous workup (Scheme 1.44a). In 2014, Molander showed that the B-OH bond containing **1.311**, the product of the self-arylation reaction, could be substituted with a phenyl group with a Grignard reagent (Scheme 1.44b).⁵⁹

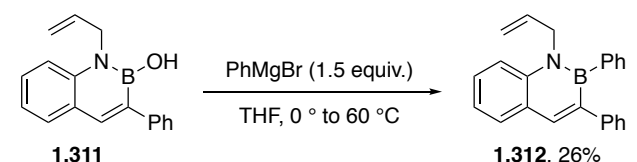
Scheme 1.44. a) Nucleophilic substitution at the boron position of 1,2-BN-naphthalene by Dewar. b) Nucleophilic substitution at the boron position of 1,2-BN-naphthalene by Molander. c) Nucleophilic substitution at the boron position of 2,1-BN-naphthalene by Cui.

(a) **Dewar (1959)**

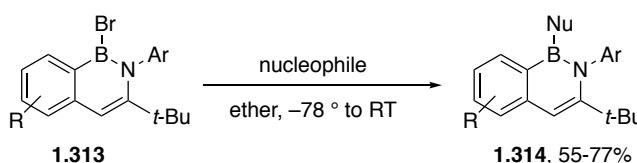


entry	nucleophile	product	yield (%)
1	LiAlH ₄	1.309	40
2	PhMgBr	1.310	43
3	MeMgBr	1.24	45

(b) **Molander (2014)**



(c) **Cui (2015) 2,1-BN-naphthalene**



Ar = phenyl and substituted phenyls
R = H, Me, F
Nu = phenyl, thienyl, naphthalenyl, alkynyl,
PhCH₂NH₂/NEt₃

In 2015, Cui reported the first synthesis and late-stage functionalization of the 2,1-BN-naphthalene.⁶⁴ The incorporation of the B-Br bond in compound **1.313** allows

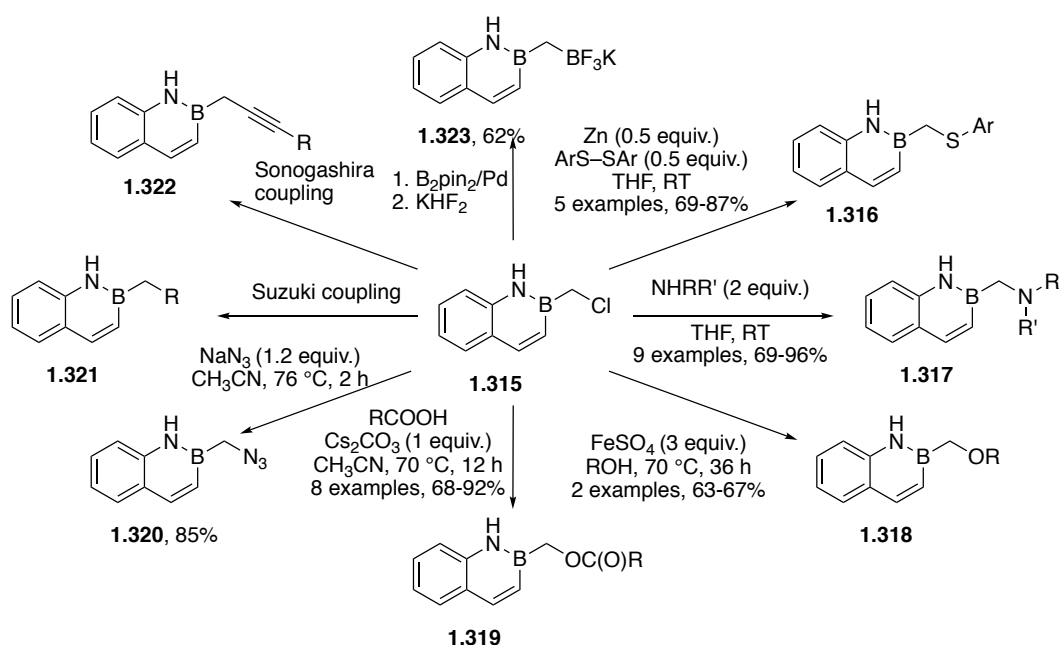
⁶⁴ Liu, X.; Wu, P.; Li, J.; Cui, C. *J. Org. Chem.* **2015**, *80*, 3737-3744.

for the relatively facile substitution with various nucleophiles to afford compound **1.314** (Scheme 1.44c).

1.4.5 Benzylic Functionalization

In 2014 Molander et al. prepared 2-chloromethyl-1,2-BN-naphthalene, a building block for benzylic functionalization.⁶⁵ Like its benzylic halide counterpart, the BN compound **1.315** undergoes nucleophilic substitutions with a wide variety of nucleophiles including amines, alcohols, carboxylic acids, thiols, and azide (Scheme 1.45). Cross-coupling reactions including Suzuki and Sonogashira reactions have also been reported.⁶⁶ Borylation and subsequent use of benzylic BF_3K reagent **1.323** as the nucleophile in cross-coupling reactions is also possible.⁶⁷

Scheme 1.45. Benzylic functionalizations of 1,2-BN-naphthalene.



conditions for Suzuki coupling: Aryl: 1.25 mol% Pd_2dba_3 , 2.5 mol% RuPhos, 2 equiv. Cs_2CO_3 , 19:1 toluene/ H_2O 80 °C, 18 h, 22 examples of (Het)Ar BF_3K , 46-92%. Alkenyl: 2 mol% Pd_2dba_3 , 4 mol% $t\text{-Bu}_2\text{MeP HBF}_4$, 2 equiv. K_2CO_3 , 12 examples, 75-90%. **conditions for Sonogashira coupling:** 2 mol% XPhos-Pd-G2, 1 equiv. Cs_2CO_3 , 19:1 toluene/ H_2O , 70 °C, 8 examples, 60-84%. **conditions for borylation:** 1. 3 mol% $(\text{Ph}_3\text{P})_2\text{PdCl}_2$, 2 equiv. K_3PO_4 , 19:1 toluene/ H_2O , 75 °C, 17h

⁶⁵ Molander, G. A.; Wisniewski, S. R.; Amani, J. *Org. Lett.* **2014**, *16*, 5636-5639.

⁶⁶ Molander, G. A.; Amani, J.; Wisniewski, S. R. *Org. Lett.* **2014**, *16*, 6024-6027.

⁶⁷ Amani, J.; Molander, G. A. *Org. Lett.* **2015**, *17*, 3624-3627.

Similar to the BN-styrenes **1.30** and **1.112** (*vide supra*, Scheme 1.27), Klausen demonstrated that *B*-vinyl, 1,2-BN-naphthalene **1.324** displays styrene-like reactivity (Scheme 1.46).⁶⁸ The reactivity of styrene and monomer **1.324** are similar enough to prepare statistical copolymers using free-radical polymerization promoted by AIBN.

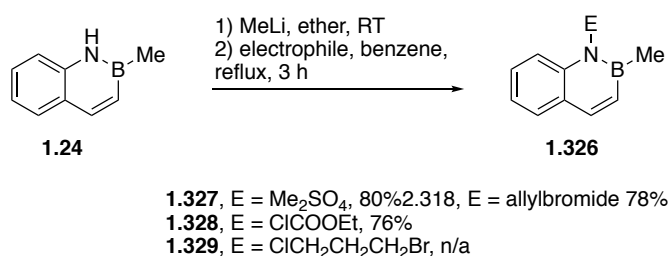
Scheme 1.46. Copolymerization of styrene and 1,2-BN-naphthalene **1.324**.



1.4.6 Electrophilic Substitution

In an effort to prepare boron-containing organic compounds for neutron capture therapy Dewar reported a procedure for the substitution of 1,2-BN-naphthalene at the nitrogen position with various electrophiles.¹² *N*-H-*B*-Me naphthalene **1.24** is first deprotonated with MeLi and then quenched with an alkyl or alkanoyl electrophile (Scheme 1.47). *N*-Me, allyl, and ethyl-ester substituted 1,2-BN-naphthalenes **1.326** were prepared in good yield.

Scheme 1.47. Electrophilic substitution at the nitrogen position of 1,2-BN-naphthalene.



1.5 BN-Polycyclic Aromatic Hydrocarbons (PAHs)

The chemistry of BN-doped polycyclic aromatic hydrocarbons encompasses a vast body of literature. The reader is encouraged to read the reviews by Piers^{1a} and

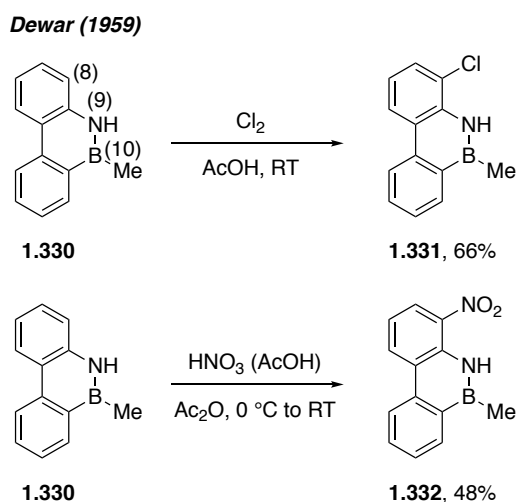
⁶⁸ van de Wouw, H. L.; Awuyah, E. C.; Baris, J. I.; Klausen, R. S. *Macromolecules* **2018**, *51*, 6359-6368.

Liu^{1b} and references therein as a starting point for this literature. Compared to the large number of publications about the assembly of BN-PAHs there are relatively few examples of late-stage functionalizations of these heterocycles. This section details the available methods for the late-stage functionalization of the 9,10 and 4a,10a-BN-phenanthrenes, 1,2 and 9a,9-BN-anthracenes, and a BN-tetraphene.

1.5.1 EAS

While halogenation of the 1,2-azaborine or BN-naphthalenes occurs at the carbon position adjacent to the boron atom, this is not generally the case for BN-PAHs. In 1959, Dewar reported that EAS occurs at the C8 position of 9,10-BN-phenanthrene (Scheme 1.48).⁶⁹ Treatment of 9,10-BN-phenanthrene **1.330** with chlorine or nitric acid affords the respective EAS product in moderate yield. 9,10-BN-phenanthrene is a remarkably stable compound, given the relatively harsh conditions of these substitution reactions by current standards.

Scheme 1.48. EAS reactions of 9,10-BN-phenanthrene.

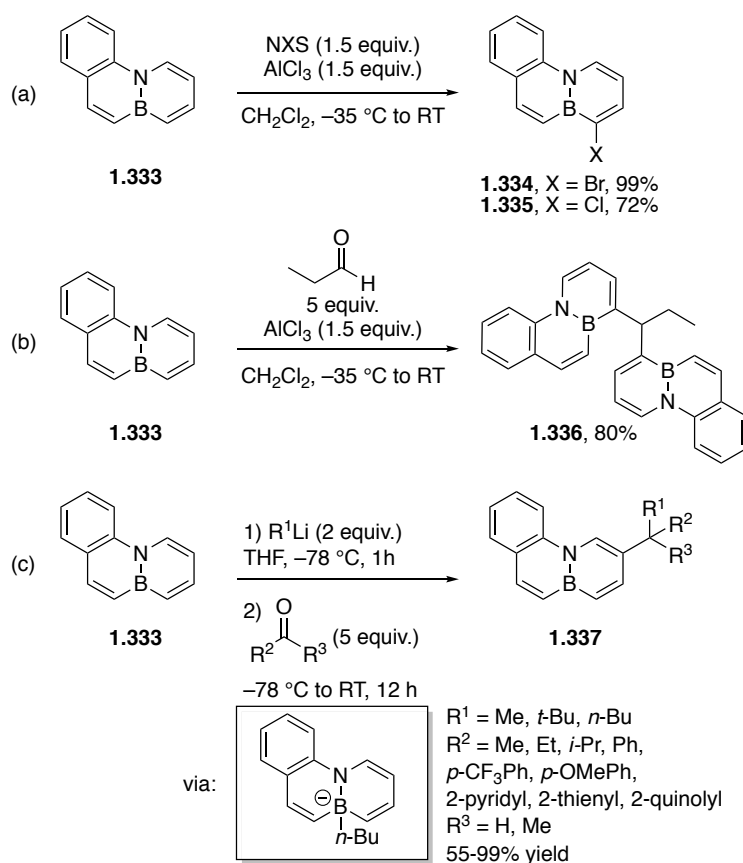


Vaquero synthesized the 4a,10a-BN-phenanthrene **1.333**, and like its simpler analogue 9,10-BN-naphthalene, it is attacked by halogen electrophiles at the carbon

⁶⁹ Dewar, M. J. S.; Kubba, V. P. *Tetrahedron* **1959**, *7*, 213-222.

position adjacent to boron (Scheme 1.49a).⁷⁰ Either a Cl or a Br can be installed in good to excellent yield. When propanal is used as the electrophile, it can be attacked by two equivalents of **1.333** to form **1.336** (Scheme 1.49b). Selectivity for the EAS reaction with aldehydes can be shifted to the carbon position β to the nitrogen atom by employing *n*-BuLi as an activator (Scheme 1.49c). The activation method is analogous to the one described in Scheme 1.35 for 9,10-BN-naphthalene. Aldehyde and ketone electrophiles are viable substrates for EAS and unlike 9,10-BN-naphthalene the reaction is completely regioselective. The resulting carbinol reacts with an additional equivalent of the alkyllithium reagent, furnishing alkylated **1.337** in moderate to excellent yields.

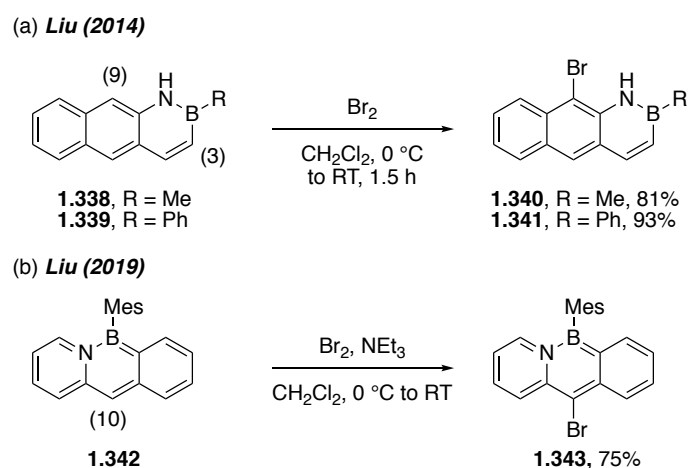
Scheme 1.49. EAS reactions of 4a,10a-BN-phenanthrene.



⁷⁰ Abengózar, A.; García-García, P.; Sucunza, D.; Frutos, L. M.; Castaño, O.; Sampedro, D.; Pérez-Redondo, A.; Vaquero, J. J. *Org. Lett.* **2017**, *19*, 3458-3461.

Liu et al. reported the first example of a BN-anthracene in 2014.⁷¹ Unlike its bi- and monocyclic analogues, EAS of the 1,2-BN-anthracene does not occur at the C3 position adjacent to B but rather at the C9 position (Scheme 1.50a). The authors found that there is a significant contribution to the HOMO from C9 but a vanishingly small one from C3. Thus, the reaction appears to be orbitally controlled which is consistent with the "soft" nature of the Br₂ electrophile. In 2019, the Liu group reported another anthracene isomer, the 9a,9 isomer.⁷² Substitution of **1.342** with bromine was selective for the apical C10 position (Scheme 1.50b). Cui prepared BN-tetraphene **1.344** and also demonstrated EAS with bromine, yielding functionalized **1.345** (Scheme 1.51).⁷³

Scheme 1.50. a) Bromination of 1,2-BN-anthracene. b) Bromination of 9a,9-anthracene.

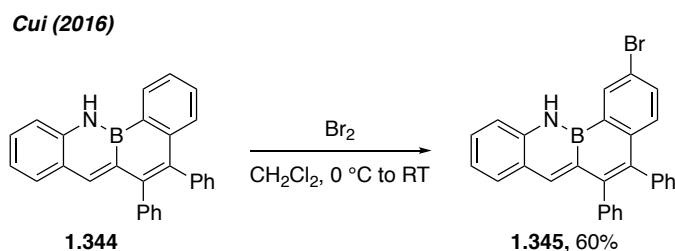


⁷¹ Ishibashi, J. S. A.; Marshall, J. L.; Mazière, A.; Lovinger, G. J.; Li, B.; Zakharov, L. N.; Dargelos, A.; Graciaa, A.; Chrostowska, A.; Liu, S.-Y. *J. Am. Chem. Soc.* **2014**, *136*, 15414-15421.

⁷² Ishibashi, J. S. A.; Darrigan, C.; Chrostowska, A.; Li, B.; Liu, S.-Y. *Dalton. Trans.* **2019**, *48*, 2807-2812.

⁷³ Huang, H.; Pan, Z.; Cui, C. *Chem. Comm.* **2016**, *52*, 4227-4230.

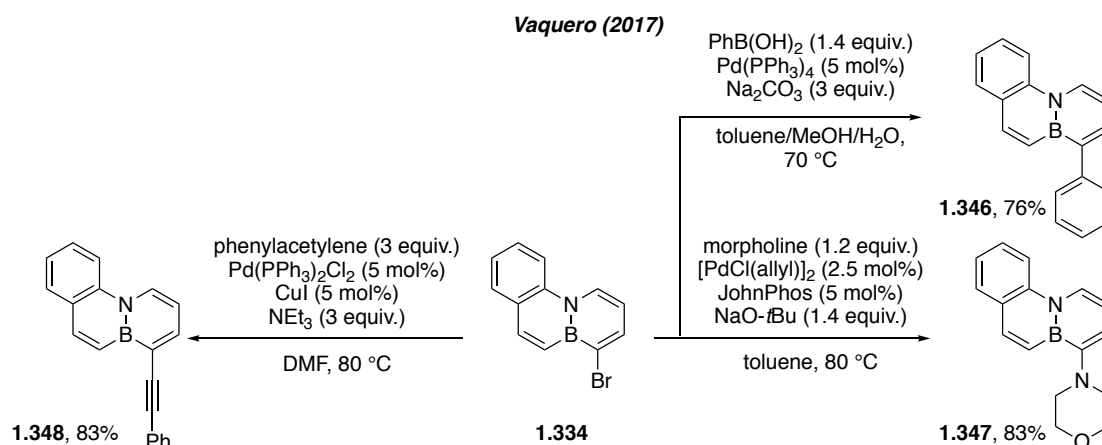
Scheme 1.51. Bromination of BN-tetraphene.



1.5.2 Cross-Coupling

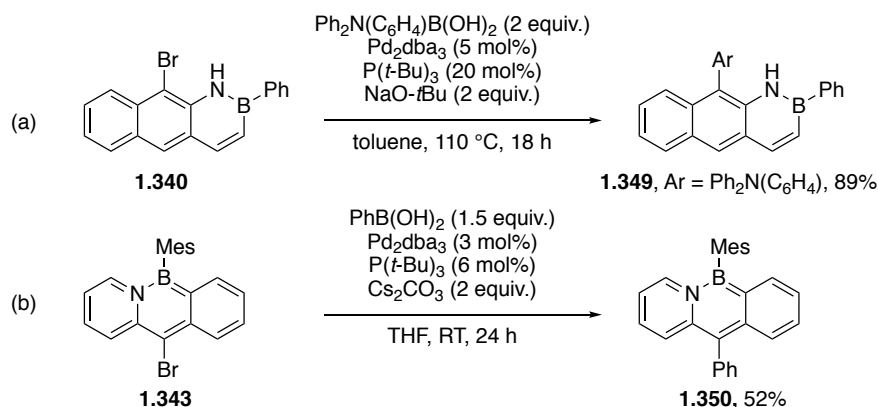
Brominated **1.334** serves as the electrophile in three different cross coupling reactions.⁷⁰ Suzuki cross-coupling leads to arylated **1.346**, Buchwald-Hartwig coupling furnishes amine-substituted **1.347**, and Sonogashira coupling installs an alkyne in product **1.348** (Scheme 1.52).

Scheme 1.52. Cross-coupling reactions of brominated BN-phenanthrene **1.334**.

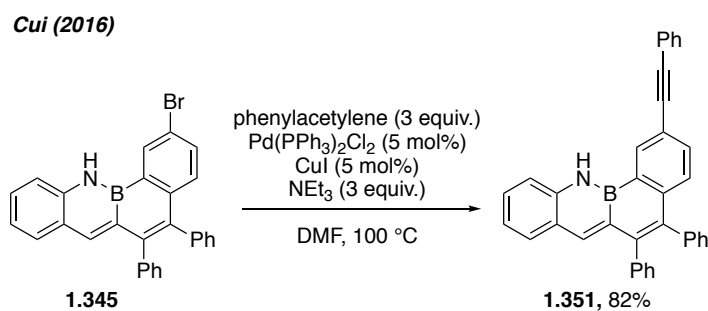


The brominated BN-anthracenes **1.340** and **1.343** also undergo Suzuki cross-coupling with arylboronic acids. An aryl group is installed at the C9 position of **1.349** (Scheme 1.53a)⁷¹ and at the C10 position of **1.350** (Scheme 1.53b).⁷² Cui reported an example of Sonogashira coupling to functionalize brominated BN-tetraphene **1.355** (Scheme 1.54).⁷³

Scheme 1.53. a) Cross-coupling at C9 position of 1,2-BN-anthracene. b) Cross-coupling at C10 position of 9a,9-BN-anthracene.



Scheme 1.54. Cross-coupling of BN-tetraphene.

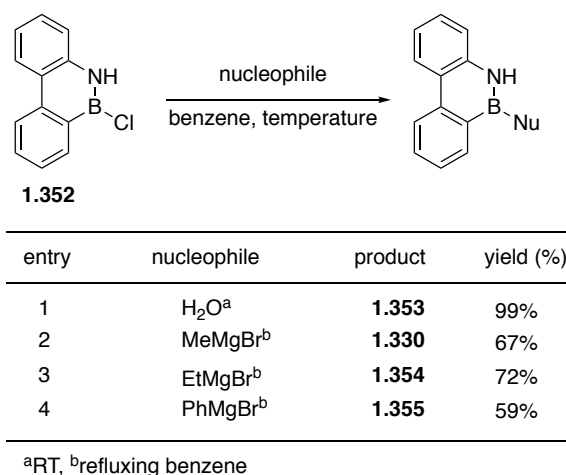


1.5.3 Nucleophilic Substitution

Synthesis of B-Cl substituted **1.352** provides a functional handle for nucleophilic substitution at the boron position. Dewar reported four examples of nucleophiles that displace the B-Cl: water, methyl Grignard, ethyl Grignard, and phenyl Grignard (Scheme 1.55).⁷⁴

⁷⁴Dewar, M. J. S.; Kubba, V. P.; Pettit, R. *J. Chem. Soc.* **1958**, 3073-3076.

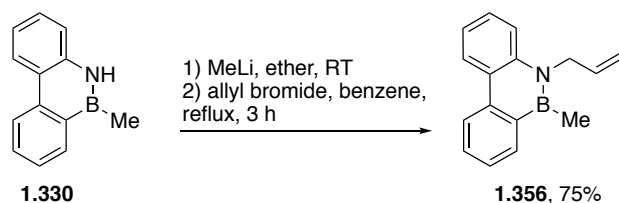
Scheme 1.55. Nucleophilic substitution of 9,10-BN-phenanthrene **1.352**.



1.5.4 Electrophilic Substitution at Nitrogen

Similar to the analogous 1,2-BN-naphthalene, a strong base will deprotonate the N-H proton of BN-phenanthrene **1.330** (Scheme 1.56).¹² The resulting amide was substituted with allylbromide in good yield.

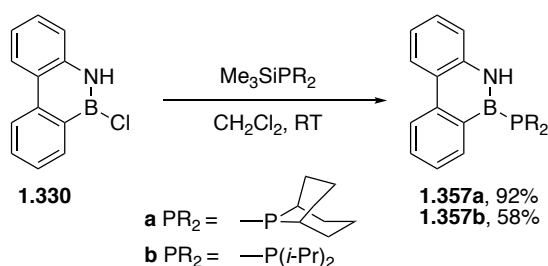
Scheme 1.56. Electrophilic substitution of N-H of 9,10-BN-phenanthrene.



1.5.5 B-X Activation

In an effort to synthesize BN-arene containing phosphine ligands, Pringle et al. discovered that B-Cl substituted BN-phenanthrene **1.352** reacts with silylphosphines at room temperature to afford BN-phosphine ligands **1.357** (Scheme 1.57).^{35b} The ease with which the B-Cl bond reacts with the P-Si bond was somewhat surprising given that formation of a P-B bond from Et₂PSiMe₃ and ClB(*n*-Pr)₂ required several hours at high temperatures (120 °C).

Scheme 1.57. Exchange reaction between B-Cl **1.330** and silylphosphines.



1.6 Distinct Reactivity of BN-Heterocycles

Replacing a CC with a BN unit renders each position of BN-heterocycles electronically distinct. As a result, the BN bond imbues distinct selectivity to a BN-heterocycle as compared to analogous reactions of its all-carbon counterpart. Based on the results presented in this review, several selectivity trends emerge for certain reactions of BN-heterocycles.

For monocyclic azaborine and BN-naphthalenes, EAS occurs at the position adjacent to boron which is the most electron-rich (Schemes 1.7, 1.31, 1.32, 1.49). Friedel-Crafts reactions can occur either adjacent to boron (Schemes 1.33, 1.49), or at the second-most electron-rich position β to nitrogen (Schemes 1.8, 1.9, 1.33, 1.34, 1.35, 1.49) depending on the conditions. EAS selectivity for BN-PAHs does not necessarily follow these trends.

The N-H bond is the most acidic position and thus can be selectively deprotonated and functionalized with electrophiles (Schemes 1.20, 1.21, 1.47). The closest C-H bond to the nitrogen atom is the most acidic and will be selectively deprotonated in the absence of an N-H bond for further functionalization (Scheme 1.35) or C-H borylation (Schemes 1.10, 1.37).

The boron atom is the most electrophilic position of a BN-heterocycle due to its partially occupied p -orbital. If a leaving group is attached, it will undergo

substitution preferentially in the presence of other carbon-based leaving-groups (Scheme 1.18).

More broadly, the presence of the boron atom provides the opportunity to perform reactions not available to all-carbon compounds. Activation of various B-X bonds is possible: B-Cl bonds undergo transmetalations (Schemes 1.23, 1.57); B-H bonds can undergo dehydrogenative borylation (Scheme 1.24); B-C bonds can undergo oxidation (Schemes 1.25, 1.26) as well as the unique self-arylation reaction (Scheme 1.41); boron atoms internal to BN-PAHs can be activated with *n*-butyllithium, which in turn activates certain C-H bonds to further functionalization (Schemes 1.35, 1.49). Finally, monocyclic 1,2-azaborines undergo Diels-Alder reactions under thermal conditions unlike their benzene-derived counterparts (Schemes 1.29, 1.30).

1.7 Conclusions

Significant progress has been made in the field of azaborine chemistry in the past two decades. The synthetic access to a continuously growing library of BN heterocyclic compounds has led to the discovery of new properties and functions in a variety of disciplines ranging from biomedical research to materials science. Despite the advances made to date, the field is still in relatively early stages of development and remains limited by the synthetic access to new BN heterocycles and their derivatives. The literature surveyed in this review highlights the distinguishing reactivity/selectivity patterns exhibited by BN heterocycles relative to their carbonaceous counterparts. It is also clear from the survey that the available synthetic toolbox for derivatizing BN heterocycles falls far short of the capabilities developed for arenes. Thus, further development in this area will undoubtedly help mature this burgeoning field. Overall, BN/CC isosterism as a general approach to create new

function has tremendous potential due to the near unlimited chemical space provided by hydrocarbon compounds. Exciting untapped opportunities related to reaction chemistry that take advantage of the distinct electronic structure of BN heterocycles include new bioconjugation chemistry and the use of BN heterocycles as synthons in organic synthesis, to name a few.

Chapter 2

Accessing New Regioisomeric Building Blocks of 1,2-Azaborine via Resolution

Chemistry Enabled by 1,2-Azaborine's Distinct Electronic Structure*

2.1 Introduction

2.1.1 Chapter Overview

The previous chapter defined the concept of late-stage functionalization as it applies to 1,2-azaborines and provided an overview of all of the available methods for decorating an assembled BN-heterocycle. In many instances, the selectivity of a given functionalization is governed by the distinct electronic structure of the 1,2-azaborine. In contrast, benzene, the symmetric all-carbon isostere of 1,2-azaborine, typically does not display high levels of regioselectivity.¹ Common strategies to induce site selectivity in the functionalization of arenes include directing groups² and ligand directing effects in transition metal catalyzed reactions.³ Efforts are on going to develop regioselective, transition metal catalyzed methods of arene C-H bond functionalization that are not promoted by directing groups.⁴ Recently, the Ritter group published a highly regioselective thianthrenation of aromatic C-H bonds that provides a versatile handle for further functional group manipulation.⁵ As evidenced in the previous chapter, the synthetic chemistry of BN-heterocycles remains in its

*The experimental work detailed in this chapter has been published in the following article:
McConnell, C. R.; Haeffner, F.; Baggett, A. W.; Liu, S.-Y. *J. Am. Chem. Soc.* **2019**, *In Press*.

¹ For reviews on C-H functionalization of arenes including discussions on regioselectivity, see: (a) Olah, G. A. *Acc. Chem. Res.* **1971**, *4*, 240-248. (b) Mkhaliid, I. A. I.; Barnard, J. H.; Marder, T. B.; Murphy, J. M.; Hartwig, J. F. *Chem. Rev.* **2010**, *110*, 890-931. (c) Yeung, C. S.; Dong, V. M. *Chem. Rev.* **2011**, *111*, 1215-1292. (d) Cheng, C.; Hartwig, J. F. *Chem. Rev.* **2015**, *115*, 8946-8975.

² (a) Colby, D. A.; Bergman, R. G.; Ellman, J. A. *Chem. Rev.* **2010**, *110*, 624-655. (b) Engle, K. M.; Mei, T.-S.; Wasa, M.; Yu, J.-Q. *Acc. Chem. Res.* **2012**, *45*, 788-802.

³ Lyons, T. W.; Sanford, M. S. *Chem. Rev.* **2010**, *110*, 1147-1169.

⁴ Kuhl, N.; Hopkinson, M. N.; Wencel-Delord, J.; Glorius, F. *Angew. Chem. Int. Ed.* **2012**, *51*, 10236-10254.

⁵ Berger, F.; Plutschack, M. B.; Riegger, J.; Yu, W.; Speicher, S.; Ho, M.; Frank, N.; Ritter, T. *Nature* **2019**, *567*, 223-228.

infancy relative to that of all-carbon arenes. Thus, many opportunities remain to develop new ways of functionalizing the 1,2-azaborine core.

In the previous chapter, strategies for functionalizing five of the six available positions of 1,2-dihydro-1,2-azaborine were described. The N1 position exhibits amide reactivity in the presence of a base (Scheme 2.1, R¹),⁶ while the electrophilic nature of the B2 permits nucleophilic substitution (Scheme 2.1, R²).⁷ Electrophilic aromatic substitution occurs at the C3 position, which provides a handle for cross-coupling chemistry (Scheme 2.1, R³).⁸ EAS, including acylation and nitration, has been demonstrated at the C5 position however the scope with respect to 1,2-azaborine remains limited (Scheme 2.1, R⁵).⁹ The C6 position of 1,2-azaborine bears the most acidic C-H bond and has been shown to undergo regioselective C-H borylation; the borylated azaborine serves as a building block where the highly versatile Bpin group can be further manipulated (Scheme 2.1, R⁶).¹⁰ Finally, there are no reported examples of late-stage C4 functionalization (Scheme 2.1, R⁴).

The lack of general functionalization strategies that have been developed for the C4 and C5 positions of the 1,2-azaborine heterocycle is a significant limitation for its envisioned application as a pharmacophore in medicinal chemistry or as a synthon in organic synthesis. This chapter will describe the development of methods for the functionalization of the C4 and C5 positions of 1,2-azaborine using a building block strategy. The distinct electronic structure of 1,2-azaborine enables the resolution of

⁶ (a) Pan, J.; Kampf, J. W.; Ashe, A. J. *Organometallics* **2004**, *23*, 5626-5629. (b) J., B. R.; Bo, L.; Monica, V.; A., D. D.; Shih-Yuan, L. *Angew. Chem. Int. Ed.* **2015**, *54*, 7823-7827. (c) Baggett, A. W.; Liu, S.-Y. *J. Am. Chem. Soc.* **2017**, *139*, 15259-15264.

⁷ (a) Marwitz, A. J. V.; Abbey, E. R.; Jenkins, J. T.; Zakharov, L. N.; Liu, S.-Y. *Org. Lett.* **2007**, *9*, 4905-4908. (b) Lamm, A. N.; Garner, E. B.; Dixon, D. A.; Liu, S.-Y. *Angew. Chem. Int. Ed.* **2011**, *50*, 8157-8160.

⁸ (a) Pan, J.; Kampf, J. W.; Ashe, A. J. *Org. Lett.* **2007**, *9*, 679-681. (b) Brown, A. N.; Li, B.; Liu, S.-Y. *J. Am. Chem. Soc.* **2015**, *137*, 8932-8935.

⁹ (a) Zhang, Y.; Dan, W.; Fang, X. *Organometallics* **2017**, *36*, 1677-1680. (b) Zhang, Y.; Sun, F.; Dan, W.; Fang, X. *J. Org. Chem.* **2017**, *82*, 12877-12887.

¹⁰ Baggett, A. W.; Vasiliu, M.; Li, B.; Dixon, D. A.; Liu, S.-Y. *J. Am. Chem. Soc.* **2015**, *137*, 5536-5541.

C4 and C5 functionalized regioisomers. In Chapter 3, the newly developed reactions are then applied to the synthesis and polymerization of BN-styrene analogues where the vinyl group is installed at the C4, C5, or C6 position of 1,2-azaborine (Figure 2.1). We investigate the effects of the positioning of the BN bond relative to the polymer backbone (Section 2.2).

Scheme 2.1. Functionalization methods of 1,2-azaborine.

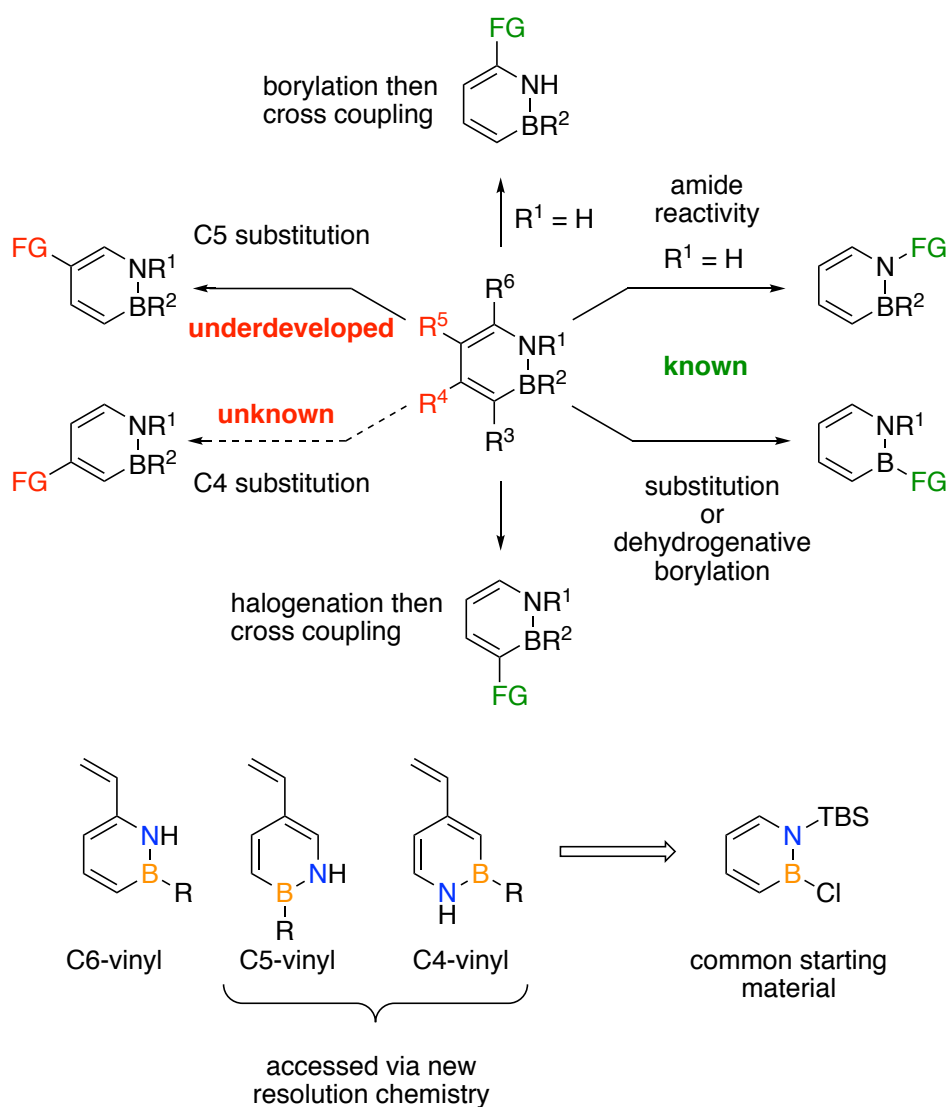
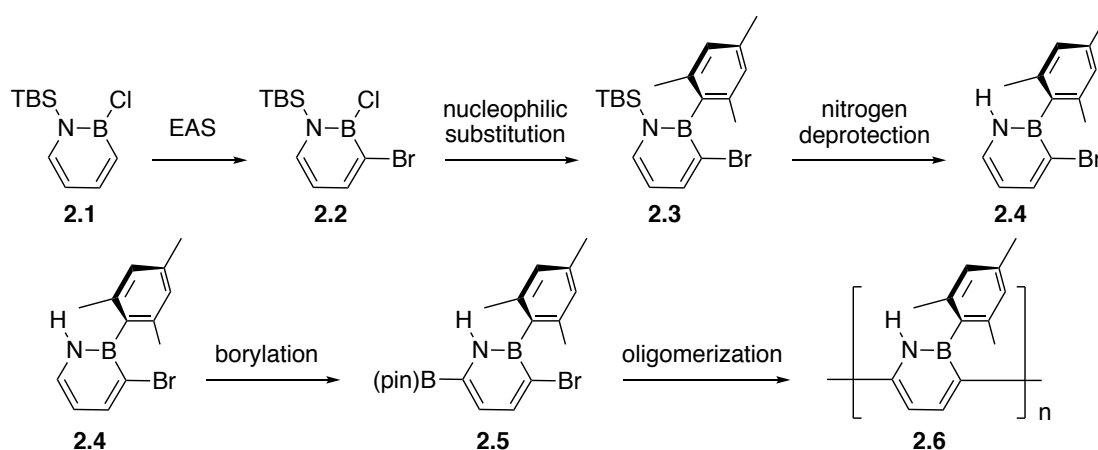


Figure 2.1. C4, C5, and C6 BN-styrene analogues (Chapter 3).

2.1.2 Building Block Approach to Azaborine Synthesis

To address the lack of functionalization methods for the C4 and C5 positions of 1,2-azaborine we sought to apply the building block strategy. Azaborines substituted with a readily modifiable Bpin or halogen group offer a foundation for constructing applications-based molecules. For example, we were able to access BN polyparaphenylene (BN-PPP) **2.6** and discover the NH...arene interaction as a new conformational orienting feature as a direct consequence of the synthetic availability of the difunctionalized C3-Br-C6-Bpin-1,2-azaborine monomer **2.5** (Scheme 2.2).¹¹

Scheme 2.2. Synthesis of oligomer **2.6** via building block **2.5**.



Synthesis of this monomer begins with commercially available synthon **2.1**. EAS reaction places a bromine at the C3 position which is followed by displacement of the Cl leaving group on boron with mesityl lithium. TBS deprotection precedes the final C-H borylation step at the C6 position. Monomer **2.5** then undergoes a Suzuki-Miyaura oligomerization process to furnish **2.6**, which adopts an all-syn conformation with respect to the heteroatoms due to the reinforcing NH...mesityl interaction between adjacent monomers.

We were drawn to C-H borylation as a potential means of functionalizing the C4 and/or C5 positions for the following reasons: 1) the reaction had already been

¹¹ Baggett, A. W.; Guo, F.; Li, B.; Liu, S.-Y.; Jäkle, F. *Angew. Chem. Int. Ed.* **2015**, *54*, 11191-11195.

established for 1,2-azaborines (*vide supra*); 2) by selecting a 1,2-disubstituted-1,2-azaborine, the C3 and C6 positions would be inaccessible to C-H borylation as selectivity is primarily determined by sterics;¹² 3) Bpin can be converted into a myriad of functional groups.¹³ The C-H borylation of monosubstituted N-H, B-R² azaborines proceeds at room temperature and is completely selective for the most acidic C6-H bond (Scheme 2.3a).^{10,14} In contrast, C-H borylation of disubstituted N-R¹, B-R² azaborines required elevated temperatures and leads to a mixture of C4 and C5 borylated isomers (Scheme 2.3b).¹⁵ While calculations indicate that the pK_a values of the C4-H and C5-H are nearly the same, a slight preference for the C5 position was observed.¹⁰ No correlation between selectivity and substitution pattern emerged from the substrate table of disubstituted 1,2-azaborines and the origin of the small amount of selectivity remains unclear. Unfortunately, the mixtures of C4 and C5 borylated isomers could not be separated with physical purification methods such as chromatography or recrystallization. At this point, we decided to turn to reaction-based methods in an effort to separate the C4 and C5-Bpin isomers.

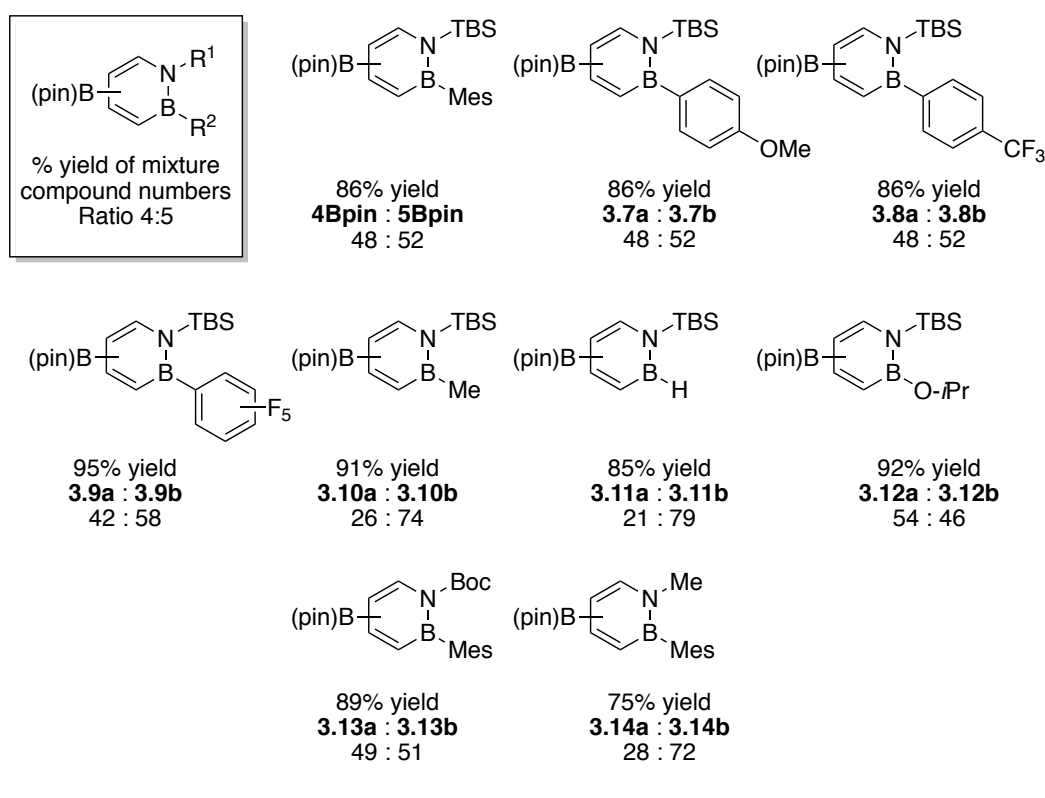
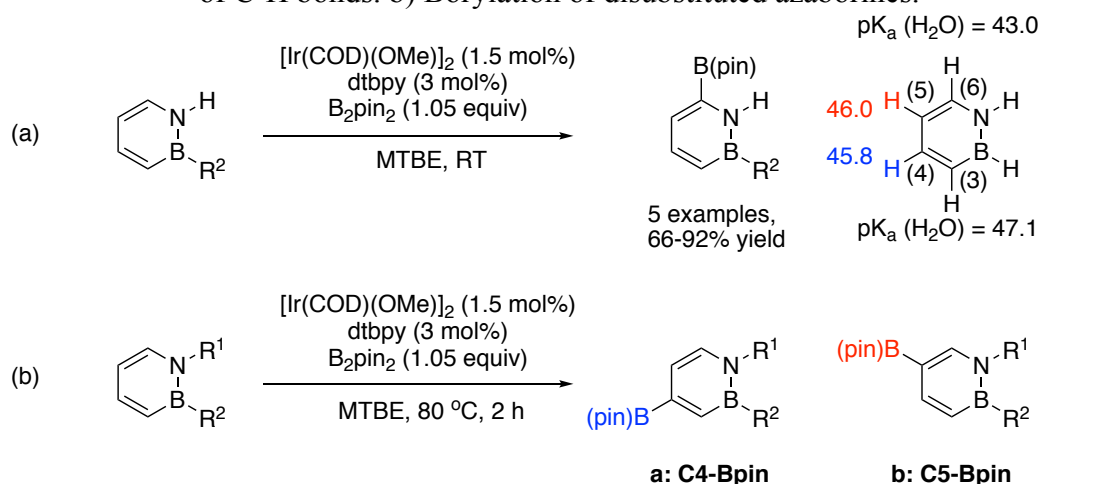
¹² For mechanistic work of Ir-catalyzed borylation, see: (a) Tamura, H.; Yamazaki, H.; Sato, H.; Sakaki, S. *J. Am. Chem. Soc.* **2003**, *125*, 16114–16126. (b) Boller, T. M.; Murphy, J. M.; Hapke, M.; Ishiyama, T.; Miyaura, N.; Hartwig, J. F. *J. Am. Chem. Soc.* **2005**, *127*, 14263–14278. (c) Larsen, M. A.; Hartwig, J. F. *J. Am. Chem. Soc.* **2014**, *136*, 4287–4299.

¹³ Sandford, C.; Aggarwal, V. K. *Chem. Comm.* **2017**, *53*, 5481–5494.

¹⁴ Vanchura, B. A.; Preshlock, S. M.; Roosen, P. C.; Kallepalli, V. A.; Staples, R. J.; Maleczka, R. E.; Singleton, D. A.; Smith, M. R., III. *Chem. Comm.* **2010**, *46*, 7724–7726.

¹⁵ Baggett, A. W. *New Strategies Enabling Diverse Functionalization of Aromatic 1,2-Azaborine Motifs*. Ph.D. Dissertation, Boston College, Chestnut Hill, MA, 2016.

Scheme 2.3. a) Borylation of monosubstituted azaborines and calculated pK_a values of C-H bonds. b) Borylation of disubstituted azaborines.



2.1.3 Regio- and Chemo-selective Reactions of Boronic Esters

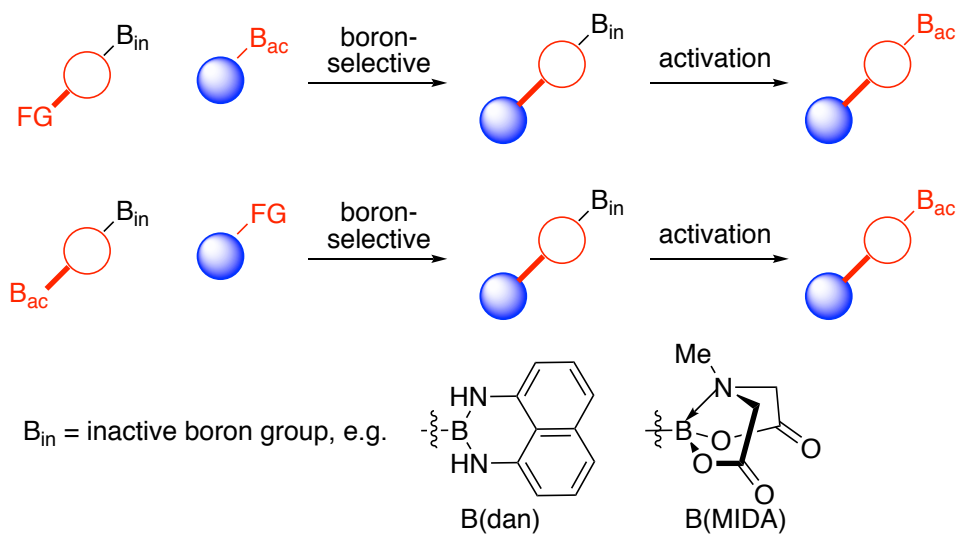
There are multiple strategies available for distinguishing between different boronyl groups in the same reaction. One well-established method to carry out a boron-selective reaction¹⁶ is to employ a boron masking group such as B(MIDA)¹⁷ or

¹⁶ For an overview, see: Xu, L.; Zhang, S.; Li, P. *Chem. Soc. Rev.* **2015**, *44*, 8848-8858.

¹⁷ Gillis, E. P.; Burke, M. D. *J. Am. Chem. Soc.* **2007**, *129*, 6716-6717.

B(dan)¹⁸ (Scheme 2.4). A boron selective reaction occurs when two or more boronyl groups are present in the reactants and their reactivity can be distinguished. For example, boronic acids and boronic acid pinacol esters readily undergo Suzuki-Miyaura cross-coupling reactions. The reactivity of these boronyl groups is predicated on the ability of an exogenous base (or palladium-hydroxyl) species to form a tetra-coordinate borate which then undergoes transmetalation with palladium.¹⁹ Masking groups such as dan or MIDA esters reduce the propensity of the boronyl group to undergo transmetalation through intramolecular dative interactions with the empty p-orbital. In this way, an iterative cross-coupling strategy can be deployed where the more reactive boronyl group can undergo a reaction in the presence of the less reactive boronyl group, which is subsequently unmasked and further functionalized.

Scheme 2.4. Boron-selective reactions using the boron masking group strategy.



B_{ac} = active boron group, e.g. B(pin), B(OH)₂, BF₃K, 9-BBN, etc.

Other strategies that distinguish between multiple boronyl groups rely on electronic and steric factors such as the hybridization of the carbon substituent or neighboring group effects. Morcken et al. published an asymmetric diboration of

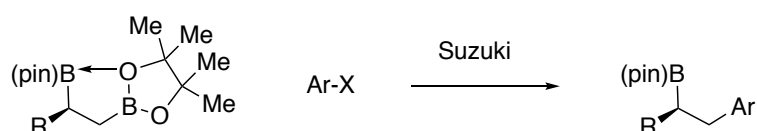
¹⁸ Noguchi, H.; Hojo, K.; Sugimoto, M. *J. Am. Chem. Soc.* **2007**, *129*, 758-759.

¹⁹ (a) Carrow, B. P.; Hartwig, J. F. *J. Am. Chem. Soc.* **2011**, *133*, 2116-2119. (b) Thomas, A. A.; Denmark, S. E. *Science* **2016**, *352*, 329-332.

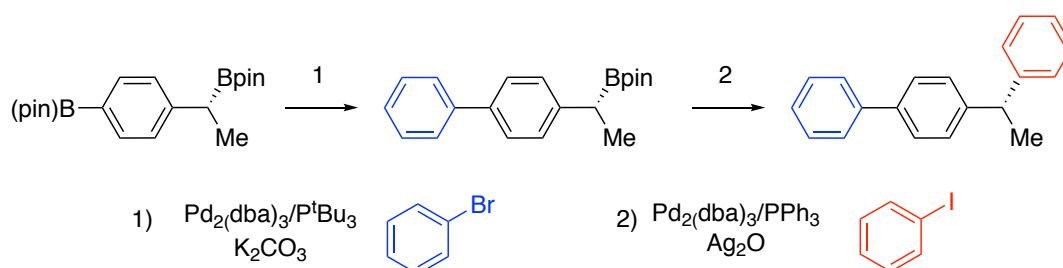
terminal alkenes.²⁰ Subsequent cross-coupling of the 1,2-bisboronate product is selective for the terminal Bpin; the selectivity can be explained by an interaction between the vicinal Bpin groups where an oxygen on the terminal pinacol donates to the internal boron atom (Scheme 2.5a). This neighboring group effect renders the terminal Bpin more Lewis acidic and thus more susceptible to attack by a palladium-hydroxyl species. Relatedly, Shibata et al. published a chemoselective and regioselective Suzuki coupling on a multisubstituted geminal diborylalkane.²¹ Another example of a chemoselective cross-coupling was published by the Crudden group. They were able to take advantage of the different rates of reactivity of B-C^{sp2} versus B-C^{sp3} in the transmetalation step of the Suzuki-Miyaura cross-coupling (Scheme 2.5b).²² In the first step of the sequence, the aryl Bpin undergoes cross-coupling in the presence of K₂CO₃; in the second step, the untouched benzylic Bpin is then cross-coupled in the presence of Ag₂O.

Scheme 2.5. a) Chemoselective cross-coupling of 1,2-bisboronates. b) Chemoselective cross-coupling of compounds containing a benzylic and aryl Bpin group.

(a) Morken, 2014



(b) Crudden, 2016



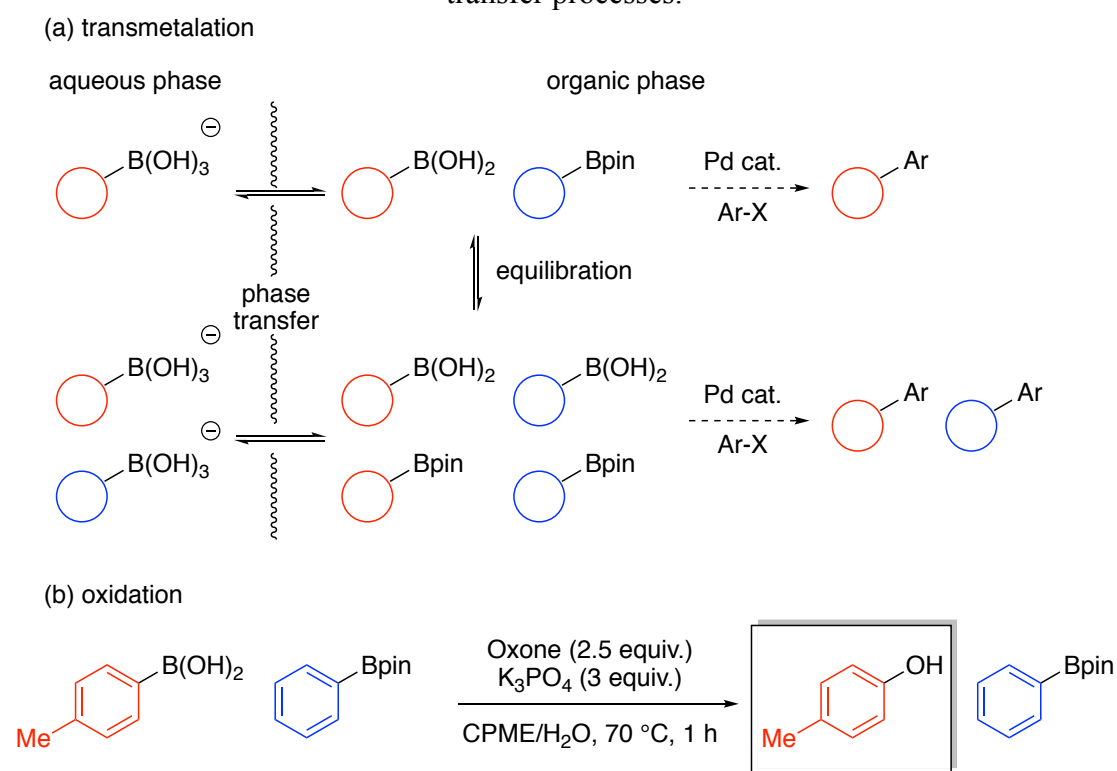
²⁰ Mlynarski, S. N.; Schuster, C. H.; Morken, J. P. *Nature* **2014**, *505*, 386-390.

²¹ Endo, K.; Ohkubo, T.; Hirokami, M.; Shibata, T. *J. Am. Chem. Soc.* **2010**, *132*, 11033-11035.

²² Crudden, C. M.; Ziebenhaus, C.; Rygus, J. P. G.; Ghozati, K.; Unsworth, P. J.; Nambo, M.; Voth, S.; Hutchinson, M.; Laberge, V. S.; Maekawa, Y.; Imao, D. *Nature Communications* **2016**, *7*, 11065.

Kinetic selection between two boronyl groups with the same, i.e. aryl, carbon moiety has also been achieved. The Watson group has published two examples of kinetic control that distinguish between boronic acids and boronic acid pinacol esters: 1) in the transmetalation step of a Suzuki coupling²³ and 2) in the oxidation of organoboron compounds.²⁴ In the first example, the key to a chemoselective transmetalation is to restrict the equivalents of water in the reaction. Limiting the amount of water slows down two key processes that regulate transmetalation: diol equilibration and phase transfer (Scheme 2.6a). Overall, the boronic acid undergoes transmetalation faster than Bpin.

Scheme 2.6. a) Chemoselective transmetalation and b) oxidation by kinetic phase transfer processes.



In addition, a discrete biphasic system tends to sequester the active borate species, slowing the reaction and increasing the relative rate of diol equilibration. As the boronic acid is consumed, the equilibrium is driven toward the initial

²³ Fyfe, J. W. B.; Fazakerley, N. J.; Watson, A. J. B. *Angew. Chem. Int. Ed.* **2017**, *56*, 1249-1253.

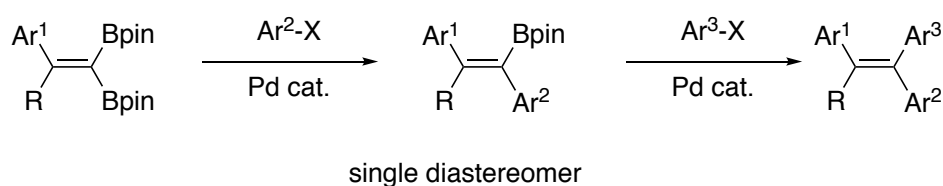
²⁴ Molloy, J. J.; Clohessy, T. A.; Irving, C.; Anderson, N. A.; Lloyd-Jones, G. C.; Watson, A. J. B. *Chem. Sci.* **2017**, *8*, 1551-1559.

B(OH)₂/Bpin mixture thus selectivity is aided by Le Chatelier's principle. The chemoselective oxidation operates by a similar principle, but instead the reaction takes place in the aqueous phase (Scheme 2.6b). In a discrete biphasic system, the boronic acid more rapidly forms the active borate species and transfers to the aqueous phase where it will be oxidized.

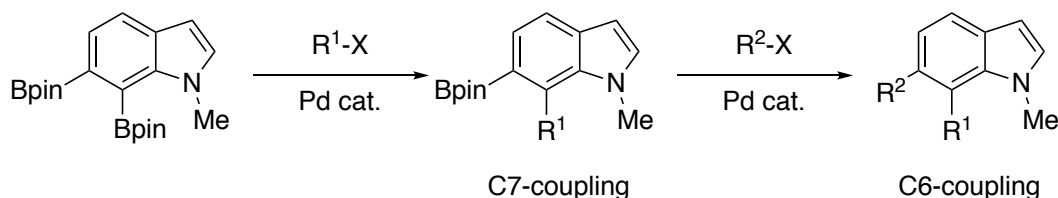
Reactions that can discriminate between two boronyl regioisomers with the same diol substituent are somewhat rare. In 2005, Hiyama showed that certain 1,1-diboryl alkenes undergo stereoselective cross-coupling (Scheme 2.7a).²⁵ While the origin of the stereoselectivity is not entirely clear, the first Suzuki coupling installs an aryl group to form the corresponding *E*-alkene; the remaining Bpin group can then be coupled with a different electrophile. Oestreich discovered that 6,7-bisborylated indole undergoes a regioselective cross-coupling at the C7-Bpin (Scheme 2.7b).²⁶ Again, the origins of the regioselectivity are unclear but the bisborylated indole can be cross-coupled with different electrophiles sequentially.

Scheme 2.7. a) Stereoselective cross-coupling of 1,1-diboryl alkenes. b) Regioselective cross-coupling of diboryl indole.

a) Hiyama, 2005



b) Oestreich, 2015

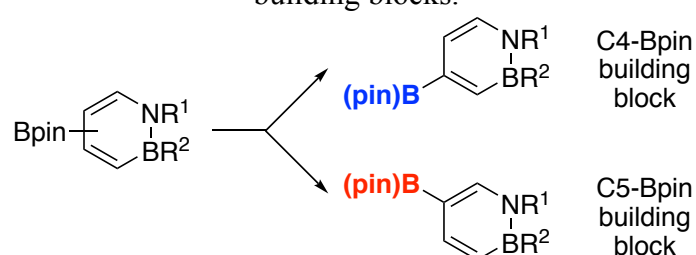


²⁵ Shimizu, M.; Nakamaki, C.; Shimon, K.; Schelper, M.; Kurahashi, T.; Hiyama, T. *J. Am. Chem. Soc.* **2005**, *127*, 12506-12507.

²⁶ Pareek, M.; Fallon, T.; Oestreich, M. *Org. Lett.* **2015**, *17*, 2082-2085.

To the best of our knowledge, there are no examples in the literature of reaction selectivity between two *mono*-borylated arenes with the same boronyl group. Nonetheless, due to the precedent of electronic factors playing a role in reaction selectivity, we hypothesized the distinct electronic structure of 1,2-azaborine would allow for the separation of the mixture of C4- and C5-borylated azaborines (Scheme 2.8).²⁷

Scheme 2.8. Separation of borylated 1,2-azaborine regioisomers into C4 and C5-Bpin building blocks.



2.2 Electronic Structure Analysis of C4- and C5- Borylated Azaborines

As mentioned previously, while C-H borylation is selective for functionalizing the C6 position of a *B*-monosubstituted-1,2-azaborine, we determined that borylation of *N,B*-disubstituted-1,2-azaborines such as **2.15** (cf. Scheme 2.3) occurs only at an elevated temperature and in a non-regioselective fashion, affording a 1:1.2-1.4 mixture of C4- and C5-borylated regioisomers (eq. 1). Because each position of the 1,2-azaborine ring is electronically distinct, we envisioned that the asymmetry of the electronic structure of 1,2-azaborine would impart differential reactivity to the two borylated regioisomers **4Bpin** and **5Bpin**. Our hypothesis is as follows: because of partial localization of nitrogen's lone pair, the C5 carbon of **5Bpin** should be more electron rich than the C4 carbon of the **4Bpin**, and the boron in the Bpin of the **5Bpin** isomer should be less Lewis acidic than the Bpin boron in **4Bpin** (Figure 2.2). The extra resonance contribution provided by the Bpin in **5Bpin** should also result in

²⁷ Chrostowska, A.; Xu, S.; Lamm, A. N.; Mazière, A.; Weber, C. D.; Dargelos, A.; Baylère, P.; Graciaa, A.; Liu, S.-Y. *J. Am. Chem. Soc.* **2012**, *134*, 10279-10285.

added stability of **5Bpin** relative to the **4Bpin** isomer.

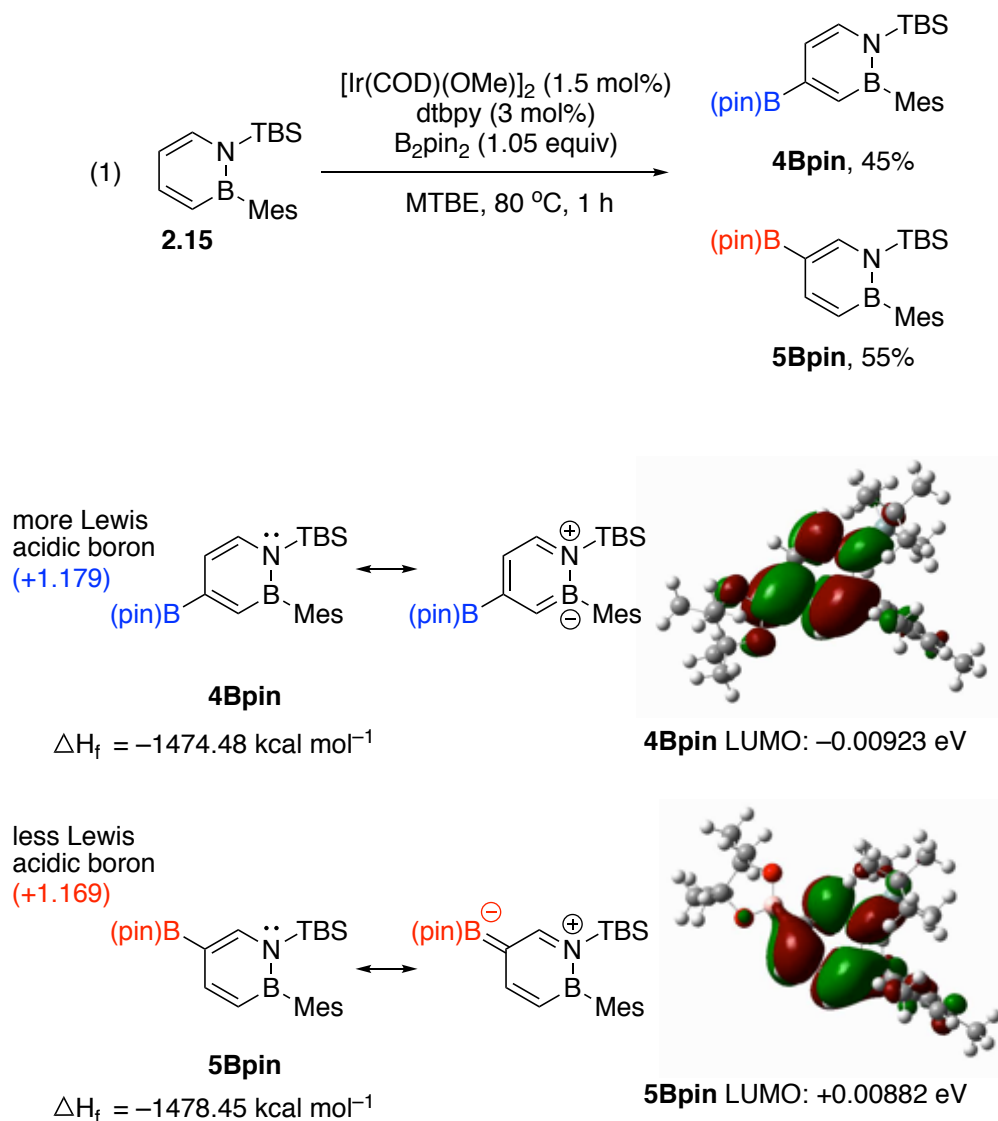


Figure 2.2. Electronic structure calculations (M062X/6-31G(d,p), computed using polarizable continuum model (PCM) simulating CH_2Cl_2 solvent): select Löwdin charges in parenthesis (a.u.), heats of formation, LUMO energies and orbital illustrations.

DFT Electronic structure calculations²⁸ were consistent with this hypothesis showing significant differences between **4Bpin** and **5Bpin**. 1) **5Bpin** is thermodynamically more stable than **4Bpin** by about 4 kcal/mol according to the calculated heats of formation (ΔH_f , see Experimental Section for details) (Figure 2.2).

²⁸ Frisch, M. J.; et al. Gaussian 09, revision B.01; Gaussian, Inc.: Wallingford, CT, 2009.

2) The p_z -atomic orbital on the boron atom in the Bpin of **4Bpin** significantly contributes to the LUMO of the molecule, in stark contrast to the corresponding orbital on the Bpin boron atom of **5Bpin**. 3) The calculated LUMO energy of **4Bpin** (-0.00923 eV) is significantly lower than the LUMO energy of **5Bpin**.²⁹ 4) The calculated Mulliken partial charge is more positive on the boron atom of the **4Bpin** than the one on the boron atom of **5Bpin**. These calculated trends are consistent with our originally stated hypothesis based on simple Lewis dot structure analysis, i.e., **5Bpin** should be thermodynamically more stable than **4Bpin**, and the Bpin boron atom in **4Bpin** should be significantly more reactive towards Lewis bases.

2.3 Oxidation with *N*-methyilmorpholine-*N*-oxide (NMO)

In our initial attempt to kinetically resolve the mixture of **4Bpin** and **5Bpin** with a Lewis basic reagent, we discovered that NMO indeed selectively oxidizes the **4Bpin** isomer over the **5Bpin** isomer.³⁰ Thus, under our optimized conditions (4 equivalents of NMO at room temperature for 24 hours in CH_2Cl_2), compound **4OH** can be isolated in 30% yield while 53% of the unreacted **5Bpin** (based on 55% available starting material) was recovered (Scheme 2.9). We independently measured the rate of oxidation of the **4Bpin** isomer and the rate of decomposition of the **5Bpin** isomer³¹ by ^1H NMR against an internal standard (*vide infra* for the isolation of the **4Bpin** compound) and determined that the rate of oxidation is approximately 29 times faster than the rate of decomposition, resulting in an effective kinetic resolution of the two borylated compounds. As a reference, we determined the rate of NMO oxidation

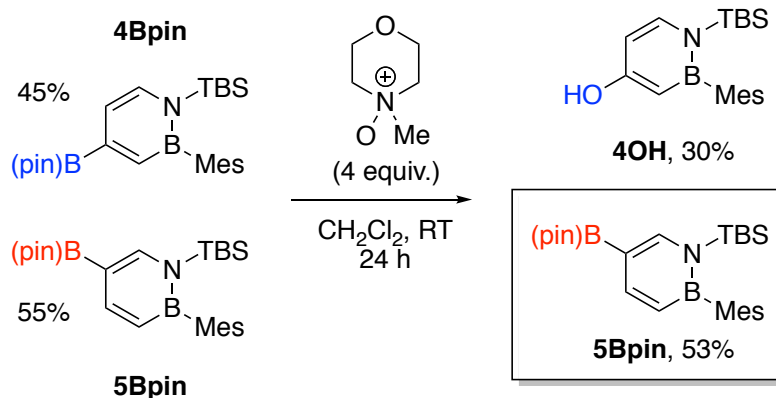
²⁹ LUMO energies > 0 eV (for **5Bpin**) have no physical meaning but are reported here to allow for direct comparison.

³⁰ For examples of oxidation of organoboron compounds with N-oxides, see: (a) Kabalka, G. W.; Hedgecock, H. C. *J. Org. Chem.* **1975**, *40*, 1776-1779. (b) Soderquist, J. A.; Najafi, M. R. *J. Org. Chem.* **1986**, *51*, 1330-1336. (c) Zhu, C.; Wang, R.; Falck, J. R. *Org. Lett.* **2012**, *14*, 3494-3497. (d) Kim, J.; Bertozzi, C. R. *Angew. Chem., Int. Ed.* **2015**, *54*, 15777-15781. (e) Gupta, S.; Sureshbabu, P.; Singh, A. K.; Sabiah, S.; Kan-dasamy, J. *Tetrahedron Lett.* **2017**, *58*, 909-913.

³¹ Attempts to convert the **5Bpin** to the 5-hydroxy compound were unsuccessful, as elevating the reaction temperature led to decomposition of **5Bpin** to unknown products.

of phenyl boronic acid pinacol ester (**PhBpin**) to be 20 fold slower than the corresponding rate for **4Bpin** (Scheme 2.9).

Scheme 2.9. Resolution of **5Bpin** and **4Bpin** via selective oxidation of **4Bpin**.



$$\text{rate (4Bpin)} = d [\text{4Bpin}]/dt = -2.89 \pm 0.16 \times 10^{-6} \text{ M s}^{-1}$$

$$\text{rate (5Bpin)} = d [\text{5Bpin}]/dt = -1.0 \pm 0.2 \times 10^{-7} \text{ M s}^{-1}$$

$$\text{selectivity (s)} = \text{rate (4Bpin)} / \text{rate (5Bpin)} = 29$$

$$\text{rate (PhBpin)} = d [\text{PhBpin}]/dt = -1.2 \pm 0.6 \times 10^{-7} \text{ M s}^{-1}$$

The experimentally observed relative rates are consistent with the calculated free energy reaction coordinate profile (M062X/6-31G(d,p); see Experimental Section for details). As can be seen from Figure 2.3, **5Bpin** is calculated to be more stable than **4Bpin** by 3.8 kcal/mol, following the same trend as was established by the calculated heats of formation. The oxidation with NMO involves the NMO-Bpin adduct as the intermediate, which then subsequently rearranges to the borate ester with concomitant release of the *N*-methyl morpholine.^{30d,e} Our DFT calculations predict the second step (C to O migration) to be the rate-determining step for both **4Bpin** and **5Bpin**. The rate-limiting activation barrier for **4Bpin** (23.8 kcal/mol) is smaller than the corresponding barrier for the **5Bpin** compound (27.7 kcal/mol), which is consistent with the selective oxidation of the **4Bpin** isomer. Overall, it appears that the extra stability of the ground state (due to additional resonance with

the lone pair of nitrogen) relative to its rate-limiting transition state exhibited by **5Bpin** as compared to **4Bpin** is responsible for the kinetic resolution.

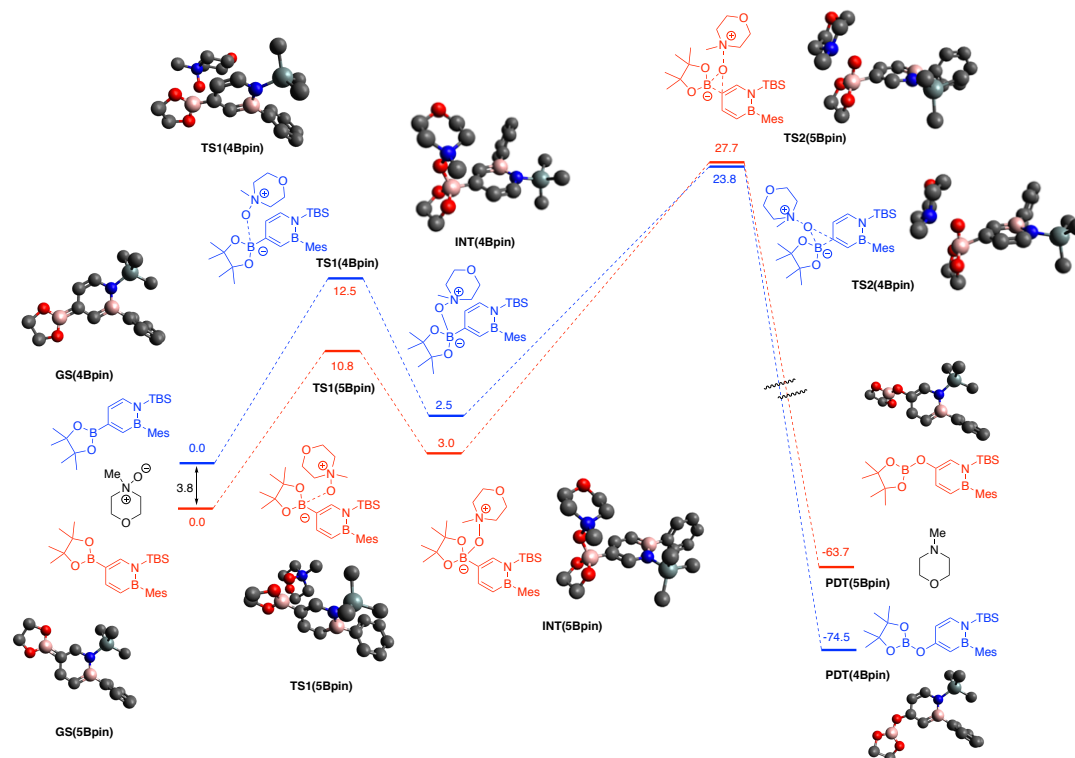


Figure 2.3. Calculated Gibbs free energy profile of the NMO oxidation of **4Bpin** and **5Bpin**, computed at 298 K and 1 atm using M062X/6-31G(d,p) method. The polarizable continuum model (PCM) was used to model the effects of the reaction by the CH_2Cl_2 solvent. Energies are in kcal mol^{-1} . All H atoms as well as the methyl on the pinacol, mesityl, and *t*-butyl substituents have been omitted for clarity.

2.4 Iridium-Catalyzed Protodeborylation

With a method for accessing the **5Bpin** isomer in hand, we pursued resolution chemistry that could be used to access **4Bpin**. Thus, we needed a reaction that would preferentially react with the less Lewis acidic and more stable **5Bpin** isomer. According to our electronic structure calculations (Figure 2.4), the C5 carbon in **5Bpin** is more electron-rich than the C4 carbon in **4Bpin**. Although the HOMO orbital energies for **4Bpin** and **5Bpin** are similar, the HOMO orbital coefficient of the C5 carbon in **5Bpin** (0.11) is significantly larger than the one for the C4 carbon in

4Bpin (0.01). Overall, the results indicate stronger nucleophilic character for the C5 carbon in **5Bpin** than the C4 carbon in **4Bpin**. Thus, we hypothesize that a transmetalation-type reaction^{32,33} would favor **5Bpin** over **4Bpin**, and we chose the Ir-catalyzed protodeborylation for our investigation.^{34,35}

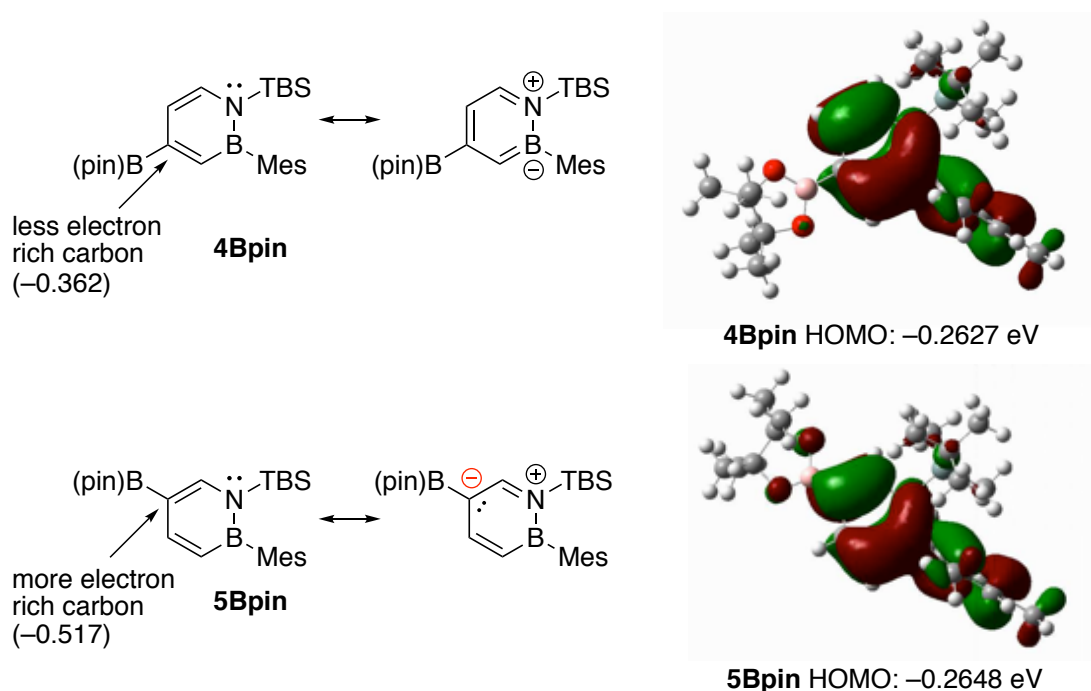


Figure 2.4. Electronic structure calculations (M062X/6-31G(d,p), computed using polarizable continuum model (PCM) simulating CH₂Cl₂ solvent): select Löwdin charges in paranthesis (a.u.), HOMO energies and orbital illustrations.

When a 1:1.4 mixture of **4Bpin** and **5Bpin** was subjected to protodeborylation catalyzed by [Ir(COD)OMe]₂ with methanol as the proton source, **4Bpin** was isolated in 25% yield based on 42% available starting material (Scheme 2.10).

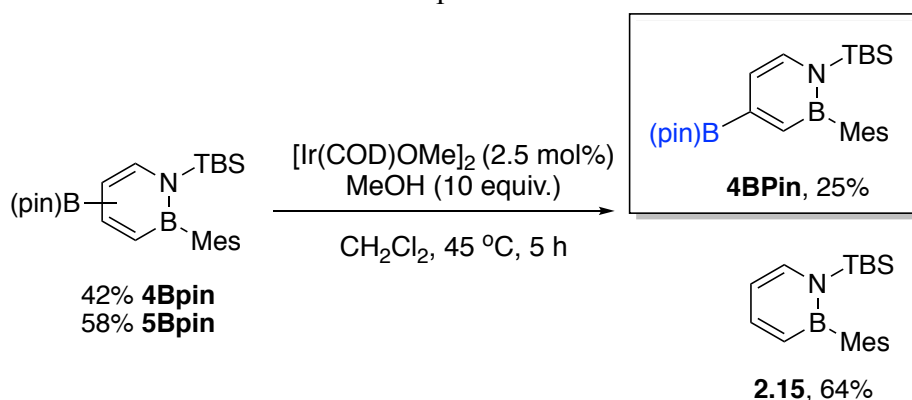
³² Electron rich organoboron compounds are known to preferentially undergo a transmetalation reaction, see: Beaumard, F.; Dauban, P.; Dodd, R. H. *Org. Lett.* **2009**, *11*, 1801-1804.

³³ For a comprehensive review on the transmetalation of unsaturated carbon nucleophiles from boron-containing species to mid to late transitions metals, see: Partyka, D. V. *Chem. Rev.* **2011**, *111*, 1529-1595.

³⁴ Movassaghi and Smith have demonstrated that certain bis-borylated heterocycles can be selectively mono-protodeborylated under mild conditions, see: (a) Loach, R. P.; Fenton, O. S.; Amaike, K.; Siegel, D. S.; Ozkal, E.; Movassaghi, M. *J. Org. Chem.* **2014**, *79*, 11254-11263. (b) Kallepalli, V. A.; Gore, K. A.; Shi, F.; Sanchez, L.; Chotana, G. A.; Miller, S. L.; Maleczka, R. E.; Smith, M. R. *J. Org. Chem.* **2015**, *80*, 8341-8353.

³⁵ (a) Nishimura, T.; Yasuhara, Y.; Hayashi, T. *Angew. Chem., Int. Ed.* **2006**, *45*, 5164-5166. (b) Nishimura, T.; Yasuhara, Y.; Hayashi, T. *J. Am. Chem. Soc.* **2007**, *129*, 7506-7507.

Scheme 2.10. Kinetic resolution via Ir-catalyzed protodeborylation. Independent rate measurements performed at 40 °C.



$$\text{rate}(\mathbf{4Bpin}) = d[\mathbf{4Bpin}]/dt = -2.7 \pm 0.3 \times 10^{-7} \text{ M s}^{-1}$$

$$\text{rate}(\mathbf{5Bpin}) = d[\mathbf{5Bpin}]/dt = -6 \pm 1 \times 10^{-6} \text{ M s}^{-1}$$

$$\text{selectivity (s)} = \text{rate}(\mathbf{5Bpin}) / \text{rate}(\mathbf{4Bpin}) = 23$$

$$\text{rate}(\mathbf{PhBpin}) = d[\mathbf{PhBpin}]/dt = -2.7 \pm 0.7 \times 10^{-7} \text{ M s}^{-1}$$

Smith observed that in the case of bisborylated compounds, the first Bpin to be installed on the molecule was also the first to be protodeborylated.^{34b} Interestingly, **5Bpin** is selectively deborylated despite the fact that both C4 and C5 positions of azaborine undergo C-H borylation with nearly equal propensity. We measured the independent rates of the protodeborylation reaction for **4Bpin** and **5Bpin** at 40 °C and found that the rate of protodeborylation of **5Bpin** is about 23 times faster than that of **4Bpin**, consistent with the kinetic resolution that occurs on the preparative scale. We also determined the rate of protodeborylation of the benchmark compound **PhBpin** to be similar to that of **4Bpin** (Scheme 2.10).

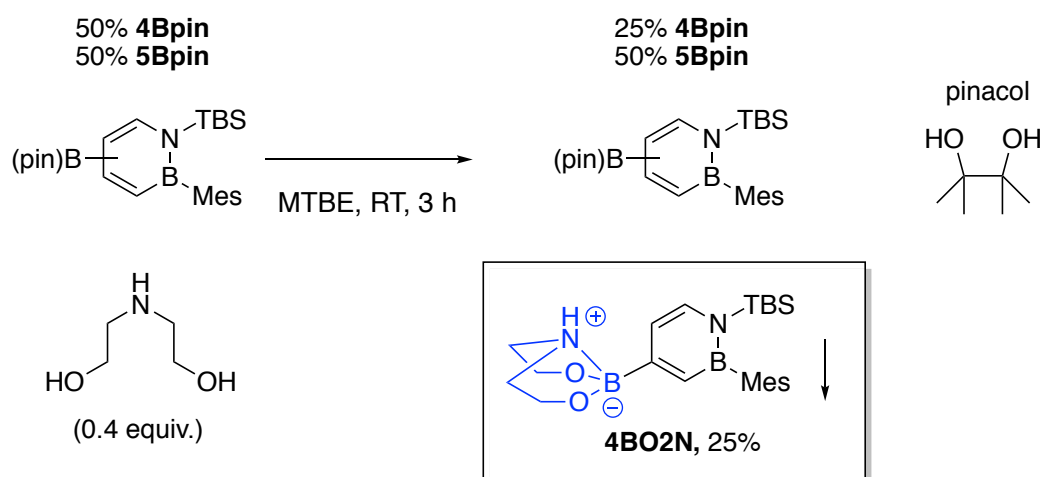
2.5 Transesterification with Diethanolamine

We also investigated the transesterification³⁶ of the boron pinacolate ester with diethanolamine with the aim to convert the mixture of the Bpin isomers into a separable mixture of differentially borylated compounds. Diethanolamine when bound to an organoboron compound typically forms a zwitterionic 4-coordinate

³⁶ Roy, C. D.; Brown, H. C. *Monatshefte für Chemie - Chemical Monthly* **2007**, *138*, 879-887.

borate. When the transesterification from pinacol to diethanolamine is performed in a non-polar ethereal solvent, the charged diethanolamine adduct tends to precipitate out of the solution.³⁷ We hypothesize that the more Lewis acidic **4Bpin** should be the favored reactant in a transesterification with diethanolamine. Thus, when we treated a 1:1 mixture of **4Bpin** and **5Bpin** with diethanolamine in methyl-*tert*-butylether (MTBE), we observed a white precipitate that was separated from the reaction mixture. The precipitate contained only the **4BO2N** isomer (50% yield, 25% based on available starting material), and the filtrate was enriched in the **5Bpin** isomer (Scheme 2.11). Addition of more equivalents of diethanolamine and changing the temperature did not drive the reaction forward to the diethanolamine product but instead resulted in an erosion of the selectivity.

Scheme 2.11. Reaction of borylated isomers with diethanolamine.

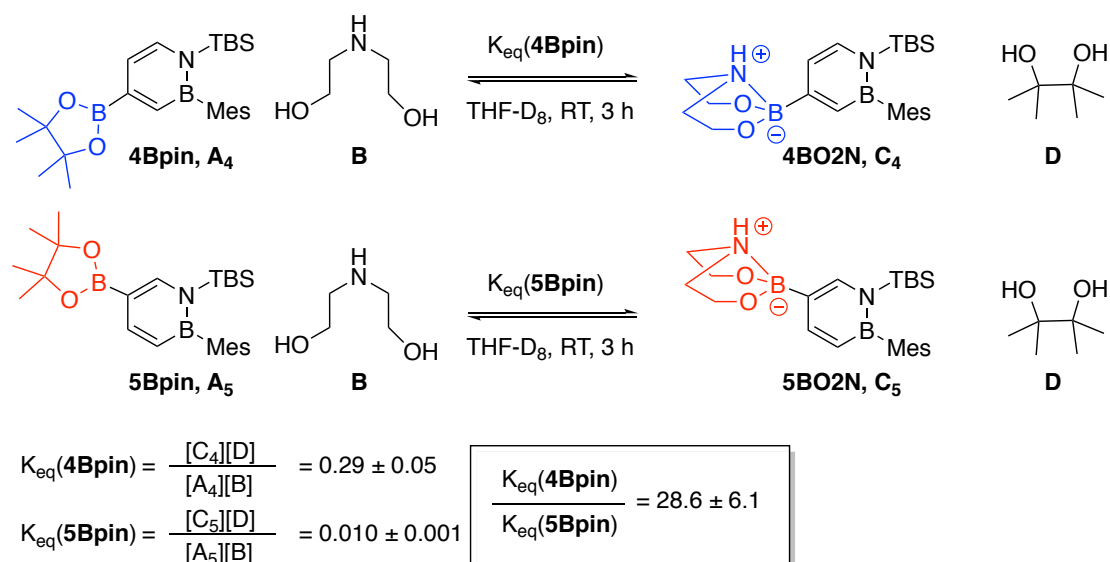


We conducted studies to determine whether the transesterification reaction is kinetically or thermodynamically controlled. Here, we used THF as the solvent to ensure that the reaction mixture formed a homogenous solution. Monitoring the transesterification reaction for each isomer independently by ¹H NMR at room temperature revealed that the transesterification had reached equilibrium within 3

³⁷ Bonin, H.; Leuma-Yona, R.; Marchiori, B.; Demonchaux, P.; Gras, E. *Tetrahedron Lett.* **2011**, 52, 1132-1136.

hours. All four components were observed in the reaction mixture: boron pinacol ester (A), free diethanolamine (B), diethanolamine adduct (C), and free pinacol (D). Initial rates of the transesterification reaction of each isomer were measured using reaction calorimetry and were found to be nearly identical (see Experimental Section for details). Determination of the concentration of each component in the reaction mixture by ^1H NMR yielded the equilibrium constant, K_{eq} for each isomer. We found that the $K_{\text{eq}}(\mathbf{4Bpin})$ is larger than the $K_{\text{eq}}(\mathbf{5Bpin})$ by a factor of 29 (Scheme 2.12). The observed relative binding propensity $K_{\text{eq}}(\mathbf{4Bpin}) : K_{\text{eq}}(\mathbf{5Bpin})$ is corroborated by DFT calculations. The Gibbs free energy of formation of $\mathbf{5BO2N}$ adduct is $\Delta G = -5.1$ kcal mol^{-1} , while the formation of $\mathbf{4BO2N}$ is more favorable with $\Delta G = -6.1$ kcal mol^{-1} . Thus, the separation of the mixture of borylated 1,2-azaborine, as illustrated in Scheme 2.11, is an example of a thermodynamically controlled resolution process.

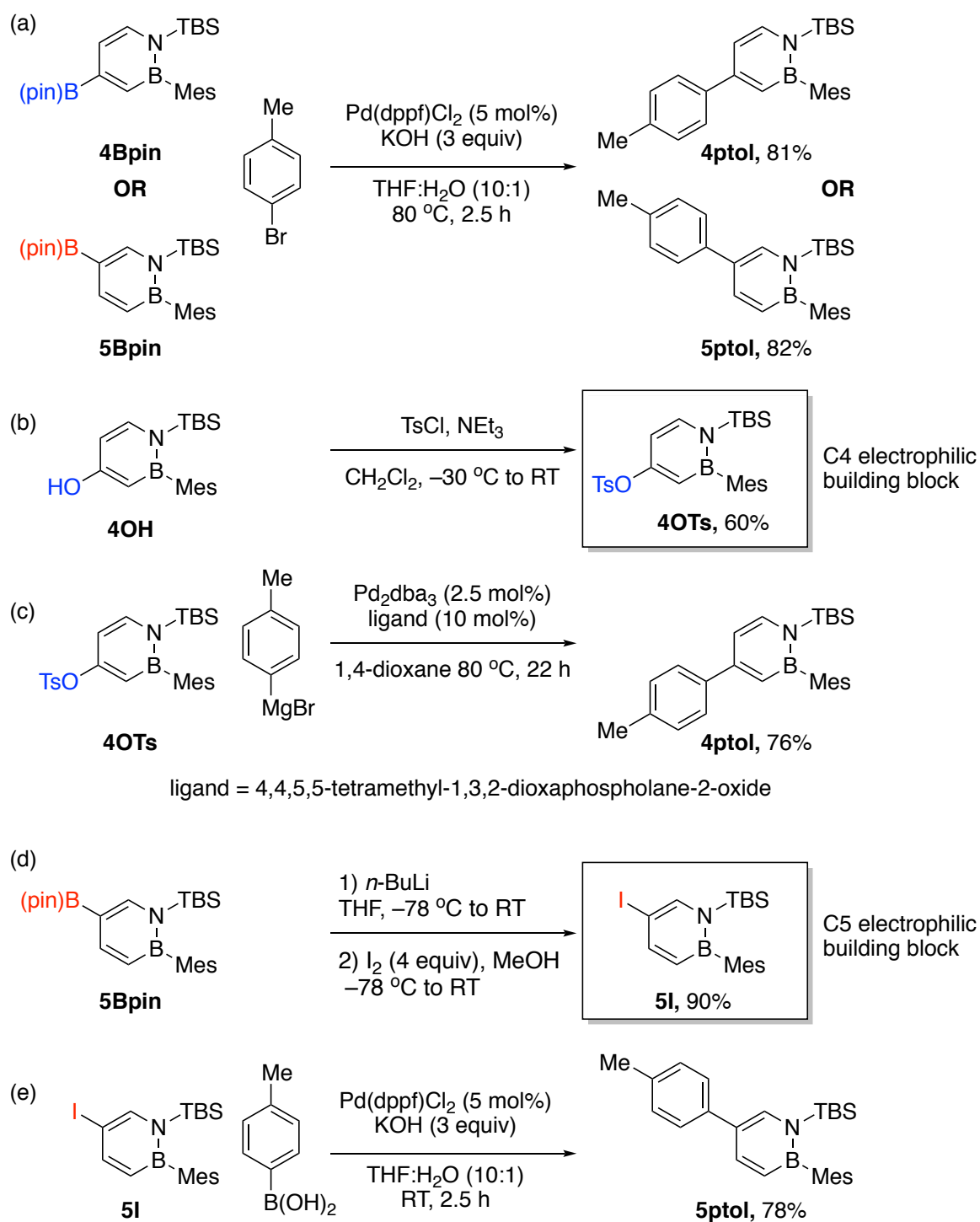
Scheme 2.12. Kinetic and thermodynamic studies of transesterification reaction.



2.6 Functionalization of the 4- and 5- Positions of the 1,2-Azaborine

The isolated $\mathbf{4Bpin}$ or $\mathbf{5Bpin}$ building blocks can undergo Suzuki-Miyaura cross-coupling with an aryl halide to afford triaryl $\mathbf{4ptol}$ or $\mathbf{5ptol}$ in good yields (Scheme 2.13a). It is also possible to generate new *electrophilic* building blocks at the

Scheme 2.13. Functionalizations of **4Bpin** and **5Bpin**.



4 and 5 positions of the 1,2-azaborine utilizing the versatile transformations of organoboron compounds. For example, compound **4OH**, generated via the NMO oxidation of **4Bpin**, can be converted into the tosylate **4OTs** (Scheme 2.13b).³⁸

³⁸ Lin, G.; Zhang, A. *Tetrahedron*, **2000**, *56*, 7163-7171.

Subsequent Kumada coupling of **4OTs** with an aryl Grignard reagent furnishes **4ptol** (Scheme 2.13c).³⁹ An iodine can be installed at the C5 position using a procedure adapted from the Evans modification of the Zweifel reaction (Scheme 2.13d).⁴⁰ **5I** undergoes facile Suzuki-Miyaura coupling at room temperature with *p*-tolylboronic acid to afford **5ptol** (Scheme 2.13e).

2.7 Conclusions

We have developed the synthesis of two new 1,2-azaborine building blocks that enables the ready diversification of 1,2-azaborine's C4 and C5 ring positions. We took advantage of 1,2-azaborine's distinct electronic structure to resolve a mixture of borylated 1,2-azaborines. By means of kinetic and thermodynamic studies and DFT calculations we have been able to rationalize the difference in reactivities of **4Bpin** and **5Bpin** at their C4 and C5 positions. NMO selectively oxidizes the more Lewis acidic **4Bpin** 1,2-azaborine isomer whereas Ir-catalyzed protodeborylation selectively deborylates the more nucleophilic **5Bpin** 1,2-azaborine isomer. Transesterification of the pinacol group with diethanolamine also favors the more Lewis acidic **4Bpin** in a thermodynamically controlled process. The aforementioned resolution methods provide access to the previously inaccessible C4-Bpin and C5-Bpin building blocks which could be further functionalized using cross-coupling chemistry. The availability of a general approach to the functionalization of the C4- and C5- positions of the 1,2-azaborine will undoubtedly advance BN/CC isosterism as a versatile strategy for expanding the currently available chemical space and enable emerging applications in the biomedical and materials science fields.

³⁹ Ackermann, L.; Kapdi, A. R.; Fenner, S.; Kornhaass, C.; Schulzke, C. *Chem. -Eur. J.* **2011**, *17*, 2965-2971.

⁴⁰ Evans, D. A.; Crawford, T. C.; Thomas, R. C.; Walker, J. A. *J. Org. Chem.* **1976**, *41*, 3947-3953.

2.8 Experimental Section

2.8.1 General

All oxygen- and moisture-sensitive manipulations were carried out under an inert atmosphere using either standard Schlenk techniques or a glove box.

THF, Et₂O, CH₂Cl₂ and pentane were purified by passing through a neutral alumina column under argon. Methanol, CD₂Cl₂, and C₆D₆ were purified by distillation after drying over calcium hydride. THF-D₈ was purified by distillation after drying over sodium/benzophenone.

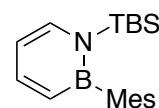
All other chemicals and solvents were purchased (TCI, Aldrich, Acros, AK Scientific, or Strem) and used as received.

¹H NMR spectra were recorded on a Varian Inova 600 spectrometer or Varian VNMRS 500 spectrometer. ¹³C NMR spectra were recorded on a Varian Inova 600 spectrometer or Varian VNMRS 500 spectrometer. ¹H and ¹³C were referenced internally to solvent signals (CD₂Cl₂: 5.32 ppm for ¹H NMR, 53.84 ppm for ¹³C NMR; C₆D₆: 7.16 ppm for ¹H NMR, 128.06 ppm for ¹³C NMR; THF-D₈: 3.58 ppm for ¹H NMR, 67.21 ppm for ¹³C NMR). ¹¹B NMR spectra were recorded on a Varian Inova 600 spectrometer or Varian Inova 500 spectrometer at ambient temperature. ¹¹B NMR shifts were externally referenced to BF₃•Et₂O (δ 0). High-resolution mass spectrometry data were obtained at the Boston College mass spectrometry facility on a JEOL AccuTOF instrument (JEOL USA, Peabody, MA), equipped with a DART ion source (IonSense, Inc., Danvers, MA) in positive ion mode. IR spectra were recorded on a Bruker Alpha FT-IR instrument with OPUS software.

2.8.2 Syntheses

Borylation of Compound N-TBS-B-Mes-1,2-Azaborine 2.15

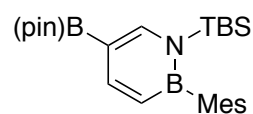
Compound 2.15 was synthesized as a white solid according to a published procedure. Spectra of the isolated compound matched published values.¹⁰



Mixture of Compounds 5Bpin and 4Bpin. Inside a glove box, a 150 mL pressure vessel was charged with [Ir(OMe)(cod)]₂ (72 mg, 0.11 mmol), 4,4'-di-*tert*-butyl-2,2'-bipyridine (dtbpy) (58 mg, 0.22 mmol), bis(pinacolato)diboron (B₂pin₂) (2.00 g, 7.95 mmol), and MTBE (35.0 mL). The catalyst mixture was aged for 2 minutes. Neat **2.15** (2.25 g, 7.23 mmol) was added to the catalyst mixture and the reaction vessel was sealed. The reaction mixture was transferred to a fume hood heated at 80 °C for 1 hour, at which point the reaction was determined to be complete by ¹H NMR. After cooling, volatiles were removed under reduced pressure and the crude residue was purified by silica gel chromatography with 99:1 pentane:ether as the eluent. A 1.2:1 C5:C4 mixture of borylated isomers was obtained as a white solid in 92% yield. The ratio was determined by ¹H NMR integration against a 1,3,5-trimethoxybenzene internal standard.

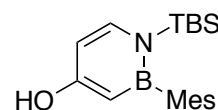
Preparatory Scale Separations of Borylated Isomers

Compound 5Bpin (via NMO oxidation). Inside a glovebox, a 250 mL round bottom flask was charged with a 1.2:1 mixture of **5Bpin** (5.31 g, 12.1 mmol) and **4Bpin** (4.35 g, 9.9 mmol), NMO (5.69 g, 48.6 mmol), and CH₂Cl₂ (80.0 mL).



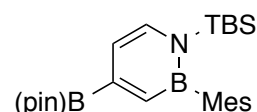
The reaction mixture was allowed to stir at room temperature for 24 hours. Reaction progress was monitored by ¹H NMR. The reaction mixture was removed from the glovebox and saturated NaHCO₃ solution was added and the crude product was extracted with excess dichloromethane. The organic layer was dried over Na₂SO₄, passed through a Buchner funnel lined with filter paper, and concentrated under reduced pressure. Pure **5Bpin** was recovered as a white solid after purification by silica gel chromatography with 95:5 pentane:ether as the eluent (5.14 g, 11.8 mmol, 97% based on 12.1 mmol starting material). ¹H NMR (500 MHz, CD₂Cl₂) δ 8.04 (s, 1H), 7.81 (dd, J = 10.8, 1.3 Hz, 1H), 6.78 (s, 2H), 6.54 (m, 1H), 2.28 (s, 3H), 2.06 (s, 6H), 1.32 (s, 12H), 0.92 (s, 9H), 0.03 (s, 6H). 30.71. ¹³C NMR (126 MHz, CD₂Cl₂) δ 148.11, 146.43, 138.47, 136.29, 126.73, 83.17, 27.05, 24.58, 23.02, 20.81, 18.97, -3.63. (the C3, C5, and mesityl carbons adjacent to boron were not observed). ¹¹B NMR (160 MHz, CD₂Cl₂) δ 40.45, 30.71. FTIR (thin film): ν cm⁻¹ = 2976, 2931, 2860, 1604. HRMS (DART) calcd. for C₂₅H₄₂B₂NO₂Si ([M+H]⁺) 438.31654, found 438.31624.

Compound 4OH (via NMO oxidation). From the same mixture of products, pure **4OH** was obtained as a yellow oil after purification by silica gel chromatography with 4:1 pentane:ether as the eluent (2.1 g, 6.4 mmol, 65% yield based on 9.9 mmol starting material).



¹H NMR (500 MHz, CD₂Cl₂): δ 7.47 (d, J = 7.5 Hz, 1H), 6.82 (s, 2H), 6.10 (m, 2H), 5.49 (d, J = 3.0 Hz, 1H), 2.32 (s, 3H), 2.15 (s, 6H), 0.97 (s, 9H), 0.04 (s, 6H). ¹³C NMR (126 MHz, CD₂Cl₂): δ 166.3, 142.7, 139.4, 136.8, 127.4, 105.5, 27.9, 23.8, 21.6, 19.8, -2.9 (C-3 and mesityl C-signal not observed). ¹¹B NMR (160 MHz, CD₂Cl₂): δ 40.9. FTIR (thin film): ν cm⁻¹ = 3390, 2959, 2929, 2857, 1613. HRMS (DART) calcd. for C₁₉H₃₁BNOSi [M+H]⁺ 328.22680, found 328.22734.

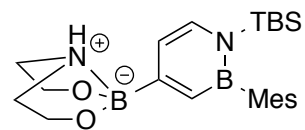
Compound 4Bpin (via protodeborylation). Inside a glovebox, a 150 mL pressure vessel was charged with a 1:1.4 mixture of **4Bpin** (2.06 g, 4.71 mmol) and **5Bpin** compounds (2.84 g, 6.49 mmol), methanol (1.51 g, 47 mmol), [Ir(COD)OMe]₂ (78 mg, 0.12 mmol), and CH₂Cl₂ (30.0 mL). The reaction vessel was sealed and transferred to a fume hood. The reaction mixture was heated at 45 °C for 5 hours.



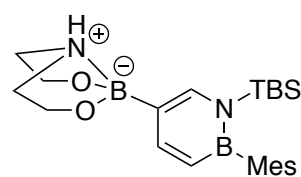
Reaction progress was monitored by ¹H NMR. Volatiles were removed under reduced pressure. The product was obtained as a white solid after purification by silica gel chromatography with hexanes as the eluent (1.22 g, 2.78 mmol 60% based on 4.71 mmol starting material). (2.25 g, 7.21 mmol, 111% of **Compound 2.15** was also recovered based on 6.49 mmol of **5Bpin** starting material). ¹H NMR (500 MHz, CD₂Cl₂) δ 7.45 (dd, J = 6.7, 1.5 Hz, 1H), 7.14 (s, 1H), 6.78 (s, 2H), 6.66 (dt, J = 6.9, 1.7 Hz, 1H), 2.28 (s, 3H), 2.06 (s, 6H), 1.32 (s, 12H), 0.92 (s, 9H), 0.02 (s, 6H). ¹³C NMR (126 MHz, CD₂Cl₂) δ 138.52, 136.94, 136.09, 126.66, 114.43, 83.75, 27.14, 24.65, 23.18, 20.81, 18.99, -3.64. (the C3, C4, and mesityl carbons adjacent to boron were not observed). ¹¹B NMR (160 MHz, CD₂Cl₂) δ 39.62, 30.35. FTIR (thin film): ν

cm^{-1} = 2978, 2932, 2860, 1610. HRMS (DART) calcd. for $\text{C}_{15}\text{H}_{19}\text{BN}$ ($[\text{M}+\text{H}]^+$) 438.3171, found 438.3184.

Compound 4BO2N. Inside a glovebox, a 100 mL round bottom flask was charged with a 1:1 mixture of **4Bpin** and **5Bpin** (1.50 g, 3.46 mmol), diethanolamine (0.144 g, 1.37 mmol, 0.4 equiv), and MTBE (15.0 mL). The reaction mixture was allowed to stir at room temperature for 4 hours. The formation of a precipitate was observed. Then, the reaction mixture was diluted with pentane and passed through a medium-grained fritted funnel. The collected precipitate was washed copiously with diethyl ether and then dried under reduced pressure. The desired product was obtained as a white solid (0.370 g, 0.87 mmol, 51%, based on 1.72 mmol starting material). ^1H NMR (500 MHz, CD_2Cl_2) δ 7.39 (d, J = 6.8 Hz, 1H), 6.79 (s, 2H), 6.66 (s, 1H), 6.61 (d, J = 6.7 Hz, 1H), 4.45 (s, 1H), 4.09 (m, 2H), 3.93 (d, J = 5.3 Hz, 2H), 3.26 (m, 2H), 2.85 (s, 2H), 2.30 (s, 3H), 2.10 (s, 6H), 0.95 (s, 9H), 0.02 (s, 6H). ^{13}C NMR (126 MHz, CD_2Cl_2) δ 138.67, 136.44, 135.74, 126.58, 114.99, 63.16, 51.80, 27.23, 26.69, 23.31, 20.79, -3.59. (the carbons adjacent to boron were not observed). ^{11}B NMR (160 MHz, CD_2Cl_2) δ 39.06, 11.09. FTIR (thin film): ν cm^{-1} = 3084, 2959, 2929, 2857, 1606. HRMS (DART) calcd. for $\text{C}_{23}\text{H}_{38}\text{B}_2\text{N}_2\text{O}_2\text{Si}$ ($[\text{M}+\text{H}]^+$) 425.2967, found 425.2987.

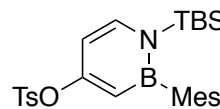


Compound 5BO2N. Inside a glovebox, a 20 mL round bottom flask was charged with **5Bpin** (400 mg, 0.91 mmol), diethanolamine (77 mg, 0.73 mmol), and MTBE (5.0 mL). The reaction mixture was allowed to stir at room temperature for 4 hours. The formation of a precipitate was observed. Then, the reaction mixture was diluted with pentane and passed through a medium-grained fritted funnel. The collected precipitate was washed copiously with diethyl ether and then dried under reduced pressure. The desired product (1:1 mixture with diethanolamine) was obtained as a white solid (170 mg, 33%). ^1H NMR (500 MHz, THF-D_8) δ 7.74 (d, J = 4.8 Hz, 1H), 7.71 (d, J = 1.3 Hz, 1H), 6.69 (s, 2H), 6.37 (d, J = 10.7 Hz, 1H), 6.08 (s, 1H), 3.97 (s, 2H), 3.86 (s, 2H), 3.14 (s, 2H), 2.81 (s, 2H), 2.22 (s, 3H), 2.04 (s, 6H), 0.94 (s, 9H), -0.03 (s, 6H). ^{13}C NMR (126 MHz, THF-D_8) δ 150.54, 143.89, 139.98, 136.96, 128.25, 65.26, 52.86, 29.03, 24.75, 22.14, 20.72, -1.86. (the carbons adjacent to boron were not observed). ^{11}B NMR (160 MHz, CD_2Cl_2) δ 36.67, 8.81. FTIR (thin film): ν cm^{-1} = 3297, 3085, 2930, 2860, 1599. HRMS (DART) calcd. for $\text{C}_{23}\text{H}_{38}\text{B}_2\text{N}_2\text{O}_2\text{Si}$ ($[\text{M}+\text{H}]^+$) 425.29614, found 425.29588.

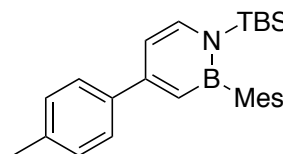


Electrophilic 1,2-Azaborine Building Blocks and their Cross-Coupling Reactions

Compound 4OTs. Inside a glovebox, a 50 mL round bottom flask was charged with **4OH** (2.00 g, 6.11 mmol), triethylamine (3.09 g, 30.55 mmol, 4.26 mL), triethylamine hydrochloride (10 mg), and CH₂Cl₂ (10.0 mL). The reaction mixture was cooled to -30 °C. A solution of 4-methylbenzenesulfonyl chloride (0.93 g, 4.89 mmol) in CH₂Cl₂ (2.0 mL) was then added. The reaction mixture was allowed to warm to room temperature over a period of one hour. The reaction mixture was then removed from the glovebox and washed with aqueous NaHCO₃. The organic layer was extracted with excess ether, dried over MgSO₄, and passed through a Buchner funnel lined with filter paper. Volatiles were removed under reduced pressure, and the desired product was obtained as a white solid after purification by silica gel chromatography with 9:1 pentane:ether as the eluent (1.76 g, 60%). ¹H NMR (500 MHz, CD₂Cl₂) δ 7.70 (d, *J* = 7.8 Hz, 2H), 7.48 (d, *J* = 7.3 Hz, 1H), 7.28 (d, *J* = 8.0 Hz, 2H), 6.73 (s, 2H), 6.25 (dd, *J* = 7.4, 3.0 Hz, 1H), 5.84 (d, *J* = 3.0 Hz, 1H), 2.40 (s, 3H), 2.24 (s, 3H), 1.92 (s, 6H), 0.86 (s, 9H), -0.03 (s, 6H). ¹³C NMR (126 MHz, CD₂Cl₂) δ 159.38, 145.30, 142.25, 138.47, 136.72, 129.74, 129.52, 128.36, 126.77, 106.99, 26.95, 22.84, 21.29, 20.76, 18.90, -3.75. (the carbons adjacent to boron were not observed). ¹¹B NMR (160 MHz, CD₂Cl₂) δ 41.41. FTIR (thin film): ν cm⁻¹ = 2960, 2930, 2860, 1607, 1521. HRMS (DART) calcd. for C₂₆H₃₇BNO₃SSi ([M+H]⁺) 482.23617, found 482.23618.



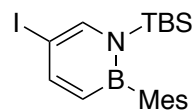
Compound 4ptol (from 4Bpin). A 4 mL pressure vessel was charged with **4Bpin** (200 mg, 0.46 mmol), 4-bromotoluene (78 mg, 0.46 mmol), Pd(dppf)Cl₂ (16 mg, 0.023 mmol), KOH (77 mg, 1.37 mmol), H₂O (0.2 mL), and THF (2.0 mL). The KOH pellets were ground into a powder and the H₂O was sparged with argon for 1 hour prior to use. The reaction mixture was then heated at 80 °C for 2.5 hours. The organic layer was decanted, and the reaction mixture was concentrated under reduced pressure. The desired product was obtained as a white solid after purification by silica gel chromatography with 99:1 pentane:ether as the eluent (149 mg, 81%).



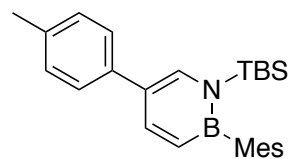
Compound 4ptol (from 4OTs). A 4 mL pressure vessel was charged with **4OTs** (100 mg, 0.21 mmol), *p*-tolylmagnesium bromide 1.0 M THF solution (0.415 mL, 0.415 mmol), Pd₂dba₃ (5.0 mg, 0.0050 mmol), 4,4,5,5-tetramethyl-1,3,2-dioxaphospholane-2-oxide (2.0 mg, 0.010 mmol), and 1,4-dioxane (1.0 mL). The reaction mixture was then heated at 80 °C for 22 hours. At the conclusion of the reaction, the reaction mixture was concentrated under reduced pressure. The desired product was obtained as a white solid after purification by silica gel chromatography with 99:1 pentane:ether as the eluent (64 mg, 76%).

¹H NMR (500 MHz, CD₂Cl₂) δ 7.56 (m, 3H), 7.22 (d, *J* = 7.9 Hz, 2H), 6.79 (s, 2H), 6.76 (s, 1H), 6.70 (d, *J* = 7.0 Hz, 1H), 2.37 (s, 3H), 2.28 (s, 3H), 2.11 (s, 6H), 0.94 (s, 9H), 0.04 (s, 6H). ¹³C NMR (126 MHz, CD₂Cl₂) δ 153.09, 139.39, 138.75, 138.70, 138.01, 136.21, 129.17, 126.73, 126.53, 110.48, 27.16, 23.19, 20.82, 20.8, 19.07, -3.64. (the carbons adjacent to boron were not observed). ¹¹B NMR (160 MHz, CD₂Cl₂) δ 37.07. FTIR (thin film): ν cm⁻¹ = 2961, 2930, 2859, 1611, 1570. HRMS (DART) calcd. for C₂₆H₃₆BNSi ([M+H]⁺) 402.27828, found 402.27944.

Compound 5I. A 100 mL round bottom flask was charged with THF (10 mL) and cooled to -78°C . *n*-Butyllithium 2.5 M hexanes solution (0.89 mL, 2.2 mmol) was added via syringe. **5Bpin** (750 mg, 1.72 mmol) was dissolved in THF (5.0 mL) and added dropwise via syringe to the flask containing *n*-butyllithium at -78°C . The reaction mixture was allowed to warm to room temperature, whereupon the formation of the borate was confirmed by ^{11}B NMR (δ 2.83). The reaction mixture was again cooled to -78°C . I_2 (1.75 g, 6.88 mmol) was dissolved in methanol (10 mL) and added via syringe to the flask containing the borate. The reaction mixture was allowed to stir at -78°C for 30 minutes, then the mixture was allowed to warm to room temperature over a period of 1 hour. At the conclusion of the reaction, the reaction mixture was quenched with aqueous Na_2SO_3 and then extracted with hexanes. The organic layer was then washed with brine. Finally, the organic layer was dried over MgSO_4 , passed through a Buchner funnel lined with filter paper, and concentrated *in vacuo*. The desired product was obtained as a highly viscous yellow oil after purification by silica gel chromatography with hexanes as the eluent (676 mg, 90%). ^1H NMR (500 MHz, C_6D_6) δ 7.84 (s, 1H), 7.70 (dd, $J = 11.5, 1.7$ Hz, 1H), 6.79 (s, 2H), 6.53 (d, $J = 11.5$ Hz, 1H), 2.22 (s, 3H), 2.12 (s, 6H), 0.75 (s, 9H), -0.14 (s, 6H). ^{13}C NMR (126 MHz, CD_2Cl_2) δ 150.01, 143.41, 138.57, 136.63, 126.83, 109.99, 26.96, 23.07, 20.80, 18.96, -3.75. (the carbons adjacent to boron were not observed). ^{11}B NMR (160 MHz, C_6D_6) δ 38.96. FTIR (thin film): $\nu\text{ cm}^{-1} = 2959, 2930, 2859, 1609, 1584$. HRMS (DART) calcd. for $\text{C}_{19}\text{H}_{30}\text{BNSi}$ ($[\text{M}+\text{H}]^+$) 438.1285, found 438.1281.



Compound 5ptol (From **5Bpin**). A 4 mL pressure vessel was charged with **5Bpin** (200 mg, 0.46 mmol), 4-bromotoluene (78 mg, 0.46 mmol), $\text{Pd}(\text{dppf})\text{Cl}_2$ (16 mg, 0.023 mmol), KOH (77 mg, 1.37 mmol), H_2O (0.2 mL), and THF (2.0 mL). The KOH pellets were ground into a powder and the H_2O was sparged with argon for 1 hour prior to use. The reaction mixture was then heated at 80°C for 2.5 hours. The organic layer was decanted, and the reaction mixture was concentrated under reduced pressure. The desired product was obtained as a white solid after purification by silica gel chromatography with 99:1 pentane:ether as the eluent (152 mg, 82%).



Compound 5ptol (from **5I**). A 4 mL vial was charged with **5I** (85 mg, 0.19 mmol), *p*-tolylboronic acid (27 mg, 0.19 mmol), $\text{Pd}(\text{dppf})\text{Cl}_2$ (7 mg, 0.010 mmol), KOH (33 mg, 0.58 mmol), H_2O (0.15 mL), and THF (1.5 mL). The KOH pellets were ground into a powder and the H_2O was sparged with argon for 1 hour prior to use. The reaction mixture was then allowed to stir at room temperature 1.5 hours. The organic layer was decanted, and the reaction mixture was concentrated under reduced pressure. The desired product was obtained as a white solid after purification by silica gel chromatography with 99:1 pentane:ether as the eluent (61 mg, 78%).

^1H NMR (500 MHz, CD_2Cl_2) δ 7.87 (dd, $J = 11.2, 1.8$ Hz, 1H), 7.67 (d, $J = 1.8$ Hz, 1H), 7.38 (d, $J = 8.0$ Hz, 2H), 7.23 (d, $J = 7.8$ Hz, 2H), 6.79 (s, 2H), 6.66 (d, $J = 11.2$ Hz, 1H), 2.37 (s, 3H), 2.28 (s, 3H), 2.10 (s, 6H), 0.95 (s, 9H), 0.05 (s, 6H). ^{13}C NMR (126 MHz, CD_2Cl_2) δ 143.19, 138.69, 137.75, 136.76, 136.30, 135.89, 129.39, 126.75, 126.12, 124.76, 27.25, 23.17, 20.82, 20.67, 19.02, -3.48. (the carbons adjacent to boron were not observed). ^{11}B NMR (160 MHz, CD_2Cl_2) δ 36.55. FTIR (thin film): $\nu\text{ cm}^{-1} = 2960, 2930, 2959, 1613, 1558$. HRMS (DART) calcd. for $\text{C}_{26}\text{H}_{36}\text{BNSi}$ ($[\text{M}+\text{H}]^+$) 402.27828, found 402.27851.

2.8.3 Kinetic and Thermodynamic Experiments

Rate Determination of NMO Oxidation by ^1H NMR

General Experimental Procedure for ^1H NMR

In a glovebox, a J-Young tube was charged with 250 μL of a stock solution in CD_2Cl_2 containing both: 1) internal standard 1,3,5-trimethoxybenzene (24.7 mg : 2.0 mL; 3.1 mg, 0.018 mmol) and 2) **5Bpin**, **4Bpin**, or **PhBpin** (110 mg : 2.0 mL; 13.8 mg, 0.032 mmol) and 100 μL of CD_2Cl_2 . Immediately prior to collecting the ^1H NMR spectrum, 250 μL of a stock solution in CD_2Cl_2 containing NMO (240 mg : 2.0 mL; 30 mg, 0.253 mmol, 8 equiv.) was added to the J-Young tube. A ^1H NMR spectrum was collected every 100 seconds and conversion of the starting material was determined by the internal standard method with a calibration to the measured NMR ratio of the starting material and 1,3,5-trimethoxybenzene in the prepared stock solution. The rate of reaction was determined from the first 10% of conversion.

Figure 2.5. 4Bpin oxidation kinetics.

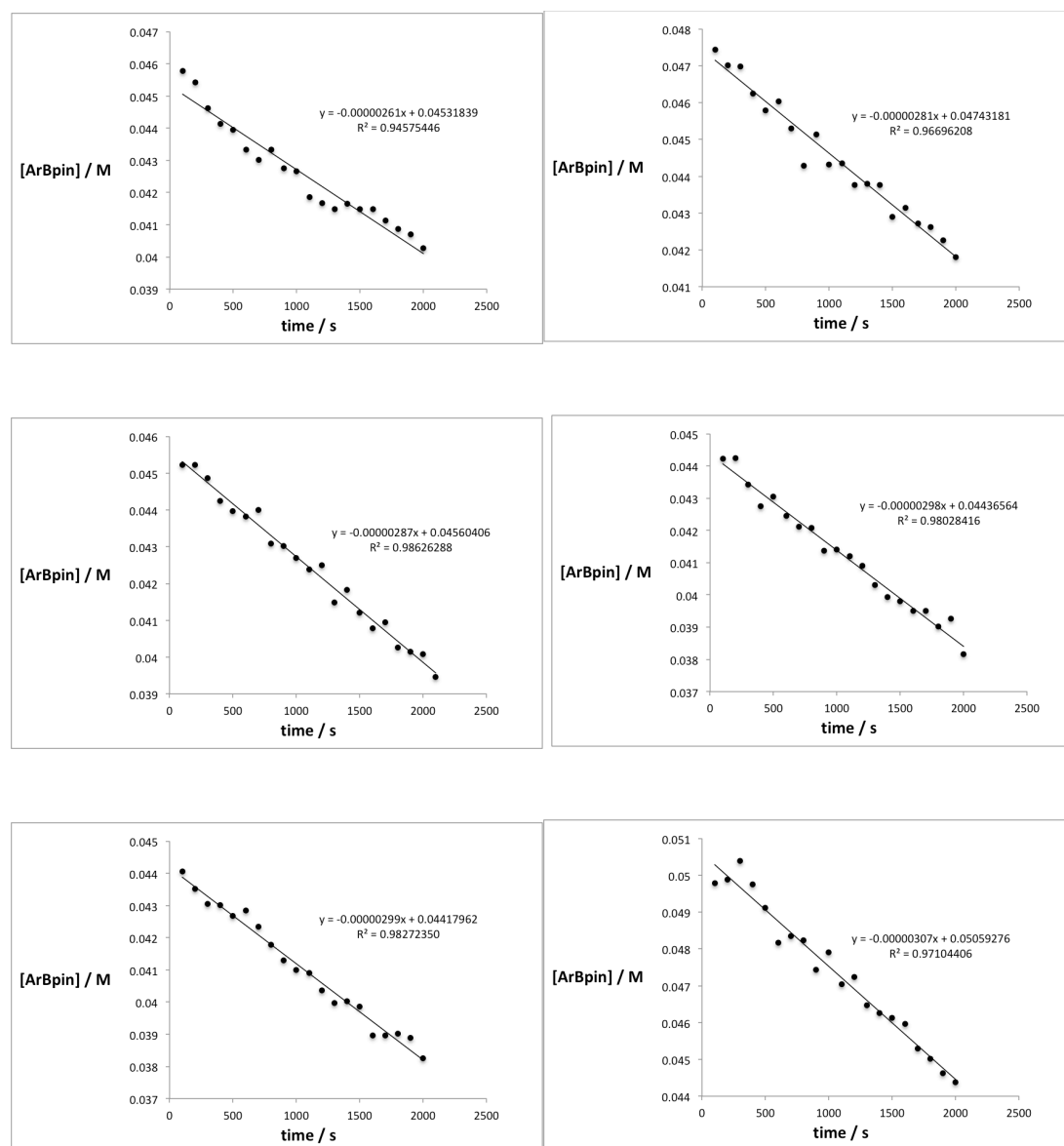


Figure 2.6. 5Bpin oxidation kinetics.

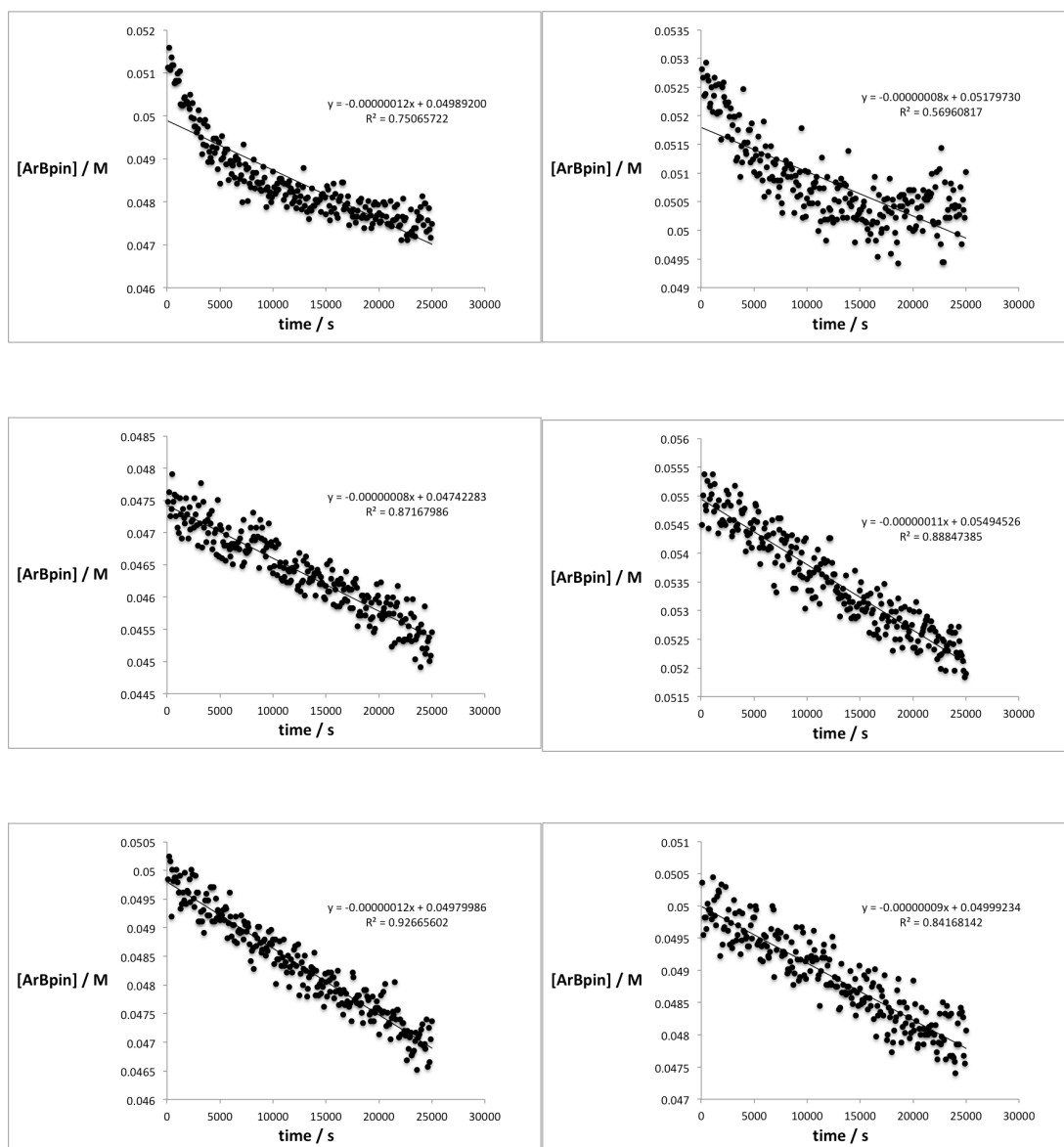


Figure 2.7. PhBpin oxidation kinetics.

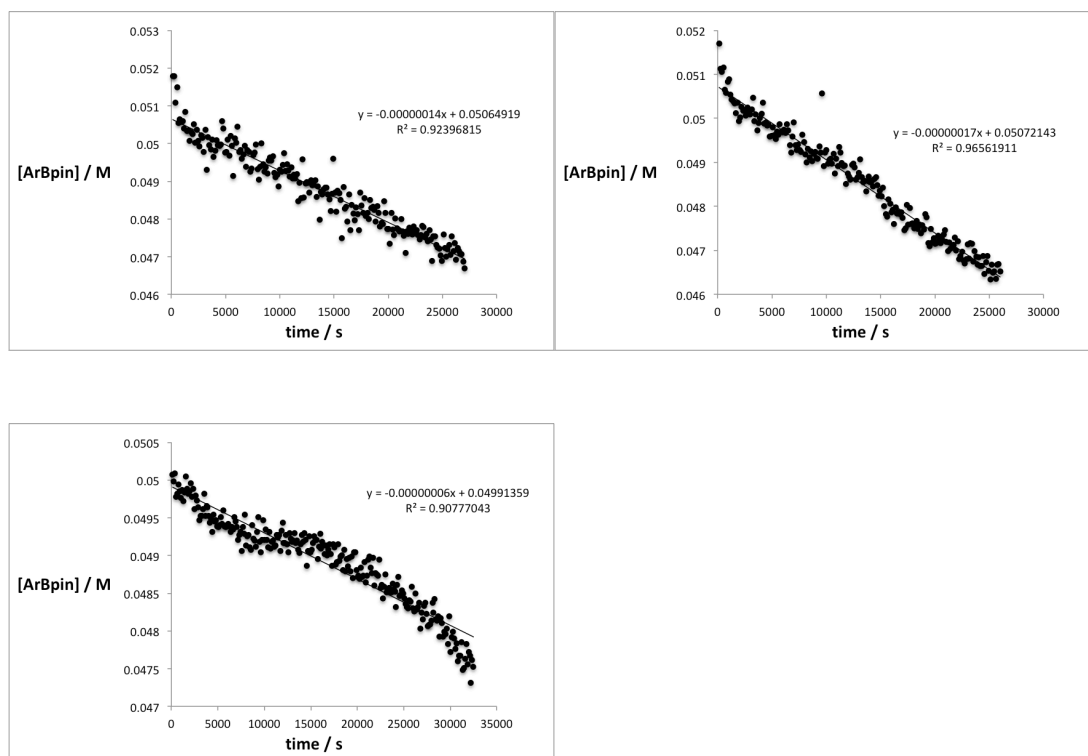


Table 2.1. Summary of oxidation kinetics.

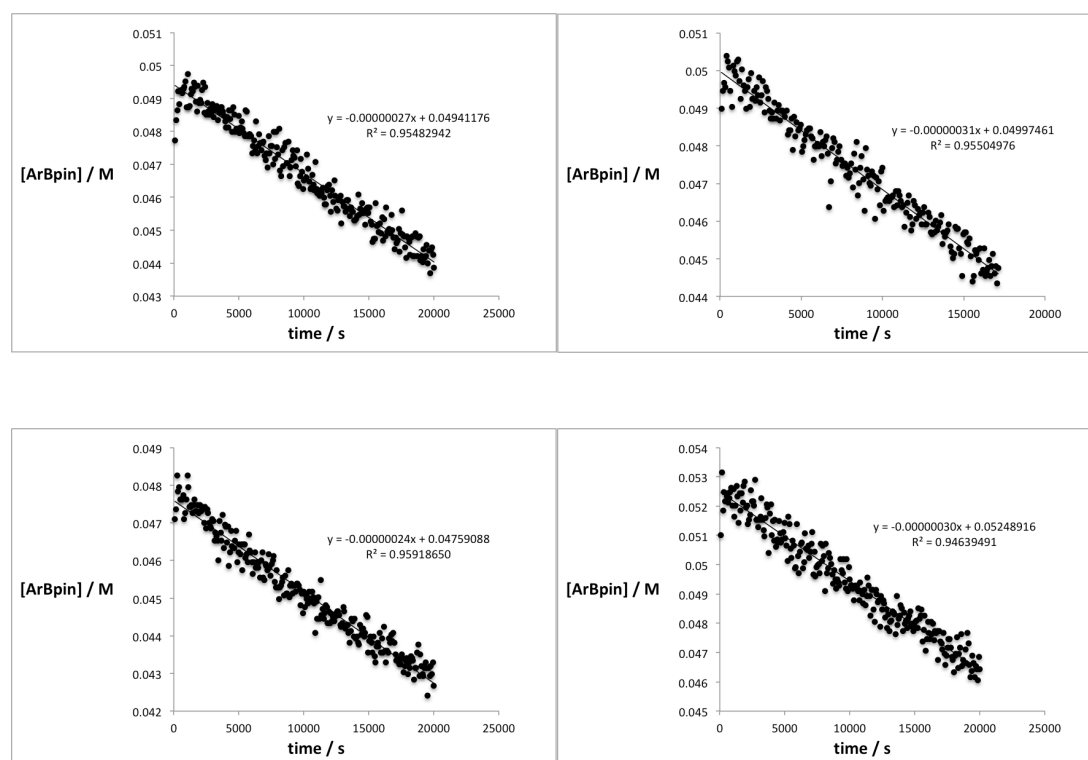
entry	rate 4Bpin (M s ⁻¹)	rate 5Bpin (M s ⁻¹)	rate PhBpin (M s ⁻¹)
1	-2.61×10^{-6}	-1.2×10^{-7}	-1.4×10^{-7}
2	-2.81×10^{-6}	-0.8×10^{-7}	-1.7×10^{-7}
3	-2.87×10^{-6}	-0.8×10^{-7}	-0.6×10^{-7}
4	-2.98×10^{-6}	-1.1×10^{-7}	—
5	-2.99×10^{-6}	-1.2×10^{-7}	—
6	-3.07×10^{-6}	-0.9×10^{-7}	—
average ± std. dev.	$-2.89 \pm 0.16 \times 10^{-6}$	$-1.0 \pm 0.2 \times 10^{-7}$	$-1.2 \pm 0.6 \times 10^{-7}$
rate 4Bpin rate 5Bpin	28.9 ± 5.7		

Rate Determination of Protodeborylation Reactions by ^1H NMR

General Experimental Procedure for ^1H NMR

In a glovebox, a J-Young tube was charged with 250 μL of a stock solution in CD_2Cl_2 containing **4Bpin** or **5Bpin** (110 mg : 2.0 mL; 13.8 mg, 0.032 mmol), 100 μL of a stock solution in CD_2Cl_2 containing internal standard 1,3,5-trimethoxybenzene (41.6 mg : 2.0 mL; 5.2 mg, 0.031 mmol), and 100 μL of a stock solution in CD_2Cl_2 containing methanol (80 mg : 2.0 mL; 10 mg, 0.31 mmol), and 50 μL of CD_2Cl_2 . Immediately prior to collecting the ^1H NMR spectrum, 100 μL of a stock solution in CD_2Cl_2 containing $[\text{Ir}(\text{OMe})(\text{cod})]_2$ (4 mg : 2.0 mL; 0.5 mg, 0.0008 mmol) was added to the J-Young tube. The reaction mixture was heated to 40 $^\circ\text{C}$. A ^1H NMR spectrum was collected every 80 seconds and conversion of the starting material was determined by the internal standard method with a calibration to the measured NMR ratio of the starting material and 1,3,5-trimethoxybenzene in the prepared stock solution. The rate of reaction was determined from the first 10% of conversion.

Figure 2.8. 4Bpin protodeborylation kinetics.



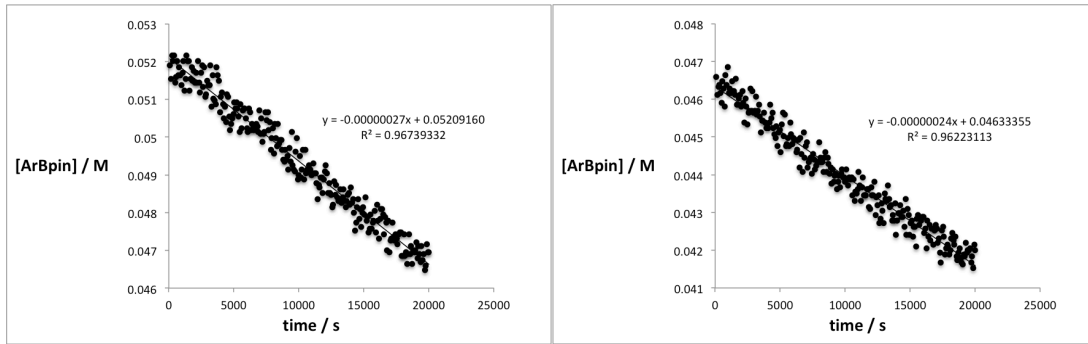


Figure 2.9. 5Bpin protodeborylation kinetics.

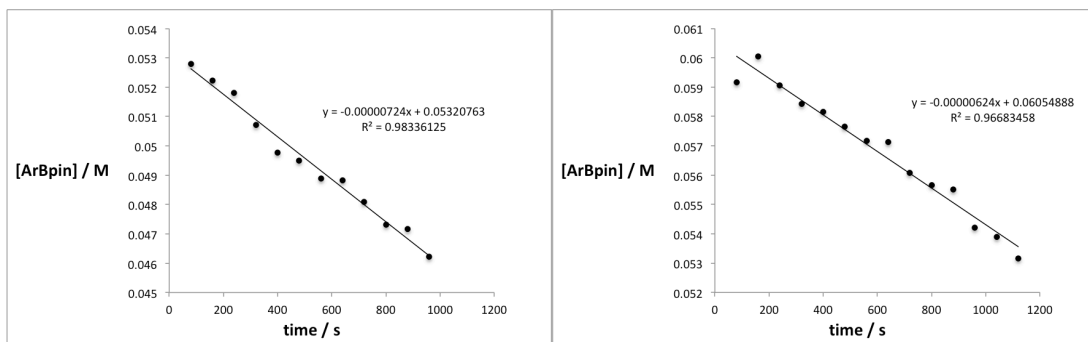
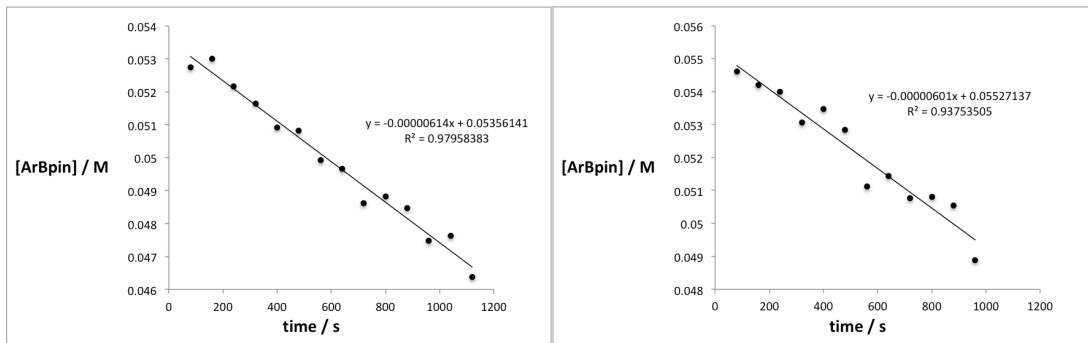
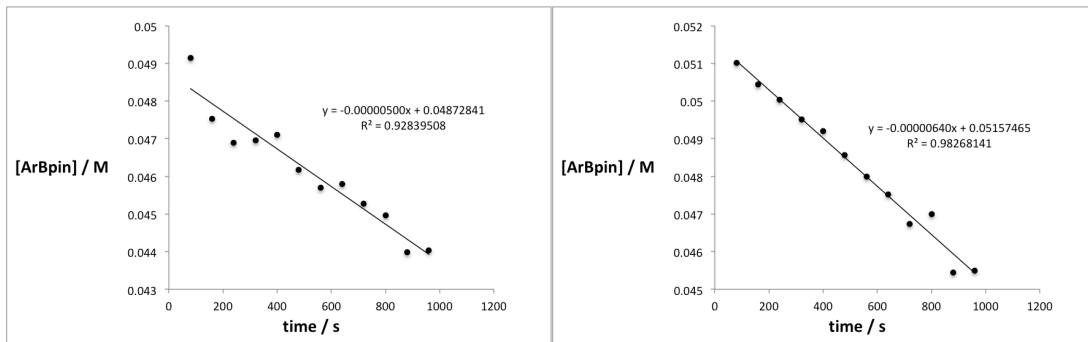


Figure 2.10. PhBpin protodeborylation kinetics.

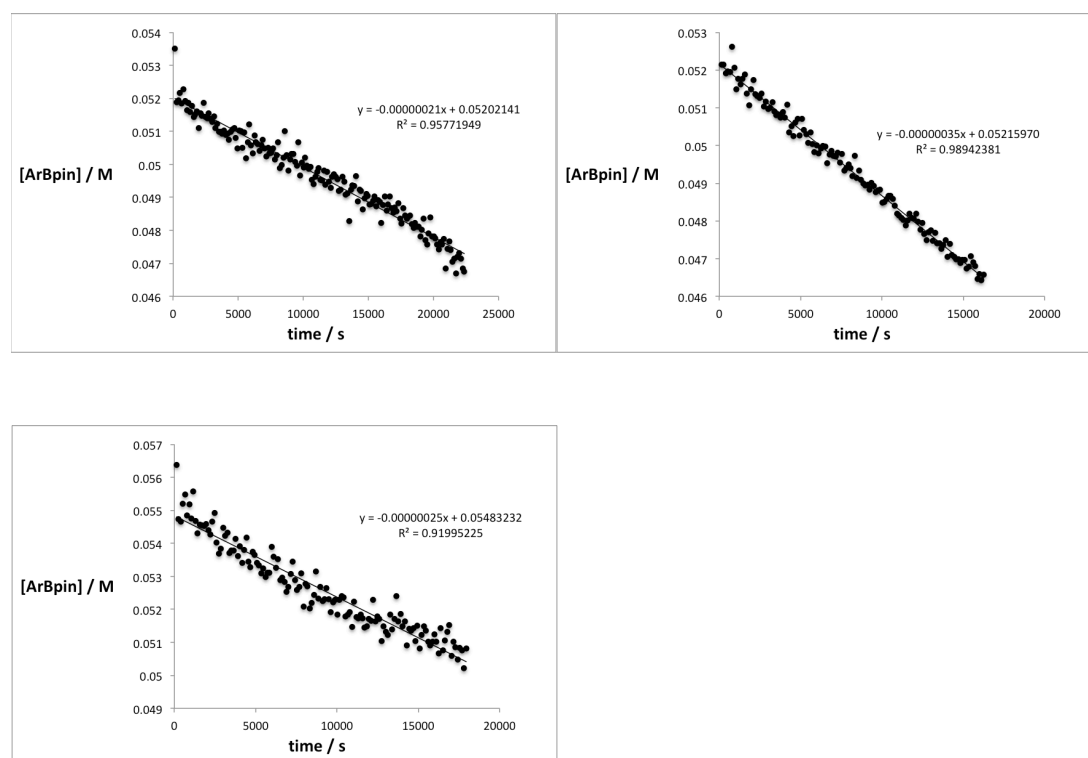


Table 2.2. Summary of protodeborylation kinetics.

entry	rate 4Bpin (M s ⁻¹)	rate 5Bpin (M s ⁻¹)	rate PhBpin (M s ⁻¹)
1	-2.7×10^{-7}	-5.0×10^{-6}	-2.1×10^{-7}
2	-3.1×10^{-7}	-6.4×10^{-6}	-3.5×10^{-7}
3	-2.4×10^{-7}	-6.1×10^{-6}	-2.5×10^{-7}
4	-3.0×10^{-7}	-6.0×10^{-6}	—
5	-2.7×10^{-7}	-7.2×10^{-6}	—
6	-2.4×10^{-7}	-6.2×10^{-6}	—
average ± std. dev.	$-2.7 \pm 0.3 \times 10^{-7}$	$-6 \pm 1 \times 10^{-6}$	$-2.7 \pm 0.7 \times 10^{-7}$
rate 5Bpin rate 4Bpin	22.7 ± 3.6		

Rate and Equilibrium Constant Determination of Transesterification Reactions

General Experimental Procedure for Rate Determination with Reaction Calorimetry

Reactions were performed in a Setaram C80 Calvet calorimeter with Setsoft 2000 software. In a glove box, a stainless steel mixing cell (approx. volume 4.6 mL) was charged with 250 μL of a stock solution in THF- D_8 containing diethanolamine (50.5 mg : 2.0 mL; 6.3 mg, 0.060 mmol) and 100 μL of THF- D_8 . To the upper chamber was added 250 μL of a stock solution in THF- D_8 containing both: 1) internal standard 1,3,5-trimethoxybenzene (101.5 mg : 5.0 mL; 5.1 mg, 0.030 mmol) and 2) **4Bpin** or **5Bpin** (526.5 mg : 5.0 mL; 26 mg, 0.060 mmol). The reference cell was left empty under air. Both cells were loaded into the calorimeter at 27 $^\circ\text{C}$ and the heat flow was allowed to equilibrate (approx. 2h). Data collection was initiated, and both plungers were depressed. Heat flow measurements were recorded every 6s. Data collection was halted when heat flow reached equilibrium.

The thermodynamic heat of reaction was obtained through integration of the complete heat flow versus time curve and moles of limiting substrate by equation (1).

$$\Delta H_{rxn} = \frac{\int_0^{\infty} q dt}{mol} \quad (1)$$

Heat flow is directly related to rate through equation (2).

$$\text{heat flow} = q = (\Delta H_{rxn})(\text{volume})(\text{rate}) \quad (2)$$

Integration of the heat flow curve from $t=0$ to $t=t$ divided by the complete area under the curve provides conversion (equation (3)).

$$(\text{Conv})_t = \frac{\text{area to time } t}{\text{total area}} = \frac{\int_0^t q dt}{\int_0^{\infty} q dt} \quad (3)$$

Conversion can also be defined as the ratio of the concentration of starting material at $t=t$ relative to its concentration at $t=0$ (equation (4)).

$$(\text{Conv})_t = \frac{[A]_t}{[A]_0} \quad (4)$$

Because the reaction being studied is an equilibrium process, the complete consumption of starting material does not define the endpoint of the reaction as in equation (4). Equation (4) must be modified to equation (5) to define the equilibrium concentration as the new endpoint.

$$(\text{Conv})_{teq} = \frac{[A]_t - [A]_{eq}}{[A]_0 - [A]_{eq}} \quad (5)$$

Rearranging to express in terms of $[A]_t$ we obtain equation (6). $(\text{Conv})_{teq}$ is the actual value determined by reaction calorimetry according to equation (3) and $[A]_{eq}$ is determined by measuring the equilibrium concentration of the starting material (*vide infra*).

$$[A]_t = (Conv)_t([A]_0 - [A]_{eq}) + [A]_{eq} \quad (6)$$

The slope of a plot of $[A]_t$ versus time over the first 5% of conversion versus time will give a measure of the instantaneous rate of the reaction.

General Experimental Procedure for Equilibrium Constant Determination with ^1H NMR

The reaction mixture was transferred from the calorimetry cell directly to an NMR tube and analysed by ^1H NMR. The concentrations of each component were determined by the internal standard method with a calibration to the measured NMR ratio of each compound and 1,3,5-trimethoxybenzene in the prepared stock solution.

Figure 2.11. 4Bpin transesterification kinetics.

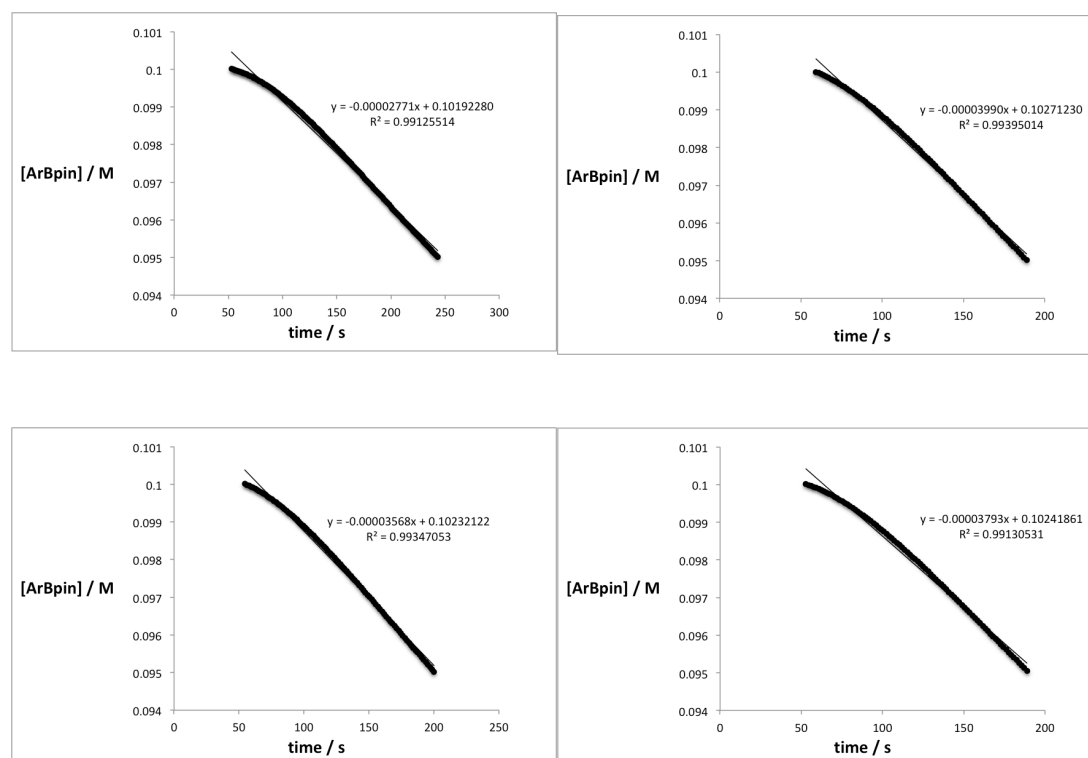


Figure 2.12. 5Bpin transesterification kinetics.

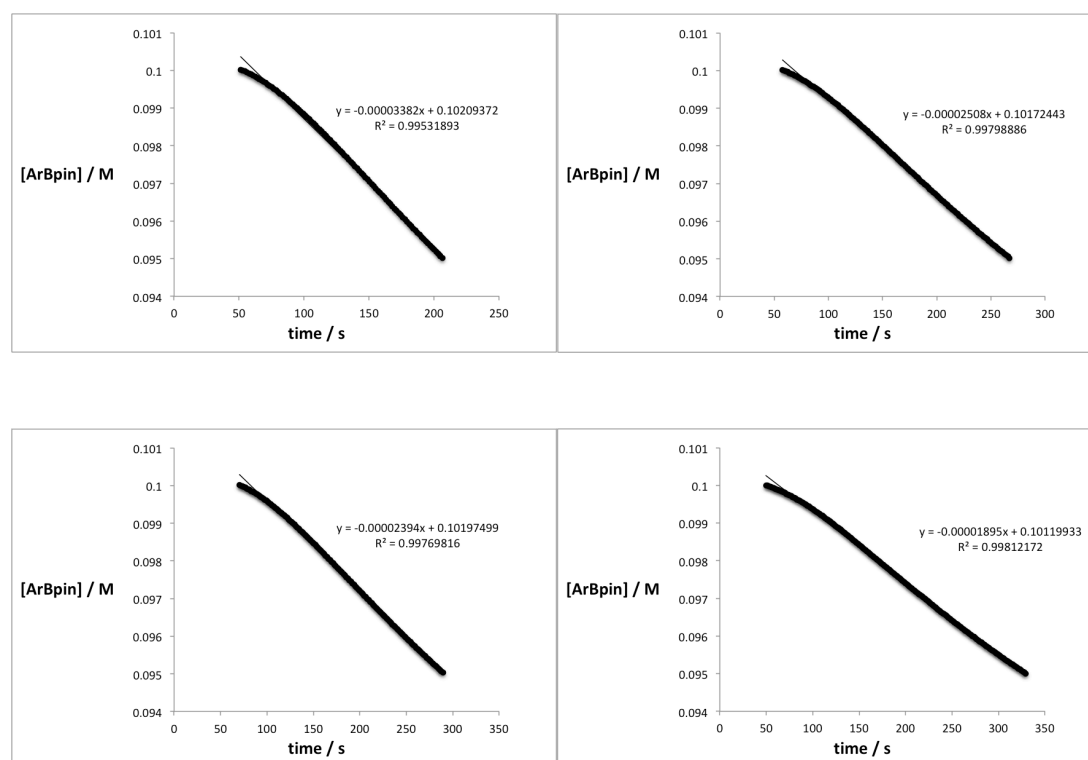
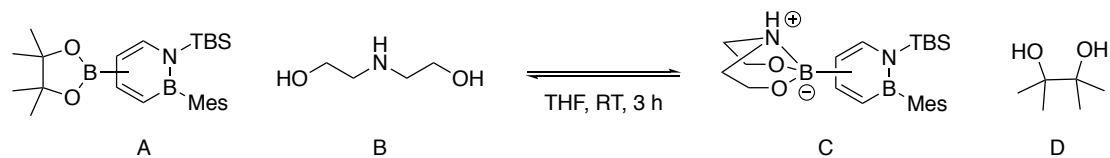


Table 2.3. Summary of transesterification rates and equilibrium constants.



$$K_{eq} = \frac{[C][D]}{[A][B]}$$

entry	rate 4Bpin ($M s^{-1}$)	rate 5Bpin ($M s^{-1}$)	K_{eq} 4Bpin	K_{eq} 5Bpin
1	-2.77×10^{-5}	-3.38×10^{-5}	0.22	0.011
2	-3.99×10^{-5}	-2.51×10^{-5}	0.35	0.010
3	-3.57×10^{-5}	-2.39×10^{-5}	0.29	0.011
4	-3.79×10^{-5}	-1.90×10^{-5}	0.30	0.009
average \pm std. dev.	$-3.5 \pm 0.5 \times 10^{-5}$	$-2.5 \pm 0.6 \times 10^{-5}$	0.29 ± 0.05	0.010 ± 0.001

$$\frac{K_{eq} \text{ 4Bpin}}{K_{eq} \text{ 5Bpin}} = 28.6 \pm 6.1$$

2.8.4 Computational Details

All calculations were performed using the Gaussian 09 program:

Full Reference for Gaussian 09

Frisch, M. J.; Trucks, G. W.; Schlegel, H. B.; Scuseria, G. E.; Robb, M. A.; Cheeseman, J. R.; Scalmani, G.; Barone, V.; Mennucci, B.; Petersson, G. A.; Nakatsuji, H.; Caricato, M.; Li, X.; Hratchian, H. P.; Izmaylov, A. F.; Bloino, J.; Zheng, G.; Sonnenberg, J. L.; Hada, M.; Ehara, M.; Toyota, K.; Fukuda, R.; Hasegawa, J.; Ishida, M.; Nakajima, T.; Honda, Y.; Kitao, O.; Nakai, H.; Vreven, T.; Montgomery, J. A., Jr.; Peralta, J. E.; Ogliaro, F.; Bearpark, M.; Heyd, J. J.; Brothers, E.; Kudin, K. N.; Staroverov, V. N.; Kobayashi, R.; Normand, J.; Raghavachari, K.; Rendell, A.; Burant, J. C.; Iyengar, S. S.; Tomasi, J.; Cossi, M.; Rega, N.; Millam, J. M.; Klene, M.; Knox, J. E.; Cross, J. B.; Bakken, V.; Adamo, C.; Jaramillo, J.; Gomperts, R.; Stratmann, R. E.; Yazyev, O.; Austin, A. J.; Cammi, R.; Pomelli, C.; Ochterski, J. W.; Martin, R. L.; Morokuma, K.; Zakrzewski, V. G.; Voth, G. A.; Salvador, P.; Dannenberg, J. J.; Dapprich, S.; Daniels, A. D.; Farkas, O.; Foresman, J. B.; Ortiz, J. V.; Cioslowski, J.; Fox, D. J. Gaussian 09, Revision C.01; Gaussian Inc., Wallingford, CT, 2010.

Electronic Structure Calculations of 4Bpin and 5Bpin

Structures **4Bpin** and **5Bpin** were optimized at the M062X/6-31G(d,p) level and computed using the polarized continuum model simulating CH₂Cl₂ solvent. The coordinates can be found in the next section, **NMO Oxidation**, with the identifiers **GS(4Bpin)** and **GS(5Bpin)**.

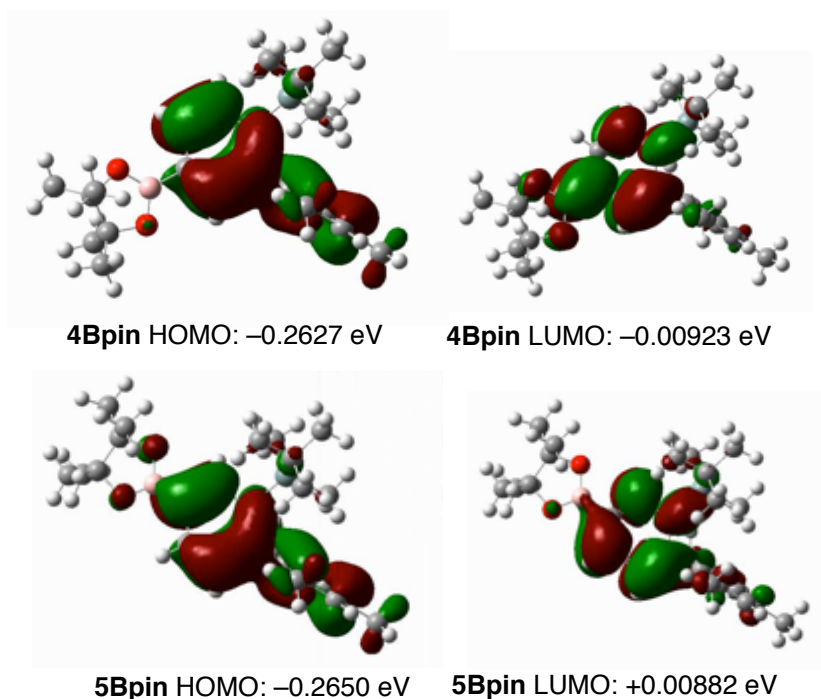


Figure 2.13. HOMO and LUMO energies and orbital illustrations of **4Bpin** (**GS(4Bpin)**) and **5Bpin** (**GS(5Bpin)**).

Table 2.4. Orbital coefficients for the C4 carbon atom of the HOMO of **4Bpin** (orbital 119) and for the C5 carbon atom of the HOMO of **5Bpin** (orbital 119).

Atomic Orbital	C4 Orbital Coefficient	C4 (Orbital Coefficient) ²	C5 Orbital Coefficient	C5 (Orbital Coefficient) ²
1s	0.00378	1.43 x 10 ⁻⁵	0.00077	5.93 x 10 ⁻⁷
2s	-0.00847	7.17 x 10 ⁻⁵	-0.0021	4.41 x 10 ⁻⁶
2px	0.03214	1.03 x 10 ⁻³	0.00313	9.80 x 10 ⁻⁶
2py	0.01161	1.35 x 10 ⁻⁴	0.122219	1.49 x 10 ⁻²
2pz	-0.06358	4.04 x 10 ⁻³	-0.2207	4.87 x 10 ⁻²
3s	-0.02233	4.99 x 10 ⁻⁵	-0.005	2.50 x 10 ⁻⁵
3px	0.01332	1.77 x 10 ⁻⁵	0.00219	4.80 x 10 ⁻⁶
3py	0.00266	7.08 x 10 ⁻⁶	0.1011	1.02 x 10 ⁻²
3pz	-0.06775	4.59 x 10 ⁻³	-0.17566	3.09 x 10 ⁻²
4xx	0.00174	3.03 x 10 ⁻⁶	-0.00071	5.04 x 10 ⁻⁷
4yy	0.00744	5.54 x 10 ⁻⁵	0.0069	4.76 x 10 ⁻⁵
4zz	-0.00808	6.53 x 10 ⁻⁵	-0.00668	4.46 x 10 ⁻⁵
4xy	-0.00064	4.10 x 10 ⁻⁷	-0.00197	3.88 x 10 ⁻⁶
4xz	0.00445	1.98 x 10 ⁻⁵	0.00225	5.06 x 10 ⁻⁶
4yz	-0.01424	2.03 x 10 ⁻⁴	-0.00606	3.67 x 10 ⁻⁵
sum	—	0.011	—	0.105

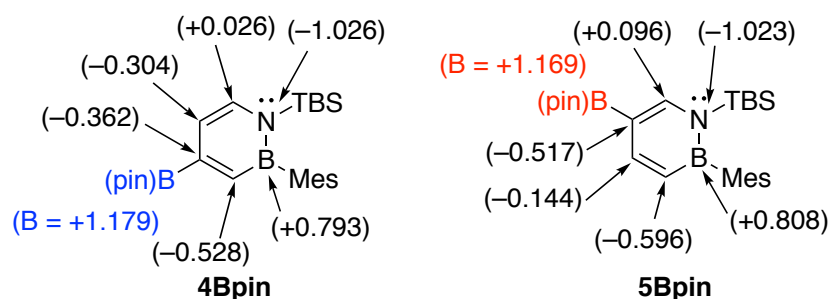


Figure 2.14. Löwdin charges for selected atoms of **4Bpin** (GS(**4Bpin**)) and **5Bpin** (GS(**5Bpin**)).

NMO Oxidation

All structures for the potential energy surface of the NMO oxidation reaction were optimized at the M062X/6-31G(d,p) level and computed using the polarized continuum model simulating CH₂Cl₂ solvent. The coordinates are reproduced here.

Table 2.5. Gibbs free energies of structures for the free energy profile for the oxidation of **5Bpin** and **4Bpin** with NMO. CounterPoisson basis set superposition errors (BSSE) are included for selected structures.

Structure	Gibbs Free Energy (Hartree)	Gibbs Free Energy Relative to GS (kcal mol ⁻¹)	CounterPoise BSSE (kcal mol ⁻¹)	Corrected Energy Value (kcal mol ⁻¹)
NMO	-401.954235	–	–	–
GS(4Bpin)	-1520.904048	–	–	–
GS(4Bpin) + NMO	-1922.858283	0.0	–	0.0
TS1(4Bpin)	-1922.849537	5.5	7.0	12.5
INT(4BPin)	-1922.867865	-6.0	8.5	2.5
TS2(4Bpin)	-1922.829616	18.2	5.5	23.8
PDT(4Bpin)	-1596.142556	–	–	–
NMM	-326.834433	–	–	–
PDT(4Bpin) + NMM	-1922.976989	-74.5	–	-74.5
GS(5Bpin)	-1520.91015	–	–	–
GS(5Bpin) + NMO	-1922.86314	0.0	–	0.0
TS1(5Bpin)	-1922.857888	4.1	6.7	10.8
INT(5BPin)	-1922.873288	-5.6	8.6	3.0
TS2(5Bpin)	-1922.829203	22.1	5.6	27.7
PDT(5Bpin)	-1596.131506	–	–	–
PDT(5Bpin) + NMM	-1922.965939	-63.7	–	-63.7

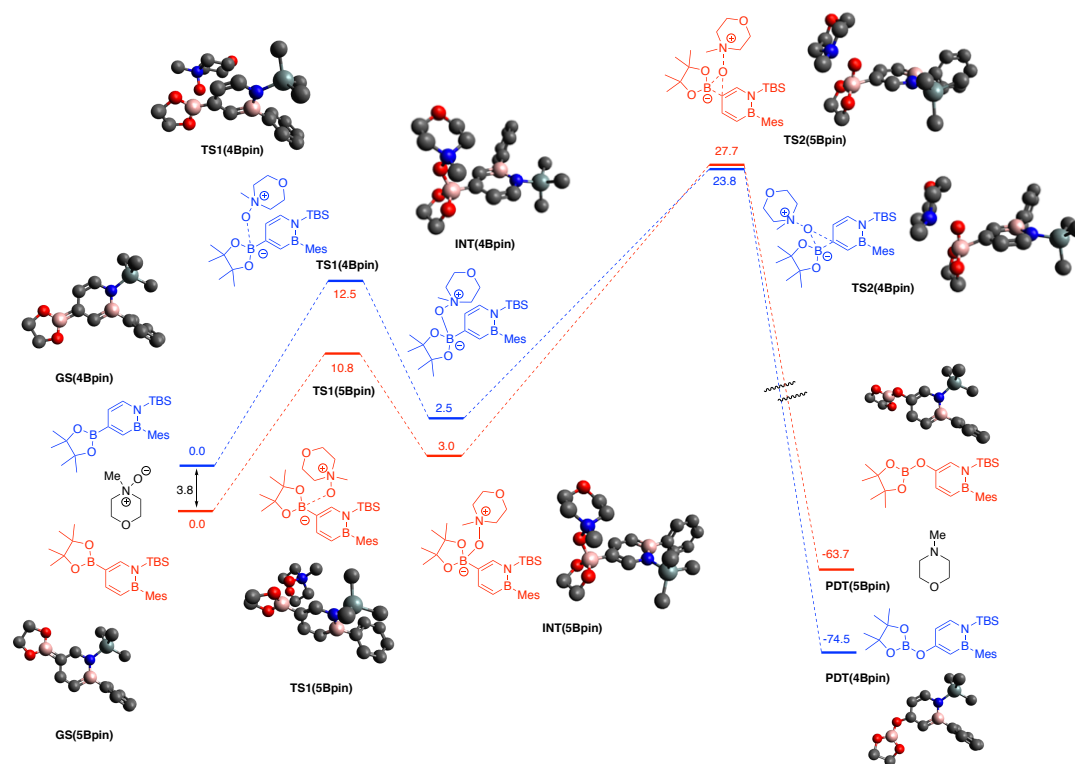
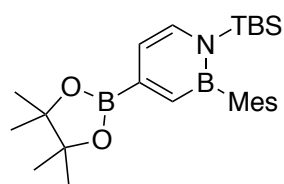


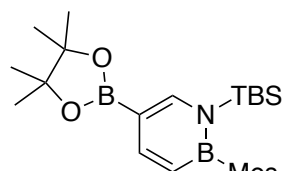
Figure 2.15. Calculated free energy profile (in kcal/mol) for the oxidation of **4Bpin** and **5Bpin** with NMO. H atoms as well as methyl-carbons on the mesityl, pinacol, and *tert*-butyl groups omitted for clarity.

Figure 2.16. Coordinates for optimized geometries for NMO oxidation.



	GS(4Bpin)		
B	-3.461	-0.300	0.014
O	-4.421	-1.267	0.168
C	-5.690	-0.658	-0.172
C	-6.779	-1.258	0.700
H	-6.527	-1.184	1.759
H	-7.730	-0.745	0.527
H	-6.910	-2.314	0.449
C	-5.406	0.858	0.085
C	-5.611	1.258	1.543
H	-5.090	0.569	2.215
H	-6.672	1.269	1.806
H	-5.203	2.260	1.695
C	-6.146	1.810	-0.839
H	-5.886	2.841	-0.586
H	-7.228	1.691	-0.718
H	-5.887	1.635	-1.884
C	-5.949	-0.972	-1.644
H	-5.931	-2.056	-1.781
H	-6.923	-0.596	-1.966
H	-5.175	-0.531	-2.279
C	-1.927	-0.604	0.051
C	-1.483	-1.953	0.216
H	-2.205	-2.754	0.329
C	-0.157	-2.259	0.234
H	0.152	-3.293	0.359
N	0.853	-1.324	0.104
Si	2.511	-2.059	-0.029
C	3.915	-0.845	0.234
H	3.946	-0.042	-0.506
H	4.846	-1.418	0.168
H	3.878	-0.385	1.224
C	2.661	-2.834	-1.762
C	2.570	-1.731	-2.824
H	3.349	-0.972	-2.694
H	1.597	-1.228	-2.787
H	2.687	-2.160	-3.827
C	4.030	-3.528	-1.859
H	4.858	-2.823	-1.731
H	4.143	-3.991	-2.848
H	4.138	-4.321	-1.110
C	1.564	-3.872	-2.036
H	0.567	-3.420	-2.043
H	1.727	-4.328	-3.021
H	1.568	-4.681	-1.296
C	2.631	-3.374	1.312
H	3.682	-3.646	1.456

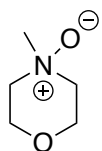
H	2.255	-2.985	2.264
H	2.082	-4.292	1.082
B	0.501	0.079	-0.015
C	1.583	1.234	0.016
C	2.120	1.616	1.268
C	1.684	0.904	2.528
H	2.115	1.372	3.416
H	0.594	0.912	2.630
H	1.989	-0.149	2.521
C	3.053	2.643	1.346
H	3.459	2.923	2.317
C	3.481	3.330	0.204
C	4.490	4.444	0.315
H	5.365	4.127	0.890
H	4.062	5.311	0.828
H	4.830	4.771	-0.670
C	2.924	2.974	-1.019
H	3.224	3.511	-1.917
C	1.973	1.950	-1.125
C	1.395	1.653	-2.489
H	0.540	0.974	-2.429
H	2.141	1.195	-3.147
H	1.060	2.575	-2.975
C	-0.992	0.396	-0.063
H	-1.354	1.419	-0.176
O	-3.984	0.951	-0.181



GS(5BPin)

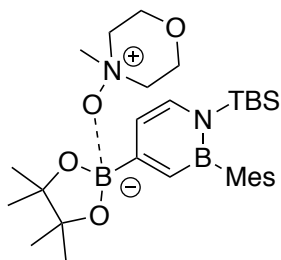
C	1.969	1.928	-1.320
C	1.533	1.223	-0.189
C	2.053	1.586	1.075
C	1.567	0.886	2.323
H	1.987	1.344	3.222
H	0.475	0.924	2.398
H	1.845	-0.174	2.325
C	3.012	2.587	1.177
H	3.404	2.854	2.157
C	3.485	3.262	0.046
C	4.539	4.332	0.180
H	4.225	5.106	0.887
H	5.478	3.913	0.556
H	4.743	4.810	-0.781
B	0.414	0.107	-0.249
N	0.723	-1.311	-0.114
C	-0.312	-2.206	-0.012
H	-0.041	-3.252	0.123
C	-1.644	-1.882	-0.070
B	-2.688	-3.014	0.047

O	-2.359	-4.327	0.294
C	-3.554	-5.108	0.058
C	-3.572	-6.290	1.013
H	-3.457	-5.967	2.048
H	-4.513	-6.841	0.917
H	-2.752	-6.970	0.769
C	-4.685	-4.057	0.297
C	-5.056	-3.912	1.771
H	-4.161	-3.782	2.387
H	-5.606	-4.786	2.131
H	-5.688	-3.030	1.890
C	-5.931	-4.259	-0.549
H	-6.667	-3.487	-0.309
H	-6.378	-5.236	-0.341
H	-5.701	-4.198	-1.614
C	-3.491	-5.590	-1.389
H	-2.562	-6.147	-1.533
H	-4.332	-6.245	-1.629
H	-3.495	-4.744	-2.083
O	-4.041	-2.822	-0.098
C	-2.009	-0.510	-0.257
H	-3.072	-0.280	-0.315
Si	2.358	-2.106	-0.214
C	2.420	-3.398	1.151
H	2.108	-2.959	2.105
H	3.449	-3.750	1.269
H	1.791	-4.272	0.962
C	3.795	-0.931	0.037
H	3.760	-0.441	1.012
H	4.709	-1.534	0.002
H	3.862	-0.152	-0.726
C	2.489	-2.914	-1.934
C	3.842	-3.639	-2.022
H	3.932	-4.426	-1.265
H	4.685	-2.950	-1.900
H	3.947	-4.113	-3.006
C	1.371	-3.935	-2.194
H	1.352	-4.729	-1.438
H	0.382	-3.464	-2.219
H	1.531	-4.414	-3.168
C	2.422	-1.827	-3.014
H	3.223	-1.088	-2.898
H	1.464	-1.295	-2.983
H	2.524	-2.274	-4.011
C	-1.063	0.470	-0.347
H	-1.391	1.501	-0.474
C	2.945	2.926	-1.190
H	3.278	3.459	-2.079
C	1.419	1.643	-2.699
H	0.518	1.026	-2.658
H	1.168	2.575	-3.214
H	2.155	1.120	-3.319



NMO

H	1.873	2.023	-0.165
H	-0.046	1.214	-1.508
C	-0.097	1.213	-0.418
C	1.297	1.164	0.189
H	-0.670	2.081	-0.086
O	1.986	0.000	-0.225
H	1.257	1.214	1.288
H	-0.046	-1.214	-1.508
O	-2.044	0.000	-0.860
N	-0.919	0.000	-0.093
C	1.298	-1.164	0.189
C	-0.097	-1.213	-0.418
H	1.873	-2.023	-0.165
C	-1.329	0.000	1.339
H	-1.940	0.890	1.484
H	1.257	-1.214	1.288
H	-0.670	-2.081	-0.086
H	-0.477	0.000	2.020
H	-1.940	-0.890	1.484

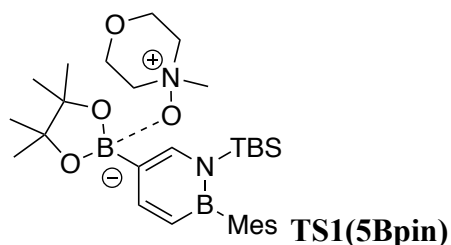


TS1(4Bpin)

H	1.809	-3.807	0.381
H	3.390	-3.075	0.670
C	2.367	-2.867	0.341
H	4.020	-4.589	-1.466
H	1.918	-2.178	1.064
H	1.459	-4.960	-1.747
C	4.004	-4.103	-2.448
H	-0.015	-3.102	-0.809
C	1.547	-4.453	-2.715
H	4.174	-4.880	-3.204
H	1.764	-5.222	-3.469
Si	2.405	-2.079	-1.370
H	4.849	-3.408	-2.498
C	2.664	-3.400	-2.716
C	-0.278	-2.133	-1.223
H	0.574	-4.015	-2.961
H	-2.342	-2.471	-0.955
H	4.740	-1.430	-1.183
C	-1.588	-1.778	-1.314
C	3.828	-0.860	-1.395

H	-1.631	-0.782	1.935
H	3.724	-0.104	-0.613
N	0.774	-1.319	-1.610
H	-0.934	0.040	0.515
H	1.739	0.737	0.290
H	-7.039	-1.990	-1.733
C	-1.396	0.184	1.490
C	2.702	-2.727	-4.092
H	-5.794	-2.008	-3.821
O	-4.511	-1.051	-1.790
C	-6.907	-0.915	-1.585
C	1.612	1.746	-0.121
H	2.904	-3.470	-4.875
H	-0.744	0.765	2.144
O	-3.506	0.046	0.515
H	3.952	-0.341	-2.347
C	-1.980	-0.498	-1.819
H	-6.789	-0.724	-0.517
H	2.106	2.453	0.550
B	0.474	-0.010	-2.165
H	3.482	-1.959	-4.152
H	0.535	1.954	-0.106
C	-5.765	-0.915	-3.810
H	1.743	-2.252	-4.322
B	-3.503	-0.108	-1.806
C	-5.685	-0.443	-2.359
N	-2.701	0.871	1.262
H	-3.445	0.202	3.103
H	-7.810	-0.407	-1.940
C	-1.001	0.360	-2.262
C	2.145	1.851	-1.531
H	-4.885	-0.591	-4.373
H	-1.940	1.965	-0.357
C	1.612	1.026	-2.546
H	-6.662	-0.538	-4.309
C	-3.395	1.149	2.563
C	-2.508	2.180	0.551
C	3.156	2.762	-1.821
H	3.564	3.380	-1.023
H	-1.722	1.931	3.721
H	-5.464	1.129	-0.074
H	-0.820	2.947	1.700
C	-5.387	1.093	-2.232
O	-3.946	1.133	-2.221
C	-2.715	2.247	3.369
H	-4.402	1.452	2.274
H	-1.319	1.331	-2.648
C	2.075	1.201	-3.858
C	-5.883	1.689	-0.915
C	-1.852	3.226	1.439
H	0.654	-0.200	-4.711
H	-3.515	2.491	0.271
H	-6.975	1.689	-0.864
C	3.662	2.898	-3.117

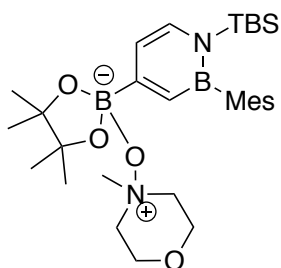
C	1.480	0.445	-5.024
H	2.228	-0.179	-5.523
C	3.102	2.117	-4.123
H	-3.326	2.472	4.246
H	5.460	3.973	-2.595
O	-2.613	3.438	2.614
C	-5.887	1.930	-3.401
H	-5.439	1.613	-4.343
H	-1.816	4.176	0.901
C	4.745	3.902	-3.419
H	-6.976	1.858	-3.486
H	-5.540	2.727	-0.852
H	3.464	2.225	-5.144
H	5.291	3.635	-4.327
H	1.091	1.144	-5.771
H	-5.628	2.979	-3.233
H	4.321	4.901	-3.570



H	-5.301	-2.839	0.525
H	-4.519	-1.667	1.610
H	-3.931	-3.337	1.533
C	-4.343	-2.513	0.944
H	-5.674	-0.350	-0.083
H	-2.868	2.701	2.496
H	-0.978	1.350	3.222
C	-4.690	0.057	-0.336
H	-4.174	0.383	0.569
C	-3.371	-2.145	-0.166
C	-2.273	3.134	1.691
C	-0.367	1.771	2.424
H	-5.468	-1.974	-2.107
H	-3.819	4.289	0.758
H	-3.860	-3.888	-1.392
O	-1.977	0.944	0.954
H	-1.722	4.009	2.049
H	-2.483	-4.095	-0.290
C	-3.134	3.483	0.488
C	-2.985	-3.393	-0.962
H	-3.706	2.598	0.191
H	-4.835	0.926	-0.986
C	-3.844	-0.971	-1.085
O	-2.164	-1.627	0.415
H	0.149	2.674	2.756
N	-1.277	2.079	1.292
C	-4.562	-1.411	-2.353
H	0.345	1.028	2.063

H	2.511	0.068	3.252
H	-4.855	-0.530	-2.931
B	-1.674	-0.653	-0.455
C	2.328	-1.000	3.096
H	-2.291	-3.137	-1.769
H	2.834	-1.538	3.904
H	-3.921	-2.034	-2.979
O	-2.597	-0.355	-1.454
H	0.382	-1.307	1.133
O	-2.343	3.948	-0.590
H	5.311	-1.720	2.287
C	-0.476	2.625	0.140
H	1.255	-1.182	3.202
H	5.083	-0.126	1.552
C	4.870	-1.191	1.435
C	-1.421	2.950	-0.999
C	0.760	-0.853	0.219
H	-1.946	2.037	-1.312
H	0.029	3.530	0.490
C	-0.143	-0.478	-0.737
H	0.256	1.867	-0.133
Si	3.033	-1.552	1.442
H	5.370	-1.529	0.522
N	2.125	-0.675	0.139
H	-0.853	3.356	-1.840
C	0.353	0.102	-1.947
H	-0.380	0.349	-2.716
C	2.758	-3.421	1.170
B	2.673	0.020	-1.015
C	3.636	2.274	0.621
C	1.683	0.371	-2.120
C	4.599	1.597	-0.327
C	4.183	0.490	-1.092
H	2.002	0.844	-3.048
H	6.217	2.920	0.174
C	5.910	2.066	-0.427
C	5.103	-0.102	-1.975
C	6.835	1.464	-1.279
C	4.679	-1.257	-2.850
C	6.412	0.378	-2.048
C	8.242	1.992	-1.398
H	7.119	-0.101	-2.724
H	3.362	1.613	1.454
H	2.704	2.541	0.113
H	4.069	3.183	1.044
H	8.326	2.697	-2.232
H	8.954	1.184	-1.581
H	8.546	2.519	-0.490
H	4.189	-2.042	-2.266
H	5.533	-1.699	-3.369
H	3.956	-0.929	-3.605
C	1.317	-3.865	1.467
C	3.700	-4.183	2.119
C	3.103	-3.792	-0.278

H	2.449	-3.277	-0.992
H	2.981	-4.872	-0.431
H	4.142	-3.541	-0.522
H	3.514	-3.932	3.170
H	4.753	-3.979	1.901
H	3.543	-5.263	2.008
H	0.998	-3.578	2.476
H	1.251	-4.959	1.402
H	0.598	-3.454	0.753

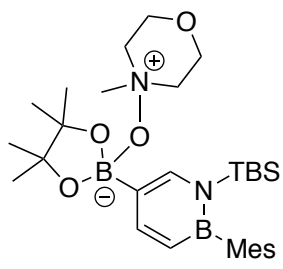


INT(4Bpin)

C	1.095	-0.504	-0.172
C	0.167	0.284	0.475
H	0.541	0.997	1.214
B	-1.317	0.183	0.170
C	-2.370	1.190	0.797
C	-2.835	1.090	2.118
C	-2.354	0.002	3.052
H	-2.044	0.429	4.011
H	-1.503	-0.540	2.633
H	-3.146	-0.724	3.263
C	-3.762	2.018	2.607
H	-4.121	1.919	3.631
C	-4.224	3.073	1.825
C	-5.250	4.043	2.355
H	-5.145	4.180	3.434
H	-6.266	3.678	2.168
H	-5.158	5.019	1.873
C	-3.711	3.204	0.532
H	-4.030	4.043	-0.084
C	-2.800	2.285	0.017
C	-2.278	2.466	-1.390
H	-1.185	2.397	-1.416
H	-2.572	3.435	-1.801
H	-2.653	1.686	-2.064
N	-1.710	-0.818	-0.814
Si	-3.388	-1.363	-1.225
C	-3.704	-3.010	-0.319
C	-3.593	-2.784	1.193
H	-4.298	-2.021	1.543
H	-3.813	-3.714	1.734
H	-2.583	-2.466	1.472
C	-5.125	-3.486	-0.662
H	-5.887	-2.783	-0.312
H	-5.321	-4.451	-0.178
H	-5.260	-3.626	-1.741

C	-2.708	-4.104	-0.729
H	-2.965	-5.044	-0.224
H	-1.682	-3.849	-0.446
H	-2.728	-4.296	-1.808
C	-4.735	-0.143	-0.764
H	-4.806	0.047	0.309
H	-5.683	-0.570	-1.108
H	-4.605	0.819	-1.263
C	-3.455	-1.595	-3.093
H	-4.497	-1.719	-3.404
H	-3.061	-0.707	-3.598
H	-2.898	-2.464	-3.454
C	-0.720	-1.563	-1.422
H	-1.046	-2.289	-2.164
B	2.684	-0.413	0.149
O	2.965	-0.448	1.565
C	4.134	-1.238	1.756
C	4.077	-1.875	3.138
H	4.172	-1.102	3.906
H	3.127	-2.392	3.290
H	4.894	-2.592	3.274
C	5.373	-0.343	1.650
H	5.261	0.489	2.351
H	6.290	-0.888	1.899
H	5.463	0.070	0.642
C	4.042	-2.252	0.574
C	3.064	-3.392	0.873
H	3.462	-4.093	1.614
H	2.114	-2.991	1.238
H	2.872	-3.940	-0.054
C	5.382	-2.821	0.124
H	5.876	-3.354	0.943
H	6.046	-2.028	-0.228
H	5.227	-3.528	-0.697
O	3.248	1.007	-0.274
N	3.204	1.464	-1.591
C	4.320	2.469	-1.688
C	4.051	3.628	-0.742
H	4.059	3.270	0.294
H	4.834	4.377	-0.870
O	2.819	4.248	-1.052
C	1.746	3.337	-0.905
H	1.684	2.964	0.125
H	0.827	3.877	-1.145
H	5.236	1.935	-1.433
H	4.353	2.814	-2.724
C	1.900	2.170	-1.863
H	1.108	1.431	-1.740
H	1.943	2.519	-2.898
C	3.421	0.375	-2.585
H	4.330	-0.152	-2.305
H	2.574	-0.306	-2.534
H	3.495	0.833	-3.572
O	3.493	-1.458	-0.471

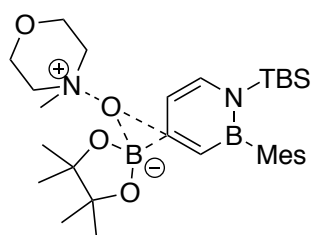
C	0.608	-1.439	-1.140
H	1.311	-2.086	-1.657



INT(5Bpin)

H	7.857	2.219	-1.731
H	8.177	0.667	-0.961
H	5.875	2.317	-0.056
C	7.629	1.151	-1.776
H	3.842	2.856	0.991
C	5.388	1.584	-0.698
H	8.019	0.757	-2.718
C	3.237	2.084	0.509
C	6.147	0.902	-1.652
H	2.886	1.397	1.288
C	4.022	1.346	-0.551
H	2.346	2.558	0.082
H	2.058	-0.370	2.738
H	4.339	-0.943	0.757
C	5.497	-0.018	-2.473
H	4.329	-2.616	1.344
H	2.029	-2.053	3.282
C	1.626	-1.356	2.540
C	3.912	-1.934	0.596
H	-1.132	2.590	2.069
H	-0.590	3.964	0.073
C	3.376	0.401	-1.368
H	6.068	-0.549	-3.233
O	-2.522	4.320	0.596
C	4.129	-0.269	-2.346
C	-1.537	3.422	0.118
C	-1.385	2.245	1.063
H	0.544	-1.293	2.697
H	4.229	-2.277	-0.393
Si	2.050	-1.938	0.803
H	-3.469	2.846	2.630
H	-0.644	1.528	0.711
B	1.814	0.165	-1.242
H	-2.359	0.865	3.152
H	2.767	-4.559	2.010
N	1.226	-0.807	-0.344
C	-3.783	3.685	0.660
C	-3.746	2.513	1.627
H	-4.500	4.421	1.029
C	0.836	0.994	-2.072
C	-2.599	0.420	2.186
H	1.183	1.732	-2.795

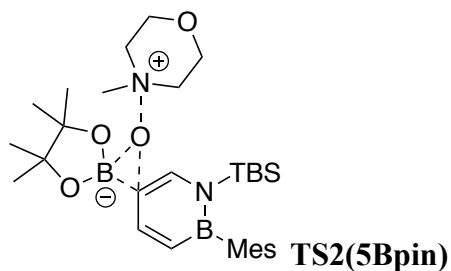
H	-1.792	3.062	-0.886
N	-2.704	1.518	1.185
C	3.458	-1.276	-3.250
C	2.472	-4.704	0.964
H	3.369	-4.617	0.344
H	-1.816	-0.261	1.858
C	-0.155	-0.895	-0.273
H	0.327	-3.884	2.452
C	1.373	-3.714	0.533
H	4.161	-1.701	-3.970
C	-0.509	0.806	-1.917
H	3.026	-2.099	-2.668
H	-4.693	1.973	1.650
H	-4.098	3.340	-0.331
H	-0.556	-1.629	0.422
H	-3.552	-0.104	2.202
H	2.631	-0.817	-3.802
C	-1.042	-0.141	-0.983
C	0.129	-4.023	1.384
O	-3.160	1.060	-0.051
H	2.099	-5.732	0.868
H	-1.227	1.382	-2.506
H	-0.741	-3.412	1.122
H	1.936	-3.804	-1.580
C	1.053	-3.955	-0.949
B	-2.620	-0.285	-0.715
H	-0.160	-5.072	1.236
O	-2.987	-1.431	0.114
H	0.261	-3.291	-1.310
H	0.718	-4.991	-1.097
O	-3.415	-0.362	-1.919
H	-5.401	-0.214	-0.067
C	-3.774	-2.301	-0.693
H	-2.241	-3.813	-0.677
H	-2.157	-2.720	-2.073
C	-2.839	-3.272	-1.418
H	-4.175	-3.735	0.860
H	-5.332	-2.394	0.813
C	-4.454	-1.308	-1.688
C	-5.658	-0.600	-1.056
C	-4.739	-3.072	0.197
H	-5.937	0.246	-1.691
H	-6.519	-1.270	-0.969
H	-3.391	-4.005	-2.015
C	-4.861	-1.924	-3.020
H	-5.418	-3.688	-0.403
H	-3.988	-2.297	-3.559
H	-5.350	-1.168	-3.641
H	-5.565	-2.750	-2.872



TS2(4Bpin)

H	-2.412	-4.837	2.562
H	-3.668	-3.658	2.980
C	-2.828	-3.858	2.306
H	7.383	-1.077	0.889
H	4.503	-1.921	2.720
H	2.060	-2.393	3.036
H	-5.029	-5.099	1.302
H	-3.603	-5.979	0.718
H	-2.055	-3.105	2.471
C	-4.191	-5.064	0.600
H	0.883	-1.650	1.940
C	6.743	-1.924	1.155
C	1.881	-1.542	2.372
C	4.277	-1.699	1.677
C	-3.286	-3.858	0.854
H	-5.755	-2.610	1.577
H	7.146	-2.805	0.644
H	6.826	-2.089	2.231
C	5.313	-1.669	0.749
C	2.947	-1.467	1.302
H	-3.621	-1.226	2.114
H	1.879	-0.641	2.994
H	-4.597	-5.039	-0.417
O	-2.143	-3.970	0.002
H	-0.909	-7.257	-1.696
C	-5.462	-2.474	0.531
C	-3.948	-2.519	0.383
C	-3.327	-1.294	1.063
H	-3.001	-5.845	-1.640
H	-5.943	-3.247	-0.071
H	-2.234	-1.322	1.004
C	-0.966	-6.289	-2.200
H	0.441	-3.127	-0.391
H	-0.582	-5.508	-1.530
C	4.989	-1.415	-0.588
C	-2.413	-5.979	-2.548
C	2.634	-1.169	-0.033
H	-5.833	-1.500	0.197
B	-2.319	-3.091	-1.113
H	1.552	1.688	2.410
H	-2.843	-6.798	-3.144
C	0.203	-2.120	-0.734
H	-3.672	-0.394	0.544
O	-3.613	-2.489	-1.005
C	3.678	-1.170	-0.983
C	0.507	1.793	2.097
H	5.783	-1.417	-1.334

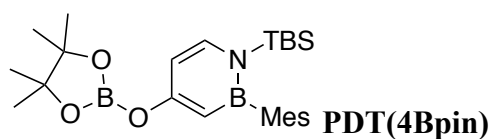
H	-0.052	2.217	2.943
B	1.156	-0.943	-0.547
H	3.378	1.312	0.826
O	-0.178	-6.381	-3.373
H	0.107	0.790	1.904
C	-1.019	-1.910	-1.313
H	-4.424	-4.240	-2.742
O	-1.757	-3.371	-2.371
N	-2.487	-4.740	-3.333
C	3.194	1.898	-0.078
C	-3.849	-4.339	-3.664
H	1.962	4.059	1.516
C	-0.182	-5.146	-4.065
N	0.671	0.355	-0.978
H	3.822	1.488	-0.871
C	3.385	-0.903	-2.442
H	-4.317	-5.080	-4.325
H	0.227	-4.350	-3.428
C	0.368	2.693	0.864
C	-1.376	-0.624	-1.817
H	3.517	2.929	0.103
C	0.917	4.092	1.188
C	-1.595	-4.776	-4.496
Si	1.388	1.966	-0.571
H	0.334	4.543	2.002
H	2.523	-1.482	-2.788
H	4.243	-1.158	-3.069
C	-0.549	0.438	-1.621
H	-1.977	-5.517	-5.214
H	-3.814	-3.369	-4.163
H	0.450	-5.267	-4.947
H	3.145	0.153	-2.620
C	-1.122	2.819	0.517
H	-2.332	-0.480	-2.310
H	-1.652	3.304	1.347
H	-1.586	1.841	0.355
H	-1.611	-3.787	-4.961
H	0.853	4.765	0.325
H	-0.849	1.421	-1.976
C	1.250	3.048	-2.106
H	-1.288	3.430	-0.378
H	1.564	2.494	-2.996
H	1.918	3.909	-1.998
H	0.243	3.433	-2.285



O	-3.692	-2.502	-5.381
---	--------	--------	--------

H	-5.241	-3.168	-4.254
C	-4.472	-2.395	-4.203
H	-3.854	-2.556	-3.309
H	-2.086	-1.670	-6.296
C	-2.655	-1.539	-5.373
H	-1.994	-1.700	-4.511
C	-5.125	-1.027	-4.113
C	-3.223	-0.127	-5.319
H	-5.817	-0.884	-4.957
H	-5.673	-0.933	-3.175
H	-3.799	0.082	-6.233
N	-4.104	0.025	-4.157
H	-2.418	0.607	-5.228
O	-2.907	-0.222	-2.775
C	-4.641	1.371	-4.014
H	-5.308	1.612	-4.853
H	-5.182	1.438	-3.070
H	-3.809	2.077	-3.991
H	-2.835	-0.236	1.254
H	-1.191	2.832	0.698
H	-4.070	0.315	2.410
H	-0.230	3.413	-1.951
C	-3.583	0.537	1.455
H	-3.065	1.496	1.545
H	-4.368	-1.953	1.544
C	-0.456	2.496	1.441
H	2.195	-1.001	3.267
H	-0.676	3.020	2.381
H	0.919	-0.758	2.058
C	0.769	2.993	-2.101
H	0.429	4.721	0.116
H	1.459	3.831	-2.243
C	1.795	-1.362	2.315
H	-0.620	1.425	1.606
H	0.756	2.406	-3.025
H	1.438	-2.386	2.475
C	-5.344	-1.723	1.112
C	1.156	4.306	0.820
H	1.014	4.811	1.784
C	-4.601	0.638	0.315
H	-5.986	-1.303	1.894
H	-5.794	-2.658	0.766
C	0.982	2.788	0.998
O	-4.262	-1.283	-0.990
B	-3.424	-0.211	-1.453
C	-1.298	-1.870	-1.094
C	-5.210	-0.757	-0.059
C	-1.746	-0.527	-1.277
H	-2.034	-2.662	-1.233
Si	1.377	1.940	-0.663
C	-0.010	-2.130	-0.722
O	-3.918	1.009	-0.882
C	-0.860	0.509	-1.150
H	-6.244	1.405	1.506

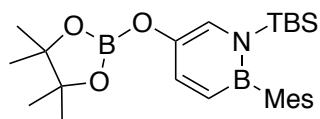
B	0.969	-0.978	-0.539
H	-5.116	2.638	0.916
C	-5.630	1.709	0.652
C	2.844	-1.339	1.226
H	0.290	-3.166	-0.568
N	0.460	0.367	-0.787
H	2.160	4.564	0.462
H	-1.217	1.517	-1.350
H	4.465	-1.568	2.621
C	1.957	2.311	2.085
C	4.189	-1.500	1.570
H	1.690	2.761	3.050
C	2.475	-1.223	-0.124
H	1.939	1.224	2.207
C	-6.563	-0.623	-0.759
C	3.236	1.777	-0.826
H	-6.286	1.912	-0.197
H	3.637	2.796	-0.757
H	-6.829	-1.585	-1.207
H	-7.352	-0.339	-0.057
H	3.540	1.368	-1.792
H	2.987	2.602	1.855
C	5.183	-1.590	0.597
C	3.467	-1.370	-1.113
H	-6.524	0.133	-1.550
H	6.748	-2.265	1.924
H	3.688	1.175	-0.036
C	6.635	-1.722	0.982
C	4.799	-1.546	-0.745
H	2.450	-2.192	-2.831
H	7.203	-2.249	0.210
C	3.083	-1.335	-2.574
H	2.506	-0.436	-2.817
H	7.096	-0.737	1.114
H	5.558	-1.645	-1.519
H	3.965	-1.359	-3.219



C	-1.397	-2.478	0.357
H	-2.036	-3.342	0.489
C	-0.046	-2.621	0.327
H	0.379	-3.616	0.432
N	0.840	-1.576	0.167
B	0.299	-0.227	0.056
C	-1.210	-0.070	0.070
H	-1.689	0.898	-0.020
C	1.248	1.041	0.029
C	1.798	1.494	1.250
C	1.470	0.777	2.540
H	1.909	1.290	3.400

H	0.387	0.716	2.691
H	1.843	-0.254	2.536
C	2.642	2.599	1.273
H	3.060	2.933	2.222
C	2.965	3.294	0.102
C	3.905	4.472	0.147
H	4.900	4.166	0.485
H	3.548	5.234	0.846
H	4.010	4.934	-0.837
C	2.384	2.872	-1.088
H	2.594	3.419	-2.006
C	1.519	1.770	-1.136
C	0.881	1.430	-2.465
H	0.163	0.612	-2.374
H	0.348	2.299	-2.863
H	1.632	1.144	-3.208
Si	2.570	-2.094	-0.022
C	2.874	-3.442	1.259
H	2.493	-3.133	2.237
H	3.953	-3.601	1.357
H	2.422	-4.406	1.008
C	3.826	-0.736	0.282
H	3.751	-0.332	1.294
H	4.816	-1.193	0.180
H	3.751	0.099	-0.418
C	2.780	-2.774	-1.786
C	4.221	-3.283	-1.945
H	4.455	-4.079	-1.228
H	4.955	-2.481	-1.815
H	4.360	-3.696	-2.953
C	1.813	-3.931	-2.074
H	1.943	-4.763	-1.372
H	0.768	-3.608	-2.030
H	1.994	-4.324	-3.083
C	2.519	-1.653	-2.799
H	3.187	-0.798	-2.647
H	1.487	-1.292	-2.728
H	2.676	-2.019	-3.822
C	-1.986	-1.186	0.217
O	-3.356	-1.217	0.265
B	-4.227	-0.170	0.160
O	-5.570	-0.405	0.312
C	-6.244	0.805	-0.106
C	-7.501	0.984	0.729
H	-7.276	0.954	1.797
H	-7.979	1.940	0.497
H	-8.208	0.183	0.502
C	-5.145	1.892	0.126
C	-5.100	2.391	1.567
H	-5.082	1.555	2.272
H	-5.963	3.022	1.795
H	-4.191	2.980	1.708
C	-5.187	3.060	-0.843
H	-4.382	3.760	-0.608

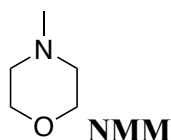
H	-6.140	3.590	-0.755
H	-5.064	2.725	-1.875
C	-6.601	0.634	-1.580
H	-7.209	-0.267	-1.693
H	-7.170	1.489	-1.954
H	-5.699	0.521	-2.190
O	-3.924	1.141	-0.097



PDT(5Bpin)

C	-2.091	-0.926	-1.403
H	-3.121	-0.797	-1.731
C	-1.673	-2.239	-1.054
O	-2.543	-3.309	-1.172
B	-3.718	-3.322	-0.480
O	-4.588	-4.375	-0.580
C	-5.809	-3.948	0.071
C	-6.462	-5.150	0.731
H	-5.767	-5.666	1.395
H	-7.338	-4.838	1.308
H	-6.793	-5.854	-0.037
C	-5.290	-2.856	1.065
C	-4.771	-3.448	2.373
H	-4.082	-4.276	2.181
H	-5.592	-3.813	2.996
H	-4.235	-2.671	2.922
C	-6.269	-1.728	1.340
H	-5.824	-1.020	2.044
H	-7.187	-2.122	1.786
H	-6.524	-1.191	0.425
C	-6.715	-3.370	-1.013
H	-6.874	-4.129	-1.783
H	-7.686	-3.079	-0.603
H	-6.256	-2.494	-1.481
O	-4.143	-2.322	0.358
C	-0.397	-2.490	-0.653
H	-0.125	-3.512	-0.409
N	0.568	-1.508	-0.542
Si	2.222	-2.162	-0.155
C	1.989	-3.423	1.223
H	1.369	-3.002	2.021
H	2.965	-3.667	1.654
H	1.530	-4.360	0.896
C	3.435	-0.871	0.456
H	3.092	-0.395	1.377
H	4.368	-1.397	0.683
H	3.646	-0.082	-0.269
C	2.905	-2.981	-1.731
C	4.277	-3.591	-1.402
H	4.208	-4.344	-0.609
H	5.000	-2.830	-1.089

H	4.687	-4.086	-2.292
C	1.987	-4.095	-2.253
H	1.822	-4.879	-1.505
H	1.012	-3.708	-2.564
H	2.448	-4.571	-3.129
C	3.067	-1.922	-2.828
H	3.727	-1.105	-2.514
H	2.099	-1.489	-3.104
H	3.500	-2.373	-3.731
B	0.215	-0.131	-0.826
C	1.208	1.073	-0.557
C	1.355	1.535	0.771
C	0.589	0.873	1.894
H	0.738	1.400	2.839
H	-0.484	0.849	1.678
H	0.902	-0.169	2.037
C	2.204	2.599	1.053
H	2.309	2.942	2.081
C	2.927	3.243	0.042
C	3.858	4.382	0.374
H	3.334	5.172	0.920
H	4.683	4.043	1.009
H	4.286	4.820	-0.530
C	2.747	2.810	-1.267
H	3.276	3.317	-2.073
C	1.888	1.748	-1.579
C	1.721	1.374	-3.034
H	0.926	0.637	-3.176
H	1.471	2.257	-3.631
H	2.644	0.956	-3.447
C	-1.213	0.115	-1.306
H	-1.567	1.110	-1.568



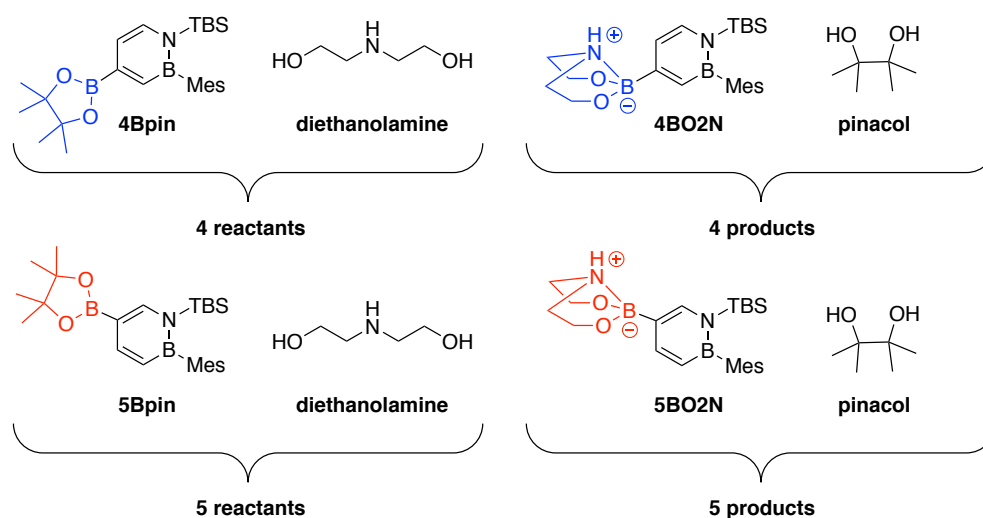
H	-1.969	0.198	1.166
H	0.384	0.619	1.037
H	-2.425	4.386	0.758
H	-0.681	4.698	0.660
N	-1.239	2.696	0.419
C	-1.503	4.113	0.238
H	-3.260	2.155	0.416
C	-2.033	0.415	0.089
C	0.254	0.824	-0.037
H	0.831	2.887	0.188
C	-2.336	1.892	-0.110
C	0.004	2.310	-0.240
H	-2.819	-0.203	-0.351
O	-0.820	0.055	-0.548
H	1.154	0.507	-0.570
H	-1.612	4.387	-0.827

H -2.489 2.087 -1.189
H -0.036 2.525 -1.325

Diethanolamine Transesterification

All structures for the transesterification reaction were optimized at the M062X/6-31G(d,p) level and computed using the polarized continuum model simulating THF. The coordinates are reproduced here.

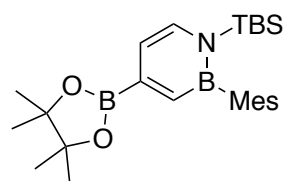
Table 2.6. Gibbs free energies for diethanolamine transesterification reaction of **4Bpin** and **5Bpin**.



Structure	Gibbs Free Energy (Hartree)
4Bpin	-1520.9036
diethanolamine	-363.937278
4 reactants	-1884.840878
4BO2N	-1497.654746
pinacol	-387.195773
4 products	-1884.850519
5Bpin	-1520.908741
5 reactants	-1884.846019
5BO2N	-1497.658469
5 products	-1884.854242

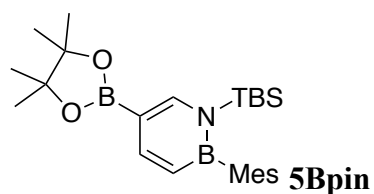
4 reactants – products = -6.05 kcal mol⁻¹ 5 reactants – products = -5.16 kcal mol⁻¹ 4 products favored by 0.89 kcal mol⁻¹

Figure 2.17. Reaction coordinates for optimized geometries for diethanolamine transesterification.



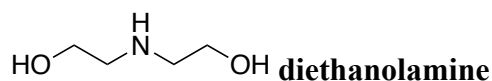
	4Bpin		
B	-3.462	-0.298	0.013
O	-4.420	-1.267	0.166
C	-5.690	-0.659	-0.173
C	-6.778	-1.263	0.698
H	-6.526	-1.191	1.758
H	-7.730	-0.752	0.526
H	-6.906	-2.319	0.445
C	-5.408	0.857	0.088
C	-5.613	1.253	1.548
H	-5.091	0.563	2.217
H	-6.674	1.262	1.811
H	-5.206	2.255	1.701
C	-6.150	1.810	-0.833
H	-5.891	2.841	-0.578
H	-7.231	1.689	-0.712
H	-5.891	1.638	-1.878
C	-5.949	-0.969	-1.645
H	-5.929	-2.053	-1.785
H	-6.924	-0.594	-1.965
H	-5.176	-0.525	-2.279
C	-1.928	-0.601	0.049
C	-1.483	-1.950	0.215
H	-2.206	-2.751	0.328
C	-0.157	-2.256	0.231
H	0.151	-3.291	0.356
N	0.852	-1.321	0.100
B	0.500	0.081	-0.020
C	1.583	1.236	0.013
C	2.118	1.617	1.265
C	1.680	0.905	2.525
H	2.109	1.374	3.413
H	0.590	0.914	2.625
H	1.986	-0.148	2.519
C	3.051	2.644	1.346
H	3.456	2.924	2.317
C	3.482	3.330	0.204
C	4.494	4.442	0.317
H	4.075	5.301	0.852
H	5.378	4.115	0.873
H	4.818	4.785	-0.668
C	2.927	2.975	-1.019
H	3.230	3.513	-1.917
C	1.976	1.951	-1.127
C	1.400	1.655	-2.493
H	0.541	0.981	-2.434

H	1.071	2.577	-2.981
H	2.146	1.192	-3.147
Si	2.510	-2.056	-0.030
C	2.631	-3.368	1.314
H	2.252	-2.978	2.264
H	3.681	-3.637	1.461
H	2.084	-4.287	1.085
C	3.913	-0.840	0.229
H	3.879	-0.381	1.219
H	4.845	-1.412	0.161
H	3.942	-0.038	-0.512
C	2.662	-2.837	-1.761
C	4.027	-3.537	-1.853
H	4.130	-4.329	-1.103
H	4.858	-2.835	-1.724
H	4.142	-4.001	-2.841
C	1.561	-3.871	-2.035
H	1.559	-4.678	-1.293
H	0.566	-3.415	-2.046
H	1.725	-4.330	-3.018
C	2.577	-1.736	-2.826
H	3.360	-0.980	-2.697
H	1.607	-1.228	-2.792
H	2.693	-2.168	-3.828
C	-0.993	0.399	-0.066
H	-1.354	1.421	-0.179
O	-3.987	0.953	-0.178

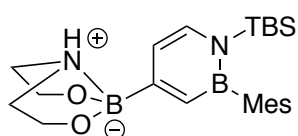


B	-3.461	-0.300	0.010
O	-4.421	-1.266	0.163
C	-5.690	-0.655	-0.174
C	-6.778	-1.253	0.702
H	-6.516	-1.188	1.759
H	-7.726	-0.731	0.541
H	-6.920	-2.306	0.445
C	-5.403	0.859	0.086
C	-5.605	1.254	1.547
H	-5.088	0.560	2.215
H	-6.666	1.267	1.809
H	-5.193	2.254	1.705
C	-6.146	1.815	-0.832
H	-5.887	2.844	-0.573
H	-7.227	1.694	-0.713
H	-5.887	1.646	-1.879
C	-5.957	-0.966	-1.644
H	-5.932	-2.050	-1.785
H	-6.936	-0.597	-1.958

H	-5.191	-0.517	-2.283
C	-1.927	-0.604	0.042
C	-1.483	-1.953	0.210
H	-2.206	-2.754	0.322
C	-0.155	-2.259	0.231
H	0.152	-3.293	0.358
N	0.854	-1.324	0.098
B	0.500	0.078	-0.026
C	1.582	1.234	0.007
C	2.119	1.609	1.260
C	1.687	0.890	2.517
H	2.109	1.361	3.407
H	0.596	0.880	2.618
H	2.007	-0.159	2.510
C	3.048	2.639	1.342
H	3.450	2.921	2.313
C	3.468	3.335	0.203
C	4.475	4.452	0.316
H	4.060	5.303	0.866
H	5.368	4.123	0.857
H	4.786	4.806	-0.669
C	2.914	2.981	-1.021
H	3.213	3.525	-1.917
C	1.971	1.953	-1.132
C	1.395	1.658	-2.499
H	0.525	1.000	-2.442
H	1.085	2.586	-2.992
H	2.136	1.181	-3.150
Si	2.513	-2.059	-0.026
C	2.627	-3.372	1.317
H	2.255	-2.982	2.270
H	3.677	-3.650	1.460
H	2.074	-4.287	1.087
C	3.918	-0.846	0.235
H	3.883	-0.385	1.223
H	4.848	-1.421	0.171
H	3.952	-0.045	-0.506
C	2.667	-2.837	-1.756
C	4.033	-3.537	-1.847
H	4.133	-4.329	-1.096
H	4.864	-2.835	-1.715
H	4.150	-4.003	-2.834
C	1.568	-3.872	-2.033
H	1.565	-4.680	-1.293
H	0.572	-3.420	-2.049
H	1.735	-4.332	-3.016
C	2.583	-1.735	-2.819
H	3.361	-0.975	-2.685
H	1.610	-1.232	-2.789
H	2.706	-2.164	-3.822
C	-0.991	0.396	-0.071
H	-1.353	1.419	-0.179
O	-3.983	0.952	-0.182

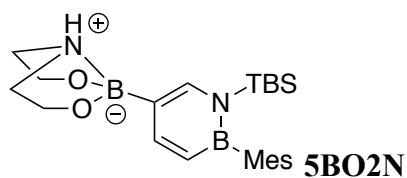


H	0.217	0.279	0.876
H	-1.506	-1.277	1.677
H	1.507	-4.178	2.197
H	0.029	-5.789	2.929
H	-0.880	-3.506	2.357
O	-1.539	0.847	0.045
C	-0.515	-0.122	0.170
C	-1.048	-1.448	0.696
C	0.755	-4.640	1.545
C	-0.420	-3.686	1.376
N	0.036	-2.407	0.849
O	0.344	-5.906	2.025
H	-2.149	0.544	-0.638
H	0.003	-0.281	-0.788
H	1.228	-4.819	0.573
H	0.455	-2.569	-0.065
H	-1.851	-1.810	0.027
H	-1.187	-4.170	0.746



H	1.435	1.442	3.373
H	0.010	0.997	2.414
H	1.692	-2.957	2.326
H	-3.650	1.875	1.377
C	1.104	0.963	2.448
H	-3.953	-0.340	1.673
H	-5.731	-1.597	1.416
H	1.381	-0.097	2.499
C	2.118	-3.371	1.406
N	-4.517	0.041	0.917
H	1.541	-4.260	1.137
C	-4.620	1.512	1.029
C	-5.802	-0.704	0.795
H	3.139	-3.696	1.631
H	-2.564	-2.665	-0.166
H	2.936	2.941	2.418
C	-1.818	-1.876	-0.191
H	-0.245	-3.247	0.187
H	-6.476	-2.009	-0.824
C	-0.513	-2.208	0.007
H	-4.576	3.002	-0.554
C	1.704	1.639	1.237
H	-5.400	1.816	1.730
C	-4.857	1.953	-0.414
H	-6.639	-0.094	1.144
C	-5.895	-1.092	-0.693

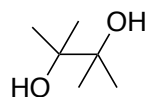
H	3.407	-0.411	1.478
C	-2.223	-0.526	-0.447
C	2.641	2.652	1.410
B	-3.781	-0.186	-0.617
N	0.526	-1.296	-0.006
Si	2.170	-2.055	0.061
B	0.211	0.109	-0.207
C	-1.252	0.447	-0.459
H	-5.924	1.857	-0.671
C	3.555	-0.868	0.497
H	-6.379	-0.292	-1.270
C	1.308	1.246	-0.063
O	-4.056	1.117	-1.206
O	-4.568	-1.291	-1.105
H	-1.576	1.470	-0.654
H	4.476	-1.459	0.542
H	1.403	-4.691	-1.278
C	3.212	3.313	0.317
H	3.950	-4.287	-0.833
H	3.807	5.237	1.093
H	5.091	4.031	1.099
C	4.233	4.401	0.529
C	1.468	-3.887	-2.020
H	3.691	-0.064	-0.229
C	2.518	-2.833	-1.642
H	0.472	-3.447	-2.135
C	3.899	-3.506	-1.600
C	1.838	1.941	-1.159
C	2.790	2.950	-0.957
H	4.700	-2.785	-1.407
H	1.738	-4.348	-2.979
H	4.601	4.790	-0.423
C	2.517	-1.733	-2.709
H	4.111	-3.980	-2.567
H	0.539	0.982	-2.606
C	1.407	1.646	-2.577
H	1.538	-1.245	-2.774
H	3.266	-0.960	-2.499
H	3.201	3.470	-1.821
H	1.142	2.571	-3.099
H	2.212	1.173	-3.149
H	2.745	-2.158	-3.696



B	-3.205	-3.033	-1.578
N	-4.105	-3.431	-0.157
H	-3.648	-3.089	0.683
C	-4.136	-4.919	-0.165
H	-3.433	-5.270	0.592

H	-5.134	-5.293	0.073
C	-3.639	-5.313	-1.566
H	-3.182	-6.307	-1.555
H	-4.472	-5.330	-2.283
C	-5.402	-2.749	-0.359
H	-6.211	-3.240	0.187
H	-5.288	-1.724	0.001
C	-5.571	-2.752	-1.878
H	-6.262	-1.964	-2.195
H	-5.988	-3.714	-2.217
C	-2.056	-1.965	-1.293
C	-0.800	-2.392	-0.957
N	0.277	-1.574	-0.676
Si	1.844	-2.477	-0.606
C	1.636	-3.890	0.619
H	1.469	-3.491	1.624
H	2.554	-4.486	0.649
H	0.811	-4.564	0.380
C	3.295	-1.440	-0.030
H	3.126	-1.002	0.956
H	4.159	-2.110	0.041
H	3.542	-0.626	-0.717
C	2.195	-3.121	-2.368
C	3.665	-3.566	-2.438
H	3.895	-4.345	-1.701
H	4.353	-2.731	-2.274
H	3.880	-3.982	-3.431
C	1.310	-4.316	-2.754
H	1.420	-5.149	-2.050
H	0.249	-4.052	-2.805
H	1.603	-4.684	-3.747
C	1.969	-1.984	-3.374
H	2.585	-1.108	-3.141
H	0.920	-1.665	-3.387
H	2.234	-2.316	-4.387
B	0.083	-0.134	-0.675
C	1.225	0.876	-0.237
C	1.509	1.035	1.139
C	0.772	0.206	2.165
H	1.011	0.528	3.181
H	1.031	-0.857	2.080
H	-0.312	0.276	2.025
C	2.478	1.942	1.556
H	2.686	2.050	2.620
C	3.193	2.719	0.638
C	4.250	3.683	1.114
H	3.828	4.422	1.802
H	5.047	3.160	1.651
H	4.702	4.220	0.277
C	2.892	2.578	-0.711
H	3.427	3.183	-1.442
C	1.912	1.680	-1.156
C	1.629	1.617	-2.641
H	0.890	0.850	-2.883

H	1.246	2.577	-3.002
H	2.541	1.401	-3.207
C	-1.307	0.355	-1.053
H	-1.547	1.416	-1.107
H	-0.620	-3.463	-0.913
C	-2.285	-0.554	-1.352
H	-3.284	-0.231	-1.651
O	-2.686	-4.341	-1.907
O	-4.291	-2.521	-2.401



pinacol

H	-2.588	0.747	1.820
O	-3.498	0.604	1.519
H	-2.947	-1.784	2.111
O	-1.091	-0.346	0.869
C	-2.566	-2.152	1.155
H	-0.643	0.200	0.211
C	-3.371	0.070	0.205
H	-2.082	1.664	-0.552
H	-1.664	-2.742	1.335
C	-2.217	-0.982	0.241
C	-3.059	1.216	-0.764
H	-3.813	1.995	-0.634
H	-3.319	-2.797	0.698
C	-4.724	-0.542	-0.138
H	-5.021	-1.275	0.615
H	-5.480	0.248	-0.158
C	-1.813	-1.486	-1.141
H	-3.075	0.890	-1.807
H	-1.030	-2.242	-1.037
H	-1.425	-0.675	-1.766
H	-4.708	-1.024	-1.119
H	-2.660	-1.939	-1.663

2.8.5 NMR Spectra

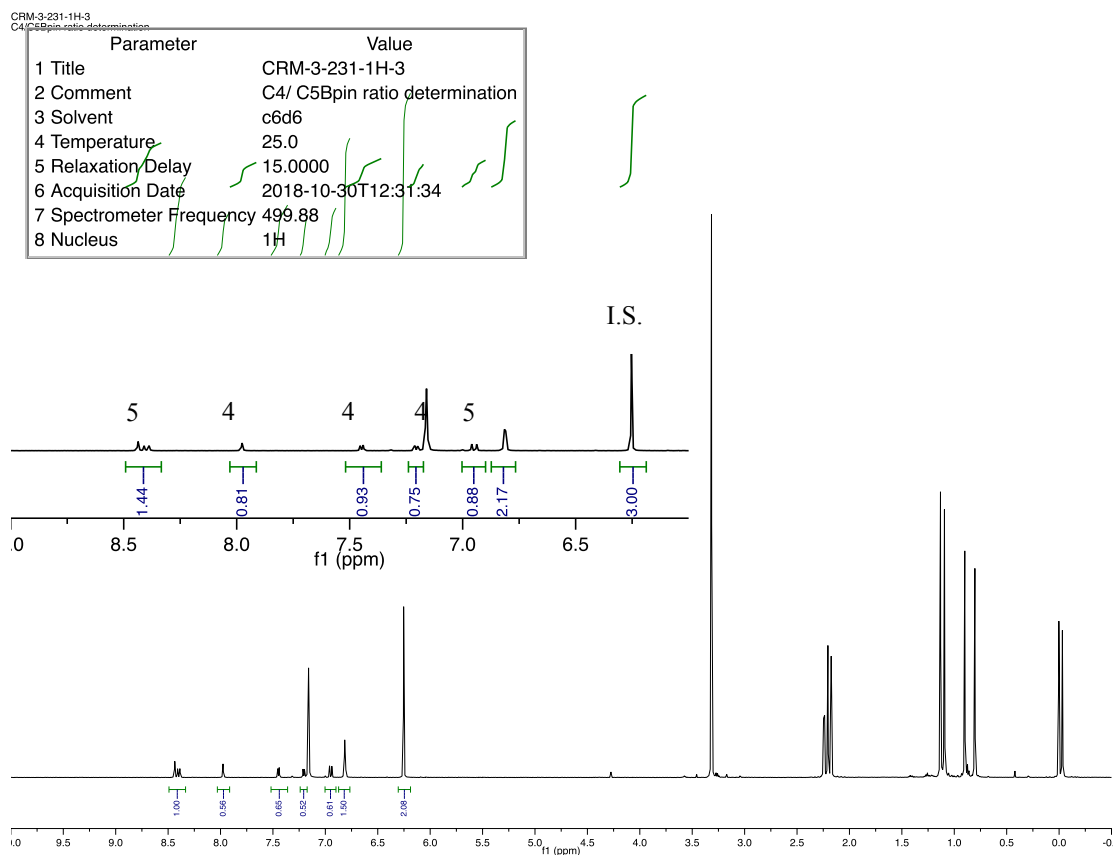


Figure 2.18. ¹H NMR of mixture of **5pin** and **4Bpin** in C₆D₆ with 1,3,5-trimethoxybenzene as internal standard.

CRM-3-177-1H-3
C5Bpin pure

Parameter	Value
1 Title	CRM-3-177-1H-3
2 Comment	C5Bpin pure
3 Solvent	c6d6
4 Temperature	25.0
5 Relaxation Delay	1.0000
6 Acquisition Date	2018-07-05T10:05:26
7 Spectrometer Frequency	499.88
8 Nucleus	1H

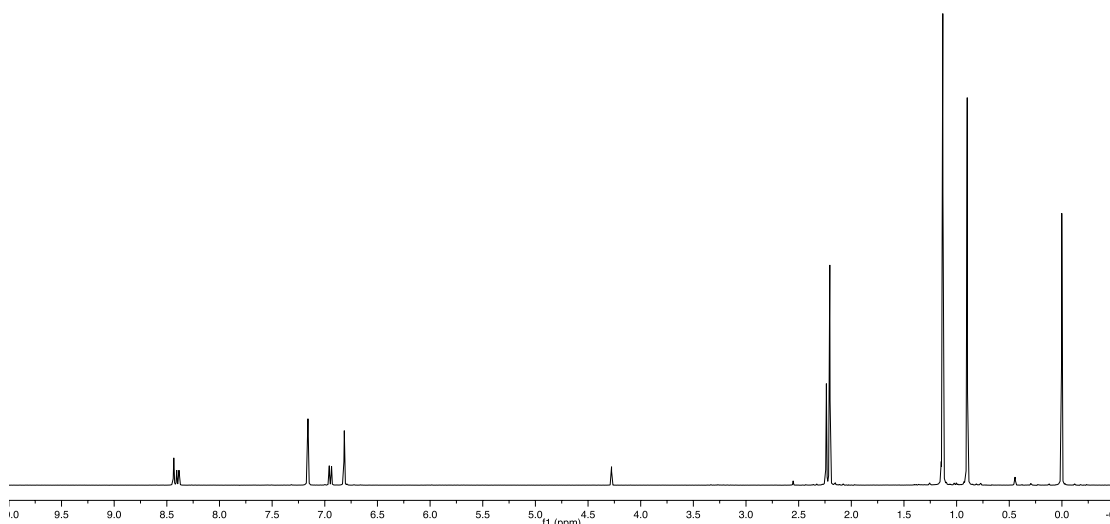


Figure 2.19. ^1H NMR of 5pin in C_6D_6 .

CRM-3-067-1H-5
C4Bpin column

Parameter	Value
1 Title	CRM-3-067-1H-5
2 Comment	C4Bpin column
3 Solvent	c6d6
4 Temperature	25.0
5 Relaxation Delay	1.0000
6 Acquisition Date	2018-03-08T16:31:07
7 Spectrometer Frequency	399.77
8 Nucleus	1H

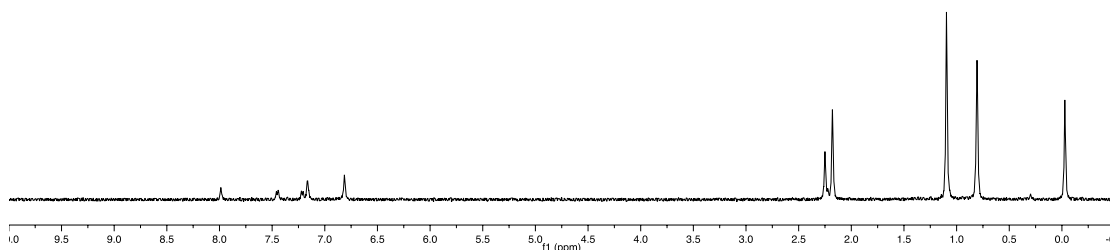
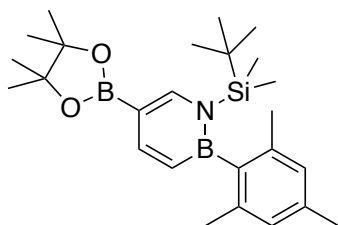
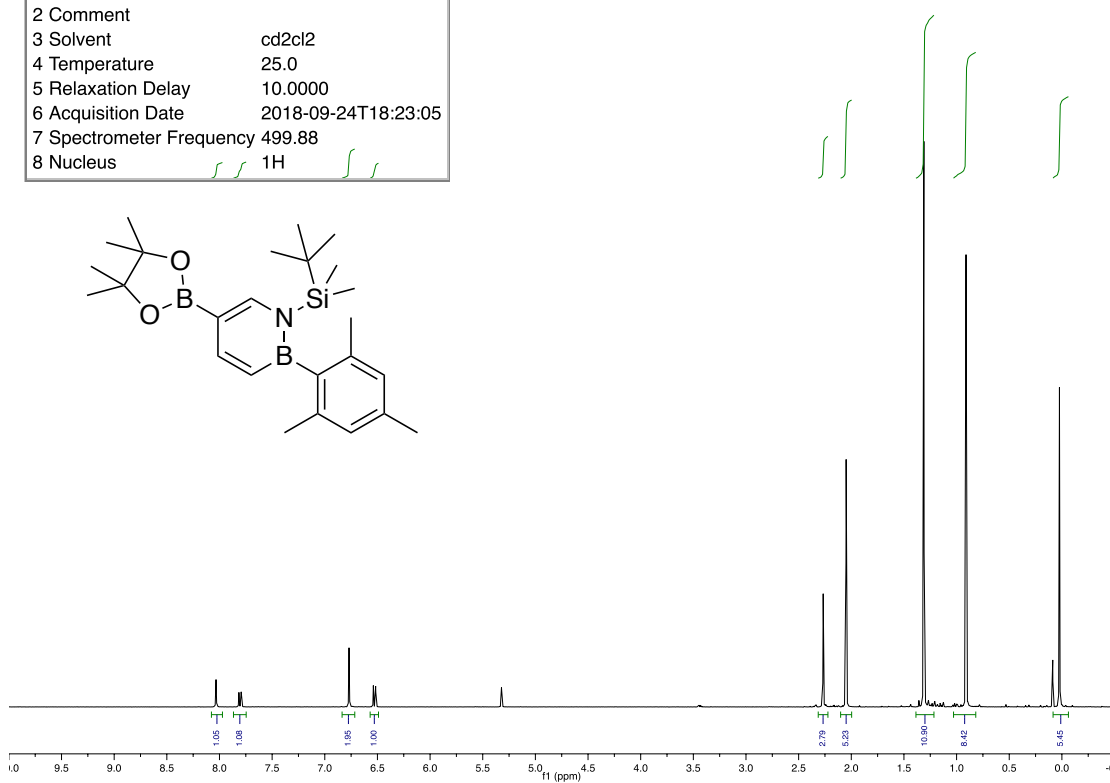


Figure 2.20. ^1H NMR of 4pin in C_6D_6 .

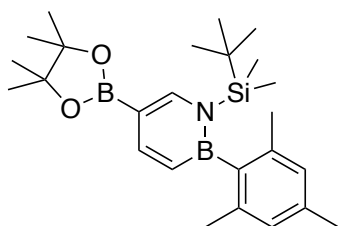
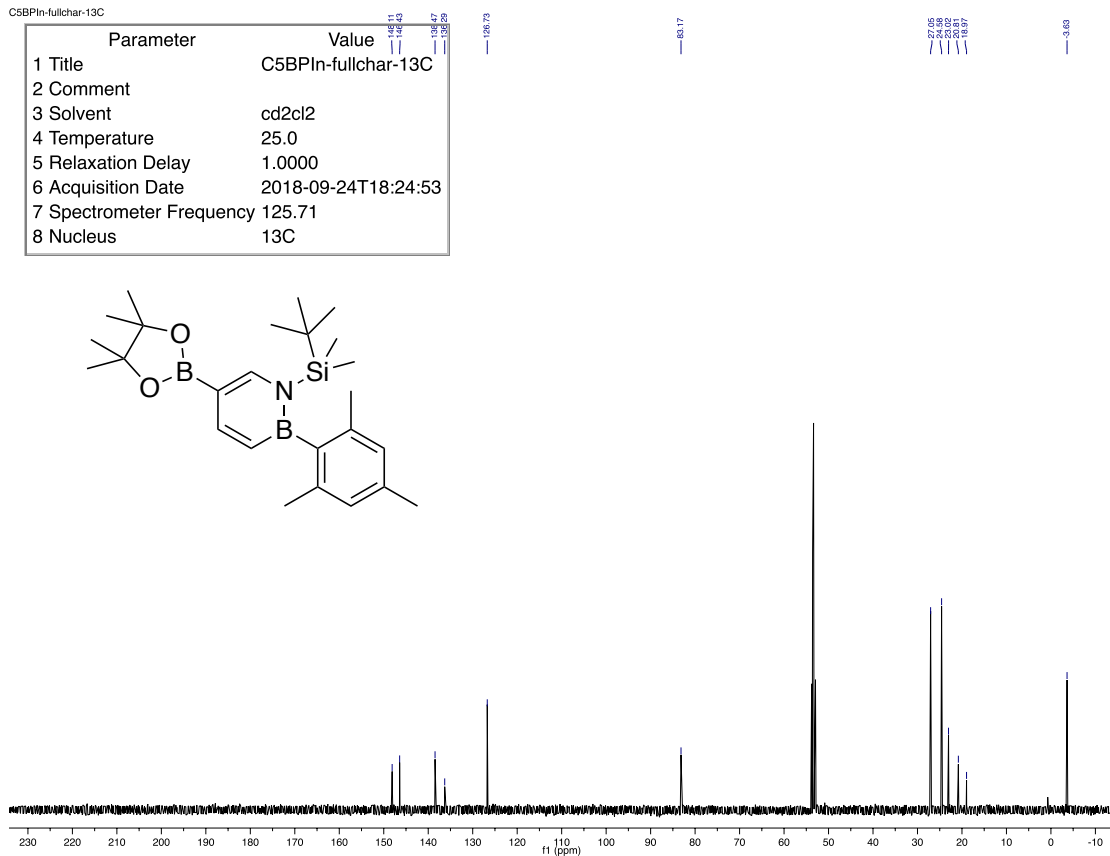
C5BPIn-fullchar-1H

Parameter	Value
1 Title	C5BPIn-fullchar-1H
2 Comment	
3 Solvent	cd2cl2
4 Temperature	25.0
5 Relaxation Delay	10.0000
6 Acquisition Date	2018-09-24T18:23:05
7 Spectrometer Frequency	499.88
8 Nucleus	1H



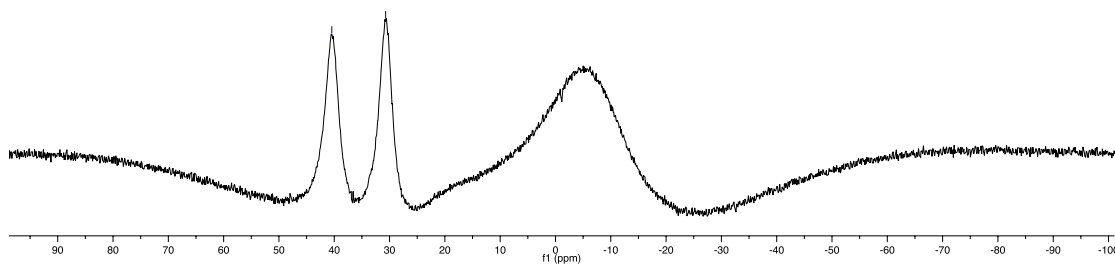
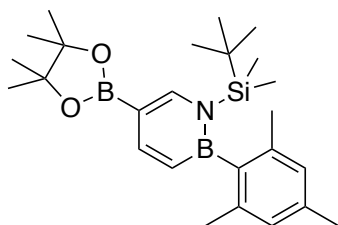
C5BPIn-fullchar-13C

Parameter	Value
1 Title	C5BPIn-fullchar-13C
2 Comment	
3 Solvent	cd2cl2
4 Temperature	25.0
5 Relaxation Delay	1.0000
6 Acquisition Date	2018-09-24T18:24:53
7 Spectrometer Frequency	125.71
8 Nucleus	13C



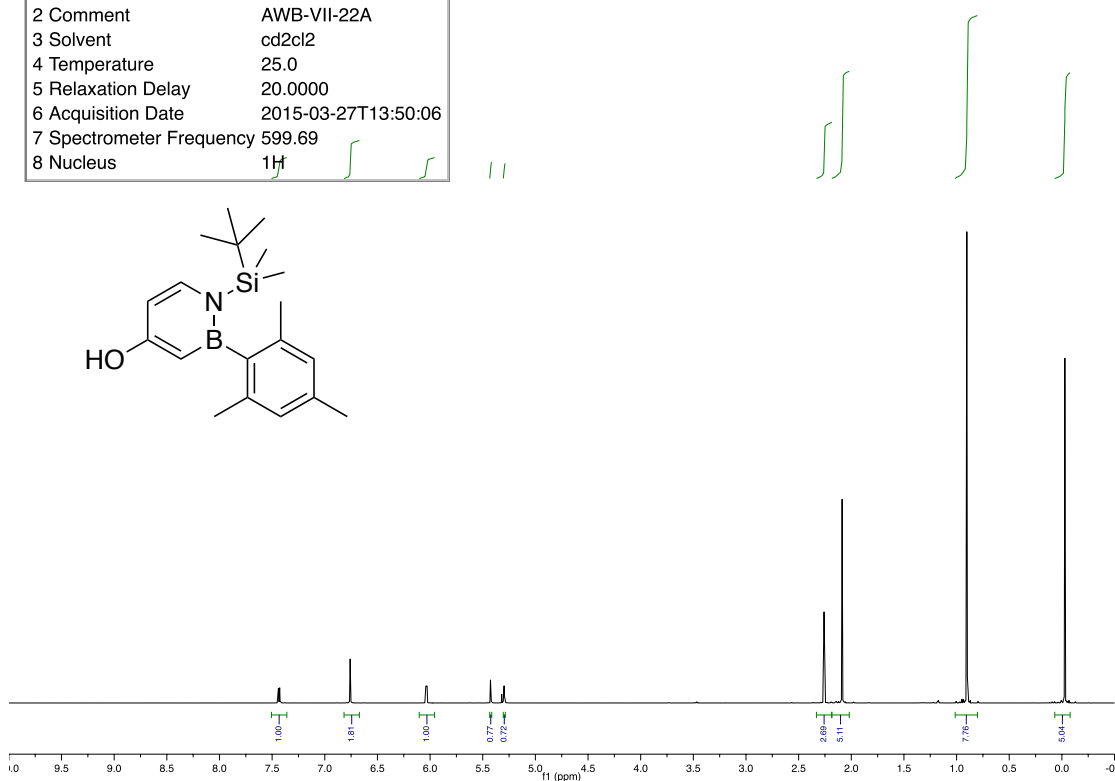
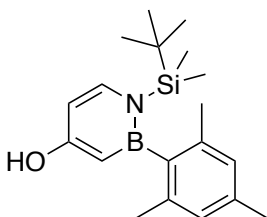
C5Bpin-fullchar-11B

Parameter	Value
1 Title	C5Bpin-fullchar-11B
2 Comment	
3 Solvent	cd2cl2
4 Temperature	25.0
5 Relaxation Delay	0.0100
6 Acquisition Date	2018-09-24T18:43:28
7 Spectrometer Frequency	160.35
8 Nucleus	11B



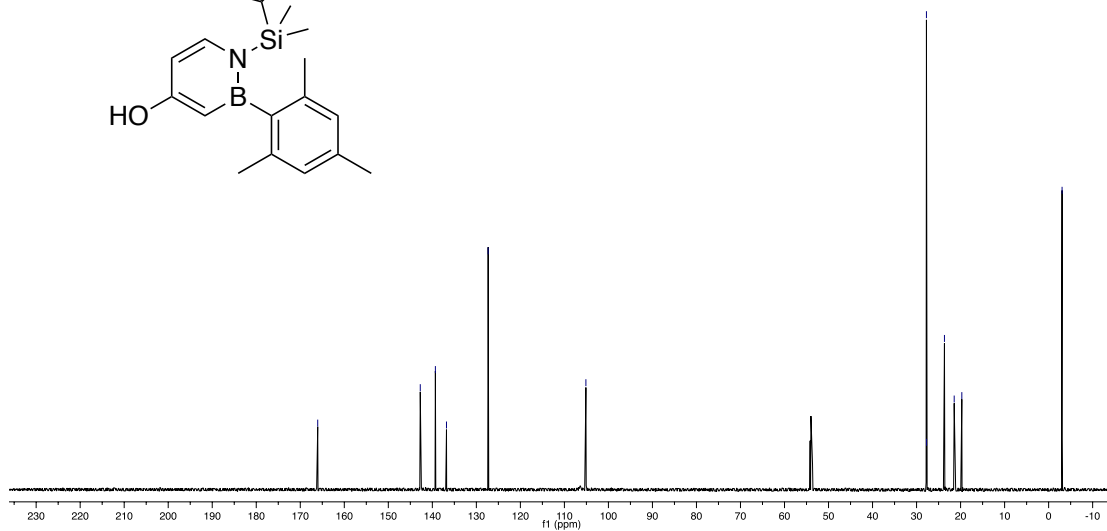
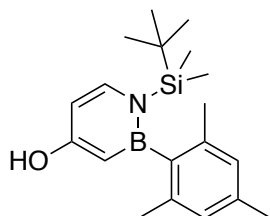
AWB-VII-22A
AWB-VII-22A

Parameter	Value
1 Title	AWB-VII-22A
2 Comment	AWB-VII-22A
3 Solvent	cd2cl2
4 Temperature	25.0
5 Relaxation Delay	20.0000
6 Acquisition Date	2015-03-27T13:50:06
7 Spectrometer Frequency	599.69
8 Nucleus	1H



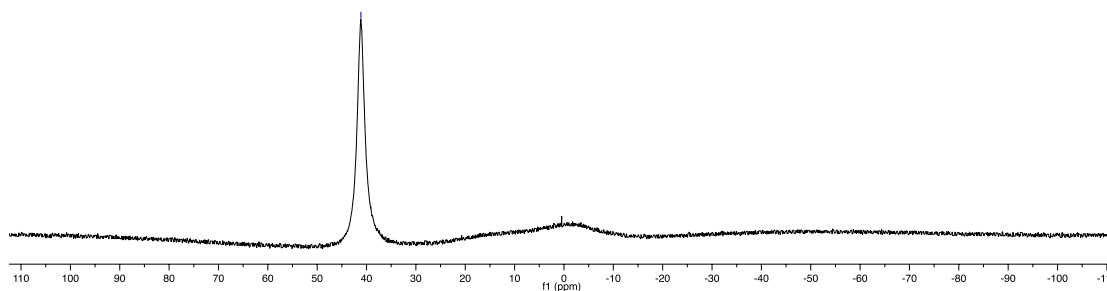
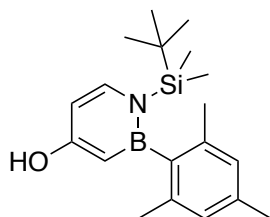
AWB-VII-22C

Parameter	Value
1 Title	AWB-VII-22C
2 Comment	AWB-VII-22C
3 Solvent	cd2cl2
4 Temperature	25.0
5 Relaxation Delay	1.0000
6 Acquisition Date	2015-03-27T13:58:50
7 Spectrometer Frequency	150.81
8 Nucleus	13C



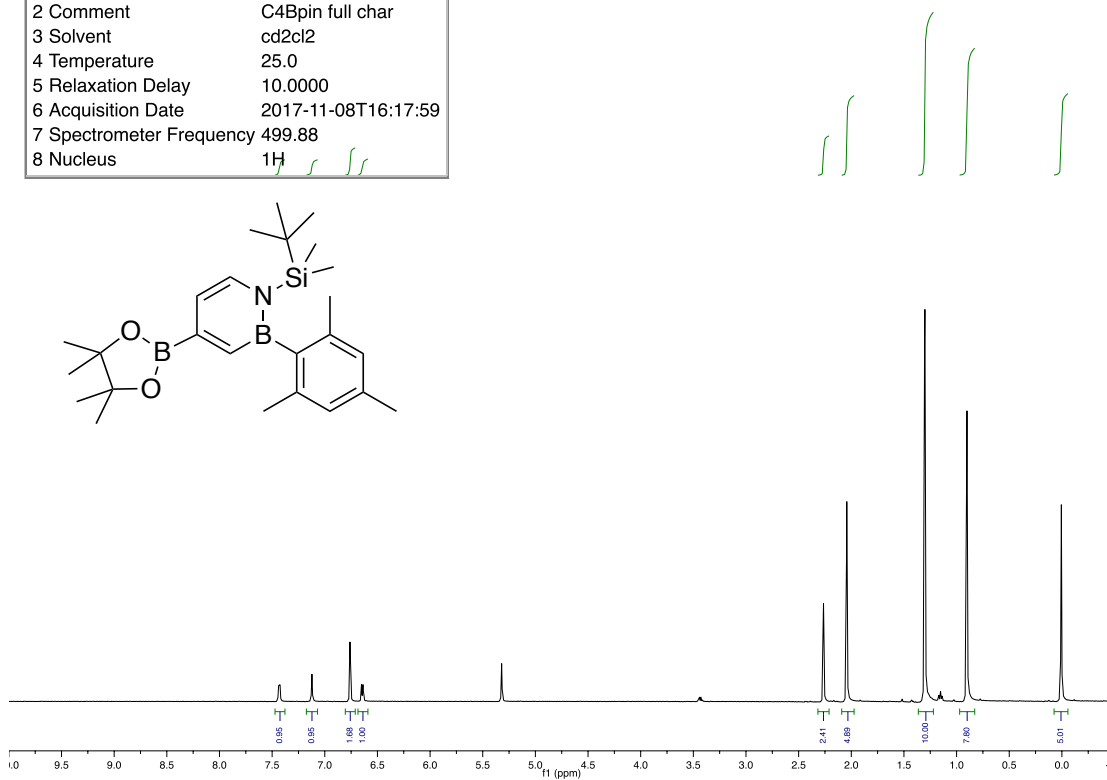
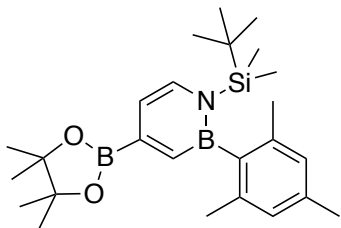
AWB-VII-22B

Parameter	Value
1 Title	AWB-VII-22B
2 Comment	AWB-VII-22B
3 Solvent	cd2cl2
4 Temperature	25.0
5 Relaxation Delay	0.1000
6 Acquisition Date	2015-03-27T13:55:13
7 Spectrometer Frequency	192.40
8 Nucleus	11B



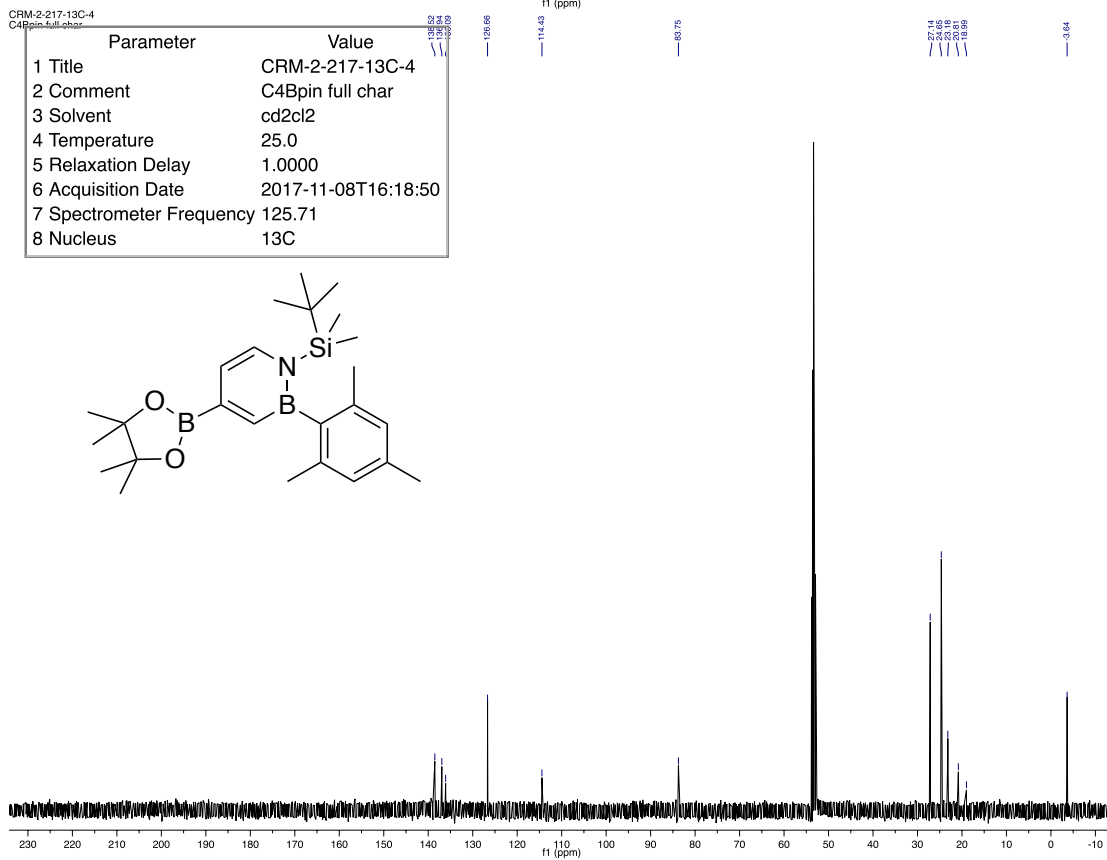
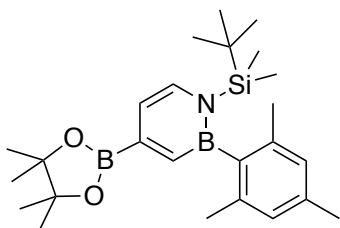
CRM-2-217-1H-3
C4Bpin full char

Parameter	Value
1 Title	CRM-2-217-1H-3
2 Comment	C4Bpin full char
3 Solvent	cd2cl2
4 Temperature	25.0
5 Relaxation Delay	10.0000
6 Acquisition Date	2017-11-08T16:17:59
7 Spectrometer Frequency	499.88
8 Nucleus	¹ H



CRM-2-217-13C-4
C4Bpin full char

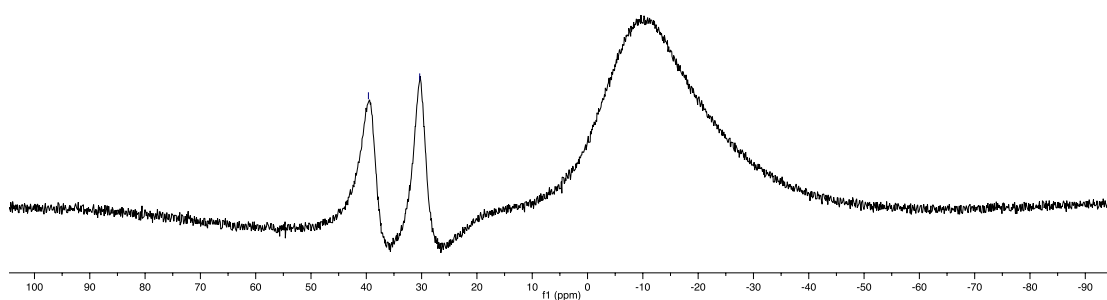
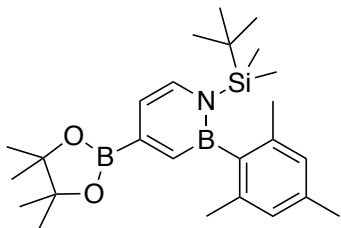
Parameter	Value
1 Title	CRM-2-217-13C-4
2 Comment	C4Bpin full char
3 Solvent	cd2cl2
4 Temperature	25.0
5 Relaxation Delay	1.0000
6 Acquisition Date	2017-11-08T16:18:50
7 Spectrometer Frequency	125.71
8 Nucleus	¹³ C



CRM-2-217-11B-2

C4Bpin full char

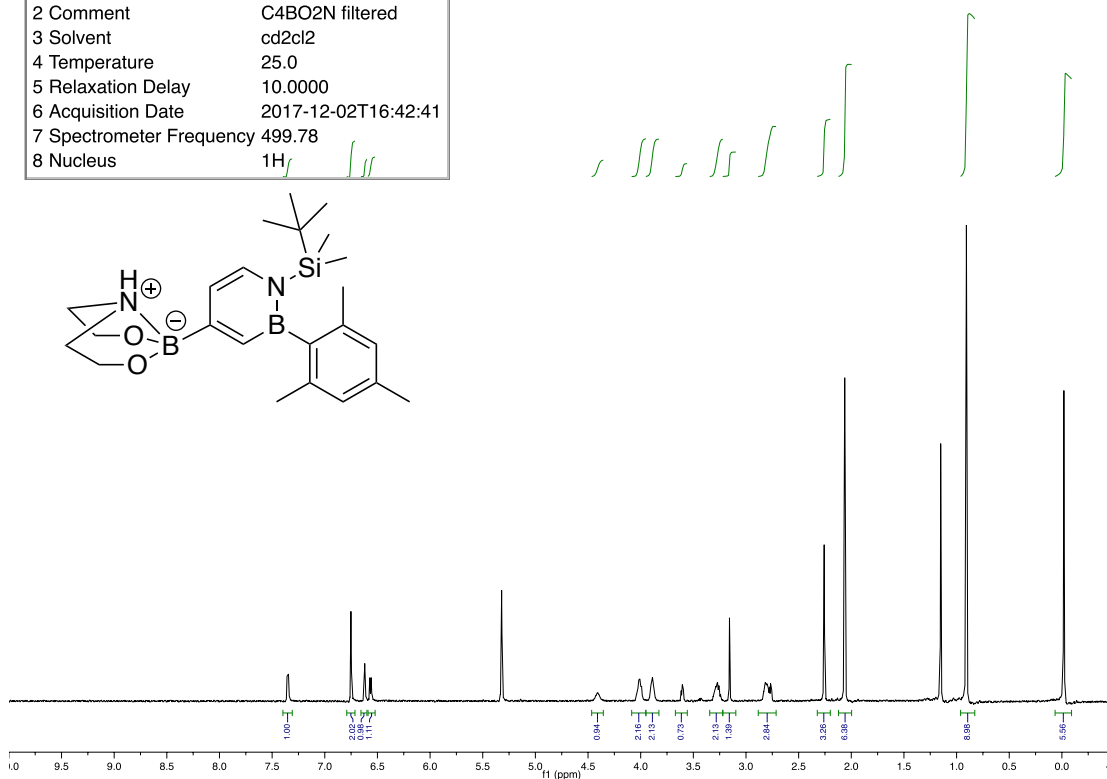
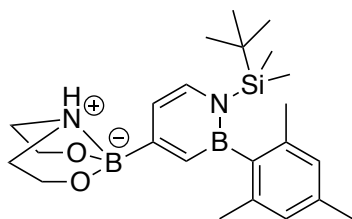
Parameter	Value
1 Title	CRM-2-217-11B-2
2 Comment	C4Bpin full char
3 Solvent	cd2cl2
4 Temperature	25.0
5 Relaxation Delay	0.0100
6 Acquisition Date	2017-11-08T15:58:11
7 Spectrometer Frequency	160.35
8 Nucleus	11B



CRM-2-234-1H-2

C4BO2N filtered

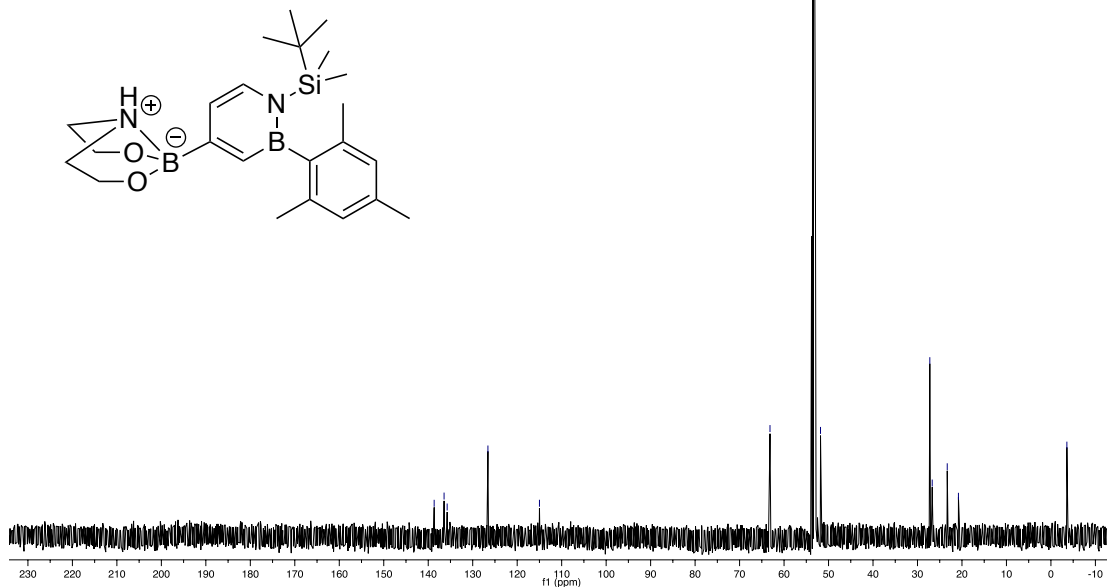
Parameter	Value
1 Title	CRM-2-234-1H-2
2 Comment	C4BO2N filtered
3 Solvent	cd2cl2
4 Temperature	25.0
5 Relaxation Delay	10.0000
6 Acquisition Date	2017-12-02T16:42:41
7 Spectrometer Frequency	499.78
8 Nucleus	1H



CRM-2-234-13C-3

C4FO2M filtered

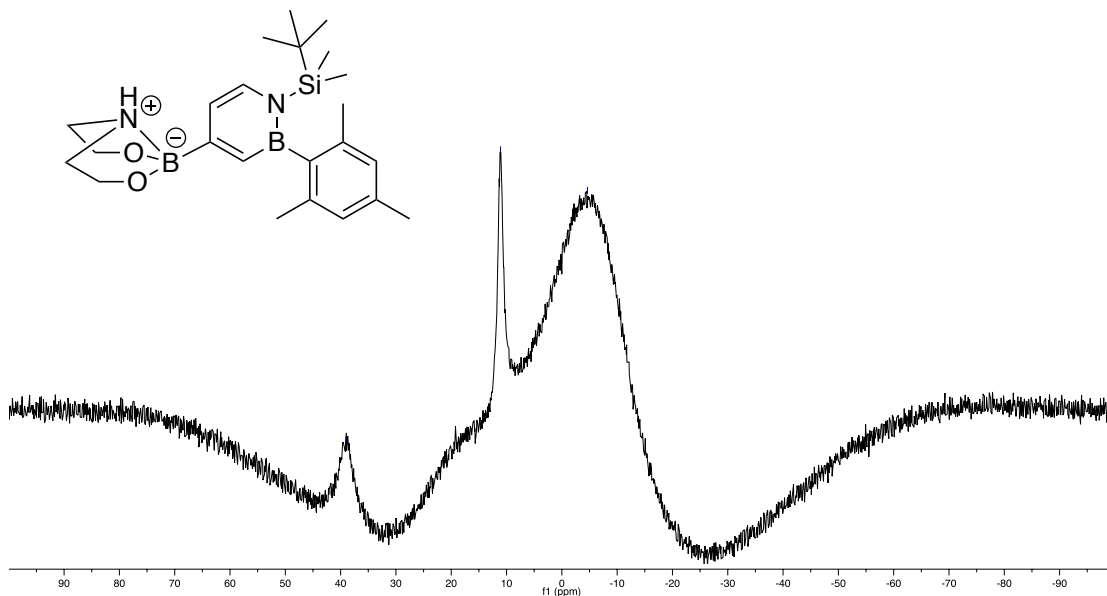
Parameter	Value
1 Title	CRM-2-234-13C-3
2 Comment	C4BO2N filtered
3 Solvent	cd2cl2
4 Temperature	25.0
5 Relaxation Delay	1.0000
6 Acquisition Date	2017-12-02T16:51:16
7 Spectrometer Frequency	125.71
8 Nucleus	13C



CRM-2-234-11B-1

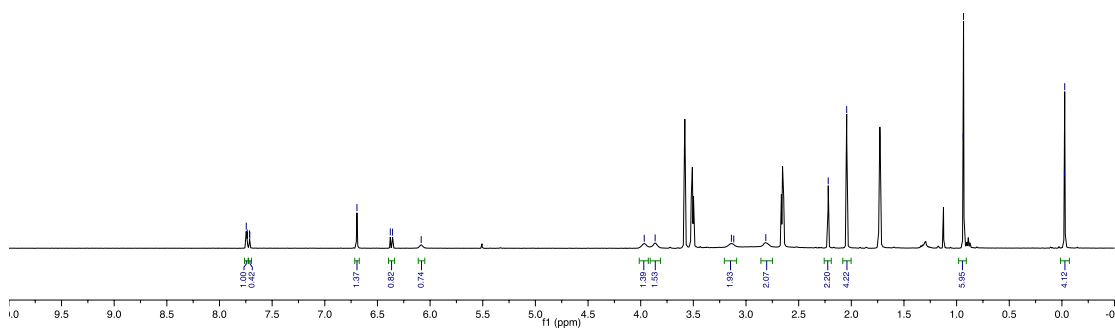
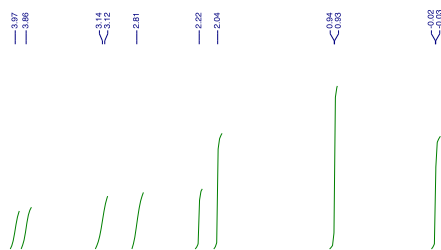
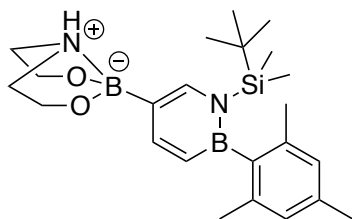
C4FO2M filtered

Parameter	Value
1 Title	CRM-2-234-11B-1
2 Comment	C4BO2N filtered
3 Solvent	cd2cl2
4 Temperature	25.0
5 Relaxation Delay	0.0100
6 Acquisition Date	2017-12-02T16:44:52
7 Spectrometer Frequency	160.35
8 Nucleus	11B



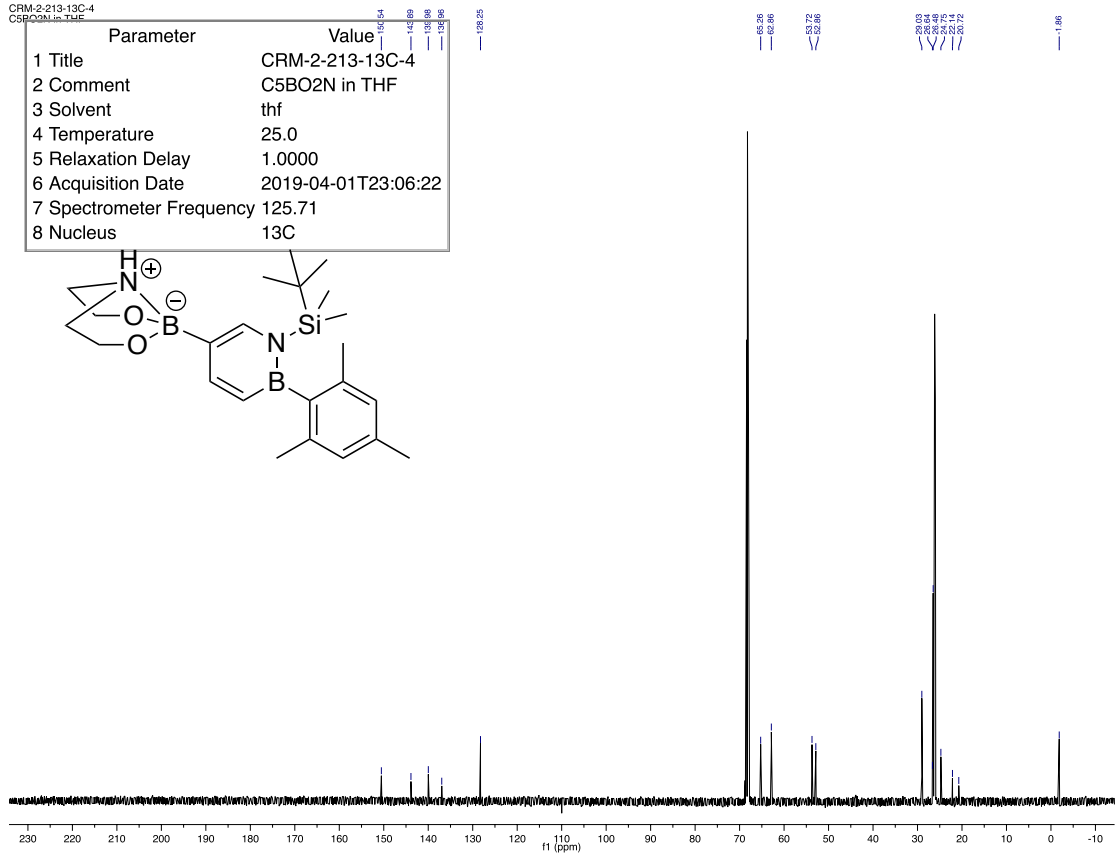
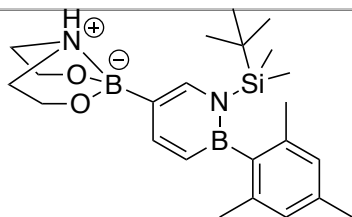
CRM-2-213-1H-5
C5BO2N in THF

Parameter	Value
1 Title	CRM-2-213-1H-5
2 Comment	C5BO2N in THF
3 Solvent	thf
4 Temperature	25.0
5 Relaxation Delay	10.0000
6 Acquisition Date	2019-04-01T23:30:40
7 Spectrometer Frequency	499.89
8 Nucleus	¹ H



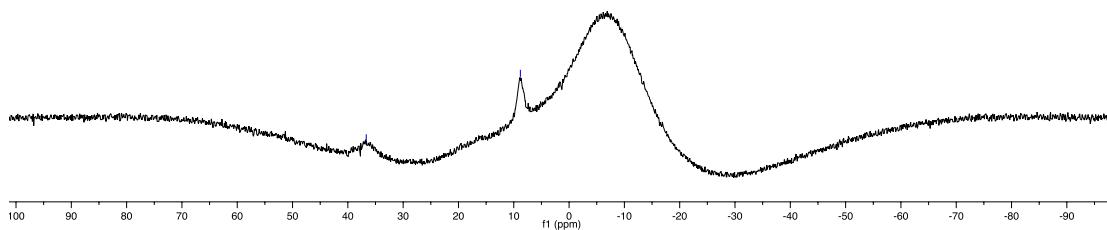
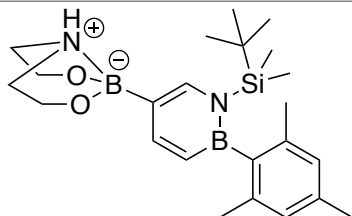
CRM-2-213-13C-4
C5BO2N in THF

Parameter	Value
1 Title	CRM-2-213-13C-4
2 Comment	C5BO2N in THF
3 Solvent	thf
4 Temperature	25.0
5 Relaxation Delay	1.0000
6 Acquisition Date	2019-04-01T23:06:22
7 Spectrometer Frequency	125.71
8 Nucleus	¹³ C



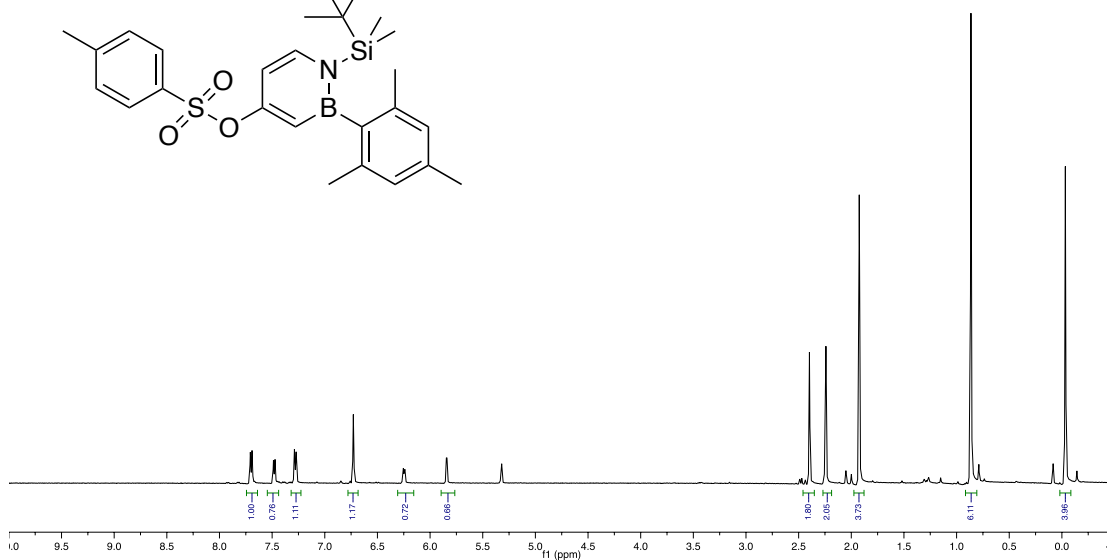
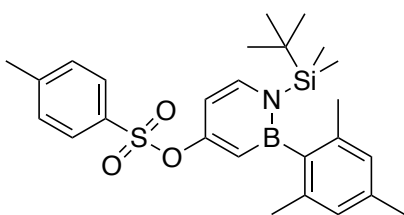
CRM-2-213-11B-6
C5BO2N full char thf

Parameter	Value
1 Title	CRM-2-213-11B-6
2 Comment	C5BO2N full char thf
3 Solvent	thf
4 Temperature	25.0
5 Relaxation Delay	0.1000
6 Acquisition Date	2019-04-02T10:53:57
7 Spectrometer Frequency	160.35
8 Nucleus	11B



CRM-2-060-1H-5
NTBSBMes C4OTs column

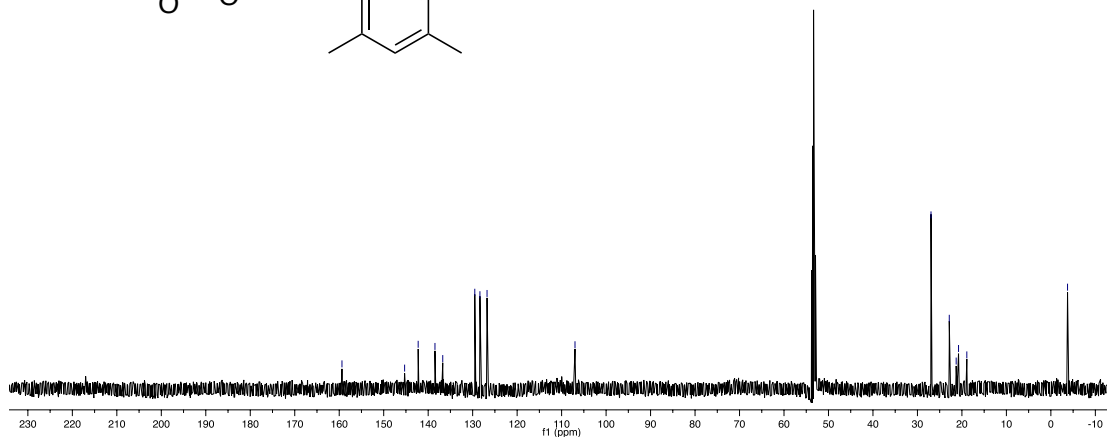
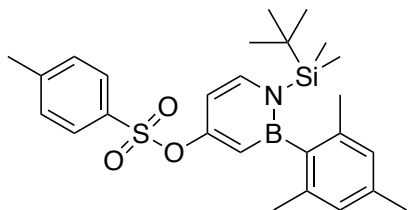
Parameter	Value
1 Title	CRM-2-060-1H-5
2 Comment	NTBSBMes C4OTs column
3 Solvent	cd2cl2
4 Temperature	23.0
5 Relaxation Delay	1.0000
6 Acquisition Date	2017-04-03T11:01:56
7 Spectrometer Frequency	499.88
8 Nucleus	1H



CRM-2-060-13C-6

NTBSBMes C4OTs column

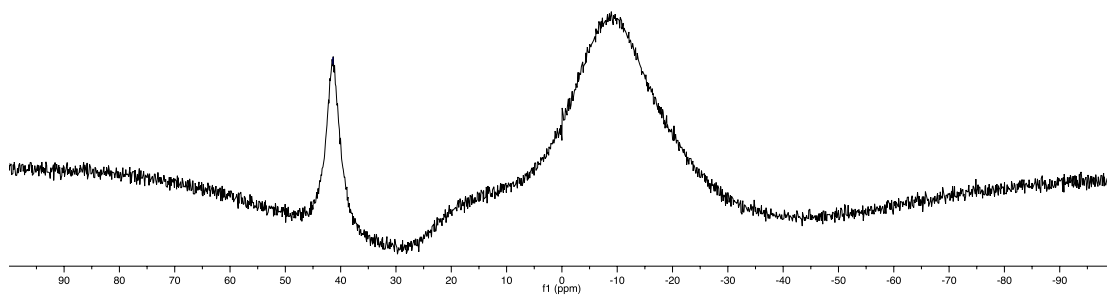
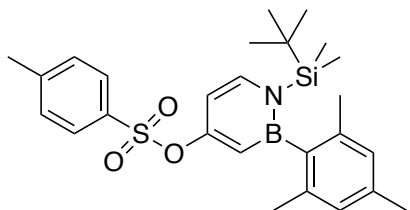
Parameter	Value
1 Title	CRM-2-060-13C-6
2 Comment	NTBSBMes C4OTs column
3 Solvent	cd2cl2
4 Temperature	23.0
5 Relaxation Delay	1.0000
6 Acquisition Date	2017-04-03T11:02:58
7 Spectrometer Frequency	125.71
8 Nucleus	13C



CRM-2-060-11B-4

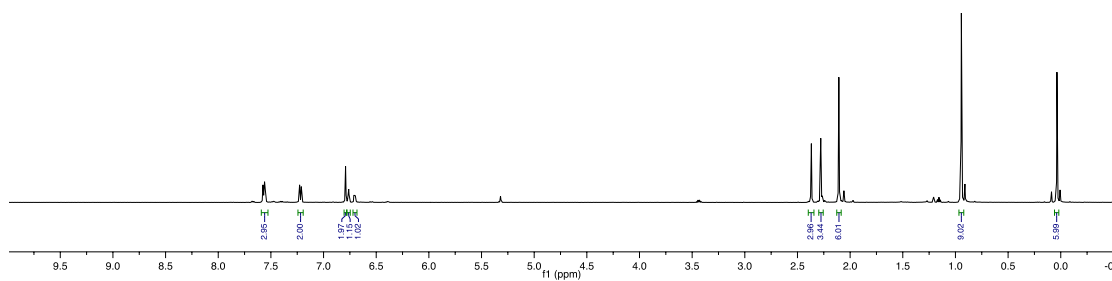
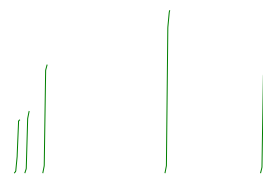
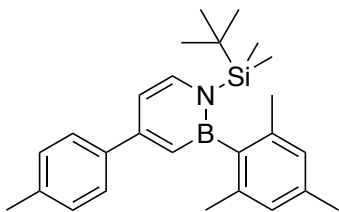
NTBSBMes C4OTs column

Parameter	Value
1 Title	CRM-2-060-11B-4
2 Comment	NTBSBMes C4OTs column
3 Solvent	cd2cl2
4 Temperature	25.0
5 Relaxation Delay	0.0100
6 Acquisition Date	2017-04-03T10:57:43
7 Spectrometer Frequency	160.35
8 Nucleus	11B



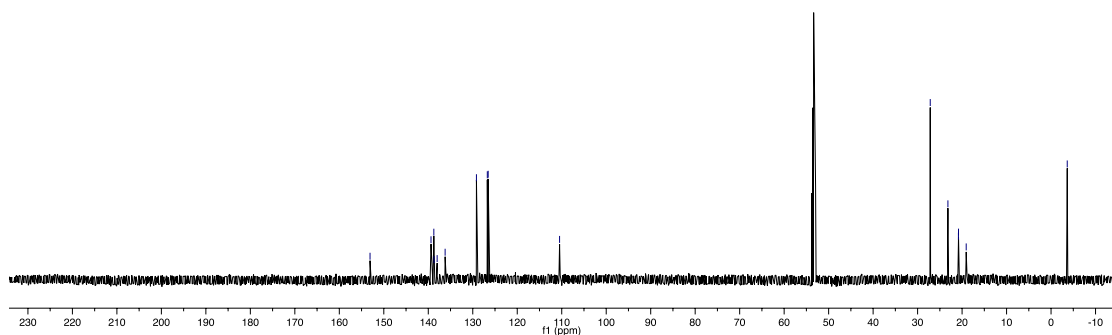
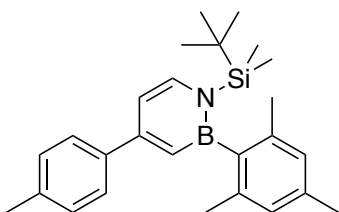
CRM-3-108-1H-4
C4ptol full char

Parameter	Value
1 Title	CRM-3-108-1H-4
2 Comment	C4ptol full char
3 Solvent	cd2cl2
4 Temperature	25.0
5 Relaxation Delay	10.0000
6 Acquisition Date	2018-04-06T11:52:12
7 Spectrometer Frequency	499.88
8 Nucleus	¹ H



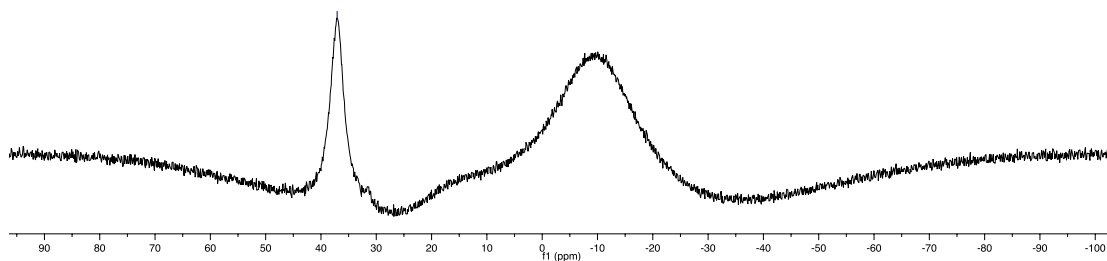
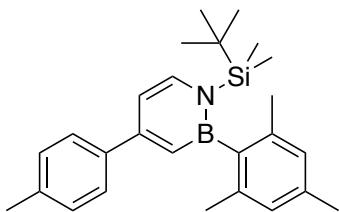
CRM-3-108-13C-5
C4ptol full char

Parameter	Value
1 Title	CRM-3-108-13C-5
2 Comment	C4ptol full char
3 Solvent	cd2cl2
4 Temperature	25.0
5 Relaxation Delay	1.0000
6 Acquisition Date	2018-04-06T11:55:22
7 Spectrometer Frequency	125.71
8 Nucleus	¹³ C



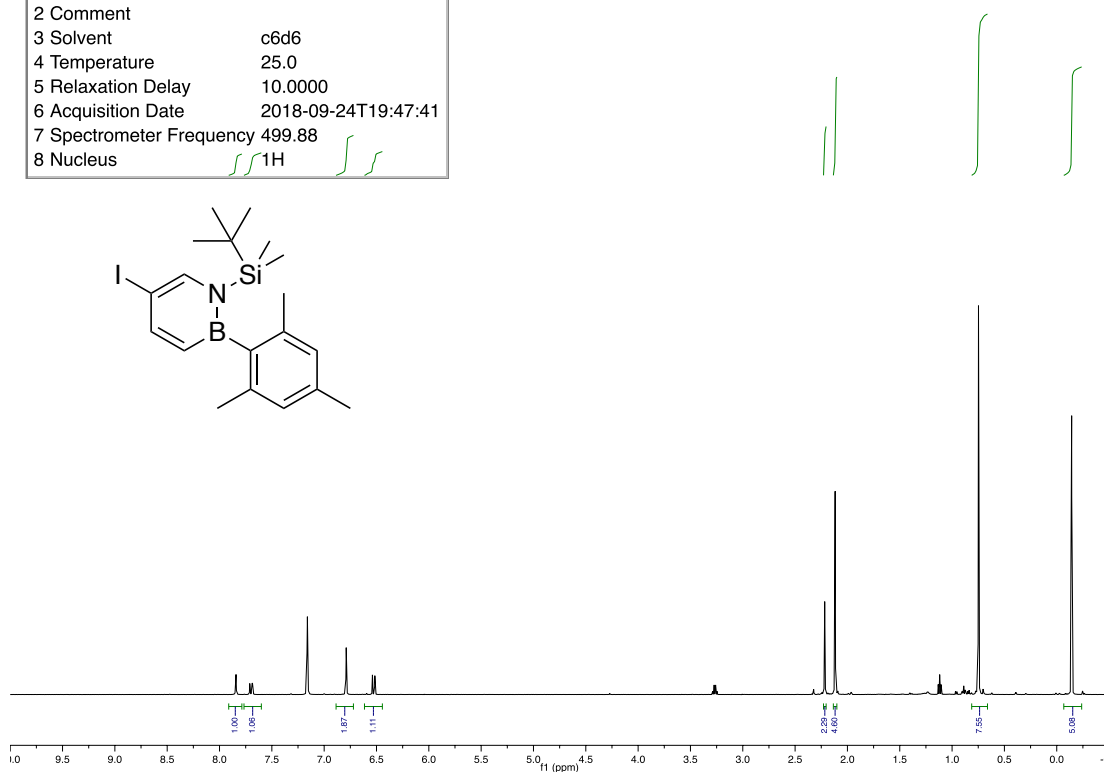
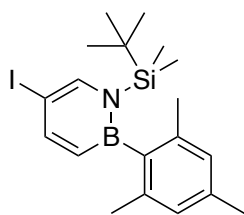
CRM-3-108-11B-3
C4ptol full char

Parameter	Value
1 Title	CRM-3-108-11B-3
2 Comment	C4ptol full char
3 Solvent	cd2cl2
4 Temperature	25.0
5 Relaxation Delay	0.0100
6 Acquisition Date	2018-04-06T10:29:06
7 Spectrometer Frequency	160.35
8 Nucleus	11B



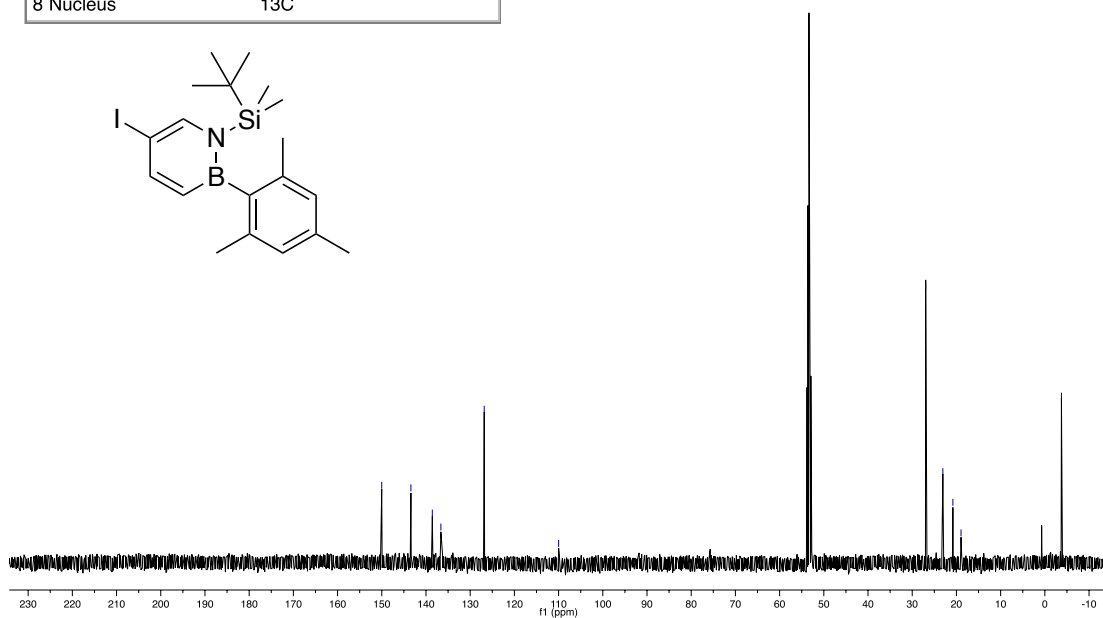
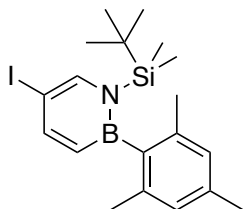
C5Iodo-fullchar-1H

Parameter	Value
1 Title	C5Iodo-fullchar-1H
2 Comment	
3 Solvent	c6d6
4 Temperature	25.0
5 Relaxation Delay	10.0000
6 Acquisition Date	2018-09-24T19:47:41
7 Spectrometer Frequency	499.88
8 Nucleus	¹ H



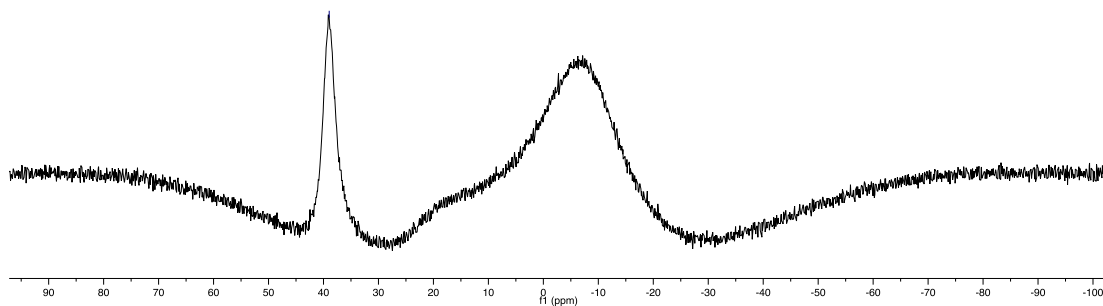
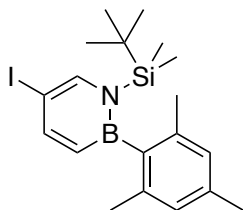
CRM-2-183-13C-7
NTBSBMes C5 iodo column

Parameter	Value
1 Title	CRM-2-183-13C-7
2 Comment	NTBSBMes C5 iodo column
3 Solvent	cd2cl2
4 Temperature	25.0
5 Relaxation Delay	1.0000
6 Acquisition Date	2017-09-29T15:40:32
7 Spectrometer Frequency	125.71
8 Nucleus	13C



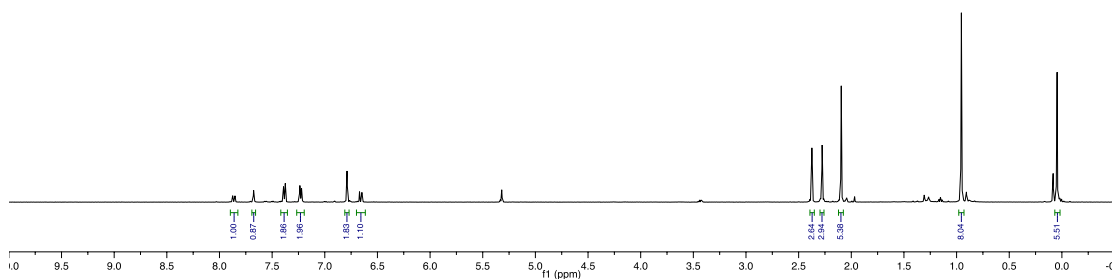
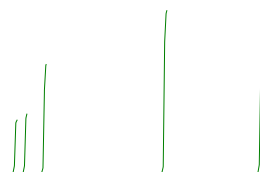
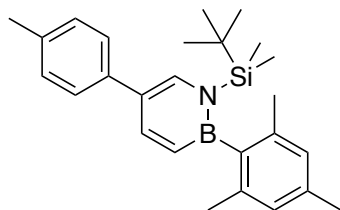
C5Iodo-fullchar-11B

Parameter	Value
1 Title	C5Iodo-fullchar-11B
2 Comment	
3 Solvent	c6d6
4 Temperature	25.0
5 Relaxation Delay	0.0100
6 Acquisition Date	2018-09-24T19:42:15
7 Spectrometer Frequency	160.35
8 Nucleus	11B



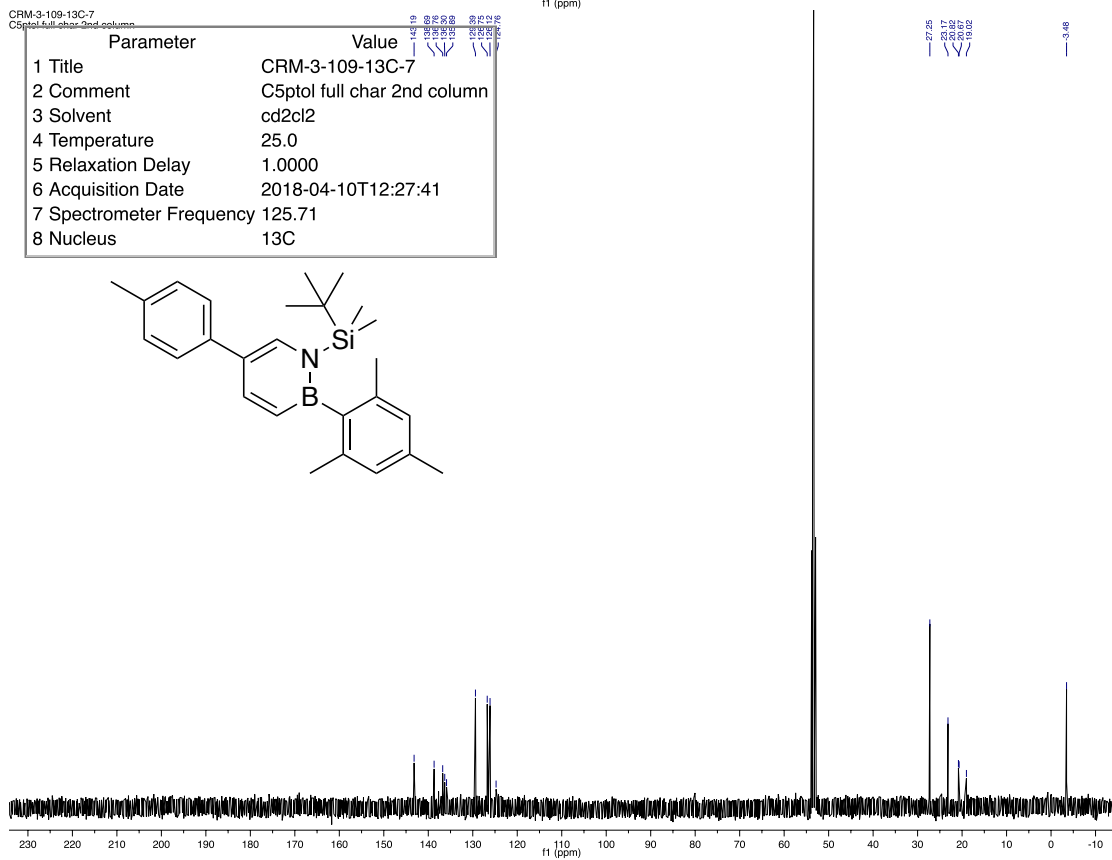
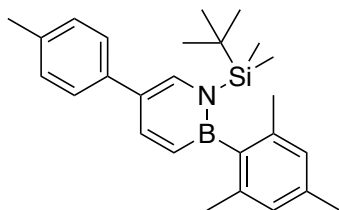
CRM-3-109-1H-6
C5ptol full char 2nd column

Parameter	Value
1 Title	CRM-3-109-1H-6
2 Comment	C5ptol full char 2nd column
3 Solvent	cd2cl2
4 Temperature	25.0
5 Relaxation Delay	10.0000
6 Acquisition Date	2018-04-10T12:25:51
7 Spectrometer Frequency	499.88
8 Nucleus	¹ H



CRM-3-109-13C-7
C5ptol full char 2nd column

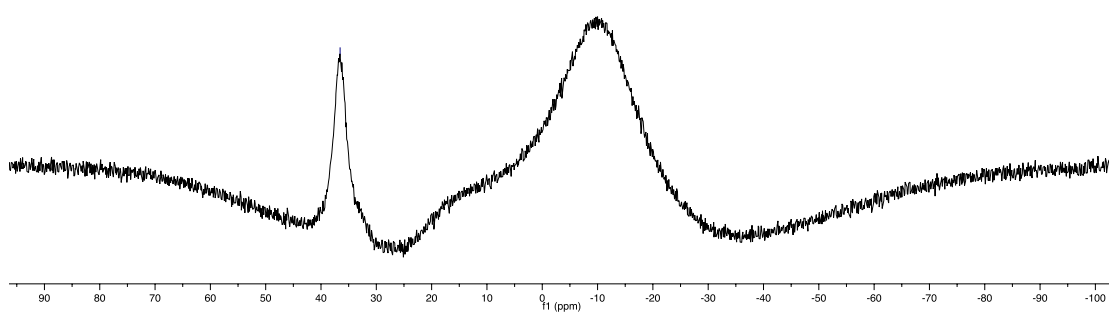
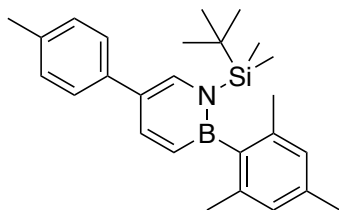
Parameter	Value
1 Title	CRM-3-109-13C-7
2 Comment	C5ptol full char 2nd column
3 Solvent	cd2cl2
4 Temperature	25.0
5 Relaxation Delay	1.0000
6 Acquisition Date	2018-04-10T12:27:41
7 Spectrometer Frequency	125.71
8 Nucleus	¹³ C



CRM-3-109-11B-3

C5ptol full char

Parameter	Value
1 Title	CRM-3-109-11B-3
2 Comment	C5ptol full char
3 Solvent	cd2cl2
4 Temperature	25.0
5 Relaxation Delay	0.0100
6 Acquisition Date	2018-04-06T10:32:20
7 Spectrometer Frequency	160.35
8 Nucleus	11B



Chapter 3

Changing up BN-Styrenes: Effect of Substitution Pattern on the Free Radical Polymerization and Polymer Properties*

3.1 Introduction: BN-Containing Polymers

The replacement of C=C for B-N units in conjugated organic systems has attracted significant recent interest, as their incorporation has led to novel electronic properties, reactivity, and applications.¹ Examples of applications range from conjugated materials for use in luminescent imaging to field effect transistors and organic solar cells.² One method of incorporating B-N bonds into polymeric materials is to replace benzene units with 1,2-azaborines; such materials have a strong potential impact given the importance of aromatic groups in polymer science. In earlier work, Sneddon had examined the polymerization of vinylborazines in an effort to generate boron-containing ceramics (Figure 3.1).³ In 2015, in collaboration with the Jäkle group, the Liu group reported the first example of an azaborine-based conjugated polymer (BN-PPP, **3.2**),⁴ a B-N analogue of poly(*p*-phenylene), and in 2016 the first example of a BN-substituted polystyrene (BN-PS, **3.4**) as well as its phenylene-expanded congener (BN-PVBP, **3.6**).⁵ Higher molecular weights and rates of incorporation into polymer were achieved for monomer **3.5** compared to monomer **3.3**, and this difference was tentatively attributed to the direct attachment of the vinyl

*The experimental work detailed in this section was performed in collaboration with Huina Lin, Berothy Jilus, and Professor Frieder Jäkle. Huina Lin performed all of the polymerization and polymer characterization experiments. Lin, H.; McConnell, C. R.; Jilus, B.; Liu, S.-Y.; Jäkle, F. *Macromolecules* **2019**, *In Press*.

¹ For reviews, see: (a) Entwistle, C. D.; Marder, T. B. *Angew. Chem. Int. Ed.* **2002**, *41*, 2927-2931. (b) Jäkle, F. *Chem. Rev.* **2010**, *110*, 3985-4022. (c) Priegert, A. M.; Rawe, B. W.; Serin, S. C.; Gates, D. P. *Chem. Soc. Rev.* **2016**, *45*, 922-953. (d) Helten, H. *Chem. -Eur. J.* **2016**, *22*, 12972-12982.

² (a) Grosche, M.; Herdtweck, E.; Peters, F.; Wagner, M. *Organometallics* **1999**, *18*, 4669-4672. (b) Zhao, R.; Dou, C.; Xie, Z.; Liu, J.; Wang, L. *Angew. Chem. Int. Ed.* **2016**, *55*, 5313-5317. (c) Zhang, W.; Li, G.; Xu, L.; Zhuo, Y.; Wan, W.; Yan, N.; He, G. *Chem. Sci.* **2018**, *9*, 4444-4450.

³ Su, K.; Remsen, E. E.; Thompson, H. M.; Sneddon, L. G. *Macromolecules* **1991**, *24*, 3760-3766.

⁴ Baggett, A. W.; Guo, F.; Li, B.; Liu, S.-Y.; Jäkle, F. *Angew. Chem. Int. Ed.* **2015**, *54*, 11191-11195.

⁵ Wan, W.-M.; Baggett, A. W.; Cheng, F.; Lin, H.; Liu, S.-Y.; Jäkle, F., *Chem. Comm.* **2016**, *52*, 13616-13619.

group to boron in monomer **3.3**, which may destabilize the propagating radical in the “benzylic” position. We also found that these polymers exhibit enhanced solubility in polar solvents, such as methanol, in comparison to the all-carbon analogs, which we ascribed to the increased polarity of the side groups and the presence of N-H moieties capable of hydrogen bonding.

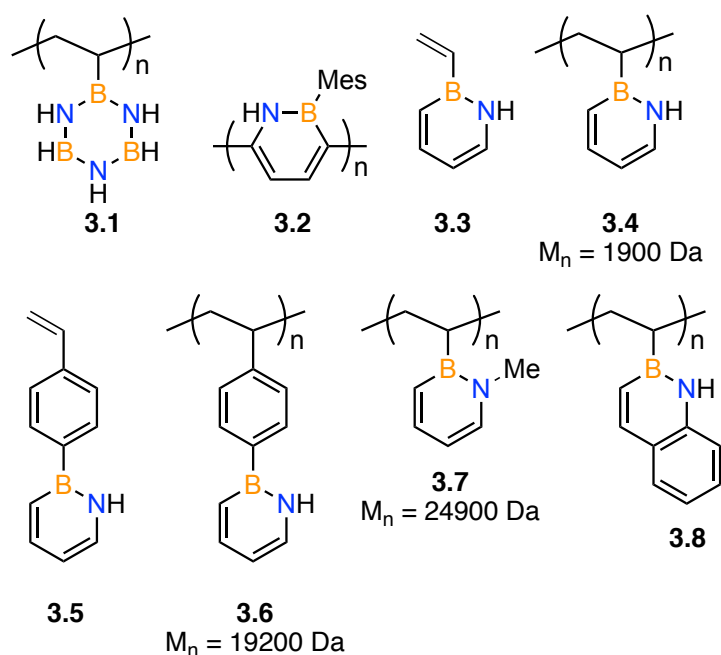


Figure 3.1. Examples of previously reported polymers that have C-C units replaced by B-N units.

In related work, Staubitz reported high molecular weight polymers **3.8**,⁶ which contain a methyl group in place of a hydrogen on N. They used the methyl group as an NMR spectroscopic handle to identify potential configurations of their overall atactic polymer. In addition, Klausen developed a gram scale synthesis of BN-substituted vinylnaphthalene polymers (**3.8**), both by free radical and syndiospecific coordination-insertion polymerization methods involving metallocene catalysts.⁷ They found that in free radical copolymerizations the reactivity of the respective BN-

⁶ Thiedemann, B.; Gliese, P. J.; Hoffmann, J.; Lawrence, P. G.; Sonnichsen, F. D.; Staubitz, A. *Chem. Comm.* **2017**, 53, 7258-7261.

⁷ (a) van de Wouw, H. L.; Lee, J. Y.; Klausen, R. S. *Chem. Comm.* **2017**, 53, 7262-7265. (b) Mendis, S. N.; Zhou, T.; Klausen, R. S. *Macromolecules* **2018**, 51, 6859-6864.

vinyl naphthalene monomer is somewhat lower but overall is in the same range as that of styrene, allowing for random incorporation into the copolymer products.⁸ Importantly, they also demonstrated that the oxidative cleavage of the BN-naphthalene moieties results in poly(styrene-*co*-vinylalcohol) copolymers that are desirable as compatibilizers due to the additional polar functional groups.⁹

The parent BN-PS (**3.4**), while showing interesting solubility and thermal characteristics, can only be obtained in modest molecular weights. This prompted us to explore the effects of placing the B-N moiety in different positions relative to the polymer backbone on the polymerizability and the polymer physical properties (Figure 3.2). Polymer **3.4** also tended to decompose in air, thus we chose to incorporate a mesityl group on the boron atom to make the azaborine heterocycle less sensitive to water and oxygen. With the newly developed late-stage functionalization methods described in Chapter 2, we were able to access monomers **4V-NBMes**, **5V-NBMes**, and **6V-NBMes**.

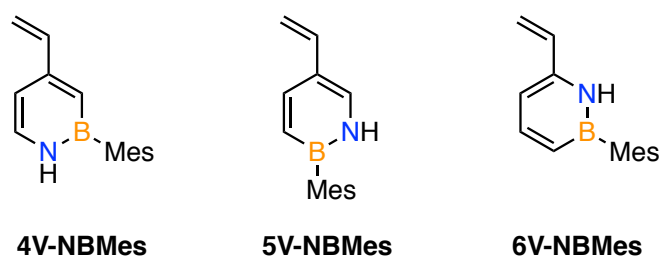


Figure 3.2. BN-styrene monomers.

Other possible isomers with the mesityl groups in *ortho*-position to the polymerizable group (1- and 3- position) were not considered as the steric bulk was presumed to prohibit polymerization. This assumption is supported by the fact that *B*-vinylborazines with Me or Ph groups attached to the nitrogens in *ortho*-position have

⁸ van de Wouw, H. L.; Awuyah, E. C.; Baris, J. I.; Klausen, R. S. *Macromolecules* **2018**, *51*, 6359-6368.

⁹ van de Wouw, H. L.; Lee, J. Y.; Awuyah, E. C.; Klausen, R. S. *Angew. Chem. Int. Ed.* **2018**, *57*, 1673-1677.

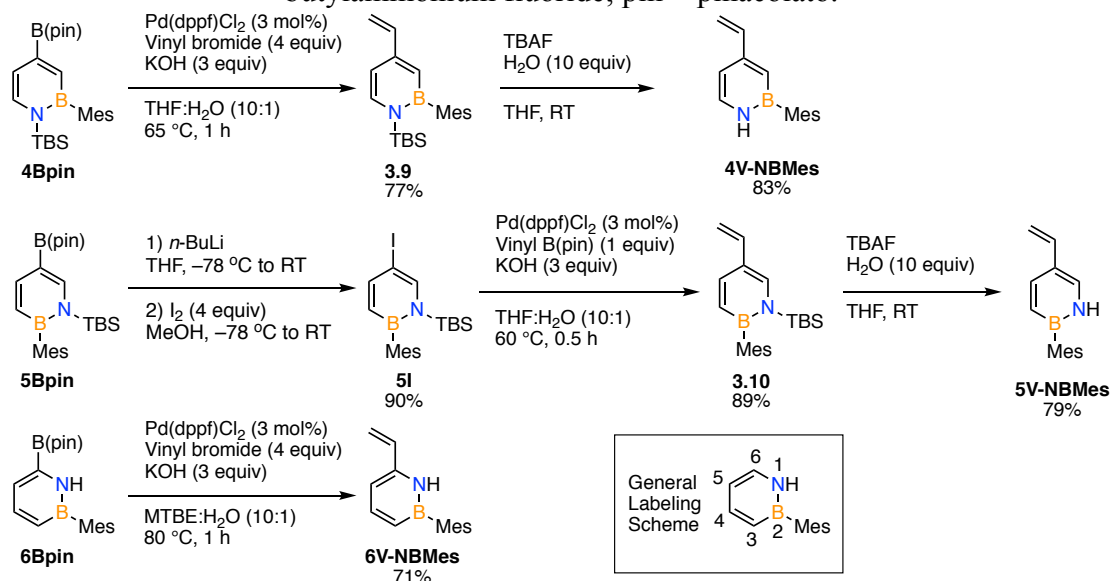
been shown not to be amenable to polymerization whereas the parent *B*-vinylborazine does undergo thermal polymerization primarily at the vinyl group.^{3,10}

3.2 Monomer Synthesis

In order to prepare the target monomers we started with borylated building blocks **4Bpin**, **5Bpin**, or **6Bpin** and installed the vinyl groups via a late-stage Suzuki-Miyaura cross-coupling (Scheme 3.1). Cross-coupling of **4Bpin** with vinyl bromide followed by removal of the *N*-TBS group yielded the product, **4V-NBMes** in 88% yield. Unexpectedly, the Suzuki coupling of **5Bpin** did not prove amenable to scale-up; this observation is puzzling, considering that cross-coupling between **5Bpin** and an aryl halide proceeded smoothly at a similar scale (Scheme 2.13). However, C5-iodo-substituted **5I** allowed for the efficient Suzuki-Miyaura coupling with vinyl pinacol boronate ester to afford **3.10**. Subsequent removal of the TBS group with tetra(*n*-butyl)ammonium fluoride (TBAF) yielded the desired **5V-NBMes** in 82% yield. Finally, the unprotected **6Bpin** afforded under Suzuki-Miyaura cross-coupling conditions with vinyl bromide the final isomer **6V-NBMes** in 71% yield. The Jäkle group also prepared *meta*-mesitylstyrene (***m*MesSt**) as a direct all-carbon analog of both **4V-NBMes** and **6V-NBMes** and *para*-mesitylstyrene (***p*MesSt**) as an analogue of **5V-NBMes**. These monomers were readily obtained by Suzuki-Miyaura cross-coupling of 2-bromomesitylene and 3- or 4-vinylphenyl boronic acid, respectively (see Experimental Section). In addition, *ortho*-mesitylstyrene (***o*MesSt**) was prepared and found to only very slowly polymerize in the presence of AIBN at 70 °C, confirming the suspicion that *ortho*-substituted monomers would not be desirable polymerization targets (see Experimental Section).

¹⁰ Jackson, L. A.; Allen, C. W. *Phosphorus Sulfur* **1989**, *41*, 341-346.

Scheme 3.1. Monomer syntheses. (TBS = *tert*-butyldimethylsilyl; dppf = 1,1'-bis(diphenylphosphino)ferrocene; MTBE = methyl *tert*-butyl ether; TBAF = tetra-*n*-butylammonium fluoride; pin = pinacolato).



3.3 Electronic Structure Calculations

When considering the propensity of these different monomers to undergo polymerization it is important to recognize that each position on the azaborine ring is electronically distinct. We performed electronic structure calculations of the azaborine isomers as well as their corresponding all-carbon counterparts using the CAM-B3LYP hybrid exchange-correlation functional with the 6-311G(d,p) basis set (Figure 3.3). Electrostatic potential (ESP) maps show the charge distribution typical of aromatic compounds, with an electron-rich surface above and below the ring and an electron deficient region around the C-H edge (Figure 3.3b). The positioning of the vinyl relative to the mesityl group does not significantly impact the charge distribution (Figure 3.3c) for the carbonaceous *m*MesSt and *p*MesSt or the C-H bond dissociation energies (BDEs, Figure 3.3d) of the respective ethyl-substituted derivatives. On the other hand, the positioning of the vinyl/ethyl group relative to the more electronegative nitrogen and less electronegative boron atoms in the azaborine ring does influence both the charge distribution and the C-H BDEs. The C α -H BDE

values for the ethyl derivatives of **6V-NBMes**, **5V-NBMes**, and **4V-NBMes** (80.1, 82.3, 83.6 kcal mol⁻¹, respectively) increase with increasing distance from the nitrogen atom of the azaborine ring in the order $\text{C}\alpha\text{-H}(\mathbf{6V}\text{-NBMes}) < \text{C}\alpha\text{-H}(\mathbf{5V}\text{-NBMes}) < \text{C}\alpha\text{-H}(\mathbf{4V}\text{-NBMes})$. The higher stability of the radical derived from **6V-NBMes** may also be related to the enhanced resonance stabilization due to conjugation with the butadiene system of the azaborine moiety. We note that these differences are relatively modest as a much larger difference in BDEs is seen when comparing *B*-ethylazaborine ($\text{C}\alpha\text{-H}$ BDE of 88.2 kcal mol⁻¹) to ethylbenzene ($\text{C}\alpha\text{-H}$ BDE of 83.0 kcal mol⁻¹),⁴⁷ indicating a significantly lower stability for the radical derived from *B*-vinylazaborine **3.3** that served as an intermediate in the synthesis of polymer **3.4** (Figure 3.1).

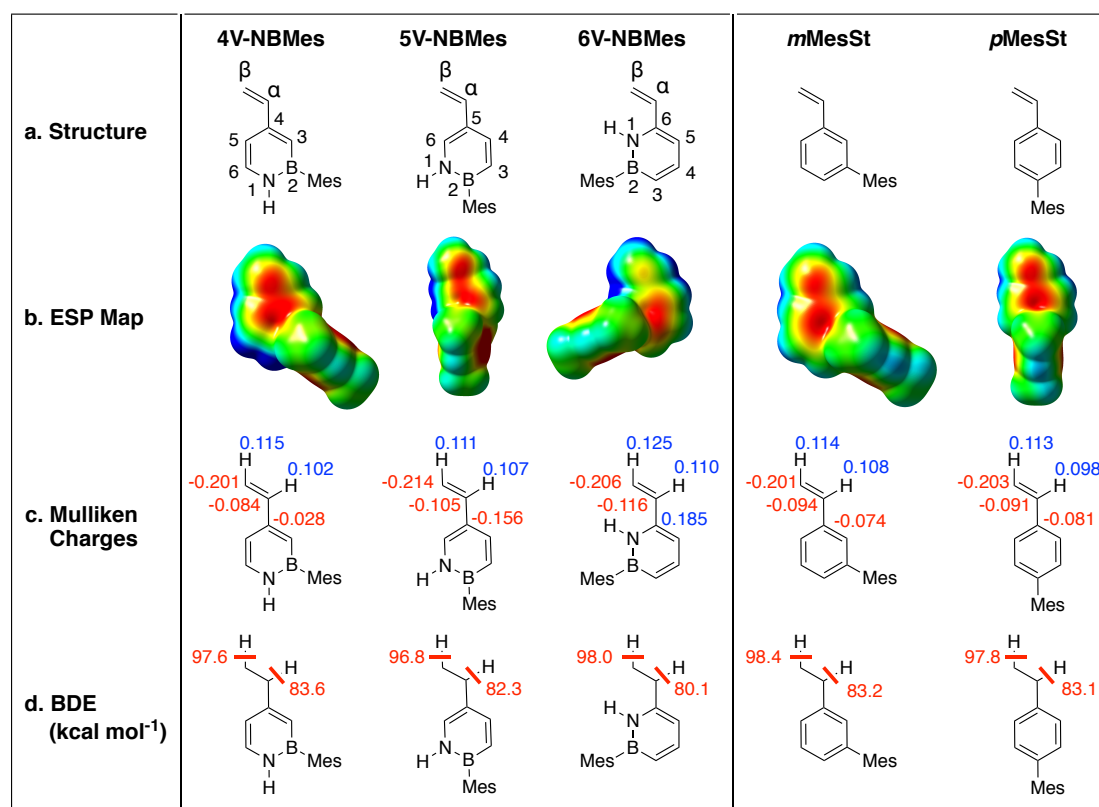


Figure 3.3. a) Structures of the *B*-mesitylazaborine and mesitylstyrene compounds; b) electrostatic potential (ESP) maps; c) Mulliken charges of selected atoms; d) calculated bond dissociation energies (BDEs).

Furthermore, as can be seen from the Mulliken charge values (Figure 3.3c), the vinyl-bound intra-ring C6 carbon (+0.185 in **6V-NBMes**) and the C4 carbon (-0.028 in **4V-NBMes**) in an 1,2-azaborine are relatively electron deficient in comparison to the intra-ring *ipso*-carbon of the mesitylstyrene derivatives (~ -0.08 for *mMesSt* and *pMesSt*). On the other hand, the vinyl-bound intra-ring C5 carbon (-0.156 in **5V-NBMes**) is significantly more electron-rich. The observed intra-ring charge distribution is consistent with the nitrogen atom exerting its inductive electron-withdrawing (-I) influence. Importantly, the mesomeric electron-donating (+M) effect is carried over into the attached vinyl group, rendering the vinyl carbons of **5V-NBMes** significantly more electron-rich than those of **4V-NBMes**. Those of **6V-NBMes** are also relatively electron-rich, due to the *linear* conjugation with the butadiene group of the azaborine moiety. The theoretically predicted differences in the Mulliken charges are nicely reflected in the ^{13}C NMR data of the azaborine monomers (Experimental Section, Table 3.23). Specifically, the ^{13}C NMR data are consistent with the notion that the C β -carbon of **5V-NBMes** (Mulliken charge -0.217, $\delta(^{13}\text{C}) = 109.6$ ppm) is the most electron-rich and the C β -carbon of **4V-NBMes** (Mulliken charge -0.201, $\delta(^{13}\text{C}) = 115.9$ ppm) the least electron-rich in this series of isomeric compounds.

3.4 Polymerizations

The Jäkle group conducted the homopolymerization of the monomers (see Experimental Section for details as well as full characterization of the homopolymers). Higher conversion of **4V-NBMes** was observed relative to the other isomers in the homopolymerization experiments. While the higher conversion indicates this monomer is more reactive, chain transfer and early termination due to trace impurities or side reactions interfere with this polymerization reaction as

indicated by the relatively high dispersities for **P4V-NBMes** and **P5V-NBMes** (Experimental Section, Table 3.2). Another indication is that under otherwise identical conditions, the polymerization of the isosteric carbonaceous mesitylstyrene analogues goes to much higher conversion over a shorter period of time (Experimental Section, Table 3.2). To better understand the differences in polymerization rates the Jäkle group investigated the free radical copolymerization of the azaborine monomers with styrene as well as with the direct isosteric carbon analogues to produce the corresponding copolymers shown in Figure 3.4. Polymerizations were conducted with 1 mol% AIBN in anisole at a monomer concentration of $[M1] = [M2] = 2.25 \text{ M}$ for 20 h at 70 °C. The conversion of the monomers in each copolymerization experiment suggested that **4V-NBMes** and **6V-NBMes** in fact polymerize preferentially compared to styrene, but **5V-NBMes** is incorporated at a lower rate than styrene (Table 3.1). This was further verified by elemental analyses of the isolated polymers, which were reasonably consistent with the conversions determined by ^1H NMR (see Experimental Section). To achieve an even more direct comparison of the B-N for C=C substitution that also takes into consideration the steric and electronic effects of the mesityl groups we also copolymerized the azaborine monomers with the respective isosteric monomers ***m*MesSt** and ***p*MesSt**, respectively. The results were qualitatively similar, further confirming these reactivity trends.

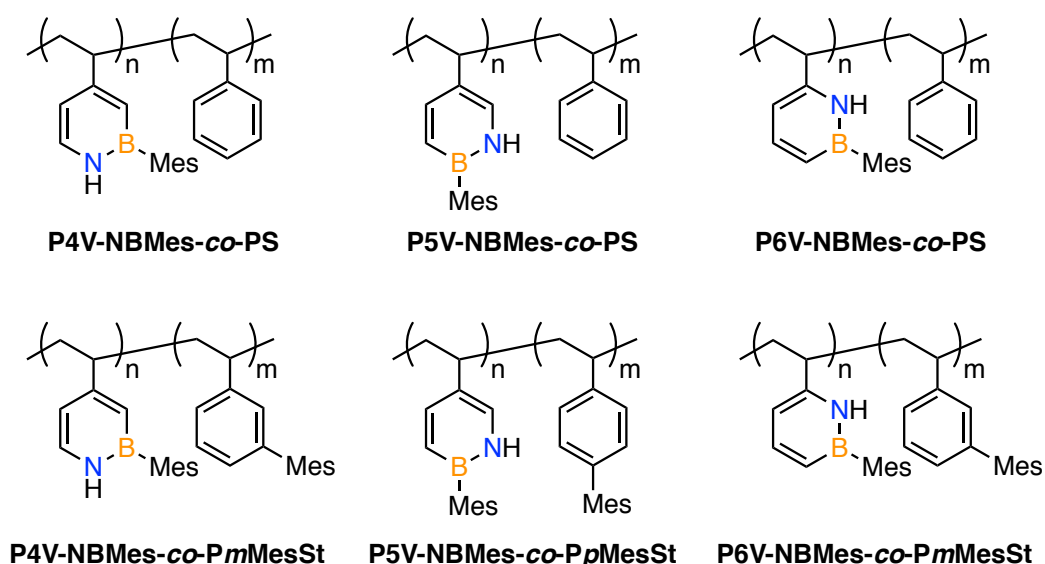


Figure 3.4. *B*-mesitylazaborine-(mesityl)styrene copolymer structures.

Table 3.1. Data for the free radical copolymerization of vinyl-functionalized azaborines with styrene (St) and mesitylstyrene (MesSt)

Copolymer	Feed ratio ^a	T / t (°C / h)	Conv (BN) ^b (%)	Conv (St) ^c (%)	M_n (kDa) ^d	M_w (kDa) ^d	D ^d
P4V-NBMes-co-PS	50:50:1	70 / 24	57	50	15.6	50.7	3.25
P5V-NBMes-co-PS	50:50:1	70 / 24	41	63	19.6	39.8	2.02
P6V-NBMes-co-PS	50:50:1	70 / 24	57	40	10.9	32.8	3.02
P4V-NBMes-co-PmMesSt	50:50:1	70 / 10	65	66	19.2	54.8	2.85
P5V-NBMes-co-PpMesSt	50:50:1	70 / 10	32	54	28.9	59.3	2.05
P6V-NBMes-co-PmMesSt	50:50:1	70 / 10	26	15	8.8	24.4	2.77
P6V-NBMes-co-PmMesSt	50:50:1	70 / 24	41	14	16.0	56.7	3.55

[a] Feed ratio of [BN monomer]:[Styrene]:[AIBN] in anisole, [M1] = [M2] = 2.25 M. [b] Conversion of azaborine monomer (BN) estimated based on ¹H NMR integration of residual BN vinyl signal before purification relative to anisole standard. [c] Conversion of styrene/mesitylstyrene estimated based on ¹H NMR integration of residual styrene vinyl signal before purification relative to anisole standard. [d] Based on GPC analysis of isolated product in THF relative to PS standards.

The results of these experiments consistently indicate that at about 50% conversion **5V-NBMes** with its vinyl group in *para*-position to Mes is incorporated to

a lesser extent than (mesityl)styrene, whereas **4V-NBMes** and **6V-NBMes**, which have vinyl groups in *meta*-position to Mes, are incorporated to a similar extent or even preferentially. These results indicate that sterics do not play a significant role in governing the relative rates of incorporation of the BN-monomers, as one would expect the more sterically-hindered **4V-NBMes** and **6V-NBMes** to be incorporated to a lesser extent than the less sterically hindered **5V-NBMes**. Thus, electronic factors, i.e. the positioning of the BN bond relative to the growing polymer chain, must primarily determine the relative rates of incorporation of BN-monomers.

The different rates of incorporation could be due to differences in the tendency of an azaborine-terminated polymer radical to add to another azaborine monomer (azaborine homopolymerization) and/or the tendency of a (mesityl)styrene-terminated polymer radical to add to the specific azaborine monomer (crossover to azaborine). In-depth reactivity ratio determinations would be necessary to further evaluate the relative monomer reactivities.^{8, 11} However, we note that the relatively lower incorporation of the **5V-NBMes** ($C\alpha$ -H BDE = 82.3 kcal mol⁻¹) isomer does not correlate well with the calculated BDE trends (see Figure 3.3), which suggested that the radical derived from **6V-NBMes** ($C\alpha$ -H BDE = 80.1 kcal mol⁻¹) is the most stabilized and that of **4V-NBMes** ($C\alpha$ -H BDE = 83.6 kcal mol⁻¹) the least stabilized (Table 3.1). The difference in reactivity for **5V-NBMes** is therefore more likely related to a radical polarity mismatch¹¹ in that a nucleophilic benzylic radical is predicted to react more slowly with a relatively electron rich monomer such as **5V-NBMes**. The partial charges on the $C\beta$ -position, the presumed site of attack by the nucleophilic benzylic radical, of the monomers support the radical polarity mismatch hypothesis. The partial charge of the $C\beta$ -position for **5V-NBMes** is -0.214, while for

¹¹ P. C. Hiemenz and T. P. Lodge, *Polymer Chemistry*, Second Edition., CRC Press, Boca Raton, FL, 2007.

the other two BN-monomers as well as the CC-monomers the partial charges of their C β -positions fall between -0.201 and -0.206 (Figure 3.3).

3.5 Thermal and Spectral Properties of Monomers and Polymers

As a precaution, the azaborine polymers were stored under N₂ atmosphere. However, based on ¹H and ¹¹B NMR analyses, the polymers proved to be perfectly stable over a period of over one week in air either as a solid or in aerated chloroform solution. The thermal stability of the polymers was established by thermogravimetric analysis (TGA), while glass transition temperatures (*T_g*) were determined by differential scanning calorimetry (DSC) (Experimental Section, Figure 3.72).

Finally, we investigated the photophysical properties of the new polymers and their precursors. The monomers **4V-NBMes**, **5V-NBMes**, and **6V-NBMes** showed the longest wavelength absorption maxima at 298, 299 and 303 nm, respectively, and a second higher energy absorption at ca. 240 to 250 nm. For the polymers, the longest wavelength absorptions were slightly blue-shifted to 273, 288 and 286 nm due to the smaller π -system of the chromophores (vinylazaborine vs azaborine) after polymerization (Figure 3.5). The longest wavelength absorption maxima of the BN compounds are red-shifted in relation to the CC compounds, a typical effect of BN/CC isosterism.¹² Among the isomeric azaborine monomers and polymers, the absorption maxima are similar. However, intriguingly, the **5V-NBMes** monomer exhibits absorption behavior that is distinct from the other isomers in that its lowest-energy absorption peak at 299 nm has a significantly smaller extinction coefficient than its absorption peak at ~260 nm. TD-DFT calculations are consistent with this observation, revealing that the oscillator strength of the first excited state of **5V-NBMes** is significantly smaller than that of the other monomers and about one order

¹² Marwitz, A. J. V.; Matus, M. H.; Zakharov, L. N.; Dixon, D. A.; Liu, S.-Y. *Angew. Chem. Int. Ed.* **2009**, *48*, 973-977.

of magnitude smaller than its second excited state (see Experimental Section). The unusual absorption behavior of the **5V-NBMes** isomer is perhaps due to the fact that it is the only isomer in which the vinyl group is linearly conjugated with the nitrogen lone pair.

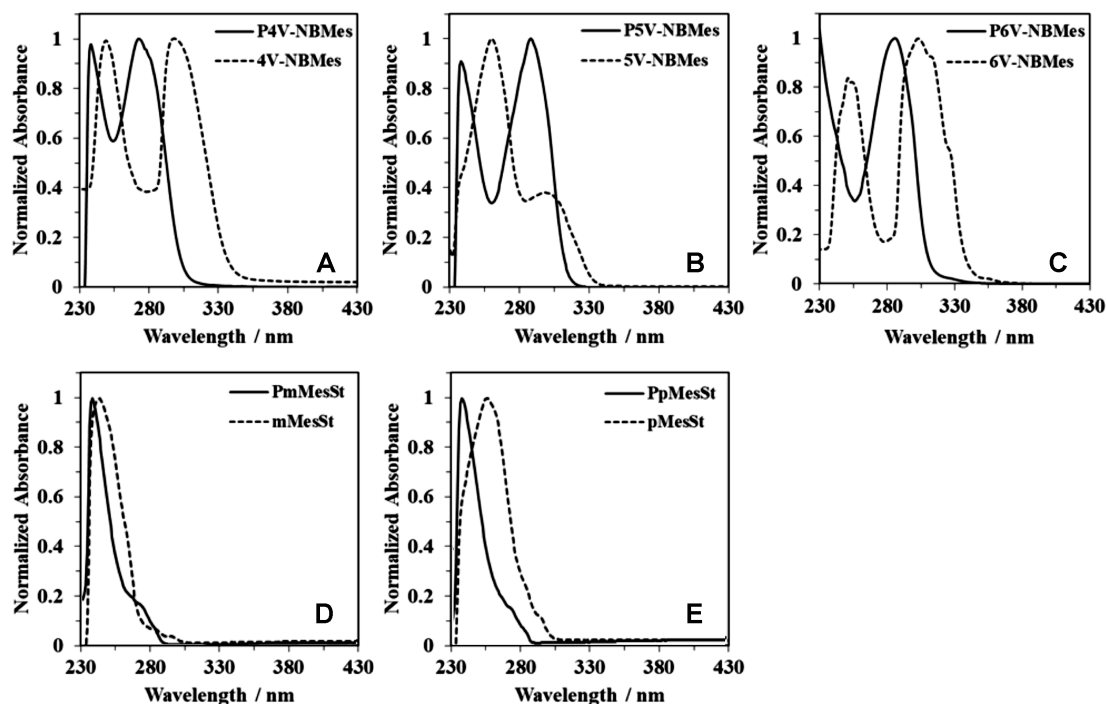


Figure 3.5. Comparison of UV-Vis spectra of B-mesityl azaborine (A-C) and mesitylstyrene (D-E) homopolymers with those of the respective monomers in THF solution.

The TD-DFT calculations also revealed distinct differences in regard to the nature of the lowest energy absorptions of the isomeric vinyl azaborine monomers and the respective ethyl derivatives that serve as models for the polymers (Figure 3.6).

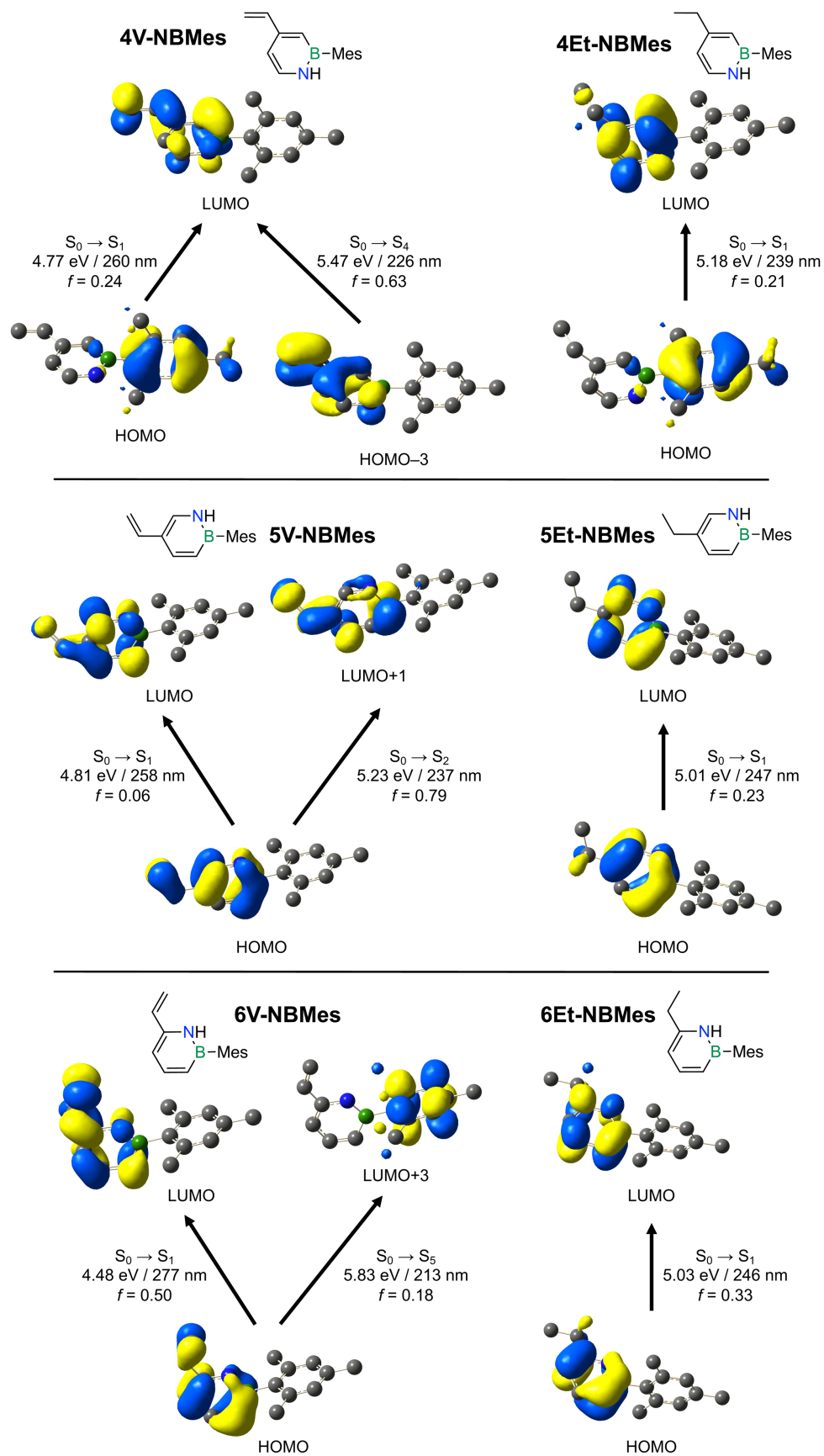


Figure 3.6. Illustration of the calculated electronic excitations for the isomeric vinyl azaborine monomers (left) and the respective ethyl-substituted model compounds (right).

For **5V-NBMe**s, both the very weak lowest energy HOMO to LUMO and the more intense higher energy HOMO to LUMO+1 transition is primarily due to π - π^* excitations localized on the vinylazaborine moiety. The LUMO shows relatively modest contributions of the vinyl group whereas the LUMO+1 is primarily centered on the vinyl group and empty p-orbital on boron. The S_0 - S_1 transition for **5Et-NBMe**s is localized on the azaborine moiety. A similar picture emerges for **6V-NBMe**s and **6Et-NBMe**s, except for that the higher energy absorption for **6V-NBMe**s involves a charge transfer to the mesityl group (LUMO+3). In sharp contrast, for **4V-NBMe**s and **4Et-NBMe**s, which are identical to **5V-NBMe**s and **5Et-NBMe**s other than that the positions of B and N in the ring system are switched, the lowest energy absorptions primarily result from charge transfer from the electron-rich mesityl group to the azaborine moiety.

3.6 Conclusions

In order to demonstrate the utility of our newly developed resolution methods we synthesized three isomeric B-mesityl vinylazaborines, substituted at the C4, C5, and C6 positions of the 1,2-azaborine ring. To examine the influence of the vinyl group position on the polymerization activity and the polymer properties we compared the three isomeric B-mesityl vinylazaborines, as well as the carbon analogues with a mesityl group attached in the *meta*- or *para*-position of styrene. The monomers have all been successfully converted into high molecular weight polymers by AIBN-initiated standard free radical polymerization. In order to better understand the effect of the BN-bond position on the rate of polymerization, we conducted copolymerization experiments between the BN-monomers and styrene as well as their mesityl-containing counterparts. Our results indicate that the **4V-NBMe**s and **6V-NBMe**s monomers are incorporated preferentially, while the **5V-NBMe**s monomer is

not copolymerized as readily as the carbonaceous compounds. With the aid of detailed computational studies, we posit that the differences in the relative rates of copolymerization can be explained by a radical polarity mismatch between the electron-rich **5V-NBMes** monomer and the nucleophilic benzylic radical.

Overall, our results demonstrate that isomeric azaborine monomers exhibit similar reactivity as the styrene analogs, while offering tunability as a result of attachment of the vinyl groups to different carbon atoms in the heterocyclic framework. The new polymers described herein add to a growing but still underdeveloped class of aromatic polymers, in which a C-C unit is replaced by an isoelectronic but polarized B-N unit. The favorable stability and facile copolymerization suggest that many new functional materials with azaborine moieties replacing styrenic groups can be accessed.

3.7 Experimental Section

3.7.1 General Methods

All oxygen- and moisture-sensitive manipulations were carried out under an inert atmosphere using either standard Schlenk techniques or a glove box. NMR data were acquired at 25 °C. 499.9 MHz ^1H and 160.4 MHz ^{11}B NMR data were recorded on a 500 MHz Bruker AVANCE spectrometer, 500.2 MHz ^1H and 125.8 MHz ^{13}C NMR data on a 500 MHz Bruker Auto AVANCE spectrometer, and 599.7 MHz ^1H , 150.8 MHz ^{13}C and 192.4 MHz ^{11}B NMR data on a Varian INOVA 600 spectrometer. ^{11}B NMR spectra were acquired with boron-free quartz NMR tubes either on the Varian INOVA 600 with a boron-free 5 mm dual broadband gradient probe (Nalorac, Varian Inc., Martinez, CA) or the 500 MHz Bruker Auto Avance with a 5mm PH SEX 500S1 11B-H/F-D probe. ^1H and ^{13}C NMR spectra were referenced internally to solvent signals (CDCl_3 : 7.26 ppm for ^1H NMR, 77.16 ppm for ^{13}C NMR) and all other NMR spectra externally to SiMe_4 (0 ppm). IR spectra were recorded on a Bruker Alpha FT-IR instrument with OPUS software.

High-resolution mass spectrometry data were obtained at the Boston College mass spectrometry facility on a JEOL AccuTOF instrument (JEOL USA, Peabody, MA), equipped with a DART ion source (IonSense, Inc., Danvers, MA) in positive ion mode.

GPC-RI analyses were performed in THF (1.0 mL/min, 35 °C) using a Viscotek GPCmax with a VE 2001 GPC solvent/sample module, a 2600 UV-PDA detector, and a TDA 305 triple detector array. A set of two columns consisting of one PLgel 5 mm mixed-D and one PLgel 5 mm mixed-C column was used for separation and ten polystyrene standards (580 Da – 364000 Da, Polymer Laboratories, Varian Inc.) for calibration. Differential scanning calorimetry (DSC) measurements were performed on a TA Instruments Discovery Series system at a scan rate of 20 °C / min. The results reported are from the second heating cycle. Thermogravimetric analyses (TGA) were performed on a TA Instruments Discovery Series analyzer at a heating rate of 10 °C min^{-1} . UV-visible absorption data were acquired on a Varian Cary 5000 UV-Vis/NIR spectrophotometer.

3.7.2 Materials

THF was distilled from Na/benzophenone, anisole and chlorinated solvents were distilled from CaH_2 . Toluene and hexanes were purified using a solvent purification system (Innovative Technologies). Azobisisobutyronitrile (AIBN) initiator was recrystallized in methanol. Benzyl dithiobenzoate (BDTB) RAFT agent was purified by column chromatography on silica gel using hexanes as the eluent. Azaborines **4BPin**, **5BPin**, **6Bpin**, and **5I** were prepared according to previously reported procedures (Chapter 2). 3-Vinylphenylboronic acid and 4-vinylphenylboronic acid were purchased from Combi Blocks and 2-bromomesitylene from Acros Organics. All other solvents and chemicals were purchased from commercial sources and used without further purification unless noted otherwise.

3.7.3 Monomer Synthesis

Compound 3.9. A 75 mL pressure vessel was charged with **4Bpin** (0.510 g, 1.20 mmol), bromo-ethylene 1.0 M THF solution (4.81 mL, 4.81 mmol), Pd(dppf)Cl₂ (0.044 g, 0.60 mmol), KOH (0.202 g, 3.61 mmol), H₂O (1.0 mL), and THF (5.0 mL). The KOH pellets were ground into a powder and the H₂O was sparged with argon for 1 hour prior to use. The reaction mixture was then heated at 70 °C for 1 hour. The organic layer was decanted, and the reaction mixture was concentrated under reduced pressure. The desired product was obtained as a yellow oil after purification by silica gel chromatography with 99:1 pentane:ether as the eluent (0.312 g, 77%). ¹H NMR (400 MHz, CD₂Cl₂) δ 7.45 (d, *J* = 7.1 Hz, 1H), 6.77 (s, 2H), 6.62 (m, 1H), 6.54 (m, 1H), 6.44 (s, 1H), 5.79 (dd, *J* = 17.6, 1.1 Hz, 1H), 5.30 (m, 1H), 2.26 (s, 3H), 2.06 (s, 6H), 0.91 (s, 9H), -0.00 (s, 6H). ¹³C NMR (126 MHz, CD₂Cl₂) δ 149.67, 138.96, 138.94, 138.63, 136.23, 126.72, 115.67, 108.18, 27.13, 23.08, 20.81, 19.04, -3.69 (the carbons attached to boron were not observed). ¹¹B NMR (160 MHz, CD₂Cl₂) δ 40.00. FTIR (thin film): ν cm⁻¹ = 2960, 2930, 2859, 1630, 1604. HRMS (DART) calcd. for C₂₁H₃₂BNSi ([M+H]⁺) 338.2475, found 338.248.

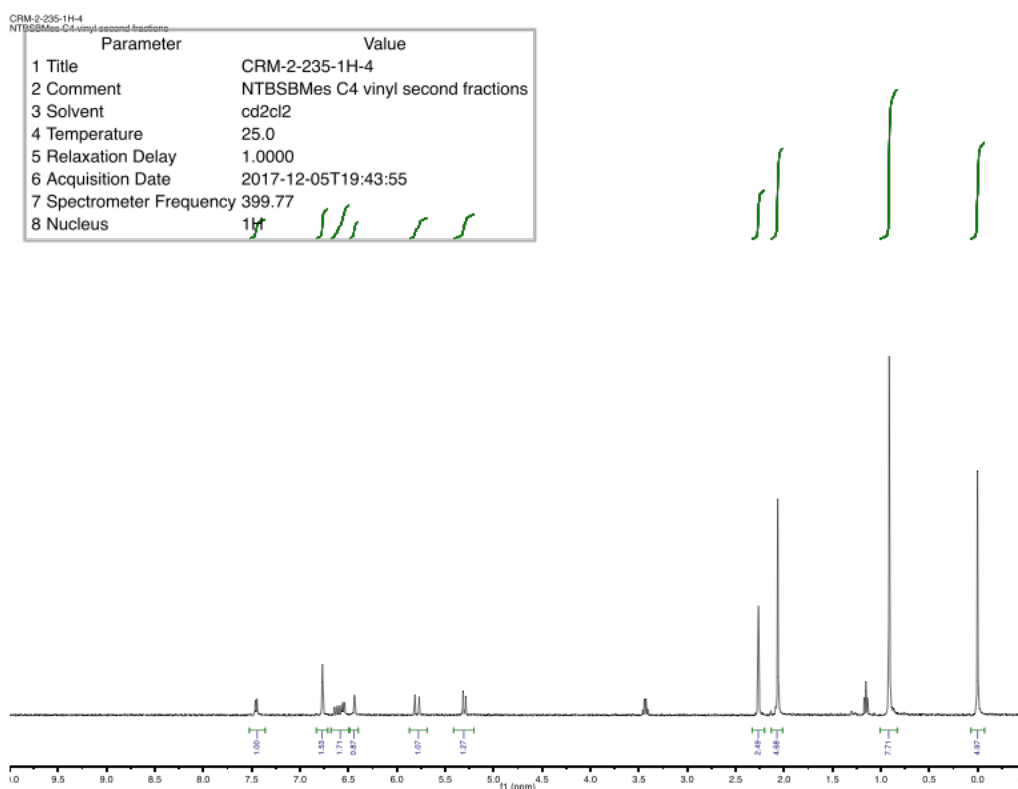
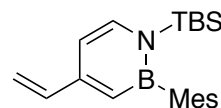


Figure 3.7. ¹H NMR spectrum of **3.9** in CD₂Cl₂.

CRM-2-235-13C-3
NTBSBMesC4vinyl full char

Parameter	Value
1 Title	CRM-2-235-13C-3
2 Comment	NTBSBMesC4vinyl full char
3 Solvent	cd2cl2
4 Temperature	25.0
5 Relaxation Delay	1.0000
6 Acquisition Date	2017-12-05T19:49:13
7 Spectrometer Frequency	125.71
8 Nucleus	13C

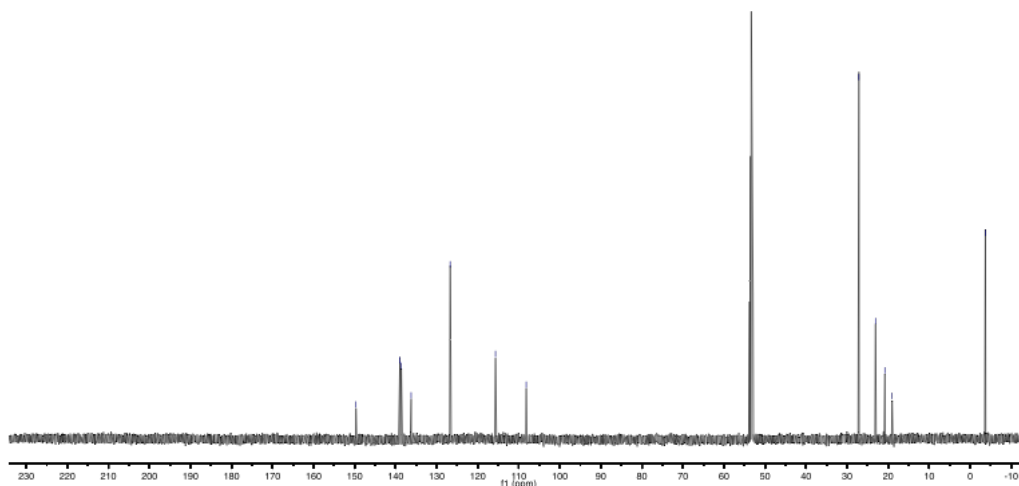


Figure 3.8. ^{13}C NMR spectrum of **3.9** in CD_2Cl_2 .

CRM-2-235-11B-2
NTBSBMesC4vinyl full char

Parameter	Value
1 Title	CRM-2-235-11B-2
2 Comment	NTBSBMesC4vinyl full char
3 Solvent	cd2cl2
4 Temperature	25.0
5 Relaxation Delay	0.0100
6 Acquisition Date	2017-12-05T20:03:25
7 Spectrometer Frequency	160.35
8 Nucleus	11B

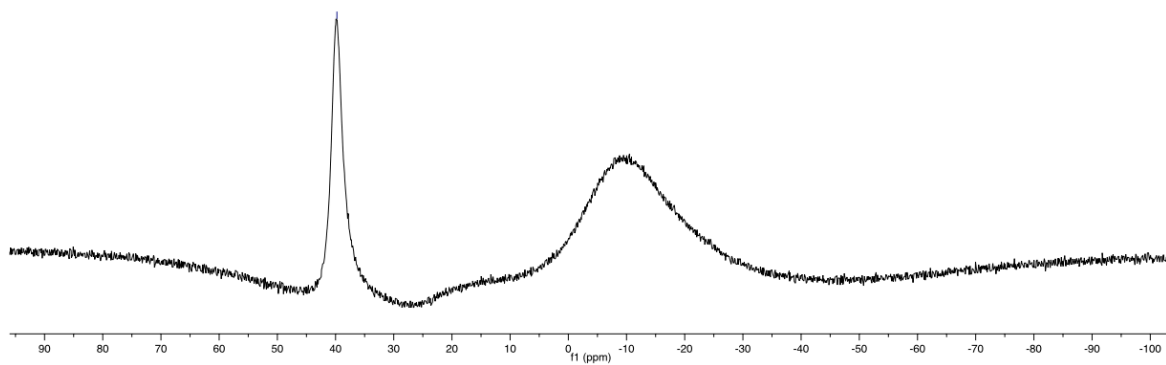


Figure 3.9. ^{11}B NMR spectrum of **3.9** in CD_2Cl_2 .

Compound 3.10. A 150 mL pressure vessel was charged with **5I** (2.00 g, 4.57 mmol), 4,4,5,5-tetramethyl-2-vinyl-1,3,2-dioxaborolane (1.06 g, 6.86 mmol), Pd(dppf)Cl₂ (0.167 g, 0.229 mmol), KOH (0.77 g, 13.7 mmol), H₂O (2.8 mL), and THF (28 mL). The reaction mixture was heated at 60 °C for 30 minutes. The organic layer was decanted, and volatiles were removed *in vacuo*. The product was obtained as a pale yellow oil after purification by silica gel chromatography with 99:1 pentane:ether as the eluent (1.38 g, 89%). ¹H NMR (500 MHz, CD₂Cl₂) δ 7.88 (dd, *J* = 11.2, 1.8 Hz, 1H), 7.42 (s, 1H), 6.77 (s, 2H), 6.59 (m, 2H), 5.52 (d, *J* = 17.6 Hz, 1H), 5.03 (d, *J* = 11.0 Hz, 1H), 2.27 (s, 3H), 2.06 (s, 6H), 0.92 (s, 9H), 0.02 (s, 6H). ¹³C NMR (126 MHz, CD₂Cl₂) δ 139.52, 138.94, 138.59, 136.38, 135.50, 121.88, 109.99, 108.61, 27.11, 23.04, 20.81, 18.96, -3.66 (the boron-bound carbons were not observed). ¹¹B NMR (160 MHz, CD₂Cl₂) δ 40.32. FTIR (thin film): ν cm⁻¹ = 2961, 2931, 2859, 1633, 1609. HRMS (DART) calcd. for C₂₁H₃₃BNSi ([M+H]⁺) 338.2475, found 338.248.

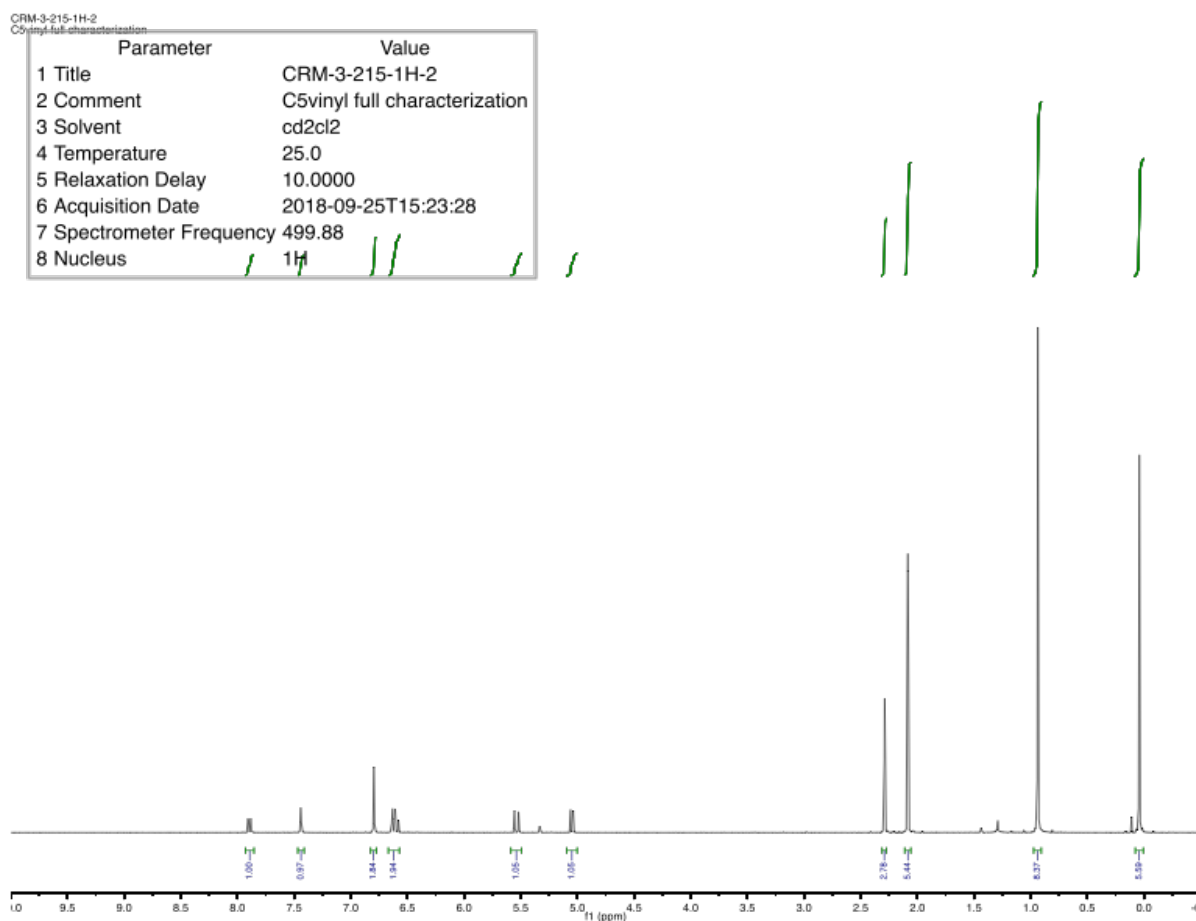
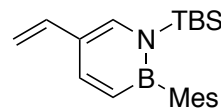


Figure 3.10. ¹H NMR spectrum of **3.10** in CD₂Cl₂.

Compound 4V-NBMes. A 100 mL round bottom flask was charged with **3.9** (1.28 g, 3.79 mmol), H₂O (0.683 g, 37.9 mmol) and THF (30 mL). The reaction mixture was allowed to stir at room temperature, and a 1.0 M solution of tetrabutylammonium fluoride in THF (3.79 mL, 3.79 mmol) was added dropwise via syringe. More H₂O was added and the crude product was extracted with diethyl ether. The organic layer was dried over magnesium sulfate, passed through a Buchner funnel lined with filter paper, then concentrated *in vacuo*. The product was obtained as a clear, colorless oil after purification by silica gel chromatography with 99:1 pentane:ether as the eluent (0.70 g, 83%). ¹H NMR (599.7 MHz, CDCl₃) δ = 7.73 (s, 1H), 7.36 (t, *J* = 7.2 Hz, 1H), 6.88 (s, 2H), 6.77 (s, 1H), 6.71 (dd, *J* = 17, 11 Hz 1H), 6.54 (d, *J* = 6.6 Hz, 1H), 5.80 (d, *J* = 17 Hz, 1H), 5.32 (d, *J* = 11 Hz, 1H), 2.31 (s, 3H), 2.18 (s, 6H). ¹³C NMR (150.8 MHz, CDCl₃) δ = 151.2, 140.4, 139.7, 137.4, 134.3, 129.1 (br), 115.9, 107.6, 23.2, 21.3 (the mesityl carbon adjacent to boron was not observed). ¹¹B NMR (160.4 MHz, CDCl₃) δ = 36.3. FTIR (thin film): ν cm⁻¹ = 3359, 2979, 2916, 2856, 1609. HRMS (DART) calcd. for C₁₅H₁₉BN ([M+H]⁺) 224.1611, found 224.1621. UV-Vis (THF): λ_{max} = 298, 249 nm.

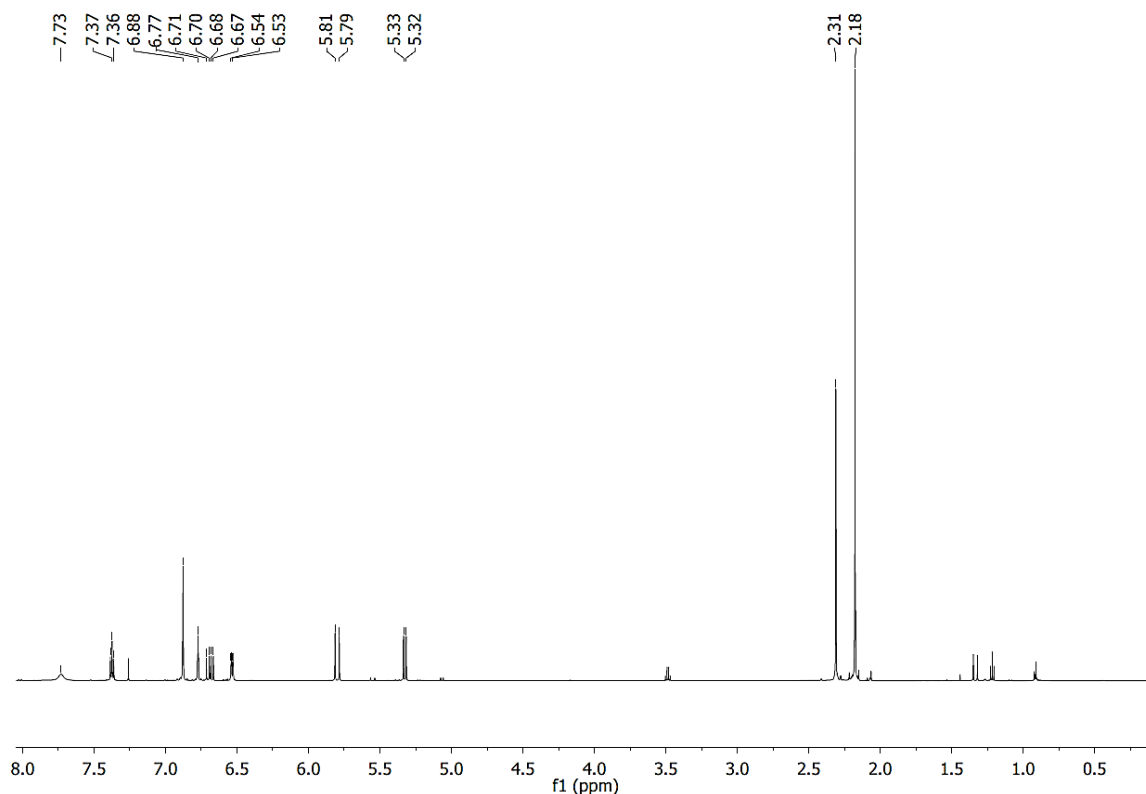
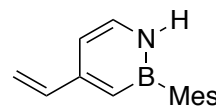


Figure 3.13. ¹H NMR spectrum of **4V-NBMes** monomer in CDCl₃.

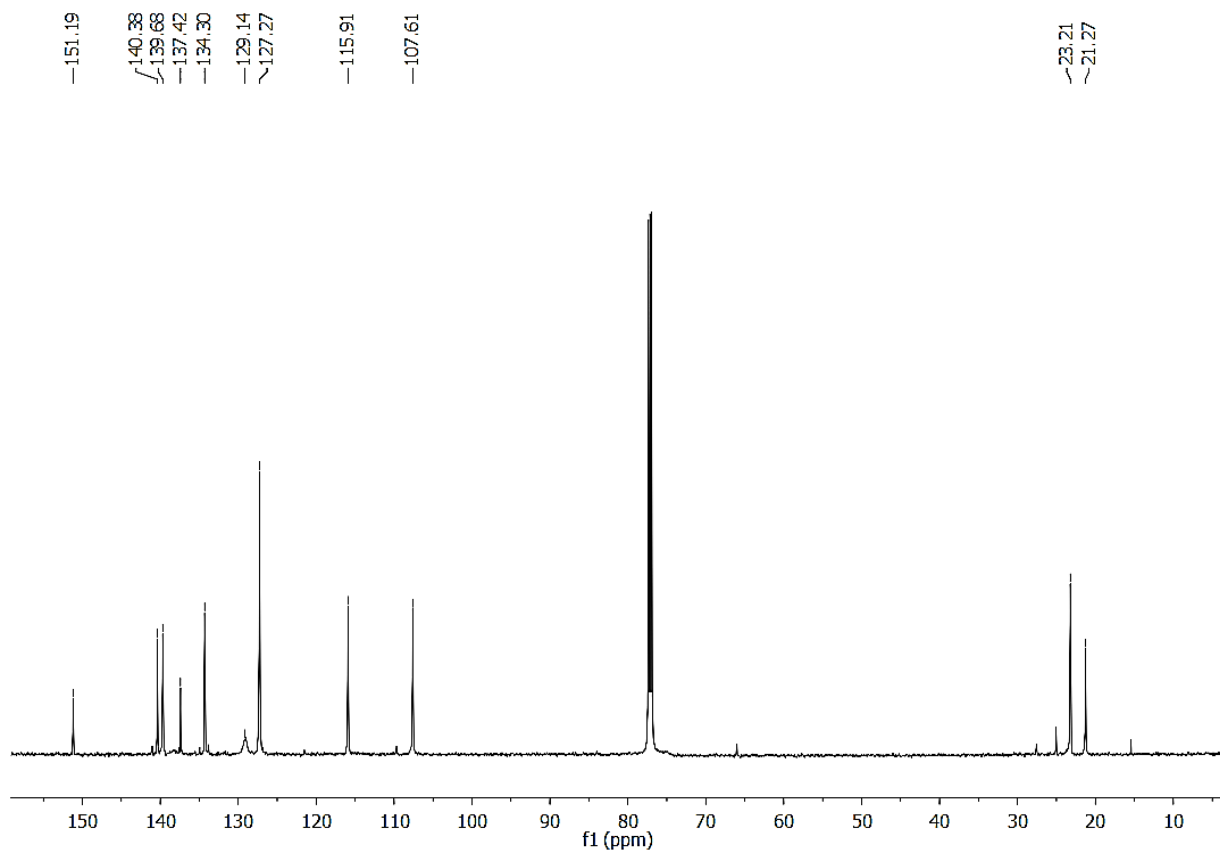


Figure 3.14. ^{13}C NMR spectrum of 4V-NBMes monomer in CDCl_3 .

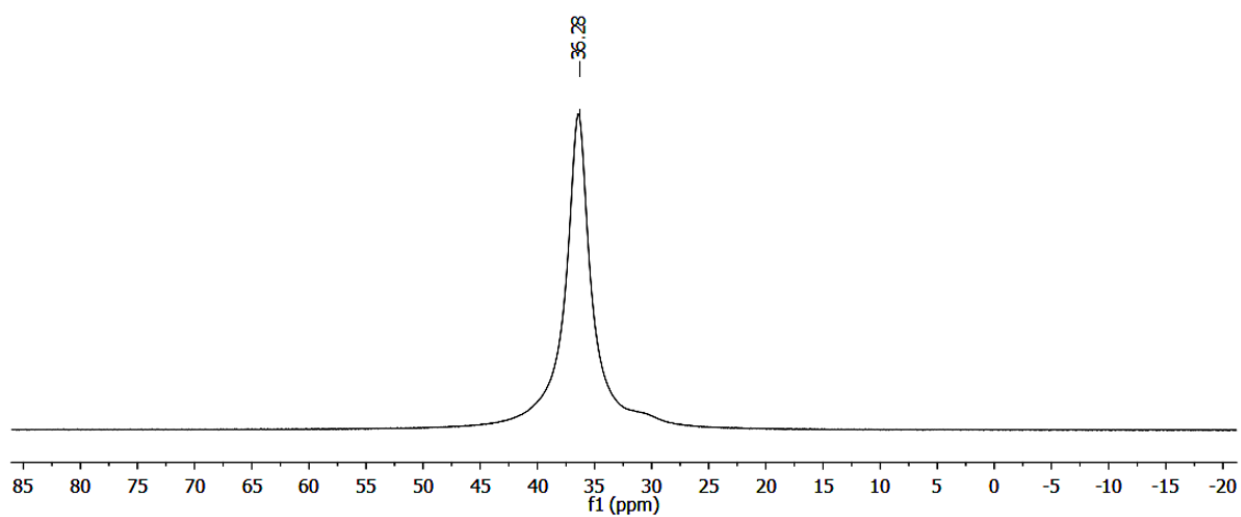


Figure 3.15. ^{11}B NMR spectrum of 4V-NBMes monomer in CDCl_3 .

Compound 5V-NBMes. A 50 mL round bottom flask was charged with **3.10** (620 mg, 1.84 mmol), H₂O (331 mg, 18.4 mmol) and THF (12 mL). The reaction mixture was allowed to stir at room temperature and a 1.0 M solution of tetrabutylammonium fluoride in THF (1.84 mL, 1.84 mmol) was added dropwise via syringe. More H₂O was added, and the crude product was extracted with diethyl ether. The organic layer was dried over magnesium sulfate, passed through a Buchner funnel lined with filter paper, and concentrated *in vacuo*. The product was obtained as a clear, colorless oil after purification by silica gel chromatography with 99:1 pentane:ether as the eluent (325 mg, 79%). ¹H NMR (599.7 MHz, CDCl₃) δ = 8.38 (d, *J* = 13 Hz, 1H), 8.11 (s, 1H), 7.69 (d, *J* = 7.8 Hz, 1H), 7.27 (m, 1H), 7.25 (s, 2H), 6.92 (dd, *J* = 17, 11 Hz, 1H), 5.91 (d, *J* = 18 Hz, 1H), 5.43 (d, *J* = 11 Hz, 1H), 2.68 (s, 3H), 2.54 (s, 6H). ¹³C NMR (150.8 MHz, CDCl₃) δ = 141.0, 140.3, 137.5, 134.9, 133.7, 131.3 (br), 127.3, 121.4, 109.6, 23.1, 21.3. (the mesityl carbon adjacent to boron was not observed). ¹¹B NMR (160.4 MHz, CDCl₃) δ = 36.1. FTIR (thin film): ν cm⁻¹ = 3353, 2915, 2855, 1635, 1608. HRMS (DART) calcd. for C₁₅H₁₉BN ([M+H]⁺) 224.1611, found 224.1621. UV-Vis (THF): λ_{max} = 299, 260 nm.

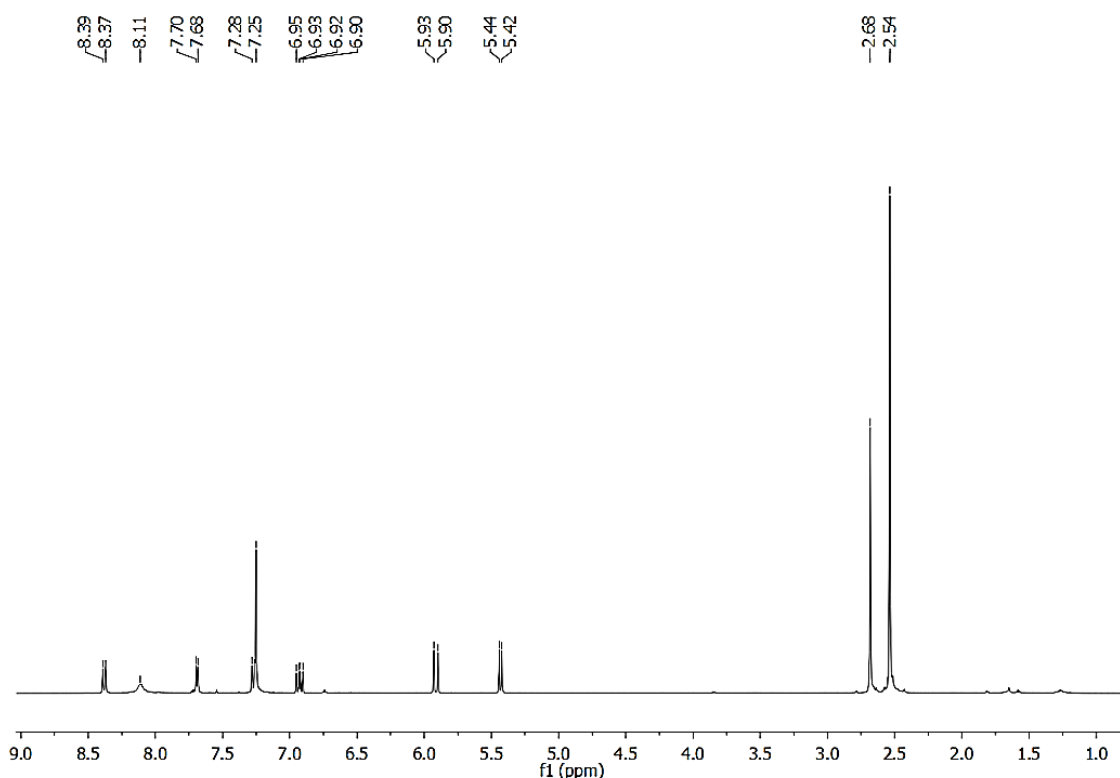
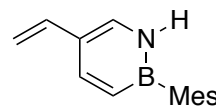


Figure 3.16. ¹H NMR spectrum of **5V-NBMes** monomer in CDCl₃.

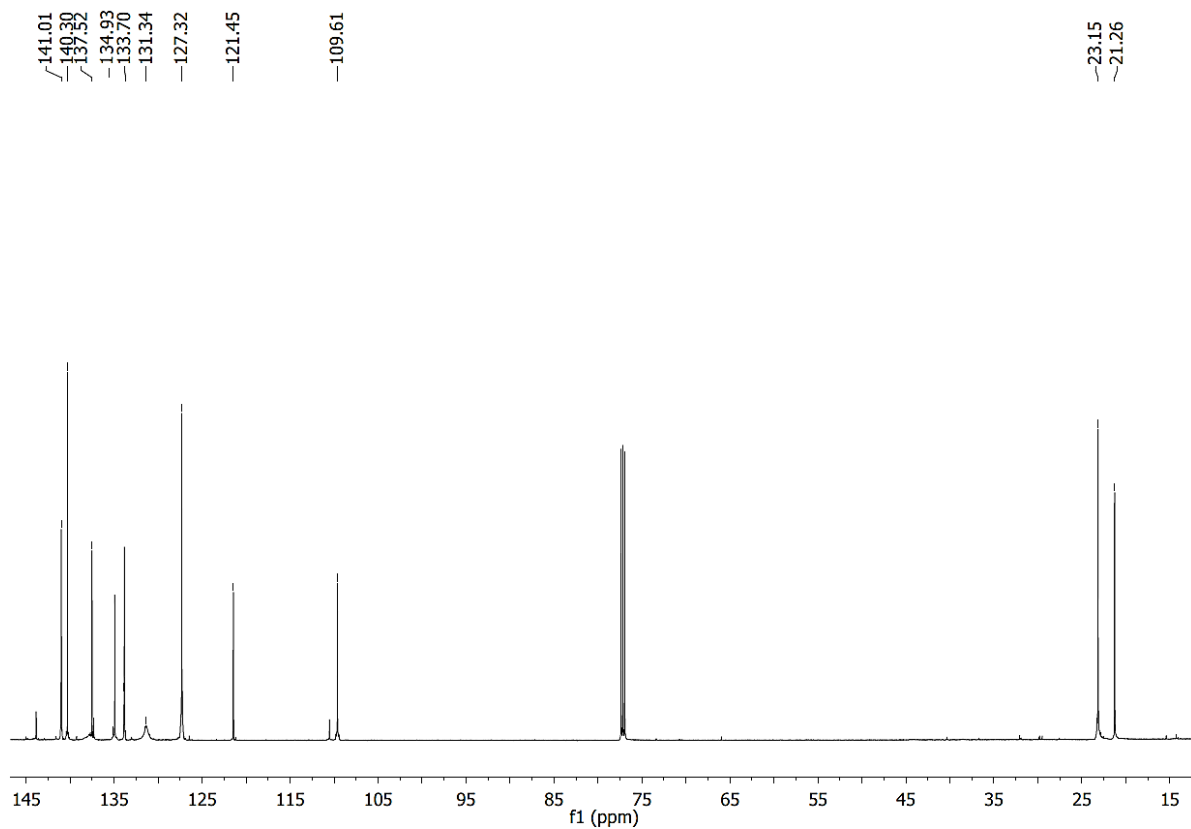


Figure 3.17. ^{13}C NMR spectrum of **5V-NBMes** monomer in CDCl_3 .

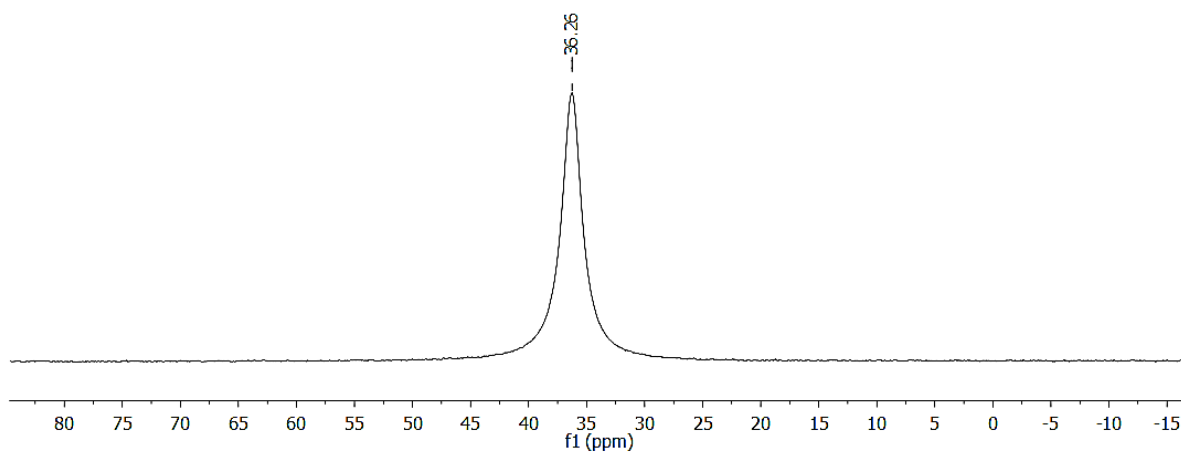


Figure 3.18. ^{11}B NMR spectrum of **5V-NBMes** monomer in CDCl_3 .

Compound 6V-NBMes. A sealed reaction vessel was charged with **6Bpin** (1.50 g, 4.64 mmol), bromoethylene solution (1.0 M THF solution, 18.6 mL, 18.6 mmol), Pd(dppf)Cl₂ (0.102 g, 0.139 mmol), KOH (0.782 g, 13.9 mmol), H₂O (5.0 mL), and MTBE (45 mL). The KOH pellets were ground into a powder and the H₂O was purged with argon for 1 hour prior to use. The reaction mixture was then heated at 80 °C for 1 hour. The organic layer was decanted, and the reaction mixture was concentrated under reduced pressure. The desired product was obtained as a yellow oil after purification by silica gel chromatography with 95:5 pentane:dichloromethane as the eluent (0.74 g, 71%). ¹H NMR (599.7 MHz, CDCl₃) δ = 8.02 (br s, 1H), 7.72 (dd, *J* = 11, 6.6 Hz, 1H), 6.92 (s, 2H), 6.87 (d, *J* = 11 Hz, 1H), 6.59 (dd, *J* = 17, 11 Hz, 1H), 6.37 (d, *J* = 6.6, 1H), 5.57 (d, *J* = 18 Hz, 1H), 5.35 (d, *J* = 11 Hz, 1H), 2.34 (s, 3H), 2.22 (s, 6H). ¹³C NMR (151 MHz, CD₂Cl₂) δ = 144.2, 141.2, 140.5, 138.3 (br), 137.6, 134.0, 132.0 (br), 127.3, 113.2, 112.0, 23.3, 21.3. ¹¹B NMR (160.4 MHz, CDCl₃) δ = 36.3. FTIR (thin film): ν cm⁻¹ = 3381, 3020, 2916, 2855, 1609. HRMS (DART) calcd. for C₁₅H₁₉BN ([M+H]⁺) 224.1611, found 224.1607. UV-Vis (THF): λ_{max} = 303, 251 nm.

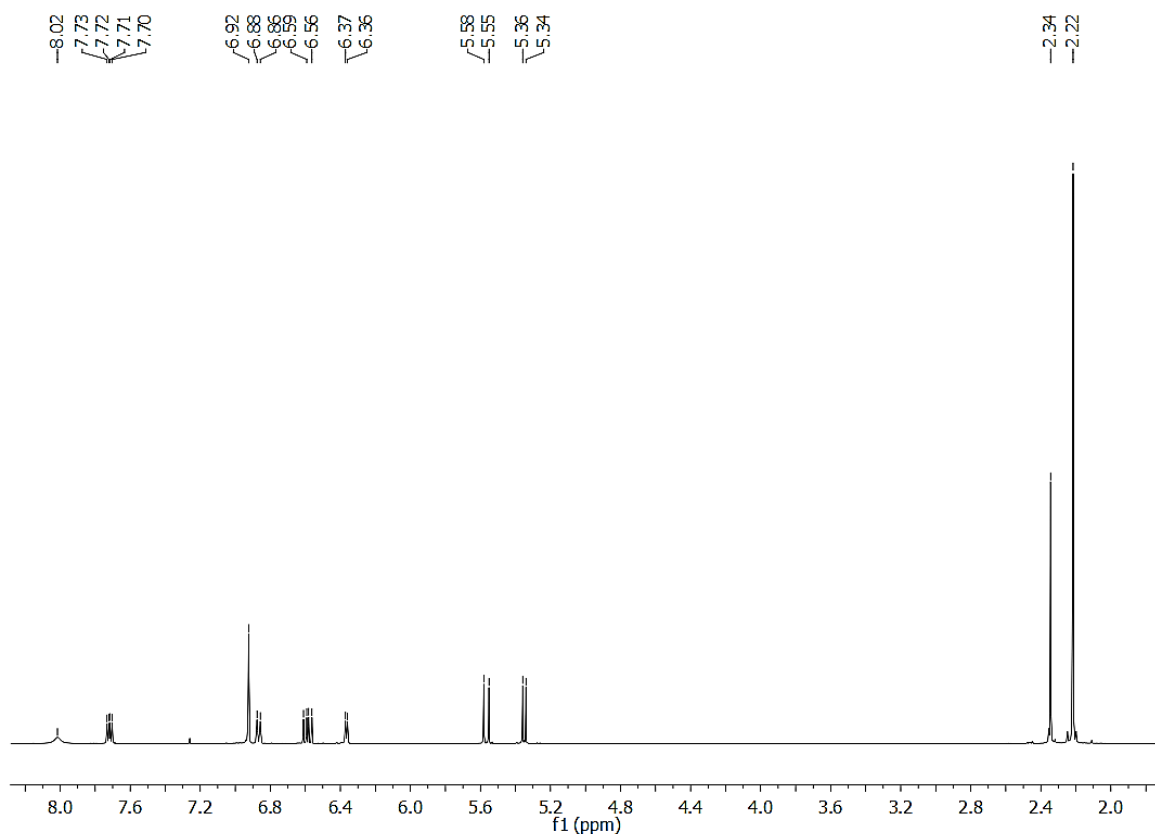
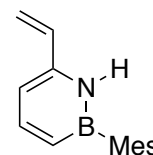


Figure 3.19. ¹H NMR spectrum of **6V-NBMes** monomer in CDCl₃.

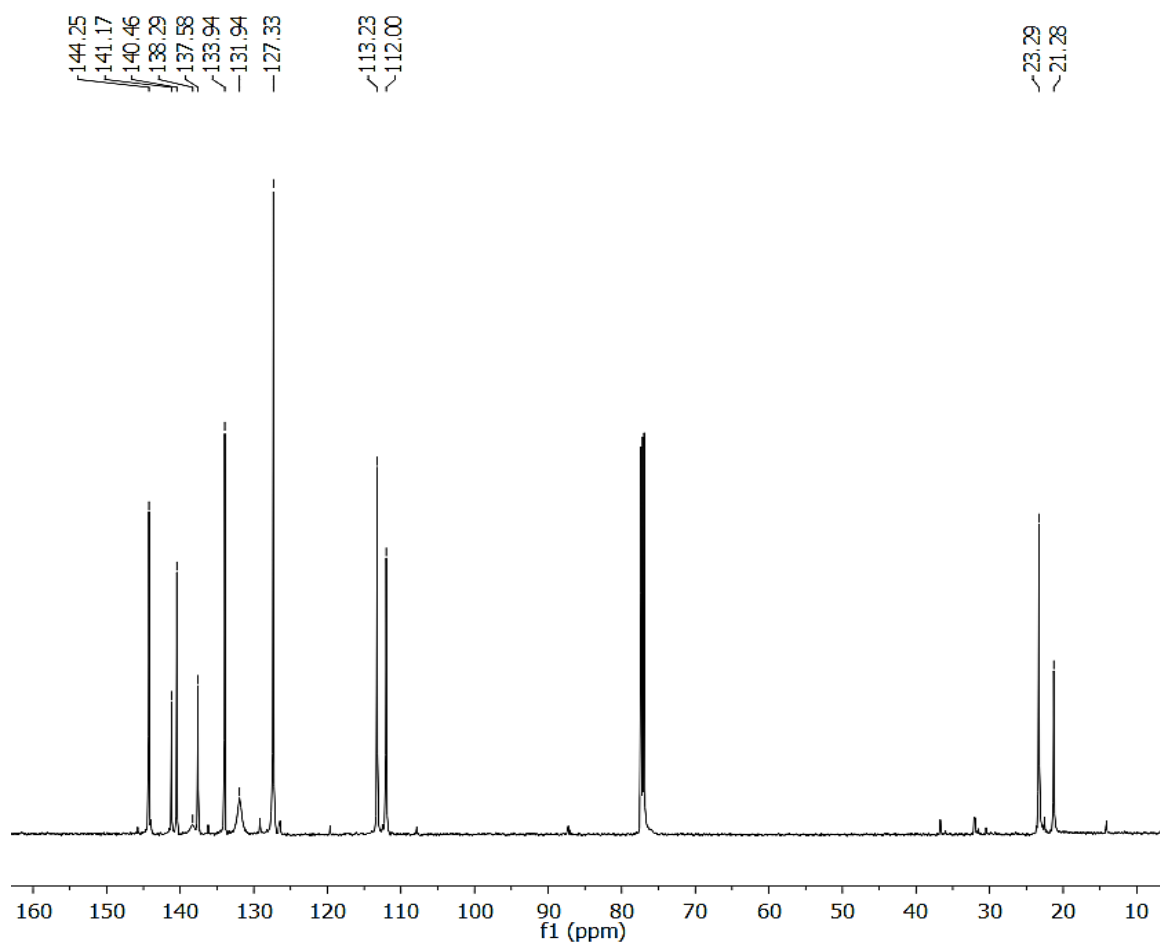


Figure 3.20. ^{13}C NMR spectrum of **6V-NBMes** monomer in CDCl_3 .

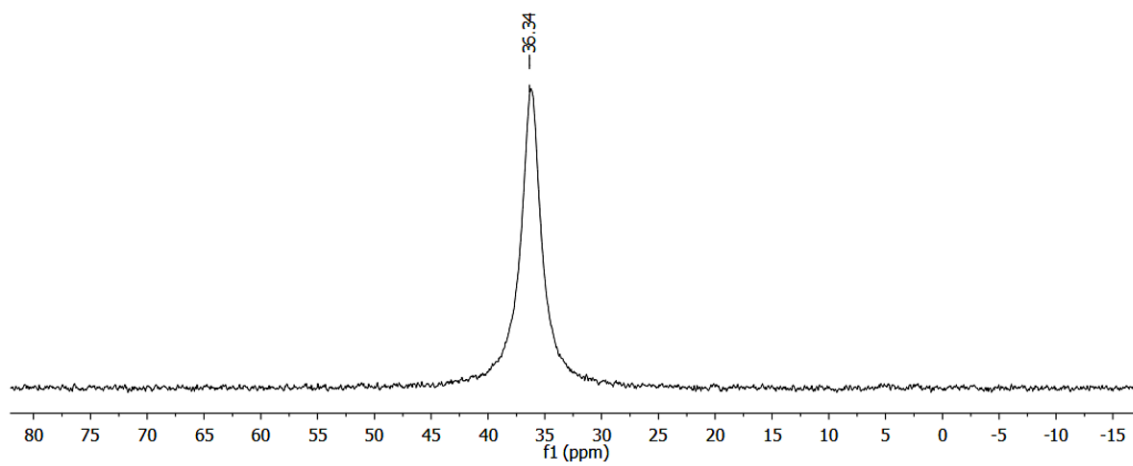


Figure 3.21. ^{11}B NMR spectrum of **6V-NBMes** monomer in CDCl_3 .

Compound *m*MesSt. A 500 mL two-neck Schlenk flask was charged with *meta*-vinylphenylboronic acid (2.66 g, 18.1 mmol), 2-bromomesitylene (3.00 g, 15.1 mmol) and Na₂CO₃ (6.40 g, 60.4 mmol). Toluene (100 mL), ethanol (20 mL), and H₂O (70 mL) were then added to the reaction vessel. The reaction mixture was purged with N₂ for 20 min. A suspension of Pd(PPh₃)₄ (0.52 g, 0.45 mmol) in toluene (10 mL) was then added by syringe. The reaction mixture was heated to 95 °C for 16 hours under nitrogen flow. After cooling to room temperature, water was added to the reaction mixture, and the mixture extracted with dichloromethane. The organic layer was collected, washed with water, and the solvent removed under reduced pressure. The product was obtained as a colorless oil by column chromatography (silica gel, hexanes). Yield: 1.25 g (37%). ¹H NMR (500.0 MHz, CDCl₃): 7.37 (m, 2H), 7.20 (s, 1H), 7.04 (m, 1H), 6.95 (s, 2H), 6.74 (dd, J = 18, 11 Hz, 1H), 5.75 (d, J = 18 Hz, 1H), 5.43 (d, J = 11 Hz, 1H), 2.33 (s, 3H), 2.01 (s, 6H). ¹³C NMR (125.8 MHz, CDCl₃) δ = 141.4, 138.8, 137.6, 137.0, 136.7, 136.0, 128.9, 128.6, 128.1, 127.2, 124.5, 113.8, 21.0, 20.8. FTIR (thin film): ν cm⁻¹ = 3006, 2950, 2917, 2854, 1612, 1597. UV-Vis (THF): λ_{max} = 244 nm.

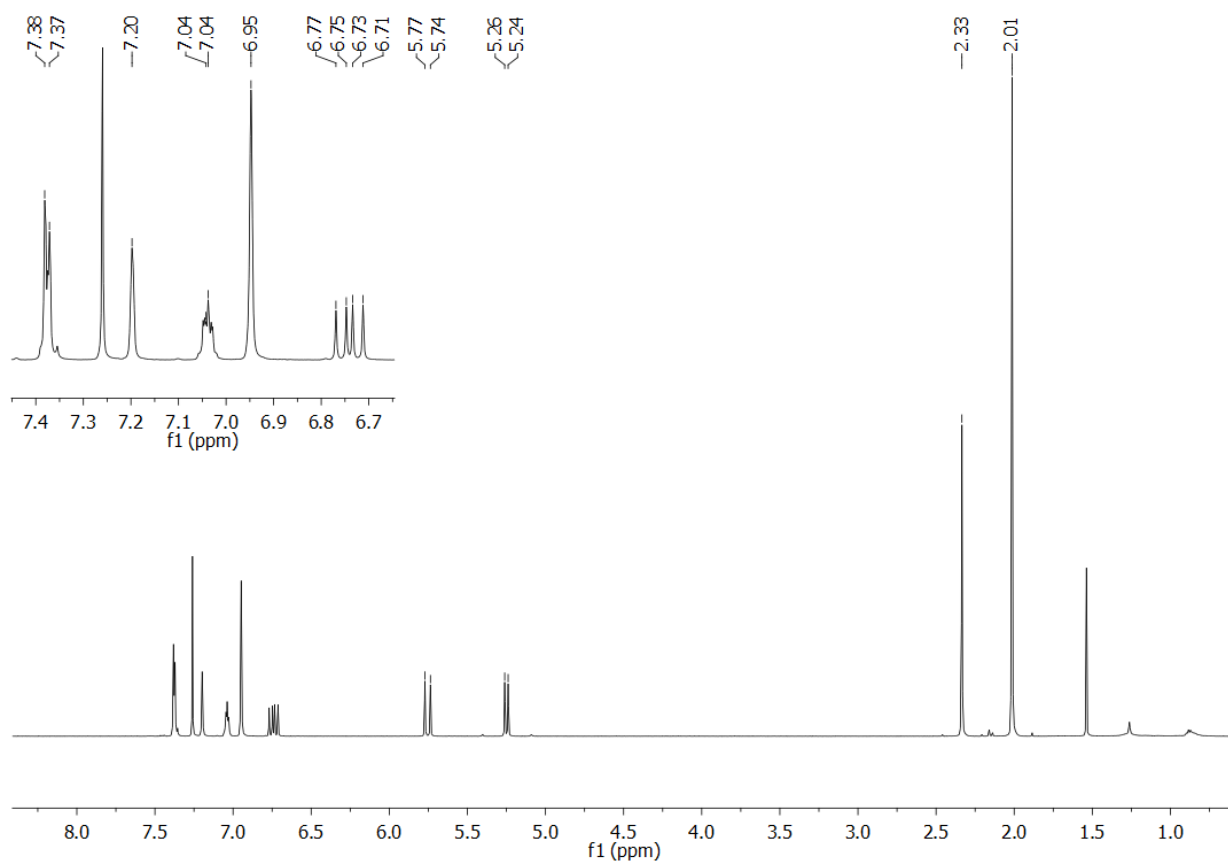
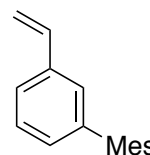


Figure 3.22. ¹H NMR spectrum *meta*-mesitylstyrene (*m*MesSt) in CDCl₃.

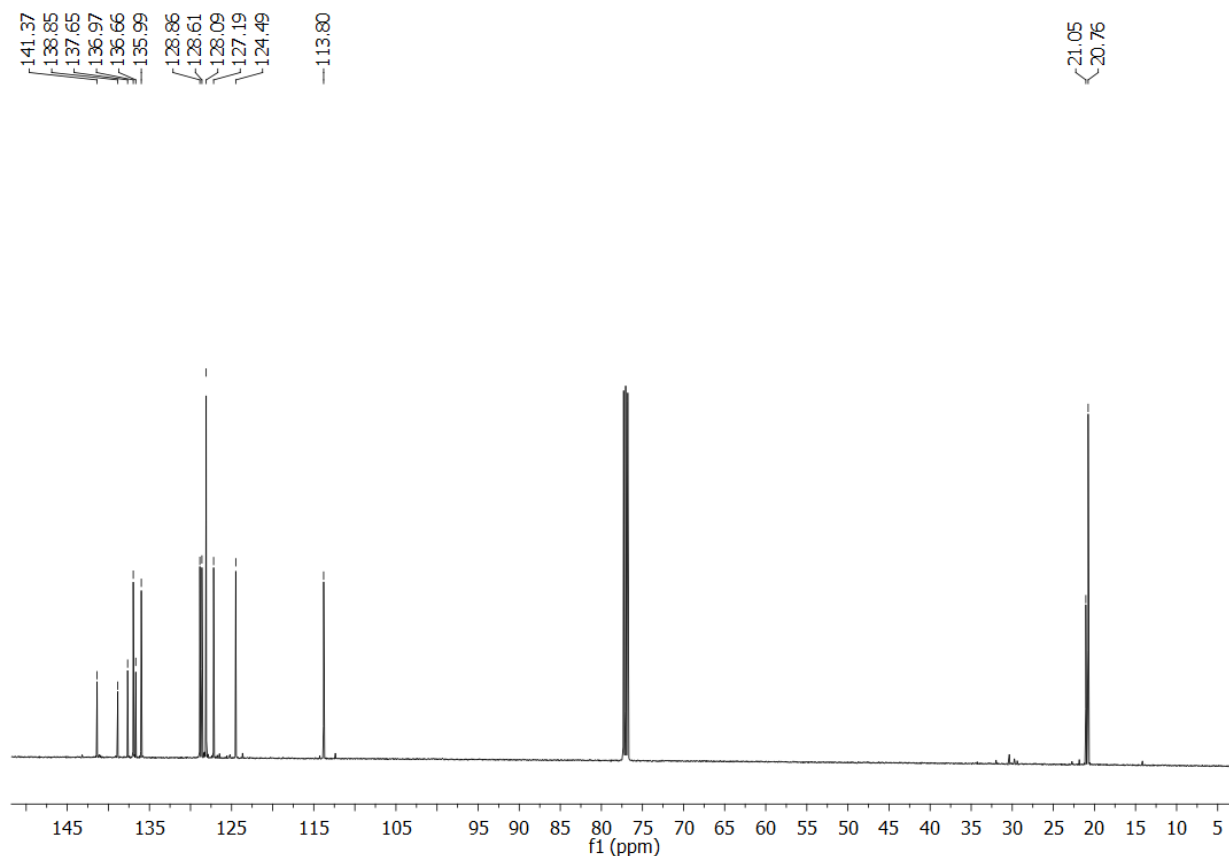
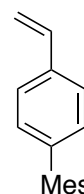


Figure 3.23. ^{13}C NMR spectrum of *meta*-mesitylstyrene (***mMesSt***) in CDCl_3 .

Compound *pMesSt*. A 500 mL two-neck Schlenk flask was charged with *para*-vinylphenylboronic acid (4.43 g, 30.1 mmol), 2-bromomesitylene (5.00 g, 25.1 mmol) and Na_2CO_3 (10.6 g, 0.10 mol). Toluene (150 mL), ethanol (25 mL), and H_2O (80 mL) were then added. The mixture was purged with N_2 for 20 min. A suspension of $\text{Pd}(\text{PPh}_3)_4$ (0.87 g, 0.75 mmol) in toluene (10 mL) was then added by syringe. The mixture was heated to 95 $^\circ\text{C}$ for 16 hours under nitrogen flow. After cooling to room temperature, water was added to the reaction mixture, and the mixture extracted with dichloromethane. The organic layer was collected, washed with water, and the solvent removed under reduced pressure. The residue was purified by column chromatography (silica gel, hexanes), and the product was recrystallized from hexanes to give colorless crystals. Yield: 1.12 g (33%). ^1H NMR (500.0 MHz, CDCl_3): 7.46 (d, $J = 8.0$ Hz, 2H), 7.10 (d, $J = 8.0$ Hz, 2H), 6.94 (s, 2H), 6.77 (dd, $J = 18, 11$ Hz, 1H), 5.79 (d, $J = 18$ Hz, 1H), 5.26 (d, $J = 11$ Hz, 1H), 2.33 (s, 3H), 2.01 (s, 6H). ^{13}C NMR (125.8 MHz, CDCl_3) $\delta = 140.9, 138.8, 136.9, 136.8, 136.1, 135.9, 129.7, 128.2, 126.4, 113.5, 21.1, 20.8$. The NMR data are consistent with those previously reported for the synthesis of *para*-mesitylstyrene obtained through a different synthetic route.¹³ UV-Vis (THF): $\lambda_{\text{max}} = 257$ nm.



¹³ Bolliger, J. L.; Frech, C. M. *Chem.-Eur. J.* **2010**, *16*, 11072-11081.

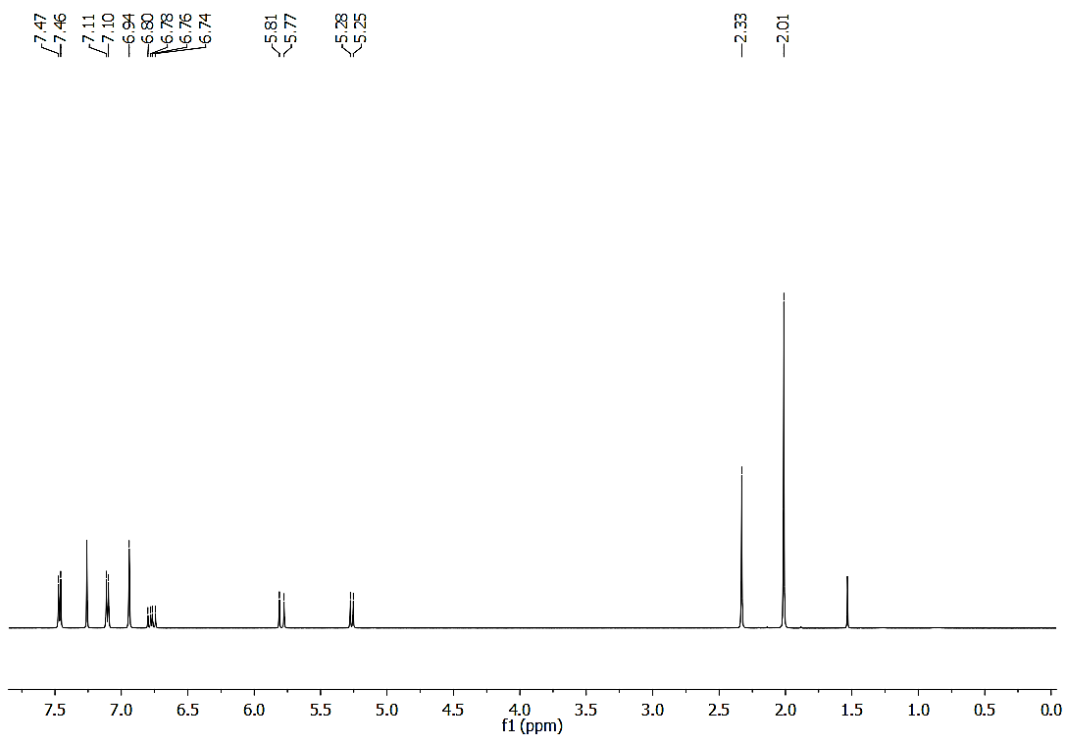


Figure 3.24. ^1H NMR spectrum of *para*-mesitylstyrene (*p*MesSt) in CDCl_3 .

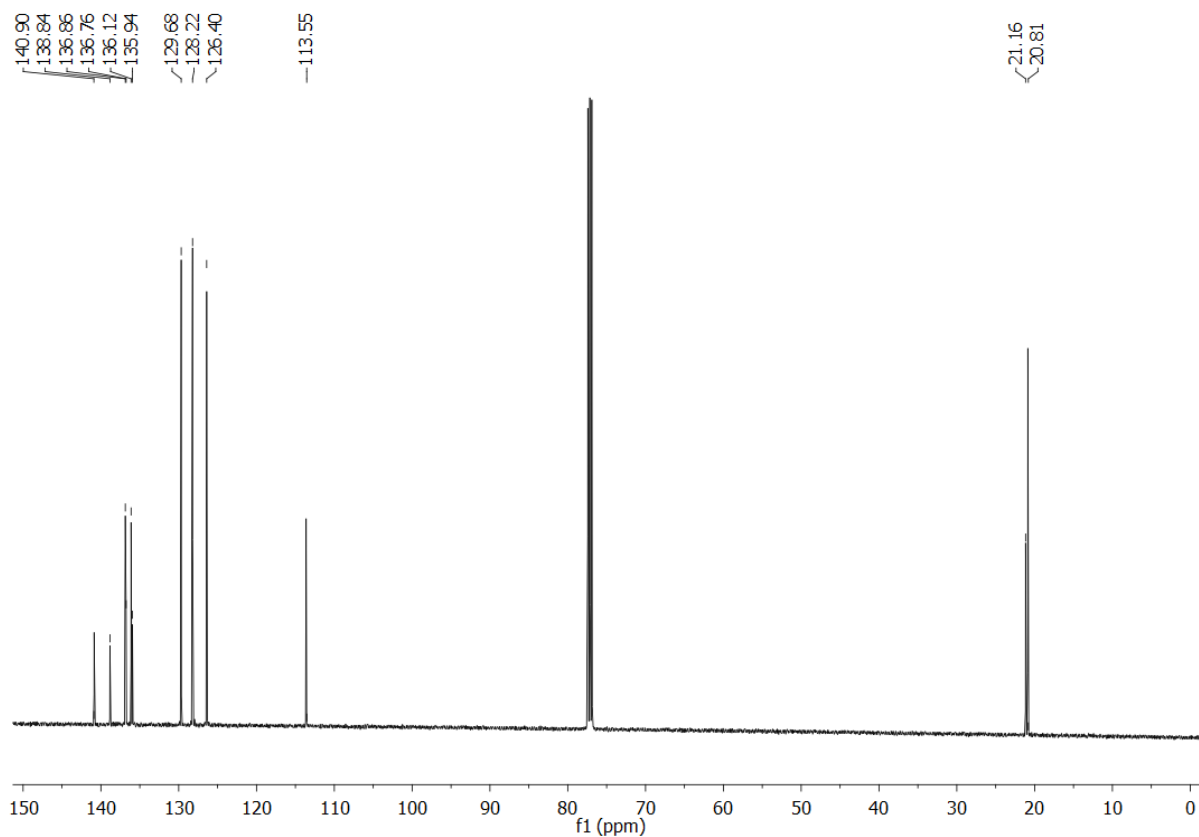


Figure 3.25. ^{13}C NMR spectrum of *para*-mesitylstyrene (*p*MesSt) in CDCl_3 .

Compound *o*MesSt.

A 250 mL three-neck Schlenk flask was charged with *ortho*-vinylphenylboronic acid (0.88 g, 7.68 mmol), 2-bromomesitylene (1.00 g, 5.02 mmol) and Na₂CO₃ (2.13 g, 0.02 mol). Toluene (20 mL), ethanol (20 mL), and H₂O (70 mL) were then added. The mixture was purged with N₂ for 20 min. A suspension of Pd(PPh₃)₄ (0.17 g, 0.15 mmol) in toluene (10 mL) was then added by syringe. The mixture was heated to 95 °C for 16 hours under nitrogen flow. After cooling to room temperature, water was added to the reaction mixture, and the mixture extracted with dichloromethane. The organic layer was collected, washed with water, and the solvent removed under reduced pressure. The residue was purified by column chromatography (silica gel, hexanes), giving the product as a colorless oil. Yield: 0.35 g (31%). ¹H NMR (500.0 MHz, CDCl₃): 7.68 (d, J = 7.0 Hz, 1H), 7.32 (m, 2H), 7.05 (d, J = 7.0 Hz, 1H), 6.94 (s, 2H), 6.33 (dd, J = 18, 11 Hz, 1H), 5.64 (d, J = 18 Hz, 1H), 5.07 (d, J = 11 Hz, 1H), 2.35 (s, 3H), 1.92 (s, 6H). ¹³C NMR (125.8 MHz, CDCl₃) δ = 139.9, 137.4, 136.8, 136.3, 136.0, 134.8, 129.9, 128.1, 128.0, 127.3, 125.0, 114.4, 21.2, 20.4. GC-MS (retention time 13 min) calcd. for C₁₇H₁₈ (m/z) 222.1, found 222.2.

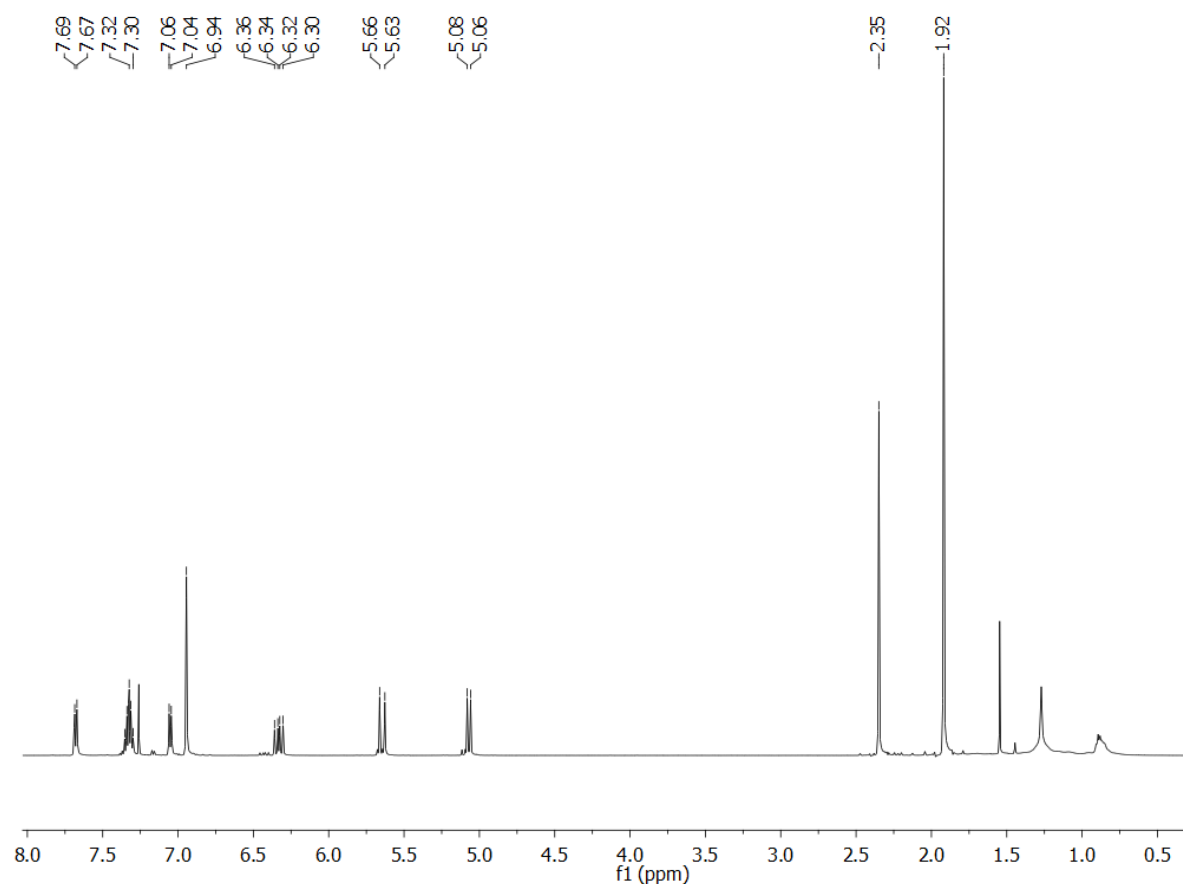


Figure 3.26. ¹H NMR spectrum of *ortho*-mesitylstyrene (*o*MesSt) in CDCl₃.

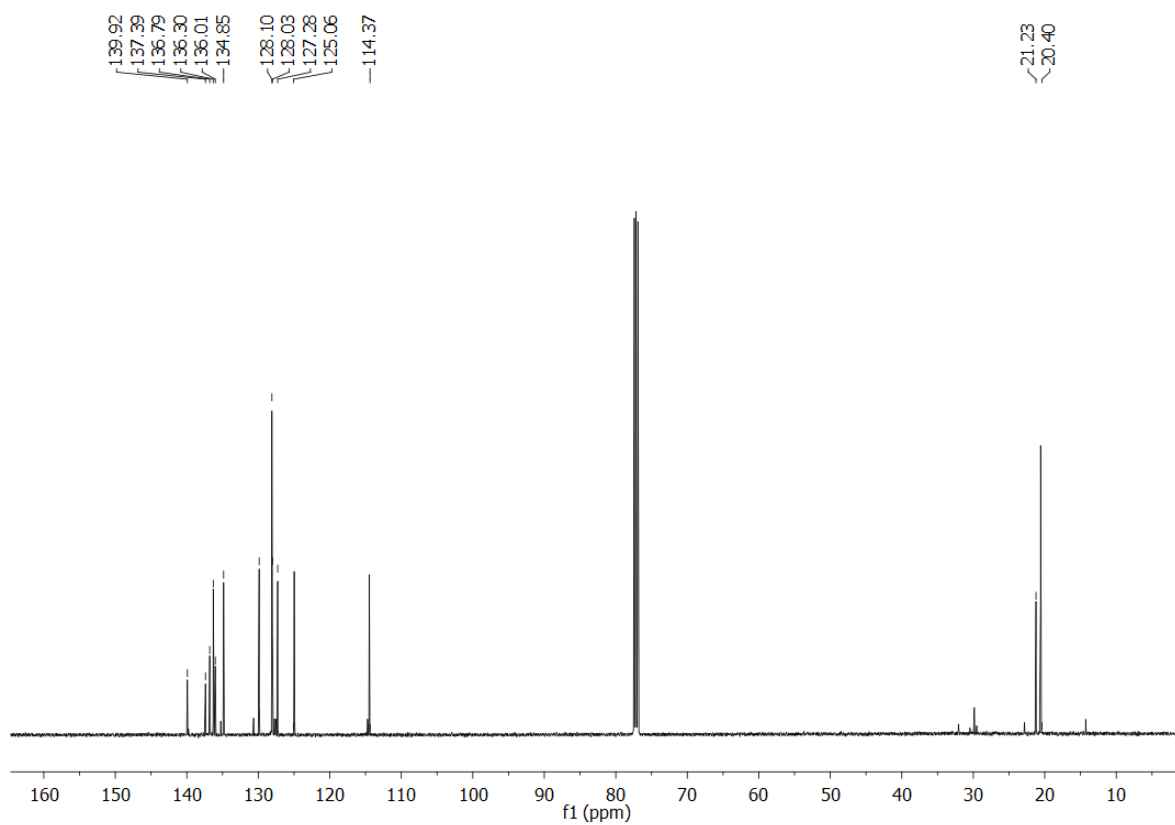


Figure 3.27. ^{13}C NMR spectrum of *ortho*-mesitylstyrene (*oMesSt*) in CDCl_3 .

3.7.4 Homopolymerizations

Free Radical Polymerization of 4V-NBMes (P4V-NBMes). Into a 10 mL Schlenk tube were loaded **4V-NBMes** monomer (50 mg, 224 μmol), 20 μL of an 0.37 M AIBN solution in anisole, and 30 μL of anisole ($[\text{4V-NBMes}]/[\text{AIBN}] = 50/1$). After 3 freeze-pump-thaw cycles, the tube was fully immersed in a 70 $^{\circ}\text{C}$ oil bath and kept stirring for 24 h. The tube was placed in liquid nitrogen to terminate the reaction. One drop of the polymerization solution was taken for ^1H NMR measurement to determine the monomer conversion (76%). The polymer was then precipitated in a 10-fold volume of hexanes at -20 $^{\circ}\text{C}$, redissolved in toluene, precipitated in a 10-fold volume of cold hexanes again, and freeze-dried in benzene. After drying in high vacuum, the polymer P4V-NBMes was obtained as an off-white powder. Yield: 22.0 mg (44%). ^{11}B NMR (160.4 MHz, CDCl_3): $\delta = 29.1$. ^{13}C NMR (150.8 MHz, CDCl_3) $\delta = 161.9, 140.2, 139.0, 136.8, 133.4, 127.1, 111.8, 42.8, 23.3, 21.3$. GPC-RI: $M_{n,\text{GPC}} = 26900 \text{ g mol}^{-1}$, $M_{w,\text{GPC}} = 130400 \text{ g mol}^{-1}$, $D = 4.84$. $X_{n,\text{GPC}} = 119$. UV-Vis (THF): $\lambda_{\text{max}} = 273, 238 \text{ nm}$.

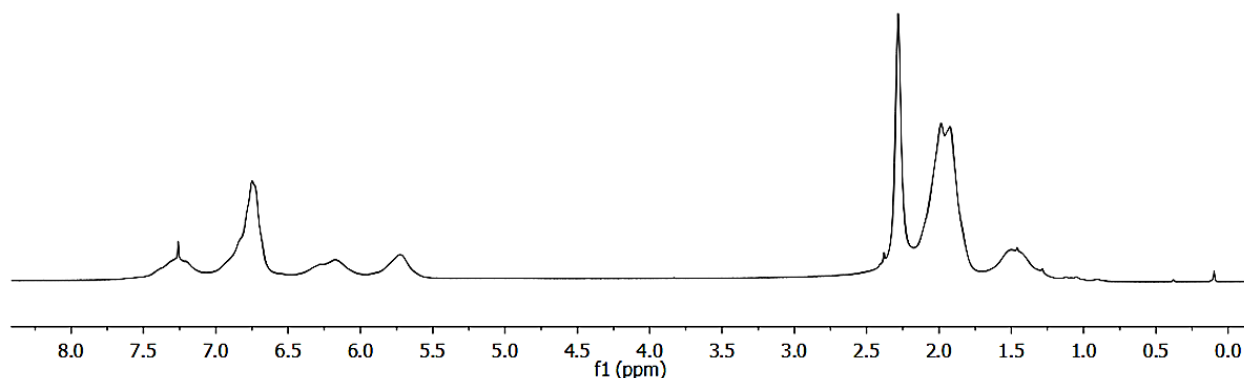
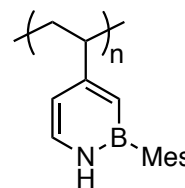


Figure 3.28. ^1H NMR spectrum of **P4V-NBMes** polymer in CDCl_3 .

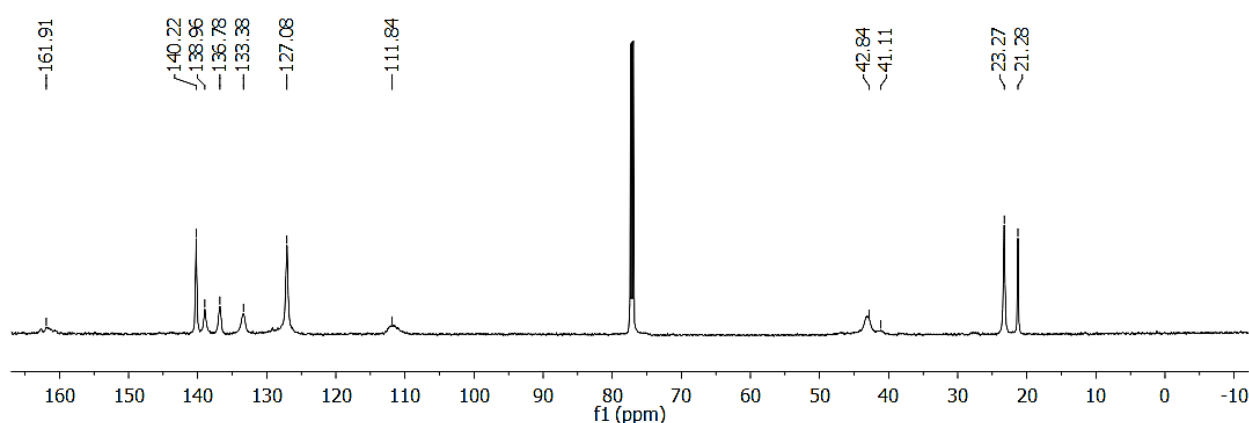


Figure 3.29. ^{13}C NMR spectrum of **P4V-NBMes** polymer in CDCl_3 .

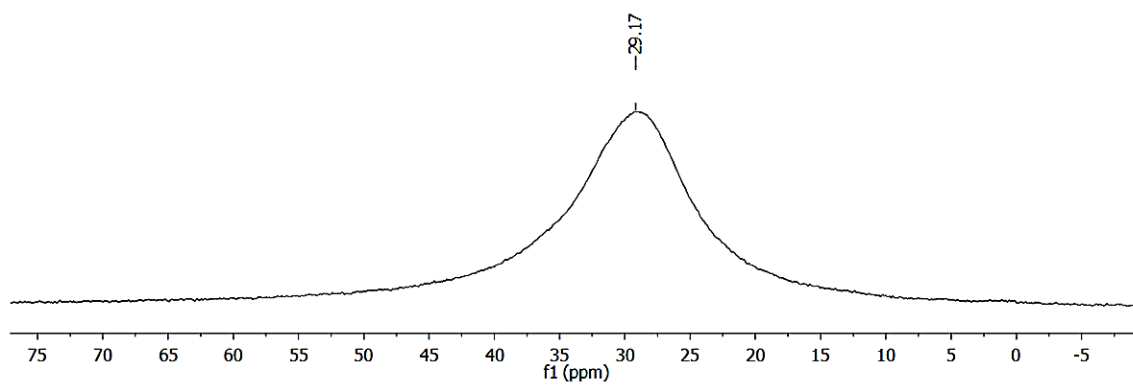


Figure 3.30. ^{11}B NMR spectrum of P4V-NBMes polymer in CDCl_3 .

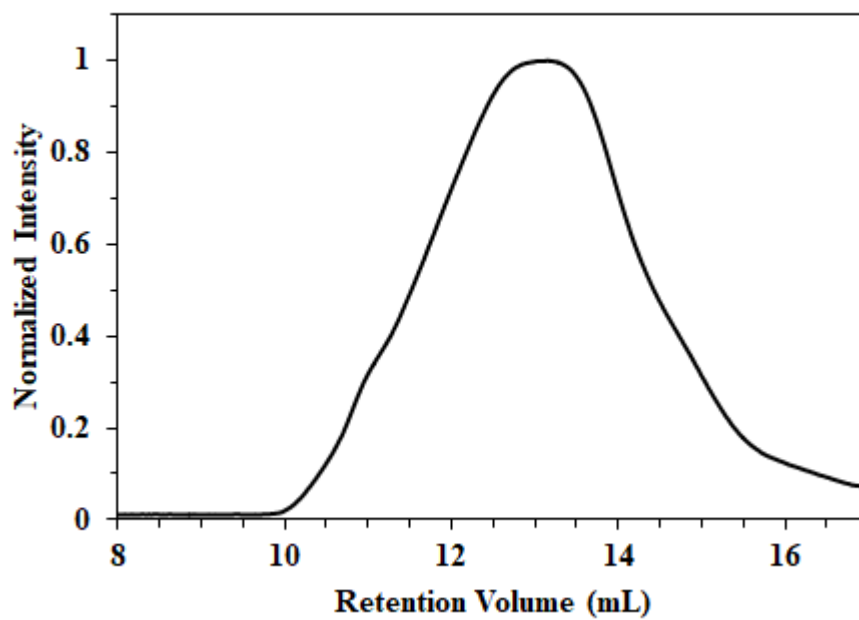


Figure 3.31. GPC trace of P4V-NBMes obtained from conventional free radical polymerization; eluent: THF, 1 mL min^{-1} .

Free Radical Polymerization of 5V-NBMes (P5V-NBMes). Into a 10 mL Schlenk tube were loaded **5V-NBMes** monomer (50 mg, 224 μmol), 20 μL of 0.37 M AIBN solution in anisole, and 30 μL of anisole ($[\text{5V-NBMes}]/[\text{AIBN}] = 50/1$). After 3 freeze-pump-thaw cycles, the tube was immersed in a 70 $^{\circ}\text{C}$ oil bath and kept stirring for 24 h. The tube was placed in liquid nitrogen to terminate the reaction. One drop of the polymerization solution was taken for ^1H NMR measurement to determine the monomer conversion (63%). The polymer was then precipitated in a 10-fold volume of hexanes at -20 $^{\circ}\text{C}$, redissolved in toluene, precipitated in a 10-fold volume of cold hexanes again, and freeze-dried in benzene. After drying in high vacuum, the polymer P4V-NBMes was obtained as a light brown powder. Yield: 21.0 mg (42%). ^{11}B NMR (160.4 MHz, CDCl_3): $\delta = 28.9$. ^{13}C NMR (150.8 MHz, CDCl_3) $\delta = 144.0, 140.0, 138.1, 137.3, 132.0, 131.3, 127.3, 125.7, 41.4, 38.3, 23.2, 21.2$. GPC-RI: $M_{n,\text{GPC}} = 11600 \text{ g mol}^{-1}$, $M_{w,\text{GPC}} = 46100 \text{ g mol}^{-1}$, $D = 3.98$. $X_{n,\text{GPC}} = 52$. UV-Vis (THF): $\lambda_{\text{max}} = 288, 238 \text{ nm}$.

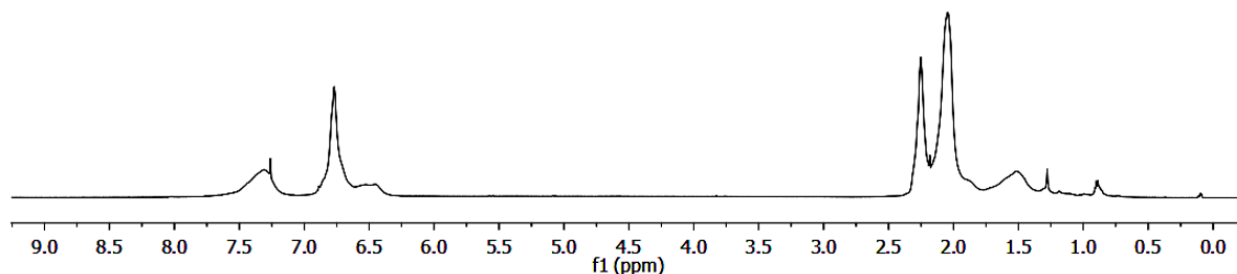
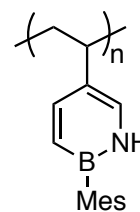


Figure 3.32. ^1H NMR spectrum of **P5V-NBMes** polymer in CDCl_3 .

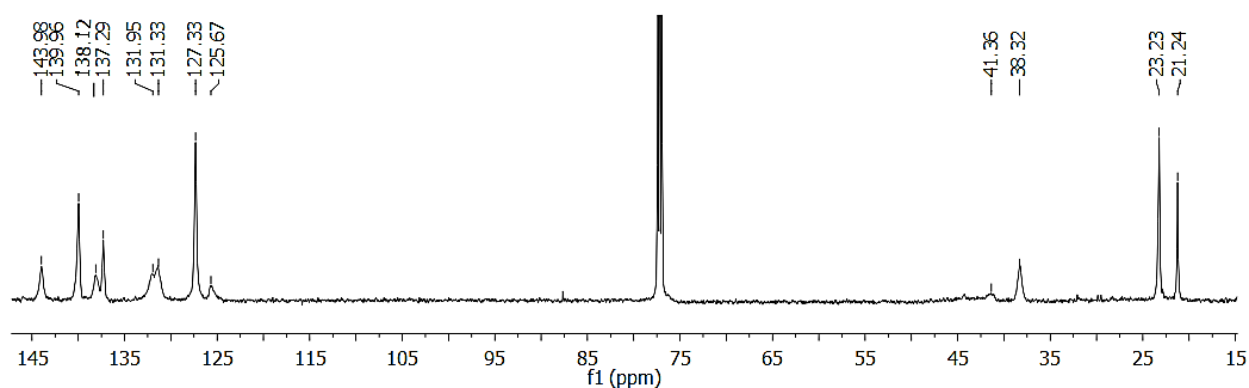


Figure 3.33. ^{13}C NMR spectrum of **P5V-NBMes** polymer in CDCl_3 .

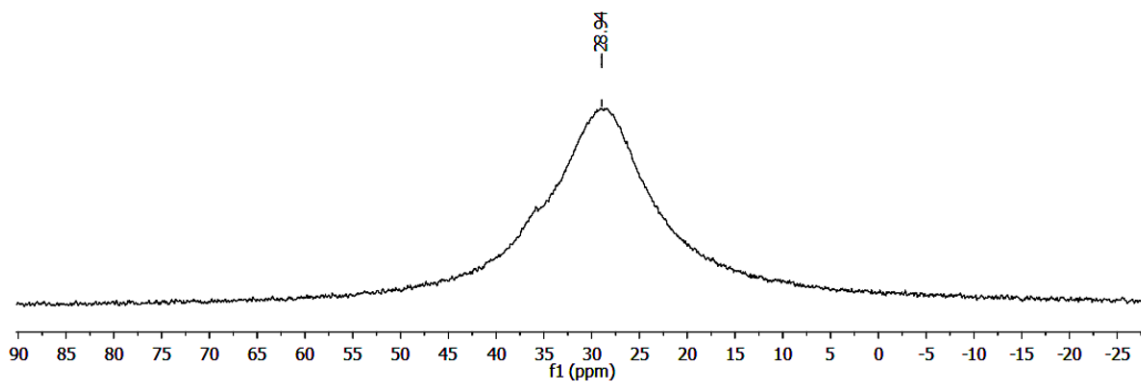


Figure 3.34. ^{11}B NMR spectrum of **P5V-NBMes** polymer in CDCl_3 .

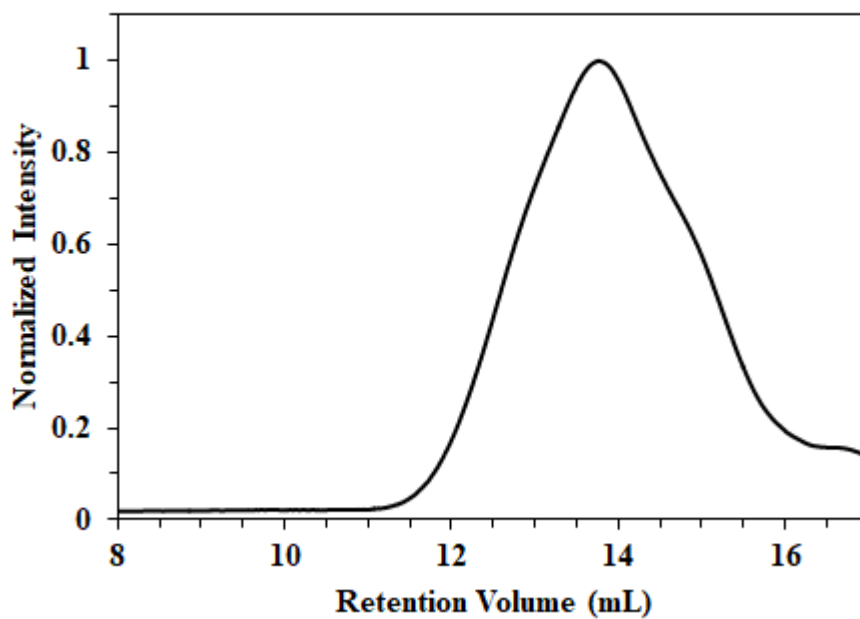


Figure 3.35. GPC trace of **P5V-NBMes** obtained from conventional free radical polymerization; eluent: THF, 1 mL min^{-1} .

Free Radical Polymerization of 6V-NBMes (P6V-NBMes). Into a 5 mL Schlenk tube were loaded **6V-NBMes** monomer (50.0 mg, 224 μmol), 20 μL of an 0.37 M AIBN solution in anisole, and 30 μL of anisole ($[\text{6V-NBMes}]/[\text{AIBN}] = 50/1$). After 3 freeze-pump-thaw cycles, the tube was immersed in a 70 $^{\circ}\text{C}$ oil bath and kept stirring for 24 h. The tube was placed in liquid nitrogen to terminate the reaction. One drop of the polymer solution was taken for ^1H NMR measurement to determine the monomer conversion (51%). The polymer was then precipitated in a 10-fold volume of hexanes, redissolved in toluene, precipitated in a 10-fold volume of cold hexanes again, and freeze-dried in benzene. After drying in high vacuum, the polymer P6V-NBMes was obtained as an off-white powder. Yield: 16.1 mg (32%). ^{11}B NMR (160.4 MHz, CDCl_3): $\delta = 29.5$. ^{13}C NMR (150.8 MHz, CDCl_3) $\delta = 146.7, 144.1, 140.0, 137.6, 129.5, 127.4, 109.8, 41.3, 23.4, 21.3$. GPC-RI: $M_{n,\text{GPC}} = 18200 \text{ g mol}^{-1}$, $M_{w,\text{GPC}} = 44400 \text{ g mol}^{-1}$, $D = 2.44$, $X_{n,\text{GPC}} = 80$. UV-Vis (THF): $\lambda_{\text{max}} = 286 \text{ nm}$.

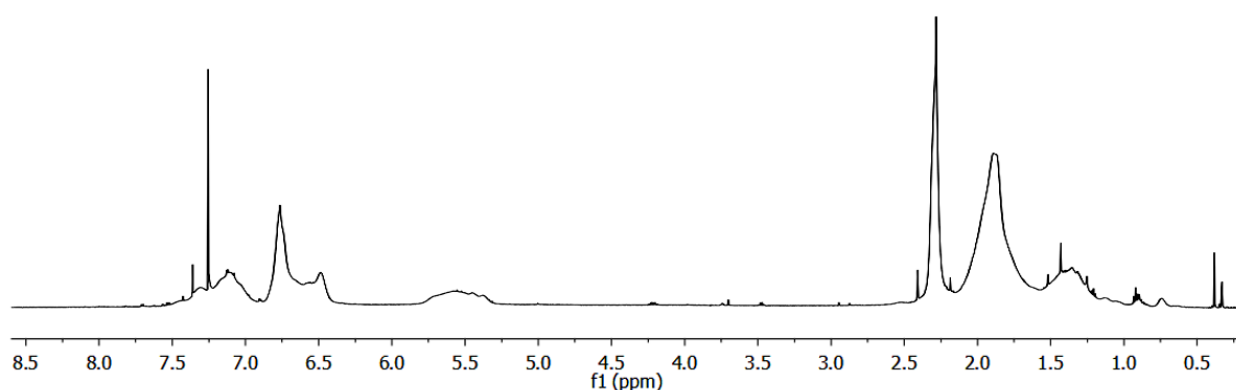
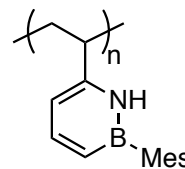


Figure 3.36. ^1H NMR spectrum of **P6V-NBMes** polymer in CDCl_3 .

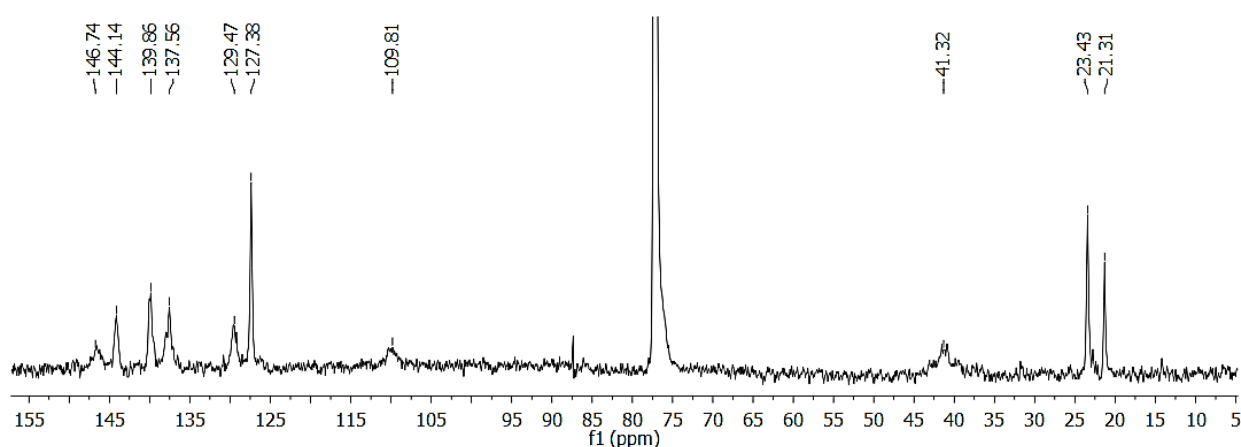


Figure 3.37. ^{13}C NMR spectrum of **P6V-NBMes** polymer in CDCl_3 .

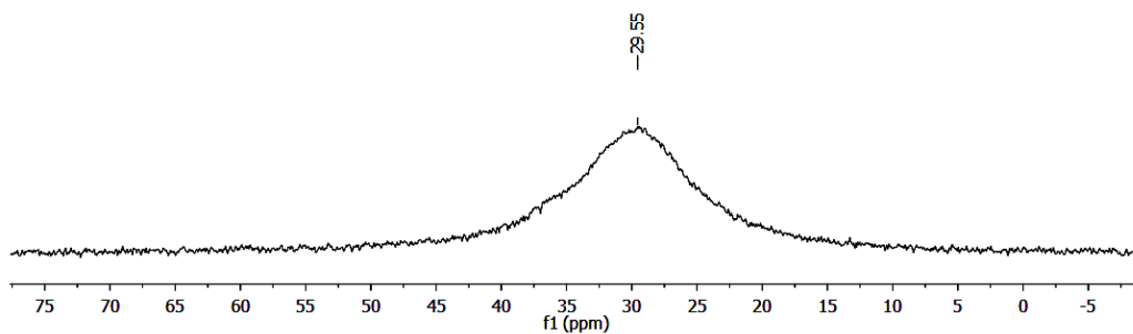


Figure 3.38. ^{11}B NMR spectrum of **P6V-NBMes** polymer in CDCl_3 .

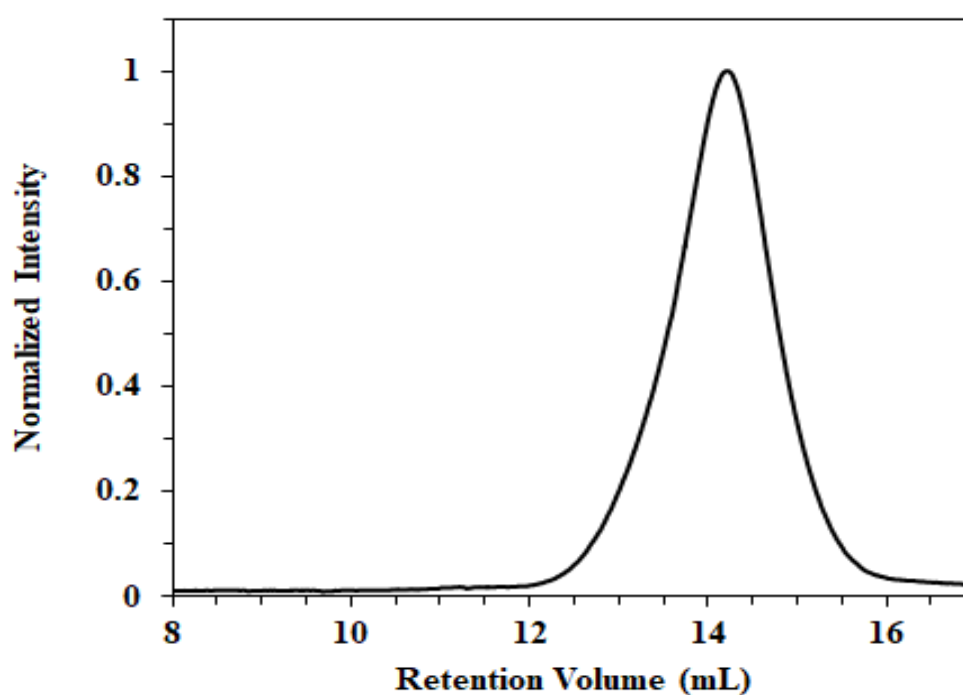


Figure 3.39. GPC trace of **P6V-NBMes** obtained from conventional free radical polymerization; eluent: THF, 1 mL min^{-1} .

Free Radical Polymerization of *meta*-Mesitylstyrene (**PmMesSt**).

Into a 10 mL Schlenk tube were loaded 3-mesitylstyrene (*m*MesSt) monomer (100 mg, 448 μmol), 20 μL of an 0.45 M AIBN solution in anisole, and 80 μL of anisole ($[m\text{MesSt}]/[\text{AIBN}] = 50/1$). After 3 freeze-pump-thaw cycles, the tube was fully immersed in a 70 $^{\circ}\text{C}$ oil bath and kept stirring for 6.5 h. The tube was placed in liquid nitrogen to terminate the reaction. One drop of the polymerization solution was taken for ^1H NMR measurement to determine the monomer conversion ($>95\%$). The polymer was then precipitated in a 10-fold volume of hexanes, redissolved in toluene, precipitated in a 10-fold volume of cold hexanes again, and freeze-dried in benzene. After drying in high vacuum, the polymer **PmMesSt** was obtained as an off-white powder. Yield: 56.1 mg (56%). ^{13}C NMR (125.8 MHz, CDCl_3) $\delta = 146.0, 145.0, 144.6, 140.8, 139.2, 136.1, 135.8, 128.0, 126.7, 40.5, 21.2, 20.8$. GPC-RI: $M_{n,\text{GPC}} = 29700 \text{ g mol}^{-1}$, $M_{w,\text{GPC}} = 61300 \text{ g mol}^{-1}$, $D = 2.07$. $X_{n,\text{GPC}} = 134$. UV-Vis (THF): $\lambda_{\text{max}} = 239 \text{ nm}$.

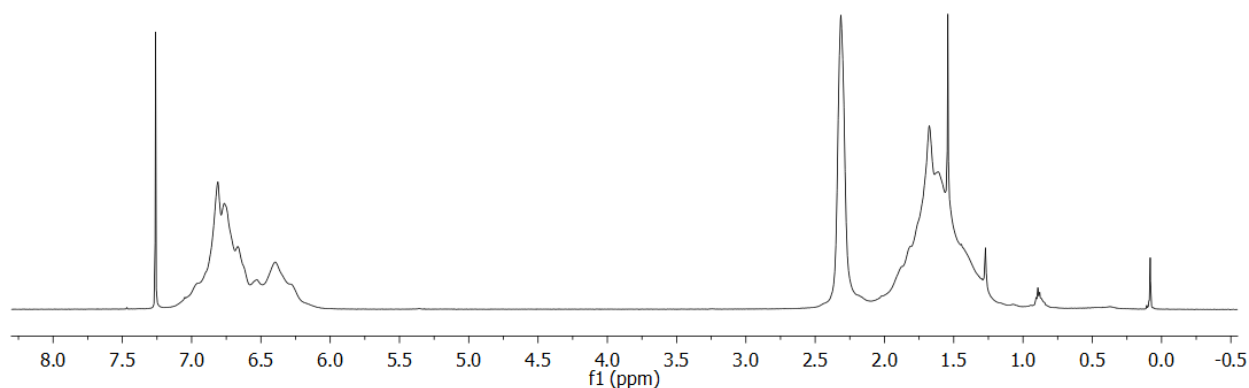
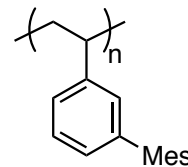


Figure 3.40. ^1H NMR spectrum of **PmMesSt** polymer in CDCl_3

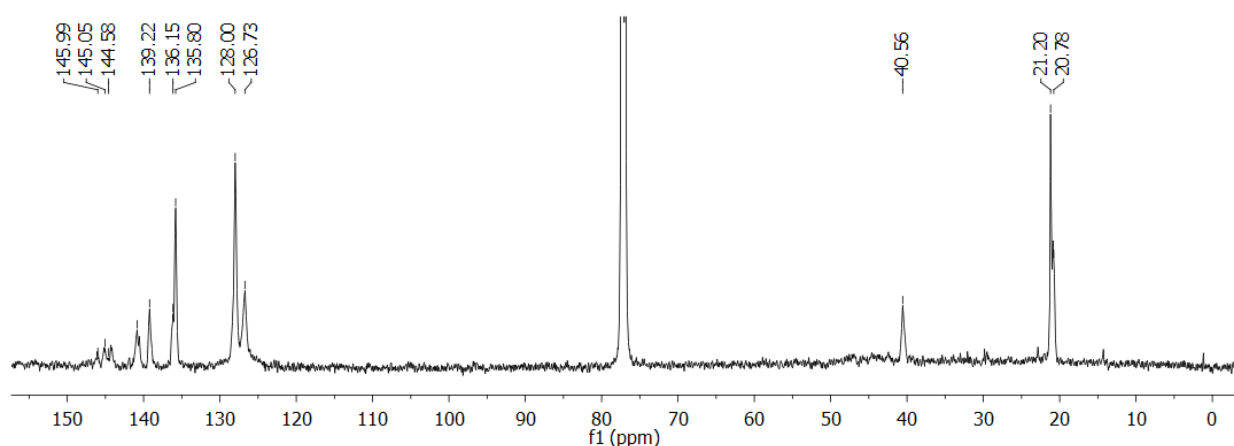


Figure 3.41. ^{13}C NMR spectrum of **PmMesSt** polymer in CDCl_3 .

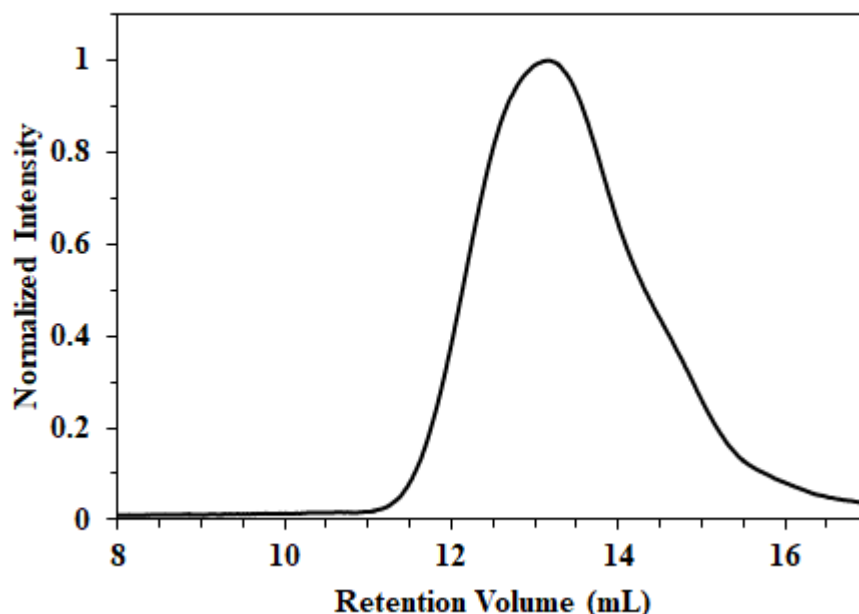


Figure 3.42. GPC trace of **PpMesSt** obtained from conventional free radical polymerization; eluent: THF, 1 mL min⁻¹.

Free Radical Polymerization of *para*-Mesitylstyrene (PpMesSt**).** Into a 10 mL Schlenk tube were loaded *para*-mesitylstyrene (**pMesSt**) monomer (200 mg, 896 μmol), 40 μL of an 0.45 M AIBN solution in anisole, and 160 μL of anisole ($[pMesSt]/[AIBN] = 50/1$). After 3 freeze-pump-thaw cycles, the tube was fully immersed in a 70 °C oil bath and kept stirring for 6.5 h. The tube was placed in liquid nitrogen to terminate the reaction. One drop of the polymerization solution was taken for ¹H NMR measurement to determine the monomer conversion (82%). The polymer was then precipitated in a 10-fold volume of hexanes, redissolved in toluene, precipitated in a 10-fold volume of cold hexanes again, and freeze-dried in benzene. After drying in high vacuum, the polymer **PpMesSt** was obtained as an off-white powder. Yield: 103.0 mg (51%). ¹³C NMR (125.8 MHz, CDCl₃) δ = 144.9, 143.5, 142.8, 139.1, 138.5, 136.3, 136.0, 129.0, 128.1, 40.6, 21.1, 20.8. GPC-RI: $M_{n,GPC} = 21600 \text{ g mol}^{-1}$, $M_{w,GPC} = 42000 \text{ g mol}^{-1}$, $D = 1.95$. $X_n GPC = 97$. UV-Vis (THF): $\lambda_{max} = 239 \text{ nm}$.

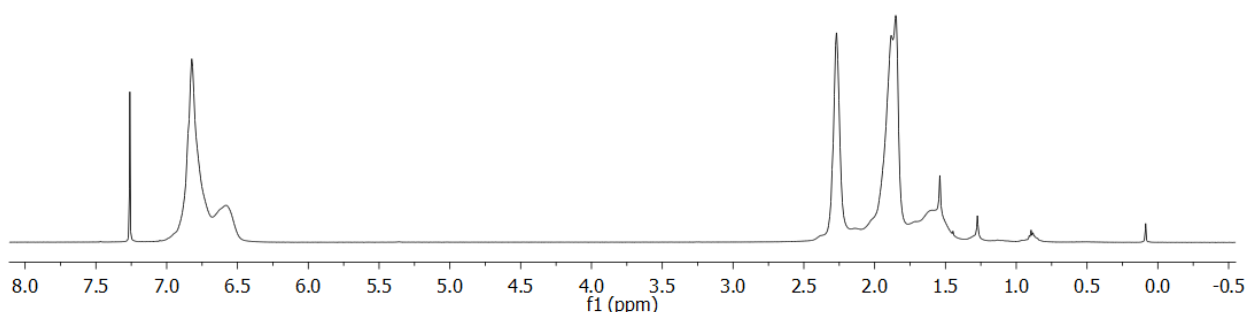
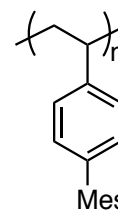


Figure 3.43. ¹H NMR spectrum of **PpMesSt** polymer in CDCl₃.

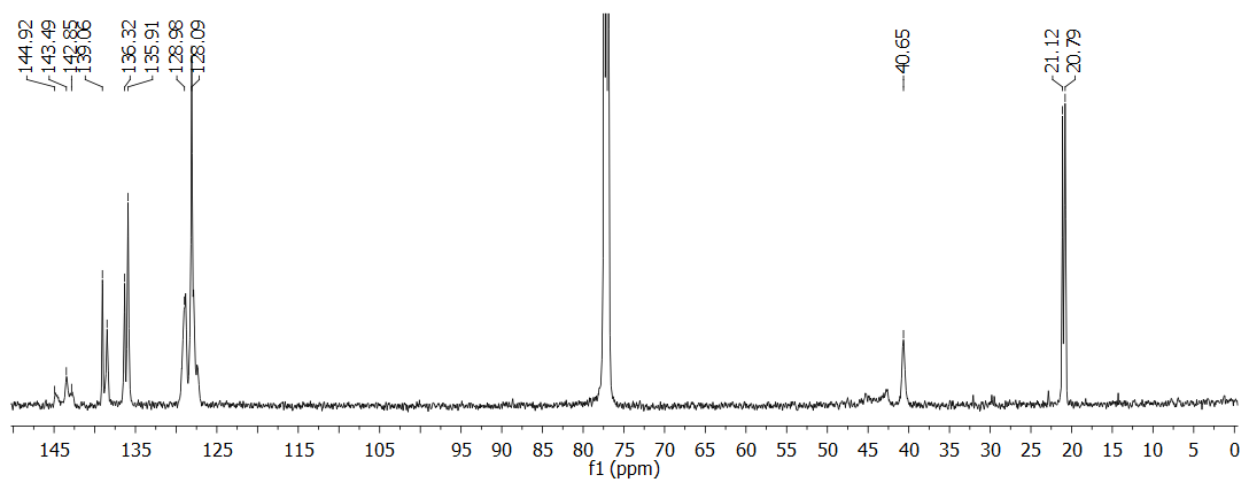


Figure 3.44. ^{13}C NMR spectrum of **PpMesSt** polymer in CDCl_3 .

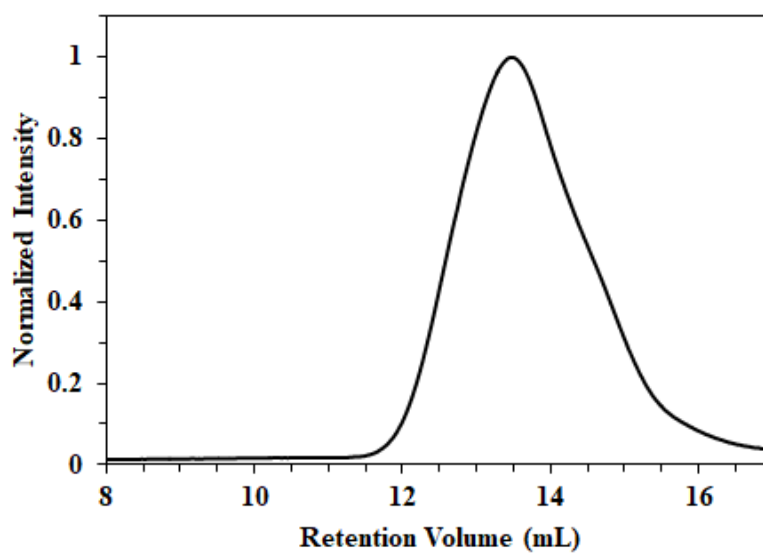


Figure 3.45. GPC trace of **PpMesSt** obtained from conventional free radical polymerization; eluent: THF, 1 mL min^{-1} .

Homopolymerization of *ortho*-Mesitylstyrene (*o*MesSt)

Scale: 100 mg of Monomer *o*MesSt, [*o*MesSt]/[AIBN] = 50/1. The reaction time was extended to 21 h.

Monomer conversion: 27%; from ^1H NMR integration of residual vinyl group signals of monomer relative to Me group of anisole.

Isolated yield: ca. 5 mg.

GPC-UV: $M_{n,\text{GPC}} = 5000 \text{ g mol}^{-1}$, $M_{w,\text{GPC}} = 7000 \text{ g mol}^{-1}$, $D = 1.39$. $X_{n,\text{GPC}} = 22$.

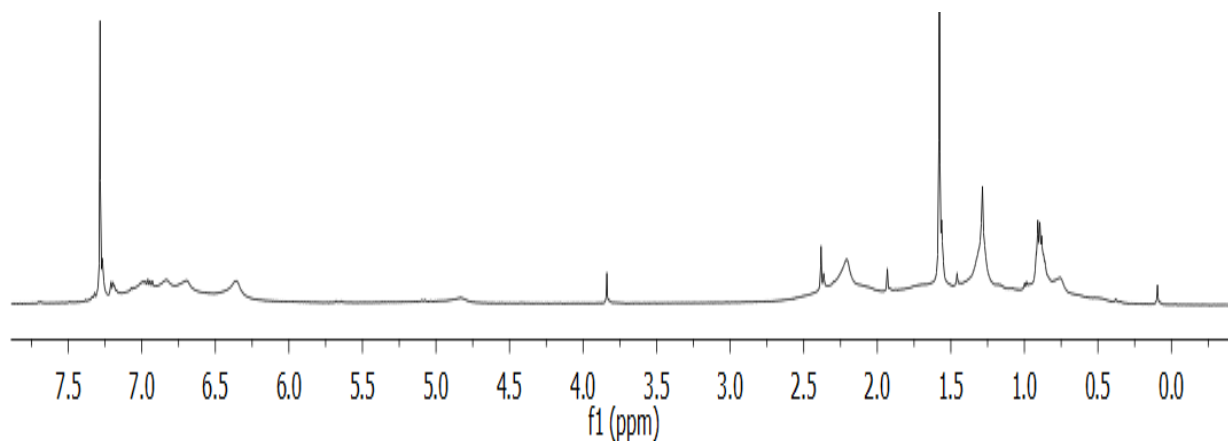


Figure 3.46. ^1H NMR spectrum of *o*MesSt polymer in CDCl_3

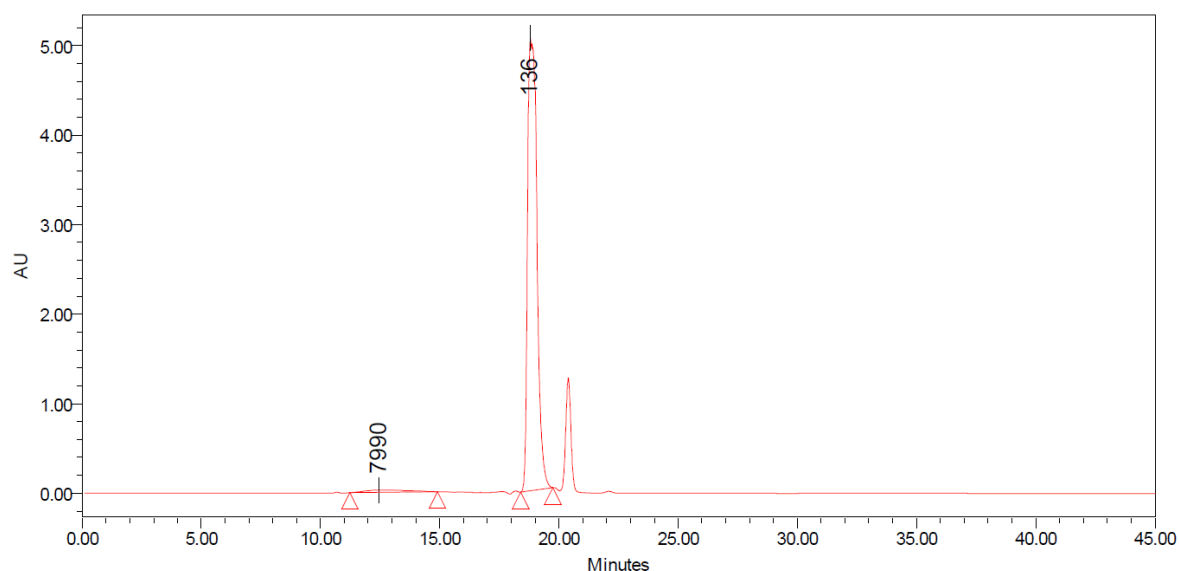


Figure 3.47. GPC-UV trace of crude mixture for *o*MesSt polymerization; eluent: THF, 1 mL min^{-1} (peak at 136 Da corresponds to residual monomer)

Table 3.2. Summary of data for the free radical polymerization of vinyl-functionalized azaborines and their all-carbon analogues.

Monomer	Feed ratio ^a	<i>T</i> / <i>t</i> (°C / h)	Conv ^b (%)	<i>M_n</i> (kDa) ^c	<i>M_w</i> (kDa) ^c	<i>D</i> ^c	<i>X_n</i> ^c
4V-NBMes	50:1	70 / 24	76	26.9	130.4	4.82	119
6V-NBMes	50:1	70 / 24	51	18.2	44.4	2.44	80
<i>m</i>MesSt	50:1	70 / 6.5	>95	29.7	61.3	2.07	134
5V-NBMes	50:1	70 / 24	63	11.6	46.1	3.98	52
<i>p</i>MesSt	50:1	70 / 6.5	82	21.6	42.1	1.95	97

[a] Feed ratio of [Monomer]:[AIBN] in anisole, [M] = 4.5 M. [b] Conversion estimated based on ¹H NMR integration of residual monomer before purification relative to anisole standard. [c] Dispersity (*D*) and average degree of polymerization (*X_n*) based on GPC analysis of isolated product in THF relative to PS standards.

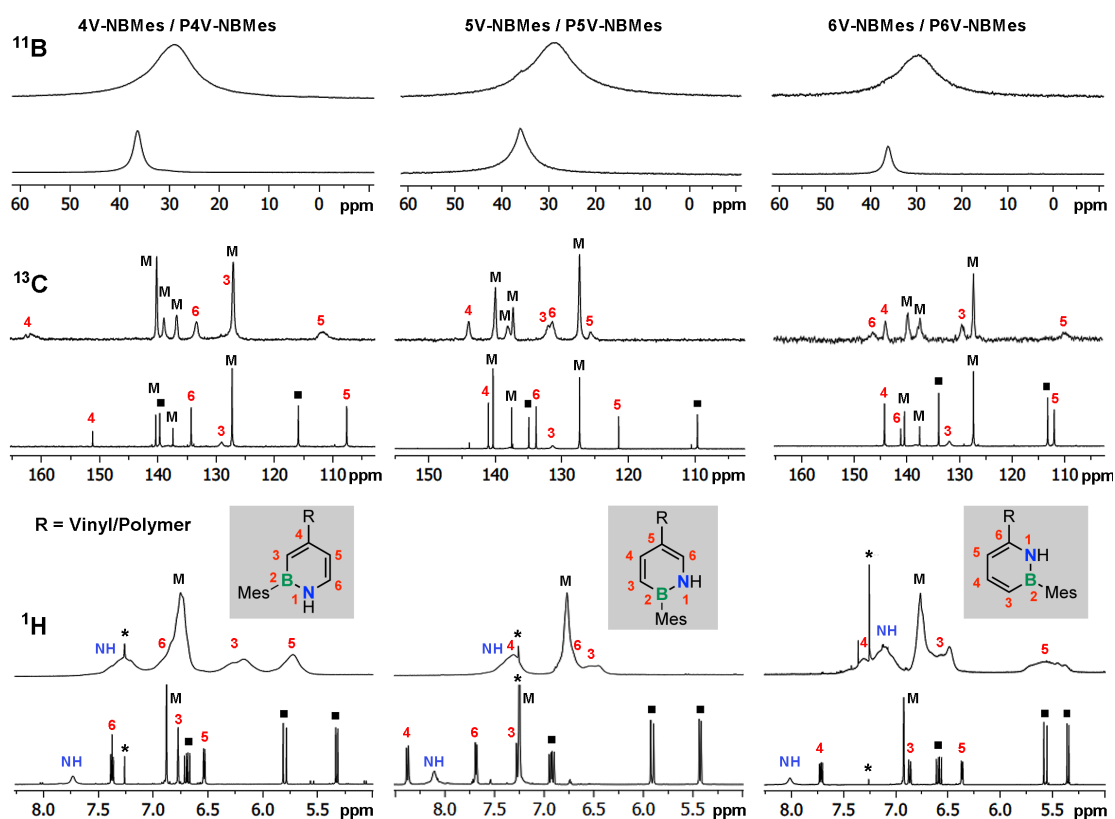


Figure 3.48. ¹H, ¹³C (aromatic region), and ¹¹B NMR spectra of monomers (bottom) and polymers (top) in CDCl₃ (*). Vinyl groups are indicated with a black square, and signals attributed to the pendent mesityl groups with “M”.

3.7.5 2D NMR Spectra

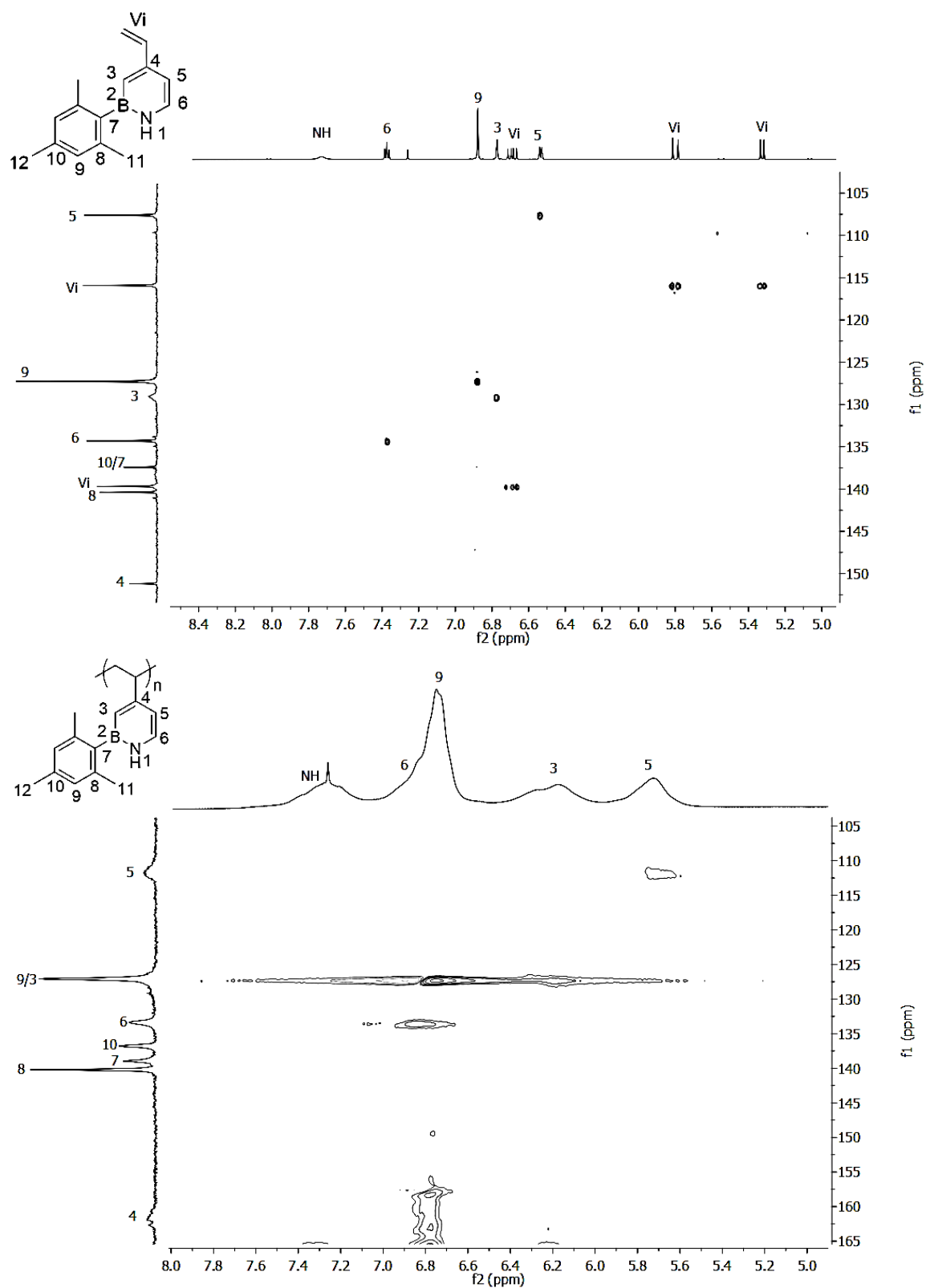


Figure 3.49. Comparison of ^1H , ^{13}C -HMQC NMR spectra of 4V-NBMe and P4V-NBMe in CDCl_3

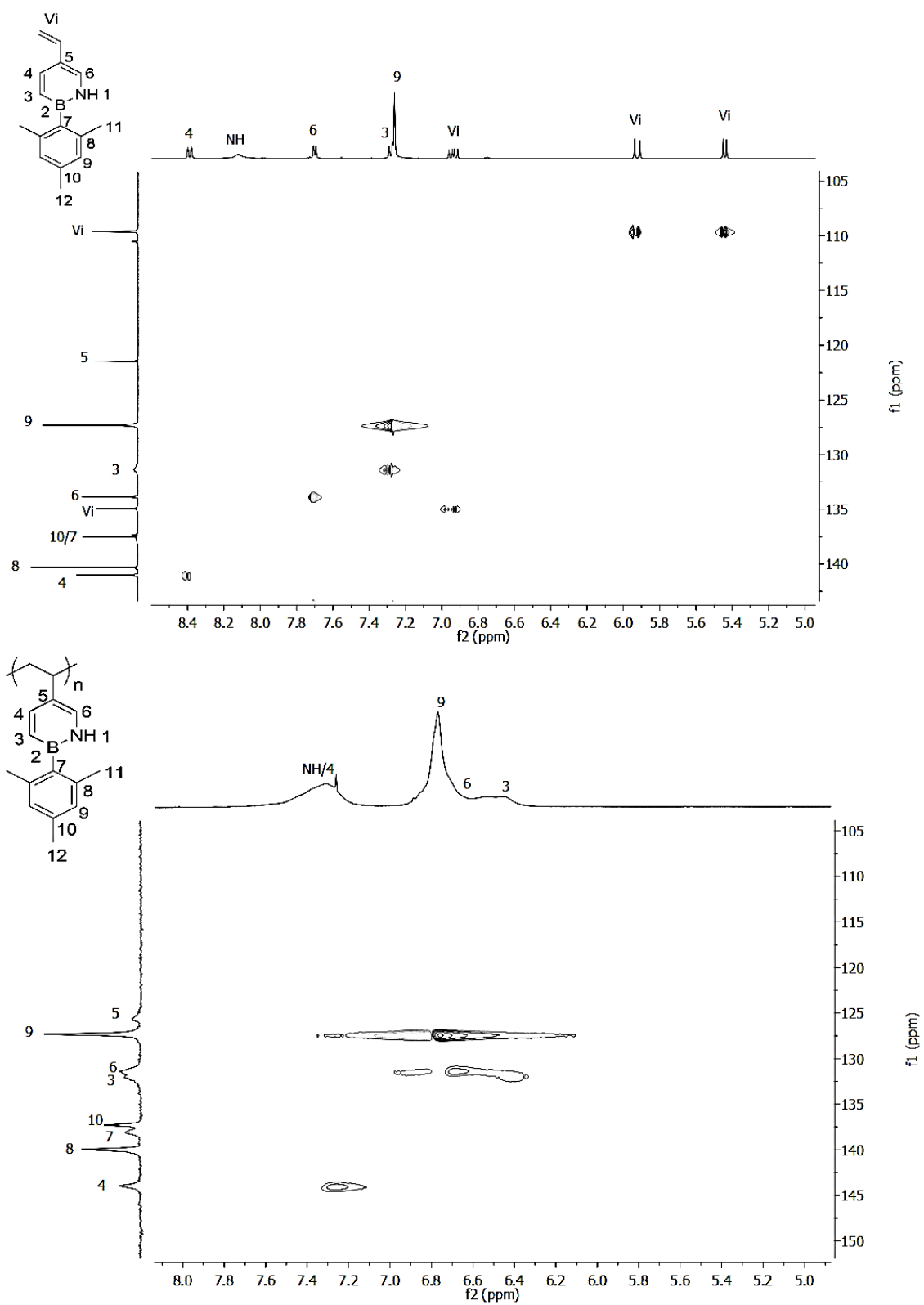


Figure 3.50. Comparison of ^1H , ^{13}C -HMQC NMR spectra of 5V-NBMes and P5V-NBMes in CDCl_3

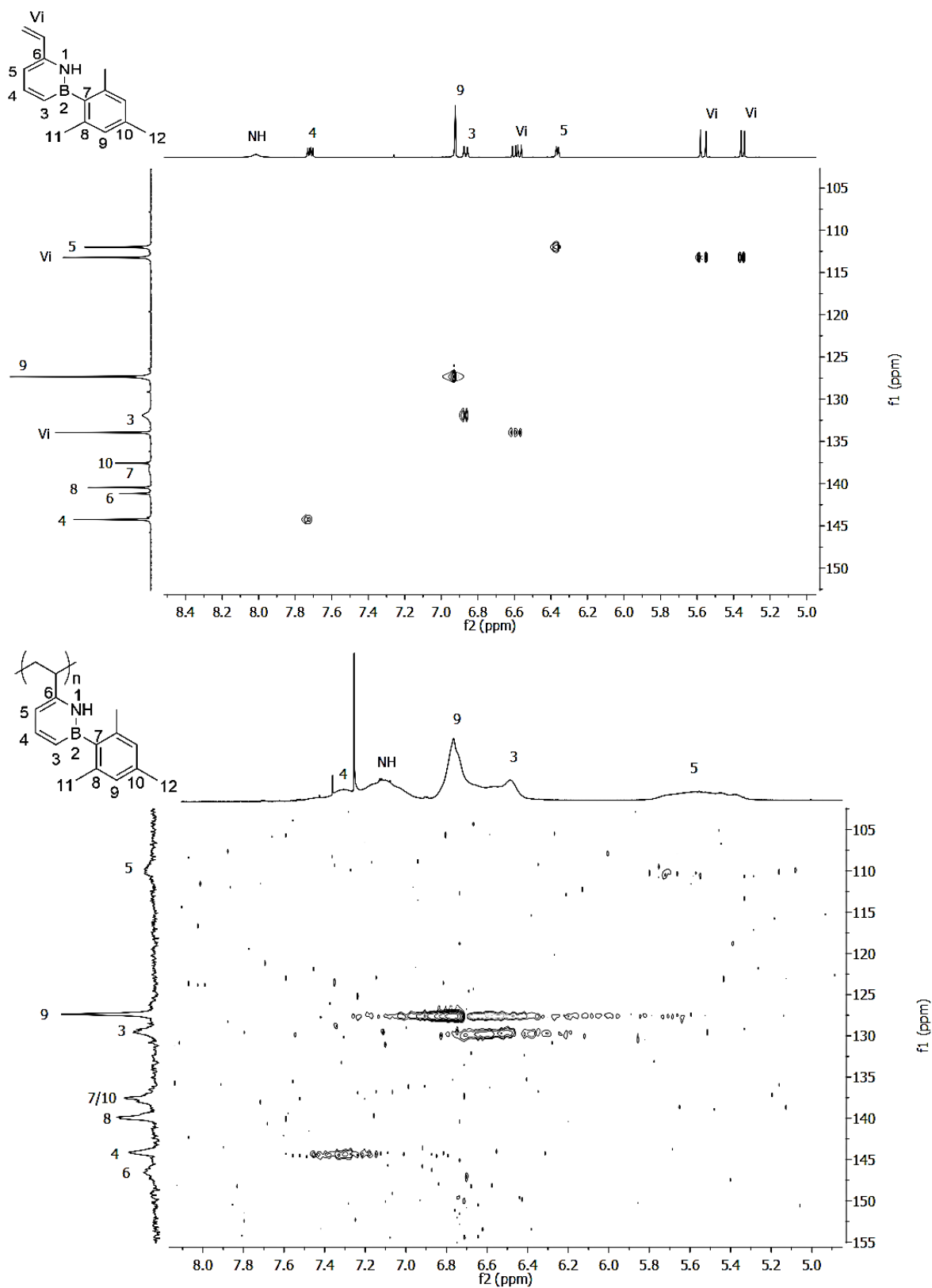


Figure 3.51. Comparison of ^1H , ^{13}C -HMQC NMR spectra of 6V-NBMes and P6V-NBMes in CDCl_3

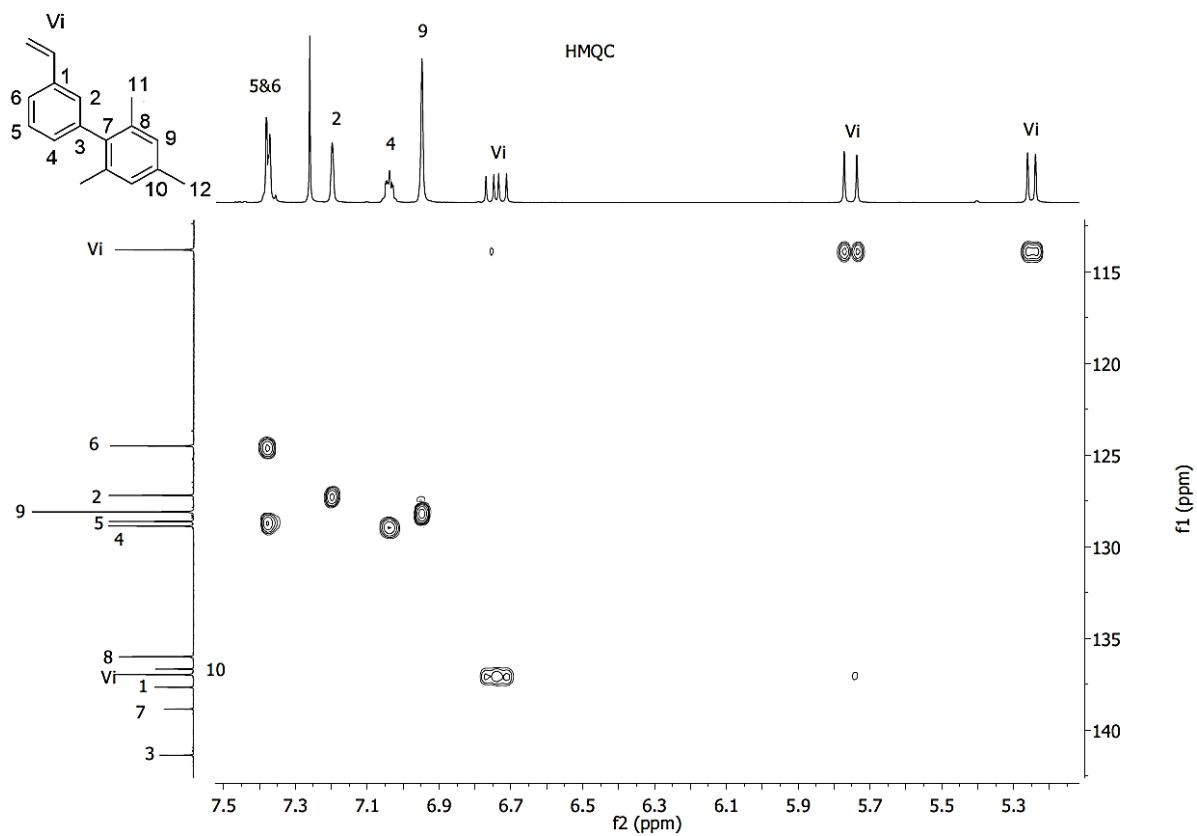
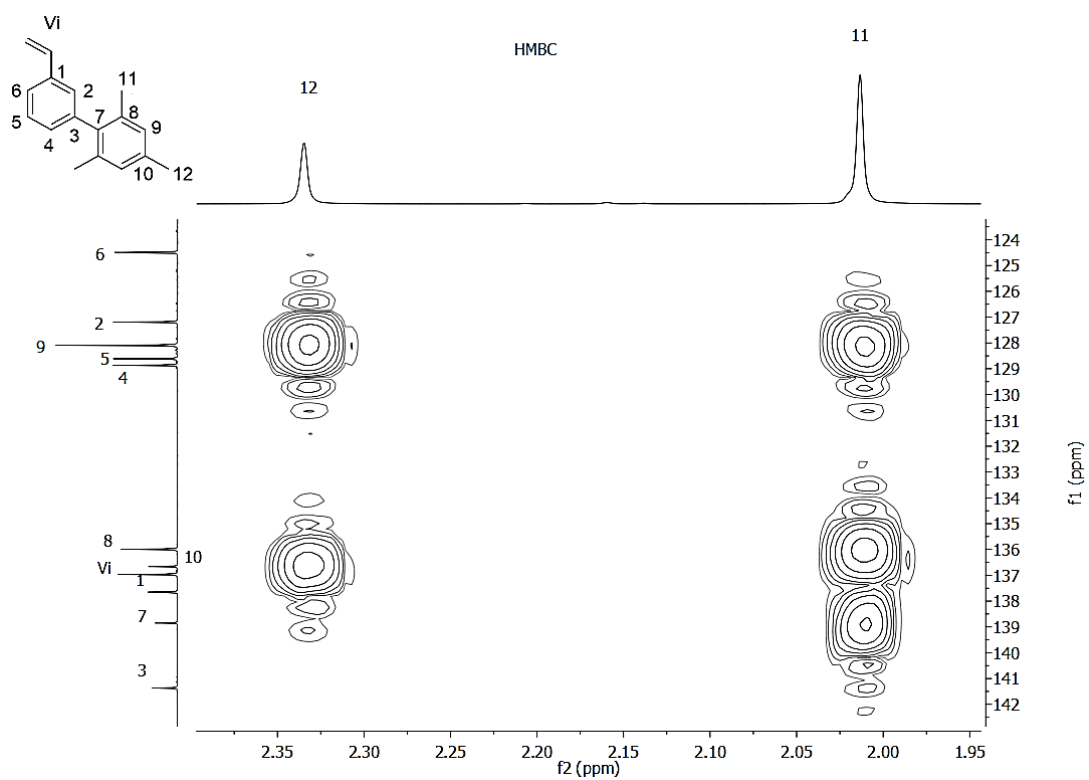


Figure 3.52. ^1H , ^{13}C -HMQC NMR spectrum of *m*MesSt in CDCl_3



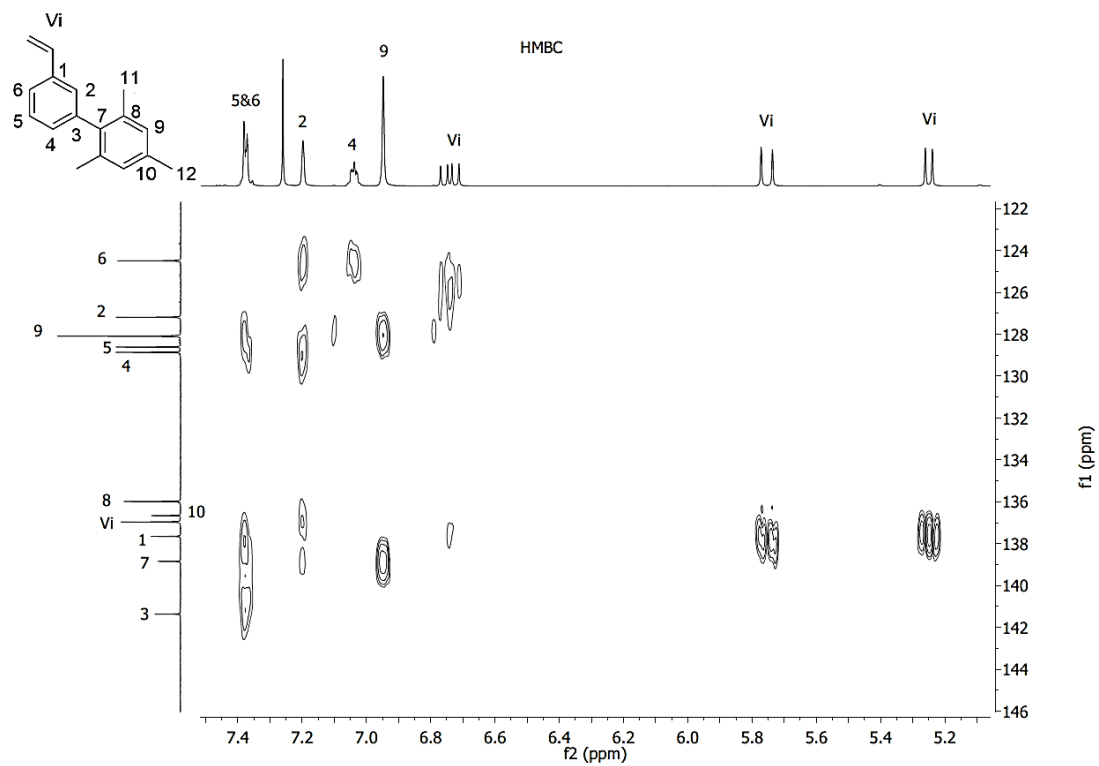


Figure 3.53. ^1H , ^{13}C -HMBC NMR spectrum of *m*MesSt in CDCl_3

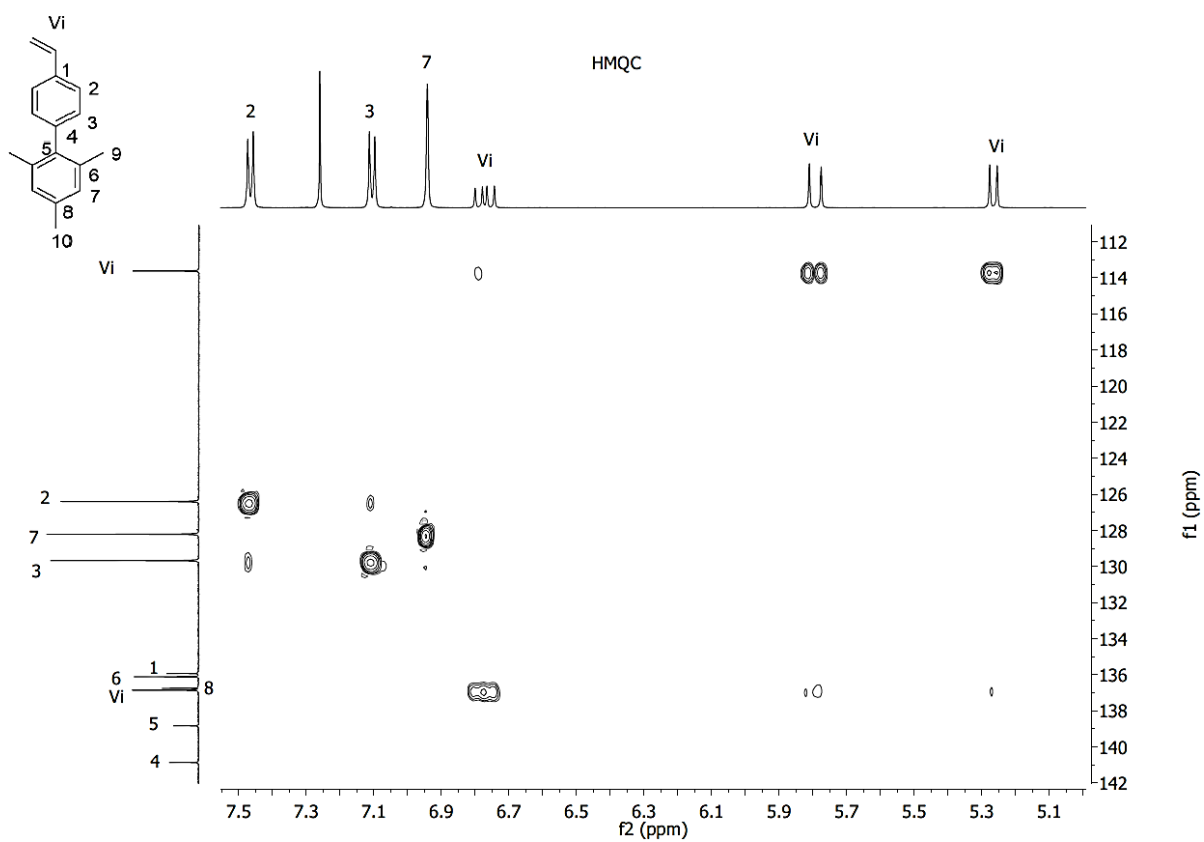


Figure 3.54. ^1H , ^{13}C -HMQC NMR spectrum of *p*MesSt in CDCl_3

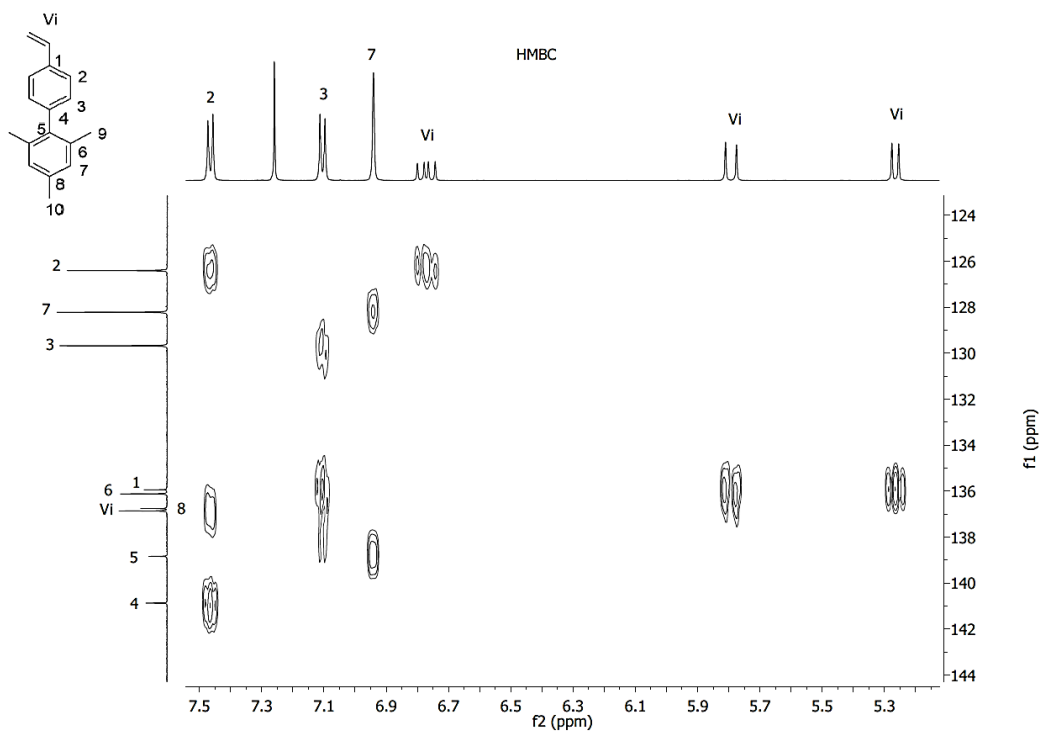
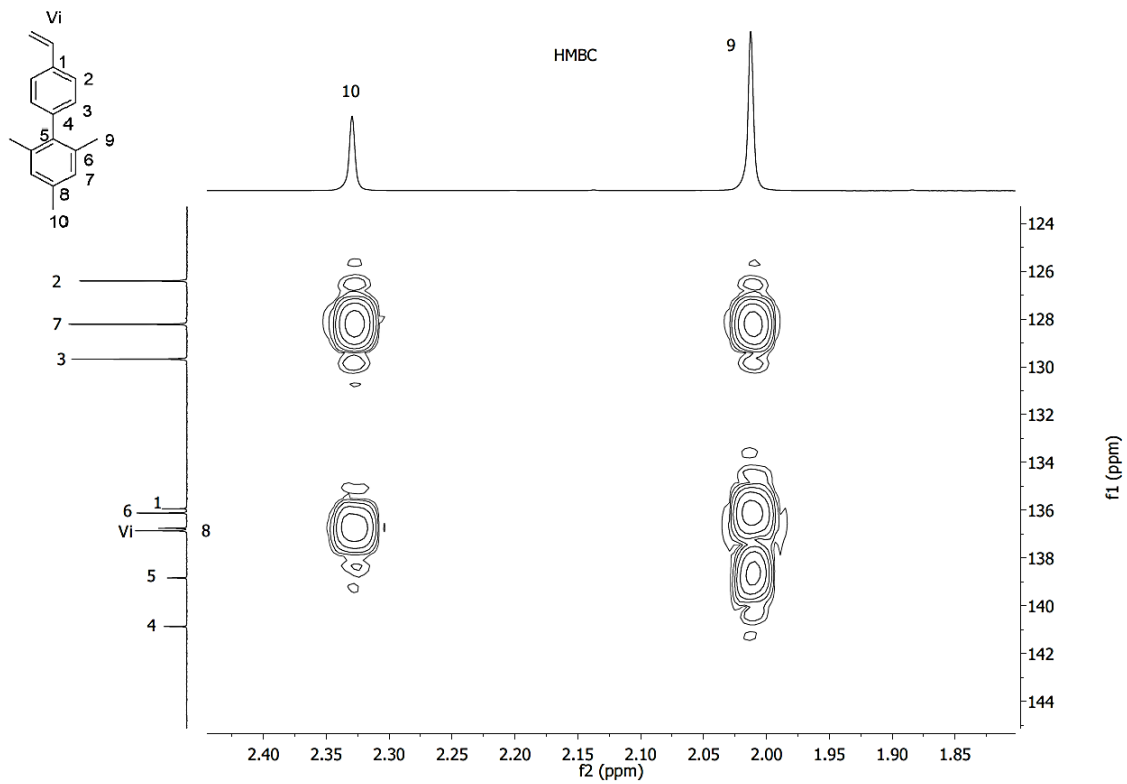


Figure 3.55. ^1H , ^{13}C -HMBC NMR spectrum of *p*MesSt in CDCl_3

3.7.6 Copolymerizations

General Procedure for the Free Radical Copolymerization of Azaborine Monomers with Styrene. Into a 10 mL Schlenk tube were loaded the azaborine monomer (50 mg, 224 μmol), styrene monomer (23.3 mg, 224 μmol), 40 μL of an 0.11 M AIBN solution in anisole, and 60 μL of anisole ($[\text{azaborine}]/[\text{St}]/[\text{AIBN}] = 50/50/1$). After 3 freeze-pump-thaw cycles, the tube was fully immersed in a 70 $^{\circ}\text{C}$ oil bath and the mixture kept stirring for 20 h. The tube was placed in liquid nitrogen to terminate the reaction. One drop of the polymerization solution was taken for ^1H NMR measurement to determine the conversion of the monomers. The polymer was then precipitated in a 10-fold volume of hexanes, redissolved in toluene, precipitated in a 10-fold volume of cold hexanes again, and freeze-dried in benzene. After drying in high vacuum, the copolymers were obtained as off-white powders. They were analyzed by ^1H NMR, elemental analysis, GPC-RI, and DSC.

General Procedure for the Free Radical Copolymerization of Azaborine Monomers with Mesitylstyrene Derivatives. Into a 10 mL Schlenk tube were loaded the azaborine monomer (50 mg, 224 μmol), MesSt monomer (50.0 mg, 224 μmol), 40 μL of an 0.11 M AIBN solution in anisole, and 60 μL of anisole ($[\text{azaborine}]/[\text{MesSt}]/[\text{AIBN}] = 50/50/1$). After 3 freeze-pump-thaw cycles, the tube was fully immersed in a 70 $^{\circ}\text{C}$ oil bath and kept stirring for 10 h. The tube was placed in liquid nitrogen to terminate the reaction. One drop of the polymerization solution was taken for ^1H NMR measurement to determine the conversion of the monomers. The polymer was then precipitated in a 10-fold volume of hexanes, redissolved in toluene, precipitated in a 10-fold volume of cold hexanes again, and freeze-dried in benzene. After drying in high vacuum, the copolymers were obtained as off-white powders. They were analyzed by ^1H NMR, elemental analysis, and GPC-RI.

Copolymerization of 4V-NBMes and styrene

Scale: 50 mg of each monomer, [azaborine]/[St]/[AIBN] = 50/50/1.

Monomer conversion: 4V-NBMes: 57%; styrene: 50% from ^1H NMR integration of residual vinyl group signals of monomers relative to Me group of anisole.

Isolated yield: 40.0 mg.

GPC-RI: $M_{n,\text{GPC}} = 15600 \text{ g mol}^{-1}$, $M_{w,\text{GPC}} = 50700 \text{ g mol}^{-1}$, $D = 3.25$.

Elemental analysis: Calcd for $(\text{C}_{15}\text{H}_{18}\text{B}_1\text{N}_1)_n(\text{C}_8\text{H}_8)_m$ with $n/m = 1.14/1$ (from monomer conversion by ^1H NMR integration): C 84.09; H 8.02; N 4.45. Found: C 83.39; H 7.96; N 4.64.

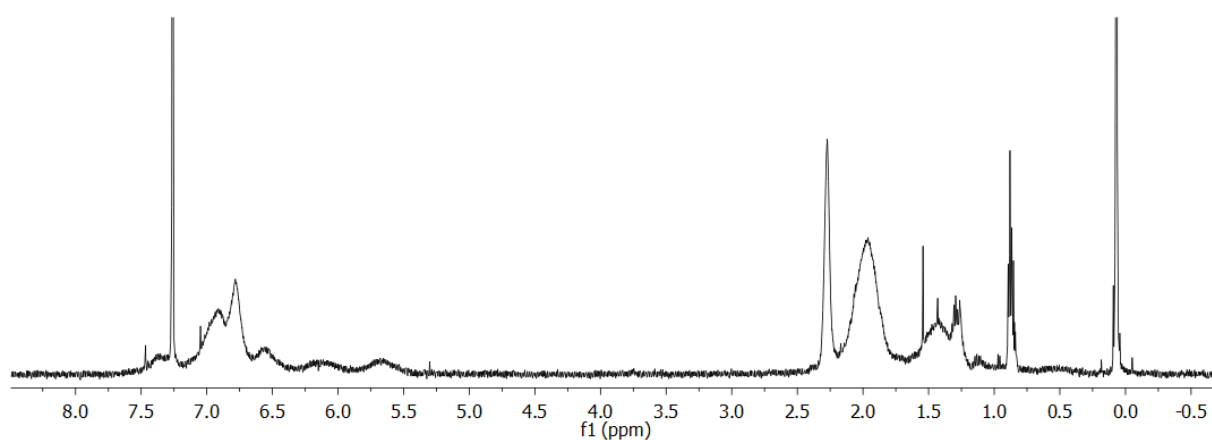


Figure 3.56. ^1H NMR spectrum of isolated P4V-NBMes-co-PS in CDCl_3

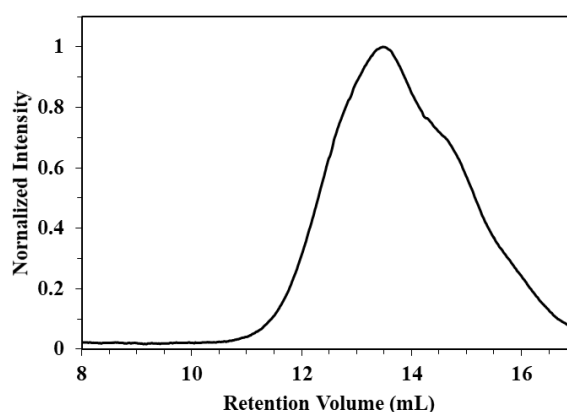


Figure 3.57. GPC trace of isolated P4V-NBMes-co-PS; eluent: THF, 1 mL min^{-1} .

Copolymerization of 5V-NBMes and styrene

Scale: 50 mg of each monomer, [azaborine]/[St]/[AIBN] = 50/50/1.

Monomer conversion: 5V-NBMes: 41%; styrene: 63% from ^1H NMR integration of residual vinyl group signals of monomers relative to Me group of anisole.

Isolated yield: 43.0 mg.

GPC-RI: $M_{n,\text{GPC}} = 19600 \text{ g mol}^{-1}$, $M_{w,\text{GPC}} = 39800 \text{ g mol}^{-1}$, $D = 2.02$.

Elemental analysis: Calcd for $(\text{C}_{15}\text{H}_{18}\text{B}_1\text{N}_1)_n(\text{C}_8\text{H}_8)_m$ with $n/m = 0.65/1$ (from monomer conversion by ^1H NMR integration): C 85.56; H 7.97; N 3.65. Found C 85.53; H 7.88; N 3.44.

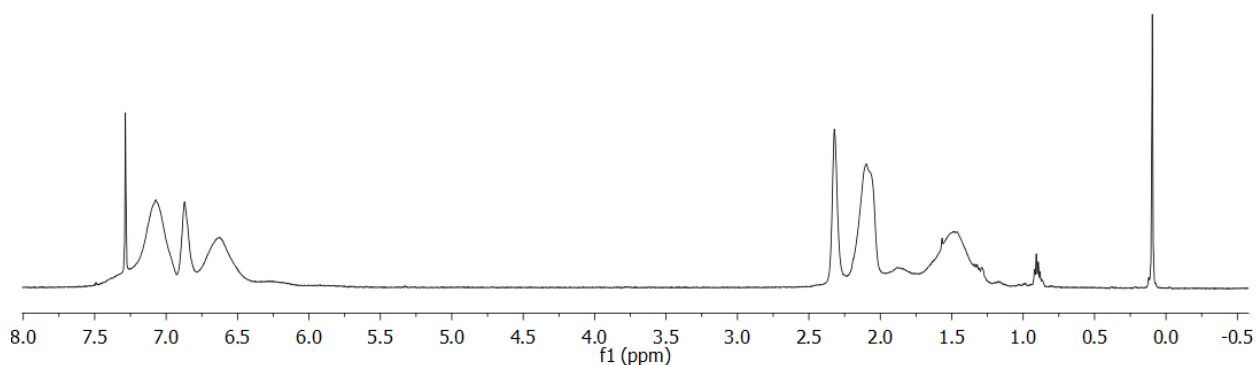


Figure 3.58. ^1H NMR spectrum of P5V-NBMes-co-PS polymer in CDCl_3

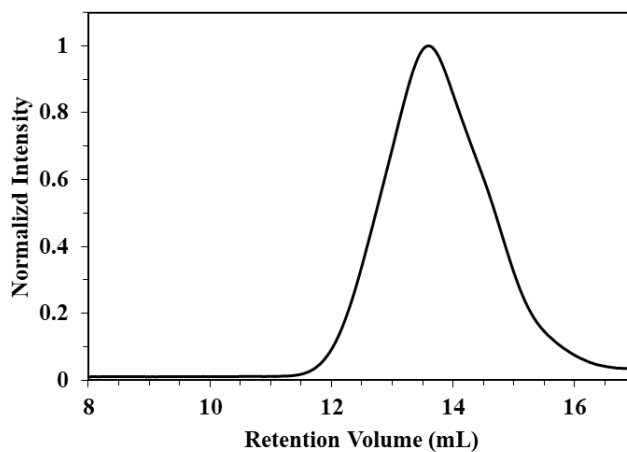


Figure 3.59. GPC trace of P5V-NBMes-co-PS; eluent: THF, 1 mL min^{-1} .

Copolymerization of 6V-NBMes and styrene

Scale: 50 mg of each monomer, [azaborine]/[St]/[AIBN] = 50/50/1.

Monomer conversion: 6V-NBMes: 57%; styrene: 40% from ^1H NMR integration of residual vinyl group signals of monomers relative to Me group of anisole.

Isolated yield: 34.4 mg.

GPC-RI: $M_{n,\text{GPC}} = 10900 \text{ g mol}^{-1}$, $M_{w,\text{GPC}} = 32800 \text{ g mol}^{-1}$, $D = 3.02$.

Elemental analysis: Calcd for $(\text{C}_{15}\text{H}_{18}\text{B}_1\text{N}_1)_n(\text{C}_8\text{H}_8)_m$ with $n/m = 1.42/1$ (from monomer conversion by ^1H NMR integration): C 83.59; H 8.04; N 4.72. Found C 82.00; H 7.84; N 4.85.

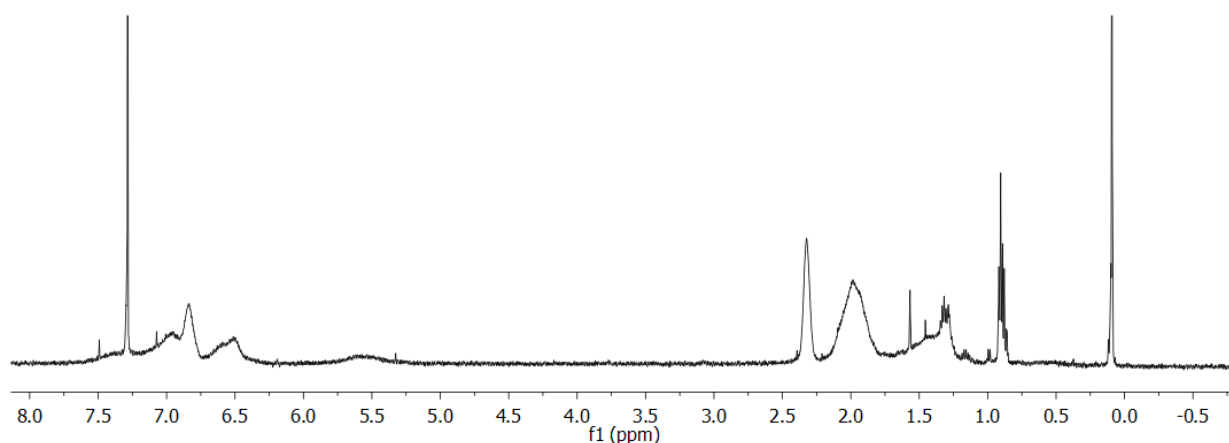


Figure 3.60. ^1H NMR spectrum of P6V-NBMes-co-PS polymer in CDCl_3

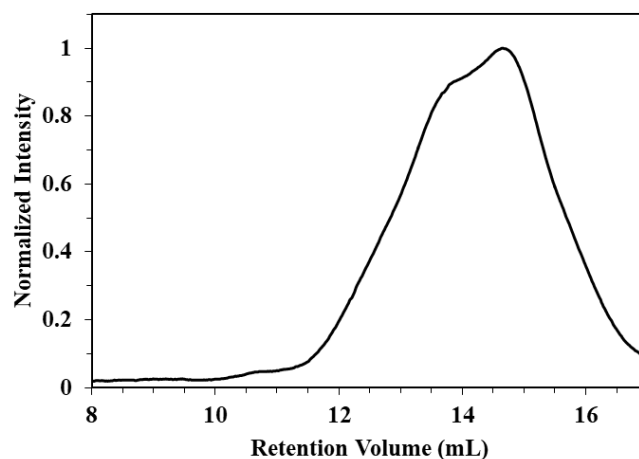


Figure 3.61. GPC trace of P6V-NBMes-co-PS; eluent: THF, 1 mL min^{-1} .

Copolymerization of 4V-NBMes and *meta*-mesitylstyrene (*m*MesSt)

Scale: 50 mg of each monomer, [azaborine]/[MesSt]/[AIBN] = 50/50/1.

Monomer conversion: 4V-NBMes: 65%; *m*MesSt: 66% from ^1H NMR integration of residual vinyl group signals of monomers relative to Me group of anisole.

Isolated yield: 58.0 mg (58%).

GPC-RI: $M_{n,\text{GPC}} = 19200 \text{ g mol}^{-1}$, $M_{w,\text{GPC}} = 54800 \text{ g mol}^{-1}$, $D = 2.85$.

Elemental analysis: Calcd for $(\text{C}_{15}\text{H}_{18}\text{B}_1\text{N}_1)_n(\text{C}_{17}\text{H}_{18})_m$ with $n/m = 1/1$ (from monomer conversion by ^1H NMR integration): C 86.28; H 8.15; N 3.14. Found C 84.91; H 8.12; N 3.12.

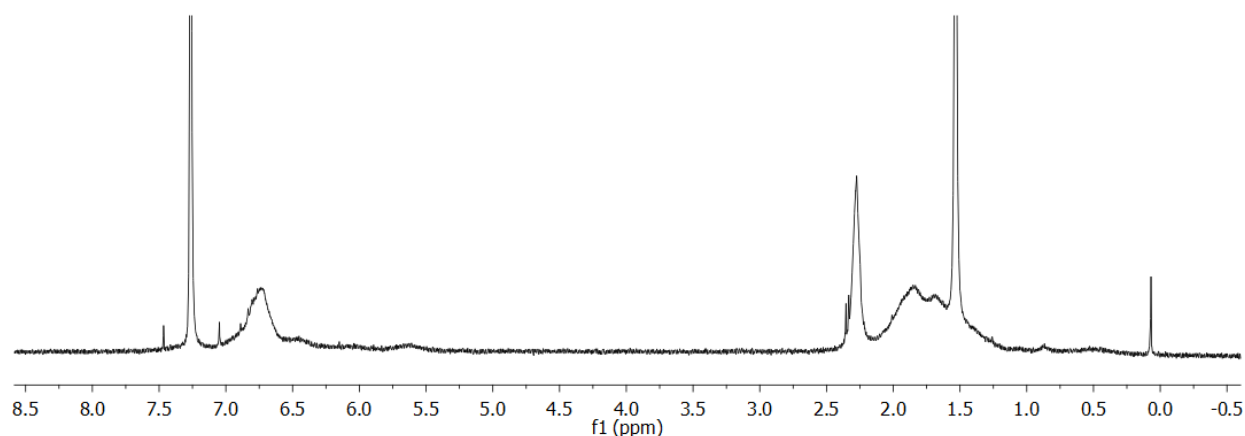


Figure 3.62. ^1H NMR spectrum of P4V-NBMes-co-P*m*MesSt polymer in CDCl_3

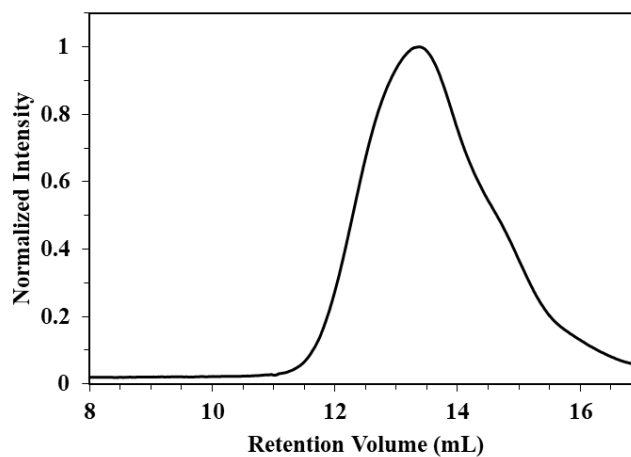


Figure 3.63. GPC trace of P4V-NBMes-co-P*m*MesSt; eluent: THF, 1 mL min^{-1} .

Copolymerization of 5V-NBMes and *para*-mesitylstyrene (*p*MesSt)

Scale: 50 mg of each monomer, [azaborine]/[MesSt]/[AIBN] = 50/50/1.

Monomer conversion: 5V-NBMes: 32%; *p*MesSt: 54% from ^1H NMR integration of residual vinyl group signals of monomers relative to Me group of anisole.

Isolated yield: 71.6 mg (72%).

GPC-RI: $M_{n,\text{GPC}} = 28900 \text{ g mol}^{-1}$, $M_{w,\text{GPC}} = 59300 \text{ g mol}^{-1}$, $D = 2.05$.

Elemental analysis: Calcd for $(\text{C}_{15}\text{H}_{18}\text{B}_1\text{N}_1)_n(\text{C}_{17}\text{H}_{18})_m$ with $n/m = 0.59/1$ (from monomer conversion by ^1H NMR integration): C 87.71; H 8.15; N 2.33. Found C 87.71; H 8.15; N 2.20.

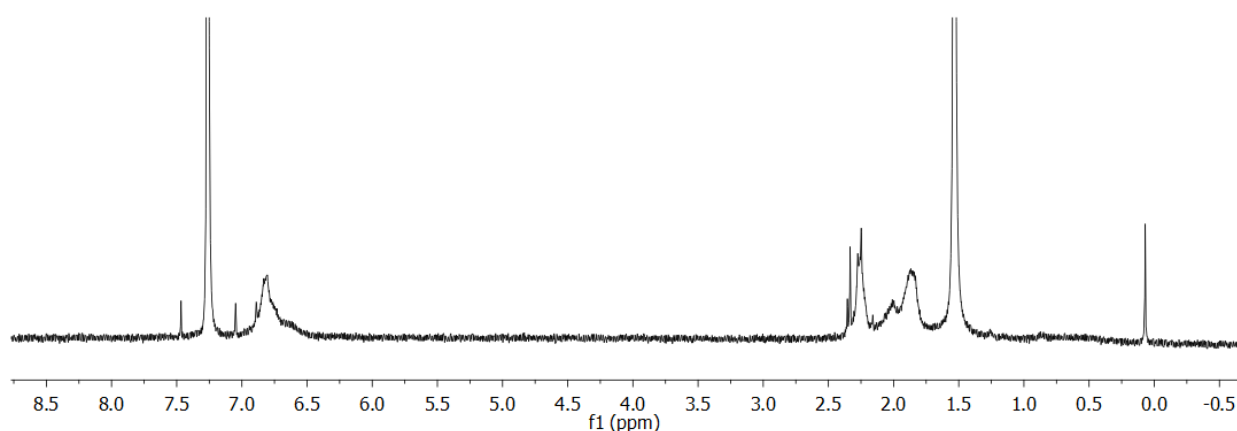


Figure 3.64. ^1H NMR spectrum of P5V-NBMes-co-PpMesSt polymer in CDCl_3

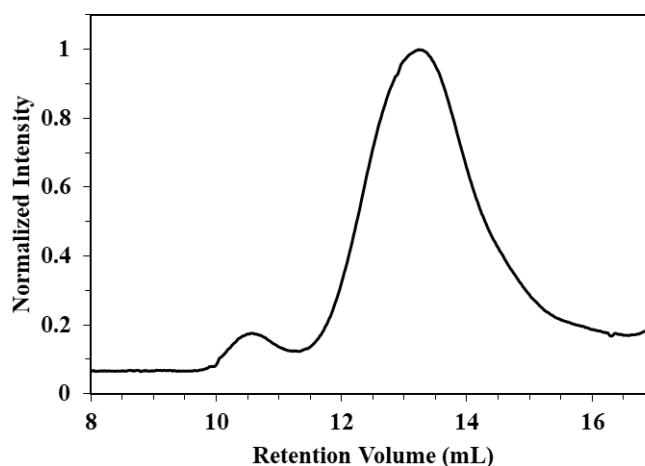


Figure 3.65. GPC trace of P5V-NBMes-co-PpMesSt; eluent: THF, 1 mL min^{-1} .

Copolymerization of 6V-NBMes and *meta*-mesitylstyrene (*m*MesSt)

Scale: 50 mg of each monomer, [azaborine]/[MesSt]/[AIBN] = 50/50/1.

Monomer conversion: 6V-NBMes: 26%; *m*MesSt: 15% from ^1H NMR integration of residual vinyl group signals of monomers relative to Me group of anisole after 10 hours. In another experiment the polymerization time was extended to 24 h (monomer conversion: 6V-NBMes: 41%; *m*MesSt: 14% from ^1H NMR integration). All analytical data provided correspond to the experiment with a 10 h reaction time.

Isolated yield: 27.6 mg (28%).

GPC-RI: $M_{n,\text{GPC}} = 8800 \text{ g mol}^{-1}$, $M_{w,\text{GPC}} = 24400 \text{ g mol}^{-1}$, $D = 2.77$.

Elemental analysis: Calcd for $(\text{C}_{15}\text{H}_{18}\text{B}_1\text{N}_1)_n(\text{C}_{17}\text{H}_{18})_m$ with $n/m = 1.73/1$ (from monomer conversion by ^1H NMR integration): C 84.80; H 8.14; N 3.98. Found C 85.71; H 8.12; N 3.52. Note that the elemental analysis is more consistent with a ratio of $n/m = 1.25/1$.

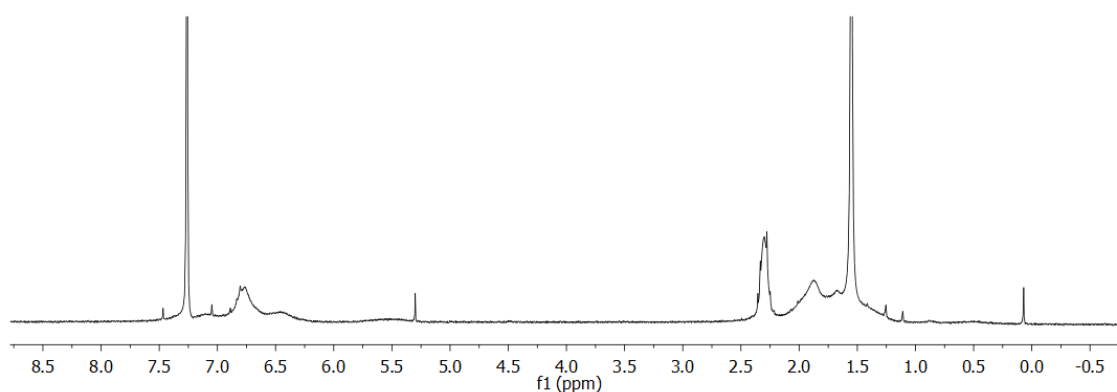


Figure 3.66. ^1H NMR spectrum of P6V-NBMes-co-P*m*MesSt polymer in CDCl_3 .

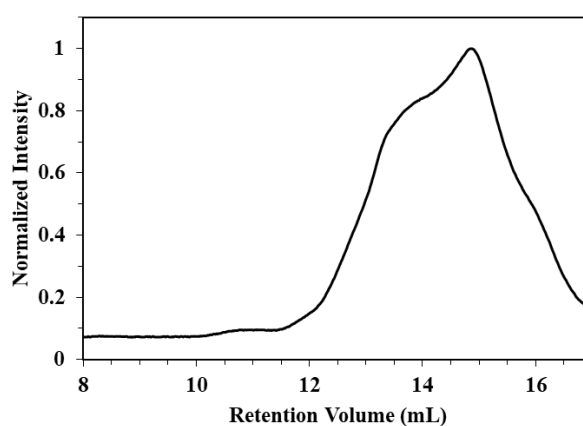


Figure 3.67. GPC trace of P6V-NBMes-co-P*m*MesSt; eluent: THF, 1 mL min^{-1} .

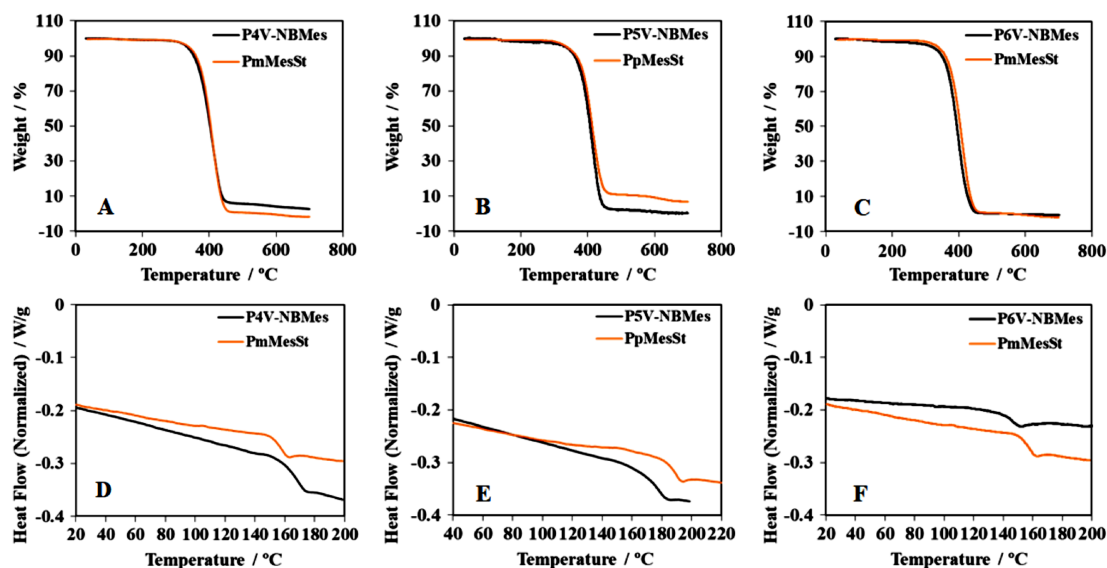


Figure 3.68. Comparisons of TGA traces (A-C) and DSC traces (D-F) for azaborine polymers with those of the respective isosteric carbon analogs. TGA data were acquired at scan rates of $10\text{ }^{\circ}\text{C min}^{-1}$ and DSC data at $20\text{ }^{\circ}\text{C min}^{-1}$.

Table 3.3. Comparison of copolymer glass transition temperatures to predicted values based on the relative composition using the Fox equation $1/T_{g,\text{calc}} = (w_{\text{BN}}/T_{g,\text{BN}}) + (w_{\text{St}}/T_{g,\text{St}})$ where w_{BN} and w_{St} are the weight fractions of vinyl azaborine and styrene respectively as determined from the monomer conversion.

	$T_{g,\text{obs}}$ (K)	$T_{g,\text{calc}}$		w_{BN}	w_{St}	$T_{g,\text{BN}}$ (K)	$T_{g,\text{St}}$ (K)
		(K)					
P4V-NBMes-co-PS	425	413		0.71	0.29	433	371
P5V-NBMes-co-PS	423	408		0.58	0.42	440	371
P6V-NBMes-co-PS	408	399		0.72	0.28	411	371

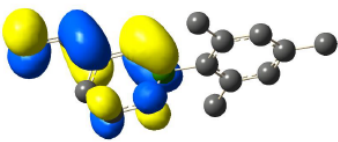
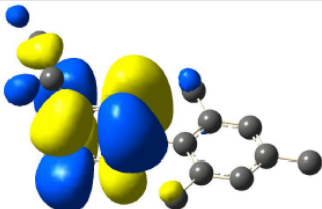
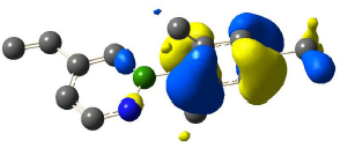
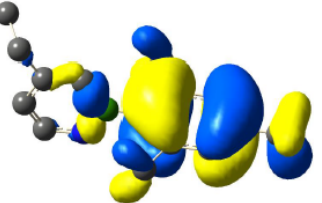
Note: The slightly lower calculated values may be a reflection of the fact that the measured $T_{g,\text{BN}}$ for the azaborine homopolymers is lower than that at infinite molecular weight.

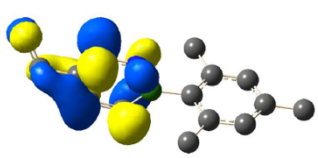
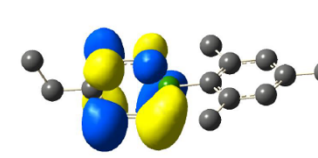
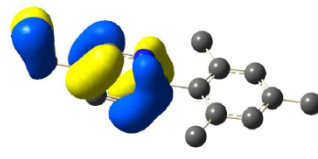
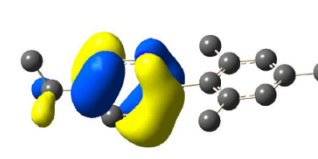
3.7.7 Calculations

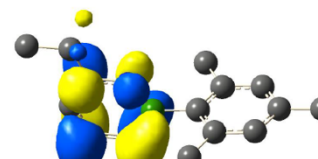
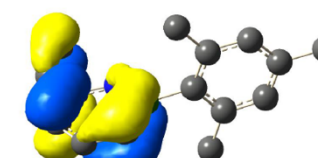
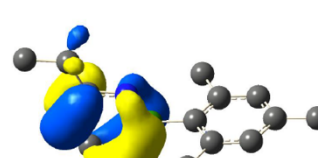
Density Functional Theory (DFT) calculations were performed using the Gaussian 09 program package. Geometries were optimized using the restricted or unrestricted CAM-B3LYP hybrid exchange-correlation functional with the 6-311(d,p) basis set in the gas phase. Frequency calculations were carried out at the same level of theory on fully optimized geometries. Energies reported are the sum of electronic and thermal enthalpies at 298 K and are converted to kcal mol⁻¹ from Hartrees (1 E_h = 627.509608 kcal mol⁻¹). Visualization of electrostatic potential maps were performed using GaussView 5.0.9.

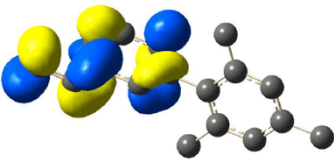
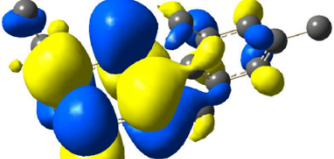
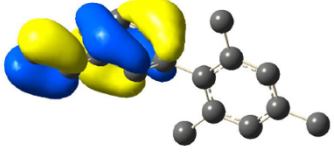
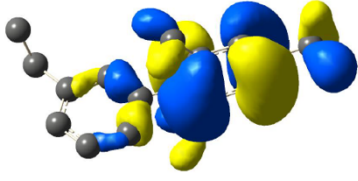
DFT and TD-DFT Calculations

Table 3.4. HOMO-LUMO orbital plots for B-mesityl vinylazaborines (cam-b3lyp/6-311g(d,p))

	4V-NBMes	4Et-NBMes
LUMO	 -0.04 eV	 0.63 eV
HOMO	 -7.53 eV	 -7.48 eV

	5V-NBMes	5Et-NBMes
LUMO	 <p>0.32eV</p>	 <p>0.60eV</p>
HOMO	 <p>-7.29 eV</p>	 <p>-7.41eV</p>

	6V-NBMes	6Et-NBMes
LUMO	 <p>-0.30 eV</p>	 <p>0.60 eV</p>
HOMO	 <p>-7.36 eV</p>	 <p>-7.42eV</p>

	<i>m</i> MesSt	<i>m</i> Mes-PhEt
LUMO	 <p>0.14 eV</p>	 <p>1.01 eV</p>
HOMO	 <p>-7.69 eV</p>	 <p>-7.72 eV</p>

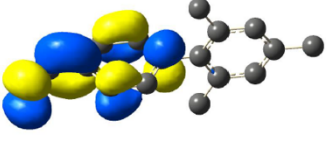
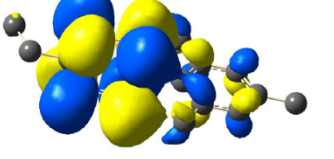
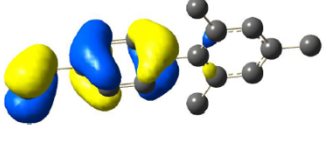
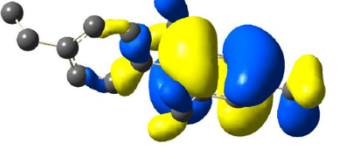
	<i>p</i> MesSt	<i>p</i> Mes-PhEt
LUMO	 <p>0.15 eV</p>	 <p>1.00 eV</p>
HOMO	 <p>-7.61 eV</p>	 <p>-7.71 eV</p>

Table 3.5. Summary of TD-DFT data (cam-b3lyp/6-311g(d,p))

Compound	Transition ^[a]	E_{ex} (eV)	λ (nm)	Oscillator strength f	Assignment (%)
4V-NBMes	$S_0 \rightarrow S_1$	4.77	260.1	0.242	H-3 \rightarrow L (0.12) H \rightarrow L (0.67)
	$S_0 \rightarrow S_4$	5.47	226.5	0.632	H-3 \rightarrow L (0.67) H-1 \rightarrow L+1 (0.10) H \rightarrow L (-0.11)
4Et-NBMes	$S_0 \rightarrow S_1$	5.18	239.5	0.209	H-3 \rightarrow L+3 (-0.14) H \rightarrow L (0.68)
	$S_0 \rightarrow S_3$	5.86	211.7	0.130	H-2 \rightarrow L+2 (0.34) H-1 \rightarrow L (-0.10) H-1 \rightarrow L+1 (0.60)
5V-NBMes	$S_0 \rightarrow S_1$	4.81	257.8	0.063	H-3 \rightarrow L+1 (0.11) H \rightarrow L (0.68) H \rightarrow L+1 (-0.10)
	$S_0 \rightarrow S_2$	5.23	236.9	0.791	H \rightarrow L (0.11) H \rightarrow L+1 (0.68)
5Et-NBMes	$S_0 \rightarrow S_1$	5.01	247.3	0.228	H-3 \rightarrow L+3 (0.12) H \rightarrow L (0.69)
	$S_0 \rightarrow S_4$	5.85	211.9	0.140	H-2 \rightarrow L+2 (0.34) H-1 \rightarrow L+1 (0.61)
	$S_0 \rightarrow S_5$	6.25	198.3	0.250	H-3 \rightarrow L (-0.29) H-2 \rightarrow L (-0.16) H-2 \rightarrow L+2 (-0.11) H \rightarrow L+3 (0.59)
6V-NBMes	$S_0 \rightarrow S_1$	4.48	277.0	0.499	H \rightarrow L (0.69) H \rightarrow L+3 (0.10)
	$S_0 \rightarrow S_5$	5.83	212.7	0.177	H-3 \rightarrow L (-0.34) H-2 \rightarrow L (-0.17) H \rightarrow L (-0.11) H \rightarrow L+3 (0.56)
	$S_0 \rightarrow S_6$	5.85	211.8	0.113	H-3 \rightarrow L (-0.11) H-2 \rightarrow L (-0.11) H-2 \rightarrow L+2 (0.33) H-1 \rightarrow L+1 (0.60)
6Et-NBMes	$S_0 \rightarrow S_1$	5.03	246.4	0.327	H-3 \rightarrow L+3 (-0.12) H \rightarrow L (0.68)
	$S_0 \rightarrow S_4$	5.86	211.7	0.109	H-2 \rightarrow L+2 (0.35) H-1 \rightarrow L+1 (-0.22)
	$S_0 \rightarrow S_5$	6.31	196.5	0.184	H-3 \rightarrow L (0.27) H-2 \rightarrow L (-0.22) H-2 \rightarrow L+2 (-0.10) H \rightarrow L+1 (-0.15) H \rightarrow L+3 (0.56)

<i>m</i>MesSt	$S_0 \rightarrow S_1$	5.11	242.8	0.233	H-3 \rightarrow L (-0.38) H \rightarrow L (0.44) H \rightarrow L+1 (-0.37)
	$S_0 \rightarrow S_2$	5.19	238.9	0.296	H-3 \rightarrow L (0.34) H \rightarrow L (0.53) H \rightarrow L+1 (0.27)
	$S_0 \rightarrow S_5$	5.93	209.2	0.197	H-3 \rightarrow L (-0.10) H-2 \rightarrow L (0.11) H-2 \rightarrow L+3 (-0.34) H-1 \rightarrow L+2 (0.57) H \rightarrow L+1 (0.13)
	$S_0 \rightarrow S_6$	6.21	199.7	0.193	H-3 \rightarrow L (0.16) H-2 \rightarrow L (0.65) H-1 \rightarrow L+2 (-0.11) H \rightarrow L+1 (-0.13)
<i>m</i>Mes-PhEt	$S_0 \rightarrow S_1$	5.35	231.6	0.000	H-1 \rightarrow L+2 (0.48) H \rightarrow L (-0.19) H \rightarrow L+3 (-0.45)
	$S_0 \rightarrow S_3$	5.94	208.8	0.112	H-1 \rightarrow L (0.15) H-1 \rightarrow L+3 (0.34) H \rightarrow L+1 (-0.16) H \rightarrow L+2 (0.55)
<i>p</i>MesSt	$S_0 \rightarrow S_1$	5.04	246.0	0.536	H-3 \rightarrow L (-0.21) H \rightarrow L (0.59) H \rightarrow L+1 (-0.27)
	$S_0 \rightarrow S_2$	5.20	238.2	0.273	H-3 \rightarrow L (0.42) H \rightarrow L (0.35) H \rightarrow L+1 (0.40)
<i>p</i>Mes-PhEt	$S_0 \rightarrow S_1$	5.35	231.7	0.000	H-1 \rightarrow L+2 (0.49) H \rightarrow L (0.20) H \rightarrow L+3 (-0.46)
	$S_0 \rightarrow S_3$	5.93	209.1	0.188	H-2 \rightarrow L+1 (-0.19) H-1 \rightarrow L (-0.14) H-1 \rightarrow L+3 (0.33) H \rightarrow L+2 (0.57)
	$S_0 \rightarrow S_4$	6.07	204.1	0.124	H-3 \rightarrow L (-0.36) H-2 \rightarrow L+1 (0.55) H-1 \rightarrow L (-0.12) H-1 \rightarrow L+3 (0.15)

Table 3.6. 4V-NBMes TD-DFT (NStates=6).

Excited State 1: Singlet-A 4.7666 eV 260.11 nm f=0.2419 <S**2>=0.000
57 -> 61 0.11682
60 -> 61 0.67194

This state for optimization and/or second-order correction.

Total Energy, E(TD-HF/TD-KS) = -661.688964928

Copying the excited state density for this state as the 1-particle RhoCI density.

Excited State 2: Singlet-A 5.3058 eV 233.68 nm f=0.0003 <S**2>=0.000
58 -> 62 0.47535
59 -> 61 -0.21243
59 -> 63 -0.34839
59 -> 64 0.30338

Excited State 3: Singlet-A 5.3879 eV 230.12 nm f=0.0001 <S**2>=0.000
54 -> 61 0.11817
58 -> 62 0.15133
59 -> 61 0.64283
59 -> 63 -0.11848
59 -> 64 0.10026
59 -> 67 0.10707

Excited State 4: Singlet-A 5.4749 eV 226.46 nm f=0.6318 <S**2>=0.000
57 -> 61 0.67163
59 -> 62 0.10304
60 -> 61 -0.11228

Excited State 5: Singlet-A 5.8600 eV 211.58 nm f=0.0585 <S**2>=0.000
58 -> 61 0.24947
58 -> 63 0.25294
58 -> 64 -0.20140
59 -> 62 0.55106
60 -> 64 0.11101

Excited State 6: Singlet-A 5.8845 eV 210.69 nm f=0.0266 <S**2>=0.000
58 -> 61 0.64523
59 -> 62 -0.22361

Table 3.7. 5V-NBMes TD-DFT (NStates=6).

Excited State 1: Singlet-A 4.8085 eV 257.84 nm f=0.0631 <S**2>=0.000
57 -> 62 0.11447
60 -> 61 0.68091
60 -> 62 -0.10574

This state for optimization and/or second-order correction.

Total Energy, E(TD-HF/TD-KS) = -661.685014922

Copying the excited state density for this state as the 1-particle RhoCI density.

Excited State 2: Singlet-A 5.2340 eV 236.88 nm f=0.7910 <S**2>=0.000
60 -> 61 0.11432
60 -> 62 0.68065

Excited State 3: Singlet-A 5.3127 eV 233.38 nm f=0.0007 <S**2>=0.000
58 -> 63 0.50198
59 -> 64 -0.48140

Excited State 4: Singlet-A 5.7239 eV 216.61 nm f=0.0006 <S**2>=0.000
54 -> 61 0.11725
59 -> 61 0.57737
59 -> 62 -0.34841

Excited State 5: Singlet-A 5.8654 eV 211.38 nm f=0.0703 <S**2>=0.000
58 -> 64 0.35242
59 -> 63 0.59193

Excited State 6: Singlet-A 6.2469 eV 198.47 nm f=0.0019 <S**2>=0.000
60 -> 63 0.66597
60 -> 65 -0.14200

Table 3.8. 6V-NBMes TD-DFT (NStates=6).

Excited State 1: Singlet-A 4.4766 eV 276.96 nm f=0.4989 <S**2>=0.000
60 -> 61 0.68893
60 -> 64 0.10519

This state for optimization and/or second-order correction.

Total Energy, E(TD-HF/TD-KS) = -661.701003025

Copying the excited state density for this state as the 1-particle RhoCI density.

Excited State 2: Singlet-A 5.2730 eV 235.13 nm f=0.0000 <S**2>=0.000
58 -> 62 -0.28860
59 -> 61 0.55498
59 -> 63 0.26391
59 -> 64 0.14346

Excited State 3: Singlet-A 5.3325 eV 232.51 nm f=0.0006 <S**2>=0.000
58 -> 62 0.41399
59 -> 61 0.38123
59 -> 63 -0.40620

Excited State 4: Singlet-A 5.7516 eV 215.56 nm f=0.0038 <S**2>=0.000
57 -> 61 -0.10075
58 -> 61 0.66828
58 -> 64 0.11601
60 -> 64 0.13351

Excited State 5: Singlet-A 5.8282 eV 212.73 nm f=0.1765 <S**2>=0.000
57 -> 61 -0.34166
58 -> 61 -0.16627
60 -> 61 -0.11248
60 -> 64 0.55505

Excited State 6: Singlet-A 5.8528 eV 211.84 nm f=0.1130 <S**2>=0.000
57 -> 61 -0.11057
58 -> 61 -0.10685
58 -> 63 0.33131
59 -> 62 0.59745

Table 3.9. *m*MesSt TD-DFT (NStates=6).

Excited State 1: Singlet-A 5.1074 eV 242.76 nm f=0.2326 <S**2>=0.000
57 -> 61 -0.38181
60 -> 61 0.44062
60 -> 62 -0.36649

This state for optimization and/or second-order correction.

Total Energy, E(TD-HF/TD-KS) = -658.229542227

Copying the excited state density for this state as the 1-particle RhoCI density.

Excited State 2: Singlet-A 5.1894 eV 238.92 nm f=0.2962 <S**2>=0.000
57 -> 61 0.34155
60 -> 61 0.53270
60 -> 62 0.26983

Excited State 3: Singlet-A 5.3520 eV 231.66 nm f=0.0002 <S**2>=0.000
58 -> 63 0.49054
59 -> 61 -0.10937
59 -> 62 -0.13422
59 -> 64 0.47059

Excited State 4: Singlet-A 5.8067 eV 213.52 nm f=0.0022 <S**2>=0.000
59 -> 61 0.66505
59 -> 62 -0.12372
59 -> 67 0.13336

Excited State 5: Singlet-A 5.9262 eV 209.21 nm f=0.1967 <S**2>=0.000
57 -> 61 -0.10433
58 -> 61 0.11476
58 -> 64 -0.33993
59 -> 63 0.56986
60 -> 62 0.13192

Excited State 6: Singlet-A 6.2094 eV 199.67 nm f=0.1932 <S**2>=0.000
57 -> 61 0.16127
58 -> 61 0.65175
59 -> 63 -0.10730
60 -> 62 -0.12963

Table 3.10. *p*MesSt TD-DFT (NStates=6).

Excited State 1: Singlet-A 5.0400 eV 246.00 nm f=0.5358 <S**2>=0.000
57 -> 61 -0.21952
60 -> 61 0.59352
60 -> 62 -0.26687

This state for optimization and/or second-order correction.

Total Energy, E(TD-HF/TD-KS) = -658.232116078

Copying the excited state density for this state as the 1-particle RhoCI density.

Excited State 2: Singlet-A 5.2052 eV 238.19 nm f=0.2732 <S**2>=0.000
57 -> 61 0.42481
60 -> 61 0.35336
60 -> 62 0.40548

Excited State 3: Singlet-A 5.3517 eV 231.67 nm f=0.0002 <S**2>=0.000
58 -> 63 0.49604
59 -> 62 -0.19745
59 -> 64 -0.45751

Excited State 4: Singlet-A 5.7262 eV 216.52 nm f=0.0001 <S**2>=0.000
54 -> 61 -0.10579
59 -> 61 0.67409
59 -> 67 0.15624

Excited State 5: Singlet-A 5.9474 eV 208.47 nm f=0.0515 <S**2>=0.000
58 -> 62 0.16777
58 -> 64 0.36398
59 -> 63 0.56767

Excited State 6: Singlet-A 6.1728 eV 200.85 nm f=0.0109 <S**2>=0.000
58 -> 61 0.68171
58 -> 67 0.12684
60 -> 62 -0.10616

Table 3.11. 4Et-NBMes TD-DFT (NStates=6).

Excited State 1: Singlet-A 5.1770 eV 239.49 nm f=0.2093 <S**2>=0.000
58 -> 65 -0.14049
61 -> 62 0.67749

This state for optimization and/or second-order correction.

Total Energy, E(TD-HF/TD-KS) = -662.903715305

Copying the excited state density for this state as the 1-particle RhoCI density.

Excited State 2: Singlet-A 5.3124 eV 233.39 nm f=0.0003 <S**2>=0.000
59 -> 63 0.49876
60 -> 64 -0.48409

Excited State 3: Singlet-A 5.8562 eV 211.71 nm f=0.1295 <S**2>=0.000
59 -> 64 0.33683
60 -> 62 -0.10213
60 -> 63 0.59920

Excited State 4: Singlet-A 5.8770 eV 210.96 nm f=0.0040 <S**2>=0.000
56 -> 62 -0.12774
57 -> 62 -0.13491
60 -> 62 0.64588
60 -> 65 -0.14005

Excited State 5: Singlet-A 6.2112 eV 199.61 nm f=0.0991 <S**2>=0.000
58 -> 62 0.35497
61 -> 65 0.57416

Excited State 6: Singlet-A 6.3893 eV 194.05 nm f=0.0021 <S**2>=0.000
61 -> 63 0.67893
61 -> 66 0.10179

Table 3.12. 5Et-NBMes TD-DFT (NStates=6).

Excited State 1: Singlet-A 5.0131 eV 247.32 nm f=0.2278 <S**2>=0.000
58 -> 65 0.12440
61 -> 62 0.68855

This state for optimization and/or second-order correction.

Total Energy, E(TD-HF/TD-KS) = -662.906402768

Copying the excited state density for this state as the 1-particle RhoCI density.

Excited State 2: Singlet-A 5.3116 eV 233.42 nm f=0.0003 <S**2>=0.000
59 -> 63 0.50192
60 -> 64 -0.48416

Excited State 3: Singlet-A 5.7835 eV 214.38 nm f=0.0004 <S**2>=0.000
56 -> 62 0.14228
57 -> 62 -0.12227
60 -> 62 0.65988
60 -> 65 -0.12487

Excited State 4: Singlet-A 5.8525 eV 211.85 nm f=0.1404 <S**2>=0.000
59 -> 64 0.33881
60 -> 63 0.60920

Excited State 5: Singlet-A 6.2534 eV 198.27 nm f=0.2497 <S**2>=0.000
58 -> 62 -0.29678
59 -> 62 -0.16486
59 -> 64 -0.11042
61 -> 65 0.58948

Excited State 6: Singlet-A 6.2737 eV 197.63 nm f=0.0020 <S**2>=0.000
61 -> 63 0.67555
61 -> 66 -0.13600

Table 3.13. 6Et-NBMes TD-DFT (NStates=6).

Excited State 1: Singlet-A 5.0315 eV 246.42 nm f=0.3270 <S**2>=0.000
58 -> 65 -0.12471
61 -> 62 0.68522

This state for optimization and/or second-order correction.

Total Energy, E(TD-HF/TD-KS) = -662.910274473

Copying the excited state density for this state as the 1-particle RhoCI density.

Excited State 2: Singlet-A 5.3115 eV 233.43 nm f=0.0002 <S**2>=0.000
59 -> 63 0.49958
60 -> 64 -0.48666

Excited State 3: Singlet-A 5.8102 eV 213.39 nm f=0.0002 <S**2>=0.000
56 -> 62 0.13951
57 -> 62 -0.11746
60 -> 62 0.65930
60 -> 65 -0.14602

Excited State 4: Singlet-A 5.8575 eV 211.67 nm f=0.1094 <S**2>=0.000
59 -> 64 0.34624
60 -> 63 0.60587

Excited State 5: Singlet-A 6.3108 eV 196.46 nm f=0.1837 <S**2>=0.000
58 -> 62 0.27362
59 -> 62 -0.22008
59 -> 64 -0.10027
61 -> 63 -0.15293
61 -> 65 0.55973

Excited State 6: Singlet-A 6.3154 eV 196.32 nm f=0.0115 <S**2>=0.000
61 -> 63 0.66844
61 -> 65 0.12783

Table 3.14. *m*Mes-PhEt TD-DFT (NStates=6).

Excited State 1: Singlet-A 5.3533 eV 231.60 nm f=0.0002 <S**2>=0.000
60 -> 64 0.47751
61 -> 62 -0.19257
61 -> 65 -0.45394

This state for optimization and/or second-order correction.

Total Energy, E(TD-HF/TD-KS) = -659.450359077

Copying the excited state density for this state as the 1-particle RhoCI density.

Excited State 2: Singlet-A 5.4494 eV 227.52 nm f=0.0058 <S**2>=0.000
58 -> 62 0.18232
58 -> 63 0.39984
59 -> 62 0.46825
59 -> 63 -0.21510

Excited State 3: Singlet-A 5.9375 eV 208.82 nm f=0.1118 <S**2>=0.000
60 -> 62 0.14870
60 -> 65 0.34502
61 -> 63 -0.16443
61 -> 64 0.55230

Excited State 4: Singlet-A 6.0871 eV 203.68 nm f=0.0198 <S**2>=0.000
58 -> 62 -0.38735
58 -> 63 0.16999
59 -> 62 0.21541
59 -> 63 0.46149
59 -> 65 -0.10573
60 -> 62 0.10957
61 -> 63 0.10384

Excited State 5: Singlet-A 6.2152 eV 199.48 nm f=0.0023 <S**2>=0.000
61 -> 62 -0.28860
61 -> 63 0.58676
61 -> 64 0.16573

Excited State 6: Singlet-A 6.4773 eV 191.41 nm f=0.0670 <S**2>=0.000
60 -> 64 0.17779
61 -> 62 0.59323
61 -> 63 0.28522
61 -> 65 -0.10545

Table 3.15. *p*Mes-PhEt TD-DFT (NStates=6).

Excited State 1: Singlet-A 5.3510 eV 231.70 nm f=0.0002 <S**2>=0.000
60 -> 64 0.49424
61 -> 62 0.20327
61 -> 65 -0.45739

This state for optimization and/or second-order correction.

Total Energy, E(TD-HF/TD-KS) = -659.450352939

Copying the excited state density for this state as the 1-particle RhoCI density.

Excited State 2: Singlet-A 5.4357 eV 228.09 nm f=0.0041 <S**2>=0.000
58 -> 63 0.42160
59 -> 62 0.54578
59 -> 65 0.13111

Excited State 3: Singlet-A 5.9286 eV 209.13 nm f=0.1876 <S**2>=0.000
59 -> 63 -0.19224
60 -> 62 -0.14249
60 -> 65 0.33058
61 -> 64 0.57039

Excited State 4: Singlet-A 6.0762 eV 204.05 nm f=0.1235 <S**2>=0.000
58 -> 62 -0.36088
59 -> 63 0.55389
60 -> 62 -0.12487
60 -> 65 0.14781

Excited State 5: Singlet-A 6.2730 eV 197.65 nm f=0.0000 <S**2>=0.000
61 -> 63 0.68384

Excited State 6: Singlet-A 6.4243 eV 192.99 nm f=0.0439 <S**2>=0.000
60 -> 64 -0.15786
61 -> 62 0.66364
61 -> 65 0.12668

Bond Dissociation Energies



$$\text{BDE} = [E(\text{radical}) + E(\text{H}\cdot)] - E(\text{toluene})$$

Figure 3.69. General method for determining bond dissociation energies.

Table 3.16. Bond dissociation energies for the C_α-H and C_β-H of B-mesityl-ethylzaborine and mesityl-ethylbenzene derivatives. The exact value of -0.5 E_h was used for the energy of H atom.

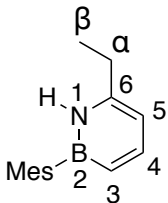
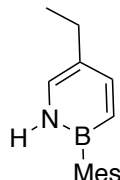
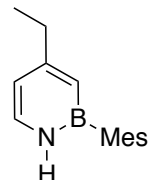
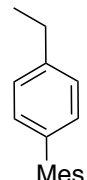
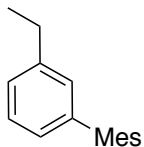
	6Et-NBMes	5Et-NBMes	4Et-NBMes	<i>p</i> Mes-PhEt	<i>m</i> Mes-PhEt
					
Closed Shell Energies (E_h)	-662.75073	-662.746294	-662.749442	-659.303407	-659.303456
Radical Species Energies (E_h)					
C _α •	-662.123109	-662.115182	-662.116293	-658.671	-658.670881
C _β •	-662.094504	-662.091969	-662.093943	-658.647584	-658.646717
Bond Dissociation Energies (kcal mol⁻¹)					
C _α -H	80.1	82.3	83.6	83.1	83.2
C _β -H	98.0	96.8	97.6	97.8	98.4

Table 3.17. Comparison of ^{13}C NMR shifts and calculated Mulliken charges for vinyl and *ipso*-carbons in azaborine and mesitylstyrene derivatives.

	<i>ipso</i> -C	Vi-C _α	Vi-C _β
4V-NBMes	151.9	139.7	115.9
Mulliken charge	-0.028	-0.084	-0.201
5V-NBMes	121.5	134.9	109.6
Mulliken charge	-0.156	-0.105	-0.214
6V-NBMes	141.2	134.0	113.2
Mulliken charge	0.185	-0.116	-0.206
<i>m</i>MesSt	137.6	137.0	113.8
Mulliken charge	-0.074	-0.094	-0.201
<i>p</i>MesSt	135.9	136.9	113.6
Mulliken charge	-0.081	-0.091	-0.203

Table 3.18 Atomic coordinates for 6Et-NBMes.

37

H	5.522	-0.887	-1.272
H	3.585	-2.135	-0.359
H	1.694	-3.363	0.169
C	5.233	-0.002	-0.702
H	5.523	0.881	-1.274
C	3.059	-1.192	-0.243
C	0.994	-2.529	0.231
H	5.819	-0.002	0.222
H	0.234	-2.675	-0.542
C	3.757	-0.001	-0.403
C	1.703	-1.206	0.066
H	0.481	-2.588	1.194
C	3.060	1.190	-0.249
C	1.004	0.001	0.222
H	3.586	2.132	-0.370
C	1.704	1.207	0.060
H	-1.163	-0.005	-1.443
B	-0.532	0.002	0.581
H	-3.364	-0.881	-2.185
N	-1.489	-0.002	-0.485
C	-3.661	-0.005	-1.596
C	-2.849	-0.001	-0.327
C	-1.151	0.007	1.961
C	0.995	2.530	0.218
H	-0.561	0.010	2.871
H	-3.364	0.867	-2.191
H	0.235	2.672	-0.556
H	-5.510	-0.886	-0.870
H	1.695	3.364	0.152
C	-3.366	0.003	0.931
C	-5.172	-0.004	-1.418
C	-2.511	0.007	2.068
H	-5.666	-0.008	-2.391
H	0.482	2.594	1.180
H	-4.437	0.004	1.069
H	-2.987	0.010	3.046
H	-5.509	0.881	-0.876

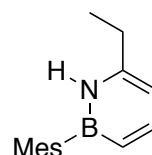


Table 3.19. Atomic coordinates for 6Et α -NBMes.

36

H	1.521	-0.213	3.364
H	0.050	0.468	2.667
C	0.824	-0.292	2.529
H	0.328	-1.263	2.594
H	-2.833	2.974	0.882
C	-3.441	2.735	0.001
C	-3.892	1.312	0.000
H	-4.290	3.418	0.001
H	3.412	0.316	2.133
C	-3.035	0.222	0.000
C	1.533	-0.125	1.207
C	-3.519	-1.099	-0.000
H	-4.592	-1.242	-0.000
C	2.887	0.193	1.191
N	-1.659	0.397	0.000
C	-2.657	-2.202	-0.001
H	-1.343	1.356	0.000
B	-0.699	-0.653	-0.000
H	-2.832	2.974	-0.880
H	-3.108	-3.192	-0.001
C	-1.289	-2.058	-0.001
H	-4.954	1.102	0.000
C	0.836	-0.287	-0.000
H	-0.674	-2.952	-0.001
H	5.343	1.236	0.885
C	3.583	0.355	0.000
C	5.057	0.665	0.000
C	1.533	-0.124	-1.207
H	5.650	-0.255	-0.003
C	2.887	0.194	-1.191
H	5.342	1.241	-0.882
C	0.824	-0.290	-2.529
H	0.049	0.469	-2.667
H	0.328	-1.262	-2.594
H	3.412	0.317	-2.133
H	1.521	-0.211	-3.364

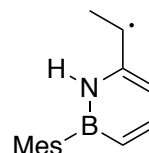


Table 3.20. Atomic coordinates for 6Et β -NBMes.

36

H	1.572	-3.329	0.545
C	0.888	-2.479	0.507
H	0.133	-2.695	-0.253
H	3.492	-2.205	-0.098
H	0.366	-2.422	1.465
H	5.543	-1.184	-0.699
C	2.986	-1.245	-0.091
C	1.626	-1.197	0.205
C	5.181	-0.155	-0.687
C	3.710	-0.095	-0.374
H	5.397	0.288	-1.664
H	-3.188	-0.739	-2.316
H	-5.361	-1.270	-0.763
H	5.765	0.397	0.054
C	0.954	0.033	0.223
C	-5.115	-0.481	-1.462
H	-1.195	-0.125	-1.455
C	-3.706	-0.045	-1.633
N	-1.531	-0.001	-0.509
B	-0.585	0.105	0.563
C	-2.890	0.043	-0.365
H	-5.881	-0.141	-2.144
C	3.038	1.122	-0.352
C	-1.219	0.275	1.926
C	-3.422	0.198	0.877
C	1.682	1.201	-0.059
C	-2.580	0.311	2.017
H	-3.674	0.927	-2.139
H	-0.637	0.366	2.838
H	-4.496	0.246	0.987
H	3.587	2.035	-0.565
H	-3.065	0.432	2.982
C	1.002	2.548	-0.047
H	0.251	2.624	-0.838
H	0.484	2.723	0.899
H	1.721	3.355	-0.194

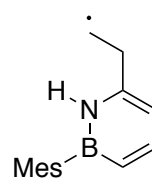


Table 3.21. Atomic coordinates for 5Et-NBMes.

37

H	-5.304	0.888	-1.640
H	-5.169	0.870	0.873
H	-6.639	0.002	-0.907
C	-5.558	0.002	-1.051
C	-4.842	-0.001	0.293
H	0.435	2.661	-0.752
H	-3.115	0.004	-1.884
H	1.818	3.364	0.090
C	-2.628	0.002	-0.917
C	1.116	2.529	0.094
C	-3.331	-0.001	0.244
H	0.510	2.602	1.001
H	-5.305	-0.880	-1.644
H	-5.169	-0.874	0.869
N	-1.260	0.002	-0.928
C	-2.601	-0.004	1.473
H	-0.829	0.004	-1.842
H	-3.190	-0.006	2.389
B	-0.443	-0.001	0.243
C	1.840	1.207	0.022
C	-1.241	-0.004	1.532
H	3.761	2.134	-0.163
C	3.224	1.191	-0.111
C	1.127	-0.000	0.088
H	-0.771	-0.006	2.510
C	3.937	0.001	-0.179
C	1.841	-1.207	0.020
H	5.801	0.900	-0.789
H	0.436	-2.659	-0.756
C	3.225	-1.190	-0.114
C	5.438	0.001	-0.289
C	1.117	-2.530	0.089
H	0.513	-2.605	0.996
H	5.903	-0.034	0.701
H	5.796	-0.866	-0.848
H	3.762	-2.132	-0.167
H	1.819	-3.364	0.081

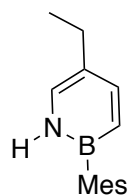


Table 3.22. Atomic coordinates for 5Et α -NBMes.

36

H	-5.471	0.883	-1.577
H	-6.711	0.001	-0.687
C	-5.653	0.002	-0.949
C	-4.793	-0.001	0.269
H	0.406	2.666	-0.768
H	-3.153	0.004	-1.908
H	1.774	3.364	0.099
C	-2.663	0.002	-0.943
C	1.072	2.529	0.088
C	-3.386	-0.001	0.243
H	0.453	2.597	0.985
H	-5.471	-0.876	-1.581
H	-5.274	-0.003	1.240
N	-1.297	0.002	-0.944
C	-2.637	-0.004	1.480
H	-0.859	0.004	-1.854
H	-3.226	-0.006	2.395
B	-0.485	-0.001	0.230
C	1.797	1.207	0.020
C	-1.284	-0.004	1.528
H	3.719	2.134	-0.156
C	3.182	1.191	-0.107
C	1.084	-0.000	0.082
H	-0.805	-0.006	2.502
C	3.895	0.001	-0.172
C	1.798	-1.207	0.017
H	5.761	0.894	-0.786
H	0.406	-2.664	-0.773
C	3.183	-1.190	-0.110
C	5.397	0.001	-0.274
C	1.073	-2.529	0.082
H	0.455	-2.600	0.981
H	5.857	-0.019	0.718
H	5.758	-0.873	-0.819
H	3.720	-2.133	-0.160
H	1.775	-3.364	0.090

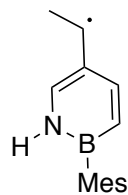


Table 3.23. Atomic coordinates for 5Et β -NBMes.

36

H	1.593	3.372	-0.039
H	3.609	2.240	0.035
C	0.936	2.503	0.005
H	0.327	2.590	0.909
H	0.250	2.554	-0.845
C	3.118	1.272	0.013
H	5.763	1.121	-0.392
C	1.729	1.218	-0.007
H	5.755	0.157	1.083
C	5.396	0.193	0.050
C	3.893	0.119	-0.002
H	-5.106	1.832	-0.255
H	5.853	-0.641	-0.485
C	1.074	-0.023	-0.043
B	-0.501	-0.103	-0.076
H	-0.721	-0.141	2.034
N	-1.221	-0.156	1.157
C	3.239	-1.106	-0.045
C	-5.580	0.859	-0.280
C	-2.582	-0.231	1.248
C	-1.395	-0.133	-1.300
C	1.851	-1.191	-0.065
H	-3.004	-0.269	2.247
H	-1.000	-0.100	-2.311
C	-3.370	-0.259	0.144
C	-2.746	-0.206	-1.140
H	-6.619	0.801	-0.579
C	-4.874	-0.338	0.254
H	3.825	-2.019	-0.068
H	-3.405	-0.225	-2.005
H	-5.144	-0.494	1.311
C	1.192	-2.548	-0.118
H	-5.236	-1.236	-0.262
H	0.587	-2.735	0.774
H	0.522	-2.632	-0.977
H	1.933	-3.345	-0.190

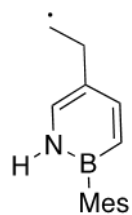


Table 3.24. Atomic coordinates for 4Et-NBMes.

37

H	-1.425	3.259	0.836
H	-3.447	2.273	0.295
C	-0.804	2.364	0.773
H	0.017	2.569	0.082
H	-5.507	1.403	-0.818
H	-0.357	2.198	1.757
C	-2.982	1.306	0.126
H	4.131	2.189	-1.193
C	-1.612	1.170	0.325
C	-5.254	0.398	-0.475
C	4.818	1.346	-1.102
C	-3.768	0.239	-0.291
H	5.630	1.490	-1.819
H	-5.642	-0.317	-1.203
H	5.247	1.375	-0.098
H	-5.786	0.229	0.466
C	-0.990	-0.069	0.104
H	1.433	0.283	-1.726
C	1.655	-0.024	-0.707
B	0.564	-0.241	0.317
C	4.089	0.024	-1.358
C	-3.145	-0.982	-0.514
H	3.684	0.019	-2.372
C	2.969	-0.215	-0.375
C	-1.777	-1.149	-0.322
N	1.045	-0.649	1.604
C	3.319	-0.626	0.948
C	2.365	-0.831	1.889
H	0.396	-0.822	2.358
H	-3.739	-1.827	-0.850
H	4.806	-0.801	-1.298
H	4.357	-0.785	1.210
H	2.613	-1.148	2.894
C	-1.151	-2.498	-0.583
H	-0.332	-2.423	-1.303
H	-0.731	-2.928	0.330
H	-1.884	-3.204	-0.977

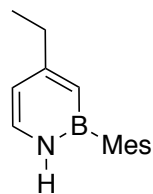


Table 3.25. Atomic coordinates for 4Et α -NBMes.

36

H	0.533	2.664	1.068
H	1.673	3.364	-0.082
C	0.991	2.529	0.084
H	0.186	2.598	-0.652
H	-5.762	0.878	-0.581
H	-2.673	0.003	3.003
H	-4.388	0.001	1.280
C	-2.406	0.002	1.952
C	-3.348	0.001	0.987
C	-5.449	-0.001	-1.156
N	-1.067	0.001	1.658
C	1.712	1.207	-0.013
C	-2.984	-0.000	-0.412
H	-0.436	0.002	2.445
H	3.620	2.133	-0.304
C	-3.980	-0.001	-1.412
H	-6.012	-0.002	-2.089
B	-0.558	0.000	0.320
C	3.088	1.191	-0.217
C	-1.627	-0.001	-0.749
H	-5.762	-0.879	-0.579
C	1.003	0.000	0.095
H	-1.383	-0.002	-1.807
H	-3.640	-0.002	-2.442
C	3.796	-0.000	-0.318
H	5.620	0.884	-1.056
C	5.289	-0.001	-0.508
C	1.712	-1.207	-0.012
H	5.808	-0.003	0.455
C	3.088	-1.191	-0.216
H	0.532	-2.662	1.070
C	0.991	-2.529	0.087
H	5.619	-0.883	-1.059
H	0.186	-2.599	-0.649
H	3.620	-2.134	-0.302
H	1.673	-3.364	-0.078

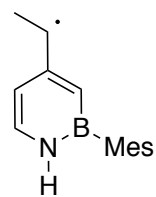


Table 3.26. Atomic coordinates for 4Et β -NBMes.

36

H	-5.758	-0.609	-0.235
H	-1.811	-3.283	-0.675
H	-3.689	-1.931	-0.650
C	-5.230	0.302	-0.524
C	-1.087	-2.530	-0.361
C	-3.107	-1.049	-0.403
H	-0.643	-2.866	0.580
H	-5.656	1.134	0.041
H	-5.441	0.481	-1.582
C	-3.749	0.177	-0.283
C	-1.734	-1.174	-0.216
H	-0.281	-2.508	-1.099
C	-2.980	1.289	0.036
C	-0.962	-0.047	0.105
H	0.461	-0.571	2.402
C	-1.605	1.194	0.229
B	0.596	-0.173	0.316
H	-3.462	2.256	0.136
N	1.098	-0.456	1.628
C	2.425	-0.585	1.912
C	1.672	-0.029	-0.737
H	2.690	-0.801	2.940
H	1.434	0.185	-1.776
C	-0.817	2.435	0.572
C	3.365	-0.449	0.946
C	2.991	-0.168	-0.404
H	-0.362	2.359	1.563
H	-1.453	3.321	0.565
H	4.670	-0.968	-1.464
H	4.411	-0.552	1.207
H	-0.003	2.597	-0.139
C	4.101	-0.031	-1.421
H	3.651	0.083	-2.418
C	5.028	1.101	-1.144
H	4.669	1.995	-0.650
H	6.026	1.112	-1.563

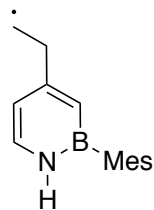


Table 3.27. Atomic coordinates for *p*Mes-PhEt.

37

H	3.075	-0.339	-2.134
H	5.099	-0.976	-0.871
H	5.120	1.541	-0.878
H	0.620	-0.157	-2.135
C	2.540	-0.294	-1.191
H	6.506	0.888	0.006
C	5.417	0.969	0.004
C	1.157	-0.192	-1.194
C	4.762	-0.415	0.004
C	3.255	-0.345	0.003
H	-0.563	-2.704	-0.882
H	5.097	-0.976	0.881
H	-0.194	2.540	-0.885
H	5.118	1.541	0.885
C	0.441	-0.139	-0.000
C	-1.199	-2.560	-0.006
C	-1.049	-0.034	-0.001
C	2.538	-0.292	1.194
C	-0.843	2.488	-0.008
C	-1.834	-1.194	-0.004
C	-1.664	1.224	-0.005
H	-1.960	-3.341	-0.007
C	1.155	-0.191	1.195
H	-1.488	3.368	-0.010
C	-3.220	-1.075	-0.008
C	-3.053	1.301	-0.008
H	-0.563	-2.706	0.870
C	-3.849	0.163	-0.007
H	-0.193	2.544	0.867
H	-3.823	-1.978	-0.013
H	3.070	-0.337	2.139
H	-3.524	2.278	-0.014
H	-5.693	1.194	-0.442
H	-5.817	-0.567	-0.504
C	-5.350	0.267	0.022
H	0.616	-0.155	2.135
H	-5.723	0.257	1.050

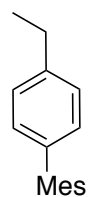


Table 3.28. Atomic coordinates for *p*Mes-PhEtα.

36

H	5.707	-0.884	-0.693
H	1.694	-3.363	-0.009
H	3.647	-2.133	-0.122
H	0.301	-2.628	-0.813
C	0.991	-2.530	0.029
C	3.109	-1.191	-0.087
C	5.327	0.000	-0.178
C	1.721	-1.212	-0.008
C	3.823	0.000	-0.124
H	5.707	0.883	-0.695
H	-0.762	0.001	-2.011
H	5.754	0.001	0.830
H	0.394	-2.630	0.937
C	-1.253	0.001	-1.044
H	-3.206	0.001	-1.898
C	1.021	-0.000	0.033
C	3.109	1.191	-0.086
C	-2.632	0.001	-0.980
H	-5.493	-0.878	-1.440
C	-0.469	-0.000	0.113
C	1.721	1.212	-0.007
H	3.647	2.133	-0.121
C	-5.641	0.000	-0.800
C	-3.307	-0.000	0.265
H	-5.493	0.879	-1.439
H	0.303	2.629	-0.812
C	-1.125	-0.001	1.351
C	0.991	2.530	0.030
C	-4.712	-0.000	0.366
C	-2.500	-0.001	1.429
H	-6.681	0.001	-0.477
H	1.694	3.363	-0.006
H	-0.533	-0.001	2.260
H	0.392	2.629	0.938
H	-5.141	-0.001	1.363
H	-2.985	-0.002	2.399

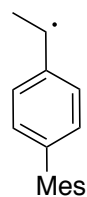


Table 3.29. Atomic coordinates for *p*Mes-PhEt β .

36

H	1.513	3.366	0.119
H	3.526	2.239	0.028
C	0.852	2.500	0.120
H	5.662	1.223	-0.083
H	0.240	2.539	1.023
C	3.036	1.271	0.007
H	0.167	2.593	-0.727
C	5.312	0.190	-0.102
C	1.646	1.221	0.047
H	5.755	-0.329	0.752
C	3.809	0.121	-0.060
H	5.704	-0.281	-1.007
C	1.008	-0.024	0.019
C	3.155	-1.106	-0.087
H	-0.602	-0.152	2.199
H	-5.018	1.786	-0.547
C	-0.484	-0.101	0.061
C	-1.165	-0.162	1.272
C	1.770	-1.198	-0.048
C	-1.234	-0.113	-1.115
C	-2.551	-0.234	1.308
H	-0.722	-0.066	-2.070
C	-5.490	0.813	-0.504
H	-3.060	-0.280	2.265
H	3.741	-2.019	-0.139
C	-2.617	-0.183	-1.077
C	-3.299	-0.246	0.136
H	-6.519	0.726	-0.828
C	-4.808	-0.328	0.165
H	-3.180	-0.187	-2.004
H	-5.136	-0.401	1.213
C	1.107	-2.551	-0.080
H	0.486	-2.712	0.805
H	0.450	-2.654	-0.946
H	1.851	-3.347	-0.122
H	-5.132	-1.269	-0.297

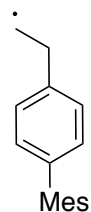


Table 3.30. Atomic coordinates for *m*Mes-PhEt.

37

H	5.338	1.510	-0.724
H	5.678	0.119	0.304
H	5.435	-0.108	-1.426
C	5.096	0.459	-0.558
C	3.621	0.267	-0.320
H	3.311	2.233	0.467
H	3.587	-1.743	-1.056
C	2.848	1.281	0.229
C	3.001	-0.938	-0.621
C	1.490	1.113	0.483
C	1.647	-1.146	-0.383
H	1.324	3.119	1.241
H	1.765	-3.159	-1.133
C	0.694	2.244	1.080
C	0.885	-0.112	0.174
C	1.021	-2.473	-0.726
H	0.254	1.960	2.038
H	0.571	-2.941	0.153
H	-0.134	2.536	0.429
H	0.223	-2.360	-1.464
C	-0.572	-0.313	0.437
H	-0.291	-1.013	2.444
H	-1.174	0.332	-1.512
C	-1.014	-0.788	1.669
C	-1.515	-0.034	-0.549
C	-2.369	-0.978	1.901
C	-2.878	-0.217	-0.332
H	-3.479	2.270	-1.459
H	-3.448	-0.068	-2.386
C	-3.294	-0.694	0.908
H	-2.704	-1.353	2.861
C	-3.882	0.133	-1.403
C	-4.329	1.596	-1.335
H	-4.789	1.818	-0.369
H	-5.058	1.821	-2.117
H	-4.351	-0.850	1.094
H	-4.754	-0.518	-1.308

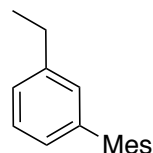


Table 3.31. Atomic coordinates for *m*Mes-PhEt α .

36

H	-1.587	3.363	0.080
H	-3.509	2.137	-0.294
H	-0.111	2.642	-0.574
C	-0.891	2.529	0.182
H	-5.633	0.924	-0.295
H	-5.340	-0.071	-1.720
C	-2.979	1.194	-0.209
C	-5.158	0.006	-0.644
C	-1.610	1.212	0.039
H	-0.400	2.613	1.154
C	-3.682	0.005	-0.346
H	-5.660	-0.838	-0.167
H	1.100	0.016	-1.631
C	-0.921	-0.001	0.154
H	3.330	0.024	-2.467
C	-2.980	-1.188	-0.224
C	1.461	0.006	-0.608
C	3.756	0.014	-1.470
C	0.548	-0.004	0.430
C	-1.612	-1.212	0.023
C	2.860	0.003	-0.381
H	5.724	0.021	-2.316
H	5.603	0.885	-0.782
C	5.241	0.012	-1.339
H	-3.512	-2.129	-0.321
C	1.021	-0.017	1.747
C	3.300	-0.010	0.964
C	2.390	-0.020	2.001
H	0.313	-0.025	2.568
C	-0.895	-2.532	0.149
H	-0.112	-2.633	-0.605
H	5.602	-0.872	-0.800
H	4.361	-0.012	1.181
H	-1.591	-3.363	0.030
H	2.744	-0.030	3.026
H	-0.409	-2.630	1.122

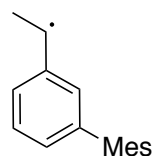


Table 3.32. Atomic coordinates for *m*Mes-PhEt β .

36

H	5.402	-0.123	-1.390
H	5.311	1.487	-0.668
C	5.059	0.436	-0.517
C	3.582	0.252	-0.295
H	5.631	0.080	0.345
H	3.274	2.219	0.490
H	3.543	-1.757	-1.033
C	2.808	1.270	0.247
C	2.958	-0.950	-0.604
H	-1.204	0.398	-1.518
C	1.447	1.109	0.486
C	1.601	-1.151	-0.379
H	-3.733	2.377	-2.071
H	-3.511	-0.052	-2.418
H	1.283	3.115	1.245
H	1.711	-3.158	-1.145
H	0.171	-2.352	-1.466
H	-0.171	2.540	0.419
C	0.839	-0.112	0.171
C	0.650	2.243	1.076
C	0.970	-2.473	-0.731
C	-4.233	1.681	-1.410
C	-1.554	0.010	-0.566
C	-3.916	0.224	-1.442
C	-0.622	-0.305	0.418
C	-2.920	-0.164	-0.360
H	-4.830	2.087	-0.602
H	-4.830	-0.362	-1.298
H	0.200	1.960	2.030
H	0.521	-2.947	0.145
C	-1.079	-0.803	1.636
C	-3.353	-0.664	0.863
H	-0.363	-1.054	2.411
C	-2.436	-0.981	1.855
H	-4.413	-0.809	1.038
H	-2.783	-1.374	2.804

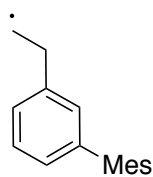


Table 3.33. Atomic coordinates for 4V-NBMes.

35

H	-5.750	-0.001	0.457
H	-5.562	-0.883	-1.057
H	-5.562	0.884	-1.055
C	-5.232	0.000	-0.507
C	-3.738	-0.000	-0.316
H	-3.563	-2.133	-0.302
H	-3.562	2.133	-0.302
C	-3.030	-1.191	-0.215
C	-3.030	1.191	-0.215
C	-1.655	-1.207	-0.010
C	-1.655	1.207	-0.011
H	-1.614	-3.364	-0.088
H	-1.614	3.364	-0.089
C	-0.934	-2.529	0.088
C	-0.946	-0.000	0.098
C	-0.934	2.530	0.088
H	-0.485	-2.669	1.075
H	-0.485	2.669	1.075
H	-0.122	-2.595	-0.641
H	-0.122	2.595	-0.641
B	0.614	-0.000	0.324
H	0.489	-0.000	2.448
N	1.123	-0.000	1.661
H	1.448	-0.001	-1.799
C	1.691	-0.000	-0.740
C	2.455	-0.000	1.957
C	3.019	-0.000	-0.397
H	2.724	-0.000	3.006
C	3.395	-0.000	0.984
H	3.647	-0.001	-2.466
C	4.046	-0.001	-1.455
H	4.436	-0.000	1.275
C	5.364	0.001	-1.295
H	6.027	-0.000	-2.151
H	5.837	0.002	-0.320

Table 3.34. Atomic coordinates for 5V-NBMes.

35

H	5.283	0.953	-1.635
C	5.677	0.402	-0.787
H	6.754	0.318	-0.719
H	3.166	-0.086	-1.975
H	-0.302	2.669	-0.659
H	-1.648	3.362	0.245
C	2.688	-0.074	-1.004
C	-0.967	2.513	0.195
H	0.875	-0.017	-1.889
C	4.887	-0.134	0.136
N	1.327	-0.038	-0.986
C	3.416	-0.118	0.148
H	-0.340	2.529	1.090
C	-1.723	1.211	0.079
H	5.348	-0.630	0.987
H	-3.624	2.189	-0.033
B	0.533	-0.055	0.207
C	-3.109	1.233	-0.032
C	2.714	-0.164	1.392
C	-1.038	-0.014	0.080
C	1.354	-0.128	1.477
H	-5.698	1.002	-0.739
C	-3.850	0.063	-0.140
H	3.321	-0.223	2.294
C	-5.353	0.104	-0.224
C	-1.780	-1.199	-0.029
C	-3.166	-1.145	-0.138
H	-0.433	-2.655	-0.899
H	-5.745	-0.765	-0.755
H	0.902	-0.162	2.463
C	-1.087	-2.541	-0.030
H	-5.800	0.107	0.775
H	-3.726	-2.072	-0.223
H	-0.461	-2.665	0.857
H	-1.810	-3.358	-0.049

Table 3.35. Atomic coordinates for 6V-NBMes.

35

H	1.502	-0.384	-3.348
H	0.033	0.339	-2.689
C	0.804	-0.416	-2.510
H	0.304	-1.388	-2.525
C	-3.558	2.705	-0.146
C	-3.919	1.429	-0.077
H	-4.302	3.489	-0.188
C	1.514	-0.183	-1.199
H	3.395	0.196	-2.147
H	-4.975	1.184	-0.063
C	-3.034	0.262	-0.014
C	-3.547	-1.002	0.054
H	-2.525	3.034	-0.164
C	2.869	0.128	-1.199
N	-1.676	0.428	-0.023
H	-1.348	1.382	-0.074
B	-0.720	-0.634	0.034
H	-4.622	-1.128	0.060
C	-2.695	-2.135	0.115
C	-1.336	-2.018	0.108
H	5.331	1.170	-0.951
C	0.815	-0.276	0.016
H	-3.167	-3.113	0.166
H	-0.739	-2.923	0.157
C	3.567	0.351	-0.019
C	5.042	0.652	-0.035
C	1.514	-0.052	1.212
C	2.869	0.258	1.178
H	0.035	0.631	2.638
H	5.630	-0.270	0.021
H	5.330	1.275	0.813
C	0.804	-0.140	2.541
H	3.395	0.429	2.113
H	0.301	-1.104	2.659
H	1.502	-0.021	3.370

Table 3.36. Atomic coordinates for *mMesSt*.

35

H	1.560	3.359	-0.125
H	0.065	2.611	-0.698
C	0.861	2.540	0.047
H	0.392	2.692	1.022
H	3.468	2.095	-0.434
H	-3.324	0.028	-2.489
C	1.566	1.210	-0.025
C	2.931	1.163	-0.285
C	-3.813	-0.043	-1.521
H	-5.708	-0.214	-2.408
H	5.421	0.784	-1.219
H	-1.160	-0.057	-1.618
C	-5.133	-0.182	-1.492
C	-2.900	0.016	-0.367
C	-1.524	-0.004	-0.597
C	3.621	-0.039	-0.360
C	5.105	-0.065	-0.611
C	0.866	0.012	0.165
C	-0.601	0.039	0.445
C	-3.348	0.092	0.954
H	-4.410	0.125	1.165
C	-1.077	0.108	1.751
C	-2.444	0.136	1.999
H	-5.691	-0.275	-0.568
H	5.661	-0.018	0.331
H	5.406	-0.981	-1.123
C	2.907	-1.216	-0.174
C	1.542	-1.212	0.088
H	-0.372	0.144	2.574
H	-2.804	0.196	3.019
H	3.426	-2.167	-0.235
C	0.811	-2.515	0.283
H	0.013	-2.640	-0.452
H	0.341	-2.567	1.267
H	1.494	-3.360	0.188

Table 3.37. Atomic coordinates for *p*MesSt.

35

H	1.652	-3.363	0.003
H	5.709	-0.882	0.311
H	3.606	-2.133	-0.066
C	0.948	-2.531	0.033
H	0.342	-2.631	0.937
C	5.283	0.001	-0.167
C	3.066	-1.191	-0.050
H	5.613	0.001	-1.210
C	1.677	-1.212	0.002
C	3.780	0.001	-0.079
H	0.266	-2.631	-0.814
H	5.709	0.885	0.311
H	-0.617	-0.001	2.225
C	0.977	-0.000	0.028
C	3.066	1.192	-0.049
C	-1.188	-0.001	1.304
C	-0.516	-0.001	0.085
C	1.676	1.213	0.003
C	-2.573	-0.001	1.350
H	-3.076	-0.002	2.311
H	3.605	2.134	-0.065
C	-1.278	-0.001	-1.084
C	-3.338	-0.001	0.184
H	-0.773	-0.001	-2.043
C	-2.660	-0.001	-1.037
C	0.947	2.531	0.035
H	-5.184	-0.006	1.310
H	0.341	2.630	0.938
C	-4.806	-0.001	0.291
H	1.650	3.363	0.005
H	-3.218	-0.002	-1.966
C	-5.686	0.004	-0.703
H	0.265	2.631	-0.812
H	-6.749	0.003	-0.503
H	-5.390	0.009	-1.746

Chapter 4

Synthesis, Electronic Structure Characterization, and Comparative Analysis of 1,2-Azaborine-Containing Phosphine Ligands

4.1 Introduction: Phosphine Ligands

4.1.1 The Role of Phosphine Ligands in Catalysis

Transition-metal catalyzed reactions form a cornerstone of modern organic chemistry.^{1,2,3} Homogeneous catalysis is an essential tool for the synthetic chemist from the exploratory scale to the largest industrial processes.^{1,2,3} The ligands of homogeneous catalysts alter the structure and reactivity of the transition metals to which they are bound.^{1,2,3} By changing the catalyst structure, ligands change the activation energies of elementary steps in a catalytic cycle.^{1,2,3} Additionally, ligands improve metal solubility in organic solvents and prevent catalyst degradation pathways like metal aggregation and precipitation.⁴ Ligand structure is largely responsible for homogeneous catalyst reactivity, and minor structural changes can lead to significant reactivity and selectivity changes. Some of the most utilized transition metal-catalyzed reactions involve phosphorus-based ligands. Such reactions include hydroformylation,⁵ Buchwald-Hartwig coupling,⁶ and cross-coupling reactions.⁷ Another indicator of the preeminent role of phosphine ligands is their presence in three Nobel Prizes in Chemistry awarded in the previous decade: in 2001

¹ Crabtree, R. H. *The Organometallic Chemistry of the Transition Metals*, 6th ed.; Wiley: New York, 2014.

² Hartwig, J. F. *Organotransition Metal Chemistry, from Bonding to Catalysis*; University Science Books: New York, 2010.

³ Kamer, P. C. J.; van Leeuwen, P. W. N. M. *Phosphorus(III) Ligands in Homogeneous Catalysis: Design and Synthesis*, Wiley: New York, 2012.

⁴ Henrici-Olivé, G.; Olivé, S. *Angew. Chem. Int. Ed.*, **1971**, *10*, 105-116.

⁵ (a) Slaugh, L. H.; Mullineaux, R. D. *J. Organomet. Chem.* **1968**, *13*, 469-477. For a review see: (b) Franke, R.; Selent, D.; Börner, A. *Chem. Rev.* **2012**, *112*, 5675-5732.

⁶ For reviews see: (a) Schlummer, B.; Scholz, U. *Adv. Synth. Cat.* **2004**, *346*, 1599-1626. (b) Surry, D. S.; Buchwald, S. L. *Angew. Chem. Int. Ed.* **2008**, *47*, 6338-6361.

⁷ For reviews see: (a) Nicolaou, K. C.; Bulger, P. G.; Sarlah, D. *Angew. Chem. Int. Ed.* **2005**, *44*, 4442-4489. (b) Torborg, C.; Beller, M. *Adv. Synth. Cat.* **2009**, *351*, 3027-3043.

for asymmetric hydrogenation,⁸ in 2005 for olefin metathesis,⁹ and in 2010 for cross-coupling reactions¹⁰ (Figure 4.1).

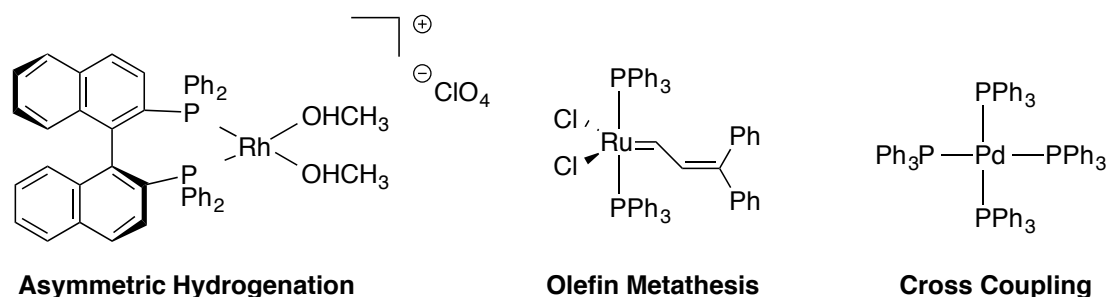


Figure 4.1. Representative transition metal-phosphine complexes from the 2001, 2005, and 2010 Nobel Prizes in Chemistry, respectively.

Phosphine ligands usually act as strong, L-type, sigma donors that bind to a variety of transition metals but do not usually participate directly in the reaction.^{1,2,3} Apart from their ability to function as sigma donors that can stabilize multiple metal oxidation states, phosphine ligands can be prepared with a staggering variety of C, N, and O-based substituents.³ The vast array of ligand structures correlates with a wide array of applications. Small changes to the structure of the phosphine ligand can drastically affect the activity, yield, product distribution, and selectivity of a given reaction.¹¹ The importance of phosphine ligands, in particular tertiary phosphines, in harnessing the reactivity of transition metals cannot be overstated.¹²

4.1.2 Measuring the Properties of Phosphine Ligands

Since the discovery of some of the first homogeneous catalysts supported by phosphine ligands, namely Wilkinson's Catalyst in the 1960's,¹³ significant research efforts have been undertaken to discern the effects of phosphine ligands on transition

⁸ (a) Miyashita, A.; Yasuda, A.; Takaya, H.; Toriumi, K.; Ito, T.; Souchi, T.; Noyori, R. *J. Am. Chem. Soc.* **1980**, *102*, 7932-7934. (b) Knowles, W. S. *Acc. Chem. Res.* **1983**, *16*, 106-112.

⁹ Nguyen, S. T.; Johnson, L. K.; Grubbs, R. H.; Ziller, J. W. *J. Am. Chem. Soc.* **1992**, *114*, 3974-3975.

¹⁰ (a) Heck, R. F.; Nolley, J. P. *J. Org. Chem.* **1972**, *37*, 2320-2322. (b) Negishi, E.; King, A. O.; Okukado, N. *J. Org. Chem.* **1977**, *42*, 1821-1823. (c) Miyaura, N.; Yamada, K.; Suzuki, A. *Tett. Lett.* **1979**, *20*, 3437-3440.

¹¹ (a) Martin, R.; Buchwald, S. L. *Acc. Chem. Res.* **2008**, *41*, 1461-1473. (b) Fu, G. C. *Acc. Chem. Res.* **2008**, *41*, 1555-1564. (c) Wu, K.; Doyle, A. G. *Nat. Chem.* **2017**, *9*, 779-784.

¹² Dias, P. B.; de Piedade, M. E. M.; Simões, J. A. M. *Coord. Chem. Rev.* **1994**, *135-136*, 737-807.

¹³ Osborn, J. A.; Jardine, F. H.; Young, J. F.; Wilkinson, G. *J. Chem. Soc. A.* **1966**, 1711-1732.

metal catalyst activity. Wilkinson published such a study in 1968, where the researchers measured the effects on the rate of Rh-catalyzed alkene hydrogenation caused by changing substituents on the triarylphosphine ligands.¹⁴ A change from tri-(*p*-fluorophenyl)phosphine ligand to tri-(*p*-methoxyphenyl)phosphine ligand on the Rh catalyst led to a 10-fold increase in the rate of hydrogenation. The observed rate difference was explained by electronic differences between the more electron-donating *p*-methoxy substituents and the less electron-donating *p*-fluoro substituents, which affected both the olefin binding affinity to the catalyst and the rate of oxidative addition of hydrogen. Specifically, more electron density on the metal center stabilizes the metal in its lower oxidation state. The increased electron density favors solvent displacement by the olefin, which was found to be the rate-limiting step. In addition, the lower oxidation state of the metal favors oxidative addition of H₂. However, simply increasing electron density on Rh by employing triethylphosphine in place of triarylphosphine dramatically lowers hydrogenation activity, suggesting that steric factors also play a role in determining reactivity.¹⁴ Developing a system to quantitatively compare properties of phosphines would be useful in studying their effects on catalysis. At this early stage in the development of transition metal catalysis researchers had identified two ligand properties, sterics and electronics, which primarily govern organometallic complex reactivity.

Studies in the late 1950's had already made some progress in quantifying the electronic properties of phosphines by showing that changing substituents on phosphine ligands caused a change in the carbonyl stretching frequencies of M(CO)_nL_n complexes.¹⁵ Wilkinson observed that increasing the number of Cl substituents on ligands of the type P(Ph)_{3-x}(Cl)_x caused a corresponding increase in

¹⁴ Montelatici, S.; van der Ent, A.; Osborn, J. A.; Wilkinson, G. *J. Chem. Soc. A* **1968**, 1054-1058.

¹⁵ Abel, E. W.; Bennett, M. A.; Wilkinson, G. *J. Chem. Soc.* **1959**, 2323-2327.

the CO infrared stretching frequency of complexes of the type $(\text{PR}_3)_3\text{Mo}(\text{CO})_3$.¹⁵ In an extensive study on the mechanism of ligand substitution by tertiary phosphines on nickel carbonyl complexes, Meriwether and Fiene noted that the carbonyl infrared bands of nickel dicarbonyl complexes were strongly influenced by the nature of the phosphine ligands.¹⁶ They concluded that the trend of decreasing carbonyl frequencies followed the decreasing π -back bonding ability of the phosphine ligands. In 1967, Strohmeier published a paper focussed exclusively on establishing the trend of π -accepting capability of phosphine ligands.¹⁷ In this publication, carbonyl stretching frequencies for a large variety of phosphine ligands and metal-carbonyl complexes containing phosphine ligands were reported, establishing a general ranking of phosphines where tri-aryl or alkyl phosphines have the least π -accepting character while PF_3 has the most. The aforementioned methods laid some groundwork for determining electronic properties of phosphines, namely measuring the effects of phosphine substituents on metal-carbonyl infrared stretching frequencies.

In 1970, Tolman presented methods for quantifying both the steric and the electronic parameters of phosphine ligands. The pair of papers proposed two modelling systems that could be applied to any phosphine ligand and independently determine its electronic parameter, ν ,¹⁸ as well as its steric parameter, θ .¹⁹ The Tolman electronic parameter provides a measure of the electronic properties of ligands using the A_1 infrared stretching frequency of the carbonyl groups of $\text{Ni}(\text{CO})_3\text{L}$ complexes, defined $\nu_{\text{CO}}(A_1)$. Carbonyl stretching frequencies change as a function of the electronics of the ligand/metal interactions. An increase in electron density on the metal from more electron-donating ligands will cause a decrease in the CO stretching

¹⁶ Meriwether, L. S.; Fiene, M. L. *J. Am. Chem. Soc.* **1959**, *81*, 4200-4208.

¹⁷ Strohmeier, W.; Müller, F.-J., *Chem. Ber.* **1967**, *100*, 2812-2821.

¹⁸ Tolman, C. A. *J. Am. Chem. Soc.* **1970**, *92*, 2953-2956.

¹⁹ Tolman, C. A. *J. Am. Chem. Soc.* **1970**, *92*, 2956-2965.

frequency. That is, the metal increases back donation into the CO π^* orbital which weakens the CO bonds resulting in a lower stretching frequency. A relatively less electron-donating ligand causes the opposite effect. The Tolman cone angle, or simply the cone angle, measures the steric bulk of a phosphine ligand. A Ni atom placed 2.28 Å away from the P atom constitutes the apex of the cone; the sum of the clearance angles to the left and right of the apex that touch the outer edges of the Van der Waals radii of the ligand substituents form the apex angle of the cone (Figure 4.2). In the original publication,¹⁹ θ was determined using space-filling models where the substituents were folded inwards to minimize steric repulsion. These simple and effective measuring systems allow researchers to compare phosphine ligands, tune their properties, and rationally select ligands for a particular reaction. The measuring techniques detailed in the 1970 papers, later expanded in a 1977 review,²⁰ are now termed the Tolman electronic parameter (TEP) and Tolman cone angle or simply cone angle.

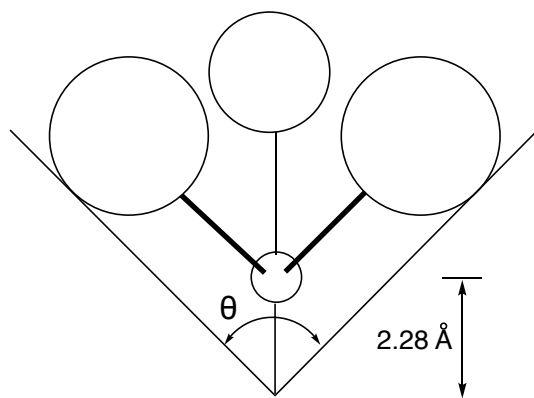


Figure 4.2. The ligand cone as defined by Tolman.

While some improvements have been made to the methodologies employed by Tolman, the underlying principles for determining steric and electronic properties of

²⁰ Tolman, C. A. *Chem. Rev.* **1977**, *77*, 313-348.

phosphines remain the same. Sophisticated DFT calculations,²¹ Sterimol steric parameters,²² buried volume cells,²³ and crystal structure data have replaced the space-filling models for determining θ . Meanwhile, other metal carbonyl complexes, such as *trans*-[Rh(CO)Cl(PX₃)₂],²⁴ have replaced the toxic and sometimes volatile Ni(CO)_x based complexes for determining v . These improved measuring techniques have helped researchers further our understanding of the role of phosphine ligands in the new catalytic reactions developed and optimized since the publication of Tolman's papers (*vide supra*). The work of Tolman and others established sterics and electronics as rationally tuneable characteristics of phosphines in addition to providing methods of quantifying them. Other important characteristics of phosphine ligands include the coordination mode, e.g. monodentate, bidentate, tridentate, tetradentate, hemilabile etc., and the bite angle (Figure 4.3). A ligand's natural bite angle, β_n , is the chelation angle determined by the multidentate-phosphine backbone when it binds to the metal.²⁵ Casey used molecular mechanics to determine the bite angle; Kamer and Van Leeuwen further developed the concept.²⁶

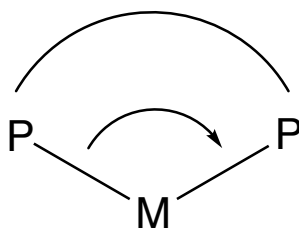


Figure 4.3. The bite angle of a bidentate phosphine ligand.

²¹ Fey, N.; Orpen, A. G.; Harvey, J. N. *Coord. Chem. Rev.* **2009**, *253*, 704-722.

²² Brethomé, A. V.; Fletcher, S. P.; Paton, R. S. *ACS Catal.* **2019**, *9*, 2131-2323.

²³ Hillier, A. C.; Sommer, W. J.; Yong, B. S.; Petersen, J. L.; Cavallo, L.; Nolan, S. P. *Organometallics* **2003**, *22*, 4322-4326.

²⁴ Roodt, A.; Otto, S.; Steyl, G. *Coord. Chem. Rev.* **2003**, *245*, 121-137.

²⁵ Casey, C. P.; Whiteker, G. T. *Isr. J. Chem.* **1990**, *30*, 299-304.

²⁶ Kranenburg, M.; van der Burgt, Y. E. M.; Kamer, P. C. J.; van Leeuwen, P. W. N. M.; Goubitz, K.; Fraanje, J. *Organometallics* **1995**, *14*, 3081-3089.

In summary, the aforementioned methods of determining steric and electronic properties are a powerful set of tools that provide a convenient benchmark with which ligands can be classified and compared.

4.1.3 The Effect of Ligand Choice on Palladium-Catalyzed Cross-Couplings

One particular class of reactions where the properties of phosphine ligands and their effects on reactivity have been studied extensively is in the area of palladium-catalyzed cross-coupling reactions.²⁷ Ligand effects for each step in the prototypical palladium-catalyzed cross-coupling reaction mechanism have been evaluated (Figure 4.4). The active palladium species will first undergo oxidative addition with the electrophile, followed by transmetalation with the nucleophilic partner and finally reductive elimination occurs to generate the product and regenerate the catalyst.

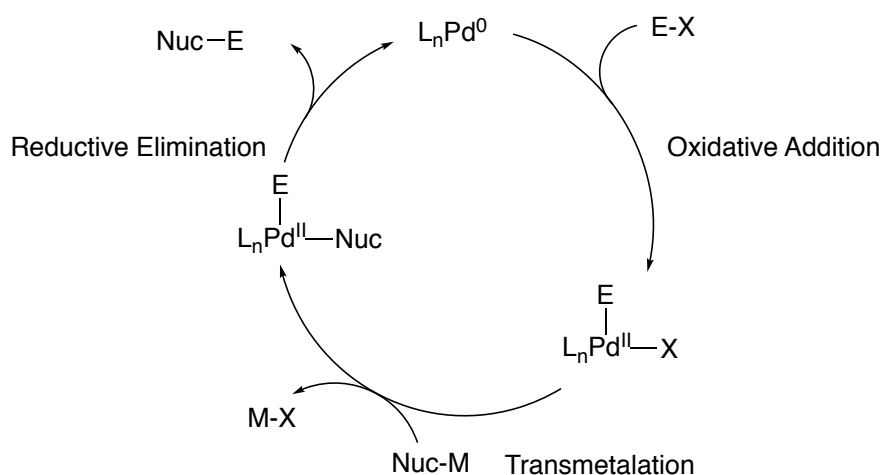


Figure 4.4. Generic palladium-catalyzed cross-coupling mechanism.

More basic, electron-donating phosphine ligands favor oxidative addition to the metal center. Amatore conducted a Hammett analysis for the oxidative addition of phenyl iodide to palladium triarylphosphine complexes.²⁸ He demonstrated a strong linear correlation between the rate of oxidative addition and substituents at the *para* position of the triarylphosphine ligands, finding that the rate increased with increasing

²⁷ Clarke, M. L.; Frew, J. J. R. *Organometallic Chemistry: Volume 35*, The Royal Society of Chemistry: London, 2009, 19-46.

²⁸ Amatore, C.; Carre, E.; Jutand, A.; M'Barki, M. A. *Organometallics* **1995**, *14*, 1818-1826.

electron-donating ability (Figure 4.5). Fu published a comprehensive study on the factors that affect the reactivity of palladium alkylphosphine complexes in the oxidative addition of alkyl electrophiles, including kinetic studies on the effects from the solvent, the sterics of the electrophile, and the leaving group of the electrophile.²⁹

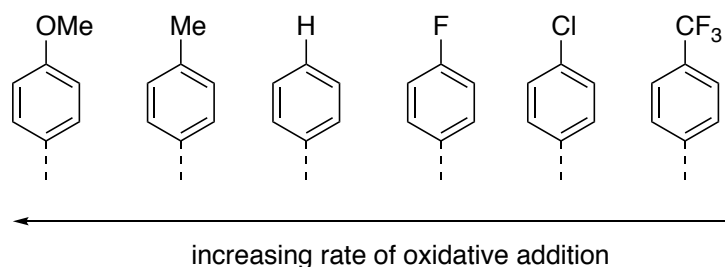


Figure 4.5. Hammett analysis for oxidative addition to Pd(PR₃)_n complexes.

The activation parameters of the oxidative addition of alkyl electrophiles to Pd for various phosphines were also determined, revealing that the oxidative addition process is quite sensitive to the steric demand of the ligand (Table 4.1). The difference in reactivity between P(*t*Bu)₂Me and P(*t*Bu)₂Et is striking and cannot be simply explained by differences in cone angle. DFT calculations for the preferred ligand conformation reveal that in the case of the ethyl-containing ligand, the energetically preferred conformation sterically hinders the approach of the electrophile (Figure 4.6).

Table 4.1: Effect of the phosphine on the activation barrier for oxidative addition.

Entry	L	θ	ΔG^\ddagger [kcalmol ⁻¹]
1	P(<i>t</i> Bu) ₂ Me	161°	19.5 (0 °C)
2	PCy ₃	170°	20.0 (0 °C)
3	P(<i>t</i> Bu) ₂ Et	165°	25.4 (60 °C)
4	P(<i>t</i> Bu) ₃	182°	>28.4 (60 °C)

²⁹ Hills, I. D.; Netherton, M. R.; Fu, G. C. *Angew. Chem. Int. Ed.* **2003**, *42*, 5749-5752.

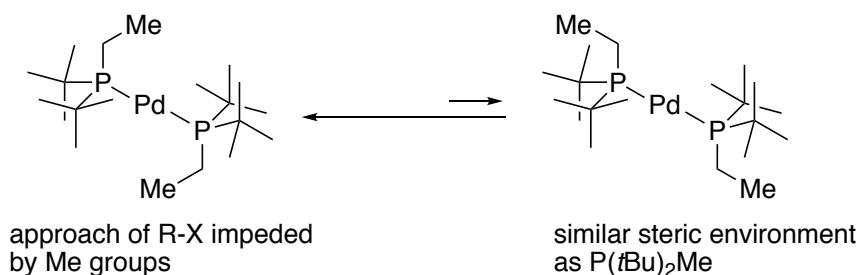


Figure 4.6. Conformational analysis of $P(tBu)_2Et$.

Ligand effects in the transmetalation step are the least well understood in most palladium-catalyzed cross-coupling cycles, with the exception of the Stille cross-coupling.³⁰ More electron-poor ligands, such as tri-2-furylphosphine and triphenylarsine exhibit significant improvements in reactivity between iodobenzene and vinyltributyltin compared to triphenylphosphine.²⁸ The improved reactivity was further explained in later studies through the discovery that more bulky, less electron-rich ligands encourage the formation of the monoligated palladium species $Pd(L)(Ar)I$ which undergoes transmetalation with the organotin species much faster than the bisphospholigated palladium species.³¹

Electron-withdrawing ligands promote reductive elimination.^{2, 32} Ligand effects on the reductive elimination step in the Buchwald-Hartwig cross-coupling reaction have been thoroughly investigated. In the case of diaryl-ether synthesis, more electron-withdrawing ligands improved reaction yields.³³ In a study published by Hartwig, reaction yields in the cross-coupling between phenol and 4-bromobenzonitrile increase as the substituent in the *para* position of the phenyl rings on the DPPF ligand becomes more electron-withdrawing (Figure 4.7a). Other ligand properties were shown to have a significant impact on reductive elimination, and

³⁰ Farina, V.; Krishnan, B. *J. Am. Chem. Soc.* **1991**, *113*, 9585-9595.

³¹ Amatore, C.; Bahsoun, A. A.; Jutand, A.; Meyer, G.; Ndedi Ntepe, A.; Ricard, L. *J. Am. Chem. Soc.* **2003**, *125*, 4212-4222.

³² Korenaga, T.; Abe, K.; Ko, A.; Maenishi, R.; Sakai, T. *Organometallics* **2010**, *29*, 4025-4035.

³³ Mann, G.; Hartwig, J. F. *Tett. Lett.* **1997**, *38*, 8005-8008.

further studies by the Hartwig group led to a re-evaluation of the importance of ligand electronics as opposed to sterics and coordination mode.³⁴ By conducting stoichiometric studies on the thermal chemistry of reductive elimination from isolated arylpalladium aryloxide complexes, the Hartwig group was able to discern the relative effects of ligand sterics and electronics.³² C-O reductive elimination occurred only 2 times faster from a palladium complex bearing a diphosphino ferrocene complex with *para*-trifluoromethylphenyl substituents than the corresponding palladium DPPF complex (Figure 4.7b). On the other hand, reductive elimination was 100 times faster from a palladium complex bearing a diphosphino ferrocene ligand with *tert*-butyl substituents. Taken together, these results indicate that in fact more electron-poor ligands do not significantly impact the rate of C-O coupling. The much more electron-rich and bulky *t*-butyl-bearing ligand dramatically increased the rate, demonstrating the importance of sterics in this reaction. Although great care must be taken when attempting to draw conclusions about the effect of ligand properties on catalytic activity, especially at points in the catalytic cycle that occur after the rate-determining step, evaluating ligand properties can nonetheless provide valuable information for understanding reaction mechanism and improving catalyst function.

³⁴ Mann, G.; Shelby, Q.; Roy, A. H.; Hartwig, J. F. *Organometallics* **2003**, *22*, 2775-2789.

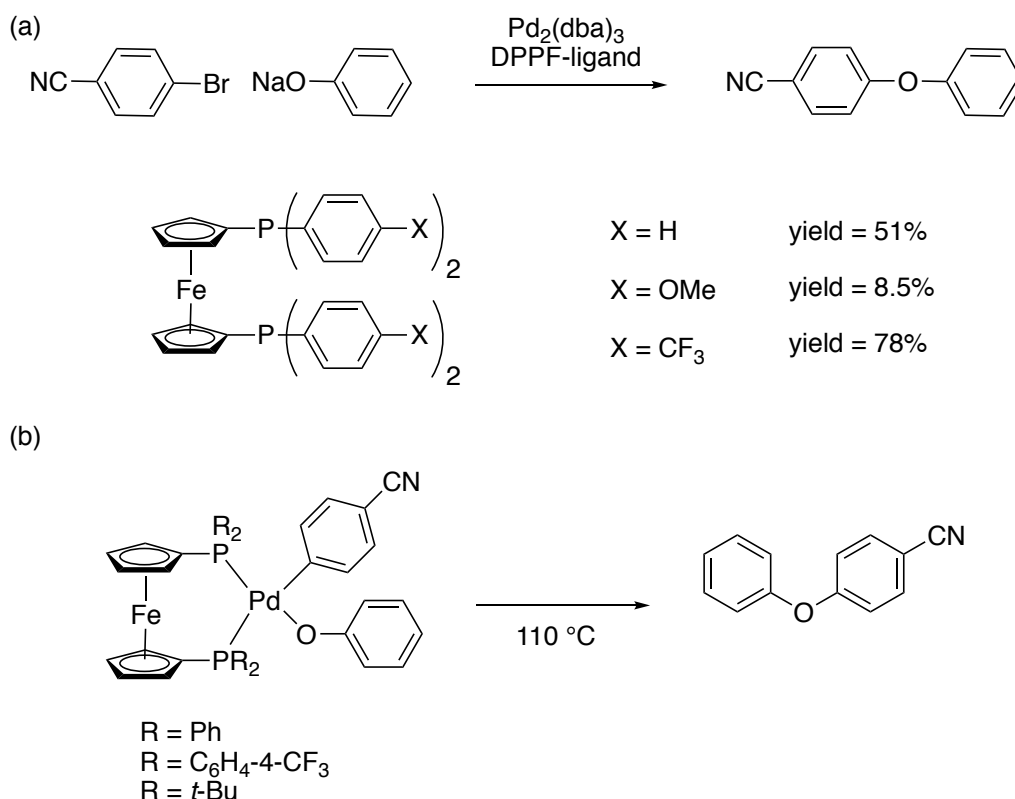


Figure 4.7. a) Effect of DPPF ligand electronics on the yield of diarylether. b) Differentiation of steric and electronic effects of DPPF ligands on rate of C-O reductive elimination.

In addition to improving transition-metal catalyst reactivity, applying ligand-property measuring techniques can help classify the plethora of new phosphine ligand architectures being added to the literature.³⁵ The wide variety of possible substituents on phosphorus translates to a correspondingly wide range in both electronic and steric parameters. Ligands at the extremes of the cone angle and TEP scales are of fundamental interest. Boron is one of the least electronegative main group elements (H: 2.2; B: 2.04; C: 2.55; P: 2.19)³⁶ and its incorporation into a ligand with a P-B bond should render such a ligand extremely electron rich. The following section contains details on the history of P-B bond containing ligands and will be followed by a section about the development of a new P-B containing ligand through the use of BN/CC isosterism.

³⁵ Balueva, A. S.; Musina, E. I.; Karasik, A. A. *Organophosphorus Chemistry: Volume 47*, The Royal Society of Chemistry: London, 2018, 1-49.

³⁶ Allen, L. C. *J. Am. Chem. Soc.* **1989**, *111*, 9003-9014.

4.1.4 Prior Examples of P-B Containing Ligands

Tolman reported the parameters for the most electron-deficient phosphine ligand, PF₃, in his initial paper.¹⁸ However, ligands containing a bond between P and B were not investigated until a decade later. The absence of a phosphine ligand containing a P-B bond in Tolman's review may have been due to the reactive nature of P-B bonds. Compounds containing a P-B bond have long been known, especially where both P and B are 4-coordinate,³⁷ but such compounds cannot bind to metals in the manner of a traditional monodentate, L-type phosphine ligand as the lone pair is tied up in a dative bond with empty p-orbital of boron. Phosphinoboranes with the simple formula R₂BPR'₂, where both the P and B atoms are 3-coordinate, have also been prepared and studied but require bulky substituents to prevent oligomerization.³⁵ In 1985 Malisch published the first report of a P-B bond-containing metal complex that was prepared by reacting Cp*Fe(CO)₂(PPh₂) with borane-THF complex.³⁸ However, the first example of a P-B ligand resembling traditional tertiary phosphines came from the Fu group who accomplished the synthesis and characterization of a boratabenzene containing, anionic, triarylphosphine ligand.³⁹ Diphenylphosphidoboratabenzene is an anionic analogue of the ubiquitous triphenylphosphine (Figure 4.8). Several transition-metal complexes were prepared via a substitution reaction between **4.2** and the corresponding metal halide (Scheme 4.1). Crystal structure data of Zr complex **4.3** and Fe complex **4.4** revealed that the P-C bond distances in the DPB ligand were about 0.12 Å shorter than the P-B bond distance, while in the case of **4.5** the difference was only about 0.6 Å, presumably due

³⁷ Pestana, D. C.; Power, P. P. *J. Am. Chem. Soc.* **1991**, *113*, 8426-8437.

³⁸ Angerer, W.; Sheldrick, W. S.; Malisch, W. *Chem. Ber.* **1985**, *118*, 1261-1266.

³⁹ For the synthesis of boratabenzene see: (a) Hoic, D. A.; Davis, W. M.; Fu, G. C. *J. Am. Chem. Soc.* **1995**, *117*, 8480-8481. For boratabenzene reactivity studies and phosphine ligand synthesis see: (b) Qiao, S.; Hoic, D. A.; Fu, G. C. *J. Am. Chem. Soc.* **1996**, *118*, 6329-6330. For studies of the phosphine ligand and its transition metal complexes see: (c) Hoic, D. A.; Davis, W. M.; Fu, G. C., *J. Am. Chem. Soc.* **1996**, *118*, 8176-8177.

to the reduced Lewis acidity of the Rh metal. Rh metal. Complexes $[\text{CpFe}(\text{CO})_2(\text{PPh}_3)]^+$ and $[\text{CpFe}(\text{CO})_2(\text{PPh}_2)]$ are isoelectronic with **4.4**. Comparison of the two C-O stretching frequencies on each iron complex places **4.4** (1982, 2024 cm^{-1}) between the least electron-rich PPh_3 complex (2025, 2070 cm^{-1}) and most electron rich PPh_2 complex (1966, 2015 cm^{-1}). Some caution should be exercised when comparing these iron carbonyl complexes, as the complex containing PPh_3 is cationic while the other two are neutral. Additionally, it should be noted that diphenylphosphide has an additional lone pair of electrons to donate to the metal compared to the two L-type donors.

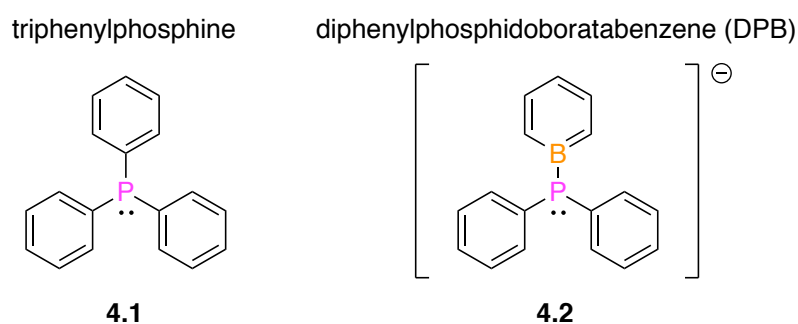
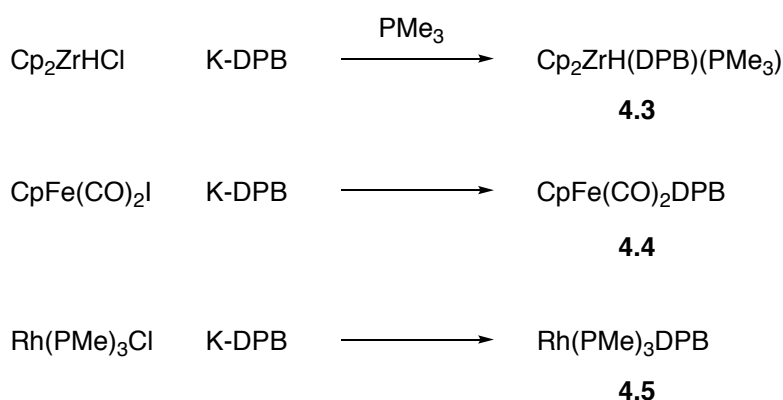


Figure 4.8. Structures of PPh_3 and Fu's DPB ligand.

Scheme 4.1. Synthesis of DPB transition-metal complexes.



Following the work by Fu, investigations into two transition metal-catalyzed reactions led to the discovery of two new complexes containing anionic phosphanylborohydride ligands. Brown reported the reactive intermediate in the Pd-catalyzed coupling between secondary phosphine borane adducts and aryl halides to

be a square planar complex bound at P of the type $L_3Pd(PPh_2BH_3)$.⁴⁰ As part of an effort to polymerize phosphine boranes, Manners found that both primary and secondary phosphine boranes underwent P-H oxidative addition with Pt^0 to form complexes of the form $L_2HPt(PRPhBH_3)$.⁴¹ In the wake of the publication of the two phosphanylborohydride containing complexes and directly inspired by the work of Fu, the Wagner group decided to investigate the ligand properties of phosphanylborohydrides $[BH_3PRR']$ in a series of publications.^{40,41,42}

In an initial study, Wagner sought to establish the Lewis basicity of $[BH_3PRR']^-$ type ligands by comparing them to their isosteric methyl analogues $[CH_3PRR']$.⁴² The following series of compounds, along with a few derivatives, were prepared and characterized using NMR and X-ray crystallography: $K[PPh_2]$, $HPPH_2$, CH_3PPh_2 , $BH_3(H)PPh_2$, $BBr_3(H)PPh_2$, $BH_3(CH_3)PPh_2$, $BBr_3(CH_3)PPh_2$, $[H_2PPh_2]I$, $[CH_3(H)PPh_2]I$, $[(CH_3)_2PPh_2]I$, and $K[(BH_3)_2PPh_2]$. Based on spectroscopic data, including P-B, P-H, and P-C NMR coupling constants as well as C-P-C bond angles from X-ray crystallography, the authors concluded that $[BH_3PPh_2]^-$ forms dative bonds of the highest p character in the series. Higher p character in a dative bond indicates greater Lewis basicity. In a follow up study, the electron donating ability of $[BH_3PPh_2]^-$ was measured in relation to two isosteric ligands, PPh_2Me and $SiPh_2Me^-$ by comparing the C-O stretching frequencies in their corresponding $[CpFe(CO)_2L]$ complexes (Figure 1.9).⁴³ Silyl complex **4.8** was the most electron- rich, followed by **4.7** then **4.6**. In a separate publication, complex **4.9** was reported to be slightly more electron rich than its monometallic counterpart **4.7**.⁴⁴

⁴⁰ Gaumont, A.-C.; M. Brown, J.; B. Hursthouse, M.; J. Coles, S. *Chem. Comm.* **1999**, 63-64.

⁴¹ Dorn, H.; Jaska, C. A.; Singh, R. A.; Lough, A. J.; Manners, I. *Chem. Comm.* **2000**, 1041-1042.

⁴² Dornhaus, F.; Bolte, M.; Lerner, H.-W.; Wagner, M. *Eur. J. Inorg. Chem.* **2006**, 2006, 1777-1785.

⁴³ Kückmann, T. I.; Dornhaus, F.; Bolte, M.; Lerner, H.-W.; Holthausen, M. C.; Wagner, M., *Eur. J. Inorg. Chem.* **2007**, 2007, 1989-2003.

⁴⁴ Dornhaus, F.; Bolte, M.; Lerner, H.-W.; Wagner, M. *J. Organomet. Chem.* **2007**, 692, 2949-2955.

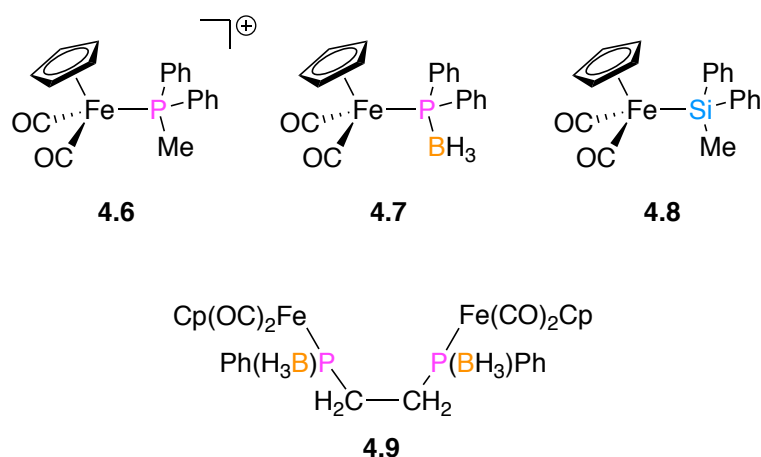


Figure 4.9. Fe(CO) complexes prepared by Wagner.

In order to study P-B ligands containing a coordinatively unsaturated B atom, care must be taken to prevent cleavage of the reactive P-B bond. In the case of phosphinoboranes **4.10** and **4.11**, Stephan showed that electron-donating substituents on P and electron-accepting substituents on B could stabilize the P-B bond.⁴⁵ The geometries about B and P are pseudotrigonal planar as the sum of the angles about B and P are 360.0° and 359.07°, respectively.⁴³ Compounds **4.10** and **4.11** demonstrated alkene-type behavior when bound to Pt (Scheme 1.2).⁴⁶ The bonding situation in **4.12** and **4.13** is considered to be a superposition of two types of metal-ligand interactions. The first is a Pt to borane interaction supported by P coordination while the second is a combination of $\pi(\text{PB})$ to Pt donation and Pt to $\pi^*(\text{PB})$ back-donation. This mixed bonding mode lies in contrast to other examples of B and P containing ligands which interact with metals as boryl ligands⁴⁷ or as Z-type ligands.⁴⁸

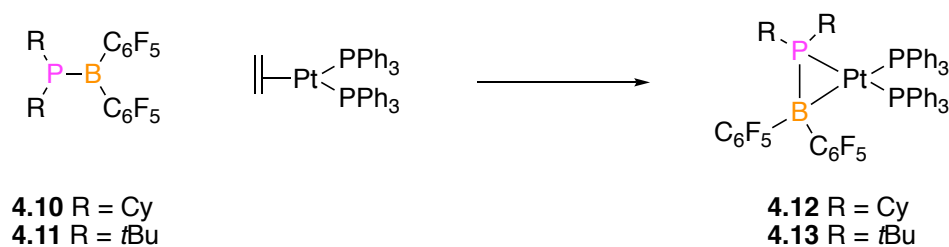
⁴⁵ Geier, S. J.; Gilbert, T. M.; Stephan, D. W. *J. Am. Chem. Soc.* **2008**, *130*, 12632-12633.

⁴⁶ Amgoune, A.; Ladeira, S.; Miqueu, K.; Bourissou, D. *J. Am. Chem. Soc.* **2012**, *134*, 6560-6563.

⁴⁷ Notable examples: (a) Nöth, H.; Schmid, G. *Angew. Chem. Int. Ed.* **1963**, *2*, 623-623. (b) Baker, R. T.; Ovenall, D. W.; Calabrese, J. C.; Westcott, S. A.; Taylor, N. J.; Williams, I. D.; Marder, T. B. *J. Am. Chem. Soc.* **1990**, *112*, 9399-9400. (c) Knorr, J. R.; Merola, J. S. *Organometallics* **1990**, *9*, 3008-3010. (d) Braunschweig, H.; Radacki, K.; Seeler, F.; Whittell, G. R. *Organometallics* **2004**, *23*, 4178-4180. (e) Segawa, Y.; Yamashita, M.; Nozaki, K. *J. Am. Chem. Soc.* **2009**, *131*, 9201-9203.

⁴⁸ Notable examples: (a) Hill, A. F.; Owen, G. R.; White, A. J. P.; Williams, D. J. *Angew.*

Scheme 4.2. Coordination of phosphinoboranes to Pt.



In 2012 the Fontaine group investigated another hybrid binding mode of a P-B ligand to a metal center by preparing complexes with a *t*-Bu derivative of Fu's boratabenzene ligand.⁴⁹ Complexes **4.3**, **4.4**, and **4.5** (Scheme 4.1) displayed η^1 coordination at P, likely due to the fact that **4.3** and **4.4** are $18e^-$ complexes and **4.5** is a square planar, $16e^-$ Rh complex. On the other hand, Ni **4.15** and Pt **4.16** complexes of ligand **4.14** involve η^6 or η^3 π complexation with the boratabenzene portion of the ligand, respectively (Figure 4.10).

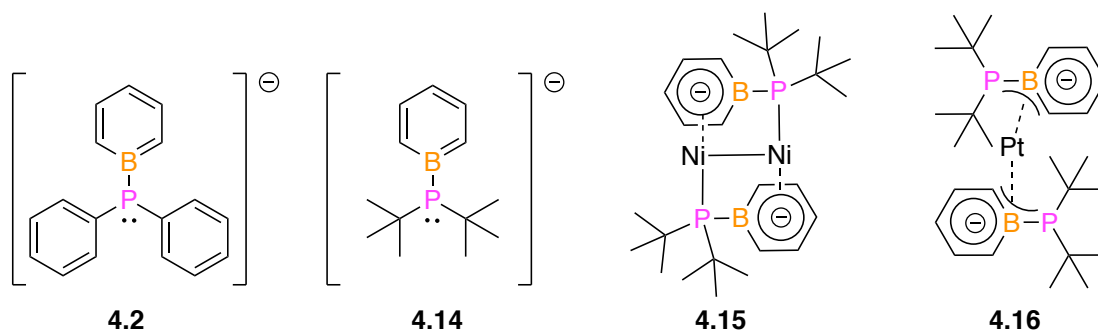


Figure 4.10. di-*tert*-butylphosphidoboratabenzene ligand and two of its metal complexes.

DFT calculations corroborated the observed binding modes by demonstrating that the HOMO is centered mostly on the ring system. In **4.15** the dimeric Ni is bridged by an η^6 interaction with the π cloud of the boratabenzene ring while in **4.16** the Pt is bound in an η^3 fashion to the P as well as the adjacent B and C atoms of the ring. The TEP was also calculated for **4.14** and compared to **4.2** as well as some

Chem. **1999**, 111, 2920–2923. (b) Bontemps, S.; Gornitzka, H.; Bouhadir, G.; Miqueu, K.; Bourissou, D. *Angew. Chem. Int. Ed.* **2006**, 45, 1611–1614. (c) Shih, W.-C.; Gu, W.; MacInnis, M. C.; Timpa, S. D.; Bhuvanesh, N.; Zhou, J.; Ozerov, O. V. *J. Am. Chem. Soc.* **2016**, 138, 2086–2089.

⁴⁹ Macha, B. B.; Boudreau, J.; Maron, L.; Maris, T.; Fontaine, F.-G. *Organometallics* **2012**, 31, 6428–6437.

phosphines and an NHC ligand (Table 4.2). The stretching frequency for **4.14** is quite low, indicating that it is even more electron rich than the highly donating NHC ligand.

ligand	A ₁ stretching frequency (cm ⁻¹)
PF ₃	2111.3
PPh ₃	2067.5
P(<i>t</i> Bu) ₃	2055.3
ICy	2049.8
4.2	2035.3
4.14	2026.4

Gaussian 03 MPW1PW91 functional 6-311+G(2d) (Ni),
6-311+G(dp) (C, H, B, O, P).

Table 4.2. DFT Calculated ν_{CO} Stretching Frequencies of CO Bonds in LNi(CO)₃

Another extremely electron rich P-B ligand was prepared by the Buchwald group and features a carborane substituent (Figure 4.11).⁵⁰ Three-dimensional aromatic icosahedral dicarba-*closo*-dodecaborane clusters, or carboranes, transmit vastly different electronic properties to their substituents depending on the vertex to which they are attached. C-connected carborane phosphine ligands, first reported in 1963,⁵¹ are electron poor while the B-connected phosphine ligands reported by Buchwald demonstrated an electron-rich TEP. A carborane-based ligand represents a system where the electronic properties of the ligand can be dramatically altered without changing the steric parameter.

⁵⁰ Spokoiny, A. M.; Lewis, C. D.; Teverovskiy, G.; Buchwald, S. L. *Organometallics* **2012**, *31*, 8478-8481.

⁵¹ Alexander, R. P; Schroeder, H. *Inorg. Chem.* **1963**, *2*, 1107–1110.

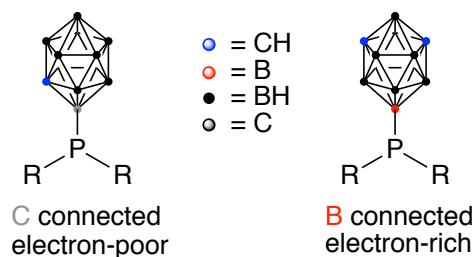


Figure 4.11. Carborane-based phosphine ligands.

The dearth of phosphine ligands containing a P-B bond relative to the vast quantity of phosphine ligands containing other main-group substituents is due to the reactivity of the P-B bond. Thus far we have seen strategies to occupy, shield, or otherwise prevent reaction with the empty p-orbital on the B atom in order to help stabilize the P-B bond. Such strategies include occupying the p-orbital with a covalent bond that forms a 4-coordinate borate ligand,³⁷ incorporating the B atom into an aromatic system,^{39,48} placing electron-donating substituents on P and electron-withdrawing substituents on B,⁴⁵ attaching π -donating NR_2 substituents to B,⁵² and incorporating the B atom into a carborane.⁵⁰ The Pringle group employed BN/CC isosterism as a strategy to incorporate and stabilize a B atom in a phosphine ligand.

Pringle chose readily prepared BN-phenanthrene **4.17**⁵³ as the B-containing arene scaffold for the target phosphine ligands (Scheme 4.3).⁵⁴ Treatment of the electrophilic B-Cl moiety with secondary phosphide nucleophiles did not result in formation of the desired ligand, likely due to side reactions with the protic N-H bond. Instead, reaction with SiMe_3PR_2 furnished the target ligands, azaborinylphosphines **4.18a** and **4.18b**. The all-carbon analogues **4.20a** and **4.20b** were prepared via addition of lithiate **4.19** to secondary chlorophosphines. With the desired BN-phosphine ligands as well as their direct all-carbon analogues in hand, the authors

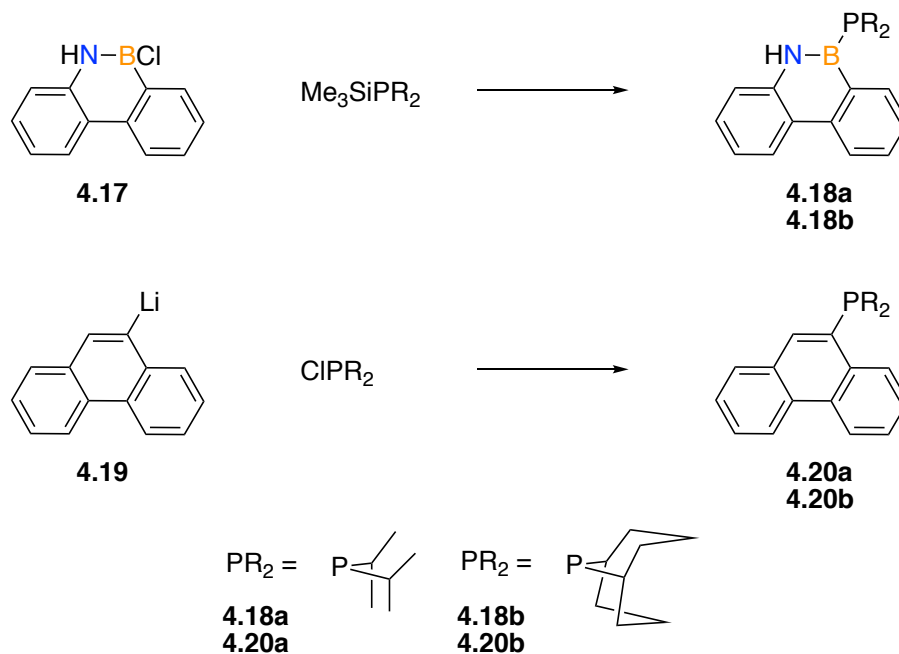
⁵² Kaaz, M.; Bender, J.; Forster, D.; Frey, W.; Nieger, M.; Gudat, D. *Dalton Trans.* **2014**, *43*, 680-689.

⁵³ Dewar, M. J. S.; Kubba, V. P.; Pettit, R., 624. *J. Chem. Soc.* **1958**, 3073-3076.

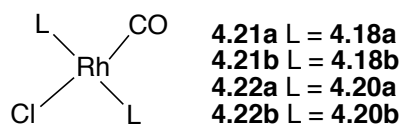
⁵⁴ Bailey, J. A.; Haddow, M. F.; Pringle, P. G. *Chem. Comm.* **2014**, *50*, 1432-1434.

then compare their structural and electronic parameters as well as evaluated their catalytic performance in the hydrogenation of alkenes.

Scheme 4.3. Synthesis of BN- and CC-phenanthrene ligands.



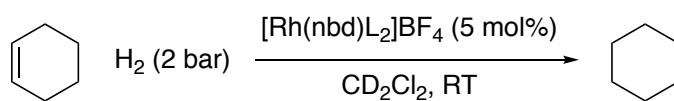
In order to compare the electron donating capacity of the two ligands, the CO stretching frequencies of the *trans*-[RhCl(CO)L₂] complexes were measured (Table 4.3). The P-B containing ligands are more electron-donating than their all-carbon counterparts. According to the crystal structure data of the Rh complexes the BN and CC ligands are sterically similar with the exception of bonds connected to the B atom, which are slightly elongated compared to their all-C analogues. For example, the P-B bond in **4.21a** (1.957(3) Å) is more than 0.1 Å longer than the P-C bond in **4.22a** (1.843(2) Å).

Table 4.3. ν_{CO} of trans-RhCl(CO)L₂.

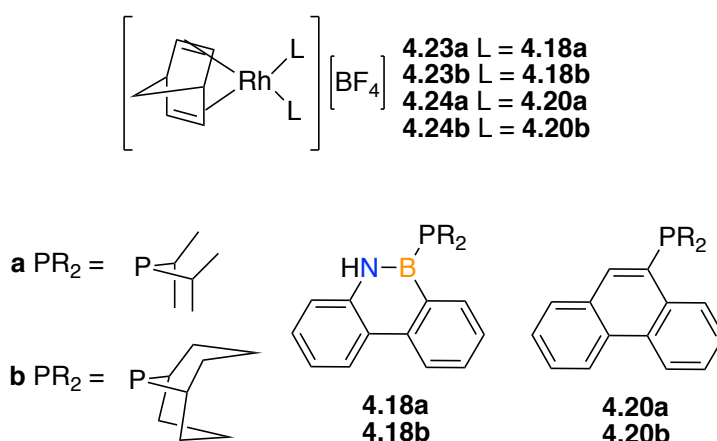
complex	stretching frequency (cm ⁻¹)
4.21a	1951
4.21b	1946
4.22a	1966
4.22b	1951

Rh-carbonyl complexes **4.21** and **4.22** served to compare the steric and electronic parameters of the BN ligands **4.18** to their CC counterparts **4.20**. In order to evaluate the performance of compounds **4.18** and **4.20** as supporting ligands in homogenous catalysis, Rh-norbornadiene complexes **4.23** and **4.24** were prepared (Table 4.4). In the first example of homogeneous catalysis with a phosphino-borane ligand, cationic, Rh-norbornadiene complexes **4.23** and **4.24** were evaluated in the hydrogenation of alkenes. The more electron-rich **4.23** were found to be more efficient catalysts than their counterparts **4.24**. In order to discount the possibility that adventitious water cleaved the easily hydrolyzed P-B bond to form the active catalyst, the authors performed the reaction in the presence of water and observed a dramatic decrease in TOF.

Table 4.4. Catalytic performance of Rh complexes in the catalytic hydrogenation of cyclohexene with H₂.



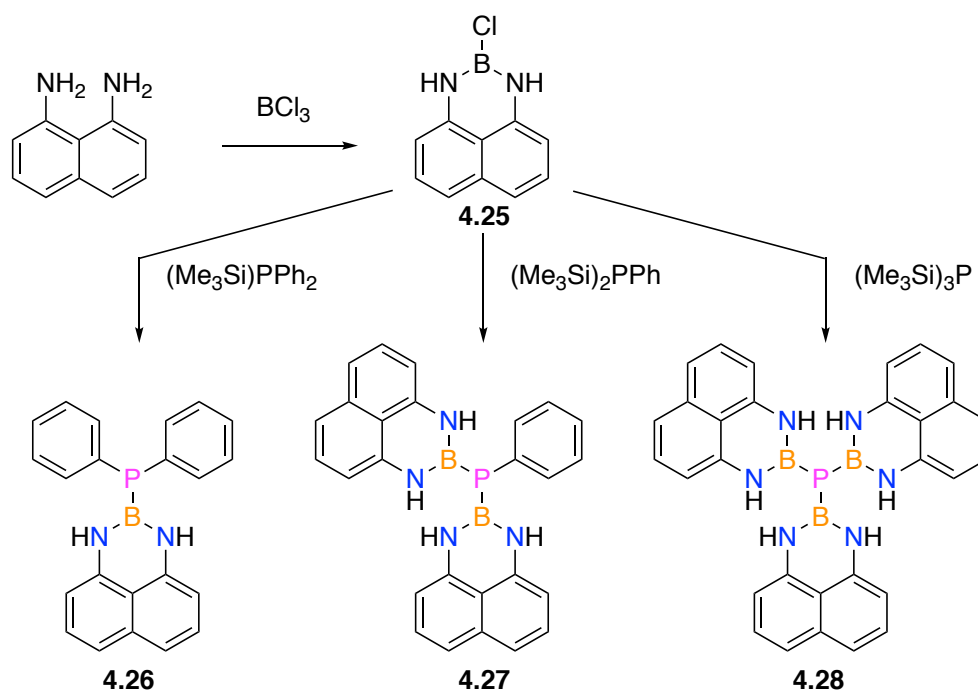
complex	Rel. TOF
4.23a	15
4.23b	>30
4.24a	1
4.24b	12



In a subsequent publication, the Pringle group extended their exchange reaction between B-Cl and Si-P species to the preparation of a new class of P-B ligands (Scheme 4.4).⁵⁵ Reaction between 1,8-diaminonaphthalene and boron trichloride resulted in the formation of chloroborane **4.25**, the B source for mono, bi, and triborylphosphine ligands **4.26**, **4.27**, and **4.28**, respectively.

⁵⁵ Bailey, J. A.; Ploeger, M.; Pringle, P. G., *Inorg. Chem.* **2014**, *53*, 7763-7769.

Scheme 4.4. Synthesis of 1,8-diaminonaphthylboronamide-based ligands.



According to the crystal structures of the ligands, the planarity of the phosphine as measured by the P-B bond angles increased with increasing B substitution while the P-B bonds became shorter in length. According to nucleus independent chemical shift (NICS) calculations the heterocyclic ring of **4.29** can be considered antiaromatic (Figure 4.12). This antiaromaticity is in contrast to **4.31** where the heterocyclic ring has aromatic character. The closest neutral CC analogue, pyrene **4.30**, has significant aromatic character while borazine **4.32** displays only a modest diatropic ring current. Complexes of the type $[\text{Mo}(\text{L}_2)(\text{CO})_4]$ were prepared to measure ν_{CO} (Table 4.5). As expected, increasing the number of B substituents increases the electron donating ability of the ligand.

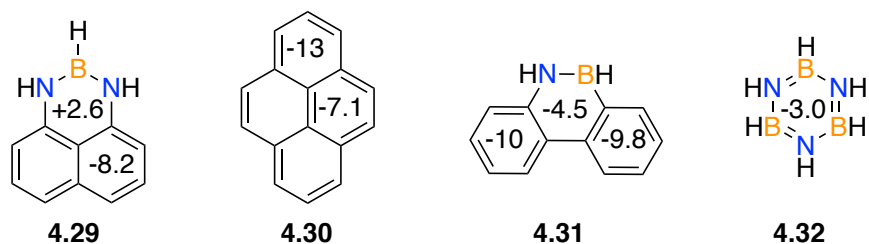


Figure 4.12. NICS-1 values (calculated at the B3LYP/6-311+G(2d) level).

Table 4.5. ν_{CO} of $[\text{Mo}(\text{L})_2(\text{CO})_4]$.

L	complex	ν_{CO} (cm^{-1})
PPh₃	4.33	2022
4.26	4.34	2018.1
4.27	4.35	2015.8
4.28	4.36	2012.8

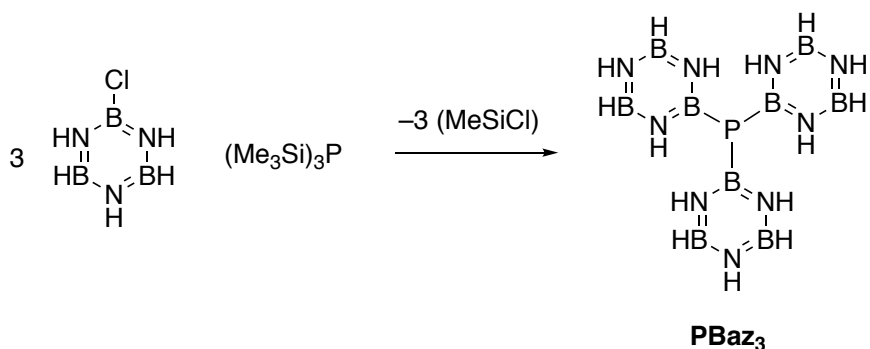
Pringle and coworkers have very recently published the inorganic version of triphenylphosphine, where the phenyl groups have been replaced with their inorganic analogue borazine.⁵⁶ Similar to previously reported methods, elimination of chlorosilane from a reaction between a monochloroborazine and a trisilylphosphine furnished the inorganic triphenylphosphine, or **PBaz₃** (Scheme 4.5). As previously discussed, borazine has much less aromatic stabilization than benzene. Key structural differences can also be seen from the crystal structures of the two compounds. The P-B bonds are about 0.1 Å longer than the corresponding P-C bonds, consistent with the larger covalent radius of boron.⁵⁷ Compared to triphenylphosphine, the geometry around P in **PBaz₃** is flatter due to increased π and decreased p character of the P-B bond. The flattening observed in **PBaz₃** is consistent with Bent's Rule, which predicts

⁵⁶ Gorman, A. D.; Bailey, J. A.; Fey, N.; Young, T. A.; Sparkes, H. A.; Pringle, P. G. *Angew. Chem. Int. Ed.* **2018**, *57*, 15802-15806.

⁵⁷ Pyykkö, P.; Atsumi, M. *Chem. -Eur. J.* **2009**, *15*, 12770-12779.

that the p-character of P-X σ -bonds decreases with decreasing electronegativity.⁵⁸ The lengthening of the P-B bonds also reduces the crowding around the P, as evidenced by the cone angle of PBaz₃ (137°), which is reduced compared to that of triphenylphosphine (154°). In addition to these structural parameters, the authors also wanted to compare the Lewis basicity of PBaz₃ with PPh₃. When either the Ph₃P•BH₃ or Baz₃P•BH₃ adduct was mixed with the other free ligand in THF solution, an equilibrium was slowly established that favored the PPh₃ adduct by 3 kcal mol⁻¹. It was concluded that PPh₃ is slightly more Lewis basic than PBaz₃.

Scheme 4.5. Synthesis of inorganic triphenylphosphine **PBaz₃**.

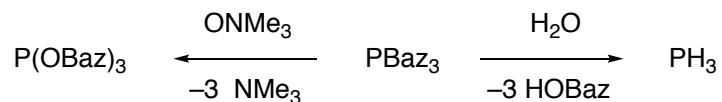


The reactivity of the P-B bond in PBaz₃ towards water and oxidizing agents was also investigated. In direct contrast to the relatively stable P-C bonds in PPh₃, the P-B bonds in PBaz₃ are easily hydrolysed or oxidized (Scheme 4.6). PBaz₃ reacts with water in a rapid and quantitative fashion to yield PH₃. PPh₃ is inert to water; the driving force for the hydrolysis of P-B bonds is the formation of a strong B-O bond (130 kcal mol⁻¹), as opposed to the much weaker C-O bond (85 kcal mol⁻¹). While PPh₃ undergoes oxidation with ONMe₃ to yield O=PPh₃, PBaz₃ undergoes direct O insertion into the P-B bond to furnish an inorganic triphenylphosphite, P(OBaz)₃.

⁵⁸ Bent, H. A. *Chem. Rev.* **1961**, 61, 275 – 311.

Interestingly, PBaz₃ catches fire when exposed to air while PPh₃ is indefinitely air stable.

Scheme 4.6. Hydrolysis and oxidation reactions of PBaz₃



4.1.5 Proposal for a New 1,2-Azaborine Containing Phosphine Ligand

Generally, introducing a boron atom that is bound to the phosphorus of a phosphine ligand furnishes an electron-rich ligand relative to its closest all-carbon analogue. Many of the studies presented thus far include comparative analyses between P-B ligands and their approximate all-C analogues, which serve as benchmarks to evaluate the effect of introducing a boron atom. The most common benchmark for comparing the properties of the new P-B ligands is the ubiquitous triphenylphosphine. Triarylphosphines are immensely important in synthetic chemistry, acting as ligands, stoichiometric reagents, and even as catalysts in their own right.⁵⁹ Benzene and its functionalized derivatives comprise the most important class of aryl groups in triarylphosphines; compounds such as triphenylphosphine and tri-*o*-tolylphosphine are fundamental examples. To this point, comparable, but not direct, single-boron-containing analogues have been reported. Fu's anionic boratabenzene ligand is isostructural but not isoelectronic with triphenylphosphine, while Pringle's phenanthrene-based BN ligand is isoelectronic but not isostructural with triphenylphosphine (Figure 4.13). A BN isostere (isoelectronic and isostructural) of a triarylphosphine ligand would provide a valuable comparison with two major benefits: the comparison would draw on a wealth of data for the monocyclic all-carbon compound and also grant an opportunity to investigate the effects of changing

⁵⁹ Matthew, T. H.; Jason, M. H.; Ralph Nicholas, S. *Curr. Org. Synth.* **2007**, *4*, 31-45.

the electronic parameter without perturbing the steric parameter of the ligand. Modifying electronic properties while retaining similar steric properties is a hallmark of BN/CC isosterism, a concept that will be introduced presently.

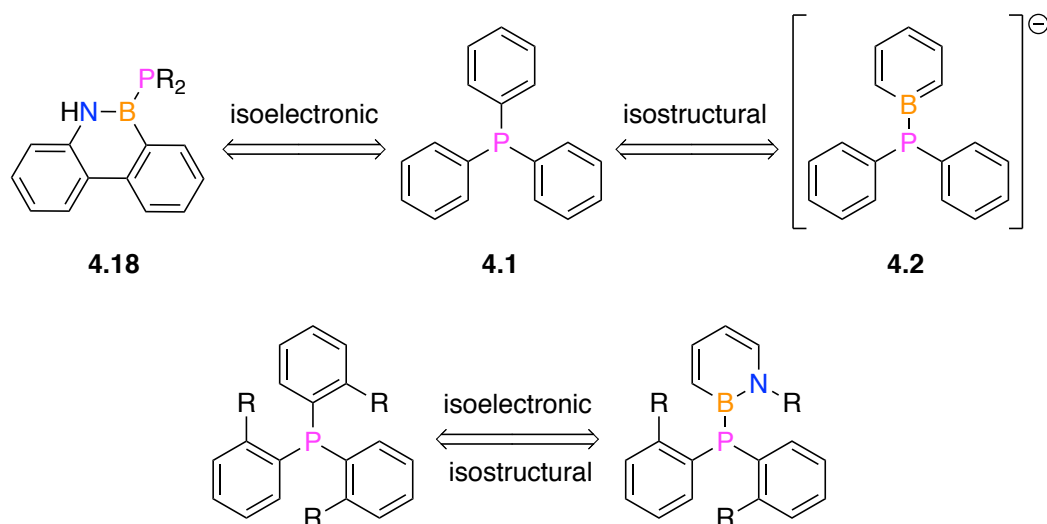


Figure 4.13. Isoelectronic, isostructural, and isosteric relationships between ligands.

4.2 Synthesis and Characterization of BN-Phosphine Ligands⁶⁰

4.2.1 Synthesis of BN-Phosphine Ligands

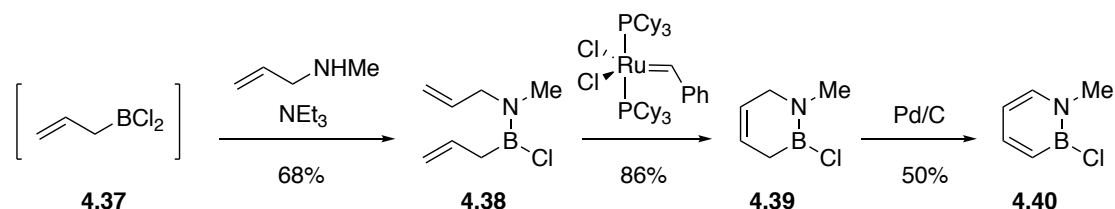
In order to prepare a 1,2-azaborine-containing phosphine ligand, a strategy coupling a nucleophilic, diaryl phosphide with an electrophilic boron chloride-containing azaborine was employed. The azaborine electrophile **4.40** was prepared according to the literature (Scheme 4.7).⁶¹ *In-situ* generated allylborondichloride **4.37** underwent reaction with N-methylallylamine in the presence of triethylamine to furnish adduct **4.38**. Ring closing metathesis with Grubbs' first generation catalyst yielded ring-closed product **4.39**. Finally, an oxidation was carried out with palladium on carbon in cyclohexene, a hydrogen acceptor, to afford the desired azaborine **4.40**. The key B-P bond forming reaction was accomplished by first deprotonating either

⁶⁰ The following section details the following published article: McConnell, C. R.; Campbell, P. G.; Fristoe, C. R.; Memmel, P.; Zakharov, L. N.; Li, B.; Darrigan, C.; Chrostowska, A.; Liu, S.-Y. *Eur. J. Inorg. Chem.* **2017**, 2207-2210.

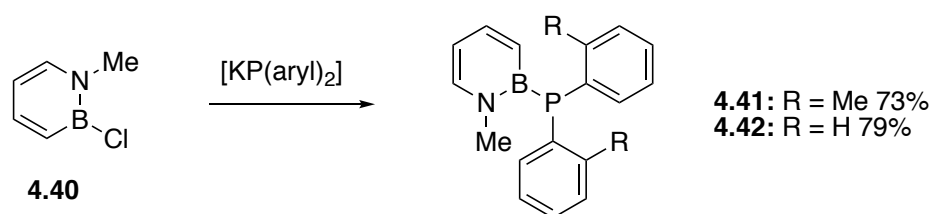
⁶¹ Chrostowska, A.; Xu, S.; Lamm, A. N.; Mazière, A.; Weber, C. D.; Dargelos, A.; Baylère, P.; Graciaa, A.; Liu, S.-Y. *J. Am. Chem. Soc.* **2012**, *134*, 10279-10285.

diphenyl or di-*o*-tolylphosphine with KH and then treating **4.40** with the resulting diarylphosphide (Scheme 4.8). Tri-*o*-tolyl BN-phosphine **4.41** and *o*-tolylbiphenyl BN-phosphine **4.42** were obtained in good yields.

Scheme 4.7. Preparation of azaborine electrophile **1.54**.



Scheme 4.8. Synthesis of BN ligands **4.41** and **4.42**.



4.2.2 Evaluation of Steric Parameters

Fortunately, we were able to obtain single crystals of BN-phosphine **4.41** suitable for X-ray diffraction, allowing us to directly compare the ligand structure to its all-carbon analogue tri-*o*-tolylphosphine **4.41c**. According to the crystal structure data, the two ligands display largely similar geometries (Figure 4.14). Two notable exceptions are the P-B (1.93 Å) and B-C (1.49 Å) bond lengths in the BN-ligand, which are elongated compared to their all-C counterparts in tri-*o*-tolylphosphine (1.84 Å and 1.39 Å, respectively).⁶² The larger covalent radius of the B atom vs. the carbon atom accounts for the increased bond lengths.⁵⁷ In spite of the differences in the geometric parameters, the steric parameter as measured by the ligand cone angle was nearly the same between the two ligands. For BN-tri-*o*-tolylphosphine, the cone angle

⁶² Cameron, T. S.; Dahlen, B. *J. Chem. Soc., Perkin Trans. 2* **1975**, 1737–1751.

was determined to be 191⁶³ which is similar to the published value of 194²⁰ for tri-*o*-tolylphosphine.

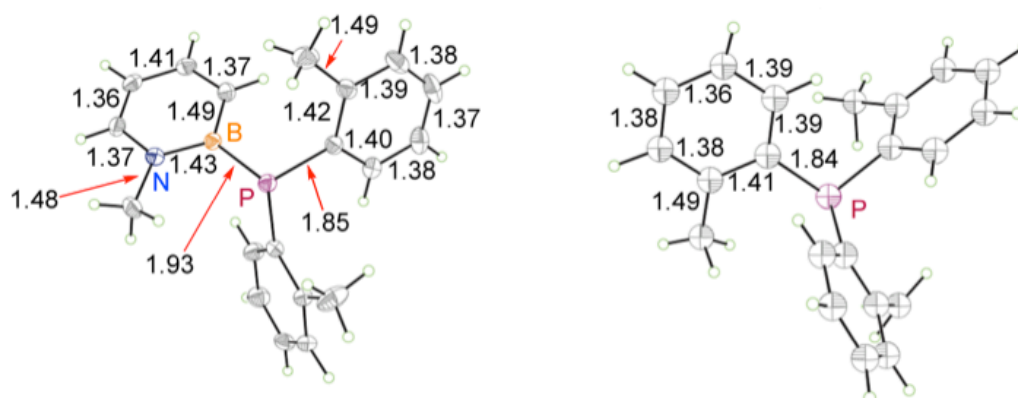


Figure 4.14. Structures and selected bond lengths of BN phosphine **4.41** (thermal ellipsoids displayed at 50% probability) and tri-*o*-tolylphosphine **4.41c**.⁶²

4.2.3 Evaluation of Electronic Parameters

4.2.3.1 UV-PES and DFT Studies

In order to learn more about their electronic structure, ligands **4.41** and **4.41c** were subjected to UV-PES studies supported by DFT calculations. These experiments were performed by the Chrostowska group (Univ. Pau et des Pays de l'Adour), who are experts in studying BN-heterocycles with UV-PES.^{61,64} The UV-photoelectron spectrum of **4.41** (Figure 4.15a) displays the low energy band at 7.3 eV, which is attributed to the ionization of the phosphorous lone pair. In the case of **4.41c** (Figure 4.15b) the first band is located at 7.64 eV and is also due to the phosphorous lone pair

⁶³ The ligand cone angle was determined according to a published procedure: Muller, T. E.; Mingos, D. M. P. *Transition Met. Chem.* **1995**, *20*, 533-539.

⁶⁴ (a) Lemierre, V.; Chrostowska, A.; Dargelos, A.; Chermette, H. *J. Phys. Chem. A* **2005**, *109*, 8348–8355; (b) Chrostowska, A.; Maciejczyk, M.; Dargelos, A.; Baylère, P.; Weber, L.; Werner, V.; Eickhoff, D.; Stammner, H.-G.; Neumann, B. *Organometallics* **2010**, *29*, 5192–5198; (c) Chrostowska, A.; Xu, S.; Mazière, A.; Boknevitc, K.; Li, B.; Abbey, E. R.; Dargelos, A.; Graciaa, A.; Liu, S.-Y. *J. Am. Chem. Soc.* **2014**, *136*, 11813–11820; (d) Ishibashi, J. S. A.; Marshall, J. L.; Mazière, A.; Lovinger, G. J.; Li, B.; Zakharov, L. N.; Dargelos, A.; Graciaa, A.; Chrostowska, A.; Liu, S.-Y. *J. Am. Chem. Soc.* **2014**, *136*, 15414-15421; (e) Liu, Z.; Ishibashi, J. S. A.; Darrigan, C.; Dargelos, A.; Chrostowska, A.; Li, B.; Vasiliu, M.; Dixon, D. A.; Liu, S.-Y. *J. Am. Chem. Soc.* **2017**, *139*, 6082-6085; (f) Ishibashi, J. S. A.; Dargelos, A.; Darrigan, C.; Chrostowska, A.; Liu, S.-Y. *Organometallics* **2017**, *36*, 2494-2497; (g) Ishibashi, J. S. A.; Darrigan, C.; Chrostowska, A.; Li, B.; Liu, S.-Y. *Dalton Trans.* **2019**, *48*, 2807-2812.

ionization. Thus, the HOMO of BN-tri-*o*-tolylphosphine, which represents the phosphorus lone pair, is destabilized by 0.34 eV relative to the HOMO of all-carbon tri-*o*-tolylphosphine. The band at 9.15 eV in the spectrum of **4.41** is attributed to the phosphorus lone pair ionization in a bonding interaction with π_2 of two *o*-tolyl substituents; the corresponding phosphorous lone pair interaction with π_2 of the three *o*-tolyl substituents in **4.41c** appears at 9.4 eV. Taken together, the orbitals with significant phosphorus lone pair contribution in **4.41** are higher energy than in **4.41c**, indicating that **4.41** should be considered a more σ -donating ligand than its carbonaceous counterpart.

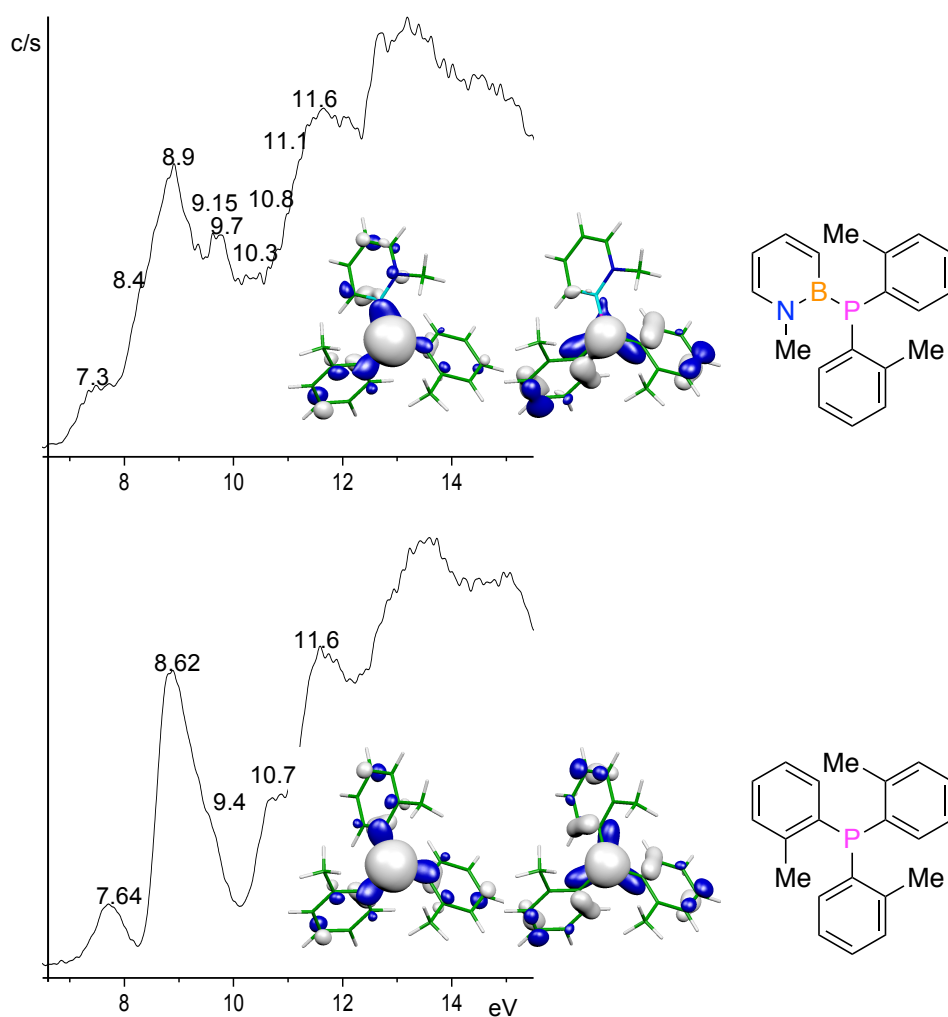
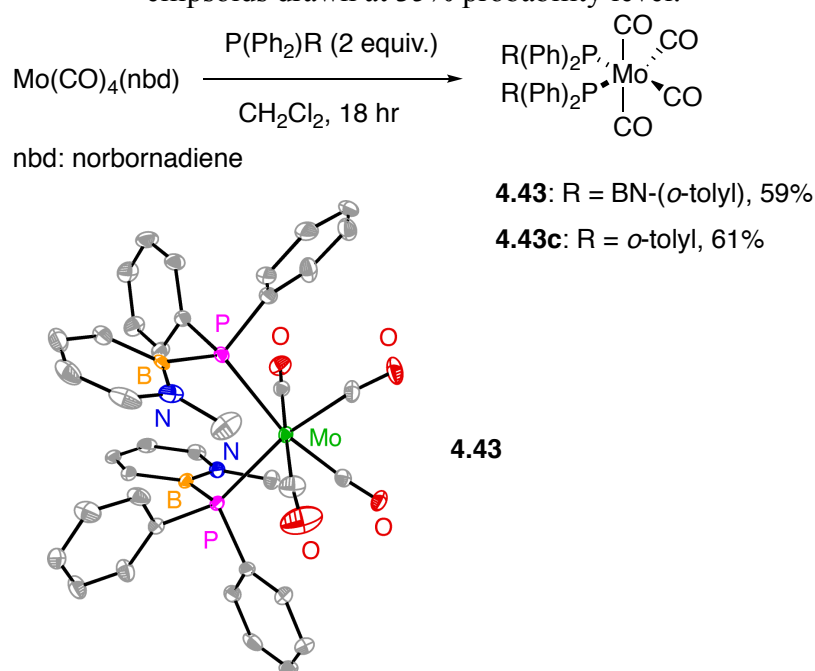


Figure 4.15. UV-photoelectron spectra of: (a) **4.41**, (b) **4.41c**.

4.2.3.2 Determination of the Tolman Electronic Parameter

To determine the Tolman electronic parameter of BN-tri-*o*-tolylphosphine and compare it to its direct all-carbon analogue tri-*o*-tolylphosphine, we prepared molybdenum-carbonyl complexes of the type *cis*-[MoL₂(CO)₄].⁵³ Attempts to prepare iridium(I)-carbonyl complexes, another commonly used complex for TEP determination, were unsuccessful due to the tendency of the P-B bond to undergo side-reaction with Ir-X bonds. Such reactivity is not possible with the Mo(0) complex. However, the steric requirements of tri-*o*-tolylphosphine prohibited the formation of a *cis*-[MoL₂(CO)₄] complex. The less sterically demanding **4.42** readily formed molybdenum-carbonyl complex **4.43** from the known precursor Mo(CO)₄(nbd) in 59% yield (Scheme 4.9).⁵⁵ Complexation of diphenyl-(*o*-tolyl)phosphine to Mo(CO)₄(nbd) analogously formed all-carbon complex **4.43c**. The structure of **4.43** was unambiguously confirmed through x-ray diffraction of a single crystal grown from a diethyl ether solution (see ORTEP with thermal ellipsoids drawn at the 35% probability level in Scheme 4.9).

Scheme 4.9. The synthesis of phosphine-molybdenum metal complexes. Thermal ellipsoids drawn at 35% probability level.



FTIR analysis of the Mo complexes **4.43** and **4.43c** allowed us to determine the TEP of the BN-phosphine ligand **4.42** and compare it to its all-carbon analogue diphenyl-(*o*-tolyl)phosphine. The convention for determining the TEP of *cis*-[MoL₂(CO)₄] complexes is to report the symmetric A¹ carbonyl vibrational mode.⁶⁵ The FTIR data for **4.43** and its all-carbon analogue **4.43c** are shown in Table 4.6 along with other selected phosphine ligands. The A¹ CO vibrational mode is highlighted in bold. The A¹ CO vibrational mode for **4.43** and **4.43c** corresponds to $\nu(\text{CO}) = 2012 \text{ cm}^{-1}$ and $\nu(\text{CO}) = 2019 \text{ cm}^{-1}$, respectively. The smaller $\nu(\text{CO})$ for **4.43** relative to **4.43c** indicates a greater net electron-donating ability for the azaborine-substituted phosphine ligand **4.42** in direct comparison to the all-carbon diphenyl-(*o*-tolyl)phosphine. In general, the net electron-donating ability of **4.42** appears to be stronger than even that of some trialkylphosphine ligands (Table 4.6).^{66,67} Ligand **4.42** is also slightly more electron-rich than the triborylphosphine ligand **4.28** reported by Pringle.⁵⁵ The greater electron-donating ability of the 1,2-azaborine-containing phosphine ligand can be rationalized by inductive effects. The incorporation of the less electronegative boron atom (P–B vs. P–C) leaves more electron density with the phosphorus. Moreover, the monocyclic 1,2-azaborine appears to be a more electron-releasing moiety when compared to other BN heterocycles that contain multiple inductively withdrawing atoms (such as N) bound to boron (e.g., in ligand **4.28**).

⁶⁵ Anton, D. R.; Crabtree, R. H. *Organometallics*, **1983**, *2*, 621-627.

⁶⁶ Poilblanc, R.; Bigorgne, M. *Compt. Rend.* **1960**, *250*, 1064-1066.

⁶⁷ Cotton, F. A.; Darensbourg, D. J.; Klein, S.; Kolthammer, B. W. S. *Inorg. Chem.* **1982**, *21*, 2661-2666.

4.4 Experimental Section

4.4.1 General Considerations

All oxygen- and moisture-sensitive manipulations were carried out under an inert atmosphere using either standard Schlenk techniques or a glove box.

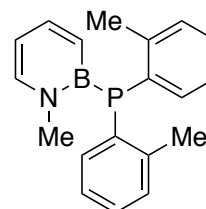
THF, Et₂O, CH₂Cl₂ and pentane were purified by passing through a neutral alumina column under argon. Cyclohexene, CD₂Cl₂, and C₆D₆ were purified by distillation after drying over calcium hydride.

Potassium hydride (Aldrich) was washed with pentane three times and pumped dry under vacuum prior to use. All other chemicals and solvents were purchased (TCI, Aldrich or Strem) and used as received.

¹¹B NMR (160 MHz) spectra were recorded on a Varian Inova 600 spectrometer, or Varian Inova 500 spectrometer at ambient temperature. ¹H NMR (500 MHz) spectra were recorded on a Varian Inova 600 spectrometer, or Varian VNMRS 500 spectrometer. ¹³C NMR (126 MHz, ¹H decoupled) spectra were recorded on a Varian Inova 600 spectrometer or Varian VNMRS 500 spectrometer. ³¹P NMR (202 MHz) spectra were recorded on a Varian VNMRS 500 spectrometer. All chemical shifts are externally referenced: ¹¹B NMR to BF₃•Et₂O (δ 0) and ³¹P NMR to 1% H₃PO₄ (δ 0). IR spectra were recorded on a Bruker Alpha FT-IR instrument with OPUS software.

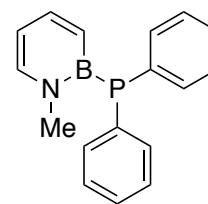
4.4.2 Synthetic Details

Compound 4.41. Di(*o*-tolyl)phosphine (0.336 g, 4.43 mmol) was deprotonated at room temperature in THF (5.0 mL) using potassium hydride (0.076 g, 1.9 mmol) to generate di(*o*-tolyl)phosphide *in situ*. After 1 hour, the phosphide solution was passed through a PTFE filter before being added dropwise via syringe to a solution of **4.40**⁶¹ (0.200 g, 4.43 mmol) in THF (10.0 mL) at -78 °C and allowed to warm to room temperature for 30 minutes. THF was removed under reduced pressure and the desired product was isolated by extraction with pentane. The pentane solution was passed through an acrodisc, then cooled to -30 °C, whereupon the desired product precipitated as a white crystalline solid (0.35 g, 73% yield). ¹H NMR (500 MHz, C₆D₆) δ 7.30 (dd, *J* = 10.9, 6.6 Hz, 1H), 7.20 (ddd, *J* = 7.7, 4.7, 1.4 Hz, 2H), 7.14 (dd, *J* = 2.1, 1.1 Hz, 1H), 7.08 (m, 3H), 6.92 (m, 2H), 6.64 (m, 2H), 6.09 (td, *J* = 6.6, 1.6 Hz, 1H), 3.09 (d, *J* = 2.8 Hz, 3H), 2.53 (t, *J* = 2.0 Hz, 6H). ¹¹B NMR (160 MHz, C₆D₆) δ 38.60. ¹³C NMR (126 MHz, CD₂Cl₂) δ 140.8 (d, *J* = 23.2 Hz), 139.8, 138.5, 134.1 (d, *J* = 6.6 Hz), 132.79, 128.2 (d, *J* = 4.9 Hz), 126.1, 124.2, 110.2, 40.8, 19.9 (the boron-bound carbon was not observed). ³¹P NMR (202 MHz, C₆D₆) δ -64.0. IR spectrum (cm⁻¹): 3056.4, 3032.1, 3001.0, 2966.4, 2935.3.

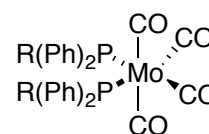


HRMS (DART) calcd. for C₁₉H₂₁BNP ([M+H]⁺) 306.15159, found 306.15143.

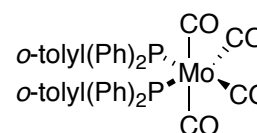
Compound 4.42. Diphenylphosphine (0.205 g, 1.10 mmol) was deprotonated at room temperature in THF (5.0 mL) using potassium hydride (0.053 g, 1.32 mmol) to generate diphenylphosphide *in situ*. After 1 hour, the phosphide solution was passed through a PTFE filter before being added dropwise to a solution of **4.40**⁶¹ (0.140 g, 1.10 mmol) in THF (10.0 mL) at -78 °C and allowed to warm to room temperature for 30 minutes. THF was removed under reduced pressure and the desired product was isolated by extraction with pentane. The pentane solution was passed through a PTFE filter then cooled to -30 °C, whereupon the desired product precipitated as a white crystalline solid (0.24 g, 79% yield). ¹H NMR (500 MHz, CD₂Cl₂): δ 7.53(m, 1H), 7.36 (m, 11H), 6.45 (m, 2H), 3.57 (s, 3H). ¹¹B NMR (160 MHz, CD₂Cl₂): δ 38.5. ¹³C NMR (126 MHz, CD₂Cl₂): δ 141.9, 140.7, 137.2, 134.7 (d, *J* = 17.2 Hz), 131 (br), 128.3 (d, *J* = 7.1 Hz), 127.4, 112.1, 43.3. ³¹P NMR (202 MHz, CD₂Cl₂): δ -49.8. IR spectrum (cm⁻¹): 3065.9, 3024.9, 3013.0, 2997.0, 2934.3. HRMS (DART) calcd. for C₁₇H₁₇BNP ([M+H]⁺) 278.12029, found 278.12113.



Compound 4.43. (R = *N*-Me-2-1,2-azaboroly). A solution of Mo(CO)₄(nbd) (0.021 g, 0.070 mmol) and **4.42** (0.039 g, 0.14 mmol) in CH₂Cl₂ (1.0 mL) was stirred at room temperature for 18 hours. The crude reaction mixture was layered with pentane and cooled to -30 °C, whereupon the desired product precipitated as a dark yellow, crystalline solid (0.032 g, 59% yield). ¹H NMR (500 MHz, CD₂Cl₂) δ 7.60 (dd, *J* = 11.1, 6.9 Hz, 2H), 7.37 (t, *J* = 8.5 Hz, 8H), 7.27 (m, 6H), 7.17 (t, *J* = 7.6 Hz, 8H), 6.62 (d, *J* = 11.0 Hz, 2H), 6.51 (t, *J* = 6.7 Hz, 2H), 3.36 (s, 6H). ¹¹B NMR (160 MHz, CD₂Cl₂): δ 36.9. ¹³C NMR (126 MHz, CD₂Cl₂) δ 215.9, 210.8, 142.4 (d, *J* = 5.7 Hz), 141.6, 135.6 (d, *J* = 28.9 Hz), 134.8 (d, *J* = 11.3 Hz), 131 (br), 128.5, 128.1 (d, *J* = 29 Hz), 113.0, 44.4 (d, *J* = 6.9 Hz). ³¹P NMR (202 MHz, CD₂Cl₂) δ -18.45. IR spectrum (cm⁻¹): 3055.0, 2943.0, 2011.6, 1886.7, 1856.1.



Compound 4.43c. A solution of Mo(CO)₄(nbd) (0.027 g, 0.090 mmol) and diphenyl(*o*-tolyl)phosphine (0.050 g, 0.18 mmol) in CH₂Cl₂ (1.0 mL) was stirred at room temperature for 18 hours. The crude reaction mixture was layered with pentane and cooled to -30 °C, whereupon the desired product precipitated as a yellow, powdery solid (0.042 g, 61% yield). ¹H NMR (500 MHz, CD₂Cl₂) δ 7.44 (m, 8H), 7.34 (q, *J* = 7.0 Hz, 6H), 7.29 (t, *J* = 7.5 Hz, 8H), 7.20 (m, 4H), 6.99 (t, *J* = 7.6 Hz,



2H), 1.98 (s, 6H). ^{13}C NMR (126 MHz, CD_2Cl_2) δ 215.6, 211.4, 142.1, 136.0, 135.9, 135.7 (m), 133.0 (t, $J = 6.4$ Hz), 132.1 (t, $J = 2.9$ Hz), 130.2, 129.3, 128.2 (t, $J = 4.5$ Hz), 125.4 (t, $J = 5.4$ Hz), 22.91. ^{31}P NMR (202 MHz, CD_2Cl_2) δ 37.56. IR spectrum (cm^{-1}): 3056.5, 2019.1, 1898.6, 1873.1.

4.4.3 X-ray Crystal Structure Determination of 4.41 and 4.43.

General Procedure

Diffraction intensity data for all compounds were collected with a Bruker Smart Apex CCD diffractometer at 173(2) K using $\text{MoK}\alpha$ - radiation (0.71073 Å). The structures were solved using direct methods, completed by subsequent difference Fourier syntheses, and refined by full matrix least-squares procedures on F^2 . All non-H atoms were refined with anisotropic thermal parameters. H atoms were found on the residual density map and refined with isotropic thermal parameters. All software and sources scattering factors are contained in the SHELXTL (6.10) program package (G.Sheldrick, Bruker XRD, Madison, WI). Crystallographic data and some details of data collection and crystal structure refinement for 4.41 and 4.43 are given in the following tables.

Crystallographic Data for Compound 4.41 (=liu97)

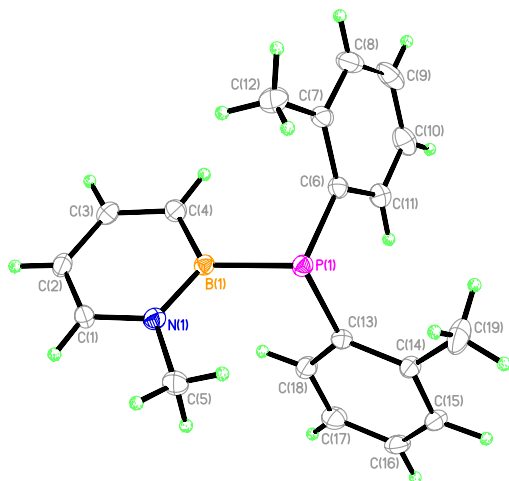


Table 4.7. Crystal data and structure refinement for liu97.

Identification code	liu97
Empirical formula	$\text{C}_{19}\text{H}_{21}\text{BNP}$
Formula weight	305.15
Temperature	173(2) K
Wavelength	0.71073 Å
Crystal system	Monoclinic
Space group	$P2(1)/n$

Unit cell dimensions	a = 7.6132(9) Å b = 7.9016(9) Å c = 28.864(3) Å	a = 90°. b = 90.407(2)°. g = 90°.
Volume	1736.3(4) Å ³	
Z	4	
Density (calculated)	1.167 Mg/m ³	
Absorption coefficient	0.154 mm ⁻¹	
F(000)	648	
Crystal size	0.25 x 0.22 x 0.16 mm ³	
Theta range for data collection	1.41 to 27.00°.	
Index ranges	-9<=h<=9, -9<=k<=10, -36<=l<=36	
Reflections collected	10512	
Independent reflections	3763 [R(int) = 0.0233]	
Completeness to theta = 27.00°	99.6 %	
Absorption correction	Semi-empirical from equivalents	
Max. and min. transmission	0.9758 and 0.9626	
Refinement method	Full-matrix least-squares on F ²	
Data / restraints / parameters	3763 / 0 / 283	
Goodness-of-fit on F ²	1.039	
Final R indices [I>2sigma(I)]	R1 = 0.0442, wR2 = 0.1101	
R indices (all data)	R1 = 0.0562, wR2 = 0.1184	
Largest diff. peak and hole	0.354 and -0.156 e.Å ⁻³	

Table 4.8. Atomic coordinates (x 10⁴) and equivalent isotropic displacement parameters (Å²x 10³) for liu97. U(eq) is defined as one third of the trace of the orthogonalized U^{ij} tensor.

	x	y	z	U(eq)
P(1)	8229(1)	-528(1)	1460(1)	26(1)
N(1)	10549(2)	-3206(2)	1151(1)	31(1)
B(1)	9526(2)	-1790(2)	1004(1)	25(1)
C(1)	11385(2)	-4216(2)	835(1)	32(1)
C(2)	11296(2)	-3914(2)	373(1)	33(1)
C(3)	10325(2)	-2534(2)	200(1)	34(1)
C(4)	9443(2)	-1479(2)	494(1)	32(1)
C(5)	10788(4)	-3662(3)	1645(1)	47(1)
C(6)	7117(2)	1078(2)	1096(1)	28(1)

C(7)	5641(2)	586(2)	824(1)	32(1)
C(8)	4797(3)	1816(3)	560(1)	44(1)
C(9)	5342(3)	3480(3)	560(1)	50(1)
C(10)	6755(3)	3962(3)	826(1)	45(1)
C(11)	7635(3)	2777(2)	1091(1)	35(1)
C(12)	4994(3)	-1198(3)	817(1)	47(1)
C(13)	9931(2)	730(2)	1760(1)	29(1)
C(14)	9534(2)	1540(2)	2182(1)	31(1)
C(15)	10842(3)	2465(2)	2407(1)	36(1)
C(16)	12512(3)	2609(3)	2232(1)	39(1)
C(17)	12914(3)	1819(3)	1819(1)	42(1)
C(18)	11640(2)	896(2)	1587(1)	36(1)
C(19)	7719(3)	1471(4)	2383(1)	55(1)

Table 4.9. Bond lengths [Å] and angles [°] for liu97.

P(1)-C(13)	1.8442(18)
P(1)-C(6)	1.8491(17)
P(1)-B(1)	1.9285(18)
N(1)-C(1)	1.372(2)
N(1)-B(1)	1.425(2)
N(1)-C(5)	1.480(2)
B(1)-C(4)	1.493(2)
C(1)-C(2)	1.357(3)
C(1)-H(1)	0.93(2)
C(2)-C(3)	1.406(3)
C(2)-H(2)	0.952(19)
C(3)-C(4)	1.369(2)
C(3)-H(3)	0.98(2)
C(4)-H(4)	0.97(2)
C(5)-H(5A)	1.03(4)
C(5)-H(5B)	0.97(3)
C(5)-H(5C)	0.90(3)
C(6)-C(11)	1.399(3)
C(6)-C(7)	1.420(2)
C(7)-C(8)	1.391(3)
C(7)-C(12)	1.493(3)

C(8)-C(9)	1.379(3)
C(8)-H(8)	0.93(2)
C(9)-C(10)	1.372(3)
C(9)-H(9)	0.93(3)
C(10)-C(11)	1.380(3)
C(10)-H(10)	0.95(3)
C(11)-H(11)	0.94(2)
C(12)-H(12A)	0.98(3)
C(12)-H(12B)	0.94(3)
C(12)-H(12C)	0.95(3)
C(13)-C(18)	1.403(2)
C(13)-C(14)	1.411(2)
C(14)-C(15)	1.392(3)
C(14)-C(19)	1.503(3)
C(15)-C(16)	1.375(3)
C(15)-H(15)	1.01(2)
C(16)-C(17)	1.383(3)
C(16)-H(16)	0.94(2)
C(17)-C(18)	1.382(3)
C(17)-H(17)	0.92(2)
C(18)-H(18)	0.96(2)
C(19)-H(19A)	1.02(4)
C(19)-H(19B)	0.93(3)
C(19)-H(19C)	0.93(3)

C(13)-P(1)-C(6)	102.36(8)
C(13)-P(1)-B(1)	103.73(8)
C(6)-P(1)-B(1)	101.65(7)
C(1)-N(1)-B(1)	121.01(14)
C(1)-N(1)-C(5)	116.32(16)
B(1)-N(1)-C(5)	122.67(15)
N(1)-B(1)-C(4)	116.13(15)
N(1)-B(1)-P(1)	119.03(12)
C(4)-B(1)-P(1)	124.68(13)
C(2)-C(1)-N(1)	122.06(17)
C(2)-C(1)-H(1)	122.5(12)
N(1)-C(1)-H(1)	115.5(12)
C(1)-C(2)-C(3)	120.45(16)

C(1)-C(2)-H(2)	117.8(12)
C(3)-C(2)-H(2)	121.7(12)
C(4)-C(3)-C(2)	120.77(16)
C(4)-C(3)-H(3)	121.8(12)
C(2)-C(3)-H(3)	117.4(12)
C(3)-C(4)-B(1)	119.58(17)
C(3)-C(4)-H(4)	119.5(11)
B(1)-C(4)-H(4)	120.8(11)
N(1)-C(5)-H(5A)	108.0(19)
N(1)-C(5)-H(5B)	111.2(19)
H(5A)-C(5)-H(5B)	107(3)
N(1)-C(5)-H(5C)	112.9(17)
H(5A)-C(5)-H(5C)	101(2)
H(5B)-C(5)-H(5C)	116(2)
C(11)-C(6)-C(7)	118.63(16)
C(11)-C(6)-P(1)	122.46(14)
C(7)-C(6)-P(1)	118.87(13)
C(8)-C(7)-C(6)	118.18(18)
C(8)-C(7)-C(12)	120.06(18)
C(6)-C(7)-C(12)	121.76(17)
C(9)-C(8)-C(7)	121.9(2)
C(9)-C(8)-H(8)	123.5(13)
C(7)-C(8)-H(8)	114.5(13)
C(10)-C(9)-C(8)	119.98(19)
C(10)-C(9)-H(9)	118.8(15)
C(8)-C(9)-H(9)	121.3(15)
C(9)-C(10)-C(11)	119.8(2)
C(9)-C(10)-H(10)	120.9(15)
C(11)-C(10)-H(10)	119.3(15)
C(10)-C(11)-C(6)	121.44(19)
C(10)-C(11)-H(11)	119.5(14)
C(6)-C(11)-H(11)	119.1(14)
C(7)-C(12)-H(12A)	112.2(15)
C(7)-C(12)-H(12B)	111.5(15)
H(12A)-C(12)-H(12B)	109(2)
C(7)-C(12)-H(12C)	111.7(17)
H(12A)-C(12)-H(12C)	106(2)
H(12B)-C(12)-H(12C)	105(2)

C(18)-C(13)-C(14)	118.01(16)
C(18)-C(13)-P(1)	122.27(13)
C(14)-C(13)-P(1)	119.71(13)
C(15)-C(14)-C(13)	118.93(16)
C(15)-C(14)-C(19)	119.72(16)
C(13)-C(14)-C(19)	121.32(17)
C(16)-C(15)-C(14)	122.17(17)
C(16)-C(15)-H(15)	120.4(11)
C(14)-C(15)-H(15)	117.4(11)
C(15)-C(16)-C(17)	119.34(18)
C(15)-C(16)-H(16)	120.9(12)
C(17)-C(16)-H(16)	119.8(12)
C(18)-C(17)-C(16)	119.79(18)
C(18)-C(17)-H(17)	121.7(14)
C(16)-C(17)-H(17)	118.6(14)
C(17)-C(18)-C(13)	121.77(17)
C(17)-C(18)-H(18)	118.5(12)
C(13)-C(18)-H(18)	119.7(12)
C(14)-C(19)-H(19A)	108.9(19)
C(14)-C(19)-H(19B)	112.5(17)
H(19A)-C(19)-H(19B)	107(3)
C(14)-C(19)-H(19C)	111.7(16)
H(19A)-C(19)-H(19C)	105(3)
H(19B)-C(19)-H(19C)	111(2)

Symmetry transformations used to generate equivalent atoms:

Table 4.10. Anisotropic displacement parameters ($\text{\AA}^2 \times 10^3$) for liu97. The anisotropic displacement factor exponent takes the form: $-2\pi^2 [h^2 a^{*2} U^{11} + \dots + 2 h k a^* b^* U^{12}]$

	U ¹¹	U ²²	U ³³	U ²³	U ¹³	U ¹²
P(1)	29(1)	26(1)	24(1)	-1(1)	0(1)	0(1)
N(1)	36(1)	30(1)	26(1)	0(1)	-3(1)	2(1)
B(1)	26(1)	23(1)	25(1)	-1(1)	-1(1)	-2(1)
C(1)	31(1)	27(1)	38(1)	-4(1)	-1(1)	5(1)
C(2)	32(1)	34(1)	34(1)	-11(1)	2(1)	-2(1)
C(3)	39(1)	37(1)	25(1)	-3(1)	0(1)	-3(1)
C(4)	36(1)	28(1)	31(1)	2(1)	-1(1)	0(1)
C(5)	66(2)	44(1)	30(1)	4(1)	-7(1)	20(1)
C(6)	26(1)	31(1)	26(1)	-1(1)	3(1)	3(1)
C(7)	26(1)	41(1)	29(1)	-2(1)	1(1)	4(1)
C(8)	30(1)	68(2)	35(1)	4(1)	-3(1)	11(1)
C(9)	46(1)	60(2)	45(1)	22(1)	9(1)	26(1)
C(10)	48(1)	35(1)	53(1)	10(1)	9(1)	10(1)
C(11)	36(1)	31(1)	38(1)	0(1)	2(1)	2(1)
C(12)	37(1)	51(1)	53(1)	-9(1)	-7(1)	-8(1)
C(13)	32(1)	29(1)	25(1)	1(1)	-4(1)	4(1)
C(14)	35(1)	30(1)	26(1)	-2(1)	-2(1)	2(1)
C(15)	45(1)	37(1)	27(1)	-4(1)	-8(1)	4(1)
C(16)	38(1)	39(1)	38(1)	-1(1)	-16(1)	-2(1)
C(17)	29(1)	54(1)	44(1)	-3(1)	-3(1)	-1(1)
C(18)	32(1)	43(1)	32(1)	-8(1)	0(1)	1(1)
C(19)	48(1)	69(2)	48(1)	-28(1)	17(1)	-10(1)

Table 4.11. Hydrogen coordinates ($\times 10^4$) and isotropic displacement parameters ($\text{\AA}^2 \times 10^3$) for liu97.

	x	y	z	U(eq)
H(1)	12020(30)	-5110(30)	959(7)	37(5)
H(2)	11880(20)	-4680(20)	172(7)	34(5)
H(3)	10320(30)	-2350(20)	-137(8)	43(6)
H(4)	8740(30)	-570(20)	369(7)	36(5)
H(5A)	11960(50)	-3160(40)	1757(12)	108(11)
H(5B)	9870(40)	-3170(40)	1835(11)	102(10)
H(5C)	10990(30)	-4770(40)	1687(9)	75(8)
H(8)	3810(30)	1430(30)	399(7)	40(5)
H(9)	4770(30)	4290(30)	381(8)	64(7)
H(10)	7150(30)	5100(30)	826(8)	63(7)
H(11)	8630(30)	3100(30)	1262(8)	51(6)
H(12A)	5790(30)	-1950(30)	652(9)	68(7)
H(12B)	3860(30)	-1270(30)	685(8)	56(7)
H(12C)	4880(30)	-1650(30)	1122(10)	78(8)
H(15)	10510(30)	3070(30)	2702(7)	41(5)
H(16)	13380(30)	3250(30)	2389(7)	42(5)
H(17)	14030(30)	1930(30)	1704(8)	52(6)
H(18)	11950(30)	330(30)	1305(7)	37(5)
H(19A)	6890(50)	2160(50)	2179(12)	111(12)
H(19B)	7270(40)	380(40)	2394(9)	75(8)
H(19C)	7680(30)	1980(40)	2673(10)	74(8)

Table 4.12. Torsion angles [°] for liu97.

C(1)-N(1)-B(1)-C(4)	-0.5(2)
C(5)-N(1)-B(1)-C(4)	178.81(18)
C(1)-N(1)-B(1)-P(1)	175.05(13)
C(5)-N(1)-B(1)-P(1)	-5.6(2)
C(13)-P(1)-B(1)-N(1)	75.57(15)
C(6)-P(1)-B(1)-N(1)	-178.45(13)
C(13)-P(1)-B(1)-C(4)	-109.26(15)
C(6)-P(1)-B(1)-C(4)	-3.28(17)
B(1)-N(1)-C(1)-C(2)	0.6(3)
C(5)-N(1)-C(1)-C(2)	-178.79(19)
N(1)-C(1)-C(2)-C(3)	-0.1(3)
C(1)-C(2)-C(3)-C(4)	-0.5(3)
C(2)-C(3)-C(4)-B(1)	0.5(3)
N(1)-B(1)-C(4)-C(3)	0.0(2)
P(1)-B(1)-C(4)-C(3)	-175.32(14)
C(13)-P(1)-C(6)-C(11)	0.54(15)
B(1)-P(1)-C(6)-C(11)	-106.51(14)
C(13)-P(1)-C(6)-C(7)	-177.04(12)
B(1)-P(1)-C(6)-C(7)	75.91(14)
C(11)-C(6)-C(7)-C(8)	1.0(2)
P(1)-C(6)-C(7)-C(8)	178.71(13)
C(11)-C(6)-C(7)-C(12)	-179.15(17)
P(1)-C(6)-C(7)-C(12)	-1.5(2)
C(6)-C(7)-C(8)-C(9)	-0.7(3)
C(12)-C(7)-C(8)-C(9)	179.45(19)
C(7)-C(8)-C(9)-C(10)	0.0(3)
C(8)-C(9)-C(10)-C(11)	0.5(3)
C(9)-C(10)-C(11)-C(6)	-0.2(3)
C(7)-C(6)-C(11)-C(10)	-0.6(3)
P(1)-C(6)-C(11)-C(10)	-178.19(14)
C(6)-P(1)-C(13)-C(18)	-92.87(15)
B(1)-P(1)-C(13)-C(18)	12.57(17)
C(6)-P(1)-C(13)-C(14)	88.20(14)
B(1)-P(1)-C(13)-C(14)	-166.35(13)
C(18)-C(13)-C(14)-C(15)	0.1(2)
P(1)-C(13)-C(14)-C(15)	179.11(13)

C(18)-C(13)-C(14)-C(19)	178.0(2)
P(1)-C(13)-C(14)-C(19)	-3.0(3)
C(13)-C(14)-C(15)-C(16)	-0.3(3)
C(19)-C(14)-C(15)-C(16)	-178.2(2)
C(14)-C(15)-C(16)-C(17)	0.3(3)
C(15)-C(16)-C(17)-C(18)	0.0(3)
C(16)-C(17)-C(18)-C(13)	-0.1(3)
C(14)-C(13)-C(18)-C(17)	0.1(3)
P(1)-C(13)-C(18)-C(17)	-178.87(15)

Crystallographic Data for Compound 4.43

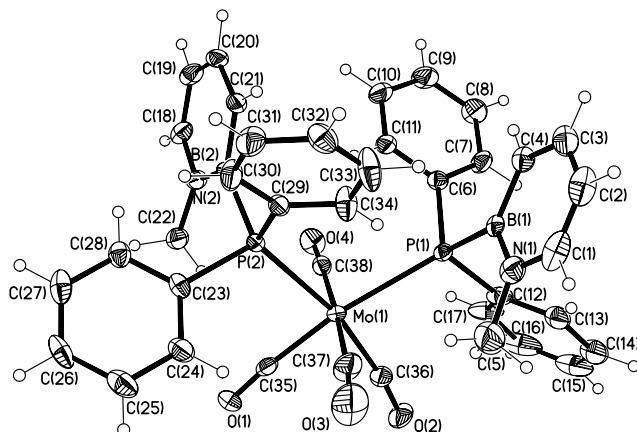


Table 4.13. Crystal data and structure refinement for **4.43**.

Identification code	MoBN	
Empirical formula	$C_{42}H_{44}B_2MoN_2O_5P_2$	
Formula weight	836.29	
Temperature	100(2) K	
Wavelength	1.54178 Å	
Crystal system	Monoclinic	
Space group	Cc	
Unit cell dimensions	$a = 12.4798(7)$ Å	$a = 90^\circ$.
	$b = 18.7635(7)$ Å	$b = 97.164(2)^\circ$.
	$c = 17.2516(7)$ Å	$c = 90^\circ$.
Volume	$4008.2(3)$ Å ³	
Z	4	
Density (calculated)	1.386 Mg/m ³	
Absorption coefficient	3.804 mm ⁻¹	

F(000)	1728
Crystal size	0.410 x 0.190 x 0.140 mm ³
Theta range for data collection	4.278 to 69.683°.
Index ranges	-14<=h<=13, -22<=k<=21, -20<=l<=18
Reflections collected	12329
Independent reflections	5732 [R(int) = 0.0252]
Completeness to theta = 67.679°	99.5 %
Absorption correction	Semi-empirical from equivalents
Max. and min. transmission	0.7532 and 0.5878
Refinement method	Full-matrix least-squares on F ²
Data / restraints / parameters	5732 / 21 / 486
Goodness-of-fit on F ²	1.054
Final R indices [I>2sigma(I)]	R1 = 0.0286, wR2 = 0.0745
R indices (all data)	R1 = 0.0286, wR2 = 0.0745
Absolute structure parameter	0.451(10)
Extinction coefficient	n/a
Largest diff. peak and hole	0.929 and -0.323 e. Å ⁻³

Table 4.14. Atomic coordinates (x 10⁴) and equivalent isotropic displacement parameters (≈²x 10³) for C₃₈H₃₄B₂MoN₂O₄P₂(C₄H₁₀O). U(eq) is defined as one third of the trace of the orthogonalized U^{ij} tensor.

	x	y	z	U(eq)
Mo(1)	4753(1)	528(1)	5142(1)	19(1)
P(1)	4009(1)	1475(1)	4063(1)	18(1)
P(2)	6036(1)	1256(1)	6157(1)	19(1)
O(1)	5133(3)	-806(2)	6221(2)	33(1)
O(2)	3461(4)	-667(2)	4164(2)	43(1)
O(3)	6813(5)	-4(3)	4426(3)	79(2)
O(4)	2721(3)	941(2)	6003(2)	38(1)
N(1)	5671(3)	1755(2)	3018(2)	33(1)
N(2)	4671(3)	1547(2)	7406(2)	25(1)
B(1)	4848(4)	2053(2)	3420(3)	19(1)
B(2)	5350(4)	1850(2)	6884(3)	22(1)
C(1)	6232(4)	2160(4)	2545(3)	44(1)
C(2)	6043(5)	2864(3)	2447(3)	43(1)

C(3)	5242(5)	3202(3)	2818(3)	39(1)
C(4)	4646(4)	2827(3)	3297(3)	28(1)
C(5)	6032(6)	1026(4)	3061(4)	55(2)
C(6)	3161(3)	2162(2)	4445(2)	22(1)
C(7)	2217(4)	2417(3)	4039(3)	31(1)
C(8)	1605(4)	2931(3)	4361(3)	39(1)
C(9)	1930(4)	3198(3)	5093(3)	38(1)
C(10)	2882(5)	2956(3)	5508(3)	38(1)
C(11)	3499(4)	2445(2)	5187(3)	29(1)
C(12)	3040(4)	1026(2)	3303(3)	30(1)
C(13)	3216(4)	1012(3)	2496(3)	35(1)
C(14)	2522(6)	637(3)	1968(4)	50(2)
C(15)	1659(5)	259(3)	2207(5)	59(2)
C(16)	1482(4)	279(3)	2977(5)	57(2)
C(17)	2144(5)	659(3)	3510(4)	40(2)
C(18)	4130(4)	1971(2)	7873(3)	29(1)
C(19)	4239(4)	2698(3)	7878(3)	32(1)
C(20)	4928(4)	3030(2)	7410(3)	29(1)
C(21)	5477(4)	2650(2)	6906(3)	26(1)
C(22)	4544(4)	774(2)	7532(3)	30(1)
C(23)	6994(4)	696(3)	6810(3)	23(1)
C(24)	7494(4)	111(2)	6507(3)	33(1)
C(25)	8244(4)	-291(3)	6977(4)	41(1)
C(26)	8503(4)	-117(3)	7758(3)	37(1)
C(27)	8031(5)	467(3)	8060(3)	35(1)
C(28)	7282(4)	873(2)	7588(3)	28(1)
C(29)	6992(4)	1883(2)	5786(3)	22(1)
C(30)	7860(5)	2171(3)	6265(3)	37(1)
C(31)	8544(5)	2653(3)	5975(3)	38(1)
C(32)	8367(4)	2865(3)	5201(3)	35(1)
C(33)	7502(5)	2588(4)	4730(3)	48(2)
C(34)	6824(4)	2087(3)	5014(3)	35(1)
C(35)	5018(4)	-288(2)	5848(3)	26(1)
C(36)	3901(5)	-193(2)	4488(3)	30(1)
C(37)	6069(5)	230(3)	4658(3)	40(1)
C(38)	3441(4)	802(2)	5684(3)	23(1)
C(1S)	10698(10)	1076(6)	9988(8)	72(3)
C(2S)	9940(11)	519(5)	10153(10)	75(4)

O(3S)	10354(9)	-160(5)	10035(7)	95(3)
C(4S)	9720(19)	-743(10)	10272(13)	128(7)
C(5S)	10168(14)	-1385(8)	9896(9)	99(5)
C(1T)	5210(20)	3938(11)	5165(14)	54(6)
C(2T)	5890(17)	4433(10)	4793(14)	53(6)
O(3T)	5193(12)	5017(7)	4528(9)	48(4)
C(4T)	4840(30)	5463(12)	5126(15)	59(6)
C(5T)	4450(20)	6109(11)	4671(14)	54(6)

Table 4.15. Bond lengths [\approx] and angles [∞] for C₃₈H₃₄B₂MoN₂O₄P₂(C₄H₁₀O).

Mo(1)-C(35)	1.960(5)
Mo(1)-C(36)	1.985(5)
Mo(1)-C(37)	2.012(5)
Mo(1)-C(38)	2.049(4)
Mo(1)-P(2)	2.6064(11)
Mo(1)-P(1)	2.6569(11)
P(1)-C(6)	1.840(4)
P(1)-C(12)	1.869(5)
P(1)-B(1)	1.947(5)
P(2)-C(29)	1.845(4)
P(2)-C(23)	1.862(5)
P(2)-B(2)	1.953(5)
O(1)-C(35)	1.164(6)
O(2)-C(36)	1.152(6)
O(3)-C(37)	1.144(7)
O(4)-C(38)	1.141(6)
N(1)-C(1)	1.371(7)
N(1)-B(1)	1.423(6)
N(1)-C(5)	1.439(7)
N(2)-C(18)	1.369(6)
N(2)-B(2)	1.429(6)
N(2)-C(22)	1.478(6)
B(1)-C(4)	1.485(7)
B(2)-C(21)	1.510(6)
C(1)-C(2)	1.348(9)
C(1)-H(1)	0.9500

C(2)-C(3)	1.403(9)
C(2)-H(2)	0.9500
C(3)-C(4)	1.373(7)
C(3)-H(3)	0.9500
C(4)-H(4)	0.9500
C(5)-H(5A)	0.9800
C(5)-H(5B)	0.9800
C(5)-H(5C)	0.9800
C(6)-C(7)	1.380(7)
C(6)-C(11)	1.402(6)
C(7)-C(8)	1.388(7)
C(7)-H(7)	0.9500
C(8)-C(9)	1.372(8)
C(8)-H(8)	0.9500
C(9)-C(10)	1.385(8)
C(9)-H(9)	0.9500
C(10)-C(11)	1.387(7)
C(10)-H(10)	0.9500
C(11)-H(11)	0.9500
C(12)-C(17)	1.396(7)
C(12)-C(13)	1.436(8)
C(13)-C(14)	1.371(8)
C(13)-H(13)	0.9500
C(14)-C(15)	1.394(12)
C(14)-H(14)	0.9500
C(15)-C(16)	1.373(12)
C(15)-H(15)	0.9500
C(16)-C(17)	1.360(9)
C(16)-H(16)	0.9500
C(17)-H(17)	0.9500
C(18)-C(19)	1.371(7)
C(18)-H(18)	0.9500
C(19)-C(20)	1.397(7)
C(19)-H(19)	0.9500
C(20)-C(21)	1.372(7)
C(20)-H(20)	0.9500
C(21)-H(21)	0.9500
C(22)-H(22A)	0.9800

C(22)-H(22B)	0.9800
C(22)-H(22C)	0.9800
C(23)-C(28)	1.385(7)
C(23)-C(24)	1.396(7)
C(24)-C(25)	1.384(7)
C(24)-H(24)	0.9500
C(25)-C(26)	1.386(8)
C(25)-H(25)	0.9500
C(26)-C(27)	1.375(9)
C(26)-H(26)	0.9500
C(27)-C(28)	1.389(8)
C(27)-H(27)	0.9500
C(28)-H(28)	0.9500
C(29)-C(34)	1.376(6)
C(29)-C(30)	1.389(7)
C(30)-C(31)	1.380(7)
C(30)-H(30)	0.9500
C(31)-C(32)	1.384(8)
C(31)-H(31)	0.9500
C(32)-C(33)	1.369(8)
C(32)-H(32)	0.9500
C(33)-C(34)	1.395(7)
C(33)-H(33)	0.9500
C(34)-H(34)	0.9500
C(1S)-C(2S)	1.462(14)
C(1S)-H(1S1)	0.9800
C(1S)-H(1S2)	0.9800
C(1S)-H(1S3)	0.9800
C(2S)-O(3S)	1.398(13)
C(2S)-H(2S1)	0.9900
C(2S)-H(2S2)	0.9900
O(3S)-C(4S)	1.440(17)
C(4S)-C(5S)	1.509(17)
C(4S)-H(4S1)	0.9900
C(4S)-H(4S2)	0.9900
C(5S)-H(5S1)	0.9800
C(5S)-H(5S2)	0.9800
C(5S)-H(5S3)	0.9800

C(1T)-C(2T)	1.46(2)
C(1T)-H(1T1)	0.9800
C(1T)-H(1T2)	0.9800
C(1T)-H(1T3)	0.9800
C(2T)-O(3T)	1.438(18)
C(2T)-H(2T1)	0.9900
C(2T)-H(2T2)	0.9900
O(3T)-C(4T)	1.44(2)
C(4T)-C(5T)	1.49(2)
C(4T)-H(4T1)	0.9900
C(4T)-H(4T2)	0.9900
C(5T)-H(5T1)	0.9800
C(5T)-H(5T2)	0.9800
C(5T)-H(5T3)	0.9800
C(35)-Mo(1)-C(36)	81.76(18)
C(35)-Mo(1)-C(37)	87.5(2)
C(36)-Mo(1)-C(37)	88.9(2)
C(35)-Mo(1)-C(38)	89.73(18)
C(36)-Mo(1)-C(38)	91.6(2)
C(37)-Mo(1)-C(38)	177.1(2)
C(35)-Mo(1)-P(2)	87.16(13)
C(36)-Mo(1)-P(2)	168.54(14)
C(37)-Mo(1)-P(2)	87.71(17)
C(38)-Mo(1)-P(2)	91.23(13)
C(35)-Mo(1)-P(1)	167.37(14)
C(36)-Mo(1)-P(1)	86.67(14)
C(37)-Mo(1)-P(1)	97.31(17)
C(38)-Mo(1)-P(1)	85.55(12)
P(2)-Mo(1)-P(1)	104.62(3)
C(6)-P(1)-C(12)	102.5(2)
C(6)-P(1)-B(1)	100.9(2)
C(12)-P(1)-B(1)	101.5(2)
C(6)-P(1)-Mo(1)	112.52(14)
C(12)-P(1)-Mo(1)	109.18(16)
B(1)-P(1)-Mo(1)	127.28(15)
C(29)-P(2)-C(23)	100.2(2)
C(29)-P(2)-B(2)	102.3(2)

C(23)-P(2)-B(2)	103.5(2)
C(29)-P(2)-Mo(1)	118.02(14)
C(23)-P(2)-Mo(1)	113.89(16)
B(2)-P(2)-Mo(1)	116.64(16)
C(1)-N(1)-B(1)	121.7(4)
C(1)-N(1)-C(5)	112.2(5)
B(1)-N(1)-C(5)	126.1(5)
C(18)-N(2)-B(2)	120.9(4)
C(18)-N(2)-C(22)	114.4(4)
B(2)-N(2)-C(22)	124.5(4)
N(1)-B(1)-C(4)	115.8(4)
N(1)-B(1)-P(1)	122.0(3)
C(4)-B(1)-P(1)	122.2(3)
N(2)-B(2)-C(21)	116.7(4)
N(2)-B(2)-P(2)	121.2(3)
C(21)-B(2)-P(2)	122.1(4)
C(2)-C(1)-N(1)	121.6(5)
C(2)-C(1)-H(1)	119.2
N(1)-C(1)-H(1)	119.2
C(1)-C(2)-C(3)	120.5(5)
C(1)-C(2)-H(2)	119.7
C(3)-C(2)-H(2)	119.7
C(4)-C(3)-C(2)	120.9(5)
C(4)-C(3)-H(3)	119.5
C(2)-C(3)-H(3)	119.5
C(3)-C(4)-B(1)	119.5(5)
C(3)-C(4)-H(4)	120.3
B(1)-C(4)-H(4)	120.3
N(1)-C(5)-H(5A)	109.5
N(1)-C(5)-H(5B)	109.5
H(5A)-C(5)-H(5B)	109.5
N(1)-C(5)-H(5C)	109.5
H(5A)-C(5)-H(5C)	109.5
H(5B)-C(5)-H(5C)	109.5
C(7)-C(6)-C(11)	118.2(4)
C(7)-C(6)-P(1)	123.6(3)
C(11)-C(6)-P(1)	118.2(3)
C(6)-C(7)-C(8)	121.1(5)

C(6)-C(7)-H(7)	119.5
C(8)-C(7)-H(7)	119.5
C(9)-C(8)-C(7)	120.5(5)
C(9)-C(8)-H(8)	119.7
C(7)-C(8)-H(8)	119.7
C(8)-C(9)-C(10)	119.5(4)
C(8)-C(9)-H(9)	120.3
C(10)-C(9)-H(9)	120.3
C(9)-C(10)-C(11)	120.2(5)
C(9)-C(10)-H(10)	119.9
C(11)-C(10)-H(10)	119.9
C(10)-C(11)-C(6)	120.5(4)
C(10)-C(11)-H(11)	119.7
C(6)-C(11)-H(11)	119.7
C(17)-C(12)-C(13)	117.6(5)
C(17)-C(12)-P(1)	120.8(4)
C(13)-C(12)-P(1)	121.6(4)
C(14)-C(13)-C(12)	119.6(6)
C(14)-C(13)-H(13)	120.2
C(12)-C(13)-H(13)	120.2
C(13)-C(14)-C(15)	120.7(7)
C(13)-C(14)-H(14)	119.6
C(15)-C(14)-H(14)	119.6
C(16)-C(15)-C(14)	119.7(6)
C(16)-C(15)-H(15)	120.1
C(14)-C(15)-H(15)	120.1
C(17)-C(16)-C(15)	120.7(6)
C(17)-C(16)-H(16)	119.7
C(15)-C(16)-H(16)	119.7
C(16)-C(17)-C(12)	121.7(6)
C(16)-C(17)-H(17)	119.2
C(12)-C(17)-H(17)	119.2
N(2)-C(18)-C(19)	121.8(4)
N(2)-C(18)-H(18)	119.1
C(19)-C(18)-H(18)	119.1
C(18)-C(19)-C(20)	120.5(4)
C(18)-C(19)-H(19)	119.8
C(20)-C(19)-H(19)	119.8

C(21)-C(20)-C(19)	121.8(4)
C(21)-C(20)-H(20)	119.1
C(19)-C(20)-H(20)	119.1
C(20)-C(21)-B(2)	118.3(4)
C(20)-C(21)-H(21)	120.9
B(2)-C(21)-H(21)	120.9
N(2)-C(22)-H(22A)	109.5
N(2)-C(22)-H(22B)	109.5
H(22A)-C(22)-H(22B)	109.5
N(2)-C(22)-H(22C)	109.5
H(22A)-C(22)-H(22C)	109.5
H(22B)-C(22)-H(22C)	109.5
C(28)-C(23)-C(24)	118.5(5)
C(28)-C(23)-P(2)	121.4(4)
C(24)-C(23)-P(2)	120.0(4)
C(25)-C(24)-C(23)	120.7(5)
C(25)-C(24)-H(24)	119.6
C(23)-C(24)-H(24)	119.6
C(24)-C(25)-C(26)	119.9(5)
C(24)-C(25)-H(25)	120.0
C(26)-C(25)-H(25)	120.0
C(27)-C(26)-C(25)	119.9(5)
C(27)-C(26)-H(26)	120.1
C(25)-C(26)-H(26)	120.1
C(26)-C(27)-C(28)	120.2(5)
C(26)-C(27)-H(27)	119.9
C(28)-C(27)-H(27)	119.9
C(23)-C(28)-C(27)	120.8(5)
C(23)-C(28)-H(28)	119.6
C(27)-C(28)-H(28)	119.6
C(34)-C(29)-C(30)	118.8(4)
C(34)-C(29)-P(2)	119.1(4)
C(30)-C(29)-P(2)	122.1(3)
C(31)-C(30)-C(29)	120.7(5)
C(31)-C(30)-H(30)	119.6
C(29)-C(30)-H(30)	119.6
C(30)-C(31)-C(32)	120.5(5)
C(30)-C(31)-H(31)	119.8

C(32)-C(31)-H(31)	119.8
C(33)-C(32)-C(31)	118.8(5)
C(33)-C(32)-H(32)	120.6
C(31)-C(32)-H(32)	120.6
C(32)-C(33)-C(34)	121.1(5)
C(32)-C(33)-H(33)	119.5
C(34)-C(33)-H(33)	119.5
C(29)-C(34)-C(33)	120.1(5)
C(29)-C(34)-H(34)	120.0
C(33)-C(34)-H(34)	120.0
O(1)-C(35)-Mo(1)	174.6(4)
O(2)-C(36)-Mo(1)	172.5(4)
O(3)-C(37)-Mo(1)	172.8(6)
O(4)-C(38)-Mo(1)	177.9(4)
C(2S)-C(1S)-H(1S1)	109.5
C(2S)-C(1S)-H(1S2)	109.5
H(1S1)-C(1S)-H(1S2)	109.5
C(2S)-C(1S)-H(1S3)	109.5
H(1S1)-C(1S)-H(1S3)	109.5
H(1S2)-C(1S)-H(1S3)	109.5
O(3S)-C(2S)-C(1S)	111.3(12)
O(3S)-C(2S)-H(2S1)	109.4
C(1S)-C(2S)-H(2S1)	109.4
O(3S)-C(2S)-H(2S2)	109.4
C(1S)-C(2S)-H(2S2)	109.4
H(2S1)-C(2S)-H(2S2)	108.0
C(2S)-O(3S)-C(4S)	115.1(13)
O(3S)-C(4S)-C(5S)	103.8(14)
O(3S)-C(4S)-H(4S1)	111.0
C(5S)-C(4S)-H(4S1)	111.0
O(3S)-C(4S)-H(4S2)	111.0
C(5S)-C(4S)-H(4S2)	111.0
H(4S1)-C(4S)-H(4S2)	109.0
C(4S)-C(5S)-H(5S1)	109.5
C(4S)-C(5S)-H(5S2)	109.5
H(5S1)-C(5S)-H(5S2)	109.5
C(4S)-C(5S)-H(5S3)	109.5
H(5S1)-C(5S)-H(5S3)	109.5

H(5S2)-C(5S)-H(5S3)	109.5
C(2T)-C(1T)-H(1T1)	109.5
C(2T)-C(1T)-H(1T2)	109.5
H(1T1)-C(1T)-H(1T2)	109.5
C(2T)-C(1T)-H(1T3)	109.5
H(1T1)-C(1T)-H(1T3)	109.5
H(1T2)-C(1T)-H(1T3)	109.5
O(3T)-C(2T)-C(1T)	105.1(16)
O(3T)-C(2T)-H(2T1)	110.7
C(1T)-C(2T)-H(2T1)	110.7
O(3T)-C(2T)-H(2T2)	110.7
C(1T)-C(2T)-H(2T2)	110.7
H(2T1)-C(2T)-H(2T2)	108.8
C(4T)-O(3T)-C(2T)	116.2(18)
O(3T)-C(4T)-C(5T)	101.8(18)
O(3T)-C(4T)-H(4T1)	111.4
C(5T)-C(4T)-H(4T1)	111.4
O(3T)-C(4T)-H(4T2)	111.4
C(5T)-C(4T)-H(4T2)	111.4
H(4T1)-C(4T)-H(4T2)	109.3
C(4T)-C(5T)-H(5T1)	109.5
C(4T)-C(5T)-H(5T2)	109.5
H(5T1)-C(5T)-H(5T2)	109.5
C(4T)-C(5T)-H(5T3)	109.5
H(5T1)-C(5T)-H(5T3)	109.5
H(5T2)-C(5T)-H(5T3)	109.5

Symmetry transformations used to generate equivalent atoms:

Table 4.16. Anisotropic displacement parameters ($\approx \times 10^3$) for C38H34B2MoN2O4P2(C4H10O). The anisotropic displacement factor exponent takes the form: $-2\pi^2 [h^2 a^{*2}U^{11} + \dots + 2 h k a^* b^* U^{12}]$

	U ¹¹	U ²²	U ³³	U ²³	U ¹³	U ¹²
Mo(1)	22(1)	15(1)	19(1)	-3(1)	2(1)	1(1)
P(1)	19(1)	18(1)	19(1)	-3(1)	1(1)	-2(1)
P(2)	20(1)	16(1)	19(1)	1(1)	0(1)	2(1)
O(1)	43(2)	20(2)	35(2)	5(1)	3(2)	4(1)
O(2)	68(3)	27(2)	31(2)	-6(2)	-2(2)	-18(2)
O(3)	67(3)	117(5)	56(3)	-6(3)	23(2)	47(3)
O(4)	33(2)	43(2)	39(2)	6(2)	12(2)	7(2)
N(1)	26(2)	41(2)	32(2)	-4(2)	-3(2)	4(2)
N(2)	26(2)	22(2)	26(2)	-4(1)	1(2)	1(1)
B(1)	16(2)	22(2)	17(2)	-2(2)	-3(2)	-6(2)
B(2)	26(3)	17(2)	22(2)	-2(2)	-2(2)	4(2)
C(1)	23(3)	80(4)	29(3)	-8(3)	4(2)	-6(3)
C(2)	34(3)	63(4)	33(3)	3(2)	5(2)	-22(3)
C(3)	44(3)	37(3)	34(3)	4(2)	-3(2)	-17(2)
C(4)	26(2)	31(2)	26(2)	-1(2)	2(2)	-5(2)
C(5)	63(4)	54(4)	48(4)	5(3)	9(3)	21(3)
C(6)	20(2)	21(2)	25(2)	-1(2)	2(2)	1(2)
C(7)	30(3)	34(2)	28(3)	-8(2)	-6(2)	3(2)
C(8)	28(3)	40(3)	46(3)	-3(2)	-4(2)	13(2)
C(9)	37(3)	35(2)	42(3)	-7(2)	9(2)	12(2)
C(10)	49(3)	31(2)	33(3)	-10(2)	-3(2)	10(2)
C(11)	34(3)	24(2)	27(2)	-5(2)	-7(2)	7(2)
C(12)	23(2)	23(2)	41(3)	-8(2)	-5(2)	5(2)
C(13)	33(3)	27(2)	41(3)	-1(2)	-14(2)	1(2)
C(14)	57(4)	34(3)	51(4)	-7(2)	-32(3)	8(3)
C(15)	37(3)	28(3)	99(6)	-16(3)	-41(4)	6(3)
C(16)	20(3)	28(3)	118(7)	-11(3)	-7(3)	1(2)
C(17)	27(3)	24(2)	73(4)	-10(3)	18(3)	0(2)
C(18)	26(2)	35(2)	26(2)	-10(2)	1(2)	2(2)
C(19)	26(2)	36(2)	34(3)	-14(2)	-2(2)	12(2)
C(20)	27(2)	20(2)	36(3)	-5(2)	-9(2)	7(2)
C(21)	26(2)	21(2)	28(2)	0(2)	-7(2)	0(2)

C(22)	39(3)	26(2)	26(2)	-2(2)	6(2)	-1(2)
C(23)	18(2)	23(2)	28(2)	8(2)	1(2)	0(2)
C(24)	32(3)	25(2)	40(3)	2(2)	-2(2)	4(2)
C(25)	29(3)	31(3)	61(4)	6(2)	-3(2)	6(2)
C(26)	22(2)	35(3)	50(3)	21(2)	-7(2)	-2(2)
C(27)	27(3)	46(3)	29(3)	12(2)	-5(2)	-16(2)
C(28)	27(2)	30(2)	28(2)	3(2)	1(2)	-3(2)
C(29)	23(2)	21(2)	22(2)	1(2)	2(2)	2(2)
C(30)	47(3)	37(3)	24(2)	6(2)	-8(2)	-17(2)
C(31)	43(3)	35(2)	36(3)	-2(2)	-2(2)	-16(2)
C(32)	33(3)	30(2)	42(3)	9(2)	5(2)	-4(2)
C(33)	37(3)	72(4)	33(3)	28(3)	-2(2)	-12(3)
C(34)	28(3)	50(3)	26(2)	10(2)	-4(2)	-7(2)
C(35)	27(2)	24(2)	25(2)	-10(2)	2(2)	1(2)
C(36)	43(3)	20(2)	28(2)	0(2)	3(2)	-5(2)
C(37)	36(3)	52(3)	35(3)	-9(2)	12(2)	12(2)
C(38)	23(2)	23(2)	22(2)	2(2)	2(2)	0(2)

Table 4.17. Hydrogen coordinates ($\times 10^4$) and isotropic displacement parameters ($\approx \times 10^3$) for C₃₈H₃₄B₂MoN₂O₄P₂(C₄H₁₀O).

	x	y	z	U(eq)
H(1)	6768	1940	2281	53
H(2)	6455	3133	2123	52
H(3)	5111	3696	2736	47
H(4)	4109	3061	3548	33
H(5A)	6156	863	2540	83
H(5B)	5480	726	3255	83
H(5C)	6706	991	3417	83
H(7)	1982	2239	3531	37
H(8)	956	3099	4072	47
H(9)	1505	3547	5313	45
H(10)	3113	3141	6014	46
H(11)	4155	2286	5473	35
H(13)	3810	1260	2330	42
H(14)	2630	634	1432	61
H(15)	1195	-11	1840	71
H(16)	890	24	3139	68
H(17)	1994	676	4036	48
H(18)	3666	1755	8202	35
H(19)	3843	2978	8203	38
H(20)	5019	3532	7442	34
H(21)	5925	2885	6580	31
H(22A)	5027	625	7995	46
H(22B)	4726	512	7075	46
H(22C)	3794	672	7610	46
H(24)	7318	-11	5972	40
H(25)	8581	-687	6764	49
H(26)	9005	-399	8085	44
H(27)	8219	592	8593	42
H(28)	6964	1277	7800	34
H(30)	7984	2035	6800	45
H(31)	9140	2841	6309	46

H(32)	8837	3197	5000	42
H(33)	7362	2740	4202	58
H(34)	6245	1885	4673	42
H(1S1)	10387	1544	10076	107
H(1S2)	11377	1018	10335	107
H(1S3)	10839	1039	9444	107
H(2S1)	9789	562	10701	90
H(2S2)	9251	582	9809	90
H(4S1)	8945	-676	10081	153
H(4S2)	9807	-791	10847	153
H(5S1)	9778	-1813	10027	148
H(5S2)	10081	-1323	9327	148
H(5S3)	10937	-1437	10088	148
H(1T1)	5635	3523	5361	81
H(1T2)	4922	4178	5601	81
H(1T3)	4606	3782	4782	81
H(2T1)	6500	4599	5171	64
H(2T2)	6182	4202	4347	64
H(4T1)	5451	5579	5533	71
H(4T2)	4258	5235	5374	71
H(5T1)	4188	6460	5023	81
H(5T2)	5046	6316	4425	81
H(5T3)	3863	5975	4267	81

Table 4.18. Torsion angles [$^{\circ}$] for C₃₈H₃₄B₂MoN₂O₄P₂(C₄H₁₀O).

C(1)-N(1)-B(1)-C(4)	-0.4(7)
C(5)-N(1)-B(1)-C(4)	178.2(5)
C(1)-N(1)-B(1)-P(1)	177.7(4)
C(5)-N(1)-B(1)-P(1)	-3.7(7)
C(18)-N(2)-B(2)-C(21)	2.8(6)
C(22)-N(2)-B(2)-C(21)	-172.9(4)
C(18)-N(2)-B(2)-P(2)	-175.2(4)
C(22)-N(2)-B(2)-P(2)	9.1(6)
B(1)-N(1)-C(1)-C(2)	1.0(8)
C(5)-N(1)-C(1)-C(2)	-177.8(6)
N(1)-C(1)-C(2)-C(3)	-1.3(8)
C(1)-C(2)-C(3)-C(4)	1.0(8)
C(2)-C(3)-C(4)-B(1)	-0.4(8)
N(1)-B(1)-C(4)-C(3)	0.2(7)
P(1)-B(1)-C(4)-C(3)	-178.0(4)
C(12)-P(1)-C(6)-C(7)	-21.6(4)
B(1)-P(1)-C(6)-C(7)	82.9(4)
Mo(1)-P(1)-C(6)-C(7)	-138.7(4)
C(12)-P(1)-C(6)-C(11)	159.0(4)
B(1)-P(1)-C(6)-C(11)	-96.5(4)
Mo(1)-P(1)-C(6)-C(11)	41.8(4)
C(11)-C(6)-C(7)-C(8)	-1.2(7)
P(1)-C(6)-C(7)-C(8)	179.4(4)
C(6)-C(7)-C(8)-C(9)	0.2(9)
C(7)-C(8)-C(9)-C(10)	0.6(9)
C(8)-C(9)-C(10)-C(11)	-0.3(8)
C(9)-C(10)-C(11)-C(6)	-0.7(8)
C(7)-C(6)-C(11)-C(10)	1.5(7)
P(1)-C(6)-C(11)-C(10)	-179.0(4)
C(6)-P(1)-C(12)-C(17)	-63.7(4)
B(1)-P(1)-C(12)-C(17)	-167.7(4)
Mo(1)-P(1)-C(12)-C(17)	55.9(4)
C(6)-P(1)-C(12)-C(13)	119.6(4)
B(1)-P(1)-C(12)-C(13)	15.6(4)
Mo(1)-P(1)-C(12)-C(13)	-120.8(4)
C(17)-C(12)-C(13)-C(14)	-1.0(7)

P(1)-C(12)-C(13)-C(14)	175.8(4)
C(12)-C(13)-C(14)-C(15)	-1.1(8)
C(13)-C(14)-C(15)-C(16)	1.9(9)
C(14)-C(15)-C(16)-C(17)	-0.4(9)
C(15)-C(16)-C(17)-C(12)	-1.8(9)
C(13)-C(12)-C(17)-C(16)	2.5(8)
P(1)-C(12)-C(17)-C(16)	-174.4(4)
B(2)-N(2)-C(18)-C(19)	-2.0(7)
C(22)-N(2)-C(18)-C(19)	174.2(5)
N(2)-C(18)-C(19)-C(20)	-1.0(8)
C(18)-C(19)-C(20)-C(21)	3.1(7)
C(19)-C(20)-C(21)-B(2)	-2.0(7)
N(2)-B(2)-C(21)-C(20)	-0.9(6)
P(2)-B(2)-C(21)-C(20)	177.1(4)
C(29)-P(2)-C(23)-C(28)	89.4(4)
B(2)-P(2)-C(23)-C(28)	-16.0(4)
Mo(1)-P(2)-C(23)-C(28)	-143.7(3)
C(29)-P(2)-C(23)-C(24)	-86.2(4)
B(2)-P(2)-C(23)-C(24)	168.4(4)
Mo(1)-P(2)-C(23)-C(24)	40.8(4)
C(28)-C(23)-C(24)-C(25)	1.4(7)
P(2)-C(23)-C(24)-C(25)	177.1(4)
C(23)-C(24)-C(25)-C(26)	0.2(8)
C(24)-C(25)-C(26)-C(27)	-1.5(8)
C(25)-C(26)-C(27)-C(28)	1.2(7)
C(24)-C(23)-C(28)-C(27)	-1.7(7)
P(2)-C(23)-C(28)-C(27)	-177.3(4)
C(26)-C(27)-C(28)-C(23)	0.4(7)
C(23)-P(2)-C(29)-C(34)	140.7(4)
B(2)-P(2)-C(29)-C(34)	-113.0(4)
Mo(1)-P(2)-C(29)-C(34)	16.5(4)
C(23)-P(2)-C(29)-C(30)	-41.1(5)
B(2)-P(2)-C(29)-C(30)	65.2(4)
Mo(1)-P(2)-C(29)-C(30)	-165.3(4)
C(34)-C(29)-C(30)-C(31)	-0.1(8)
P(2)-C(29)-C(30)-C(31)	-178.3(4)
C(29)-C(30)-C(31)-C(32)	0.9(9)
C(30)-C(31)-C(32)-C(33)	0.0(9)

C(31)-C(32)-C(33)-C(34)	-1.7(9)
C(30)-C(29)-C(34)-C(33)	-1.6(8)
P(2)-C(29)-C(34)-C(33)	176.6(5)
C(32)-C(33)-C(34)-C(29)	2.6(10)
C(1S)-C(2S)-O(3S)-C(4S)	173.0(15)
C(2S)-O(3S)-C(4S)-C(5S)	165.7(15)
C(1T)-C(2T)-O(3T)-C(4T)	69(3)
C(2T)-O(3T)-C(4T)-C(5T)	163.3(18)

4.4.4 Electronic structure analysis of azaborine-phosphine by UV-PES and quantum calculations.

UV-photoelectron spectra of 2-(N-methyl-1,2-BN-tolyl)-bis(2-methylphenyl)-phosphine (BN-phosphine) **4.41** and tri(*o*-tolyl)phosphine (phosphine) were recorded, and their UV-PES spectra are displayed at Figure 1.22. For sake of consistency and to allow a direct comparison between the BN-phosphine **4.41** and its all-carbon analogue, the latter UV-PES spectrum⁶⁸ has also been collected at a higher resolution. Also, for the reliable assignment of PE bands, different calculations of ionization energies using the 6-311G(d,p) basis set have been carried out on optimized geometrical parameters of molecular structures under investigation. Tables 4.9 and 4.10 contain calculated Kohn-Sham (CAM-B3LYP) energies of molecular orbitals (MO) ($-\epsilon^{K-S}$), Δ SCF+TD-DFT (CAM-B3LYP), OVGf, P3 and “corrected” ionization energies with the Molekel MOs visualization of **4.41** and tri(*o*-tolyl)phosphine in comparison with experimental values.

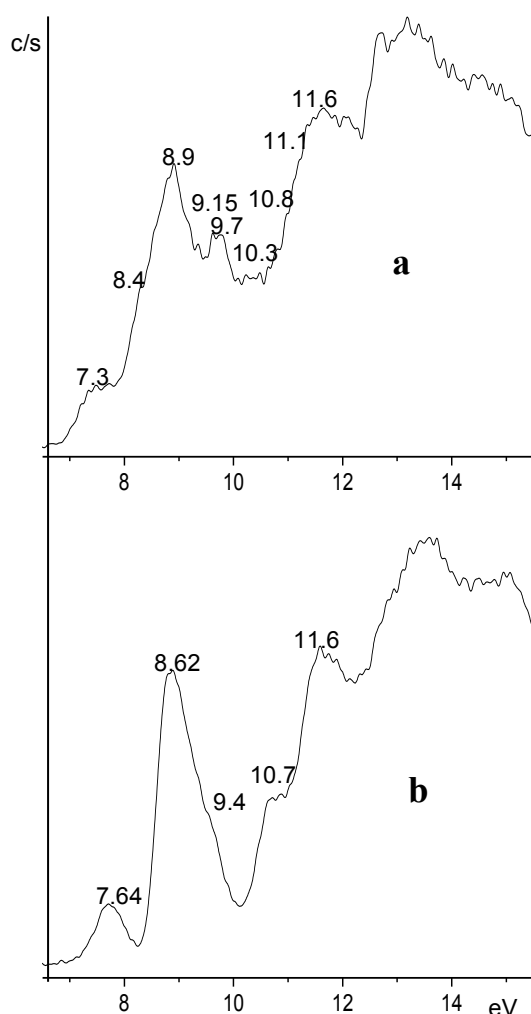


Figure 4.16. UV-photoelectron spectra of: (a) **4.41**, (b) tri(*o*-tolyl)phosphine.

⁶⁸Weiner, M. A.; Lattman, M.; Grim, S. O. *J. Org. Chem.* **1975**, *40*, 1292–1294.

Table 4.19. Calculated Kohn-Sham energies of MO ($-\epsilon^{\text{K-S}}$), $\Delta\text{SCF}+\text{TD-DFT}$ (CAM-B3LYP), OVGf and “corrected” ionization energies with the Molekel MOs visualization of **4.41** in comparison with experimental values (in eV). For all calculations 6-311G(d,p) basis set was applied.

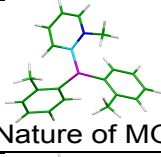
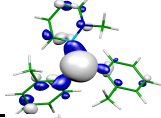
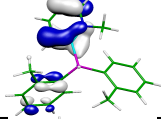
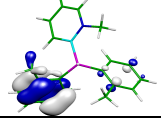
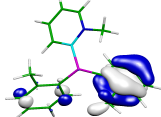
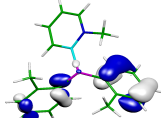
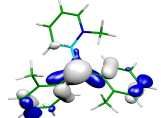
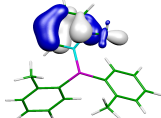
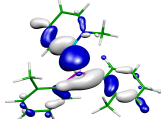
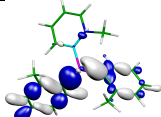
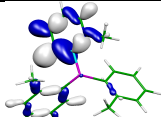
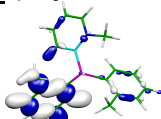
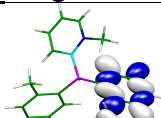
 Nature of MO	$-\epsilon^{\text{K-S}}$	$\Delta\text{SCF}+\text{TD-DFT}$	OVGF	P3	Corrected $X_{\text{exp}}=0.460$	Exp.
	6.840	7.155	7.053	7.228	7.300	7.3
	7.744	8.207	7.991	8.201	8.204	8.4
	7.966	8.493	8.219	8.465	8.426	
	8.137	8.656	8.403	8.653	8.597	8.9
	8.295	8.825	8.504	8.778	8.755	
	8.748	9.144	8.928	9.049	9.208	9.15
	9.280	9.835	9.589	9.678	9.740	9.7
	9.938	10.229	10.171	10.333	10.398	10.3
	10.147	10.477	10.444	10.682	10.607	10.8
	10.743	11.217	11.324	11.341	11.203	11.1
	10.836	11.239	11.377	11.486	11.296	11.65
	11.000	11.344	11.570	11.570	11.460	

Table 4.20. Calculated Kohn-Sham energies of MO ($-\epsilon^{K-S}$), Δ SCF+TD-DFT (CAM-B3LYP), OVGf and “corrected” ionization energies with the Molekel MOs visualization of tri(*o*-tolyl)phosphine in comparison with experimental values (in eV). For all calculations 6-311G(d,p) basis set was applied.

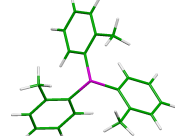
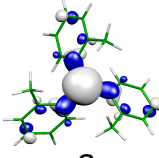
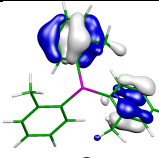
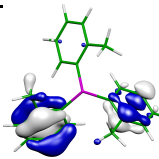
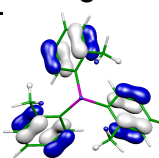
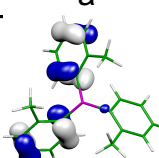
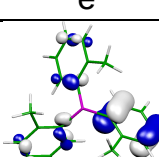
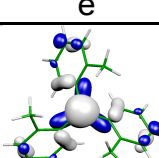
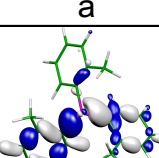
 Nature of MO	$-\epsilon^{K-S}$	Δ SCF+ TD-DFT	OVGF	P3	Corrected $X_{exp}=0.469$	Exp.
 a	7.171	7.490	7.369	7.590	7.640	7.64
 e	8.148	8.659	8.399	8.655	8.617	8.62
 e	8.148	8.659	8.399	8.655	8.617	
 a	8.273	8.848	8.549	8.781	8.742	
 e	8.455	8.946	8.644	8.933	8.924	
 e	8.455	8.946	8.644	8.933	8.924	
 a	9.030	9.417	9.222	9.332	9.499	9.4
 e	10.357	10.698	10.656	10.900	10.826	10.7

Table 4.21. Calculated [CAM-B3LYP/6-311G(d,p)] HOMO \rightarrow LUMO gap for **4.41** and tri(*o*-tolyl)phosphine.

	HOMO $\epsilon^{\text{K-S}}$ (eV)	HOMO-LUMO transition Δ_{HL} gap (eV), λ_{HL} (nm)	LUMO $\epsilon^{\text{K-S}}$ (eV)
2-(N-methyl-1,2-BN-tolyl)-bis(2-methylphenyl)-phosphine 4.41	-6.840	7.117 174.2	0.277
tri(<i>o</i> -tolyl)phosphine	-7.171	7.692 161.2	0.502

Additional computational results

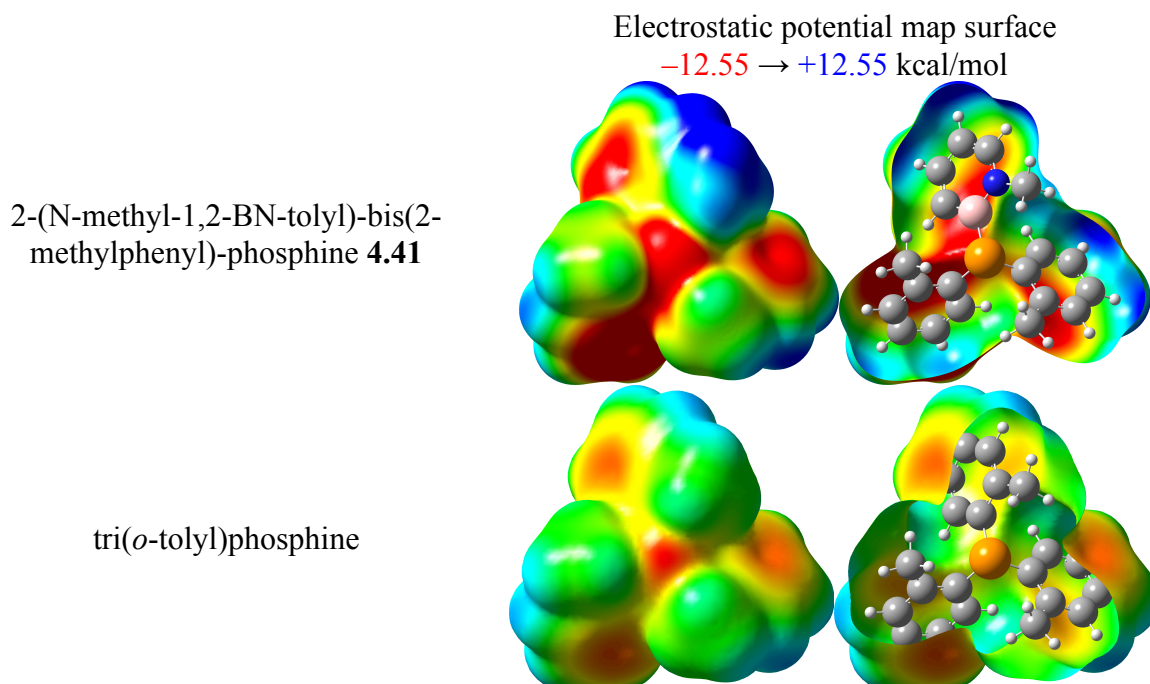
a. Ground and excited state dipole moment

Table 4.22. Dipole moments calculated for ground state [CAM-B3LYP/6-311G(d,p)] and first excited state [TD-DFT/CAM-B3LYP/6-311G(d,p)] for **4.41** and tri(*o*-tolyl)phosphine.

	Ground state dipole (debye)	First excited state dipole (debye)
2-(N-methyl-1,2-BN-tolyl)-bis(2-methylphenyl)-phosphine 4.41	2.306	3.560
tri(<i>o</i> -tolyl)phosphine	0.571	3.038

b. Electrostatic potential map surface

Table 4.23. Electrostatic potential map (from -12.55 to $+12.55$ kcal/mol) plotted on the 0.001 electron. au^{-3} isodensity surface. Calculated with [CAM-B3LYP/6-311G(d,p)] for **4.41** and tri(*o*-tolyl)phosphine.



c. Electron affinity

Table 4.24. Theoretical electron affinity (EA_{th}) and ionization energy (IE_{th}), first experimental IE_{exp} and $D(IE_{exp} + EA)$ for **4.41** and tri(*o*-tolyl)phosphine, calculated with CAM-B3LYP: 6-311G(d,p) basis set used for Δ SCF IE (neutral and cation); 6-311++G(d,p) basis set used for Δ SCF EA (neutral and anion) (all values in eV).

	Δ SCF IE_{th} (eV)	IE_{exp} (eV)	Δ SCF EA_{th} (eV)	$\Delta(IE_{exp}+EA_{th})$ (eV)
2-(N-methyl-1,2-BN-tolyl)-bis(2-methylphenyl)-phosphine 4.41	7.155	7.3	-0.401	6.90
tri(<i>o</i> -tolyl)phosphine	7.490	7.65	-0.705	6.95

Table 4.25 tri(*o*-tolyl)phosphine

Atomic coordinates for [CAM-B3LYP/6-311G(d,p)] optimized geometry:

Point group: C_3

C	-1.47142	2.37380	-0.61331
C	-0.40699	1.61323	-0.09372
C	0.34024	2.12496	0.96638
C	0.05552	3.36740	1.51420
C	-0.99268	4.11556	1.00517
C	-1.74548	3.61477	-0.04626
H	1.15812	1.54222	1.37122
H	0.65155	3.74433	2.33680
H	-1.22595	5.08797	1.42271
H	-2.56577	4.20205	-0.44424
P	0.00000	0.00000	-0.89364
C	1.60059	-0.45415	-0.09372
C	1.67015	-1.35713	0.96638
C	2.79148	0.08739	-0.61331
C	2.88849	-1.73178	1.51420
H	0.75654	-1.77407	1.37122
C	4.00323	-0.29575	-0.04626
C	4.06052	-1.19809	1.00517
H	2.91690	-2.43642	2.33680
H	4.92197	0.12100	-0.44424
H	5.01929	-1.48228	1.42271
C	-1.19360	-1.15908	-0.09372
C	-2.01039	-0.76783	0.96638
C	-1.32006	-2.46119	-0.61331
C	-2.94402	-1.63562	1.51420
H	-1.91466	0.23185	1.37122
C	-2.25774	-3.31902	-0.04626
C	-3.06784	-2.91747	1.00517
H	-3.56846	-1.30790	2.33680
H	-2.35620	-4.32305	-0.44424
H	-3.79334	-3.60569	1.42271
C	-0.45620	-2.95244	-1.74456
H	-0.78984	-3.93187	-2.08833
H	-0.47895	-2.26294	-2.59114
H	0.58870	-3.04362	-1.43606
C	-2.32879	1.87130	-1.74456
H	-1.72029	1.54626	-2.59114
H	-2.93020	1.01199	-1.43606
H	-3.01018	2.64996	-2.08833
C	2.78499	1.08114	-1.74456
H	2.19924	0.71669	-2.59114
H	2.34151	2.03164	-1.43606
H	3.80002	1.28191	-2.08833

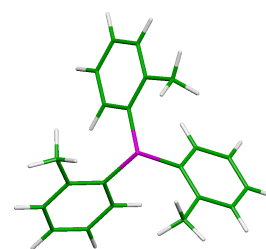
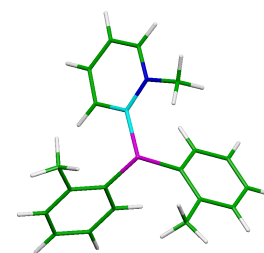


Table 4.26. compound 4.41

Atomic coordinates for [CAM-B3LYP/6-311G(d,p)] optimized geometry: Point group: C₁

C	-1.52004	1.93229	-0.89442
C	-1.72334	3.20312	-1.35119
C	-0.91095	4.27681	-0.91228
C	0.08997	4.05315	-0.02174
H	-2.16098	1.14020	-1.26592
H	-2.51201	3.41842	-2.06701
H	-1.07613	5.28276	-1.27368
H	0.72151	4.86219	0.32663
P	-0.03750	-0.05164	0.91338
C	-1.25766	-1.16517	0.08616
C	-0.90211	-1.98360	-0.98530
C	-2.57514	-1.21815	0.57722
C	-1.81801	-2.84544	-4.43003
H	0.10910	-1.94557	-1.37043
C	-3.48230	-2.08416	-0.02718
C	-3.11605	-2.89616	-1.08951
H	-1.51484	-3.47164	-2.40093
H	-4.49781	-2.12461	0.35199
H	-3.84203	-3.56505	-1.53658
C	4.43311	-0.56920	0.17193
C	2.15126	0.12616	-0.89181
C	2.26360	-1.66740	0.71934
C	3.39088	-0.22826	-1.40426
H	1.61638	0.95639	-1.33840
C	3.50256	-2.01450	0.18744
C	4.07078	-1.30461	-0.85940
H	3.81526	0.33025	-2.23020
H	4.03392	-2.86072	0.60915
H	5.03917	-1.59613	-1.24881
C	1.68803	-2.48592	1.84389
H	2.41008	-3.22452	2.19350
H	1.39815	-1.85502	2.68633
H	0.78880	-3.01881	1.52407
C	1.48580	2.72828	1.42282
H	1.29084	1.94962	2.15891
H	2.40953	2.48079	0.89635
H	1.61476	3.67665	1.94432
C	-3.02928	-0.35422	1.72386
H	-2.34644	-0.43003	2.57295
H	-3.06667	0.70067	1.43776
H	-4.02707	-0.64407	2.05514
B	-0.40778	1.66895	0.08734
N	0.36067	2.81791	0.48971



4.4.5 Cone Angle Determination

Cone angles for **4.41** and tri-*o*-tolylphosphine were determined using structures optimized by DFT calculations (*vide supra*). In the Avogadro program, a Ni atom was placed 2.28 Å away from the phosphorus atom. The distance (*d*) from the Ni atom to the outermost H atom of each aryl group along with the angle between the rotation axis and *d* (α) were measured (Figure 4.17).

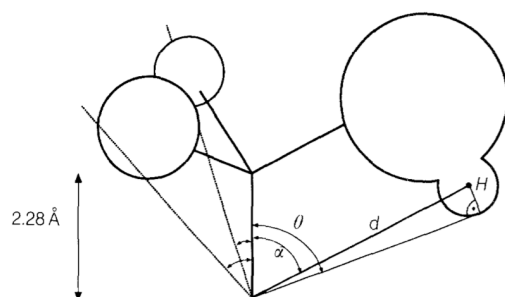


Figure 4.17. Scheme detailing the measurements used for determining cone angle.

The angle of interest (θ) was determined using equation 1:

$$\theta = \alpha + 180/\pi \times \sin^{-1}(V_r/d) \quad (1)$$

where V_r is the van-der-Waals radius of hydrogen, or 1.00 Å. The final cone angle was then determined according to equation 2:

$$\text{cone angle} = 2/3 \sum \theta_{1,2,3} \quad (2)$$

Table 4.28. Cone Angle Determination for **4.41** and tri-*o*-tolylphosphine
Compound 4.41

atom	α (°)	<i>d</i> (Å)	θ (°)
H37	70.9	4.359	84
H39	76.0	2.377	101
H32	76.8	2.4	101

Tri-*o*-tolylphosphine

atom	α (°)	<i>d</i> (Å)	θ (°)
H41	72.1	2.578	95
H37	75.8	2.390	101
H34	74.3	2.467	98

Cone angle for **4.41** = 191°

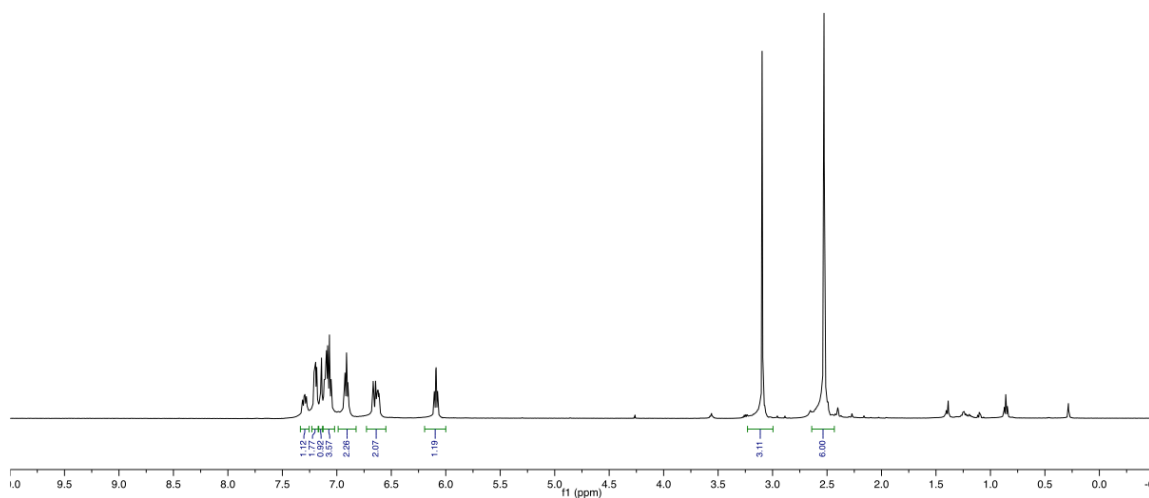
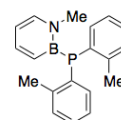
Cone angle for tri-*o*-tolylphosphine = 196°

Muller, T. E.; Mingos, D. M. P. Determination of the Tolman cone angle from crystallographic parameters and a statistical analysis using the Crystallographic Data Base. *Transition Met. Chem.* **1995**, 20, 533-539.

4.4.6 NMR Spectra

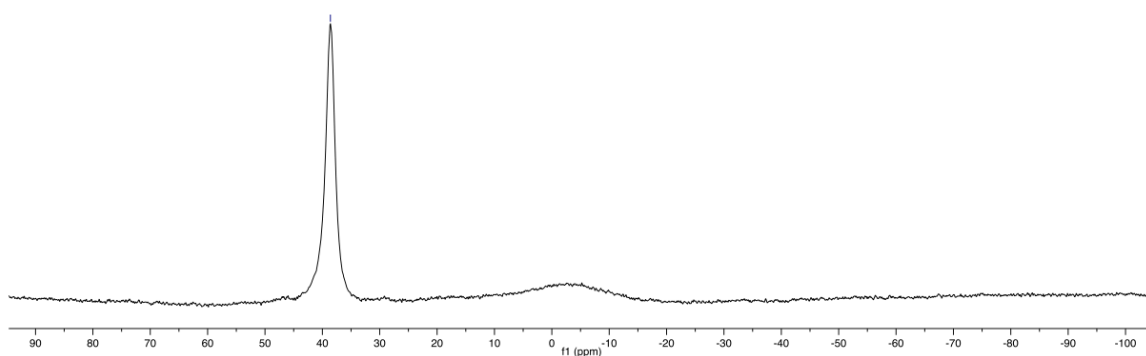
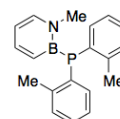
CRM-1-209-1H-10
triotolylphosphine ligand
recrystallized

Parameter	Value
1 Title	CRM-1-209-1H-10
2 Comment	triotolylphosphine ligand recrystallized
3 Solvent	c6d6
4 Temperature	25.0
5 Relaxation Delay	5.0000
6 Acquisition Date	2014-11-15T16:18:06
7 Nucleus	1H



CRM-1-209-11B-9
triotolylphosphine ligand
recrystallized

Parameter	Value
1 Title	CRM-1-209-11B-9
2 Comment	triotolylphosphine ligand recrystallized
3 Solvent	benzene
4 Temperature	25.0
5 Relaxation Delay	0.1000
6 Acquisition Date	2014-11-15T16:15:38
7 Nucleus	11B



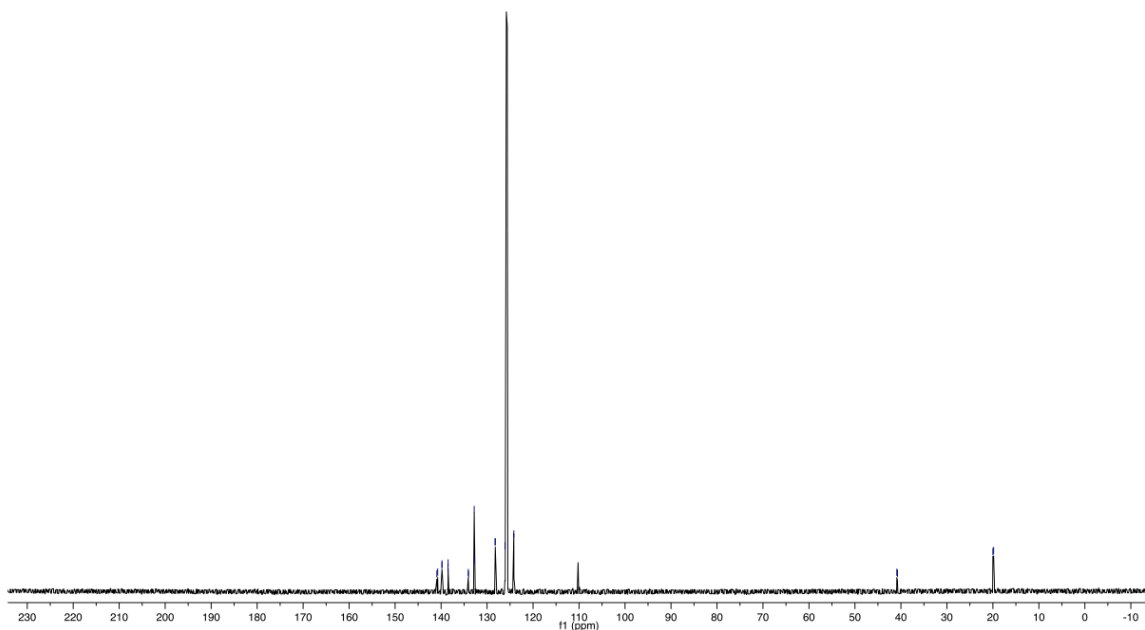
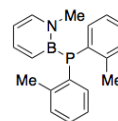
CRM-2-265-13C-7
BNtriotolyl

Parameter	Value
1 Title	CRM-2-265-13C-7
2 Comment	BNtriotolyl
3 Solvent	cd2cl2
4 Temperature	25.0
5 Relaxation Delay	1.0000
6 Acquisition Date	2017-01-13T17:43:20
7 Nucleus	13C

140.92
140.72
139.90
139.60
139.47
138.43
138.03
137.79
136.22
136.10
135.10

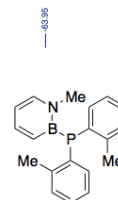
40.90
40.76

20.01
19.84

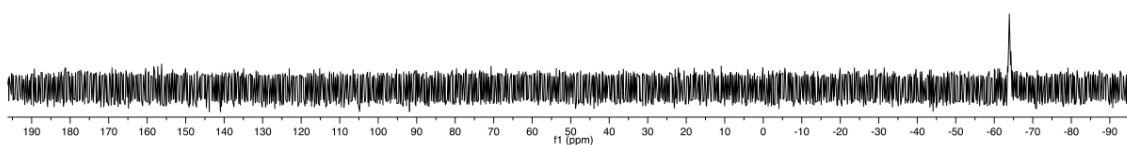


CRM-1-209-31P-8
triotolylphosphine ligand
recrystallized product

Parameter	Value
1 Title	CRM-1-209-31P-8
2 Comment	triotolylphosphine ligand recrystallized product
3 Solvent	benzene
4 Temperature	25.0
5 Relaxation Delay	1.0000
6 Acquisition Date	2014-11-15T16:12:21
7 Nucleus	31P

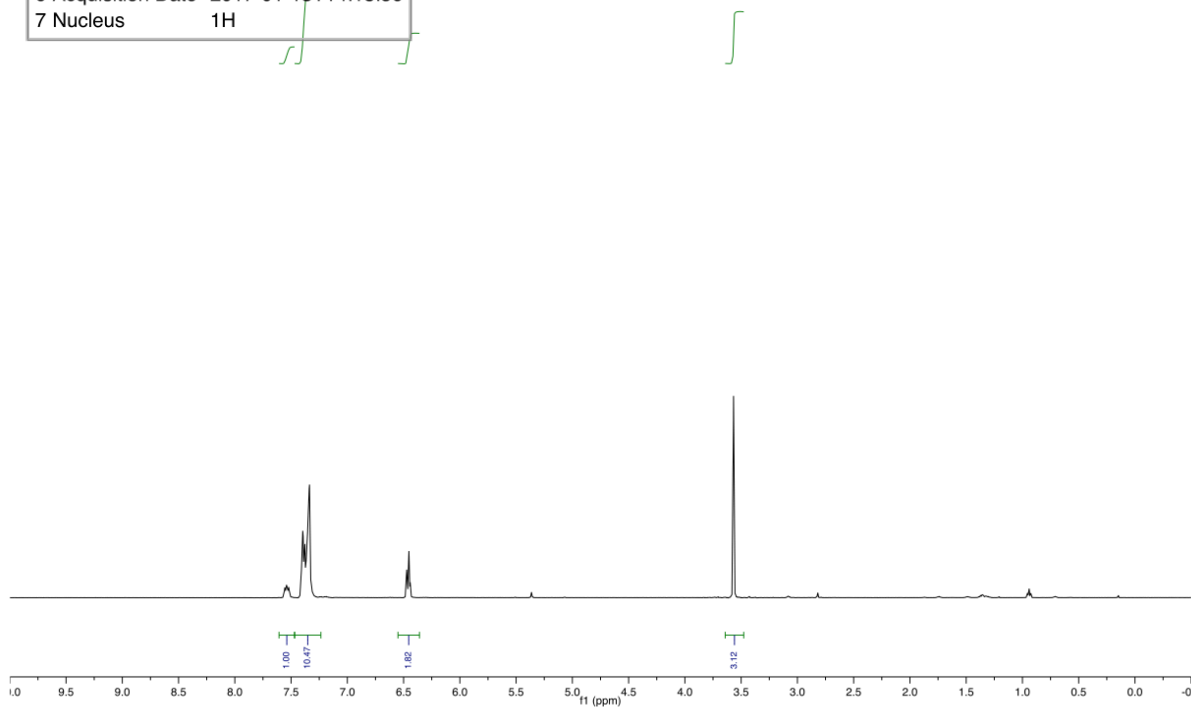
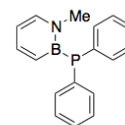


60.56



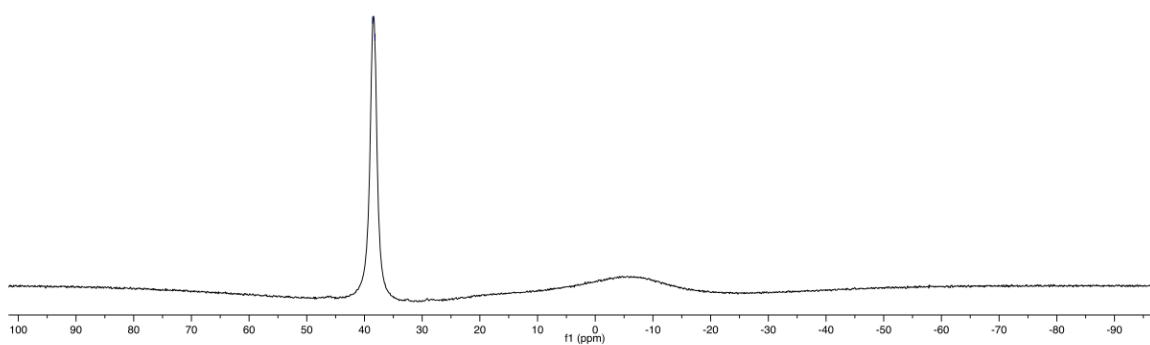
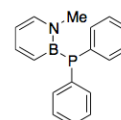
CRM-2-002-1H-6
NMeBPPPh2

Parameter	Value
1 Title	CRM-2-002-1H-6
2 Comment	NMeBPPPh2
3 Solvent	cd2cl2
4 Temperature	25.0
5 Relaxation Delay	1.0000
6 Acquisition Date	2017-01-13T14:18:56
7 Nucleus	1H



CRM-1-034-11B-4
PazaPh2 recrystallized

Parameter	Value
1 Title	CRM-1-034-11B-4
2 Comment	PazaPh2 recrystallized
3 Solvent	cd2cl2
4 Temperature	25.0
5 Relaxation Delay	0.0100
6 Acquisition Date	2016-10-18T17:31:11
7 Nucleus	11B



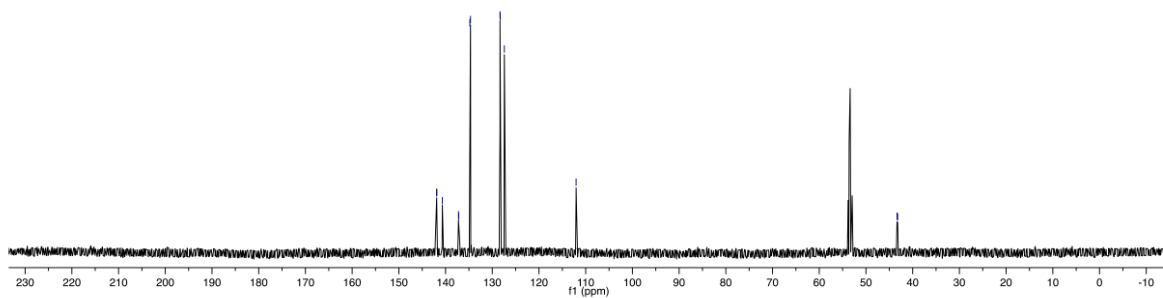
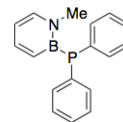
CRM-2-002-13C-6
NMePPh2 pentane wash

Parameter	Value
1 Title	CRM-2-002-13C-6
2 Comment	NMePPh2 pentane wash
3 Solvent	cd2cl2
4 Temperature	25.0
5 Relaxation Delay	1.0000
6 Acquisition Date	2017-01-12T22:41:45
7 Nucleus	13C

145.890
140.889
137.777
134.890
128.341
127.474

112.05

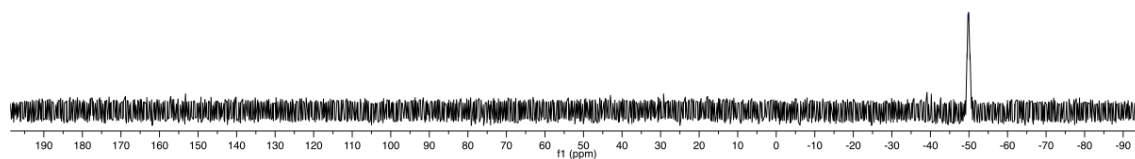
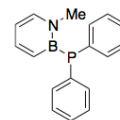
43.35
43.32



CRM-1-034-31P-6
PazaPh2 recrystallized

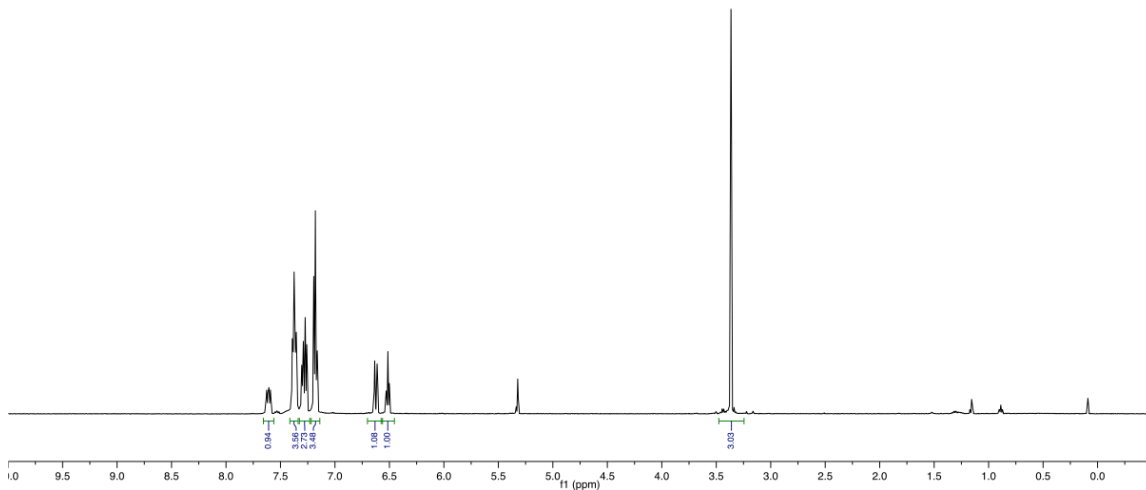
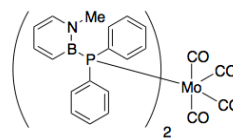
Parameter	Value
1 Title	CRM-1-034-31P-6
2 Comment	PazaPh2 recrystallized
3 Solvent	cd2cl2
4 Temperature	25.0
5 Relaxation Delay	1.0000
6 Acquisition Date	2016-10-18T17:40:01
7 Nucleus	31P

-49.89



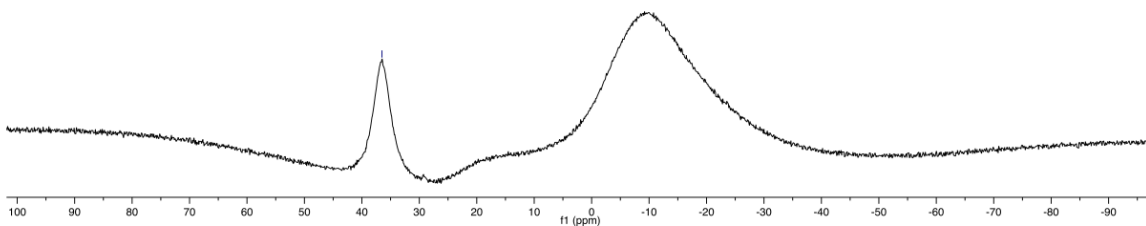
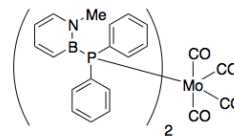
CRM-1-061-1H-3
NMeBPPH2 MoCO4 freezer crash out

Parameter	Value
1 Title	CRM-1-061-1H-3
2 Comment	NMePPh2 MoCO4 freezer crash out
3 Solvent	cd2cl2
4 Temperature	25.0
5 Relaxation Delay	1.0000
6 Acquisition Date	2017-01-12T20:54:50
7 Nucleus	1H



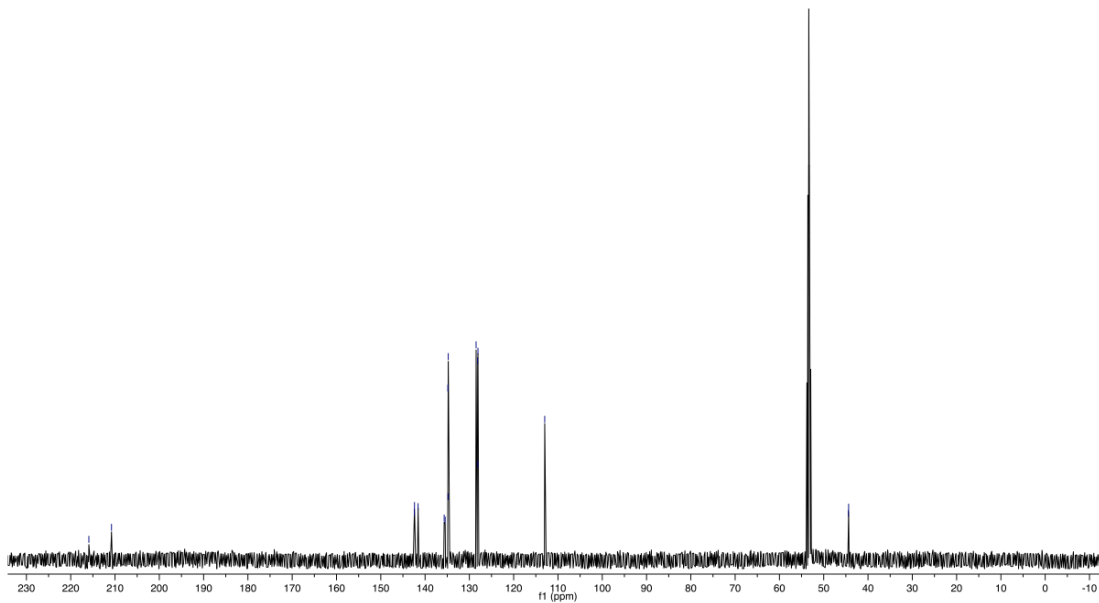
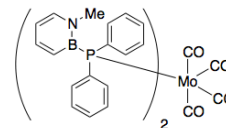
CRM-1-047-11B-10
NMeBPPH2 MoCO ether dcm rex

Parameter	Value
1 Title	CRM-1-047-11B-10
2 Comment	NMeBPPH2 MoCO ether dcm rex
3 Solvent	cd2cl2
4 Temperature	25.0
5 Relaxation Delay	0.0100
6 Acquisition Date	2017-01-04T19:01:09
7 Nucleus	11B



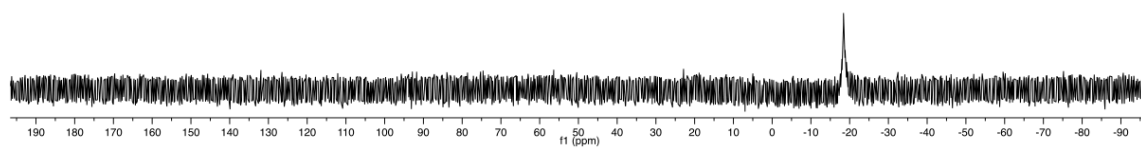
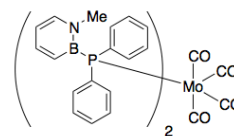
CRM-1-061-13C-4
NMePPh2 MoCO4 freezer crash out

Parameter	Value
1 Title	CRM-1-061-13C-4
2 Comment	NMePPh2 MoCO4 freezer crash out
3 Solvent	cd2cl2
4 Temperature	25.0
5 Relaxation Delay	1.0000
6 Acquisition Date	2017-01-12T20:58:07
7 Nucleus	13C



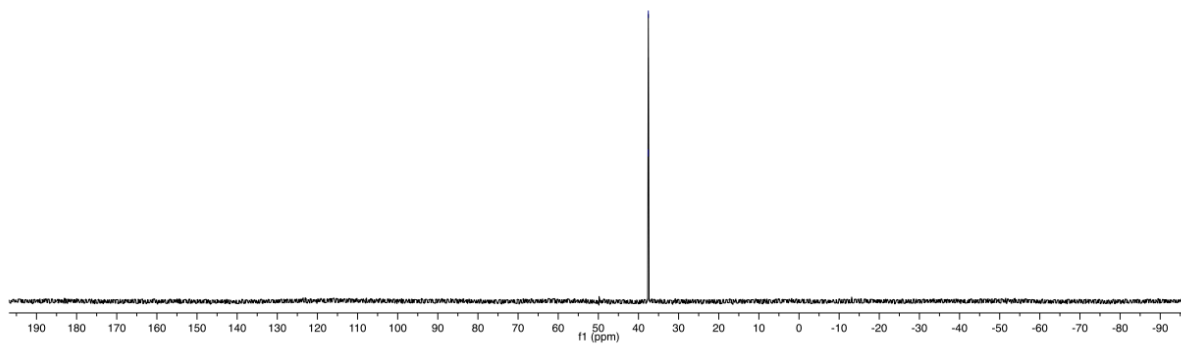
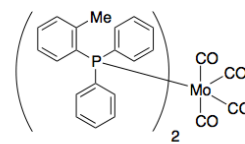
CRM-1-047-31P-1
NMeBPPPh2 addn to MoCO crude

Parameter	Value
1 Title	CRM-1-047-31P-1
2 Comment	NMeBPPPh2 addn to MoCO crude
3 Solvent	cd2cl2
4 Temperature	25.0
5 Relaxation Delay	1.0000
6 Acquisition Date	2016-11-12T15:14:13
7 Nucleus	31P

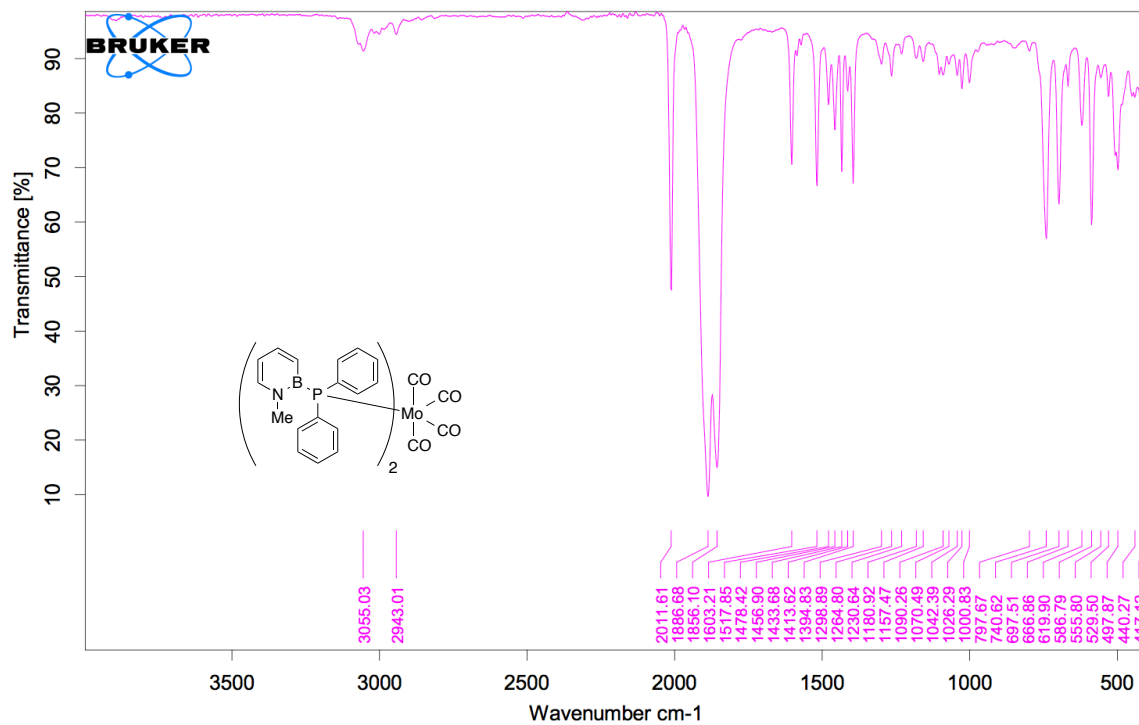


CRM-1-062-31P-2
otolyIPPh2 MoCO pentane dcm layer freezer crash out

Parameter	Value
1 Title	CRM-1-062-31P-2
2 Comment	otolyIPPh2 MoCO pentane dcm layer freezer crash out
3 Solvent	cd2cl2
4 Temperature	25.0
5 Relaxation Delay	1.0000
6 Acquisition Date	2017-01-05T11:37:51
7 Nucleus	31P



4.4.7 IR Spectra of 4.43 and 4.43c.



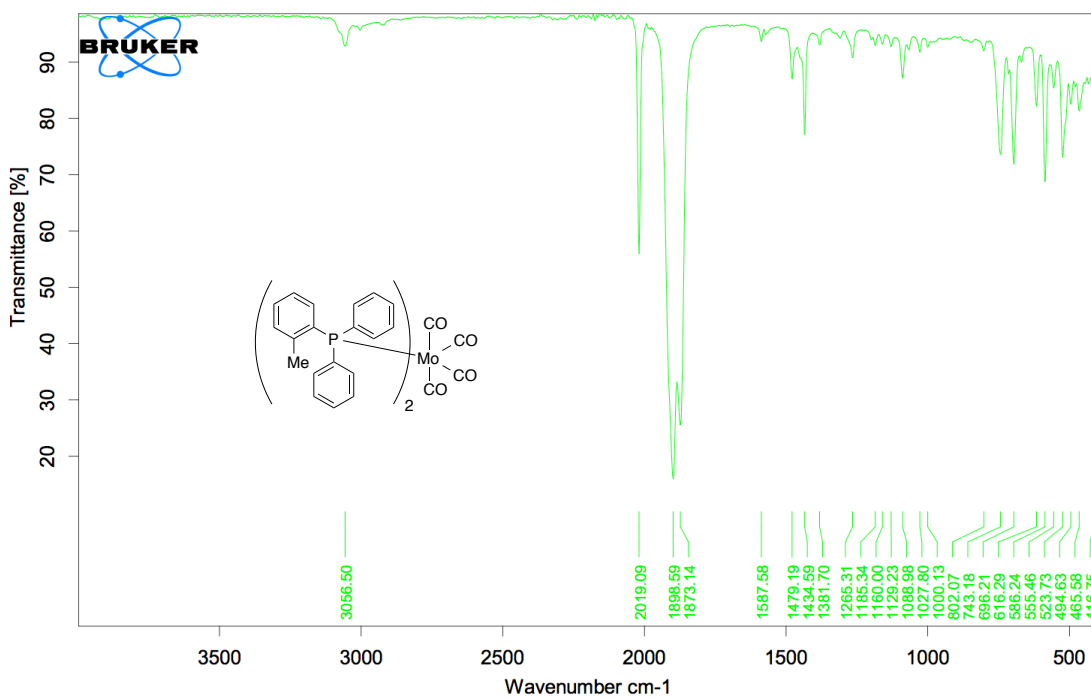
C:\OPUS_7.2.139.1294\MEAS\Sample description.264

Sample description

Instrument type and / or accessory

1/6/2017

Page 1/1



C:\OPUS_7.2.139.1294\MEAS\Sample description.265

Sample description

Instrument type and / or accessory

1/6/2017

Page 1/1